DOES IT CLICK?

Interfacial Click Reactions and H–bonded arrays as Studied by Ambient Mass Spectrometry and X–ray Photoelectron Spectroscopy

Digvijay Gahtory

Thesis committee

Promotor

Prof. Dr Han Zuilhof

Professor of Organic Chemistry

Wageningen University & Research

Co-promotor

Dr Maarten M.J. Smulders

Assistant professor, Laboratory of Organic Chemistry

Wageningen University & Research

Other members

Prof. Dr Harry Bitter, Wageningen University & Research

Prof. Dr Bart Jan Ravoo, University of Münster, Germany

Prof. Dr Floris P.J.T. Rutjes, Radboud University Nijmegen

Dr Dmitri Filippov, Leiden University

This research was conducted under the auspices of the Graduate School of VLAG (Advanced studies in Food Technology, Agrobiotechnology, Nutrition and Health Sciences).

DOES IT CLICK?

Interfacial Click Reactions and H–bonded Arrays as Studied by Ambient Mass Spectrometry and X–ray Photoelectron Spectroscopy

Digvijay Gahtory

Thesis

submitted in fulfillment of the requirements for the degree of doctor
at Wageningen University
by the authority of the Rector Magnificus,
Prof. Dr A.P.J. Mol,
in the presence of the
Thesis Committee appointed by the Academic Board
to be defended in public
on Wednesday 30 May 2018
at 4 p.m. in the Aula.

Digvijay Gahtory

Does it Click? Interfacial Click Reactions and H–bonded Arrays as Studied by Ambient Mass Spectrometry and X–ray Photoelectron Spectroscopy,

509 pages.

PhD thesis, Wageningen University, Wageningen, the Netherlands (2018)

With references, with summary in English

DOI: https://doi.org/10.18174/440360

ISBN: 978-94-6343-245-0

TABLE OF CONTENTS

PROPOSITIONS

1. The direct extrapolation of a reaction's kinetics and efficiency in solution to sterically hindered systems, such as surfaces and polymers, is not generally correct.

   (this thesis)

2. The most desirable characteristic of a true click reaction is orthogonality.

   (this thesis)

3. Seitz' 'universally applicable'-claim of FIT probes for single nucleotide polymorphism detection is not true. (*ChemBioChem* **2005**, *6*, 69)

4. Interfacial kinetics data without mentioning the reaction yields can be highly misleading. (Yatvin *et al*. *Angew. Chem. Int. Ed*. **2015**, *54*, 13370)

5. Simple rinsing instead of sonication, although extensively practised, is not rigorous enough to eliminate non–specific interactions. (Sanyal et al. *Langmuir*, **2004**, *20*, 5958; Park et al. *J. Am. Chem. Soc*. **2002**, *124*, 13366)

6. The aversion of reputed chemists towards public debates on science reflects in their say in policy making.

7. The ever increasing academic push towards scientific publications will eventually lead to the demise of curiosity-driven research.

8. Chasing a perfect scientific story is akin to chasing a proverbial ghost.

Propositions belonging to the thesis entitled

"Does it Click? Interfacial Click Reactions and H–bonded Arrays as Studied by Ambient Mass Spectrometry and X–ray Photoelectron Spectroscopy"

Digvijay Gahtory

Wageningen, 30 May 2018

CHAPTER 1

Introduction

AUTHOR'S PREFACE

This thesis narrates an approach towards amalgamation of synthetic organic and material chemistry. It explores the frontiers of covalent surface modification and subsequent chemical functionalization from an organic chemist's perspective. In the author's opinion, organic surface chemistry is basically performing organic reactions at a nanoscale under sterically confined conditions. Hence, provided that the analytical tools can be optimized to monitor a reaction, surfaces provide a highly complementary platform for conducting organic reactions. But some questions arise: how is surface modification usually done, and how can use of newer organic chemistry tools such as novel reactions add to the existing knowledge. For example, can the reaction efficiencies be increased or can the reactions be made orthogonal, etc.

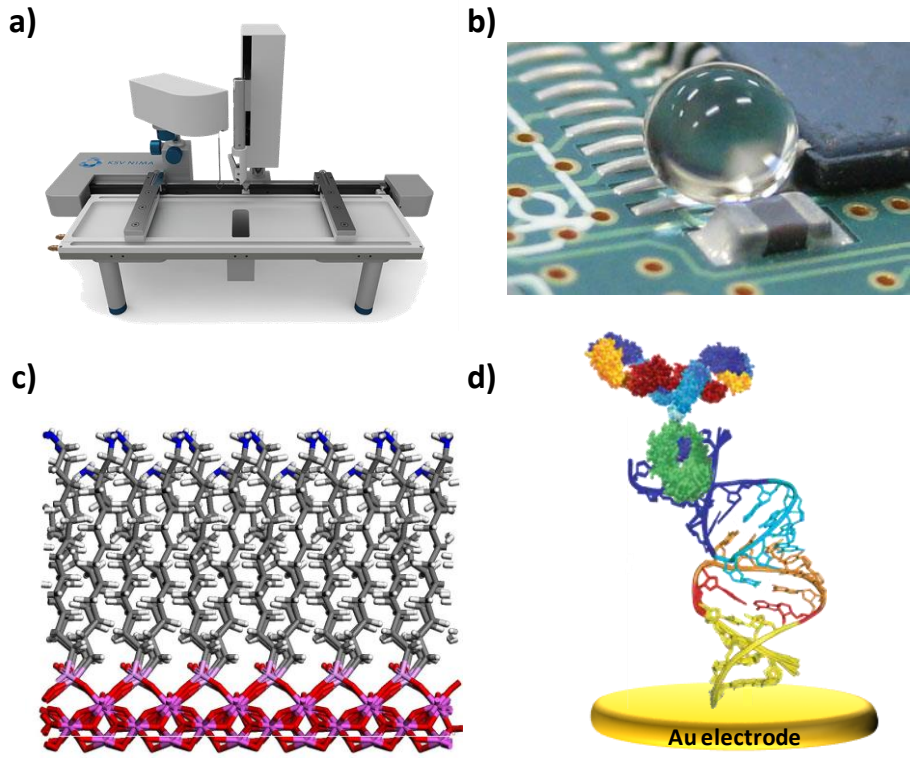

Figure 1. Tools and surface constructs to study surface interactions, a) Langmuir–Blodgett trough, b) superhydrophobic surface, (source for a and b: internet) c) 3D model depicting a covalently attached self–assembled monolayer on an aluminum surface with metal (Al–P) phosphonate ester bonds, and d) schematic of an antibody capture onto a DNA-functionalized gold electrode.

Solid surfaces are diverse in their characteristics - this diversity also applies to the need for diverse modification and functionalization methodologies. In fact, surface coatings have ubiquitous commercial applicability ranging from non–stick pans and canned food cases to antifouling coatings for marine vessels. Ever since the discovery of the Langmuir–Blodgett film deposition process[1] (Figure 1a), continual efforts have been made to systematically improve surface modification procedures to get a grip on surface behavior (Figure 1b). This involves control over surface properties such as adhesiveness, wettability, responsiveness, stability, redox capability, etc. The requirement of a tunable surface spans diverse applications like in electronics, battery science, bio–sensors, etc. Thus, development of effective strategies for surface functionalization is an ever–growing domain.

Generally speaking, surface modification usually involves either deposition of physisorbed overlayers, or formation of covalent bonds between the exposed surficial groups (for example created by plasma activation) and a reagent in either solution or gas phase to form strongly bound mono- or polymeric layers. These overlayers then provide a platform for further functionalization that can be done in two ways: covalently or non–covalently, both offering distinct advantages and disadvantages. While non–covalent interactions are weaker but allow dynamicity, covalent reactions are static but form more stable structures. Covalent surface modification with self–assembled monolayers (Figure 1c) offers an attractive alternative to physisorbed/deposited overlayers as they typically provide an increased molecular control. A typical example is the facile Au–S bond formation, which provides excellent control during modification of Au surfaces, and allows diverse chemical functionalization (Figure 1d). Other examples, on other surfaces, include more stable covalent bonds such as Si–C, Al–P and Si–O–C functionalization strategies. Once a stable monolayer has been formed, one can easily envision further chemical functionalization for attachment of different moieties.

Simple chemical transformations – such as amide coupling,[2] ester synthesis,[3] nucleophilic substitution[4] and imine formation[5] – have been well studied for monolayer modification, e.g. for the attachment of biomolecules, polymers, electroactive functionalities, etc. However, two major challenges for on–surface reactions are the relatively small amount of the surface-bound species and the inability to remove any undesired products formed. Hence, for optimal results a successful interfacial reaction has to fulfill the stringent criterion of excellent yields and no side–products with fast kinetics. Moreover, while the simple S_N2 transformation of surficial bromo groups to azides[4] or amide coupling using NHS[6] activation in some cases does achieve 100-% efficiency, it can't be classified as an interfacial click. The main reasons for this include either the lack of stability and orthogonality of the surface-bound reactive groups or the formation of a byproduct that may interact with the surface layer. The development of reaction methodologies and tailoring of known organic reactions to suit such stringent demands of an interfacial "click" transformation are the challenges we have tried to tackle in the research reported in this thesis. To this end, we focus on several reactions that are orthogonally reactive, fast, form stable products and yielding little to no byproducts.

The gold standards for quantitative surface analysis normally are X–ray photoelectron spectroscopy (XPS) and grazing angle attenuated total reflection–Fourier transform infrared (GATR–FTIR) spectroscopy. However, major limitations exist with these techniques, as XPS measurements require long and non–ambient measurement conditions, while infrared measurements are often limited to polar groups such as azides, cyano groups or isocyanates, and not generally applicable. We combat this challenge by using a new quantitative surface analysis technique based on ambient mass spectrometry, namely the direct analysis in real time–high resolution mass spectrometry (DART-HRMS) technique.[7] To summarize, the research in this thesis revolves around development of novel reaction methodologies that allow easy and efficient

surface functionalization and elaborates on the thorough analysis of these reactions.

CLICK CHEMISTRY

The term ‘click chemistry’ was first used by Kolb, Finn and Sharpless in their seminal review,[8] in which they introduced a new approach for organic transformations. The ‘guiding principles’ that a transformation should meet to be formally labelled click were described as modularity, high yields, wide scope, minimal side–products and mild reaction conditions. The earliest example of such reactions is the Huisgen dipolar cycloaddition of azides and alkynes published in 1967.[9] This reaction was further improved by the introduction of the copper–catalyzed azide–alkyne cycloaddition (CuAAC), independently by the groups of Sharpless[10] and Meldal[11] as the first organic click reaction, with excellent reaction yields (typically >90%).[12] Since its discovery, the reaction has been continually enriched and improved in methodology[13] and application.[14,15]

Scheme 1. a) Thermal 1,3 dipolar cycloaddition of azides and alkynes, and b) Copper-catalyzed azide–alkyne cycloaddition (CuAAC).

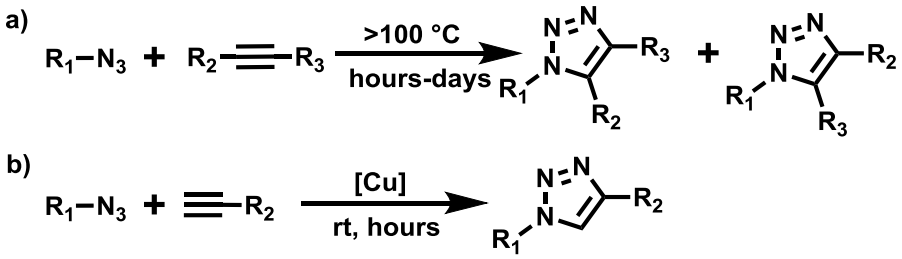

Probably, the next major advancement in the field of click chemistry was the use of reactant selectivity offered by a click reaction for cellular engineering by Bertozzi and co–workers.[16] Their strategy involved installing an azide motif onto a cell surface or to proteins by tricking the cellular biosynthetic machinery with azido tags that could be incorporated into the metabolic pathway.[17] The incorporated azide moieties then underwent a facile Staudinger ligation followed by an *in–situ* electrophilic capture to yield a stable amide linkage.[18]

The next breakthrough in this direction was the invention of the copper-free azide alkyne click reaction using strained cyclooctynes (the so-called SPAAC reaction), again by the group of Bertozzi.[19] Use of strained alkynes allowed for a fast and catalyst-free alternative to this high-yielding click reaction, which could then be conducted under physiological conditions free from the Cu(I)-mediated generation of reactive oxygen species (ROS) from O_2. The group developed a difluorinated cyclooctyne analogue (DIFO) which permitted a fast cycloaddition with second–order rate constant (k_2) of 7.6×10^{-2} $M^{-1}s^{-1}$.[19] As shown in Scheme 2b, several other strained alkyne analogues have been reported in the following years, which proffer distinct advantages that can be put to use for different applications.

Scheme 2. a) Strain-promoted azide–alkyne cycloaddition (SPAAC) and b) commonly used cycloctynes for SPAAC reactions.

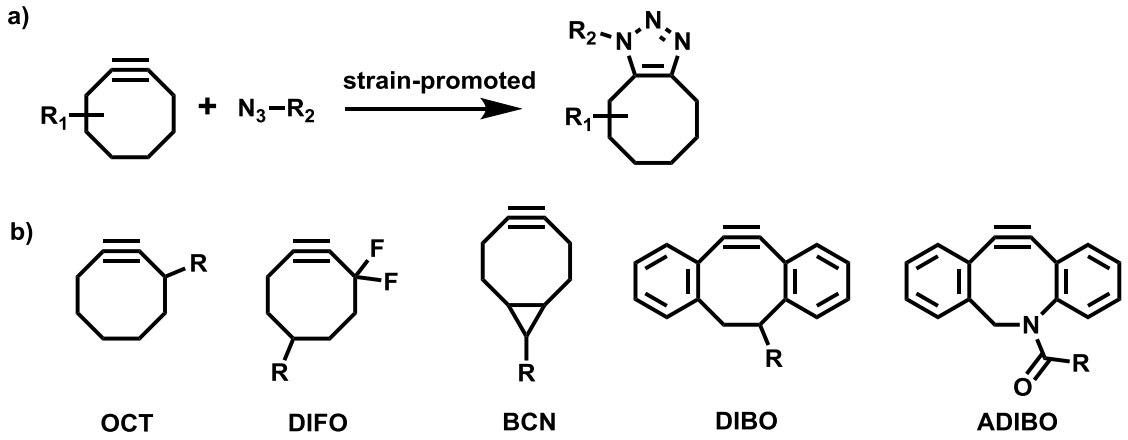

Another reaction category that has become a regular tool in the click toolbox is the inverse electron demand Diels–Alder (IEDDA) reaction (Scheme 3).[20] First discovered by Bachmann and Deno in 1949,[21] its click potential was realized independently by the groups of Hilderbrand[22] and Fox[23] in 2008. Although the actual mechanism of IEDDA reactions is disputed,[24] when compared to a normal Diels–Alder (DA) reactions in terms of frontier orbitals, they involve a dominant interaction of the LUMO of the diene with the HOMO of the dienophile (Scheme 3a).[25] The most successful IEDDA candidate for click purposes has been the cycloaddition of olefins with tetrazines (Scheme 3b). This reaction offers

advantages such as reactant stability, rapid kinetics, bio–orthogonal nature and catalyst–free conditions.[26] Notably, the use of strained alkenes and alkynes such as *trans*–cyclooctene (TCO),[27] bicyclononyne (BCN)[28] and norbornene[29] has gained prominence for a variety of bio–conjugation applications such as cancer cell labelling,[30] DNA modification,[31] polymer functionalization,[32] site–specific protein labelling,[33] etc.

Scheme 3. a) Frontier orbital model of normal DA and IEDDA. reactions. b) An IEDDA reaction between a tetrazine and an alkene.

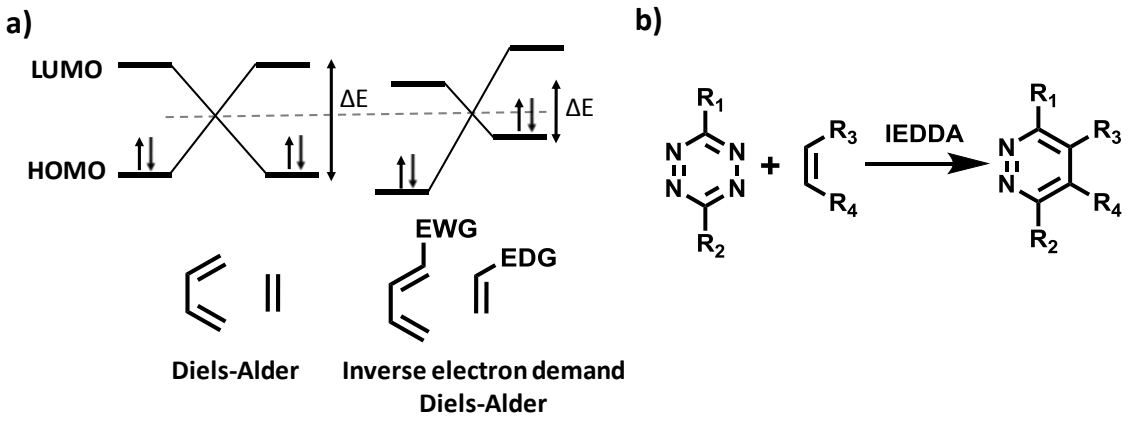

The tetrazine–TCO click is also one of the fastest known click conjugations[34] with second-order rate constants (k_2) generally in the order of 10^6 $M^{-1}s^{-1}$, making it an ideal candidate for rapid *in–vivo* click application[20] as per Houk's classification of metal-free click reactions.[35] A major disadvantage of this reaction, however, is the relatively easy isomerization of TCO to the unreactive *cis* isomer under physiological conditions (half–life of 3.26 h at 37 °C).[36] In contrast, more stable strained alkenes, such as norbornene, afford a much lower reaction rate (k_2 ~ 1 $M^{-1}s^{-1}$).[37] A lot of research has been devoted to the discovery of other TCO variants that offer better stability such as a conformationally strained dioxolane–fused trans-cyclooctene by Fox and co–workers.[38] A radical alternative has been provided by the group of Devaraj, who reported the use of 1–methyl–3–substituted cyclopropenes for rapid *in–vivo* cell labelling with tetrazines.[39] The use of cyclopropenes provides a more stable alternative albeit with a slightly slower kinetics (k_2 ~ 1–10 $M^{-1}s^{-1}$).[40] Further application of this click strategy was

shown by Patterson et al. for biorthogonal metabolic labelling.[41] They demonstrated that – while other strained alkenes and alkynes were less successful given their large sizes and incompatibility under physiological conditions – cyclopropenes stood out for metabolic labelling in living systems due to their small steric demands.

Scheme 3. IEDDA reactions between a tetrazine and different strained partners (only one regioisomer is shown for simplicity).

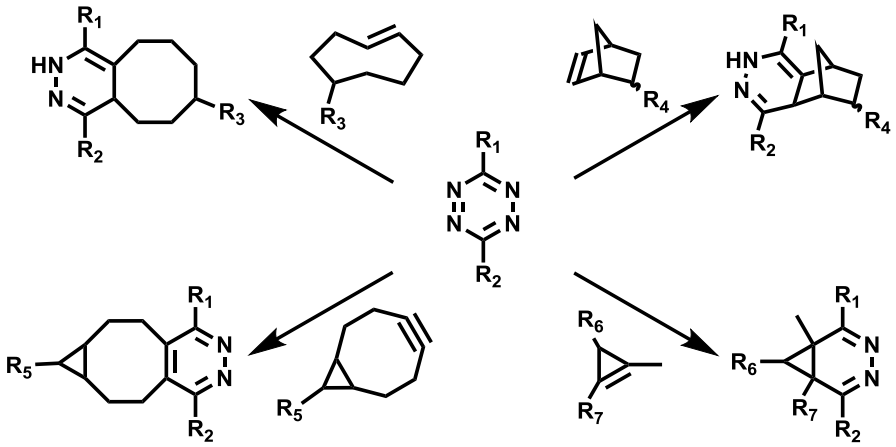

Several other strain-promoted click strategies have also been developed in subsequent years that have found increasing applications as bio–conjugation tools such as the strain-promoted alkyne nitrone (SPANC)[42] and nitrile oxide (SPANOC)[43] cycloaddition. However, an important drawback of several such click reactions is the lack of inducibility or temporal control of activation. This characteristic can be of great use especially during site-specific labelling of a biomolecule, such as in antibody drug conjugate (ADC) synthesis. Some strategies overcome this limitation by using a phototriggered click reaction such as UV-mediated cyclopropene–tetrazole click at 365 nm,[44] and photoactivation of an unreactive cyclooctyne analogue to the reactive counterpart at 350 nm for SPAAC.[45]

An alternative method was reported by Van Delft and co–workers,[46] who introduced the strain-promoted oxidation-controlled cyclooctyne–1,2–quinone cycloaddition (SPOCQ) [scheme 4a]. The reaction takes advantage of the easy

oxidation of catechol moieties into o-quinones by chemical,[47] enzymatic[48] or electrochemical[49] means, followed by a facile and rapid click with BCN.[50] The o-quinone motif can also be generated from genetically encoded tyrosine on proteins,[51] thereby providing an inducible click handle for protein labelling. Since its inception, this click strategy has been widely utilized for site specific protein bio–conjugation,[51] cell labelling[52] and hydrogel cross–linking.[53]

Scheme 4. a) SPOCQ reaction between BCN–OH and a quinone, and b) General scheme for a SuFEx reaction as catalyzed by DBU.

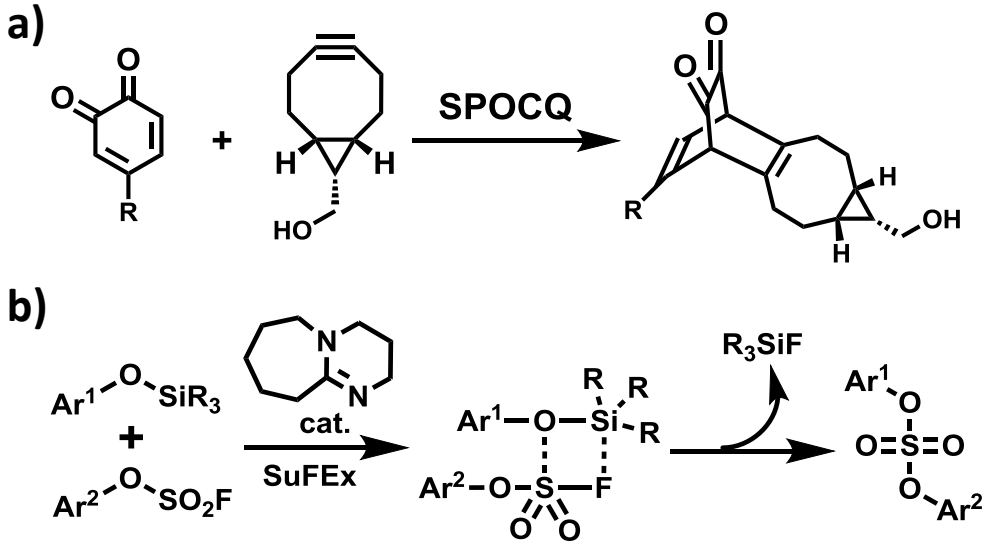

Most of the aforementioned click reactions involve formation of a new chemical entity by bringing together two species of which one can be regarded as having a high energetic nature (e.g. by ring strain), i.e. the reaction is driven by reactant destabilization. In contrast, the sulfur fluoride exchange (SuFEx) chemistry rediscovered by Sharpless and coworkers[54] utilizes a different approach, namely product stabilization, with the same effect, i.e. obtaining a click product. The reaction basically involves exchange of an S–F bond in sulfonyl fluorides with aryl silyl ethers or amines (Scheme 4b),[55] in the presence of certain catalysts such as di-azabicycloundec-7-ene (DBU),[56] 2-tert-butyl-imino-2-diethylamino-1,3-dimethyl- perhydro-1,3,2-diaza-phosphorine (BEMP),[56] or the HF_2^- anion.[57] The reaction offers distinct advantages such as exceptional chemical stability of

sulfonyl fluorides,[54] easy synthesis of the reactant modules[58] and a specialized reaction mechanism that involves fluoride anion stabilization,[54] hereby allowing control over reactivity. The reaction has shown excellent promise in solution especially for polymer synthesis,[59] with a rarely precedented reaction efficiency (>99.99%).[58]

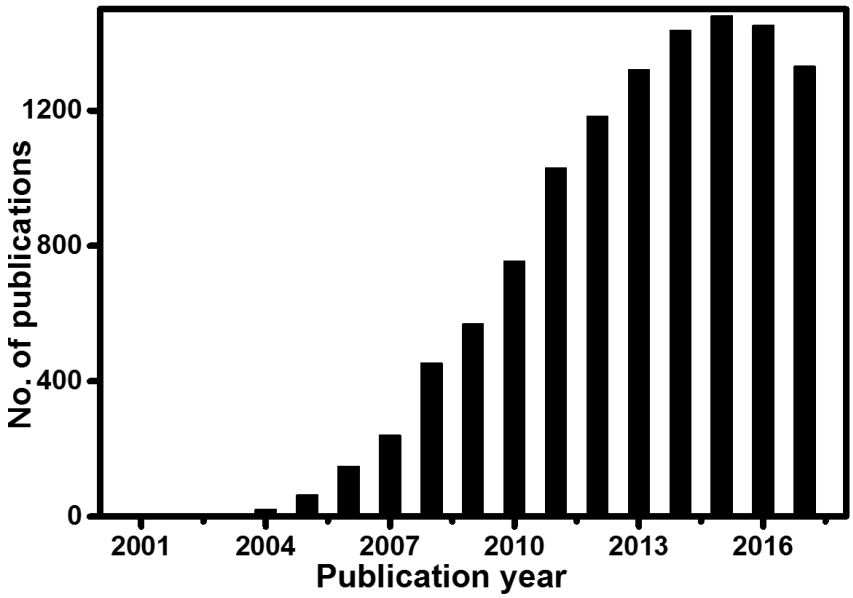

Figure 2. Number of publications per year as available in SCOPUS until 2017 under the search term “click chemistry”.

As shown in Figure 2, a plethora of literature has been published till date on click chemistry with several new reactions emerging every year with high efficiencies and potential for wide applications. However, when considering a surface, not a lot of click reactions have been as successful as in solution. This is further discussed in the next section.

CLICKING AT THE SURFACE

Organic reactions at surfaces face two distinct challenges, namely preclusion of a purification step after on-surface reactions, and the relatively small amounts of the surface-bound reactant (picomol range). Thus, in order to acquire optimal control over surface properties, a 100% reaction efficiency is desirable. Surface

functionalization by click modification has thus stood out as a highly efficient and kinetically superior method.[60] For example, the interfacial CuAAC has been shown to achieve high surface yields with fast kinetics by Hoffmann *et al*.[61] and Chidsey *et al*.[62] Using a combination of X–ray photoelectron spectroscopy (XPS), grazing angle infrared spectroscopy and electrochemical measurements on gold surfaces, Chidsey *et al*. showed that CuAAC achieved complete conversion with a second-order rate constant (k_2) of 1×10^3 $M^{-1}s^{-1}$.[62]

In recent years, also for surface-bound reactions the focus has shifted more towards utility of metal–free click reactions.[63] Since the first report of interfacial SPAAC (iSPAAC)[64] for click modification of silicon oxide surfaces by Popik, Locklin *et al*.[65] the reaction has found wide application such as in carbohydrate array preparation,[66] DNA immobilization,[67] nanoparticle functionalization,[68] protein attachment,[69] etc., on a wide variety of surfaces.[70] Similarly, other reactions – such as DA,[71,72] IEDDA,[73] thiol–ene/yne click,[74] etc. – have been increasingly explored with great success. However, despite a large number of metal-free reactions for surface applications that have been labelled as 'click reactions', in fact only few proceed with (near–)quantitative yields within an organic monolayer. For example, iSPAAC, while purported to be an interfacial click reaction, only affords a 20% yield on neat and about 40% on dilute monolayers[7] as analyzed by XPS.[70] Thus achieving quantitative conversions for interfacial click reactions remains an interesting challenge. A significant part of the work described in this thesis was devoted to that challenge.

Analysis of Interfacial Click Reactions

Another important aspect of interfacial reaction analysis is an accurate determination of the kinetics in real–time. Most research groups rely on XPS, electrochemical measurements or IR for getting a grip on the rate of an interfacial reaction. However, all of these methods suffer from disadvantages that strongly hamper an efficient analysis, such as low signal/noise ratios, limited scope, long

measurement times and/or use of high–vacuum. As a result, facile yet reliable measurements under routine, preferably ambient, conditions are not possible. Recently, Sen et al. devised a new methodology for interfacial kinetics determination under ambient conditions based on direct analysis in real time–high resolution mass spectrometry (DART-HRMS).[7,75]

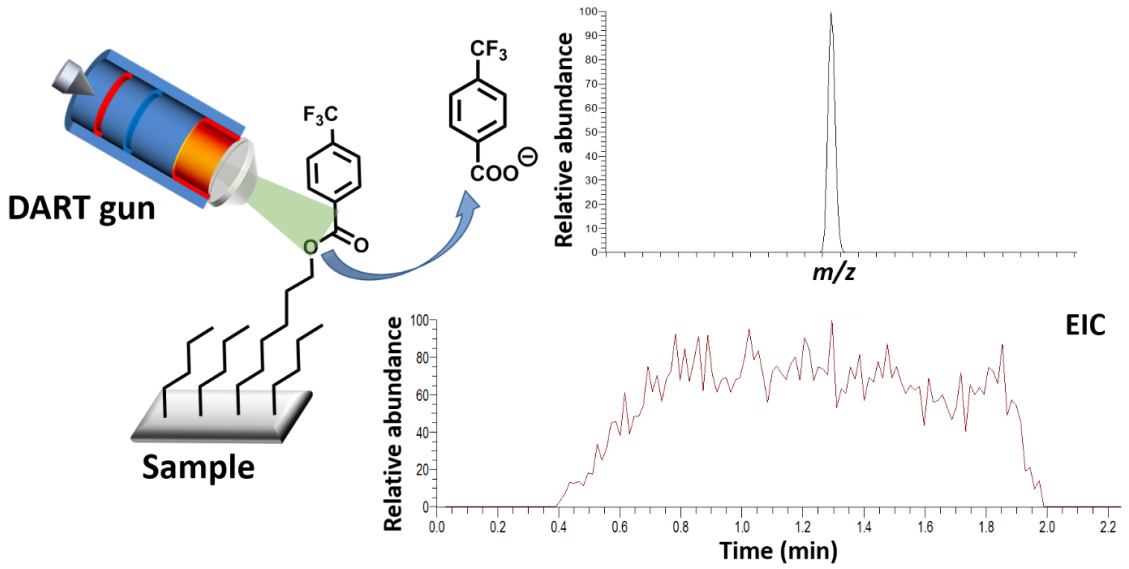

Figure 3. General methodology for kinetics measurement by DART–HRMS. Metastable He from the DART gun ionizes surface bound species which can be detected using a mass analyzer.

DART–HRMS is an ambient desorption ionization (ADI) mass spectrometry technique[75] that uses metastable helium (He) species at high temperatures to simultaneously ionize and desorb surface–bound species.[76] Using a diluted monolayer system on aluminum surfaces, our lab also showed that the reaction yield for iSPAAC could be enhanced to 37% – but also that attempts to further improvements failed – and elucidated the reaction kinetics along with the activation parameters. Using a similar methodology, they also reported the first quantitative click reaction on surfaces, the interfacial SPOCQ which achieved complete conversion in 4 h,[77] albeit only with clear reaction kinetics in the first ~25% of the reaction.

This suggested that performing click reactions on a surface offers a bigger challenge than in solution, and that a simple transposition of solution data to

reaction-bound organic transformations often fails. An important aspect of the work described in this thesis is therefore the establishment of reaction methodologies that are modular for different types of surfaces, as well as conducive to the available analytical tools. This is a challenge that we have tried to combat in this thesis.

OUTLINE OF THIS THESIS

The following six chapters will explore several click reactions and dynamic supramolecular interactions at surfaces. The primary focus will be on a fundamental study of different interactions and reaction parameters involved, on the determination of reaction efficiencies, and elucidation of interfacial kinetics.

In **chapter 2**, we validate the click character of a rather unexplored SuFEx reaction on surfaces. An analogous SuFEx reaction has been previously shown to provide excellent surface yields for post–polymerization modification on surfaces by Locklin and co–workers.[78] We develop a short route to smoothly prepare SuFExable monolayers using an easy Michael addition approach, which we follow-up on by a thorough investigation of surface yields and kinetics by XPS and DART–HRMS. Furthermore, we develop a dual–click platform whereby two successive click reactions are performed on the same chip, namely SuFEX–SPOCQ and SuFEX–CuAAC.

Chapter 3 describes a novel click reaction between 1–methyl 3–substituted cyclopropenes and quinones in solution and on surfaces. Our approach draws inspiration from the SPOCQ reaction by Van Delft and co–workers,[46] and the tetrazine cyclopropene click by the group of Devaraj.[41] We elucidate the solution and surface kinetics of the reaction, and demonstrate its utility for monolayer modification and polymer brush click functionalization.

Dynamic functionalization of surfaces with non–covalent interactions[79] provides an alternative to covalent functionalization, as such interactions provide an easily addressable handle for the quick attachment and removal of any bound

moieties,[80] which thus enables a surface-bound ON/OFF switch.[81] Multiple H–bonding arrays have garnered special interest in this regard due to their strength, specificity and reliability.[82] Thus in **chapter 4**, we explore the mechanistic details of quadruple H–bonded ureidopyrimidinone (UPy) dimers[83] on surfaces and investigate their dynamic and exchangeable nature. Using a combination of XPS, IR and DART–HRMS, we elucidate the kinetics of dimer formation and exchange, along with developing a solvent stimulus dependent ON/OFF platform that allows easy dimer attachment and removal.

In **chapter 5**, we describe a novel peptide nucleic acid (PNA)[84] sensor for single nucleotide polymorphism detection and antisense therapy based on an easy click functionalization strategy. The chapter explores a CuAAC functionalization of an azido amino acid incorporated at a specific position in a growing PNA chain that allows easy click attachment of a dye or cell-penetrating peptide.

In **chapter 6**, we showcase a novel strategy for functionalization of mica with ultrathin and ultrasmooth layers. Due to its atomic flatness, mica is a substrate of choice for atomic force microscopy (AFM) visualization of interesting biomolecules such as DNA.[85] However, the unavailability of an easy modification strategy for mica precluded a step–wise microscopic observation. Up to now! We design a mussel-based approach, and synthesize a catechol anchor that allows easy surface attachment with an amine handle for both rapid attachment and further modification. Despite the high propensity for catechols to auto–polymerize, we obtain ultrathin layers with very low roughness, and demonstrate the applicability of our strategy by observing step–wise formation of DNA minicircles.

Chapter 7 entails the study of the effect of approach of a solution reactant towards a surface-immobilized partner for the norbornene–tetrazine ligation.[29] The strategy involves a detailed physical-organic approach by studying the kinetics of the two reaction possibilities, i.e. the $\text{norbornene}_{\text{surface}}$ + $\text{tetrazine}_{\text{solution}}$

and norbornene$_{solution}$ + tetrazine$_{surface}$ using DART–HRMS and XPS. This is followed by a thorough rationalization of the results with DFT calculations and molecular mechanics studies. Furthermore, we also investigate effects of reactant stereochemistry (*exo* vs *endo*), in addition to the effect of the microenvironment.

Finally **chapter 8** contains a general summary of the research described in this thesis along with the author's opinion on future applications, further research possibilities and a delineation of some of the questions that still remain unanswered.

REFERENCES

(1) Ariga, K.; Yamauchi, Y.; Mori, T.; Hill, J. P. *Adv. Mater.* **2013**, *25*, 6477.

(2) Fabre, B.; Pujari, S. P.; Scheres, L.; Zuilhof, H. *Langmuir* **2014**, *30*, 7235.

(3) Rosso, M.; Giesbers, M.; Arafat, A.; Schroën, K.; Zuilhof, H. *Langmuir* **2009**, *25*, 2172.

(4) Debrassi, A.; Ribbera, A.; de Vos, W. M.; Wennekes, T.; Zuilhof, H. *Langmuir* **2014**, *30*, 1311.

(5) Rosso, M.; Giesbers, M.; Schroën, K.; Zuilhof, H. *Langmuir* **2010**, *26*, 866.

(6) Yang, M.; Teeuwen, R. L. M.; Giesbers, M.; Baggerman, J.; Arafat, A.; de Wolf, F. A.; van Hest, J. C. M.; Zuilhof, H. *Langmuir* **2008**, *24*, 7931.

(7) Sen, R.; Escorihuela, J.; Smulders, M. M. J.; Zuilhof, H. *Langmuir* **2016**, *32*, 3412.

(8) Kolb, H. C.; Finn, M. G.; Sharpless, K. B. *Angew. Chem. Int. Ed.* **2001**, *40*, 2004.

(9) Huisgen, R.; Szeimies, G.; Möbius, L. *Chem. Ber.* **1967**, *100*, 2494.

(10) Rostovtsev, V. V.; Green, L. G.; Fokin, V. V.; Sharpless, K. B. *Angew. Chem. Int. Ed.* **2002**, *41*, 2596.

(11) Tornøe, C. W.; Christensen, C.; Meldal, M. *J. Org. Chem.* **2002**, *67*, 3057.

(12) Feldman, A. K.; Colasson, B.; Fokin, V. V. *Org. Lett.* **2004**, *6*, 3897.

(13) Hein, J. E.; Fokin, V. V. *Chem. Soc. Rev.* **2010**, *39*, 1302.

(14) Meldal, M.; Tornøe, C. W. *Chem. Rev.* **2008**, *108*, 2952.

(15) Tiwari, V. K.; Mishra, B. B.; Mishra, K. B.; Mishra, N.; Singh, A. S.; Chen, X. *Chem. Rev.* **2016**, *116*, 3086.

(16) Saxon, E.; Bertozzi, C. R. *Science* **2000**, *287*, 2007.

(17) Kiick, K. L.; Saxon, E.; Tirrell, D. A.; Bertozzi, C. R. *Proc. Natl. Acad. Sci. USA* **2002**, *99*, 19.

(18) Chang, P. V.; Prescher, J. A.; Hangauer, M. J.; Bertozzi, C. R. *J. Am. Chem. Soc.* **2007**, *129*, 8400.

(19) Baskin, J. M.; Prescher, J. A.; Laughlin, S. T.; Agard, N. J.; Chang, P. V.; Miller, I. A.; Lo, A.; Codelli, J. A.; Bertozzi, C. R. *Proc. Natl. Acad. Sci. USA* **2007**, *104*, 16793.

(20) Oliveira, B. L.; Guo, Z.; Bernardes, G. J. L. *Chem. Soc. Rev.* **2017**, *46*, 4895.

(21) Bachmann, W. E.; Deno, N. C. *J. Am. Chem. Soc.* **1949**, *71*, 3062.

(22) Devaraj, N. K.; Weissleder, R.; Hilderbrand, S. A. *Bioconjugate Chem.* **2008**, *19*, 2297.

(23) Blackman, M. L.; Royzen, M.; Fox, J. M. *J. Am. Chem. Soc.* **2008**, *130*, 13518.

(24) Png, Z. M.; Zeng, H.; Ye, Q.; Xu, J. *Chem. Asian J.* **2017**, *12*, 2142.

(25) Knall, A.-C.; Slugovc, C. *Chem. Soc. Rev.* **2013**, *42*, 5131.

(26) Ehret, F.; Wu, H.; Alexander, S. C.; Devaraj, N. K. *J. Am. Chem. Soc.* **2015**, *137*, 8876.

(27) Devaraj, N. K.; Hilderbrand, S.; Upadhyay, R.; Mazitschek, R.; Weissleder, R. *Angew. Chem. Int. Ed.* **2010**, *49*, 2869.

(28) Lang, K.; Davis, L.; Wallace, S.; Mahesh, M.; Cox, D. J.; Blackman, M. L.; Fox, J. M.; Chin, J. W. *J. Am. Chem. Soc.* **2012**, *134*, 10317.

(29) Barker, I. A.; Hall, D. J.; Hansell, C. F.; Du Prez, F. E.; O'Reilly, R. K.; Dove, A. P. *Macromol. Rapid Commun.* **2011**, *32*, 1362.

(30) Devaraj, N. K.; Upadhyay, R.; Haun, J. B.; Hilderbrand, S. A.; Weissleder, R. *Angew. Chem. Int. Ed.* **2009**, *48*, 7013.

(31) Schoch, J.; Wiessler, M.; Jäschke, A. *J. Am. Chem. Soc.* **2010**, *132*, 8846.

(32) Hansell, C. F.; Lu, A.; Patterson, J. P.; O'Reilly, R. K. *Nanoscale* **2014**, *6*, 4102.

(33) Lang, K.; Davis, L.; Torres-Kolbus, J.; Chou, C.; Deiters, A.; Chin, J. W. *Nat. Chem.* **2012**, *4*, 298.

(34) Patterson, D. M.; Nazarova, L. A.; Prescher, J. A. *ACS Chem. biol.* **2014**, *9*, 592.

(35) Liu, F.; Liang, Y.; Houk, K. N. *Acc. Chem. Res.* **2017**, *50*, 2297.

(36) Rossin, R.; van den Bosch, S. M.; ten Hoeve, W.; Carvelli, M.; Versteegen, R. M.; Lub, J.; Robillard, M. S. *Bioconjugate Chem.* **2013**, *24*, 1210.

(37) Vrabel, M.; Kölle, P.; Brunner, K. M.; Gattner, M. J.; López-Carrillo, V.; de Vivie-Riedle, R.; Carell, T. *Chem. Eur. J.* **2013**, *19*, 13309.

(38) Darko, A.; Wallace, S.; Dmitrenko, O.; Machovina, M. M.; Mehl, R. A.; Chin, J. W.; Fox, J. M. *Chem. Sci.* **2014**, *5*, 3770.

(39) Yang, J.; Šečkutė, J.; Cole, C. M.; Devaraj, N. K. *Angew. Chem. Int. Ed.* **2012**, *51*, 7476.

(40) Yang, J.; Liang, Y.; Šečkutė, J.; Houk, K. N.; Devaraj, N. K. *Chem. Eur. J.* **2014**, *20*, 3365.

(41) Patterson, D. M.; Nazarova, L. A.; Xie, B.; Kamber, D. N.; Prescher, J. A. *J. Am. Chem. Soc.* **2012**, *134*, 18638.

(42) Ning, X.; Temming, R. P.; Dommerholt, J.; Guo, J.; Ania, D. B.; Debets, M. F.; Wolfert, M. A.; Boons, G.-J.; van Delft, F. L. *Angew. Chem. Int. Ed.* **2010**, *49*, 3065.

(43) Sanders, B. C.; Friscourt, F.; Ledin, P. A.; Mbua, N. E.; Arumugam, S.; Guo, J.; Boltje, T. J.; Popik, V. V.; Boons, G.-J. *J. Am. Chem. Soc.* **2011**, *133*, 949.

(44) Yu, Z.; Pan, Y.; Wang, Z.; Wang, J.; Lin, Q. *Angew. Chem. Int. Ed.* **2012**, *51*, 10600.

(45) Poloukhtine, A. A.; Mbua, N. E.; Wolfert, M. A.; Boons, G.-J.; Popik, V. V. *J. Am. Chem. Soc.* **2009**, *131*, 15769.

(46) Borrmann, A.; Fatunsin, O.; Dommerholt, J.; Jonker, A. M.; Löwik, D. W. P. M.; van Hest, J. C. M.; van Delft, F. L. *Bioconjugate Chem.* **2015**, *26*, 257.

(47) Ayyadurai, N.; Prabhu, N. S.; Deepankumar, K.; Jang, Y. J.; Chitrapriya, N.; Song, E.; Lee, N.; Kim, S. K.; Kim, B.-G.; Soundrarajan, N.; Lee, S.; Cha, H. J.; Budisa, N.; Yun, H. *Bioconjugate Chem.* **2011**, *22*, 551.

(48) Bruins, J. J.; Albada, B.; van Delft, F. *Chem. Eur. J.* **2017**, *23*, 1.

(49) Nematollahi, D.; Dehdashtian, S. *Tet. Lett.* **2008**, *49*, 645.

(50) Escorihuela, J.; Das, A.; Looijen, W. J. E.; van Delft, F. L.; Aquino, A. J. A.; Lischka, H.; Zuilhof, H. *J. Org. Chem.* **2018**, *83*, 244.

(51) Bruins, J. J.; Westphal, A. H.; Albada, B.; Wagner, K.; Bartels, L.; Spits, H.; van Berkel, W. J. H.; van Delft, F. L. *Bioconjugate Chem.* **2017**, *28*, 1189.

(52) George, A.; Krishna Priya, G.; Ilamaran, M.; Kamini, N. R.; Ganesh, S.; Easwaramoorthi, S.; Ayyadurai, N. *ChemistrySelect* **2017**, *2*, 7117.

(53) Jonker, A. M.; Borrmann, A.; van Eck, E. R. H.; van Delft, F. L.; Löwik, D. W. P. M.; van Hest, J. C. M. *Adv. Mater.* **2015**, *27*, 1235.

(54) Dong, J.; Krasnova, L.; Finn, M. G.; Sharpless, K. B. *Angew. Chem. Int. Ed.* **2014**, *53*, 9430.

(55) Dondoni, A.; Marra, A. *Org. Biomol. Chem.* **2017**, *15*, 1549.

(56) Li, S.; Wu, P.; Moses, J. E.; Sharpless, K. B. *Angew. Chem. Int. Ed.* **2017**, *56*, 2903.

(57) Gao, B.; Zhang, L.; Zheng, Q.; Zhou, F.; Klivansky, L. M.; Lu, J.; Liu, Y.; Dong, J.; Wu, P.; Sharpless, K. B. *Nat. Chem.* **2017**, *9*, 1083.

(58) Wang, H.; Zhou, F.; Ren, G.; Zheng, Q.; Chen, H.; Gao, B.; Klivansky, L.; Liu, Y.; Wu, B.; Xu, Q.; Lu, J.; Sharpless, K. B.; Wu, P. *Angew. Chem. Int. Ed.* **2017**, *56*, 11203.

(59) Yatvin, J.; Brooks, K.; Locklin, J. *Chem. Eur. J.* **2016**, *22*, 16348.

(60) Rusmini, F.; Zhong, Z.; Feijen, J. *Biomacromolecules* **2007**, *8*, 1775.

(61) Lummerstorfer, T.; Hoffmann, H. *J. Phys. Chem. B* **2004**, *108*, 3963.

(62) Collman, J. P.; Devaraj, N. K.; Eberspacher, T. P. A.; Chidsey, C. E. D. *Langmuir* **2006**, *22*, 2457.

(63) Escorihuela, J.; Marcelis, A. T. M.; Zuilhof, H. *Adv. Mater. Interfaces* **2015**, *2*, 1500135.

(64) Kuzmin, A.; Poloukhtine, A.; Wolfert, M. A.; Popik, V. V. *Bioconjugate Chem.* **2010**, *21*, 2076.

(65) Orski, S. V.; Poloukhtine, A. A.; Arumugam, S.; Mao, L.; Popik, V. V.; Locklin, J. *J. Am. Chem. Soc.* **2010**, *132*, 11024.

(66) Wendeln, C.; Singh, I.; Rinnen, S.; Schulz, C.; Arlinghaus, H. F.; Burley, G. A.; Ravoo, B. J. *Chem. Sci.* **2012**, *3*, 2479.

(67) Singh, I.; Wendeln, C.; Clark, A. W.; Cooper, J. M.; Ravoo, B. J.; Burley, G. A. *J. Am. Chem. Soc.* **2013**, *135*, 3449.

(68) Lai, C.-H.; Chang, T.-C.; Chuang, Y.-J.; Tzou, D.-L.; Lin, C.-C. *Bioconjugate Chem.* **2013**, *24*, 1698.

(69) Wijdeven, M. A.; Nicosia, C.; Borrmann, A.; Huskens, J.; van Delft, F. L. *RSC Adv.* **2014**, *4*, 10549.

(70) Manova, R. K.; Pujari, S. P.; Weijers, C. A. G. M.; Zuilhof, H.; van Beek, T. A. *Langmuir* **2012**, *28*, 8651.

(71) Chang, C.-M.; Liu, Y.-L. *Carbon* **2009**, *47*, 3041.

(72) Chen, C.; Fruk, L. *RSC Adv.* **2013**, *3*, 1709.

(73) Zhu, J.; Hiltz, J.; Lennox, R. B.; Schirrmacher, R. *Chem. Commun.* **2013**, *49*, 10275.

(74) Jonkheijm, P.; Weinrich, D.; Köhn, M.; Engelkamp, H.; Christianen, P. C. M.; Kuhlmann, J.; Maan, J. C.; Nüsse, D.; Schroeder, H.; Wacker, R.;

Breinbauer, R.; Niemeyer, C. M.; Waldmann, H. *Angew. Chem. Int. Ed.* **2008**, *47*, 4421.

(75) Gross, J. H. *Anal. Bioanal. Chem.* **2014**, *406*, 63.

(76) Kpegba, K.; Spadaro, T.; Cody, R. B.; Nesnas, N.; Olson, J. A. *Anal. Chem.* **2007**, *79*, 5479.

(77) Sen, R.; Escorihuela, J.; van Delft, F.; Zuilhof, H. *Angew. Chem. Int. Ed.* **2017**, *56*, 3299.

(78) Yatvin, J.; Brooks, K.; Locklin, J. *Angew. Chem. Int. Ed.* **2015**, *54*, 13370.

(79) Huang, F.; Anslyn, E. V. *Chem. Rev.* **2015**, *115*, 6999.

(80) Credo, G. M.; Boal, A. K.; Das, K.; Galow, T. H.; Rotello, V. M.; Feldheim, D. L.; Gorman, C. B. *J. Am. Chem. Soc.* **2002**, *124*, 9036.

(81) Sanyal, A.; Norsten, T. B.; Uzun, O.; Rotello, V. M. *Langmuir* **2004**, *20*, 5958.

(82) Zou, S.; Schönherr, H.; Vancso, G. J. *J. Am. Chem. Soc.* **2005**, *127*, 11230.

(83) Sijbesma, R. P.; Beijer, F. H.; Brunsveld, L.; Folmer, B. J. B.; Hirschberg, J. H. K. K.; Lange, R. F. M.; Lowe, J. K. L.; Meijer, E. W. *Science* **1997**, *278*, 1601.

(84) Egholm, M.; Buchardt, O.; Nielsen, P. E.; Berg, R. H. *J. Am. Chem. Soc.* **1992**, *114*, 1895.

(85) Rothemund, P. W. K. *Nature* **2006**, *440*, 297.

CHAPTER 2

SuFEx click chemistry delivers a quantitative and orthogonal platform for surface modification

ABSTRACT

The constraints of minute reactant amounts and the impossibility to remove any undesired surface-bound products during monolayer functionalization of a surface, necessitate selection of efficient, modular and orthogonal reactions that lead to quantitative conversions. Herein, we explore the character of sulfur–fluoride exchange (SuFEx) reactions on a surface, and explore the applicability for quantitative and orthogonal surface functionalization. To this end, we demonstrate the use of ethenesulfonyl fluoride (ESF) as an efficient SuFEx linker for creating 'SuFEx-able' monolayer surfaces, enabling three distinct approaches to utilize SuFEx chemistry on a surface. The first approach relies on a di–SuFEx loading allowing dual functionalization with a nucleophile, while the two latter approaches focus on dual (CuAAC–SuFEx/SPOCQ–SuFEx) click platforms. The resultant strategies allow facile attachment of two different substrates sequentially on the same platform. Along the way we also demonstrate the Michael addition of ethenesulfonyl fluoride to be a quantitative surface–bound reaction, indicating significant promise in materials science for also this reaction.

This work was published as:

"*SuFEx click chemistry delivers a quantitative and orthogonal platform for surface modification*" Digvijay Gahtory, Sidharam Pujari, Suhua Li, Qinhen Zheng, Rickdeb Sen, John E. Moses, K. Barry Sharpless and Han Zuilhof *Chemistry–A European Journal*, **2017**, manuscript under review.

INTRODUCTION

The facile and robust attachment of molecular functionality to surfaces is receiving increasing scientific scrunity.[1] It is of interest for a wide range of applications, including the preparation of protein-repelling surfaces,[2] the attachment of biomolecules such as DNA for biosensor fabrication,[3] dynamic surface functionalization,[4,5] nanoparticle immobilization,[6] etc. Generally, surface modification is achieved through the formation of stable self–assembled monolayers (SAMs) or polymer brushes on a solid substrate, followed by subsequent functionalization by different coupling strategies.[7] In this regard, functionalization by click chemistry has proven to be the most efficient and kinetically superior method.[8] However, the stringent criterion that a transformation should meet to be formally labelled click [modular, high yielding, wide in scope, generate minimal side–products and mild reaction conditions], inevitably limits the number of available reactions.[9] This acquires an even higher relevance in the context of modification of polymers,[10]or in case of surface functionalization, where purification after covalent on-surface reaction is not possible. In order to acquire optimal control over surface properties, a reaction efficiency of 100 % is thus desirable. For example, the surface-bound Cu(I)–catalyzed azide–alkyne cycloaddition (CuAAC)[11] has been shown to possess such characteristics by Chidsey et al.[12,13] However, the cytotoxic nature of copper catalysts along with the steric demands of the most effective Cu-ligands is limiting, and there is a growing demand for new interfacial click reactions that offer the prospect of orthogonality with other reactions.[14] This is not always trivial, and some reactions that have been shown to proceed efficiently in solution (e.g. the strain-promoted alkyne–azide cycloaddition),[15,16] do not necessarily proceed with (near–) quantitative yields within an organic monolayer.[17]

The sulfur fluoride exchange (SuFEx) family of reactions reported recently by Sharpless and coworkers,[18] is a practical metal-free click transformation with wide application.[19-23] SuFEx reactions involve the cleavage of an S–F bond of a

sulfur fluoride in a substitution reaction, often with aryl silyl ethers or amines, in the presence of certain catalysts such as diazabicycloundec–7–ene (DBU) or triazobicyclodecene (TBD)[24] or HF_2^- anion.[25] This reaction takes place in solution and in polymer synthesis, with complete selectivity and unprecedented efficiency.[26] The newly formed S–O and S–N bonds yield stable new connections, and SuFEx has proven extremely reliable in polymer synthesis[27,28] and post–polymerization modification.[29] Locklin and co–workers recently demonstrated the utility of SuFEx for the post–polymerization functionalization of polymer brushes at a surface,[30] while emphasizing its orthogonality to other click reactions.[31] However, to the best of our knowledge, there exist no examples of the application of SuFEx click chemistry in the modification of organic monolayers.

Scheme 1. a) Surface-bound SuFEx reaction with amines. b) Multiple or sequential orthogonal interfacial SuFEx click reactions as used in this study.

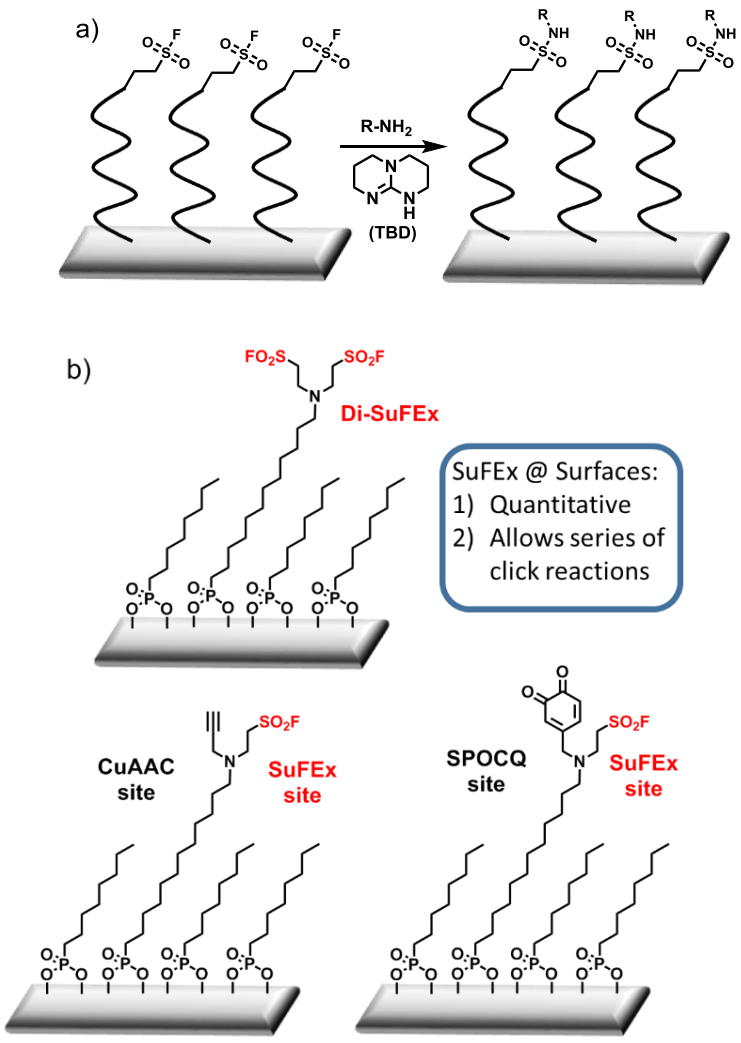

While the SuFEx chemistry of silyl ethers for surface modification is documented,[26,32] this is not the case for amines.[33] Given the abundance of available natural and synthetic amines, we envisioned that the development of an optimized SuFEx protocol for the surface immobilization of amines would be highly advantageous. Moreover, since the resulting sulfur-linked amide bond is typically more stable than a corresponding ester bond, this presents an extra advantage in terms of surface stability, as long as also the surface-bound SuFEx reaction can be shown to be a real click reaction.

In this paper, we report such a development, and demonstrate an efficient and quantitative interfacial SuFEx protocol between primary amines and a surface-tethered sulfonyl fluoride in the presence of TBD to give sulfonamide-terminated surfaces (Scheme 1a). To demonstrate the quantitative nature of the SuFEx reaction, we used – among other approaches – the sulfonamide linkage as a labile internal tag in direct analysis in real time–high resolution mass spectrometry (DART–HRMS),[34-36] and investigated three distinct approaches towards our goal (Scheme 1b). The first approach involved the preparation of a dual *'SuFExable'* platform, while the other two approaches we explored investigate the orthogonality of the surface–bound SuFEx reaction with both CuAAC and the strain-promoted oxidation–controlled cyclooctyne quinone cycloaddition (SPOCQ).[37,38] In the first example, we also provide the first evidence for the 'click' character of the Michael addition of the SuFEx linker, ethenesulfonyl fluoride (ESF), with amines at an interface. Finally, we elucidate and rationalize the kinetics of the SuFEx reaction at the solution to solid interface, and demonstrate its efficiency using X–ray photoelectron spectroscopy (XPS) and ambient desorption/ionization mass spectrometry. In this way we aim to provide a quantitative click strategy for the surface attachment of ESF and of amine–functionalized molecules.

RESULTS AND DISCUSSION

Fragmentation of SuFEx products in solution DART–HRMS. DART–HRMS is an ambient desorption ionization–mass spectrometry technique[39] that uses electronically excited metastable He species (2^3S, 19.8 eV) to generate a wide range of atmosphere–related reactive species (e.g. $O_2^{\bullet-}$, protonated water clusters, etc.). This broad set of ions can be used to obtain MS–detectable ionized fragments[40,41] from a wide range of functional groups in both solution phase[42,43] and on surfaces,[44-46] which are carried into the mass spectrometer by heated He gas. We have recently demonstrated the utility of this technique for qualitative and quantitative surface analysis of several surface-bound click reactions[17,47-49] and surface–bound hydrogen bond formation and exchange.[50]

To achieve this objective, we performed solution DART fragmentation experiments with compounds **1**–**3**,[33] via dipping of a glass capillary in a methanolic solution of the respective compound, placing the capillary in front of the mass spectrometer, and observing the fragments formed (Figure 2a). Interestingly, we found that for all three compounds, negative mode ionization showed many different fragments obtained by cleavage around the S–X (X = N, O) bond (Figure 2b). For example, compound **1** showed the fragmented sulfonate with the loss of either the morpholino (*m/z* 315.9604) or phenolate (*m/z* 308.9871) group along with a fragmentation product formed by cleavage at the S=N site (*m/z* 159.9703).[51] Interestingly, for compound **2**, we observed four different fragments that corresponded to cleavages which also occurred via bond ruptures of the various S–X links to the S–core except for the parent oxide (S=O) around the S–N bond. Most prominently, we observed the $[M–H]^-$ fragments for ethynylaniline (*m/z* 116.0481) and phenylalanine (*m/z* 164.0707).

In contrast, positive ion analysis revealed much simpler and specific modes of fragmentation to the observed ions. For example, compound **1** provided an intense $[M+H]^+$ fragment (*m/z* 161.9673) attributable to cleavage at the S=N bond. Similarly, the fragmentation of otherwise very stable sulfonamide linkage in

2 provided protonated ethynylaniline (*m/z* 118.0652) and phenylalanine (*m/z* 166.0860) in high intensities. This was fortuitous, as formation of exclusive fragments in high intensities is quite advantageous for real–time kinetic analysis of low product amounts on surfaces, especially in the early part during the course of a reaction. [For a more detailed overview and fragmentation spectra, see section 5 in Appendix 1].

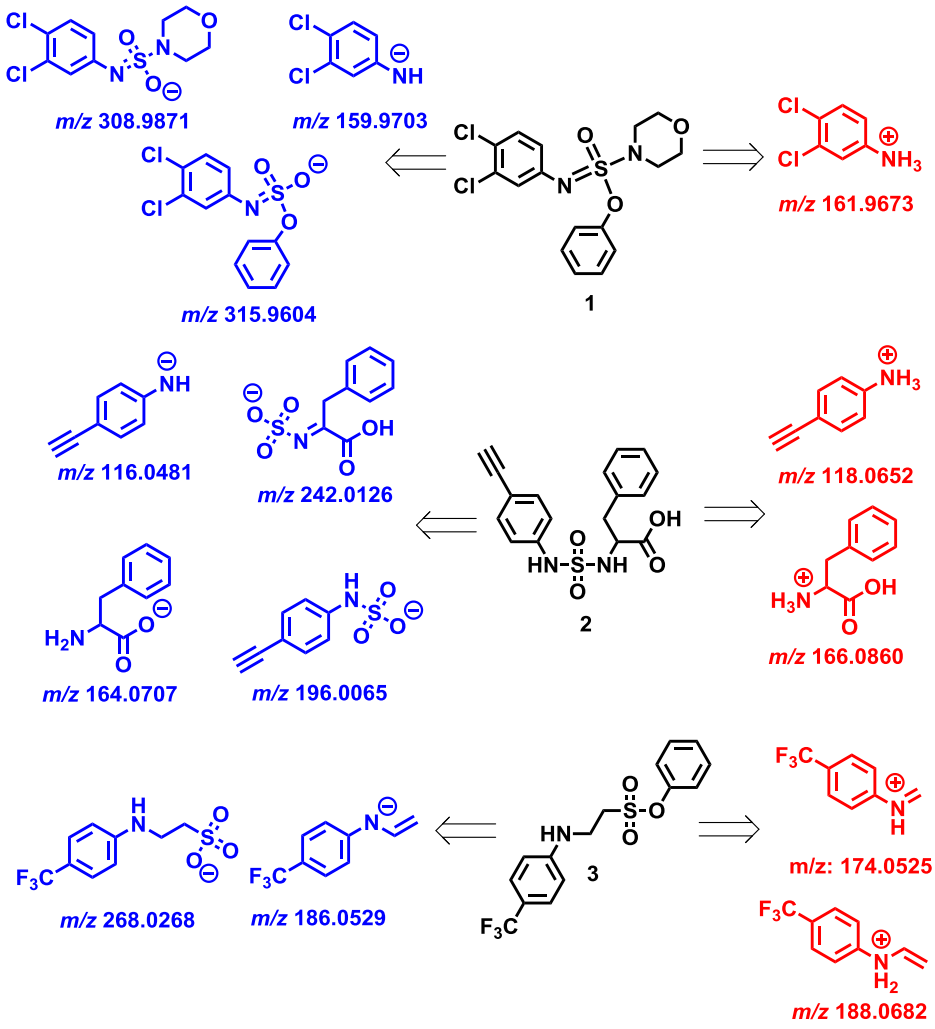

Figure 1. Fragments obtained in negative (blue) and positive (red) ion mode upon DART analysis of a selection of SuFEx products indicating cleavage of a S–N or S–OAr bond.

Based on these experiments, we could conclude that the fragmentation of SuFEx products at an interface could be anticipated around S–N or S–OAr bonds. Most importantly, we observed that for sulfonamide linkages in SuFEx products, positive mode fragmentation was more useful than negative as it exclusively yielded amine fragments in high intensities. Since, we intended to use amines as

nucleophiles for interfacial SuFEx, this knowledge was incorporated in the design of our surface experiments.

Surface aminolysis of S–F by R–NH$_2$ and kinetics determination. Our experimental design for the three SuFEx approaches involved preparation of R-SO$_2$F–terminated surfaces that could then reacted with an amine that would yield easily detectable product fragments in DART–HRMS (Scheme 2). The disappearance of the F1s signal (686.0 eV) in XPS simultaneously provides an indication of the degree of conversion via disappearance of the surface reactant (S–F). Based on our previous experience,[49] we prepared C$_{12}$–amine (**M$_1$**) and

Scheme 2. General scheme showing the design of the interfacial SuFEx, CuAAC and SPOCQ reactions under study.

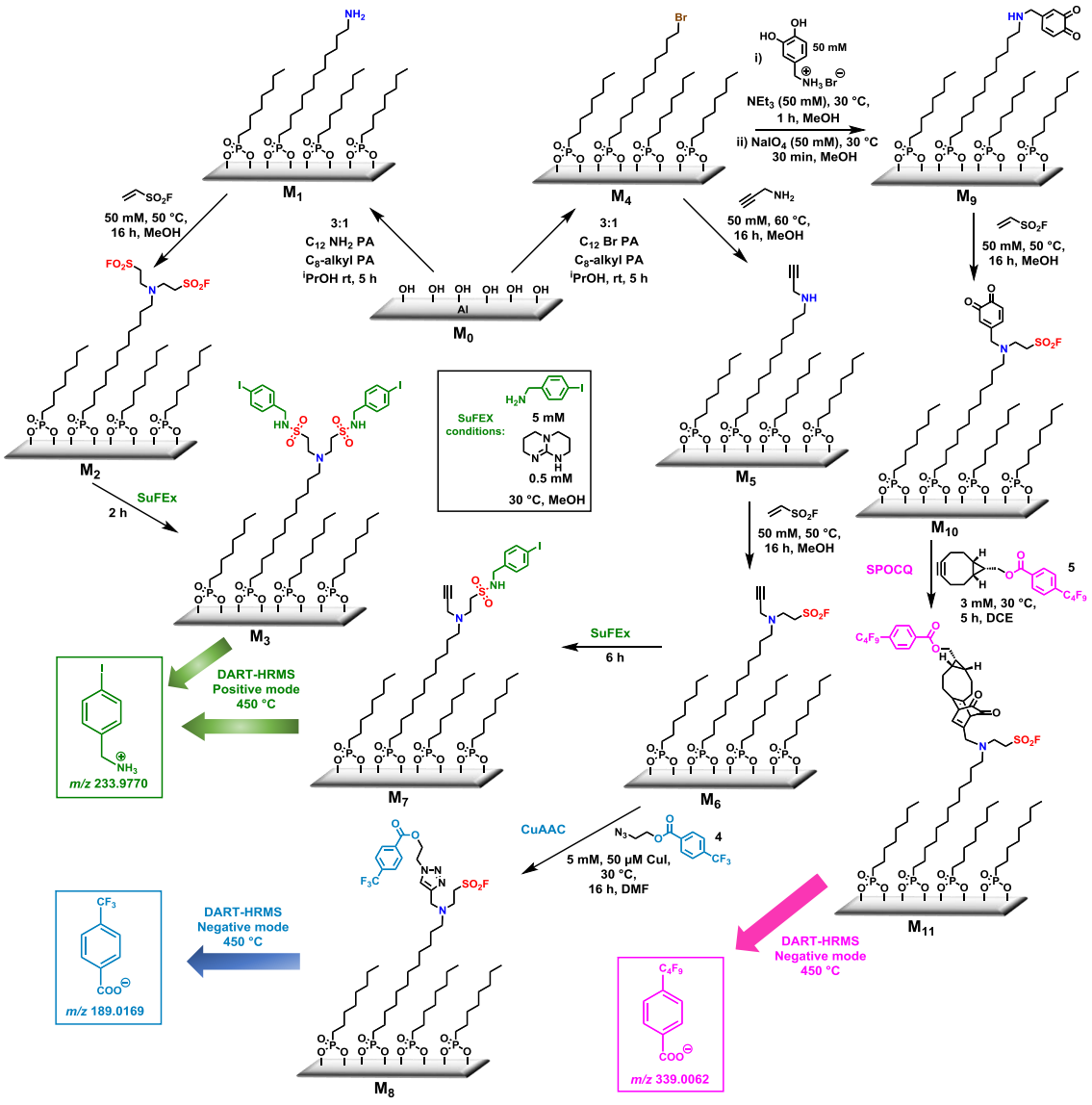

C_{12}–bromo terminated (**M_4**) phosphonic acid (PA) monolayers on aluminum oxide surfaces in a 3:1 (C_{12} amine PA:C_8 alkyl PA and C_{12} bromo PA:C_8 alkyl PA respectively) dilution ratio. The monolayer composition for **M_1** and **M_4** surfaces was confirmed by N/P (1:4) and Br/P (1:4) ratios in XPS wide scans (Figure S4.3, S4.4 and S4.5 in Appendix 1). The stability of the monolayer attachment to the surface in all following conversions was shown by an XPS-based N/P ratio that was in agreement with the theoretically expected ratio within experimental error. Amine-terminated surfaces (**M_1**) were then successfully derivatized to their Michael adducts with commercially available ESF, to quantitatively yield –$N(CH_2CH_2SO_2–F)_2$ terminated *'SuFEx-able'* surfaces (**M_2**). The appearance of a strong F1s signal (686.0 eV) in the XPS spectra (Figure 2a and Appendix 1, S4.6) along with observed F/P ratios (2:4) confirmed completion of the reaction (Appendix 1, Figure S4.7). This ratio and its corresponding error (100 ± 2 %) was derived from the reactions on six samples, prepared on different days and measured at multiple random spots on the samples using XPS. This click character of the Michael addition of ESF with surface-bound amines is in line with recent findings on dendrimer-functionalizations that show ESF-amine adducts as the most reliable embodiment of the Michael reaction known (yield > 99.7%, likely more than >99.9%).[52,53] Our findings thus indicate that the Michael addition of ESF with amines can be characterized as a true click reaction, thereby demonstrating the reliability and selectivity of this bi-functional reagent.

To study the amine-based surface-bound SuFEx reaction, we chose 4–iodobenzylamine (IBZ) as a nucleophile since the iodophenyl motif aids detection in DART–HRMS.[50] TBD, which was found to be kinetically superior to DBU and triethylamine by Locklin and co–workers,[30] was chosen as the non–nucleophilic catalyst. Upon stirring **M_2** surfaces with IBZ at 30 °C, IBZ-terminated surfaces (**M_3**) were formed in a 100 ± 3 % yield in 2 h, as indicated by the N/P ratios (3:4) observed in the XPS wide scan spectrum (Figure 2b and Appendix 1, S4.9). The corresponding full disappearance of the F1s signal was also confirmed on a hexaplet of samples to within 2 %. Furthermore, the absence of any carryover

standard error (2–3 % throughout) in the N/P ratio (changes 1:4 to 3:4 from **M₂** to **M₃**) in XPS wide scan, which would have arisen in case of any incomplete reaction (either ESF attachment or subsequent aminolysis by IBZ), confirmed the quantitative nature of both these reactions (Michael addition with ESF and SuFEx). XPS C1s narrow scan analysis (Appendix 1, Figure S4.10) of **M₃** surfaces showed the presence of carbon atoms attributable to C–S, C–N and C–I regions, and the experimental C1s spectra correlated well with simulated

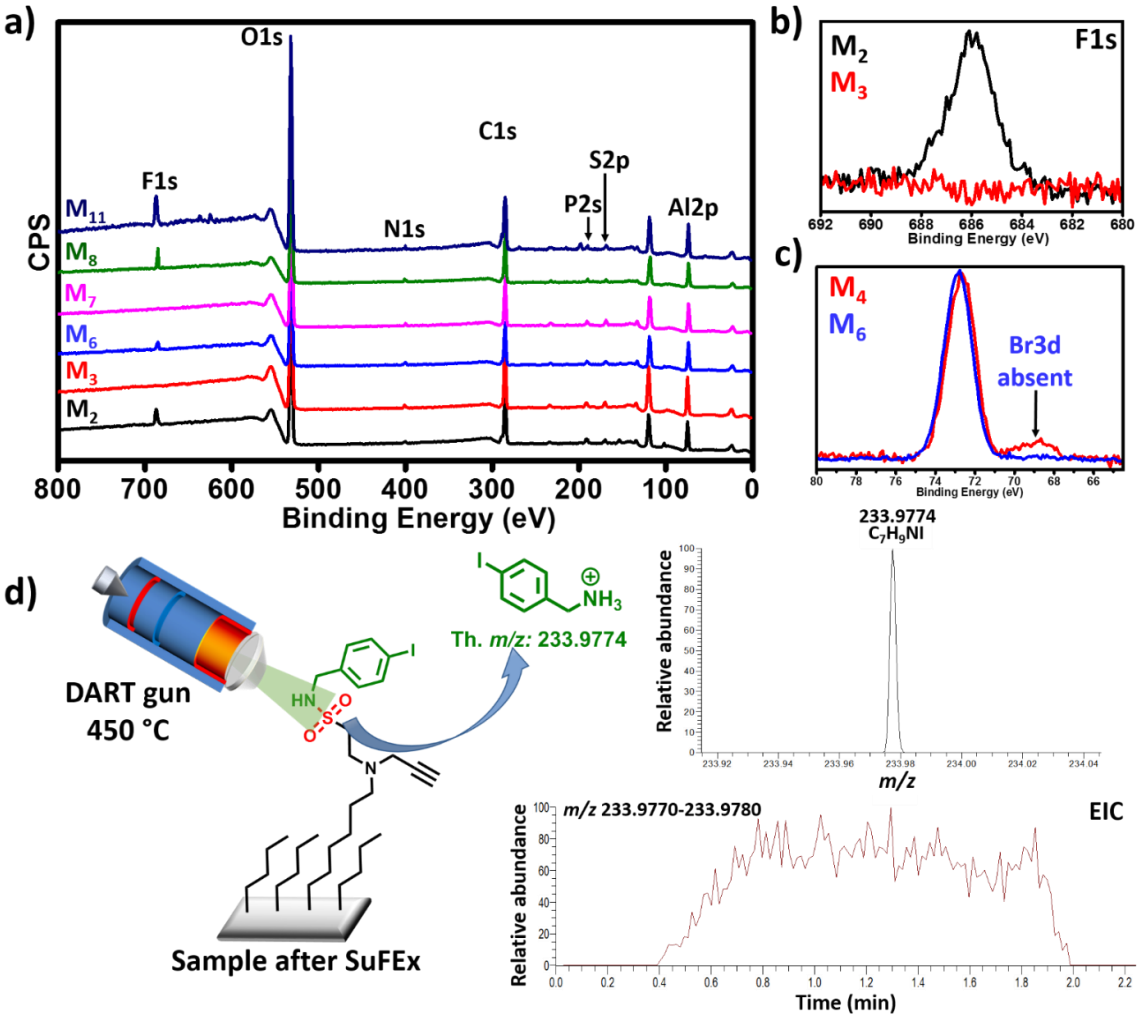

Figure 2. a) Stacked XPS wide spectra of **M₂**–**M₁₁** surfaces. b) Stacked F1s narrow spectra for **M₂** and **M₃** surfaces showing the disappearance of F1s peak upon complete reaction. c) Stacked Br3d narrow spectra for the **M₄** and **M₅** surfaces showing the disappearance of the Br3d signal upon complete propargylation. d) Schematic impression of the S–N bond fragmentation and subsequent ionization of protonated 4–iodobenzylamine (*m/z* 233.9774) by DART–HRMS.

spectra obtained using DFT calculations (Appendix 1, section 6).[54] Upon analyzing these SuFEx-derived samples by DART–HRMS, we observed a strong signal for protonated IBZ (*m/z* 233.9774) with a characteristic trace in the extracted ion chronogram (Figure 2d and Appendix 1, S4.11). This fragmentation pattern is akin to the S-N bond fragmentation observed for compound **2** in solution DART experiments. This further confirmed that SuFEx with IBZ had indeed taken place and strengthened our hypothesis that S–N bond cleavage product could be used as an 'internal tag' for reaction kinetics determination.

After thus showing that the surface–bound SuFEx reaction can be made quantitative, we next focused our attention on demonstrating the orthogonal nature of the SuFEx reaction at a surface, with two other transformations that have previously been shown to proceed in a quantitative manner, also at a surface.[47] To this aim, we chose two routes: Br–terminated surfaces (M_4) were reacted with propargylamine to yield alkyne-terminated surfaces (**M_5**), or with 3,4–dihydroxybenzylamine to yield quinone–terminated surfaces (**M_9**) upon oxidation. The formation of **M_5** surfaces was evidenced by the disappearance of Br3d signal (69.0 eV) in the narrow scan spectra of **M_5** and **M_6** (see e.g. Figure 2c and Appendix 1, S4.13). Further confirmation of propargyl attachment was obtained by the slight lowering of static water contact angle (from 103 ± 2° to 92 ± 2°; Appendix 1, Figure S4.14). Following this, **M_5** surfaces were reacted with ESF for 16 h to provide dual CuAAC–SuFEx-ready functionalities (**M_6**). The quantitative conversion to **M_6** was confirmed by the appearance of a F1s signal in the XPS wide and narrow spectrum (Figure 2a and Appendix 1, S4.15) and an eventual F/P ratio of 1:4 in the XPS wide spectrum (Appendix 1, Figure S4.16). Upon performing SuFEx with IBZ, we found that **M_6** surfaces achieved quantitative reaction within 6 h to yield the IBZ–alkyne-terminated surfaces (**M_7**), as evidenced by the complete disappearance of F1s signal and N/P ratios (2:4) in XPS wide spectra (Figure 2a and Appendix 1, S4.18). C1s narrow scan analysis of **M_7** surfaces (Appendix 1, Figure S4.19) also showed the presence of

carbons in distinct chemical environments, arising from C–S, C–N and C–I linkages, the latter attributable to the iodobenzyl motif.

Scheme 3. Surface **M_9** might undergo equilibration with aziridine surface **M_{13}**, although the Michael addition and subsequently the SPOCQ reaction will pull the equilibrium to the left.

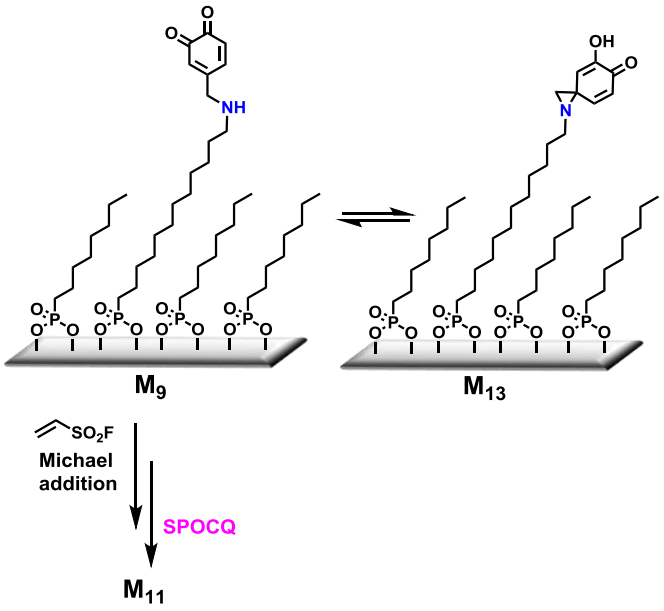

To test the dual click nature of our strategy, we also performed CuAAC on **M_6** surfaces using a fluorinated azide tag 4 that is labile under DART conditions.[48] Upon stirring **M_6** surfaces with a 5 mM solution of 4 in DMF for 16 h, we observed a 80 ± 2 % surface conversion to **M_8** as confirmed by the F/P (4:4) ratios in XPS wide scan spectra (Appendix 1, Figure S4.20). Although the reaction occurred in excellent yield, we did not achieve a quantitative conversion for surface bound CuAAC under our conditions as has been reported in literature before.[13] Furthermore, DART–HRMS analysis of **M_8** surfaces also showed the presence of the fluorinated mass tag (*m/z* 189.0169) in the EIC (Appendix 1, Figure S4.21). The dual SPOCQ–SuFEx platform was prepared by reacting the Br–terminated surfaces (**M_4**) with 3,4 dihydroxybenzylamine followed by oxidation to quinone (**M_9**) as evidenced by the N/P ratios in XPS wide scan spectrum (Appendix 1, Figure S4.22). Directly after preparation, the *o*-quinone-terminated surfaces (**M_9**) were reacted with ESF to install the SO_2F moiety (**M_{10}**). The appearance of an F1s signal in the XPS spectra with the corresponding F/P ratio (1:4) confirmed

quantitative attachment (Appendix 1, Figure S4.24) [The *o*-quinone surface **M9** may be in equilibrium with the hydroquinone surface obtained after internal nucleophilic attack of the amine N-atom to yield an aziridine surface **M13**, but upon reaction with ESF, the equilibrium should favor the *o*-quinone, which is necessary to allow the SPOCQ reaction to proceed (near-)quantitatively. See Scheme 3.].

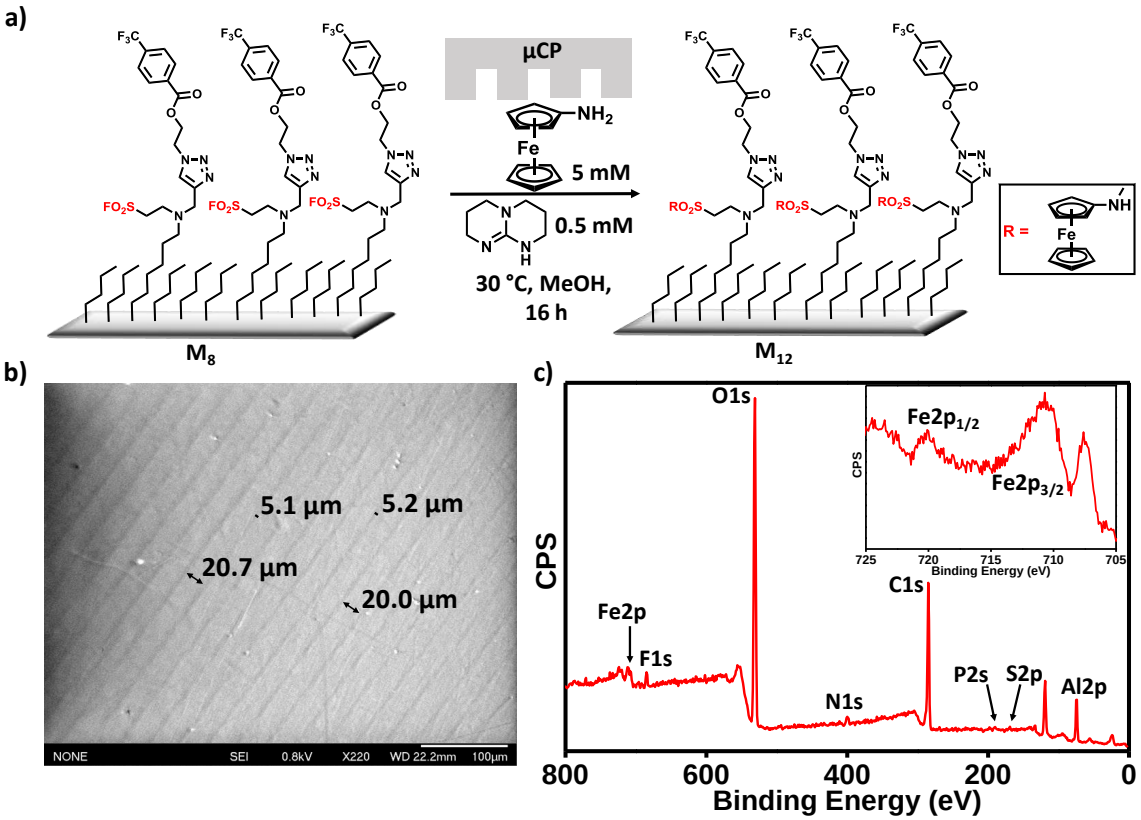

Figure 3. a) General schematic showing SuFEx reaction on **M8** surfaces by microcontact (μCP) stamping with aminoferrocene. b) SEM image obtained for **M12** surfaces after μCP showing the 5 μm patterns (scale = 100 μm). c) XPS wide spectrum for **M12** surfaces showing the Fe2p signal (inset: Fe2p narrow scan).

A subsequent SPOCQ reaction with a fluorinated BCN MS tag (**5**) provided **M11** surfaces as substantiated by a strong F1s signal in wide scan XPS spectra (Figure 2a). Furthermore, SPOCQ reaction on this platform occurred with excellent surface yield (95 ± 2 %) as quantified using the F/P ratio (10:4) in XPS wide scan (Appendix 1, Figure S4.25) within 5 h further displaying the modularity of our design. XPS C1s narrow scan analysis of **M11** surfaces showed the different fluorinated carbons attributable to the C_4F_9– chain distinctly (Appendix 1, Figure

S4.26). Presence of the expected fluorinated MS fragment (*m/z* 339.0072) in negative mode DART–HRMS analysis of SPOCQ modified **M$_{11}$** surfaces provided further proof of the reaction (Appendix 1, Figure S4.27). In a previous paper the 100% efficiency of this SPOCQ reaction at a surface has been displayed – the high, but non-perfect yield (95%) obtained in the current reaction may be due to the intermittent Michael addition, where the quinones might undergo some slight reaction with e.g. methanol.

In the spirit of further application of the dual click strategy for orthogonal functionalization, we performed a SuFEx microstamping experiment using aminoferrocene on **M$_8$** surfaces (Figure 3a). As already stated, these surfaces were CuAAC clicked with a fluorinated tag. Interestingly, after 16 h we observed a quantitative SuFEx reaction even on this sterically hindered substrate as confirmed by the N/P (5:4) and F/N (2.4:5) ratios in XPS wide scans upon aminoferrocene immobilization (Appendix 1, Figure S4.28). The patterned surface could be easily visualized using scanning electron microscopy (SEM). SEM images (Figure 3b and Appendix 1, S4.29) clearly showed regular patterns with a width of 5 μm. Moreover, XPS Fe2p narrow scan (705–725 eV) analysis clearly showed emergence of Fe2p signals (710.0 eV and 723.0 eV) characteristic of the ferrocene moiety (Appendix 1, Figure S4.30).

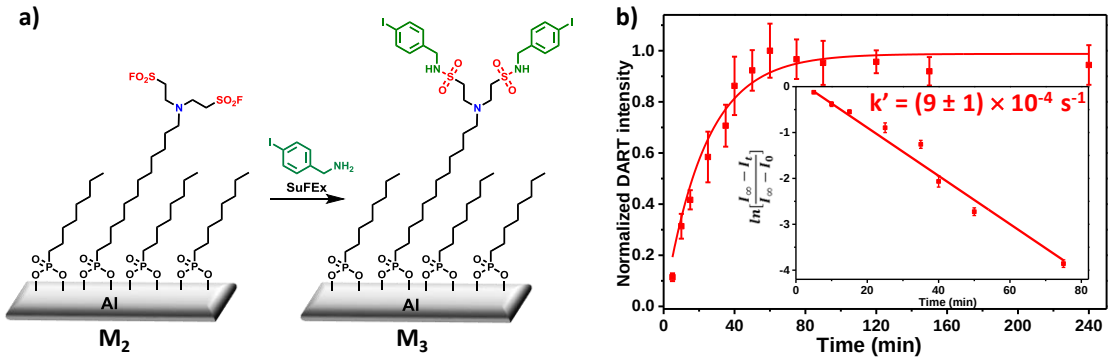

Figure 4. a) Schematic depiction of SuFEx reaction using IBZ on **M$_2$** and b) Normalized DART–HRMS intensity vs time (min) or di–SuFEx (**M$_2$** to **M$_3$**) Inserts: Linear plots of *ln* $[(I_\infty - I_t)/(I_\infty - I_0)]$ vs time (min) to obtain the pseudo-first order constants.

Having established the reaction efficiency, orthogonality and applicability of SuFEx, we finally embarked on determination of the reaction kinetics by DART–HRMS. To this end, we reacted **M₂** samples with IBZ (Figure 4a and 4b) for different time intervals (up to 4 h) and followed the signal intensity of protonated IBZ (*m/z* 233.9774) in DART– HRMS. The pseudo-first–order rate constant (k′) was calculated as the slope of the plot of $\ln|(I_t - I_\infty)/(I_0 - I_\infty)|$ versus time (t), where I_∞ corresponds to the asymptotic integrated extracted ion chronogram (EIC) intensity as obtained by exponential decay curve fitting of the data (Figure 4b). The pseudo first–order rate constant (k′) for SuFEx on **M₂** surfaces, at a concentration of 5.0 mM at 30 °C was (9 ± 1) × 10^{-4} s^{-1}, yielding a second-order rate constant of 0.18 ± 0.02 $M^{-1}s^{-1}$.

This rate constant refers to the initial well–behaved kinetic region as we observed two distinct kinetic regimes for this surface-bound SuFEx reaction: an initial fast regime followed by a slower, more complex one similar to that observed by us for surface-bound SPAAC and SPOCQ reactions previously.[17,47] However, in contrast to SPOCQ (reaction completion in 4 h), the SuFEx reaction was already quantitative on surfaces in 2 h under the conditions used in this study. These findings unequivocally demonstrate that interfacial SuFEx is indeed an excellent candidate for orthogonal surface click functionalization.

CONCLUSIONS

In summary, we have developed a new platform for surface functionalization using SuFEx click chemistry and amine nucleophiles. The hypothesis in question was whether the click character of this reaction in solution could also reflect on a surface. After thorough XPS and DART–HRMS investigations, we indeed found this to be the case. In addition, we determined the second-order rate constant for this surface-bound reaction to be 0.18 ± 0.02 $M^{-1}s^{-1}$.

We also explored the orthogonality of the SuFEx reaction by exploring a dual CuAAC/SPOCQ–SuFEx platform, whereby two click reactions could be conducted on a single chip in high yields. We found that even under sterically

challenging environments, SuFEx maintained its click nature, thus providing quantitative conversion. Along the way, we also demonstrated the quantitative nature of the surface-bound Michael addition of the SuFEx linker, ethenesulfonyl fluoride with amines. Since interfacial reactions are typically displaying rather stringent steric limitations, this finding indicates that also this reaction has significant potential in materials sciences beyond that of surface modifications. This work thus opens up exciting prospects for further application of these reactions from a surface chemist's perspective.

REFERENCES

(1) Onclin, S.; Ravoo, B. J.; Reinhoudt, D. N. *Angew. Chem. Int. Ed.* **2005**, *44*, 6282.

(2) Wang, Z.; Zuilhof, H. *Langmuir* **2016**, *32*, 6310.

(3) Zhao, W.-W.; Xu, J.-J.; Chen, H.-Y. *Chem. Rev.* **2014**, *114*, 7421.

(4) Liang, C.-K.; Dubacheva, G. V.; Buffeteau, T.; Cavagnat, D.; Hapiot, P.; Fabre, B.; Tucker, J. H. R.; Bassani, D. M. *Chem. Eur. J.* **2013**, *19*, 12748.

(5) Zou, S.; Schönherr, H.; Vancso, G. J. *J. Am. Chem. Soc.* **2005**, *127*, 11230.

(6) Tassa, C.; Liong, M.; Hilderbrand, S.; Sandler, J. E.; Reiner, T.; Keliher, E. J.; Weissleder, R.; Shaw, S. Y. *Lab on a Chip* **2012**, *12*, 3103.

(7) Pujari, S. P.; Scheres, L.; Marcelis, A. T. M.; Zuilhof, H. *Angew. Chem. Int. Ed.* **2014**, *53*, 6322.

(8) Escorihuela, J.; Marcelis, A. T. M.; Zuilhof, H. *Adv. Mater. Interfaces* **2015**, *2*, 1500135.

(9) Kolb, H. C.; Finn, M. G.; Sharpless, K. B. *Angew. Chem. Int. Ed.* **2001**, *40*, 2004.

(10) Barner-Kowollik, C.; Du Prez, F. E.; Espeel, P.; Hawker, C. J.; Junkers, T.; Schlaad, H.; Van Camp, W. *Angew. Chem. Int. Ed.* **2011**, *50*, 60.

(11) Castro, V.; Rodríguez, H.; Albericio, F. *ACS Comb. Sci.* **2016**, *18*, 1.

(12) Collman, J. P.; Devaraj, N. K.; Chidsey, C. E. D. *Langmuir* **2004**, *20*, 1051.

(13) Collman, J. P.; Devaraj, N. K.; Eberspacher, T. P. A.; Chidsey, C. E. D. *Langmuir* **2006**, *22*, 2457.

(14) Orski, S. V.; Poloukhtine, A. A.; Arumugam, S.; Mao, L.; Popik, V. V.; Locklin, J. *J. Am. Chem. Soc.* **2010**, *132*, 11024.

(15) Agard, N. J.; Prescher, J. A.; Bertozzi, C. R. *J. Am. Chem. Soc.* **2004**, *126*, 15046.

(16) Dommerholt, J.; Rutjes, F. P. J. T.; van Delft, F. L. *Top. Curr. Chem.* **2016**, *374*, 16.

(17) Sen, R.; Escorihuela, J.; Smulders, M. M. J.; Zuilhof, H. *Langmuir* **2016**, *32*, 3412.

(18) Dong, J.; Krasnova, L.; Finn, M. G.; Sharpless, K. B. *Angew. Chem. Int. Ed.* **2014**, 53, 9430.

(19) Smedley, C. J.; Barrow, A. S.; Spiteri, C.; Giel, M.-C.; Sharma, P.; Moses, J. E. *Chem. Eur. J.* **2017**, *23*, 9990.

(20) Dondoni, A.; Marra, A. *Org. Biomol. Chem.* **2017**, *15*, 1549.

(21) Chen, X.; Zha, G.-F.; Bare, G. A. L.; Leng, J.; Wang, S.-M.; Qin, H.-L. *Adv. Synth. Catal.* **2017**, *359*, 3254.

(22) Chen, W.; Dong, J.; Plate, L.; Mortenson, D. E.; Brighty, G. J.; Li, S.; Liu, Y.; Galmozzi, A.; Lee, P. S.; Hulce, J. J.; Cravatt, B. F.; Saez, E.; Powers, E. T.; Wilson, I. A.; Sharpless, K. B.; Kelly, J. W. *J. Am .Chem. Soc.* **2016**, *138*, 7353.

(23) Oakdale, J. S.; Kwisnek, L.; Fokin, V. V. *Macromolecules* **2016**, *49*, 4473.

(24) Dong, J.; Sharpless, K. B.; Kwisnek, L.; Oakdale, J. S.; Fokin, V. V. *Angew. Chem. Int. Ed.* **2014**, *53*, 9466.

(25) Gao, B.; Zhang, L.; Zheng, Q.; Zhou, F.; Klivansky, L. M.; Lu, J.; Liu, Y.; Dong, J.; Wu, P.; Sharpless, K. B. *Nat. Chem.* **2017**, doi: 10.1038/nchem.2796.

(26) Yatvin, J.; Brooks, K.; Locklin, J. *Chem. Eur. J.* **2016**, *22*, 16348.

(27) Yatvin, J.; Brooks, K.; Locklin, J. *Chem. Eur. J.* **2016**, 22*,* 16348.

(28) Wang, H.; Zhou, F.; Ren, G.; Zheng, Q.; Chen, H.; Gao, B.; Klivansky, L.; Liu, Y.; Wu, B.; Xu, Q.; Lu, J.; Sharpless, K. B.; Wu, P. *Angew. Chem. Int. Ed.* **2017**, *56*, 11203.

(29) Li, S.; Beringer, L. T.; Chen, S.; Averick, S. *Polymer* **2015**, *78*, 37.

(30) Yatvin, J.; Brooks, K.; Locklin, J. *Angew. Chem. Int. Ed.* **2015**, *54*, 13370.

(31) Brooks, K.; Yatvin, J.; McNitt, C. D.; Reese, R. A.; Jung, C.; Popik, V. V.; Locklin, J. *Langmuir* **2016**, *32*, 6600.

(32) Zhu, H.; Chen, D.; Li, N.; Xu, Q.; Li, H.; He, J.; Wang, H.; Wu, P.; Lu, J. *Chem. Eur. J.* **2017**, doi:10.1002/chem.201703309.

(33) Li, S.; Wu, P.; Moses, J. E.; Sharpless, K. B. *Angew. Chem. Int. Ed.* **2017**, *56*, 2903.

(34) Gross, J. H. Anal. *Bioanal. Chem.* **2014**, *406*, 63.

(35) Cody, R. B.; Laramee, J. A.; Durst, H. D. *Anal. Chem.* **2005**, *77*, 2297.

(36) Elena, S. C.; Morlock, G. E.; Igor, A. R. Russ. *Chem. Rev.* **2011**, *80*, 235.

(37) Borrmann, A.; Fatunsin, O.; Dommerholt, J.; Jonker, A. M.; Löwik, D. W. P. M.; van Hest, J. C. M.; van Delft, F. L. *Bioconjugate Chem.* **2015**, *26*, 257.

(38) Bruins, J. J.; Westphal, A. H.; Albada, B.; Wagner, K.; Bartels, L.; Spits, H.; van Berkel, W. J. H.; van Delft, F. L. *Bioconjugate Chem.* **2017**, *28*, 1189.

(39) Monge, M. E.; Harris, G. A.; Dwivedi, P.; Fernández, F. M. *Chem. Rev.* **2013**, *113*, 2269.

(40) Song, L.; Gibson, S. C.; Bhandari, D.; Cook, K. D.; Bartmess, J. E. *Anal. Chem.* **2009**, *81*, 10080.

(41) Song, L.; Dykstra, A. B.; Yao, H.; Bartmess, J. E. *J. Am. Soc. Mass Spectrom.* **2009**, *20*, 42.

(42) Cody, R. B. *Anal. Chem.* **2009**, *81*, 1101.

(43) Gómez-Ríos, G. A.; Gionfriddo, E.; Poole, J.; Pawliszyn, *J. Anal. Chem*. **2017**, *89*, 7240.

(44) Manova, R. K.; Joshi, S.; Debrassi, A.; Bhairamadgi, N. S.; Roeven, E.; Gagnon, J.; Tahir, M. N.; Claassen, F. W.; Scheres, L. M. W.; Wennekes, T.; Schroën, K.; van Beek, T. A.; Zuilhof, H.; Nielen, M. W. F. Anal. Chem. **2014**, 86, 2403.

(45) Sanchez, L. M.; Curtis, M. E.; Bracamonte, B. E.; Kurita, K. L.; Navarro, G.; Sparkman, O. D.; Linington, R. G. *Org. Lett.* **2011**, *13*, 3770.

(46) Zhou, S.; Forbes, M. W.; Abbatt, J. P. D. *Anal. Chem.* **2015**, *87*, 4733.

(47) Sen, R.; Escorihuela, J.; van Delft, F. L.; Zuilhof, H. *Angew. Chem. Int. Ed.* **2017**, *56*, 3299.

(48) Sen, R.; Gahtory, D.; Carvalho, R. R.; Albada, B.; van Delft, F. L.; Zuilhof, H. *Angew. Chem. Int. Ed.* **2017**, *56*, 4130.

(49) Sen, R.; Gahtory, D.; Escorihuela, J.; Firet, J.; Pujari, S. P.; Zuilhof, H. *Chem. Eur. J.* **2017**, *23*, 13015.

(50) Gahtory, D.; Sen, R.; Smulders, M. M. J.; Zuilhof, H. *Faraday Discussions* **2017**, 204, 383.

(51) Sun, M.; Dai, W.; Liu, D. Q. *J. Mass. Spectrom.* **2008**, *43*, 383.

(52) Zheng, Q.; Dong, J.; Sharpless, K. B. *J. Org. Chem.* **2016**, *81*, 11360.

(53) Zheng, Q.; Wang, H.; Wu, P.; Sharpless, K. B. Unpublished results.

(54) Giesbers, M.; Marcelis, A. T. M.; Zuilhof, H. *Langmuir* **2013**, *29*, 4782.

CHAPTER 3

Strain-promoted cycloaddition of cyclopropenes with o–quinones: a rapid click reaction

ABSTRACT

Novel click reactions are of continued interest in fields as diverse as bio–conjugation, polymer science and surface chemistry. Qualification as a proper 'click' reaction requires stringent criteria, including fast kinetics and high conversion, to be met. Herein, we report a novel strain-promoted cycloaddition between cyclopropenes and o–quinones in solution and on a surface. We demonstrate the 'click character' of the reaction in solution and on surfaces for both monolayer and polymer brush functionalization.

This work was published as:

"*Strain-promoted cycloaddition of cyclopropenes with o–quinones: a rapid click reaction*" Digvijay Gahtory, Rickdeb Sen, Andriy R. Kuzmyn, Jorge Escorihuela and Han Zuilhof *Angewandte Chemie International Edition*, **2018**, manuscript accepted.

INTRODUCTION

The discovery and application of novel click reaction strategies is a growing domain[1] that has garnered significant interest amongst (bio-)organic[2] and material chemists.[3] Since the introduction of the copper-catalyzed azide alkyne cycloaddition (CuAAC),[4,5] major advances have been made in this regard. Specifically the development of metal-free click reactions[6] that are either strain-promoted or catalyzed by simple bases is noteworthy. Examples include the strain-promoted azide–alkyne cycloaddition (SPAAC)[7] – which uses a highly strained cyclooctyne motif – a range of inverse electron-demand Diels-Alder (IEDDA) reactions such as the tetrazine–*trans*–cyclooctene (TCO)/cyclopropene click,[7] and most recently a series of sulfur-fluoride exchange (SuFEx) reactions.[8] Most of these reactions involve strained reactants (alkyne or alkene) that accelerate the reaction or a highly facile bond exchange.[9] There also has been a growing increase in the use of photochemical click reactions in this regard.[10] The advantages of such reactions include metal-free conditions,[10] faster kinetics[11] and good-to-excellent yields.[12]

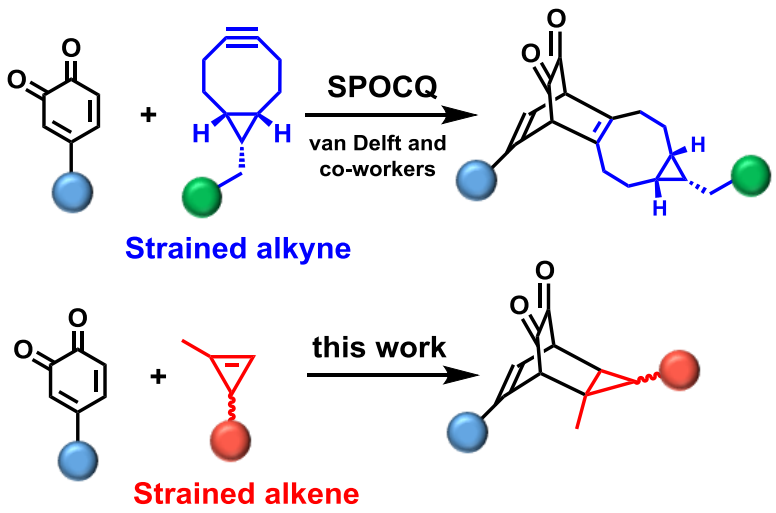

Scheme 1. Scheme showing the inspiration for strain-promoted click between quinones and cyclopropenes.

The strain-promoted oxidation–controlled cyclooctyne–1,2–quinone cycloaddition (SPOCQ)[11] shown in Scheme 1, is another example of such a click

strategy. The fast kinetics of this reaction in solution (k_2 = 496 ± 70 $M^{-1}s^{-1}$) makes it amenable for e.g. accelerated site–specific protein conjugation,[13] cell labelling[14] and hydrogel preparation.[15] An additional feature of this reaction is that quinone formation can be triggered by enzymatic[13] or electrochemical oxidation,[16] thus providing an inducible click handle. In addition, when used for surface functionalization, SPOCQ achieves a rarely obtained quantitative conversion within 4 h with high surface-bound rates (k_2 = 33 ± 2 $M^{-1}s^{-1}$).[17] A distinct feature of this reaction is, however, the use of a relatively large, hydrophobic 8–membered ring, which in itself is not necessary for bio–conjugations and typically disadvantageous in sterically crowded environments such as polymers and surfaces. Thus, a smaller, yet fast, stable and easily synthesizable alternative is quite desirable. With this goal in mind, we hypothesized that a smaller dienophile such as a strained cyclopropene could meet these criteria. 1–Methyl–3–substituted cyclopropenes have been recently reported for fast IEDDA cycloadditions with tetrazines.[18] This click reaction has been widely used for glycoprotein conjugation,[19] cell imaging,[20] etc.[21] Moreover, the higher stability of substituted cyclopropenes[22] as compared to TCO, an alternative strained alkene, is an additional advantage. Based on these findings, we envisaged that cyclopropenes could serve as a potentially novel candidate for facile conjugation with *o*–quinones both in solution and on surfaces.

Herein, we report a novel click reaction between strained alkenes, namely 1–methyl–3–substituted cyclopropenes, and *o*–quinones. We determine the rate constants for the reaction in solution using UV spectroscopy and on a surface using DART–HRMS.[17] Furthermore, we also demonstrate the quantitative nature of the reaction on surfaces and demonstrate its versatility using anti–fouling polymer brush functionalization. Finally, we use density functional theory (DFT) to study the reaction mechanism in more detail. We believe that the high solution-phase yields, minute–scale completion times for monolayer modification coupled

with the ability for polymer functionalization demonstrate the wide potential of this novel reaction.

RESULTS AND DISCUSSION

The cyclopropene probes were designed based on the balance between reactivity and stability found by Devaraj and co–workers.[22] To this end, we synthesized 1–methylcyclopropenes **2**, **5** and **7** (Scheme 2; see Appendix 2 for details). Compound 5 and 7 were derived as fluorinated aromatic ester and carbamate, respectively, from cyclopropene alcohol 3. The aromatic fluorinated head groups were chosen to ease visualization by XPS and DART–HRMS characterization after surface functionalization, based on previous experience.[23]

Following the synthesis of the cyclopropene probes, we performed a reaction between **5** and t–butyl quinone (**8**), which proceeded with good yield in solution

Scheme 2. Synthesis of methyl-substituted cyclopropenes (**2**, **5** and **7**) and reaction with t-butyl quinone, **8**. See Appendix 2 for detailed synthetic procedures.

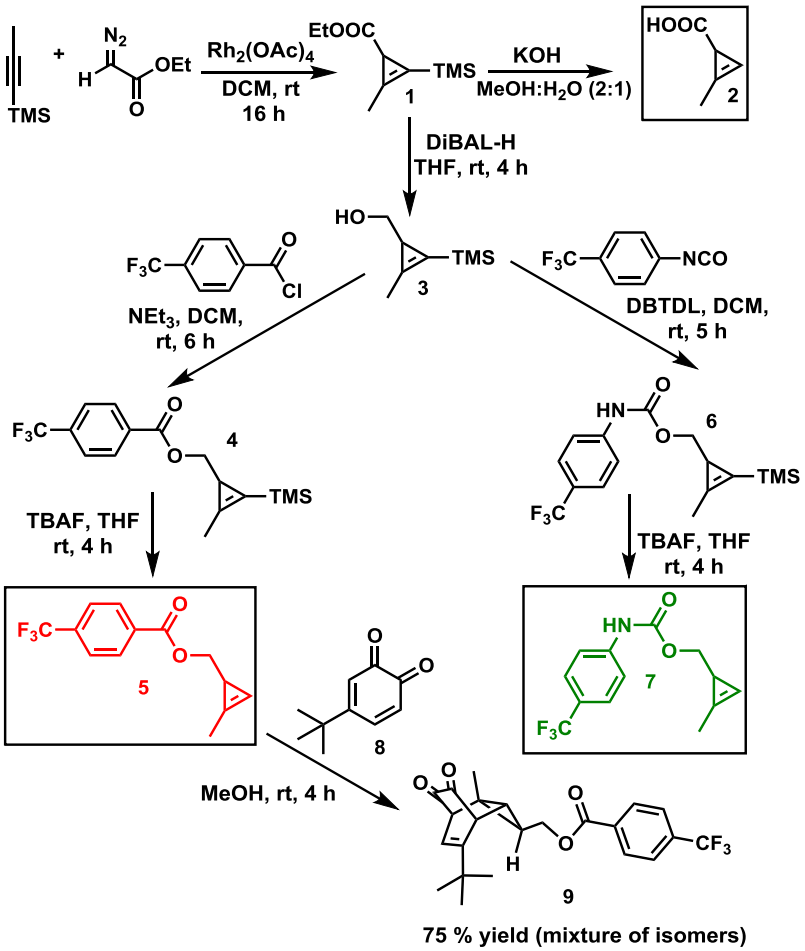

(75 %) at room temperature within 4 h. The resulting cycloadducts (mixture of isomers) were isolated and thoroughly characterized by NMR (see Appendix 2, section S2.5). Based on NOESY and COSY correlations, we deduced an *endo*–configuration of the resultant cycloadducts (three-membered ring formed away from quinone oxygen atoms; see section S5 in Appendix 2).

Next, we determined the reaction kinetics in solution for compounds **2**, **5** and **7** (see Appendix 2 for experimental conditions, section S3.1) by following the decay of the characteristic UV absorption signal for the quinone at 385 nm.[11] In accordance with literature data,[18] **2** showed a sluggish kinetics (k_2 = 0.20 ± 0.04 $M^{-1}s^{-1}$; Figure S3.1) with reaction completion in about 1 h. In contrast, the fluorinated ester **5** and carbamate **7** showed rapid kinetics (k_2 = 1.95 ± 0.02 $M^{-1}s^{-1}$ and 1.70 ± 0.01 $M^{-1}s^{-1}$; respectively) and the reaction is completed within 5 min (Figure 1 and Figure S3.1). These rates bring this reaction into the realm of potentially useful for *in vivo* application according to Houk's classification of metal-free click reactions.[24] As explained in their study, the orthogonal reactivity of 1,3 di-substituted cyclopropenes coupled with high reaction rates enables their application in multicomponent imaging as well.

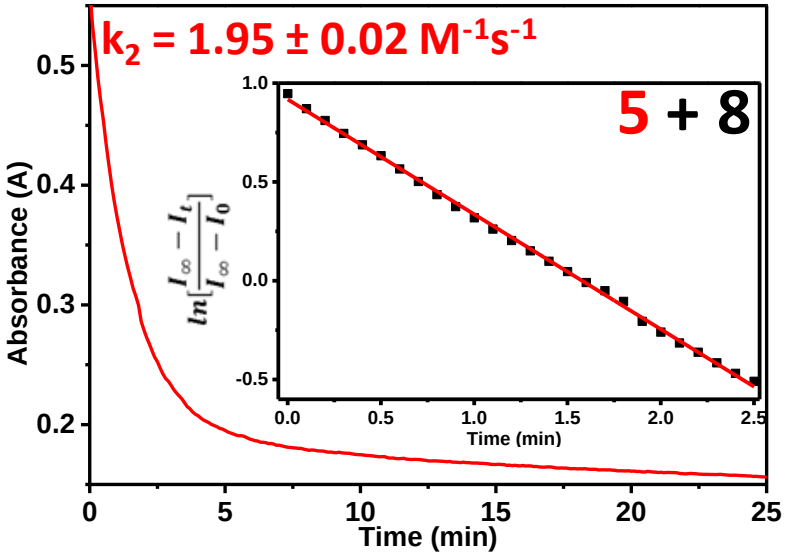

Figure 1. UV kinetics (at 385 nm) of the reaction between cyclopropenes 5 and *t*–butyl quinone 8 at 30 °C in methanol; inset: Linear plots of *ln* $[(I_\infty - I_t)/(I_\infty - I_0)]$ vs time (min), to obtain 2nd-order constants; [5] = 5 mM.

Density functional theory (DFT) calculations were performed using Gaussian 16,[25] in order to study the reaction mechanism of this exothermic reaction (ΔH_{calc} = –31 to –35 kcal/mol) in more detail. For that purpose, we used the dispersion-corrected B97D density functional, which has been proved to give accurate activation energies for SPOCQ cycloaddition reactions,[26] and the Conductor–like Polarizable Continuum Model (CPCM) to mimic methanol. These computations yield that the cycloaddition reaction proceeds through a non-synchronous transition state (TS), as shown by the distances for both new C-C bonds (see Figure 2). In addition, the activation free energies for the *endo*– cycloaddition of **5** and **8** are lower than that of the *exo*–approach (7.5 vs. 9.0 kcal/mol, respectively).

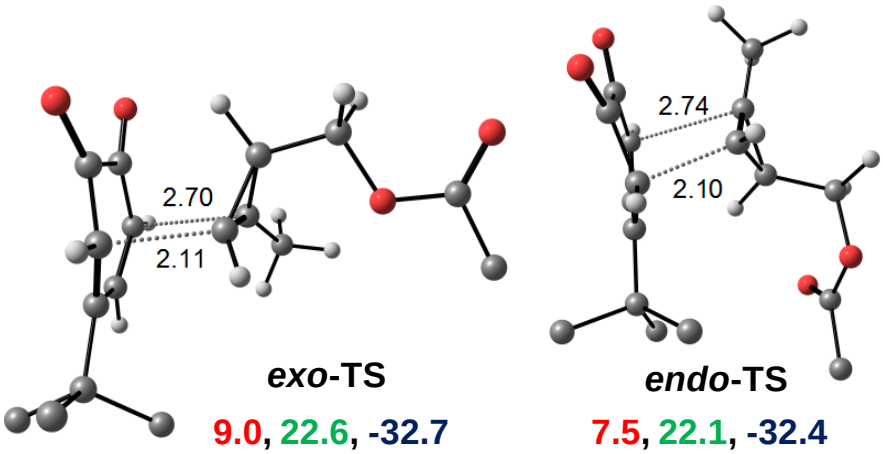

Figure 2. B97D/6-311+G(d,p) transition state geometries for the *exo*– and *endo*– attack of **5** + **8**. Bond lengths reported in Å. Solution-based activation free energies (red), distortion energies (green) and reaction free energies (blue) are in kcal/mol.

A subsequent distortion analysis shows that this difference is largely caused by the smaller distortion energy that is required to obtain the *endo* TS compared to that for the *exo*–TS (22.1 vs. 22.6 kcal/mol). The TS geometries also suggest that the cycloaddition is favored on the face away from the 3–methyl substituent of the cyclopropene ring. These activation energies are higher than those calculated for bicyclo[6.1.0]non-4-yne and cyclooctyne, with barriers of 4.9 and 6.9 kcal/mol, respectively, and rate constants of 838 and 51 $M^{-1}s^{-1}$, but lower than that of dibenzoazacyclooctyne (12.1 kcal/mol, with k_2 = 0.51 $M^{-1}s^{-1}$),[26] and

those reported for the Diels-Alder reaction of cyclopropenes and butadiene (21-27 kcal/mol).[24] The marginally slower reaction of **7** and **8**, the cycloaddition proceeds similarly via a non-synchronous *endo*–TS with an activation barrier of 7.9 kcal/mol (vs 7.5 kcal/mol for **5**; *vide supra*). In this case, the distortion energies for the cyclopropene and *o*-quinone were found to be higher (26.3 kcal/mol, respectively).

Scheme 3. Scheme for preparation of quinone-terminated surfaces (**M_3**) and reaction with **5**. See Appendix 2 for more detail.

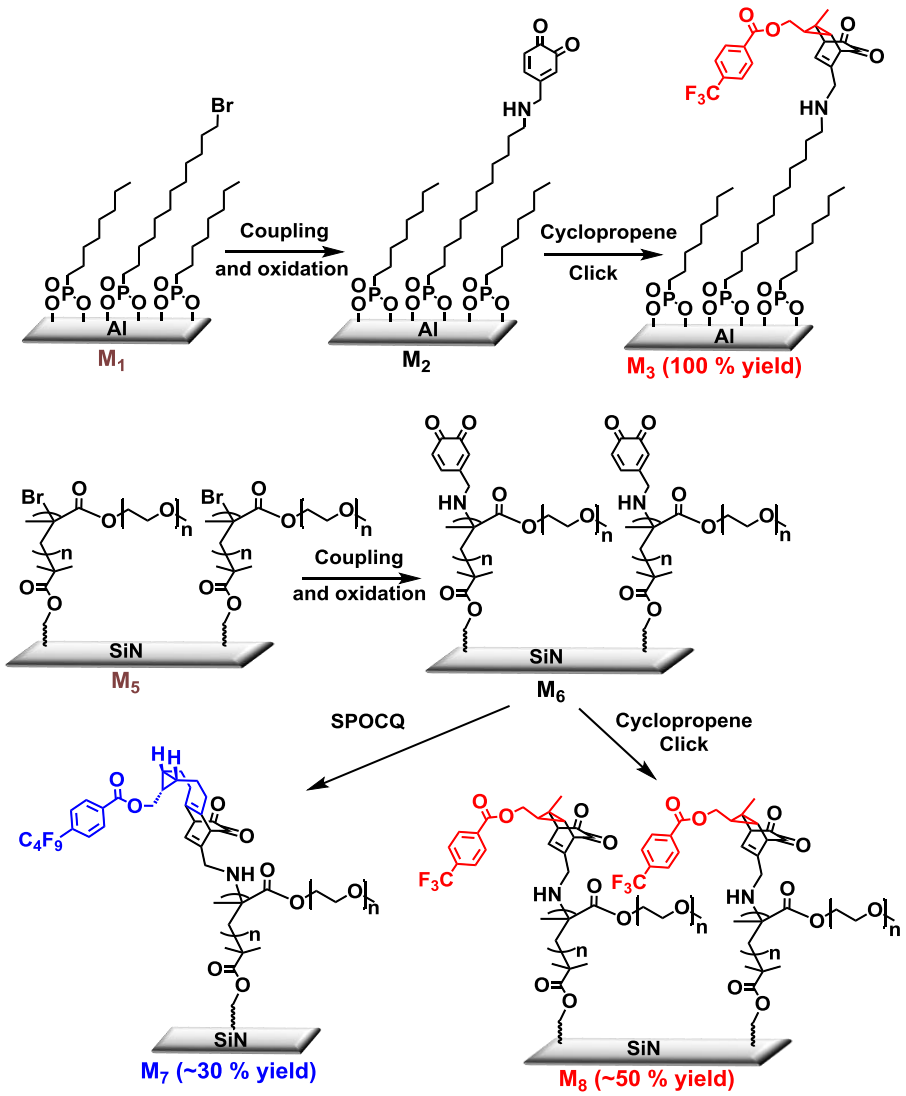

The potential of this novel click reaction should become evident in crowded environments, where the small size of cyclopropene is of relevance. Thus, we tested the applicability of this click reaction for surface functionalization. Surface functionalization provides difficult reaction conditions due to the steric constraints

and immobility of one of the reaction partners. A 100% reaction efficiency is specifically in high demand, as purification after covalent on–surface reactions is simply not possible. We envisaged that the highly efficient and fast nature of our novel reaction would also translate on a surface. For this purpose, activated aluminum (Al) surfaces (**M_0**) were modified with dodecyl (C_{12}) Br–terminated phosphonic acids diluted with octyl chains in a 3:1 ratio, to get **M_1** surfaces (Appendix 2, section S1). This was followed by coupling with 3,4-dihydroxybenzylamine hydrobromide and oxidation to *o*–quinones with $NaIO_4$ to yield **M_2** surfaces (Scheme 3).

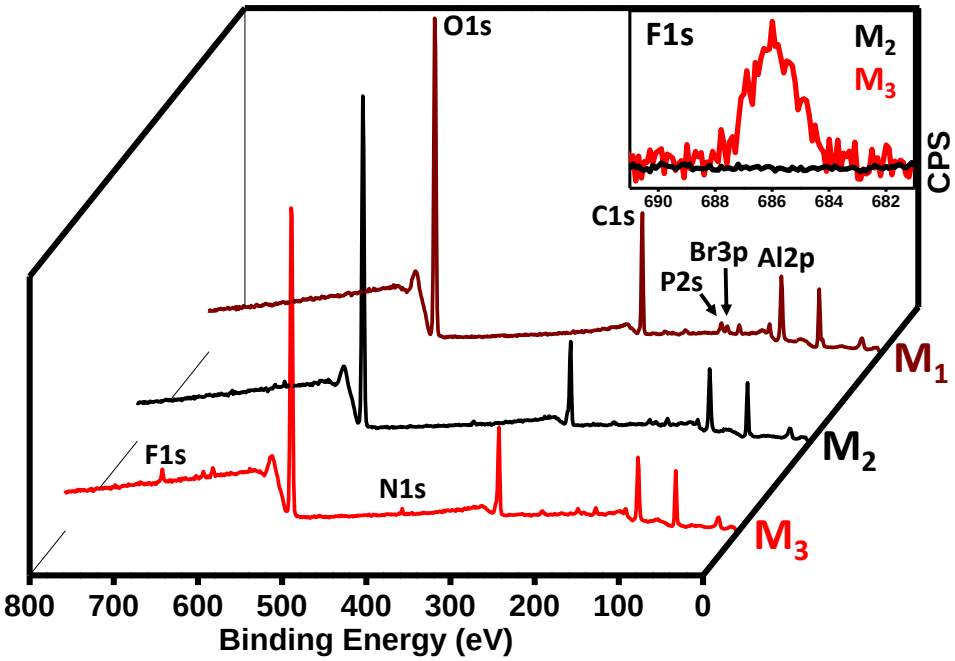

Figure 3. Stacked XPS wide scan spectra of **M_1**–**M_3** surfaces; insert: F1s narrow range spectra of **M_2** and **M_3** surfaces.

XPS wide scan analysis (Br/P = 1:4 for **M_1** and N/P = 1:4 for **M_2** surfaces, Figure S4.2–4.4) coupled with the disappearance of the Br3d signal (at 67.0 eV, Figure S4.5) in XPS narrow scan for **M_2** confirmed formation of surface-bound *o*–quinones. **M_2** surfaces were then subject to a 5 mM solution of **5**, to yield clicked **M_3** surfaces (Scheme 3). F/P ratios (3:4) in the XPS wide (Figure 3 and Figure S4.6) and narrow scan F1s and P2s analysis (Figure 4) confirmed a quantitative click reaction (100 ± 3 % yield) within 20 min. The standard deviation of the

reaction yield was determined over a hexaplet of independent samples prepared on different days to ensure rigorous reproducibility of the reaction.

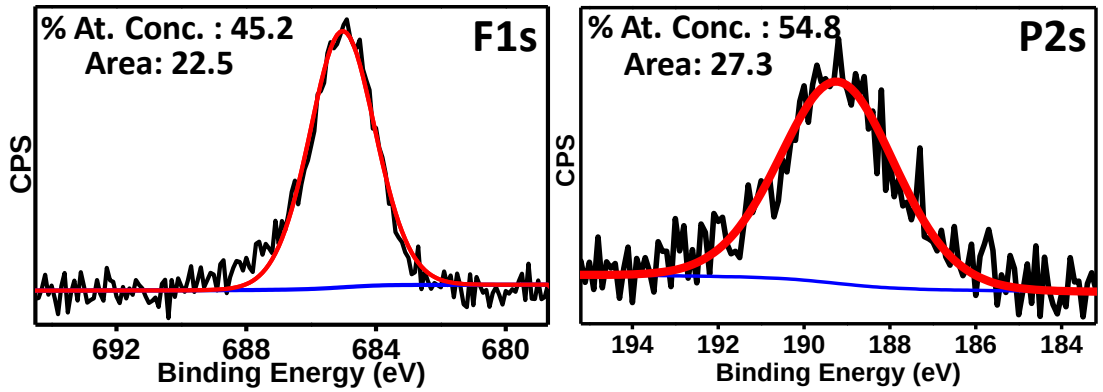

Figure 4. XPS F1s and P2s narrow scan spectra of **M_3** surfaces showing the atomic concentration of the two elements, respectively.

For testing polymer brush functionalization, we utilized poly(MeOEGMA) brushes that have been shown to possess good anti–fouling properties.[27] Bromine–ended polymer brushes (**M_5**) were prepared by SI–ATRP (Appendix 2, section 1) on silicon nitride (SiN) surfaces and analyzed by XPS (Figure S4.8–S4.13) and AFM (thickness = 11 ± 1 nm, roughness = 2.2 nm, Figure S4.14). This was followed by coupling and subsequent oxidation steps to yield *o*-quinone-terminated brushes M_6 (Scheme 3), as shown by the disappearance of the Br3d signal in the XPS wide and narrow scan analysis (Figure 3 and S4.15–S4.17). To compare the clickability of strained alkyne (BCN derivative) versus strained alkene (cyclopropene) on polymer brushes, we performed both the reactions on **M_6** surfaces and calculated the approximate conversion via the ratio of F1s (686.0 eV)/N1s (~400.7 eV) signals from narrow scan analysis (Figure S4.19 and S4.23). With a BCN–C_4F_9 analogue,[17] the reaction yielded a ~30 % yield, while the sterically advantageous cyclopropene provided ~60 % conversion (each averaged over 6 samples). This further shows the wide applicability of this approach for polymer modification.

For interfacial kinetics determination, we followed over the course of the reaction on **M_2** surfaces the growth of an MS–ionizable tag (*p*–CF_3 benzoate anion [*m/z* 189.016]) obtained by aromatic ester fragmentation from **M_3** surfaces

by DART–HRMS (Figure 5).[21a] Given the relatively short reaction time of 20 min (cf. 4 h for the previously reported SPOCQ reaction) we could follow the kinetics over the entire kinetic regime. As also confirmed by XPS results, the reaction tends to an asymptotic limit within 20 min, signaling completion. The second–order rate constant (k_2) was found to be 0.50 ± 0.01 $M^{-1}s^{-1}$ at 30 °C. Despite the slightly reduced rate, it is quite remarkable that the reaction still achieved complete conversion within 20 min. In contrast, the SPOCQ reaction (k_2 = 3.3 $M^{-1}s^{-1}$ for first 70% conversion; afterwards more complex and slower kinetics) achieves quantitative conversion only in 4 h. This further emphasizes the positive role played by smaller sterics of the cyclopropene motif as compared to a bulky cyclooctyne. We believe the "clean kinetics" of this reaction to be a significant benefit over its predecessor interfacial SPOCQ.

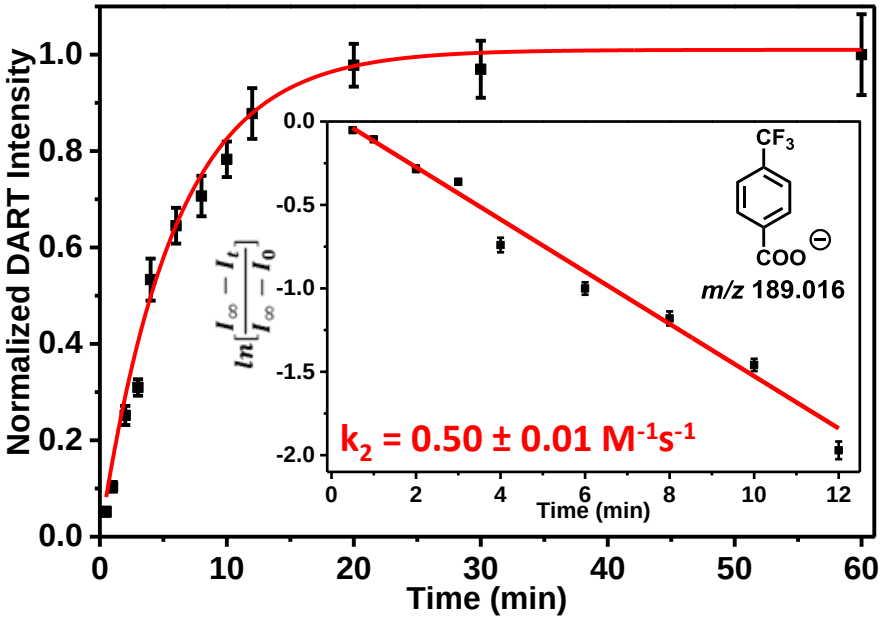

Figure 5. Normalized DART–HRMS intensity vs time (min) for reaction between $\mathbf{M_3}$ surfaces and **5**. Inset: Linear plots of $ln\ [(I_\infty - I_t)/(I_\infty - I_0)]$ vs time to obtain the pseudo-first order constants, from which k_2 was determined.

These kinetics also reveal a more general point on the difference between dilute solution data and those relevant in crowded environments. The surface-bound cyclopropene–quinone click is only 4 times lower than in solution. In contrast, the SPOCQ reaction is ~150 times slower on the surface than in

solution. In other words: the solution-based kinetics, but also quantum chemical data mimicking solutions, provide an important first indication on the relative rate in crowded environments – however, these data may still be up to two orders of magnitude off when predicting relative rates and efficiencies of different click or coupling reactions under the conditions whether these reactions are actually most useful, namely in crowded environments. One-on-one transposition of solution data to e.g. surface modification, polymer modification or bio-conjugation efficacy is therefore not generally allowed, and more detailed considerations and/or calculations are in order. Surface-bound rates might more closely mimic the rates relevant in those situations.

As suggested by Sharpless and Barner–Kowollik,[4,9] click reactions have to fulfill stringent criteria of fast rate, high efficiency, modularity and orthogonality to fit into the click category. We demonstrate that indeed our reaction proceeds with fast kinetics and high efficiencies both in solution and on surfaces for two distinct examples, monolayers and polymer brushes, thus validating its click attributes. Moreover, the products in solution can be easily characterized by NMR spectroscopy. Finally the very slow reactivity of 1,3-disubstituted cyclopropenes towards azides and nitrile imines[24] should allow a preferential and orthogonal reactivity for quinones as it does for tetrazines in presence of such groups.

CONCLUSIONS

In conclusion, we report a novel strain–promoted reaction between *o*-quinones and strained alkenes (1–methyl-3–substituted cyclopropenes) with reaction rates paralleling that of click reactions of cyclopropenes with unsymmetrical tetrazines. In addition, we show that reaction is quantitative for monolayer functionalization and high yielding for polymer brushes. Finally we show that the small size of the cyclopropene moiety is highly advantageous in crowded environments, as present in e.g. polymer and bio-conjugation reactions, and on surfaces. We believe that the use of 1–methyl–3–substituted cyclopropenes will therefore also be highly useful for bio–conjugations that require small reagents.

REFERENCES

(1) Moses, J. E.; Moorhouse, A. D. *Chem. Soc. Rev.* **2007**, *36*, 1249.

(2) Castro, V.; Rodríguez, H.; Albericio, F. *ACS Comb. Sci.* **2016**, *18*, 1.

(3) Escorihuela, J.; Marcelis, A. T. M.; Zuilhof, H. *Adv. Mater. Interfaces* **2015**, *2*, 1500135.

(4) Kolb, H. C.; Finn, M. G.; Sharpless, K. B. *Angew. Chem. Int. Ed.* **2001**, *40*, 2004.

(5) Tornøe, C. W.; Christensen, C.; Meldal, M. *J. Org. Chem.* **2002**, *67*, 3057.

(6) Laughlin, S. T.; Baskin, J. M.; Amacher, S. L.; Bertozzi, C. R. *Science* **2008**, *320*, 664.

(7) Knall, A.-C.; Slugovc, C. *Chem. Soc. Rev.* **2013**, *42*, 5131.

(8) Dong, J.; Krasnova, L.; Finn, M. G.; Sharpless, K. B. *Angew. Chem. Int. Ed.* **2014**, *53*, 9430.

(9) Li, S.; Wu, P.; Moses, J. E.; Sharpless, K. B. *Angew. Chem. Int. Ed.* **2017**, *56*, 2903.

(10) a) Kim, H. L.; Sachin, K.; Jeong, H. J.; Choi, W.; Lee, H. S.; Kim, D. W. *ACS Med. Chem. Lett.* **2015**, *6*, 402 b) T. Pauloehrl, G. Delaittre, V. Winkler, A. Welle, M. Bruns, H. G. Börner, A. M. Greiner, M. Bastmeyer, C. Barner-Kowollik, *Angew. Chem. Int. Ed.* **2012**, *51*, 1071; c) S. Arumugam, S. V. Orski, N. E. Mbua, C. Mcnitt, G-J. Boons, J. Locklin, V. V. Popik, *Pure Appl. Chem.* **2013**, *85*, 1499; d) H. Frisch, D. E. Marschner, A. S. Goldmann, C. Barner-Kowollik, *Angew. Chem. Int. Ed.* **2018**, *57*, 2036.

(11) Borrmann, A.; Fatunsin, O.; Dommerholt, J.; Jonker, A. M.; Löwik, D. W. P. M.; van Hest, J. C. M.; van Delft, F. L. *Bioconjugate Chem.* **2015**, *26*, 257.

(12) Gao, B.; Zhang, L.; Zheng, Q.; Zhou, F.; Klivansky, L. M.; Lu, J.; Liu, Y.; Dong, J.; Wu, P.; Sharpless, K. B. *Nat. Chem.* **2017**, *9*, 1083.

(13) Bruins, J. J.; Westphal, A. H.; Albada, B.; Wagner, K.; Bartels, L.; Spits, H.; van Berkel, W. J. H.; van Delft, F. L. *Bioconjugate Chem.* **2017**, *28*, 1189.

(14) George, A.; Krishna Priya, G.; Ilamaran, M.; Kamini, N. R.; Ganesh, S.; Easwaramoorthi, S.; Ayyadurai, N. *ChemistrySelect* **2017**, *2*, 7117.

(15) Jonker, A. M.; Borrmann, A.; van Eck, E. R. H.; van Delft, F. L.; Löwik, D. W. P. M.; van Hest, J. C. M. *Adv. Mater.* **2015**, *27*, 1235.

(16) Nematollahi, D.; Dehdashtian, S. *Tet. Lett.* **2008**, *49*, 645.

(17) Sen, R.; Escorihuela, J.; van Delft, F.; Zuilhof, H. *Angew. Chem. Int. Ed.* **2017**, *56*, 3299.

(18) Yang, J.; Šečkutė, J.; Cole, C. M.; Devaraj, N. K. *Angew. Chem. Int. Ed.* **2012**, *51*, 7476.

(19) Späte, A.-K. S., V. F.; Häfner, J.; Niederwieser, A.; Mayer, T. U.; Wittmann, V. *Beilstein J. Org. Chem.* **2014**, *10*, 2235.

(20) Späte, A.-K.; Bußkamp, H.; Niederwieser, A.; Schart, V. F.; Marx, A.; Wittmann, V. *Bioconjugate Chem.* **2014**, *25*, 147.

(21) Patterson, D. M.; Nazarova, L. A.; Xie, B.; Kamber, D. N.; Prescher, J. A. *J. Am. Chem. Soc.* **2012**, *134*, 18638.

(22) Yang, J.; Liang, Y.; Šečkutė, J.; Houk, K. N.; Devaraj, N. K. *Chem. Eur. J.* **2014**, *20*, 3365.

(23) Sen, R.; Gahtory, D.; Escorihuela, J.; Firet, J.; Pujari, S. P.; Zuilhof, H. *Chem. Eur. J.* **2017**, *23*, 13015.

(24) Liu, F.; Liang, Y.; Houk, K. N. *Acc. Chem. Res.* **2017**, *50*, 2297.

(25) M. J. Frisch et al. Gaussian 16, Revision A.03, Gaussian, Inc., Wallingford CT, 2016.

(26) Escorihuela, J.; Das, A.; Looijen, J.; Delft, F. L. v.; Aquino, A.; Lischka, H.; Zuilhof, H. *J. Org. Chem.* **2018**, *83*, 244.

(27) Kuzmyn, A. R.; de los Santos Pereira, A.; Pop-Georgievski, O.; Bruns, M.; Brynda, E.; Rodriguez-Emmenegger, C. *Polym. Chem.* **2014**, *5*, 4124.

CHAPTER 4

Surface-Bound Quadruple H–bonded Dimers: Formation and Exchange Kinetics

ABSTRACT

While the mechanistic details of dimerization of the self–complementary 2–ureido–4(1H)–pyrimidinone (UPy) motif are well studied in solution, no such investigation is available on a surface. Here we report an extensive study of hydrogen binding kinetics for quadruple H–bonded UPy arrays on aluminum surfaces and explore the ON/OFF capability of such arrays under externally controllable conditions. Also, we investigate the dynamic nature of this system whereby the interfacially H–bonded UPy is displaced by another UPy derivative in solution and reveal the kinetics of the exchange process.

This work was published as:

"*Surface-Bound Quadruple H–bonded Dimers: Formation and Exchange Kinetics*" Digvijay Gahtory, Rickdeb Sen, Maarten M. J. Smulders and Han Zuilhof *Faraday discussions*, **2017**, *204,* 383.

INTRODUCTION

Supramolecular chemistry, often referred to as 'chemistry beyond the molecule', utilizes reversible, non–covalent interactions for the formation of large molecular assemblies.[1,2] While the advance of supramolecular chemistry has spurred great development in various research areas, such as functional supramolecular polymers,[3] supramolecular catalysts[4] and supramolecular DNA assemblies,[5] the potential of such stable, yet dynamic interactions for surface applications is still underexplored.

Current surface attachment strategies largely rely on strong covalent bonding of a molecule of interest to self–assembled monolayers (SAMs) on the surface.[6] In this regard, several reactions have been utilized for various applications, *e.g.* preparation of protein-repellent surfaces,[7] attachment of biomolecules such as DNA,[8] preparation of carbohydrate and protein arrays[9] and nanoparticle functionalization.[10] This approach, although providing a robust attachment strategy, precludes a reversible attachment strategy that offers control by external stimuli such as solvent, light, temperature, pH and chemical influences. While supramolecular surface modification strategies allow easy manipulation of the interfacial chemical composition, architecture, topology, etc., to yield responsive and reusable surfaces, so far only a limited number of reports dealing with dynamic covalent[11] or non–covalent interactions[12] have been reported. A major advantage of any dynamic interfacial interaction is its ability to confer a stimulus-dependent ON/OFF handle for the surface. The utility of such rewritable substrates is beneficial for the development of (regeneratable) bio–sensors, electro-(de)activation of surfaces, nanofabrication platforms, etc.[13]

Non–covalent interactions such as hydrogen bonding and π–π interactions offer a distinct advantage in this regard as they provide an easily addressable handle for quick attachment and removal of the bound moiety, which thus enables a surface-bound ON/OFF switch. As a virtue of their strength, specificity and dynamic nature, arrays of multiple hydrogen bonds have garnered significant

interest for the assembly of complex supramolecular structures with useful properties in a predictable and reliable fashion.[14] Despite a ubiquitous presence of such motifs in supramolecular applications, their role in surface science is still underexamined. Reports by Ward *et al.* and Rotello *et al.* have demonstrated the utility of simple two- and three-fold hydrogen bonding arrays such as adenine–thymine[15] and thymine–diamidopyridine.[16] Although explored for different applications such as polymer attachment and attachment of electroactive groups,[13] these motifs are quite labile and several of these motifs are needed to be applied in concert.[17] In contrast, increasing the number of available hydrogen bonding groups in a motif such as for quadruple[18] or hexafold[19] bonding arrays should produce much more stable dimeric structures.

An interesting candidate among such hydrogen bonding motifs is 2–ureido–4(1H)–pyrimidinone (UPy), a self–complementary quadruple hydrogen bonding array (Scheme 1).[20] Easily synthesized and capable of strong self–dimerization[21] (K_{dim} = 6 × 10^8 M^{-1} in toluene) through a self–complementary donor–donor–acceptor–acceptor H–bonding motif, this system has been widely utilized for various applications such as polymeric materials with self–healing properties[22] and responsive nanoparticles.[23]

Despite numerous reports on aforementioned H–bonding motifs, the exploration of the UPy motif at a surface has received surprisingly little attention.[24] As shown by single-molecule force spectroscopy (SMFS), the UPy motif forms a reversible, yet strongly bonded, UPy dimer on the surface.[25] Interestingly, the dimer between surface-bound UPy and soluble UPy can also be displaced, as shown by Tolbert *et al.* for glass substrates.[26] However, their study was significantly hampered by non–specific interactions of UPy molecules with the substrate itself, in which no significant preference was observed for the UPy dimer during the exchange process.

Notwithstanding this early work, the potential for reversibility and exchangeability of the UPy motif to yield dynamic surfaces with properties that

can be easily manipulated has not been fully investigated. Moreover, while the mechanistic details of UPy dimerization and other complementary hydrogen bonding counterparts have been studied comprehensively in solution,[27] kinetics inquiries on a surface have not been conducted to the best of our knowledge. We believe that insight in the extent and kinetics of surface binding and exchange by hydrogen bonding can facilitate the design and development of functional surfaces that rely on dynamic surface modification (*e.g.* regeneratable sensor surfaces), in an analogous manner to how insight in solution–based binding has contributed to the development of tunable responsive polymers.[28]

In this study, we examine the quadruple H–bonded UPy dimer formation on aluminum surfaces and exploit its reversible attachment by ON/OFF and exchange experiments. For the characterization we primarily use X–ray photoelectron spectroscopy (XPS), grazing angle total reflection–Fourier transform infrared spectroscopy (GATR–FTIR), and direct analysis in real time–high resolution mass spectrometry (DART–HRMS).[29] Recently, we have demonstrated the potential of DART–HRMS for quantitative surface analysis by elucidating interfacial kinetics and activation parameters of strain-promoted click reactions.[30] In addition, using a combination of aforementioned techniques, we further explore the reconfigurable and dynamic nature of the UPy H–bonding system to obtain rewritable and exchangeable dynamic surfaces.

RESULTS AND DISCUSSION

Monolayer formation and Link–UPy attachment. Our experimental design involved attachment of a ureido-[2-(4-pyrimidone)] functionalized with 1-hexylisocyanate (**UPy–Link**, **1**) onto amine-terminated aluminum (Al) substrates using an isocyanate coupling (Scheme 1). The choice of substrate was based on previous experience with interfacial kinetics determination: oxide-coated Al samples are easily modified with highly stable phosphonate-based monolayers and offer a distinct advantage during DART measurements at higher temperatures (see below).[31] Amine-terminated monolayers **S1** were prepared by

linking ω-NH_2-functionalized alkyl phosphonic acids (PAs) onto hydroxylated aluminum oxide surfaces. The C/P ratio (13 ± 0.5) and N/P ratio (1.0 ± 0.3) in XPS wide scans (Figure 1a and Appendix 3, Figure S1) confirmed the formation of C_{12}–NH_2 monolayers. GATR–FTIR analysis of the monolayers showed peaks at 2925 cm^{-1} and 2854 cm^{-1}, corresponding to the antisymmetric and symmetric methylene stretching, respectively (Appendix 3, Figure S2). Simulation studies with varying degrees of monolayer attachment using Material Studio (Appendix 3, section 7) revealed that ideally about half the surface sites are bound to a phosphonate moiety (in terms of obtaining the lowest packing energy per molecule).[32]

Scheme 1. Preparation of **Link–UPy** and **Link–UPy···UPy–CF_3** surfaces, **S2** and **S3**, respectively.

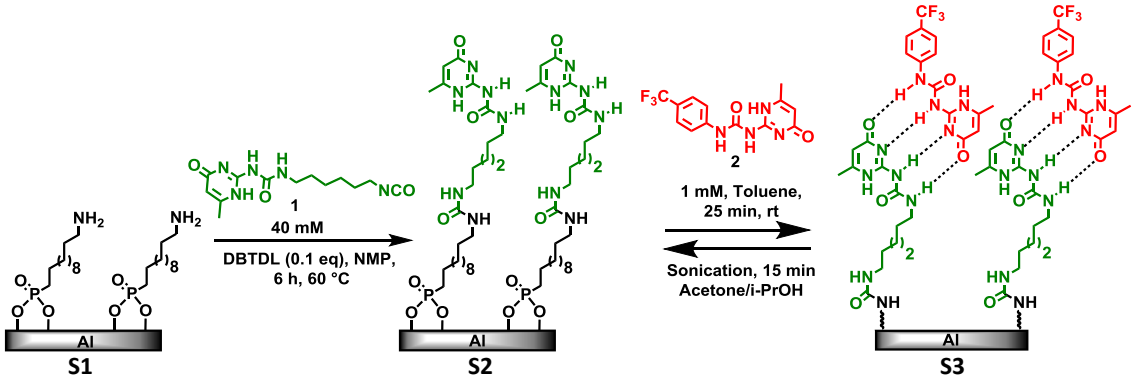

S1 substrates were reacted with a 40 mM solution of **1** in NMP for 6 h at 60 °C (Scheme 1). The successful coupling of **UPy–Link** became evident from the increase in the XPS N1s signal (Figure 1b). This signal is, after sonication only resulting from covalently bound UPy: GATR–FTIR spectra of **S3** (Appendix 3, Figure S2) showed no peak around 2270 cm^{-1} ascribable to isocyanate groups, indicating that after sonication no **Link–UPy···UPy–Link** dimer is present on the surface. Further confirmation of UPy attachment was obtained by appearance of a region corresponding to C=O in C1s narrow scan (Figure S5). While the presence of UPy was thus confirmed, it was also observed that the conversion tended to an asymptotic limit of 52 ± 5%, as determined from the N/P ratio in XPS

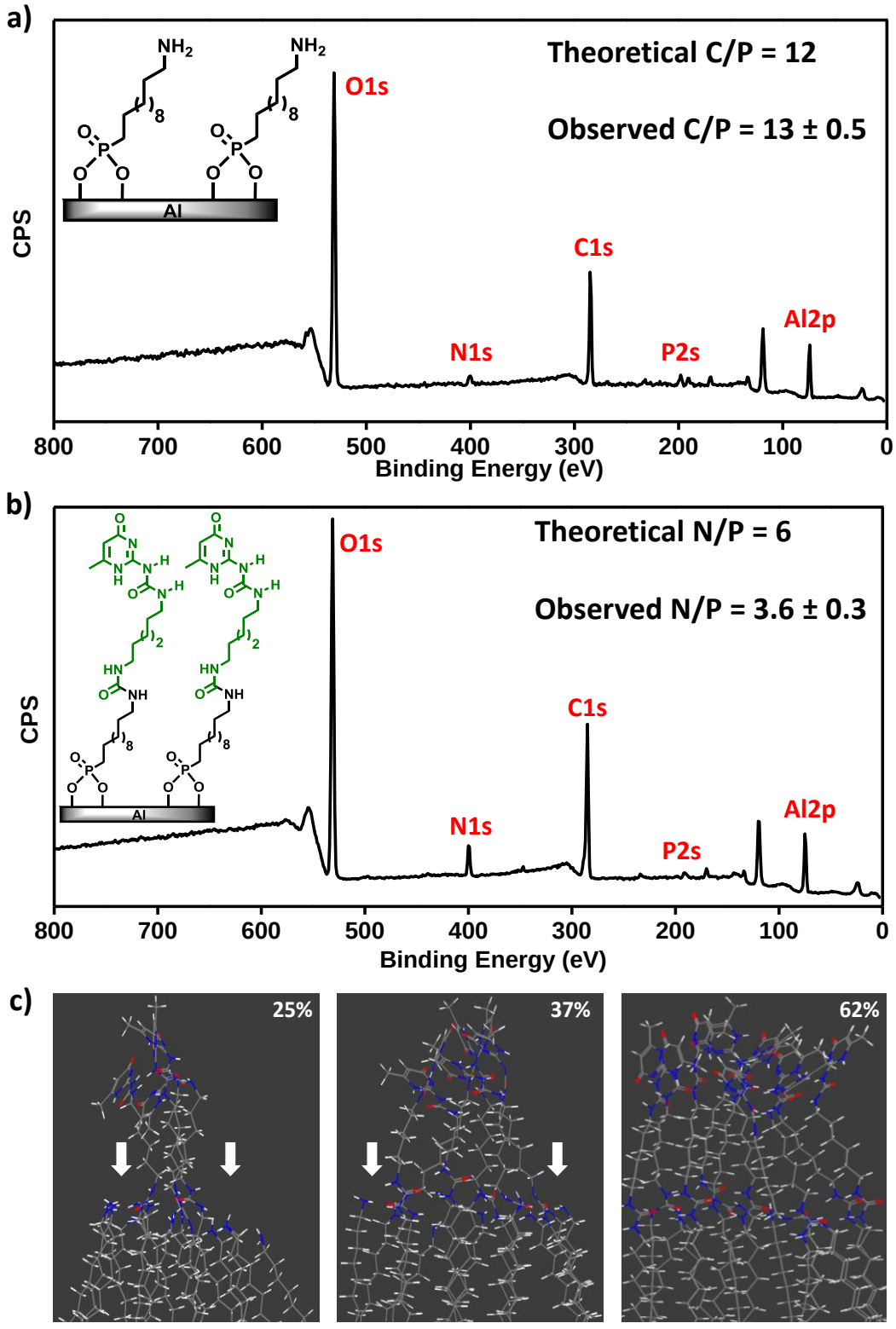

Figure 1. a) XPS wide spectra of **S2** surfaces b) Front view of simulation cell after **UPy–Link** attachment on aluminum surface with increasing coverage (25, 37 and 62%) of **UPy–Link** on aluminum surfaces. After approx. 60% coverage with **UPy–Link**, the amine groups (shown by white arrows) are completely buried and inaccessible for incoming 1–hexylisocyanate UPy molecules.

spectra (Figure 1b and Appendix 3, Figure S3–S4). Attempts to enhance the surface yield by increased reaction times or temperatures rendered no improvement. A less than 100% conversion can be rationalized by the significantly larger footprint of a UPy moiety compared to an amine. To further rationalize this asymptotic limit, the availability of surficial amine groups was compared at different yields of the surface-bound isocyanate coupling by theoretical 3D models (Figure 1c, 2 and Appendix 3, section 7). We found that at around 60% coverage the surface becomes highly crowded. Hereby, the remaining amine groups are rendered inaccessible for any further functionalization with the incoming **UPy–Link** molecules. Although evidently only qualitatively, this confirms that for steric reasons the reaction of **UPy–Link** to the amine-terminated surface is not quantitative, but is limited to around 50%.

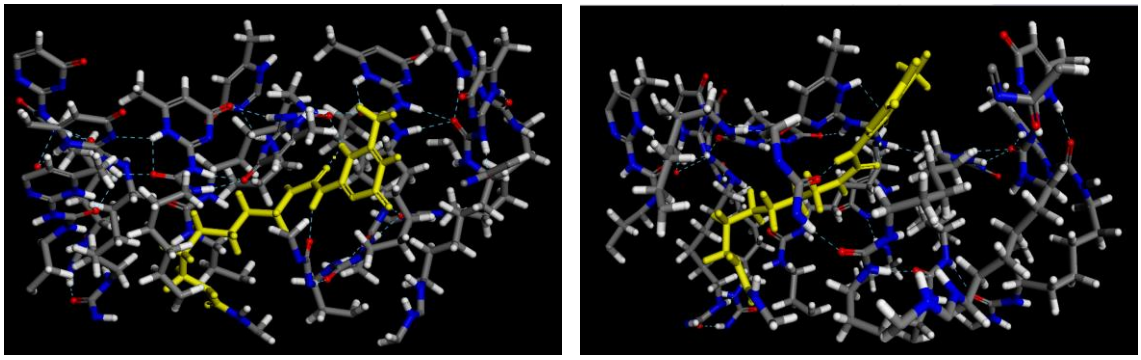

Figure 2. Different views of UPy–Link on surfaces obtained after molecular dynamics (one of the **UPy–Link** molecules has been highlighted in yellow). The intermolecular H–bonding interactions with adjacent UPy molecules can be clearly seen and possibly compete with the incoming soluble **UPy–CF_3** molecules.

Indicative 3D structures were obtained by constructing surfaces **S2** with this surface coverage of 60% in a molecular mechanics simulation program using the PCFF force field.[32] First, such a surface (with 320 UPy moieties on 512 chains) was constructed with repeating boundary conditions to eliminate edge effects. Second, a series of randomized structures was obtained by running molecular dynamics structures at temperatures of 500 °C or higher, which we subsequently optimized with geometry optimization routines. Typical structures of **S2** are

presented in Figure 2 and section 7.8 (Appendix 3), and such structures invariably show the presence of surface–bound 4–fold H–bonded UPy dimers, amidst a range of not ideally H–bonded UPy moieties. For the latter, the optimal 4–fold H–bonding is apparently hampered by the increased steric hindrance that this would cause. In summary: surface-bound UPy is partially internally H-bonded; this will influence the equilibrium with UPy moieties in solution.

Interfacial UPy dimer H–bonding and kinetics determination. In order to study the H–bonding phenomena quantitatively by XPS and DART–HRMS, we required a UPy tag that could fulfil specific roles: (1) when surface–bound it should yield a characteristic signal in XPS, and (2) it should be sufficiently volatile and ionizable to be detected in DART–HRMS. 4–(Trifluoromethyl)phenyl UPy (**UPy–CF$_3$**, **2**) was found to be a good candidate that meets both criteria (Figure 3a and 3b). For kinetics determination, **UPy–Link**-terminated samples (**S2**) were immersed in a 1 mM solution of **2** in toluene at 25 °C for different time intervals, followed by sonication for 5 min in toluene. The sonication step was necessary to ensure that all **UPy–CF$_3$** binding to the surface was specifically bound through strong (likely fourfold) hydrogen bonding, and that all weakly and nonspecifically physisorbed **UPy–CF$_3$** was removed.

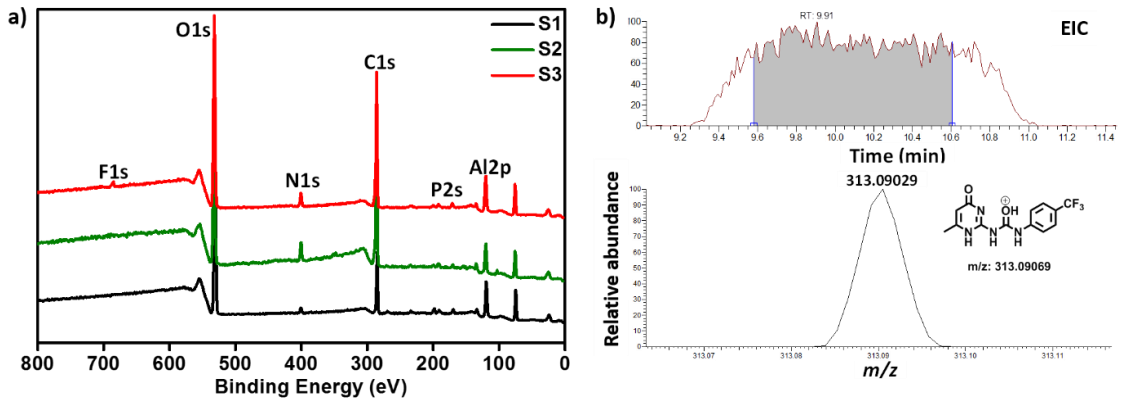

Figure 3. Analysis of surfaces **S1**, **S2** and **S3**: a) XPS wide scans and b) DART ion intensity EIC (top panel) for **Link–UPy···UPy–CF$_3$** dimers and peak of ion of interest (bottom panel).

The extent of surface immobilization was subsequently determined by XPS and DART-HRMS. Monitoring the F/P ratio in XPS versus time (Figure 3, and

Appendix 3, Figure S9) and the DART–HRMS intensity of protonated **2** (Figure 4a) both showed that the extent of H–bonding converged to a limiting value around 20 min. Careful analysis of the data revealed (pseudo-)first-order reaction kinetics, with a first-order rate constant for UPy binding to the surface, at 25 °C in toluene at [UPy] = 1 mM, of (22 ± 1) × 10^{-4} s^{-1} (Appendix 3 section 4.5). The limiting F/P ratio corresponded to about 35% coverage of all surface-bound UPy moieties with **2** (Figure 4b and Appendix 3, Figure S10).

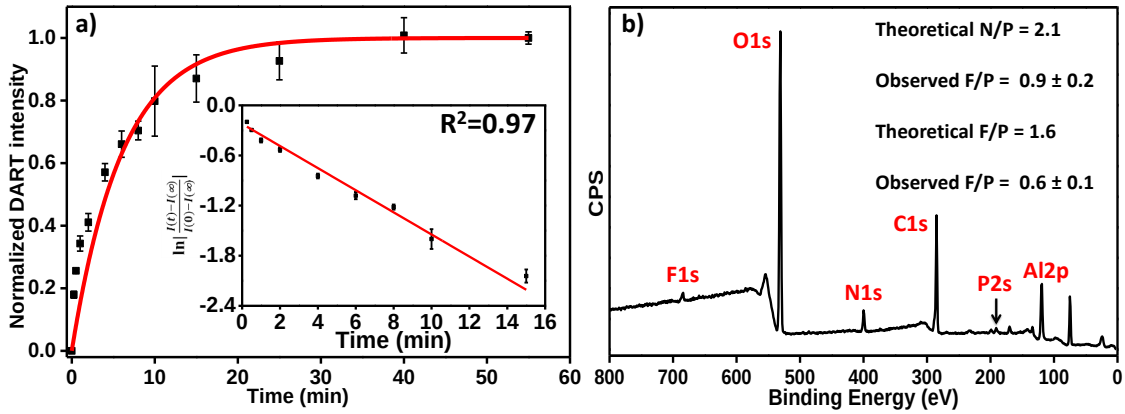

Figure 4. a) Normalized EIC intensity of protonated **2** (positive mode) for the dimerization process at 25 °C (each data point from 6–fold repetition). Inset: Plot of $\ln|(I_t - I_\infty)/(I_0 - I_\infty)|$ versus time used to obtain the first-order rate constant. b) XPS wide scan of **S3**, showing a ~40 % dimerization by **UPy–CF_3**).

Overall, this means that the monolayer covers 50% of the surface sites with amines; approximately 52% of those amine groups are reacted with 1; and 35% of the resulting surface-bound **UPy–Link** form **UPy···UPy** dimers. This yields a maximum overall dimer coverage of ~9%. This maximum value hinges on the formation of H–bonded dimers that induces additional steric constraints within the monolayer. Molecular dynamics indeed revealed that crowding at the surface by surface-bound UPy can hamper further binding (Figure 2 **and** Appendix 3, Section 7). As a result, when the steric hindrance becomes too large, binding of a surface-bound UPy with a soluble UPy will be outcompeted by the competitive equilibrium between the dimers in solution. In addition, GATR–FTIR spectra of these surfaces (Figure 3b and Appendix 3, Figure S2) displayed distinct peaks at

1582 cm^{-1} and 1653 cm^{-1}, attributable to amide I and II bands for dimeric UPy as previously reported (at ~1580 cm^{-1} and ~1660 cm^{-1} respectively).[47]

Control H–bonding experiments with NH_2-terminated surfaces (**S1**) under similar conditions were also performed, and these showed absence of any **UPy–CF_3** bonded non–specifically to the amino monolayers. This combination of XPS and DART analysis of control samples (Appendix 3, Figure S12–S13) thus confirmed that immobilization of **2** onto **S2** surfaces occurred through specific, likely fourfold, UPy···UPy hydrogen bonding, about 38% coverage of all surface-bound UPy moieties with **2** (Figure 4b and Appendix 3, Figure S10).

Surface reusability and exchange kinetics. We observed that this interfacial dimer could be disrupted upon sonication in acetone or *i*–PrOH for 15 min, yielding the UPy monomer–terminated surface (OFF state). The OFF surface thus obtained could be changed back into the ON state simply by stirring it for 20 min in a solution of 2 (in toluene). The ON/OFF process was easily monitored by following the XPS F1s signal (Figure 5 and Appendix 3, Figure S14).

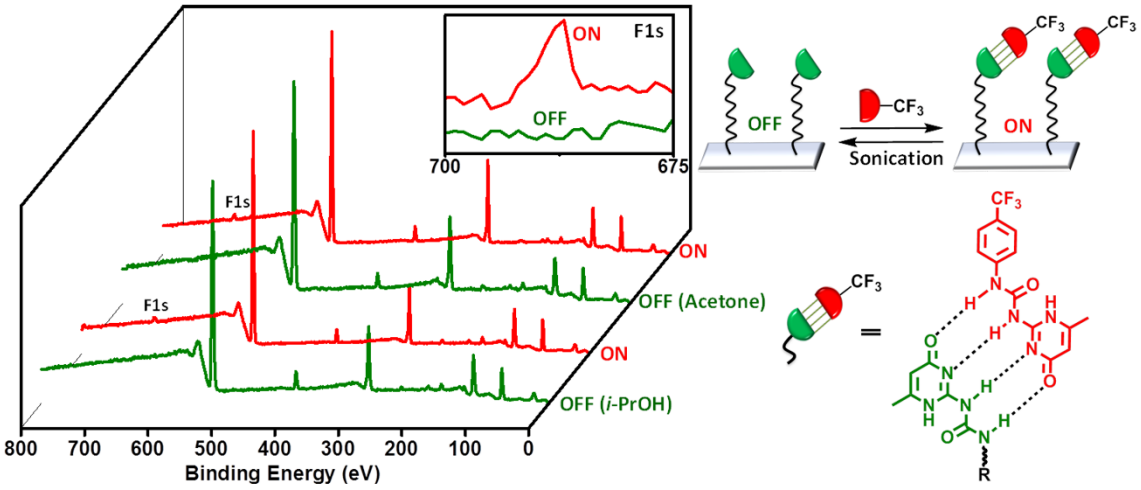

Figure 5. XPS wide scans for solvent-mediated removal and re–attachment of **UPy–CF_3**, inset: F1s region. ON refers to the dimeric state and OFF refers to the monomeric UPy.

Interestingly, the disassembly of UPy dimer showed a strong solvent dependence. Sonication in chloroform, dichloromethane and NMP was found to be ineffective in disrupting the hydrogen bonding assembly. Water like acetone

and *i*–PrOH, a competing solvent for H–bonding was expected to disrupt the interfacial H–bonds, but this was surprisingly not found to be true. This can possibly be explained by the hydrophobic 4–(trifluoromethyl)phenyl groups that hamper interaction of the solvent with surface–bound dimers. It should be noted that the observed solvent dependence may not apply to other interfacial H–bonded species. However, a useful implication is that in our case of **CF_3–UPy···UPy–Link** dimers, the system is stable under specific, easily obtainable conditions, while it can be easily dismantled in others.

Akin to their ON/OFF characteristics, dynamic systems also offer the additional advantage of exchangeability. We hypothesized that it would be possible to exchange the **Link–UPy···UPy–CF_3** complex by a different UPy motif. Hence, we synthesized 4-(iodo)phenyl UPy (**UPy–I**, **3**), which is structurally similar to **2**, but possesses a different substituent, and exchanged this for **2** on surface **S2**. The formation of **Link–UPy···UPy–I** dimers on a surface was confirmed by XPS (**Appendix 3,** Figure S15–S16), and compound **3** easily ionized in DART–HRMS as was seen upon simple dipping of a glass slide in a solution of **3** and subsequent strong signals of protonated **3** (*m/z* = 370.9986) in DART-HRMS. This allowed us to follow the growth of the signal of its protonated species over time, in order to quantify the rate of exchange.

Samples with **Link–UPy···UPy–CF_3** dimers were allowed to react with a 1 mM solution of **3** in toluene. DART–HRMS analysis of these substrates showed the presence of protonated species for both **2** and **3** (**Appendix 3,** Figure S17). The investigation of intensities thus obtained over different time intervals revealed that the decrease in DART intensity for **2** nicely correlated with the increase in signal intensity for **3** (Appendix 3, Figure 6a and 6c). After 3 h the two signals acquired a limiting value indicating that an equilibrium between the two motifs had been achieved. Monitoring the decrease of F/P ratio for the exchange process in XPS (**Appendix 3,** Figure S18–S19) also confirmed that at room temperature the exchange was slow, requiring several hours to reach equilibrium. Also, at room

temperature displacement of **UPy–CF₃** for **UPy–I** was not complete: 15-20% of **UPy–CF₃** remained surface-bound, and can likely only gradually be lost via an exchange process with a higher activation barrier.

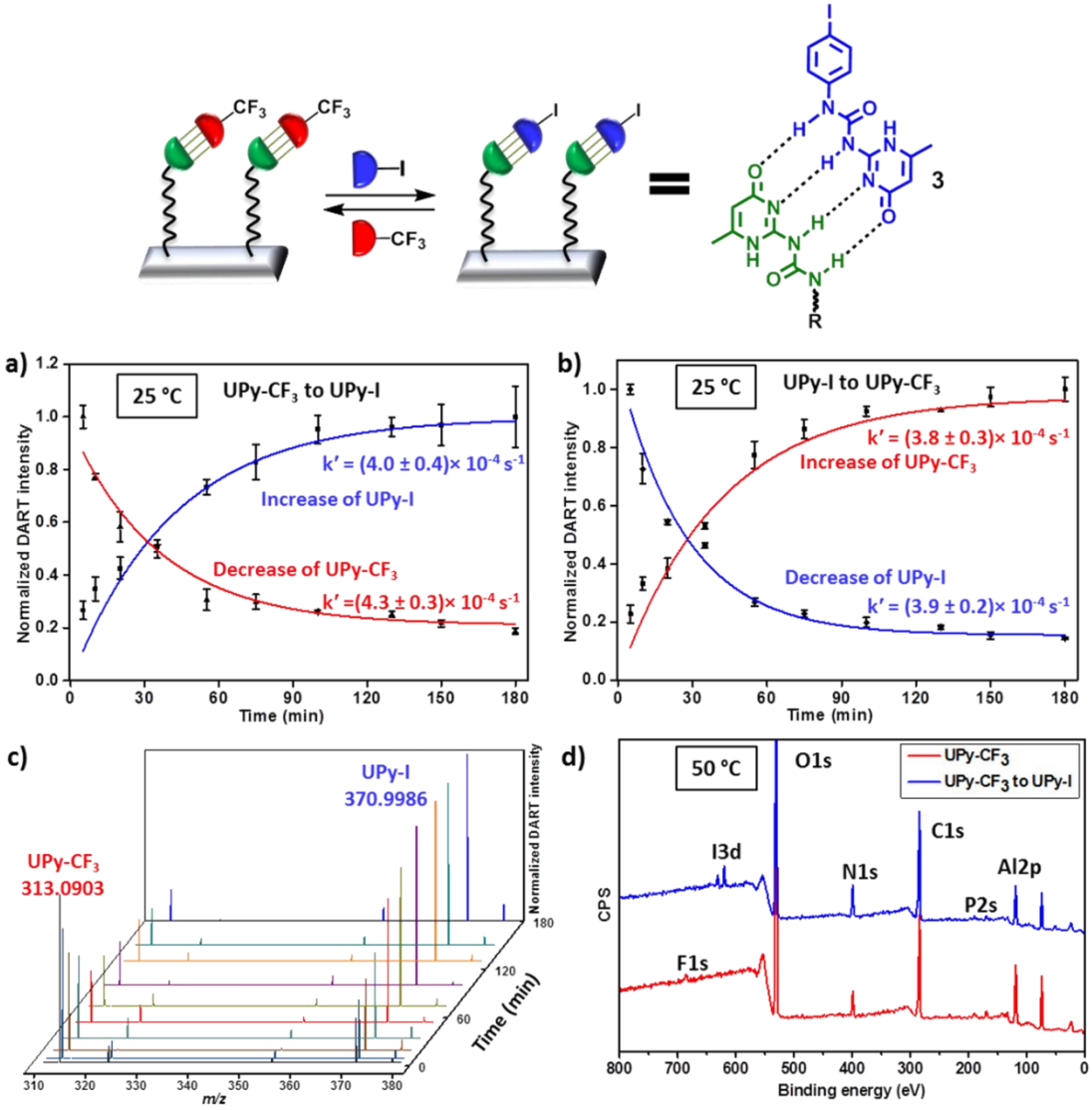

Figure 6. Normalized EIC intensity of protonated **2** (*m/z* = 313.0903) and **3** (*m/z* = 370.9986) during (a) the **UPy–CF₃** to **UPy–I** exchange, and (b) the **UPy–I** to **UPy–CF₃** exchange. c) EIC intensity plot vs time for *m/z* of **2** and **3** during **UPy–CF₃** to **UPy–I** exchange d) Stacked XPS wide spectra of the **UPy–CF₃** to **UPy–I** exchange at 50 °C

Schematically one might tentatively think about H-bonded **UPy–CF₃** that is bound via vertically oriented H-bonds at the top of the monolayer without further embedding (so that loss of **UPy–CF₃** only means breaking the four H-bonds) versus a smaller fraction of **UPy–CF₃** that is fully embedded in the monolayer, so

that loss of **UPy–CF$_3$** not only requires loss of H-bonds, but also of π–π stacking.[33] In reality, a range of dimer complexes with different degrees of embedding within the monolayer will likely be present, the ratios of which, of course, also depend on the precise composition of the monolayer and degree of H-bonding. However, at 50 °C the exchange was not only faster (completed within 2 h), but also complete as evidenced by the disappearance of the F1s signal in XPS (Figure 6d and **Appendix 3,** Figure S20) and the *m/z* intensity for 2 in DART (**Appendix 3,** Figure S21).

A similar exchange process was observed when the system was reversed: *i.e.* the initial dimeric state as **Link–UPy···UPy–I** and displacement with **UPy–CF$_3$** in solution (Figure 6b and **Appendix 3** Figure S22). The pseudo-first order rates (at [**UPy–CF$_3$**] = 1 mM) for both exchange reactions were found to be similar, 4×10^{-4} s^{-1} (Figure 4a, b), but approximately five times slower than the initial **Link–UPy···UPy–CF$_3$** dimer (**S3**) exchange process at a dimeric UPy surface than for the formation of dimers on a monomeric UPy surface. In addition during the initial H-bond forming process the total number of H–bonded complexes is increased, which drives the reaction, while the number of hydrogen bonds stays constant during the exchange process. Thirdly, we can ascertain that exchange/displacement of UPy at a surface is indeed independent of the UPy substituent and takes place with precisely determinable, slower kinetics than simple dimer formation.

Finally, we were interested in a comparison between the equilibrium constant (*K*) for dimer formation in solution and interfacial dimer formation. To this aim, we studied the rate of loss of dimers from the **Link–UPy···UPy–CF$_3$** system by XPS at 80 °C (Appendix 3, Figure S23–S26). Extrapolating the observed rate constant to 25 °C (see Appendix **3**, Figure S26), we found that the dissociation rate (k_{off}) was much slower than the dimer-forming reaction, and estimated k_{off} to be in the order of 10^{-7} s^{-1}. Based on the experimentally determined pseudo-first order rate constant for dimer formation (k_{on}') of 22×10^{-4} s^{-1} and based on the known (and

constant) UPy concentration of 1.0 mM, we could calculate a second-order rate constant of k_{on} = 2.2 M^{-1} s^{-1} (see Appendix 3, section 4.5 and Figure S26). This fixes the equilibrium constant (k_{on}/k_{off}) for interfacial H–bonded dimer formation in toluene to be in the order of 10^7 M^{-1}. This value is about an order of magnitude lower than that observed for soluble dimers in toluene (6×10^8 M^{-1}).[21] Three aspects may contribute to this observed difference between solution and surface-bound data.

First, the difference may be caused by already present H–bonds within the monolayer and the restrictions in orientation between surface-bound H–bond forming UPy moieties and the soluble UPy moieties. This likely lowers the value for surface-bound dimerization. Second, while the solution data refers to observations at low concentrations, the surface-bound data reflect highly interacting systems with varying entropy and enthalpy contributions. Given e.g. increased sterics on the one hand, but increased π–π interactions on the other hand, it is difficult to foresee the direction of this argument on *K* prior to more detailed experiments. Finally, while k_{on} is accurately determined, k_{off} is characterized with a lower precision, which simply adds uncertainty to the eventual outcome for *K*. Most important, we would therefore argue is that the value of *K* is comparable to the high value observed in solution, and that this formation of stable dimers on a surface provides potential for further studies on H-bonded responsive surfaces.

CONCLUSIONS

In summary, we have demonstrated that the fourfold hydrogen bonding UPy motif can be used for reversible surface modification. The inherently dynamic nature of this highly stable dimer (on–surface dimerization: *K* ~10^7 M^{-1}) allows straightforward switching between a surface–bound (ON state) and a surface–free (OFF state) by control over solvent. In addition, exchange of a hydrogen-bonded UPy moiety for a competing hydrogen bonding UPy motif was possible,

which yields further routes for exchangeable surface modification. By detailed kinetic analysis we have established the kinetics of binding, release and exchange. These studies not only revealed the typical time scales of these processes, but also enabled us to confirm that the strength of the quadruple hydrogen bond motif on the surface is of comparable strength to the solution-based binding. Our study provides a rational approach towards the formation of dynamically controllable complex H–bonding arrays at a surface. This also opens up new avenues for the preparation of dynamic and regeneratable surface platforms with ON/OFF capability that may find various applications in molecular electronics, bio–sensing and other applications.

REFERENCES

(1) Huang, F.; Anslyn, E. V. *Chem. Rev.* **2015**, *115*, 6999.

(2) Desiraju, G. R. *Nature* **2001**, *412*, 397.

(3) Aida, T.; Meijer, E. W.; Stupp, S. I. *Science* **2012**, *335*, 813.

(4) Schulze, M.; Kunz, V.; Frischmann, P. D.; Würthner, F. *Nat. Chem.* **2016**, *8*, 576.

(5) McLaughlin, C. K.; Hamblin, G. D.; Sleiman, H. F. *Chem. Soc. Rev.* **2011**, *40*, 5647.

(6) Pujari, S. P.; Scheres, L.; Marcelis, A. T. M.; Zuilhof, H. *Angew. Chem. Int. Ed.* **2014**, *53*, 6322.

(7) Wang, Z.; Zuilhof, H. *Langmuir* **2016**, *32*, 6310.

(8) Abi, A.; Ferapontova, E. E. *J. Am. Chem. Soc.* **2012**, *134*, 14499.

(9) Sun, X.-L.; Stabler, C. L.; Cazalis, C. S.; Chaikof, E. L. *Bioconjugate Chem.* **2006**, *17*, 52.

(10) Tassa, C.; Liong, M.; Hilderbrand, S.; Sandler, J. E.; Reiner, T.; Keliher, E. J.; Weissleder, R.; Shaw, S. Y. *Lab Chip* **2012**, *12*, 3103.

(11) Rozkiewicz, D. I.; Ravoo, B. J.; Reinhoudt, D. N. *Langmuir* **2005**, *21*, 6337.

(12) Arias, F.; Godínez, L. A.; Wilson, S. R.; Kaifer, A. E.; Echegoyen, L. *J. Am. Chem. Soc.* **1996**, *118*, 6086.

(13) Credo, G. M.; Boal, A. K.; Das, K.; Galow, T. H.; Rotello, V. M.; Feldheim, D. L.; Gorman, C. B. *J. Am. Chem. Soc.* **2002**, *124*, 9036.

(14) Brunsveld, L.; Folmer, B. J. B.; Meijer, E. W.; Sijbesma, R. P. *Chem. Rev.* **2001**, *101*, 4071.

(15) Viswanathan, K.; Long, T. E.; Ward, T. C. *Langmuir* **2009**, *25*, 6808.

(16) Jeoung, E.; Carroll, J. B.; Rotello, V. M. *Chem. Commun.* **2002**, 1510.

(17) Sanyal, A.; Norsten, T. B.; Uzun, O.; Rotello, V. M. *Langmuir* **2004**, *20*, 5958.

(18) Embrechts, A.; Velders, A. H.; Schönherr, H.; Vancso, G. J. *Langmuir* **2011**, *27*, 14272.

(19) Wedler-Jasinski, N.; Delbosc, N.; Virolleaud, M.-A.; Montarnal, D.; Welle, A.; Barner, L.; Walther, A.; Bernard, J.; Barner-Kowollik, C. *Chem. Commun.* **2016**, *52*, 8753.

(20) Beijer, F. H.; Sijbesma, R. P.; Kooijman, H.; Spek, A. L.; Meijer, E. W. *J. Am. Chem. Soc.* **1998**, *120*, 6761.

(21) Bosman, A. W.; Sijbesma, R. P.; Meijer, E. W. *Materials Today* **2004**, *7*, 34.

(22) Kushner, A. M.; Gabuchian, V.; Johnson, E. G.; Guan, Z. *J. Am. Chem. Soc.* **2007**, *129*, 14110.

(23) Foster, E. J.; Berda, E. B.; Meijer, E. W. *J. Am. Chem. Soc.* **2009**, *131*, 6964.

(24) Zou, S.; Schönherr, H.; Vancso, G. J. *J. Am. Chem. Soc.* **2005**, *127*, 11230.

(25) Zou, S.; Zhang, Z.; Förch, R.; Knoll, W.; Schönherr, H.; Vancso, G. J. *Langmuir* **2003**, *19*, 8618.

(26) Crowe, L. L.; Solntsev, K. M.; Tolbert, L. M. *Langmuir* **2007**, *23*, 6227.

(27) ten Cate, A. T.; Kooijman, H.; Spek, A. L.; Sijbesma, R. P.; Meijer, E. W. *J. Am. Chem. Soc.* **2004**, *126*, 3801.

(28) Yan, X.; Wang, F.; Zheng, B.; Huang, F. *Chem. Soc. Rev.* **2012**, ***41***, 6042.

(29) Gross, J. H. *Anal. Bioanal. Chem.* **2014**, *406*, 63.

(30) Sen, R. E., J.; van Delft, F. L.; Zuilhof, H. *Submitted* **2016**.

(31) Sen, R.; Escorihuela, J.; Smulders, M. M. J.; Zuilhof, H. *Langmuir* **2016**, *32*, 3412.

(32) Rijksen, B.; Pujari, S. P.; Scheres, L.; van Rijn, C. J. M.; Baio, J. E.; Weidner, T.; Zuilhof, H. *Langmuir* **2012**, *28*, 6577.

(33) Guo, D.; Sijbesma, R. P.; Zuilhof, H. *Org. Lett.* **2004**, *6*, 3667.

CHAPTER 5

Facile functionalization of peptide nucleic acids (PNAs) for antisense and single nucleotide polymorphism detection

ABSTRACT

A convenient on–resin functionalization of peptide nucleic acids is reported that allows sensitive detection of single-nucleotide polymorphisms (SNP). Hybridizing our thiazole orange (TO) clicked PNA probes in a circular fashion with antisense DNA provides two readout signals for increased sensitivity.

This work was published as:

"*Facile functionalization of peptide nucleic acids (PNAs) for antisense and single nucleotide polymorphism detection*" Digvijay Gahtory, Merita Murtola, Maarten M. J. Smulders, Tom Wennekes, Han Zuilhof, Roger Stromberg and Bauke Albada *Organic and Biomolecular Chemistry*, **2017**, *15,* 6710.

INTRODUCTION

Since the discovery of peptide nucleic acids (PNAs),[1] these materials have been employed for numerous applications in molecular biology,[2] antisense technology,[3] and nucleic acid detection.[4] Generally, the PNA structure is composed of a polyamide backbone consisting of N–(2–aminoethyl)glycine (Aeg)[5] or other amino acid units,[6] with the nucleobases linked via an amide linkage. This bio–mimetic structure makes them compatible with biology, yet renders them resilient to enzymatic degradation.[7] Furthermore, DNA–PNA duplexes have higher melting points than similar DNA–RNA or DNA-DNA duplexes.[8] The biomimetic properties of PNA have led to a growing interest in their utilization as carriers for the delivery of antisense DNA/RNA molecules for inhibition of gene expression, for example using penetrating peptide–PNA conjugates.[9] Seitz *et al.* reported that replacing one of the nucleobases with an intercalating fluorophore provides so–called *forced intercalation* probes that possess an excellent single-nucleotide polymorphism (SNP) detection ability.[10,11] Specifically, it was shown that alteration of the backbone structure that anchors thiazole orange (TO) to the PNA oligomer, from Aeg to D–Ornithine (^{D}Orn), increased the SNP detection ability.[12]

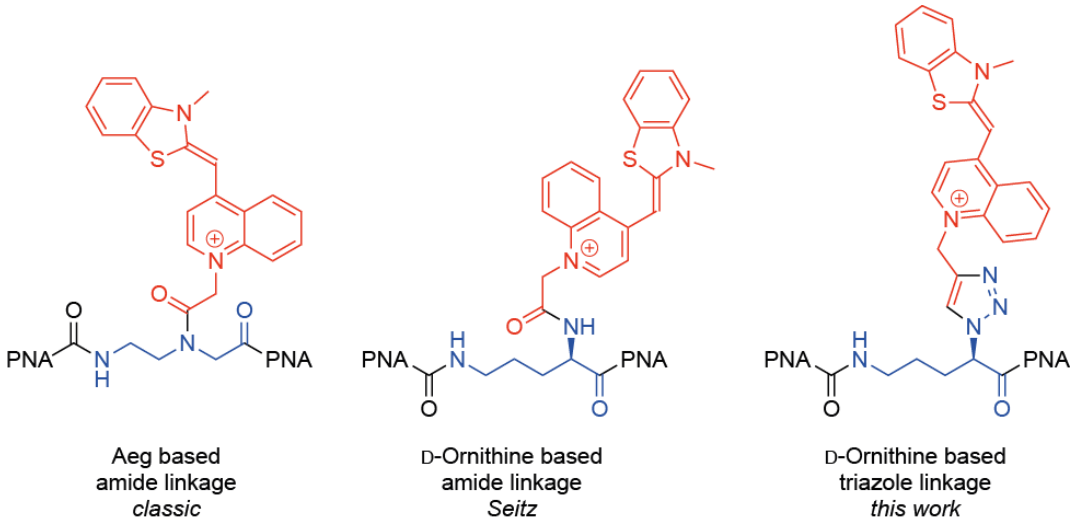

Figure 1. Structural comparison of a thiazole orange fluorophore linked to PNA by an amide on Aeg (a) and D–Orn (b), respectively, versus (c) triazole linkage.

Apart from the natural nucleobases, also non–base fragments have been linked to the PNA backbone via an amide bond (see Figure 1, a and b).[13] More recently, however, the wide repertoire of click reactions[14] has also been used to attach modified azido nucleobases[15] or a flexible azido/alkyne tether[16] for subsequent click functionalization. Since the triazole linkage is a good isostere for amide bonds,[17] we reasoned that incorporating an azide functionality directly onto the backbone without a flexible tether (see Figure 1c), although more challenging from a synthetic point of view, may have a positive effect on the sensing ability of a PNA construct due to the restricted mobility of the fluorophore at the site where sensing should occur.[18]

In this paper, we therefore report a click strategy for resin–bound PNA using a commercially available azido δ–amino acid, *i.e.* α–azido D–ornithine, that can be incorporated in the PNA chain during standard Fmoc–based solid–phase PNA synthesis. Once incorporated, the azido group allows direct attachment of thiazole orange (TO), illustrating its convenience as handle for PNA diversification. We used an on–resin copper–catalyzed azide–alkyne click (CuAAC) reaction to attach the dye to the resin–bound PNA chain. The resulting TO–PNA construct was then tested as a sensing module in (i) antisense DNA detection, and (ii) mismatch detection.

Firstly, we prepared an DNA–binding motif based on PNA. As shown by Seitz *et al.*, a D–ornithine linker successfully mimics the six–atom long building block that normally forms the PNA backbone, facilitating optimal PNA nucleobase alignment for hybridization with DNA or RNA.[12] Accordingly, resin–bound PNA that contained azido–D–ornithine (**P1**) was prepared using standard procedures (Scheme 1 and see Appendix 4, Figure S1–S3 for crude HPLC traces of **P1**). Following this, resin-bound PNA underwent a facile CuAAC with alkyne–derivatized thiazole orange **1** (see Appendix 4 for synthesis), to yield resin–bound TO–PNA conjugate **P2**. After acidic removal of TO–labeled PNA **P2** from the resin, TO–PNA conjugate **P3** was obtained in good yields (40% after HPLC

purification) (Scheme 1 and see Appendix 4, Figure S4–S6 for HPLC traces and absorbance spectrum of the conjugate).

Scheme 1. General scheme for synthesis of ^{D}Orn-containing PNA (P1) and on–resin click with thiazole orange to give clicked PNA (P2), which after acidic cleavage and deprotection yields soluble TO–PNA P3.

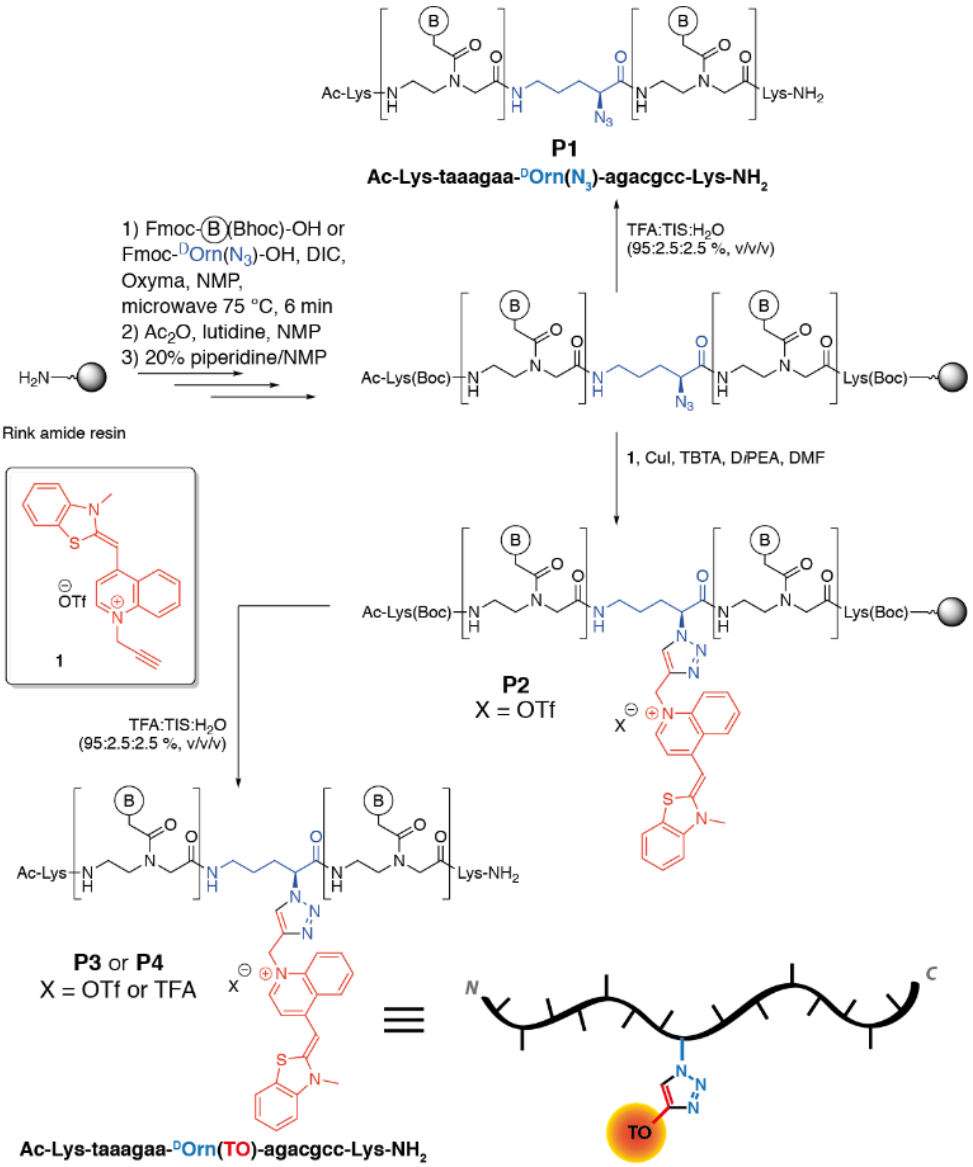

For DNA detection, we pursued partial hybridization of the PNA strand to a sequence D1 that was labelled with a fluorophore–quencher pair of Cy5 (λ_{ex} = 650 nm, λ_{em} = 668 nm) and Iowa Black quencher (Q) (λ_{max} = 667 nm), at the 5'– and 3'–ends of the oligonucleotide chain, respectively. The oligonucleotide sequence was chosen so that it would form a circular DNA–PNA heterodimer in

Scheme 2. Overview of the various sensing approaches that are described in this study. The solid wavy arrows indicate the irradiation and emission event of a fluorophore (F or TO), the dotted wavy arrow indicates low intensity emission due to quenching by a nearby organic black hole quencher (Q, panels a and b) or the larger mobility of the TO-dye (in panel c). a) Schematic representation of hybridization between azido–PNA **P1** and antisense DNA **D1**. On hybridization, the dye and quencher molecules come in close proximity due to the circular alignment of the sensor–strand **D1–P1**, leading to reduction in fluorescence. Upon addition of DNA **D2** that is complementary to **D1**, or DNA-strands that are partially complementary to **D1**, the sensor–strand is released from the PNA strand **P1**, leading to increased fluorescence. b) Schematic depiction of the FRET-assisted antisense detection system based on TO-labelled PNA **P3**. Hybridization with F and Q labelled DNA sensor strand **D1**, the dyes Cy5 and TO both are in close proximity of the quencher, leading to reduced fluorescence of TO, which results in poor FRET and concomitant emission from Cy5. Fluorescence of both TO and Cy5 is restored after replacement of the PNA **P3** with a fully complementary target strand **D2**. c) Schematic representation of hybridization between TO–PNA (**P3**) and matched/mismatched DNA, showing the single nucleotide polymorphism (SNP) detection approach in which the TO label senses the match/mismatch pair of its neighboring base.

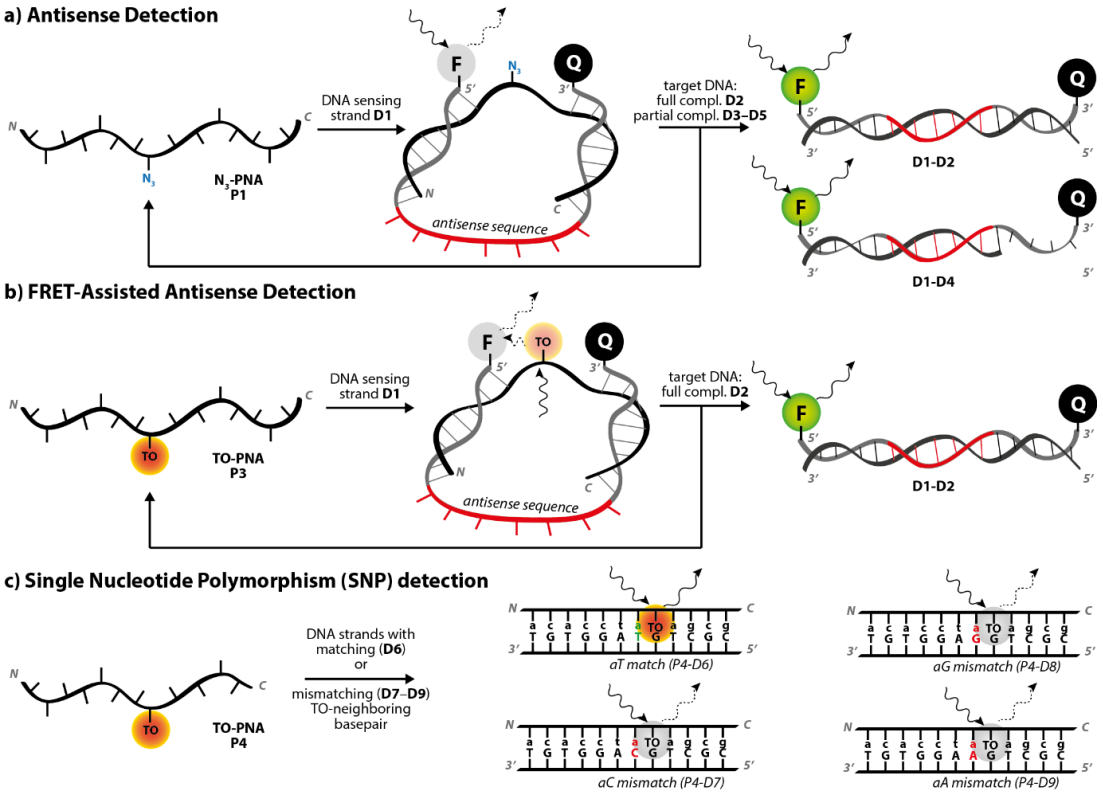

which the labeled termini of the DNA bind to the middle section of the PNA sequence, close to the azido group; an internal stretch of ssDNA would provide

the sensing sequence located on the opposite side of the circle with respect to the azido group (see Scheme 2a). Specifically, the overall design provides significant binding to two 7 bp–long termini of **P1** while providing a ssDNA docking site of 7 bp for an incoming oligonucleotide that would be complementary to **D1**. In this configuration, the fluorophore and quencher are in close proximity, which facilitates quenching of Cy5 by Iowa Black quencher.

In the presence of a DNA trigger, the F/Q–labelled DNA strand should be released from the DNA–PNA heterodimer via a competitive hybridization stimulus, resulting in the formation of a rigid dsDNA and a concomitant separation of Cy5 from Iowa Black quencher, leading to an increase in the fluorescent signal emanating from **D1**. Since the DNA–bound FRET–pair is now located next to the azido group, we created the possibility of introducing an additional FRET event, *i.e.* between a dye that was clicked to the azido group and a DNA–bound fluorophore, quencher, or both (Scheme 2b). That same design would also facilitate direct detection of single-nucleotide polymorphisms (Scheme 2c), or the azido group could function as a handle for further derivatization, *e.g.* with a bioactive moiety.

The sensing ability of the DNA–PNA duplex was tested using an antisense sequence targeting normal luciferase mRNA 5´–TTCTTTATGTTTTTGGCGTCT–3´, which was included in DNA strand **D1** (Figure 2). The sequence targeting luciferase mRNA was chosen to be applied in CPP–PNA delivery vectors.[9a] Mixing **D1** and **P1** indeed resulted in a 6–fold decrease in fluorescence intensity at 667 nm when compared to D1 alone (Figure 2a). Upon addition of **D2**, which is fully complementary to **D1**, a significant increase in fluorescence was observed. In fact, when compared to **D1** alone, a 2–fold increase in fluorescence was observed at λ_{em} = 667 nm along with a shift of λ_{em} to a higher wavelength (λ = 695 nm).

PNA

P1: Ac-Lys-taaagaaN_3agacgcc-Lys-NH_2

P3: Ac-Lys-taaagaaTOagacgcc-Lys-NH_2

P4: Ac-acacctaTOagcg-Gly-NH_2

DNA

D1: 5′-Cy5-TTCTTTATGTTTTTGGCGTCT-3IAbRQSp-3′

D2: 5′-AGACGCCAAAAACATAAAGAA-3′

D3: 5′-AGACGCCAAAAACA-3′

D4: 5′-AAAAACATAAAGAA-3′

D5: 5′-CGCCAAAAACATAAA-3′

D(6-9): 5′-CGCTGXAGGTGT-3′

X= T, C, G, A

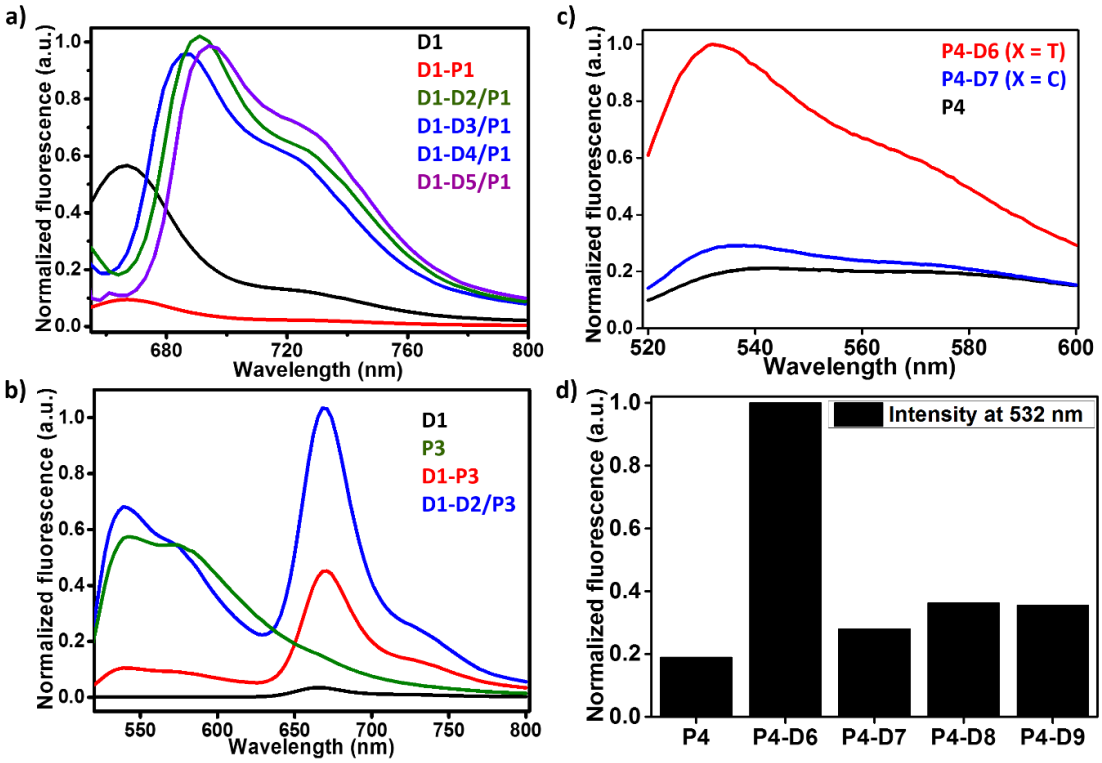

Figure 2. a) Normalized fluorescence spectra showing the binding of antisense DNA **D1** to PNA **P1** followed by release upon addition of competitive DNA strands (**D2**–**D5**), Measurement conditions: 1 µM PNA and DNA in 10 mM NaH_2PO_4, 100 mM NaCl buffer at pH = 7.0, 25 °C, λ_{ex} = 650 nm. Note: **D3** and **D4** provide indistinguishable fluorescence increase upon addition to a **P1**–**D1** hybrid (blue traces), b) Normalized fluorescence spectra showing the binding of antisense DNA **D1** to TO–labeled PNA **P3**, showing FRET observed between Cy5 and TO, λ_{ex} = 510 nm, c) Normalized fluorescence spectra of PNA **P4** before and after addition of matched (**D6**) and mismatched (**D7**) DNA and d) Normalized fluorescence showing the SNP-dependent decrease in fluorescence at 532 nm of **P4**. Measurement conditions: 1 µM PNA and DNA in 10 mM NaH_2PO_4, 100 mM NaCl buffer at pH = 7.0, 25 °C, λ_{ex} = 510 nm.

Comparing the intensity of the **D1**–**P1** duplex at 667 nm with that of the **D1**–**D2** duplex at 695 nm displays a 10–fold increase in fluorescence as result of the

sensing event. Interestingly, at 695 nm the difference in intensities was even higher (25-fold). Although not fully understood at the moment, we attribute the 28 nm redshift and increase in intensity to the change in microenvironment that occurred when the cyanine dye Cy5 moved from the PNA–DNA duplex (**P1**–**D1**) to the more polar microenvironment of dsDNA (**D1**–**D2**).

We observed a difference of 10 °C in T_M value (ΔT_M) between the two complexes (see Appendix 4, Figure S7), *i.e.* D1–P1 and D1–D2. The higher T_M for D1–D2 when compared to **D1**–**P1** shows that the former duplex was more tightly associated than the latter hybrid duplex. Although PNA–DNA duplexes usually have a higher T_M than DNA–DNA duplexes that have the same sequences, the lower T_M of the **D1**–**P1** duplex can be explained by (i) the circular design of **D1**–**P1**, and (ii) the presence of more base–pairs in **D1**–**D2** when compared to **D1**–**P1**. The redshift and increase in fluorescence was also observed after the addition of strands that are partially complementary to **D1**, *i.e.* 14–15 bp-long sequences **D3**–**D5** (Figure 2), to the **P1**–**D1** mixture (Figure 2c). Also these shorter strands compete successfully with the PNA for binding to **D1**. For all these cases we thus have two readout signals that can be used to detect the strand–displacement event, namely the increase in fluorescence intensity at 695 nm, and the notable redshift of the λ_{em} band from 667 to 695 nm.

Realizing that it would be beneficial to have the ability to directly monitor the association and dissociation of labeled DNA to the PNA, we attached TO (**1**) to the resin–bound PNA (**P2**), resulting in TO–PNA (**P3**), in order to measure FRET between TO and Cy5 (Scheme 2b). Indeed, although the fluorescence intensity for TO in the **P3**–**D1** duplex was much lower than in the single-stranded **P3**, a clear FRET from TO to Cy5 was observed (Figure 2b, red trace). Upon addition of fully complementary **D2**, the fluorescence intensity for both TO and Cy5 increased multiple times (Figure 2b, blue trace), signaling displacement of DNA strand **D1** from the TO–labeled PNA strand **P3**. As the displacement of P3 from **D1** by **D2** leads to the hydrophobic ssPNA **P3**, we tentatively attribute the

increase in Cy5 fluorescence to aggregation of the hydrophobic PNA **P3** to the Cy5 dye, which is also hydrophobic. AFM analysis of the **P3**–**D1** duplex revealed dotted structures (see Appendix 4, Figure S8), indicating formation of the expected circular DNA–PNA hybrid structures, and ruling out a considerable contribution from linear structures to the observed FRET signal in **P3**–**D1**. Since PNA–oligonucleotide hybrids usually offer higher stability towards enzymatic degradation,[7] this allows utilization of our PNA–DNA/RNA complexes for cellular delivery based on our conjugation strategy.

Lastly, we studied the performance of a TO–labeled PNA, **P4**, in single-nucleotide polymorphism (SNP) detection.[10] We envisioned that our novel triazole–linked TO–PNA conjugate could, in principle, also be used for mismatch detection (Scheme 2c). We chose a reported DNA sequence **D6** (X = T) for which upto 3-fold match/mismatch discrimination using FIT– PNA at 25 °C was reported.[19] Upon hybridization of PNA **P4** to complementary **D6** (X = T) we observed a 5–fold enhancement of fluorescence (Figure 2c). In comparison, changing the adjacent pyrimidine nucleobase into a mismatched pyrimidine (X = C, in **D7**) increased the fluorescence only 1.5 fold. Thus, we observed about 3.5–fold discrimination ability for the A–C match/mismatch pair, indicating good match/mismatch discrimination ability. Importantly, we observed a similar discriminating ability for other mismatches (X = G and A) as well, indicating the general applicability of our method.

CONCLUSIONS

In conclusion, we report a novel strategy for PNA functionalization that allows straightforward on–resin click modification. We demonstrate the applicability of the method by clicking TO at an internal position on the PNA. The modified PNA is then hybridized to a fluorescent DNA strand to form a circular complex, allowing direct and TO–assisted sensing of the target DNA strand. In addition, we explore the SNP detection ability of a triazole linked dye on a FIT–PNA and observed up

to 4–fold match vs mismatch discrimination. Since PNA–DNA hybrids generally show a higher stability towards exonuclease degradation, we believe that this work provides a platform for different cellular delivery applications. Specifically, research regarding the application of our antisense PNA–DNA hybrids in cell assays is planned.

REFERENCES

(1) Nielsen, P.; Egholm, M.; Berg, R.; Buchardt, O. *Science* **1991**, *254*, 1497.

(2) Perry-O'Keefe, H.; Yao, X.-W.; Coull, J. M.; Fuchs, M.; Egholm, M. *Proc. Natl. Acad. Sci. U.S.A* **1996**, *93*, 14670.

(3) Hanvey, J.; Peffer, N.; Bisi, J.; Thomson, S.; Cadilla, R.; Josey, J.; Ricca, D.; Hassman, C.; Bonham, M.; Au, K.; et, a. *Science* **1992**, *258*, 1481.

(4) Hövelmann, F.; Seitz, O. *Acc. Chem. Res.* **2016**, *49*, 714.

(5) Egholm, M.; Buchardt, O.; Nielsen, P. E.; Berg, R. H. *J. Am. Chem. Soc.* **1992**, *114*, 1895.

(6) Vilaivan, T. *Acc. Chem. Res.* **2015**, *48*, 1645.

(7) Demidov, V. V.; Potaman, V. N.; Frank-Kamenetskil, M. D.; Egholm, M.; Buchard, O.; Sönnichsen, S. H.; Nlelsen, P. E. *Biochem. Pharmacol.* **1994**, *48*, 1310.

(8) Hyrup, B.; Nielsen, P. E. *Bioorg. Med. Chem.* **1996**, *4*, 5.

(9) Nielsen, P. E.; Shiraishi, T. *Artificial DNA, PNA & XNA* **2011**, *2*, 90.

(10) Kohler, O.; Seitz, O. *Chem. Commun.* **2003**, 2938.

(11) Kohler, O.; Jarikote, D. V.; Seitz, O. *Chem. Commun.* **2004**, 2674.

(12) Socher, E.; Jarikote, D. V.; Knoll, A.; Röglin, L.; Burmeister, J.; Seitz, O. *Anal. Biochem.* **2008**, *375*, 318.

(13) Jarikote, D. V.; Köhler, O.; Socher, E.; Seitz, O. *Eur. J. Org. Chem.* **2005**, *2005*, 3187.

(14) Tang, W.; Becker, M. L. *Chem. Soc. Rev.* **2014**, *43*, 7013.

(15) Manicardi, A.; Accetta, A.; Tedeschi, T.; Sforza, S.; Marchelli, R.; Corradini, R. *Artificial DNA: PNA & XNA* **2012**, *3*, 53.

(16) Ditmangklo, B.; Boonlua, C.; Suparpprom, C.; Vilaivan, T. *Bioconjugate Chem.* **2013**, *24*, 614.

(17) Brik, A.; Alexandratos, J.; Lin, Y.-C.; Elder, J. H.; Olson, A. J.; Wlodawer, A.; Goodsell, D. S.; Wong, C.-H. *ChemBioChem* **2005**, *6*, 1167.

(18) Kolb, H. C.; Finn, M. G.; Sharpless, K. B. *Angew. Chem. Int. Ed.* **2001**, *40*, 2004.

(19) Köhler, O.; Jarikote, D. V.; Seitz, O. *ChemBioChem* **2005**, *6*, 69.

CHAPTER 6

Ultrathin covalently bound organic layers on mica: Formation of atomically flat bio–functionalizable surfaces

ABSTRACT

Mica is the substrate of choice for microscopic visualization of a wide variety of intricate nanostructures. Unfortunately, the lack of a facile strategy for its modification has prevented the on-mica assembly of nanostructures. Herein, we disclose a convenient catechol-based linker that enables various surface-bound metal-free click reactions, and an easy modification of mica with DNA nanostructures and a horseradish peroxidase mimicking hemin/G–quadruplex DNAzyme.

This Chapter has been published as:

"Ultrathin Covalently Bound Organic Layers on Mica: Formation of Atomically Flat Bio–functionalizable Surfaces". Digvijay Gahtory, Rickdeb Sen, Bauke Albada, Floris van Delft and Han Zuilhof. *Angewandte Chemie International Edition* **2017***, 56,* 3299.

INTRODUCTION

The atomically flat nature of mica has made it the substrate of choice for microscopic visualization of dimensional parameters of various pre–fabricated nanomaterials such as DNA origami[1] and protein conjugates,[2,3] among others. Mica is an hydrophilic aluminosilicate, which in saline solution is covered by a hydration layer with K^+ ions that are tightly bound to the anionic silicate. While widely used for atomic force microscopy (AFM) studies,[4] the surface modification and chemical functionalization of mica itself has received surprising little attention.[5]

Lately, catechol-based coatings including mussel adhesive poly-dopamine proteins have found increasing attention for mica surface modification.[6] Despite a general acceptance that the catechol moiety in mussel proteins is central to their adhesion ability,[7] its exact adhesion mechanism is still unknown.[8] Butler *et al*. recently showed that a pending amine functionality is central to binding.[9] To demonstrate this, a symmetric trichrysobactin was synthesized that bears three 2,3-dihydroxybenzoyl moieties and a lysine tail. In this 'two-punch' approach, the NH_3^+ moiety displaced the K^+ ions, followed by surface attachment of the catechol–moiety. Unfortunately, the six-step synthesis required for the scaffold hampers its widespread application. Even more, post-attachment functionalization of mica substrates with interesting biomolecules such as DNA and proteins is still uncharted domain. Such an approach would require both facile and strong adhesion, combined with the presence of a moiety that can be routinely used for post–attachment functionalization. The current approaches[7,8] do not provide such a handle, and as such there is still need for a platform that allows various surface-modification strategies and a stepwise observation of the assembly processes of biological nanostructures in a controlled fashion.[10]

In this paper, we address this unresolved problem through a dual approach via the development of a simple molecule that allows both (i) covalent modification

of mica, and (ii) post–modification stepwise growth and study of molecular assemblies. To this end, we envisaged and synthesized a surface anchor (1) that possesses the structural characteristics required to combine optimal adhesion characteristics with a handle for modular functionalization (Figure 1). We extensively characterized the modified surfaces (**M_1**) by static water contact angle (SCA), X-ray photoelectron spectroscopy (XPS) and AFM measurements. To illustrate the potential for surface functionalization, we explored several metal–free strain–promoted click reactions. Finally, to demonstrate bio–functionalization we pursued the stepwise formation of functional DNA constructs, such as G–quadruplex (GQ, G = guanine) structures on covalently modified surfaces by AFM.

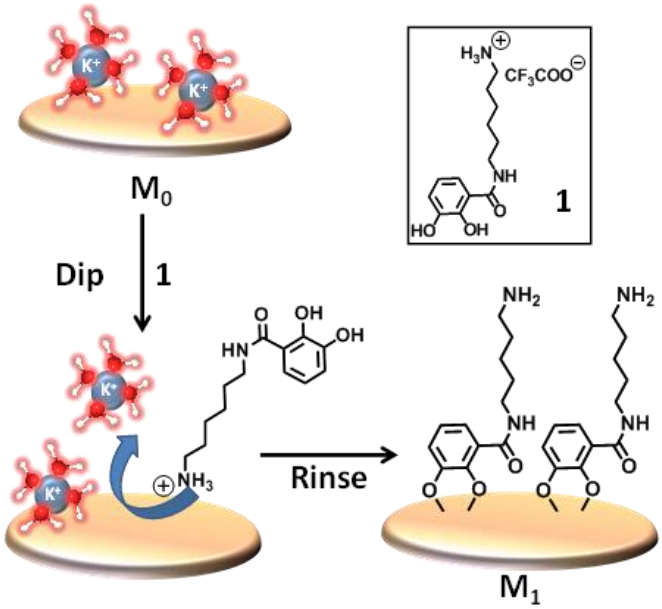

Figure 1. Tentative mechanism of mica modification by surface anchor **1**.

RESULTS AND DISCUSSION

Design and synthesis of surface anchor. As shown by Butler *et al.*[9] and Hwang *et al.*,[11] mica adhesive molecules should likely contain both catechol and amino groups. However, in their case this resulted in a poorly defined polymeric layer possibly due to intramolecular Michael–type addition reactions between the catechol and free amino groups.[12] Spencer *et al*. have tackled this issue of

polymerization by inclusion of a strongly electron-withdrawing nitro group in the catechol motif to minimize auto–oxidation.[13] Using this information, the design of our surface anchor **1** was based on the retention of the key components viz. a catechol moiety linked proximally via an electron–withdrawing amide group to a protonated amine (Figure 1). A first step forward was the synthesis of surface anchor **1**: 2,3–dihydroxybenzoic acid (DHBA) and mono–Boc–protected 1,6–hexanediamine were linked via a conventional amide coupling, followed by subsequent Boc-deprotection (Figure 2a) to afford **1** in an overall yield of 66 % (0.78 g).

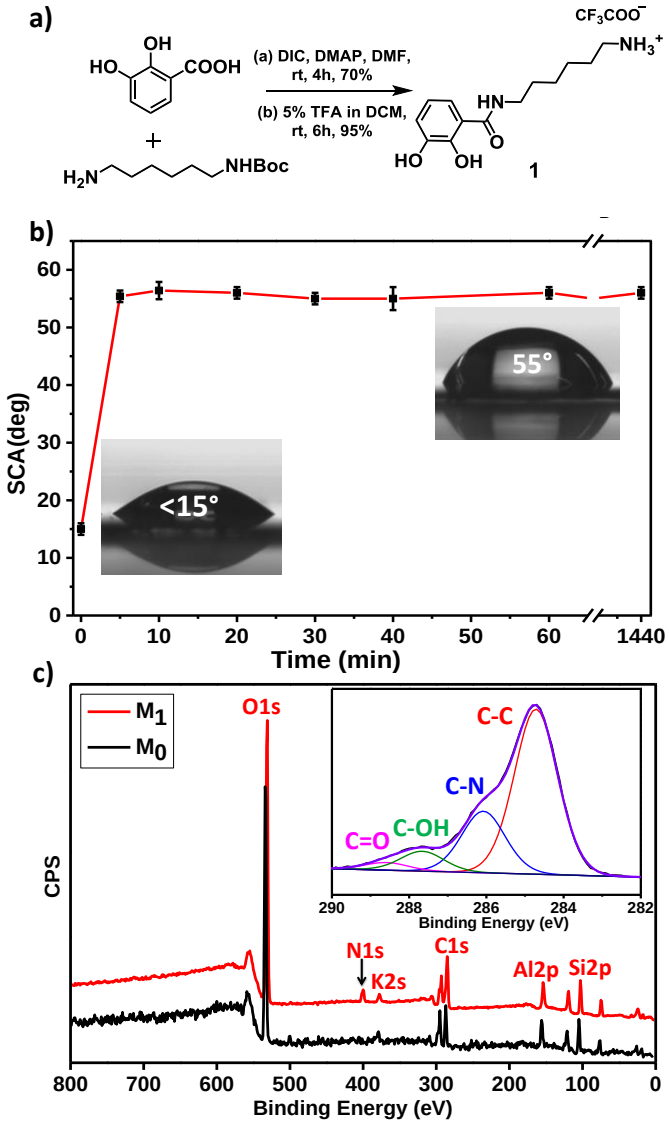

Figure 2. a) Synthesis of surface anchor **1** b) Increase of water SCA during modification process. c) XPS wide range spectra of bare ($\mathbf{M_0}$) and modified ($\mathbf{M_1}$) mica (inset: narrow scan of C1s signal).

Surface modification and characterization. A 1 mM solution of **1** in PBS buffer (pH 7.4) allowed for the simultaneous modification of large numbers of freshly cleaved mica surfaces in 24 h. A constant low water contact angle (55°) (Figure 2b), the emergence of N1s signal in XPS (Figure 2c), and the XPS analysis of subsequent modifications on **M_1** confirmed modification of the mica surfaces with surface anchor **1** (see Appendix 5). Importantly, molecules similar to surface anchor **1**, but lacking one of the mentioned components, performed inferior than anchor molecule **1** (Table S1). XPS analysis of modified surfaces also showed the overall chemical composition of M_1 to fit the molecular composition of 1 within experimental error (C/N_{XPS} = 6.8; C/N_{Theor} = 6.5) (see Appendix 5, section S4.2). As shown by Hwang *et al*., the formation of polymeric layers on mica surfaces leads to the disappearance of the Al2p, K2s and Si2p signals in the XPS spectrum.[11] Interestingly in our case, the continued high intensity of these substrate–specific signals hinted at formation of ultrathin layers (Figure 2c).

The deconvolution of the C1s narrow scan clearly revealed carbons in distinct environments, namely, C-C, C–N, C-O and C=O (Figure 2c, inset). Experimental XPS binding energy results correlated nicely with simulated values obtained from DFT calculations (Section 6.1).[14] AFM analysis of modified surfaces (M_1) displayed a remarkably low surface roughness of 0.4 nm with a layer thickness of (2.5 ± 0.5) nm (Appendix 5, Figure S1–S3). This confirms exclusive formation of ultrathin layers (length of 1 in stretched–out fashion is ca. 1.3 nm) on mica surfaces. We note that the low (0.4 nm) roughness makes our modified surfaces amenable for reliable microscopic visualization of various covalently attached nanostructured biomolecules.

Metal free click reactions on mica surface. In view of the importance of metal-free click chemistry in bio-conjugation chemistry, we performed various state-of-the-art “metal-free” strain–promoted click reactions (Figure 3). For this, amine–terminated layers M_1 were converted to azide- functionalized coatings **M_2** (see Appendix 5) by a Cu–catalyzed azide transfer reaction.[15] The resulting azide–

terminated layers underwent a facile SPAAC reaction with a fluorinated labile BCN aromatic ester. This

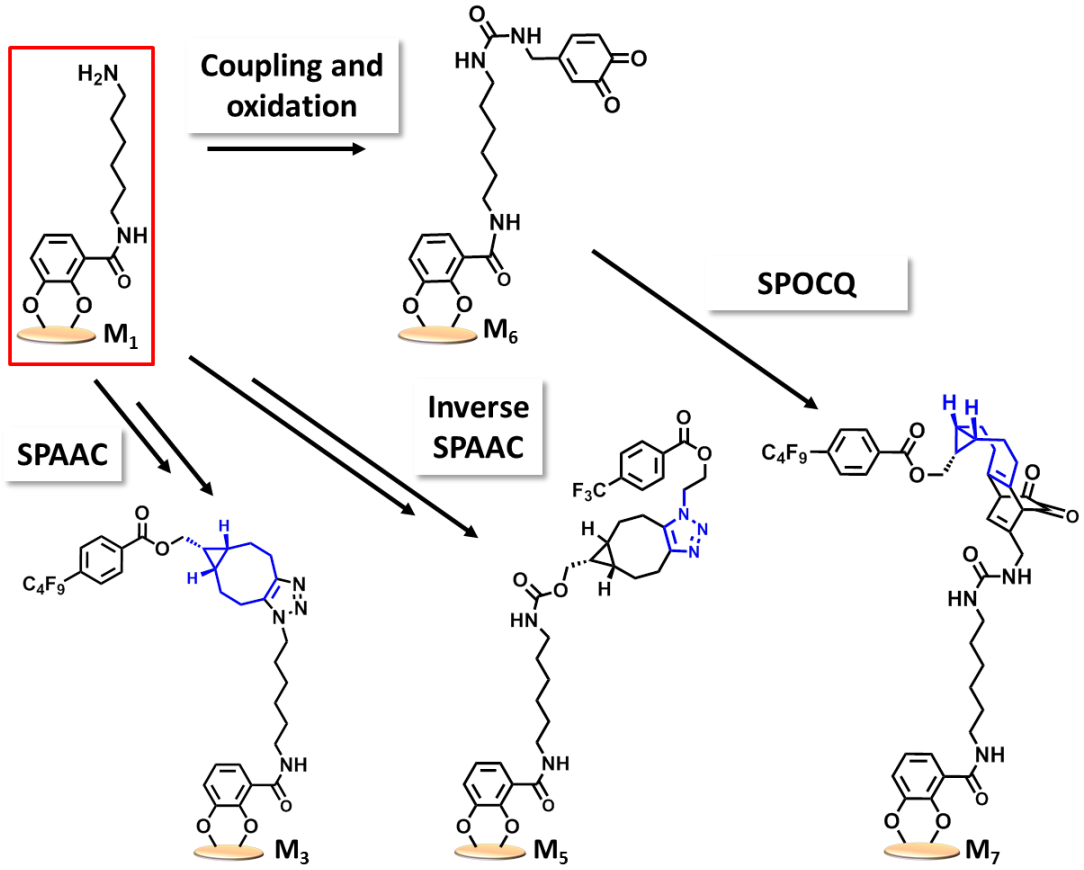

Figure 3. Functionalized mica as building block: General scheme showing the cycloaddition adducts of various metal–free click reactions on **M1**.

allowed easy characterization of the resulting surfaces **M2** by XPS and direct analysis in real time high–resolution mass spectrometry (DART–HRMS),[16] which showed the characteristic *m/z* peak of the surficial 4–perfluorinated butyl benzoate anion (339.0062) in the extracted ion chronogram (EIC; Appendix 5, Figure S4). A clear XPS F1s signal was evident at 686.0 eV, indicating a successful reaction (50 %) (Figure 4a). An inverse strategy for the surface-bound SPAAC reaction was also pursued with BCN immobilized on the surface (**M4**) and a reaction with an azide coupled to a fluorinated tail (Figure 3), to yield surface **M5**. The XPS F1s peak at 686.0 eV was used to demonstrate the extent of

reaction (83 %) (Figure 4a and Section S4.10), while also the C1s and N1s spectra confirm the success of this reaction (Figure 4b).

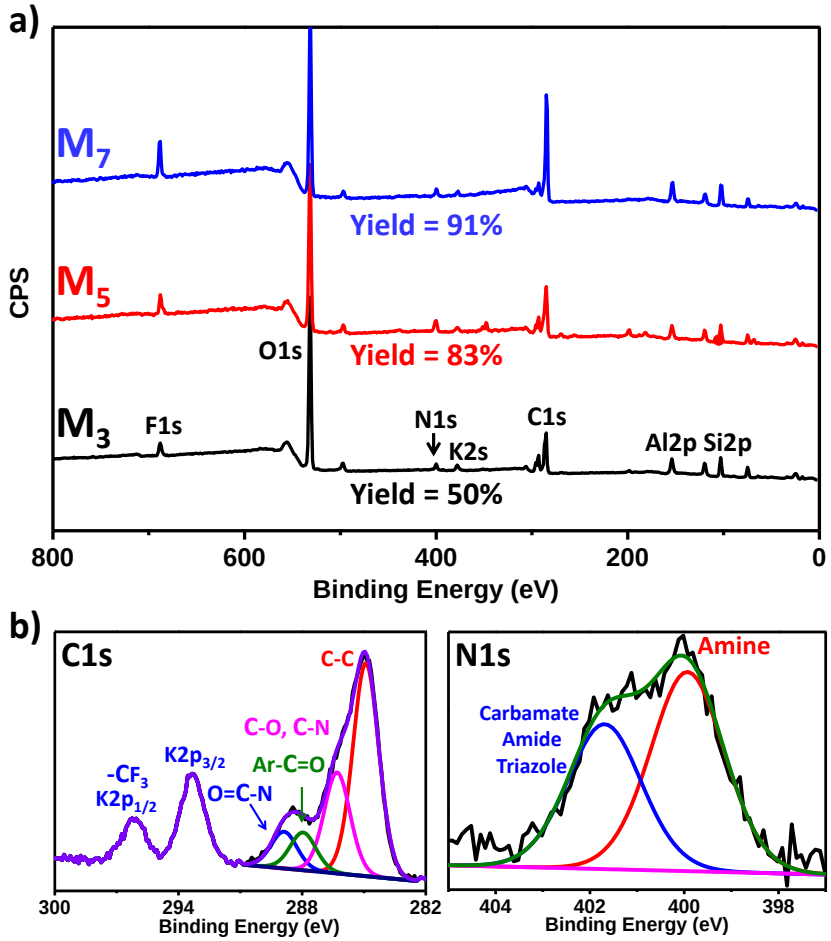

Figure 4. a) Stacked XPS wide scans of final cycloaddition adducts of SPAAC with azide on surface (**M3**; bottom), BCN on surface (**M5**; middle) and SPOCQ (**M7**; top). The F1s and N1s peaks were used for determining the yield of these reactions. b) XPS narrow scan C1s region (left) and N1s region (right) of SPAAC cycloaddition adducts (**M5**)

The strain-promoted click reaction between BCN and *ortho*–quinones (SPOCQ)[17] was investigated as a second example on mica surfaces modified by our method. To this end, 2,3-dihydroxybenzyl amine was attached to surface **M1** via a DIC coupling, and subsequently oxidized to its corresponding 1,2–quinone (**M6**) using $NaIO_4$. XPS analysis confirmed the presence of a modified anchor on mica (Section S4.13). The quinone underwent a facile SPOCQ reaction producing in excellent yield (91 %) surface **M7** in 4 h, *e.g.* as evidenced by the F/N ratio in XPS (Figure 4a and Section S4.14).

DNA mini–constructs on mica surface. Having established prominent bio-conjugation reactions on mica, we switched our attention to our other objective: the formation of AFM–observable covalently linked DNA nanostructures. Building on the insights from Famulok *et al.*, a 168–bp DNA minicircle consisting of 8 distinct DNA fragments[30] was assembled in a step–wise fashion after one of the components was tethered covalently onto mica surface **M_1**. Covalent attachment of strand **D1** (Table S2) allowed its hybridization to a preformed assembly of oligomers **D2**–**D8** (Table S2), forming circular structures. As shown in Figure 5a, 3D height images of DNA-containing surfaces revealed circular structures that possess an internal cavity (Appendix 5, Figure S8–S11). A large number of contiguous shapes with circular features was obtained, with an internal diameter of 20 ± 2 nm (Appendix 5, Figure S12), in accordance with literature (18.2 nm).[18] When significantly lower concentrations of strands **D2**–**D8** were applied (100–fold dilution, *i.e.* 0.1 μM), we observed mostly open structures, and circles of which the larger internal diameter hinted to the formation of semi-closed dimeric and trimeric structures (Figures 5b, 5c, Appendix 5, S13 and S14). Control experiments with bare mica surfaces, *i.e.* without the anchored DNA, did not show

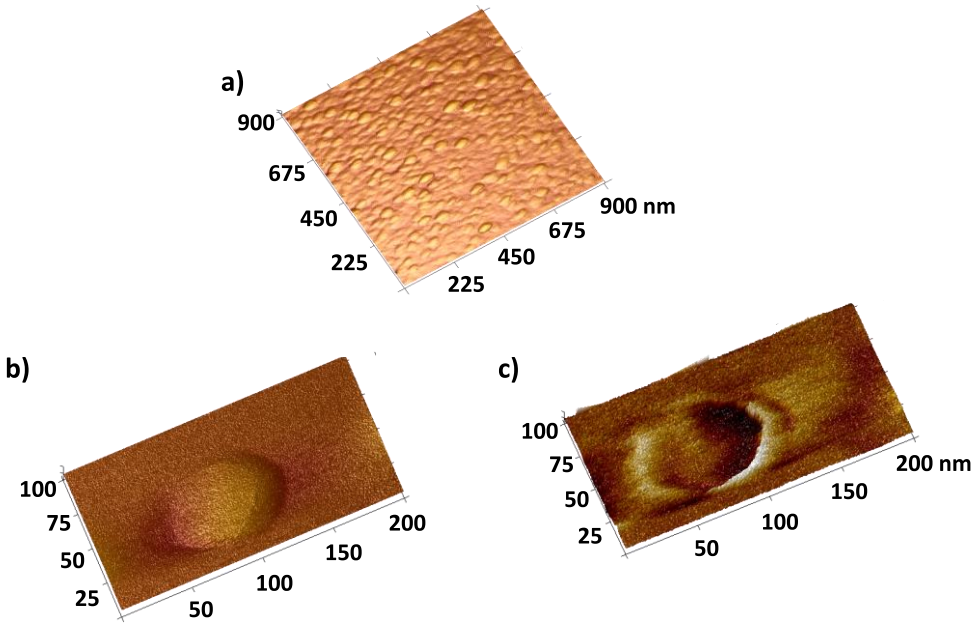

Figure 5. a) 3D height images of DNA circles assembled on mica. b) 3D height and c) quadrature image of single DNA circle.

any circles or other (linear) structures, proving the need for a covalently attached anchor.

DNAzyme activity on mica surface. Lastly, we added another dimension to our method by the attachment of functional DNA, namely the horseradish peroxidase-mimicking hemin/G-quadruplex (hGQ) DNAzyme.[19] Such a hGQ DNAzyme can oxidize a variety of organic substrates in the presence of H_2O_2.[20] To demonstrate the feasibility of hGQ catalytic activity of DNAzymes on mica surfaces, we attached the

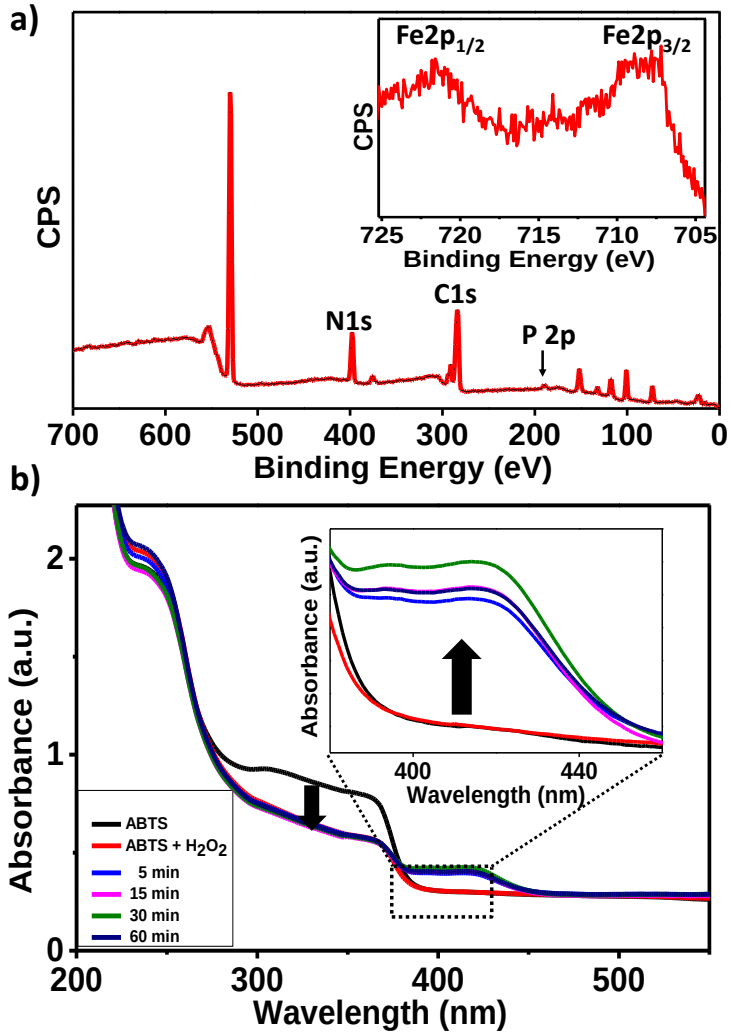

Figure 6. a) Wide scan XPS spectra of EAD2 immobilized on mica surface, (inset: Fe2p narrow spectra of the EAD2–based hGQ DNAzyme–functionalized mica). b) UV-vis spectrum of ABTS oxidation catalyzed by EAD2–hemin DNAzyme, inset: changes in the spectrum upon ABTS oxidation.

guanine-rich sequence EAD2 (Table S2) covalently to **M_1** mica surfaces. Covalent attachment of DNA was confirmed with XPS analysis by the emergence of P2s and P2p signals in the XPS wide spectra at 189.0 eV and 133.0 eV, respectively (Figure 6a). Furthermore, complexation of hemin [Fe(III)–protoporphyrin IX chloride] to the formed GQ under K^+–rich conditions was confirmed by the emergence of characteristic XPS Fe2p peaks[20] (710.0 and 721.0 eV) (Figure 6a, inset).

After validation of the covalent attachment of DNA, we assessed its HRP–mimicking ability using 2,2'–azino–bis(3–ethylbenzothiazoline–6–sulfonate) ($ABTS^{2-}$), which is converted into $ABTS^{\bullet-}$ in the presence of the hGQ DNAzyme and H_2O_2.[21] Indeed, upon addition of H_2O_2 to an ABTS-solution that contained just a single hGQ–functionalized mica slide (12 mm diameter), within 5 min a green-colored solution with λ_{max} = 414 nm (Figure 6b) was formed. Control experiments (without ABTS, without modified mica, or without H_2O_2) did not show formation of this oxidation product. Therefore, the oxidation of $ABTS^{2-}$ was solely attributable to the presence of catalytically active hGQ DNAzyme EAD2 on the surface.

CONCLUSIONS

To summarize, we demonstrate facile and covalent modification of mica using a catechol-based surface anchor with an flexibly linked amino group. This yielded robustly bound, low-roughness and ultrathin layers that are amine-terminated. We demonstrate that this approach allows for a highly flexible surface modification, using a range of metal–free click reactions as points in case. In addition, we display the potential of our strategy for microscopic imaging of functional DNA constructs, and the potential for following the formation of such constructs in a stepwise fashion. We thus believe our work opens up new avenues for the immobilization and successive visualization of a wide variety of biomolecule conjugates on mica and related surfaces.

REFERENCES

(1) Rothemund, P. W. K. *Nature* **2006**, *440*, 297.

(2) Vongchan, P.; Wutti-In, Y.; Sajomsang, W.; Gonil, P.; Kothan, S.; Linhardt, R. J. *Carbohydr. Polym.* **2011**, *85*, 215.

(3) Rusling, J. F.; Kumar, C. V.; Gutkind, J. S.; Patel, V. *Analyst* **2010**, *135*, 2496.

(4) Schönherr, H. *ACS Nano* **2015**, *9*, 12.

(5) Lego, B.; François, M.; Skene, W. G.; Giasson, S. *Langmuir* **2009**, *25*, 5313.

(6) Li, Y.; Qin, M.; Li, Y.; Cao, Y.; Wang, W. *Langmuir* **2014**, *30*, 4358.

(7) Kang, T.; Oh, D. X.; Heo, J.; Lee, H.-K.; Choy, S.; Hawker, C. J.; Hwang, D. S. *ACS Appl. Mater. Interfaces* **2015**, *7*, 24656.

(8) Brubaker, C. E.; Messersmith, P. B. *Langmuir* **2012**, *28*, 2200.

(9) Maier, G. P.; Rapp, M. V.; Waite, J. H.; Israelachvili, J. N.; Butler, A. *Science* **2015**, *349*, 628.

(10) Dunn, K. E.; Dannenberg, F.; Ouldridge, T. E.; Kwiatkowska, M.; Turberfield, A. J.; Bath, J. *Nature* **2015**, *525*, 82.

(11) Lim, C.; Huang, J.; Kim, S.; Lee, H.; Zeng, H.; Hwang, D. S. *Angew. Chem. Int. Ed.* **2016**, *55*, 3342.

(12) Hong, S.; Kim, J.; Na, Y. S.; Park, J.; Kim, S.; Singha, K.; Im, G.-I.; Han, D.-K.; Kim, W. J.; Lee, H. *Angew. Chem. Int. Ed.* **2013**, *52*, 9187.

(13) Rodenstein, M.; Zürcher, S.; Tosatti, S. G. P.; Spencer, N. D. *Langmuir* **2010**, *26*, 16211.

(14) Giesbers, M.; Marcelis, A. T. M.; Zuilhof, H. *Langmuir* **2013**, *29*, 4782.

(15) Goddard-Borger, E. D.; Stick, R. V. *Org. Lett.* **2007**, *9*, 3797.

(16) Sen, R.; Escorihuela, J.; Smulders, M. M. J.; Zuilhof, H. *Langmuir* **2016**, *32*, 3412.

(17) Borrmann, A.; Fatunsin, O.; Dommerholt, J.; Jonker, A. M.; Löwik, D. W. P. M.; van Hest, J. C. M.; van Delft, F. L. *Bioconjugate Chem.* **2015**, *26*, 257.

(18) Rasched, G.; Ackermann, D.; Schmidt, T. L.; Broekmann, P.; Heckel, A.; Famulok, M. *Angew. Chem. Int. Ed.* **2008**, *47*, 967.

(19) Li, Y.; Sen, D. *Nat. Struct. Biol.* **1996**, *3*, 743.

(20) Carvalho, R. R.; Pujari, S. P.; Gahtory, D.; Vrouwe, E. X.; Albada, B.; Zuilhof, H. *Langmuir* **2017**.

(21) Travascio, P.; Li, Y.; Sen, D. *Chem. Biol.* **1998**, *5*, 505.

CHAPTER 7

Approach matters: The kinetics of interfacial inverse–electron demand Diels–Alder reactions

ABSTRACT

Rapid and quantitative click functionalization of surfaces remains an interesting challenge. In this regard, inverse electron demand Diels Alder (IEDDA) reactions represent a promising candidate. Herein, we reveal quantitative surfaces functionalization within 15 min. Furthermore, we report the comprehensive effects of substrate stereochemistry, surrounding microenvironment and substrate order on the reaction kinetics as obtained via surface–bound mass spectrometry (DART–MS).

This Chapter has been published as:

"Approach Matters: The Kinetics of Interfacial Inverse–Electron Demand Diels–Alder Reactions". Digvijay Gahtory, Rickdeb Sen, Jorge Escorihuela, Judith Firet, Sidharam P. Pujari and Han Zuilhof *Chemistry- A European Journal* **2017***, 23,* 13015.

INTRODUCTION

The excellent kinetics, high yields, lack of by–products and high stereoselectivity of click reactions have led to their extensive use in total synthesis,[1] and biorthogonal[2] and site–specific[3,4] labelling of biomolecules. The utility of these reactions for surface modification has blossomed in recent times as evident from a significant number of reports,[5] specifically their use in biomolecular attachment and patterning.[6] Crucial for surface modification are the rate of reactions (for effective implementation) and complete conversion of the surface–bound moiety to the product of interest. The latter aspect is of importance, as surface–bound moieties cannot be removed afterwards by the standard purifications techniques so central to solution–phase chemistry (column chromatography, HPLC, etc.).

In this regard, the inverse electron demand Diels–Alder reaction (IEDDA) between 1,2,4,5–tetrazine and strained alkenes/alkynes holds great promise.[7] IEDDA reactions have been extensively studied in solution with particular focus on tuning the steric and electronic effects of a wide variety of dienes and dienophiles.[8] Such studies indicated highly interesting features such as very fast reaction kinetics[9] (among the highest for metal–free click reactions) and high chemoselectivity. Surprisingly, this facile reaction has been largely underexplored for surface functionalization with a few examples in literature using the highly reactive, but somewhat unstable *trans*–cyclooctene (TCO) reacting with tetrazine,[10] or a more stable but less reactive reactant such as norbornene reacting with tetrazines.[11,12] In studies of metal–free click reactions, a recurring but hitherto fully unresolved issue is the question whether it matters which component is better to be surface–bound or better to be in solution, i.e. in this case norbornene$_{(surf.)}$ + tetrazine$_{(soln.)}$ versus tetrazine$_{(surf.)}$ + norbornene$_{(soln.)}$. For example, for both interfacial strain promoted azide–alkyne cycloadditions[13] and surface–bound thiol–ene click reactions[14] the choice of the surface–bound reaction partner, i.e. overall reaction orientation is important but published results are inconclusive in this regard.

We have recently shown that the microenvironment around the reactive site on the surface plays an important role in the kinetics of strain–promoted click reactions, as determined by highly accurate and facile rate studies using direct analysis in real time–mass spectrometry (DART–MS).[15,16] Those studies allowed and stimulated us to investigate whether the microenvironment for the interfacial IEDDA using the more stable norbornene could be optimized to further improve the reaction rates, and possibly direct the yield of surface–bound IEDDA reactions towards 100%.

Scheme 1. a) Overall tetrazine–norbornene IEDDA reaction and b) schematic depicting the three parameters (in parentheses) under current study.

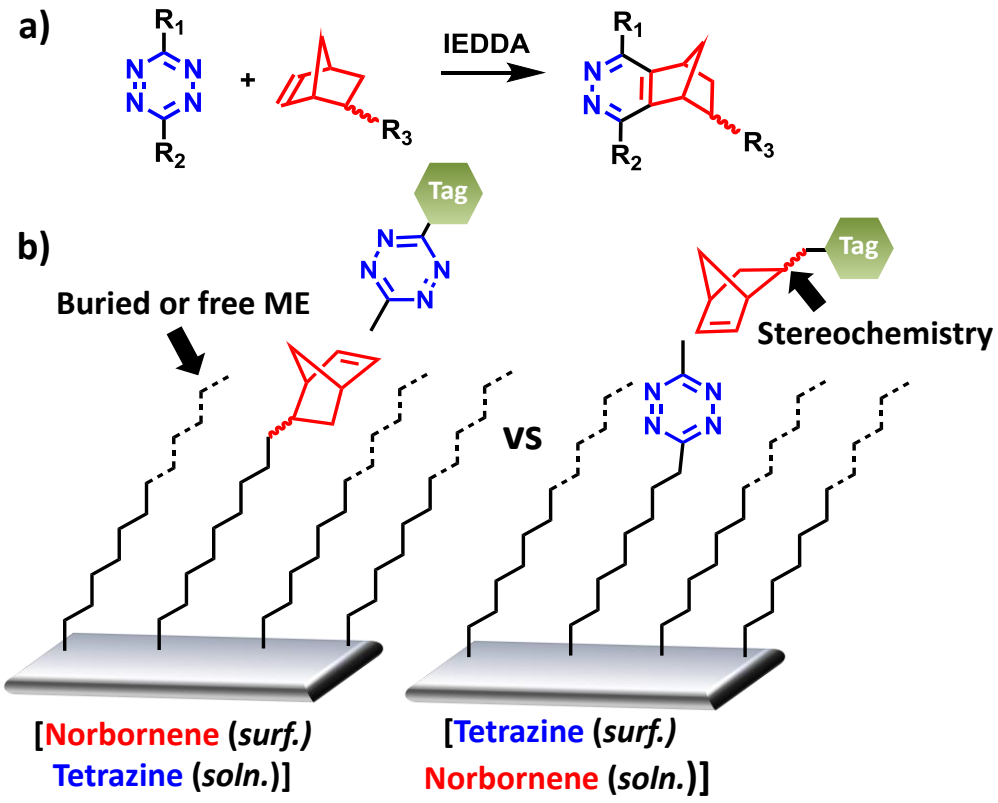

Given the high signal/noise (S/N) ratio of DART–MS, we are in this study for the first time able to systematically tune three aspects relevant for surface–bound organic conversions in detail (Scheme 1): surface–induced sterics (are the groups buried in a monolayer, or sticking out above it), stereochemistry (*endo*/*exo*–norbornene, as a means to investigate the effects of approach of the

reactant in solution) and orientation (which reactant is in the solvent and which one surface–bound).[17] Optimization of these factors yielded conditions in which the reaction is quantitative and finished within 15 min, showing the potential of both this approach and of this reaction.

RESULTS AND DISCUSSIONS

To this end, the surface of aluminum (Al) slides with its natural aluminum oxide coating were covalently modified by phosphonic acid–based monolayers by a well–established methodology.[18] For this study, we prepared 3:1 alkyl to amine–terminated monolayers (**M_1**; see Scheme 2), as previous studies indicated this to be the optimum between high density of functionalization and reactivity. The microenvironment of the reacting groups was tuned by modifying the lengths of the surrounding alkyl chains, so as to bury it in the monolayer (4 carbon atoms below the surface), or make it stick out (4 carbon atoms above the surface). The monolayer composition was confirmed by the N/P ratio (1:4) in XPS wide scans (see Appendix 6, Figure S5.1). In order to obtain a better understanding of surface coverage, a molecular mechanics study was performed that studied the average packing energy per chain in dependence of the packing density.[19] We found that ~50% coverage corresponded to the lowest packing energy per molecule (see Appendix 6, section 7.10 and 7.11). This means that ideally about half the surface sites available result in monolayer attachment.

Norbornene surfaces (**M_2**/**M_3**) were prepared by coupling 5–norbornene–2–methanol (*exo*–/*endo*–) to **M_1** surfaces by a carbamate linkage (Scheme 2 and Appendix 6, Figure S4.6, S5.2 and S5.3). For preparation of tetrazine surfaces (**M_4**), we chose an unsymmetrical tetrazine with benzyl amine and methyl substitution, again via a carbamate linkage to ensure the same freedom/buried nature as in **M_2**/**M_3**. As shown by groups of Hilderbrand and Chen, unsymmetrical tetrazines provide a better balance between stability and reactivity than their symmetric counterparts,[20] while also ensuring enough rigidity on a surface.

Scheme 2. General scheme for the surface modification followed by interfacial IEDDA reaction.

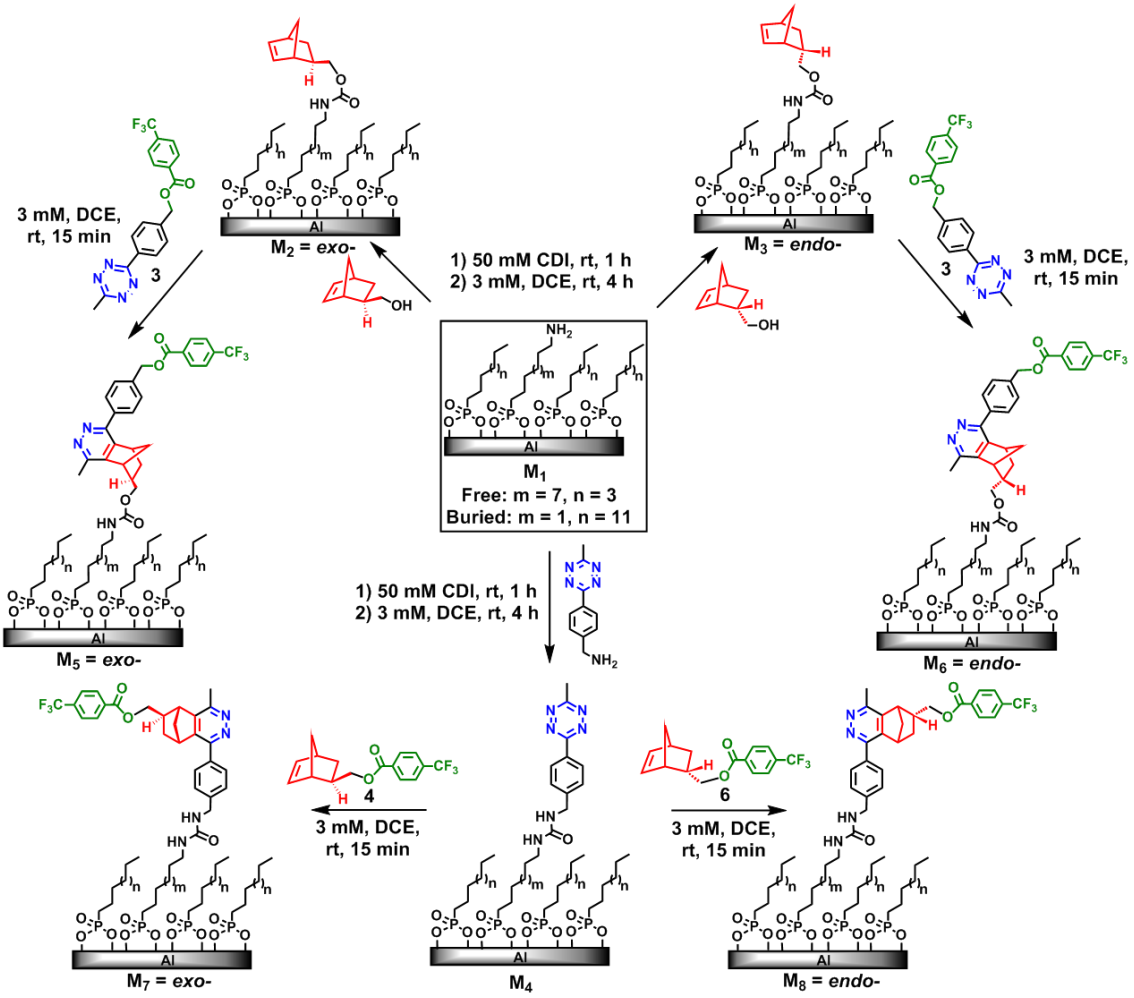

Complete surface attachment (96 ± 7 %) was obtained for this reaction as confirmed by N/P ratios (1.4 ± 0.1) in XPS analysis (Appendix 6, Figure S5.4). After confirmation of surface attachment of norbornenes and tetrazines, respectively, we embarked on exploring the IEDDA reaction. For easy analysis of the reaction progress, we synthesized fluorinated tags **3**, **4** and **6** (see Appendix 6, for synthetic details) that facilitate analysis by both XPS and DART–MS. The reactions were performed for both the reaction partners under stringently similar conditions (Scheme 2) and followed by monitoring the F/P ratio in XPS wide spectra (Figure 1). Interestingly, we found that for the "free" **M2**, **M3** and **M4** systems, a >90 % surface reaction yield was obtained within 15 min irrespective of the orientation of the reaction (Appendix 6, Figure S5.5 and S5.6). In case of the "buried" system, the crowded microenvironments around the reactive sites

slowed the reaction down, yielding a slightly lower reaction yield (~80 ± 10 %) after 15 min for "buried" exo–norbornene$_{(surf.)}$ + tetrazine$_{(soln.)}$ system (Appendix 6, Figure S5.10), but >90 % conversion was also observed for such systems after 1 h (Appendix 6, Figure S5.11).

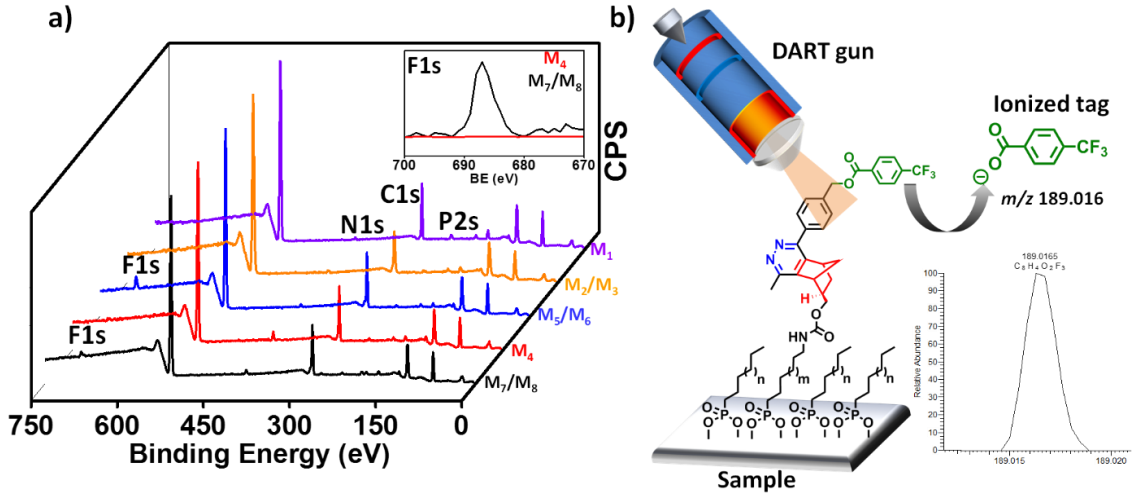

Figure 1. a) XPS wide range spectra for **M_1–M_8** surfaces showing emergence of F1s signal after the interfacial IEDDA reaction. b) Schematic impression of ionization of MS-tag (m/z 189.0163) by DART-HRMS.

To obtain accurate reaction kinetics, we reacted our samples for different time intervals (up to 20 min) and followed the signal intensity of the corresponding MS–tag (*m/z* 189.016) in DART–MS. Using such high S/N data, the first–order rate constant (k′) was calculated as the slope of the plot of $\ln|(I_t - I_\infty)/(I_0 - I_\infty)|$ versus time (t), where I_∞ corresponds to the asymptotic integrated extracted ion chronogram (EIC) intensity at obtained by exponential decay curve fitting of the data (Appendix 6, Figure S3.1–S3.8), the second-order rate constants were derived from there. The highest second-order reaction rate constant (3.62 $M^{-1}s^{-1}$ at a solute concentration of 3.0 mM, 30 °C, DCE) was observed for *exo*–norbornene$_{(surf.)}$ with tetrazine$_{(soln.)}$ **3** in a "free" microenvironment (Figure 2). Using the inverse situation, tetrazine on a surface surrounded by lower alkyl chains reacting with *exo*–norbornene **4** in solution, afforded a two–fold slower rate (Figure 2).

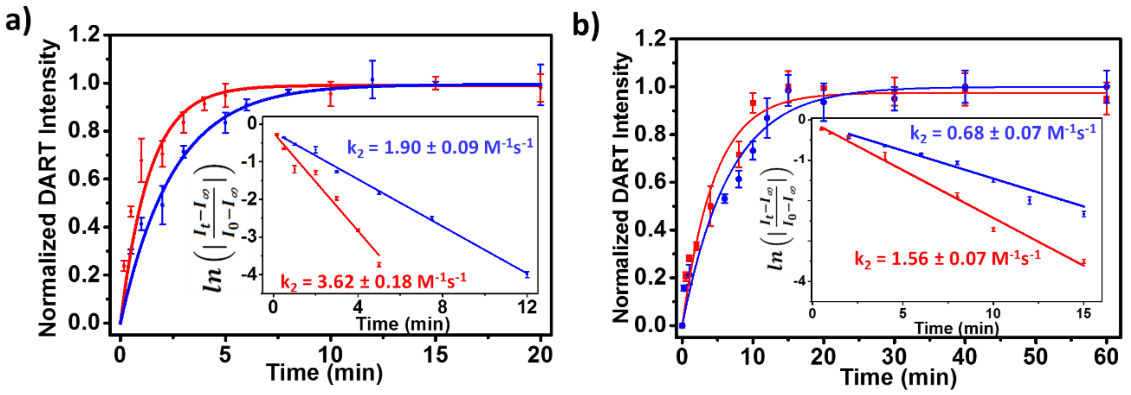

Figure 2. Normalized DART–HRMS intensity vs time (min) for IEDDA in a "free" microenvironment: a) *exo*–Norbornene surfaces (**M_2**) reacting with **3** (red) and tetrazine surfaces (**M_4**) reacting with **4** (blue). b) *endo*–Norbornene surfaces (**M_3**) reacting with **3** (red) and tetrazine surfaces (**M_4**) reacting with **6** (blue). Inserts: Linear plots of ln $[(I_\infty - I_t)/(I_\infty - I_0)]$ vs time (min) to obtain the pseudo-first order constants, and using solute concentrations of 3.0 mM the subsequently derived 2nd order rate constants (k_2).

The IEDDA reaction efficiency can be determined by comparing the atomic ratio determined by XPS with the theoretical value of 3:4 (for F/P), which corresponds to the 100% surface conversion. Interestingly, recently we reported the first 100%-yielding surface-bound metal-free click reaction (a strain–promoted cyclooctyne–quinone or SPOCQ reaction), which was further characterized by a second order rate constant (k′) of 3.3 $M^{-1}s^{-1}$.[15] While thus displaying virtually the same rate, in that case, we observed two distinct kinetic regimes: an initial fast regime followed by a slower, more complex one; the rate constant refers to the initial well–behaved kinetic regime only. The SPOCQ reaction was eventually also quantitative, but reaches full conversion only in 4 h. Here, the IEDDA reaction turned out to be a significant improvement, reaching an unprecedented complete conversion within 15 min, while the entire kinetic regime could be followed using one exponent, i.e. the IEDDA reaction displays clean kinetics.

In addition, excellent yields were obtained both in 'free' and 'buried' conditions, and independent of the orientation of the reaction, thereby showing the scope of this strategy for surface modifications. Changing the stereochemistry of the

immobilized norbornene to *endo*– in a "free" microenvironment halved the reaction rate (Figure S3.3) which is consistent with the rate differences observed in solution.[9] Interestingly, also in this case a kinetic preference (two–fold difference) was observed for immobilized norbornene reacting with tetrazine in solution than its reverse, i.e. tetrazine on the surface reacting with *endo*–norbornene **6** in solution (Table 1). This result outlines that the slowing down of reaction rate for tetrazine immobilization occurs irrespective of norbornene stereochemistry.

Table 1. Second-order rate constants k_2 ($M^{-1}s^{-1}$) of the tetrazine–norbornene IEDDA reaction in "free" and "buried" microenvironments.

Surface group		Reactant in solution	
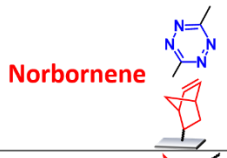 Norbornene		Tetrazine	
	Free	3.62 ± 0.18 $M^{-1}s^{-1}$ (*exo*-)	1.56 ± 0.07 $M^{-1}s^{-1}$ (*endo*-)
	Buried	0.87 ± 0.06 $M^{-1}s^{-1}$ (*exo*-)	0.57 ± 0.08 $M^{-1}s^{-1}$ (*endo*-)
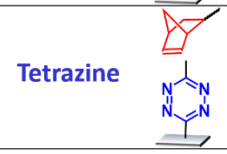 Tetrazine		Norbornene	
	Free	1.90 ± 0.09 $M^{-1}s^{-1}$ (*exo*-)	0.68 ± 0.07 $M^{-1}s^{-1}$ (*endo*-)
	Buried	0.58 ± 0.08 $M^{-1}s^{-1}$ (*exo*-)	0.61 ± 0.05 $M^{-1}s^{-1}$ (*endo*-)

Finally, we wanted to know the kinetic effects of doing the reaction 'above' the monolayer versus 'within' the monolayer. Therefore we studied the reaction in a "buried" state: surfaces were prepared with either norbornene or tetrazine moieties bound to the surface that are surrounded by long alkyl chains, and used for IEDDA reaction (Scheme 2). The rate differences again amounted to about two folds in favor of norbornene immobilization (Table 1). The highest reaction rate in this microenvironment (0.87 $M^{-1}s^{-1}$) was observed for *exo*–norbornene attached on the surface reacting with tetrazine while the lowest (0.58 $M^{-1}s^{-1}$) was observed for its reverse. Comparing the best and worst possibility, the rate constant for the *exo*–norbornene immobilization in "free" microenvironment was 6.2 fold higher than that for tetrazine immobilization in a "buried" state. It is of relevance to state that only with high S/N-techniques like DART–HRMS such relatively small rate differences can come into view and thus be rationalized.

To this latter aim, we also applied quantum chemical and molecular mechanics calculations. The reaction between unsubstituted[21] and substituted tetrazines[20] and various alkenes has been studied theoretically by Houk, Devaraj and co–workers. In our case, we modeled the IEDDA reaction between a substituted tetrazine and *exo*–/*endo*–norbornene (substituted so as to mimic their surface attachment or solution functionalities, see Figure 3). In line with previous findings, density functional theory (DFT) calculations (at M06-2X/6–311+G(d,p) level) revealed that the Diels−Alder cycloaddition, rather than the subsequent N_2 expulsion, is the rate–determining step in this reaction. In accordance with experimental results, *exo*–norbornene has a lower activation barrier than *endo*–norbornene (Figure 3a). Also, our calculations show that the reaction corresponding to norbornene$_{(surf.)}$ (*exo*– and *endo*–) and tetrazine$_{(soln.)}$ had a lower energy barrier (by ~1 kcal mol^{-1}) than the reverse orientation (Figure 3b and 3c). This energy difference is in line with the observed rate difference for the interfacial IEDDA in the "free" microenvironment.

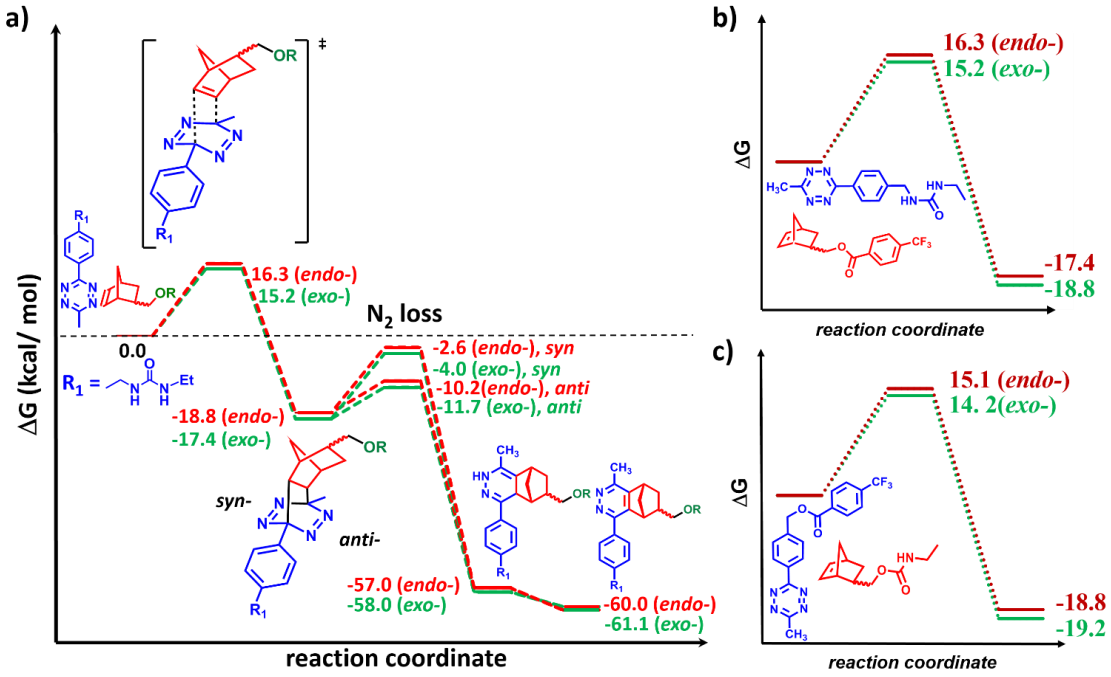

Figure 3. a) DFT calculation for the full mechanism of the multistep IEDDA reaction between an unsymmetrical tetrazine and *exo*– and *endo*–norbornene mimicking molecules used in our work, b) and c) reaction coordinate diagram for the IEDDA reaction mimicking our reaction condition showing tetrazine and *exo*–/*endo*–norbornene on surface, respectively.

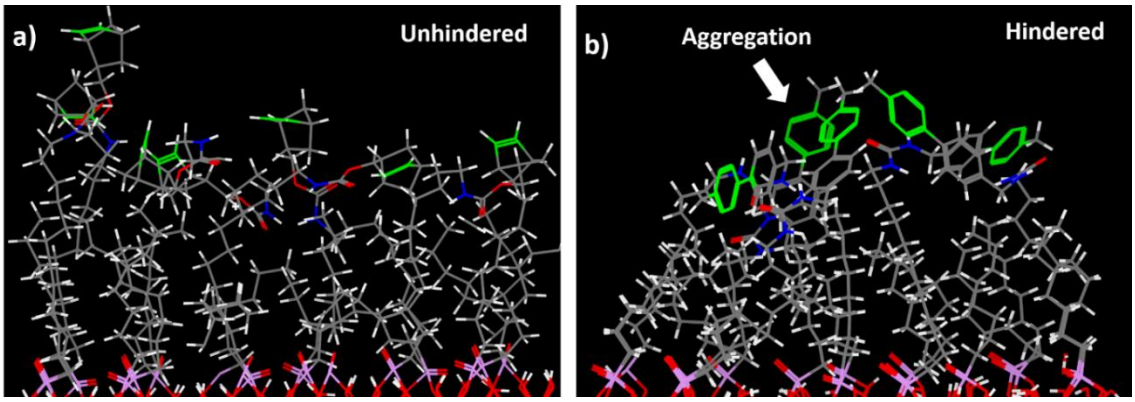

Figure 4. Comparison of surface disposition of IEDDA reactants in "free" ME after molecular dynamics of a) norbornene$_{(surf.)}$ and b) tetrazine$_{(surf.)}$.

A visual representation of the orientation of immobilized groups was obtained by performing sequential molecular dynamics and molecular mechanics optimizations of the IEDDA cycloadducts on aluminum oxide surface. The modelling was performed on large supercells obtained by attachment of the norbornene or tetrazine moieties in a random pattern followed by subsequent energy minimization (see section 7.13–7.14 in Appendix 6). Next, a series of molecular dynamics runs at 773.0 K were performed to 'shake up' the conformations of the chains, and get truly random orientations of the surface-bound moieties. Finally, those geometries were optimized by molecular mechanics, to indicate the most stable orientations of reactive groups with respect to the surface (see section 7.15–7.19 in Appendix 6). Representative geometries, from a much large set, are shown in Figure 4. For surface–bound norbornenes (Figure 4a), the surface-bound molecules prefer to be apart (no specific attractions; significant steric repulsions) with the double bond (highlighted in green) facing outwards. In contrast, tetrazines$_{(surf.)}$ in a "free" microenvironment showed a higher propensity to clump/cluster together due to additional stabilization attributable to π–π stacking (Figure 4b). These orientations and clustering (or lack thereof) will influence the reactivity and angle of approach of any reacting solute.

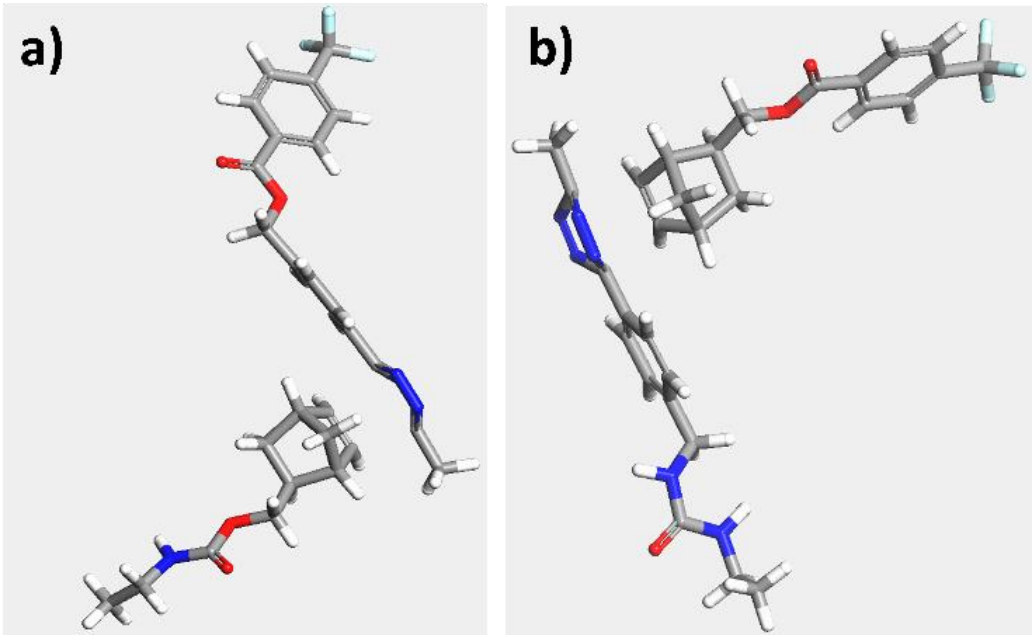

Figure 5. DFT calculation of approach of a) Norbornene$_{(surf.)}$ with tetrazine$_{(soln.)}$ and b) vice–versa, clearly showing different angles of approach to surface groups.

Based on the TS geometry obtained by DFT calculations we deduce that the approach of tetrazine$_{(soln.)}$ moieties preferentially occurs in a “top–down” manner or perpendicular to the surface (Figure 5a). In contrast, the approach of the incoming norbornene$_{(soln.)}$ should be “side–ways” or parallel to the surface (Figure 5b), and the reactant in solution thus encounters a lot more steric hindrance along the reaction path. In addition, the aggregation of surface-bound tetrazines also lowers the available number of tetrazines in statistical terms by masking one or both the available faces. Both these factors will likely contribute to the overall slower kinetics of tetrazine$_{(surf.)}$ + norbornene$_{(soln.)}$ reaction. These findings point to the overall relevance of choosing prior to immobilization which agent is surface-bound and which comes in from solution.

CONCLUSIONS

We have achieved an expeditious (within 15 min) and quantitative surface functionalization using inverse electron demand Diels–Alder reactions. The reaction displays clean pseudo-first order kinetics over the full conversion range. We found that the approach of the solution reactant towards the surface–bound

counterpart plays an important role in the course of the reaction, supporting the significance of the orientation in surface-bound reactions. Such detailed insights into surface-bound organic reactions are both required and becoming available by combining techniques like XPS and DART-MS to further improve surface modification procedures for a wide range of applications.

REFERENCES

(1) Tang, W.; Becker, M. L. *Chem. Soc. Rev.* **2014**, *43*, 7013.

(2) Ehret, F.; Wu, H.; Alexander, S. C.; Devaraj, N. K. *J. Am. Chem. Soc.* **2015**, *137*, 8876.

(3) Spicer, C. D.; Davis, B. G. *Nat. Commun.* **2014**, *5*, 4740.

(4) Sletten, E. M.; Bertozzi, C. R. *Angew. Chem. Int. Ed.* **2009**, *48*, 6974.

(5) Escorihuela, J.; Marcelis, A. T. M.; Zuilhof, H. *Adv. Mater. Interfaces* **2015**, *2*, 1500135.

(6) Godula, K.; Rabuka, D.; Nam, K. T.; Bertozzi, C. R. *Angew. Chem. Int. Ed.* **2009**, *48*, 4973.

(7) Blackman, M. L.; Royzen, M.; Fox, J. M. *J. Am. Chem. Soc.* **2008**, *130*, 13518.

(8) Karver, M. R.; Weissleder, R.; Hilderbrand, S. A. *Bioconjugate Chem.* **2011**, *22*, 2263.

(9) Vrabel, M.; Kölle, P.; Brunner, K. M.; Gattner, M. J.; López-Carrillo, V.; de Vivie-Riedle, R.; Carell, T. *Chem. Eur. J.* **2013**, *19*, 13309.

(10) Wang, P.; Na, Z.; Fu, J.; Tan, C. Y. J.; Zhang, H.; Yao, S. Q.; Sun, H. *Chem. Commun.* **2014**, *50*, 11818.

(11) Devaraj, N. K.; Upadhyay, R.; Haun, J. B.; Hilderbrand, S. A.; Weissleder, R. *Angew. Chem. Int. Ed.* **2009**, *48*, 7013.

(12) Schoch, J.; Wiessler, M.; Jäschke, A. *J. Am. Chem. Soc.* **2010**, *132*, 8846.

(13) Sen, R., Gahtory, D., Carvalho, R. R., Albada, B., van Delft, F. L. and Zuilhof, H. *Angew. Chem. Int. Ed.* **2017**, *56*, 4130.

(14) Escorihuela, J.; Banuls, M. J.; Puchades, R.; Maquieira, A. *Chem.Commun.* **2012**, *48*, 2116.

(15) Sen, R.; Escorihuela, J.; Smulders, M. M. J.; Zuilhof, H. *Langmuir* **2016**, *32*, 3412.

(16) Sen, R.; Escorihuela, J.; van Delft, F. L.; Zuilhof, H. *Angew. Chem. Int. Ed.* **2017**, *56*, 3299.

(17) Kwon, Y.; Mrksich, M. *J. Am. Chem. Soc.* **2002**, *124*, 806.

(18) Pujari, S. P.; Scheres, L.; Marcelis, A. T. M.; Zuilhof, H. *Angew. Chem. Int. Ed.* **2014**, *53*, 6322.

(19) Rijksen, B.; Pujari, S. P.; Scheres, L.; van Rijn, C. J. M.; Baio, J. E.; Weidner, T.; Zuilhof, H. *Langmuir* **2012**, *28*, 6577.

(20) Yang, J.; Liang, Y.; Seckute, J.; Houk, K. N.; Devaraj, N. K. *Chem. Eur. J.* **2014**, *20*, 3365.

(21) Törk, L.; Jiménez-Osés, G.; Doubleday, C.; Liu, F.; Houk, K. N. *J. Am. Chem. Soc.* **2015**, *137*, 4749.

(22) Frisch, M. J.; Trucks, G. W.; Schlegel, H. B.; Scuseria, G. E.; Robb, M. A.; Cheeseman, J. R.; Scalmani, G.; Barone, V.; Mennucci, B.; Petersson, G. A.; Nakatsuji, H.; Caricato, M.; Li, X.; Hratchian, H. P.; Izmaylov, A. F.; Bloino, J.; Zheng, G.; Sonnenberg, J. L.; Hada, M.; Ehara, M.; Toyota, K.; Fukuda, R.; Hasegawa, J.; Ishida, M.; Nakajima, T.; Honda, Y.; Kitao, O.; Nakai, H.; Vreven, T.; Montgomery Jr., J. A.; Peralta, J. E.; Ogliaro, F.; Bearpark, M. J.; Heyd, J.; Brothers, E. N.; Kudin, K. N.; Staroverov, V. N.; Kobayashi, R.; Normand, J.; Raghavachari, K.; Rendell, A. P.; Burant, J. C.; Iyengar, S. S.; Tomasi, J.; Cossi, M.; Rega, N.; Millam, N. J.; Klene, M.; Knox, J. E.; Cross, J. B.; Bakken, V.; Adamo, C.; Jaramillo, J.; Gomperts, R.; Stratmann, R. E.; Yazyev, O.; Austin, A. J.; Cammi, R.; Pomelli, C.; Ochterski, J. W.; Martin, R. L.; Morokuma, K.; Zakrzewski, V. G.; Voth, G. A.; Salvador, P.; Dannenberg, J. J.; Dapprich, S.; Daniels, A. D.; Farkas, Ö.; Foresman, J. B.; Ortiz, J. V.; Cioslowski, J.; Fox, D. J.; Gaussian, Inc.: Wallingford, CT, USA, 2009.

(23) Zhao, Y.; Truhlar, D. G. *Theor. Chem. Acc.* **2008**, *120*, 215.

(24) Liu, F.; Paton, R. S.; Kim, S.; Liang, Y.; Houk, K. N. *J. Am. Chem. Soc.* **2013**, *135*, 15642.

(25) Törk, L.; Jiménez-Osés, G.; Doubleday, C.; Liu, F.; Houk, K. N. *J. Am. Chem. Soc.* **2015**, *137*, 4749.

(26) Gonzalez, C.; Schlegel, H. B. *J. Phys. Chem.* **1990**, *94*, 5523.

(27) Yang, J.; Karver, M. R.; Li, W.; Sahu, S.; Devaraj, N. K. *Angew.Chem. Int. Ed.* **2012**, *51*, 5222.

CHAPTER 8

General discussion

The previous chapters described our attempts to develop new click methodologies in solution and on a surface, and their application. Moreover, it also explored new methods for surface functionalization, such as with dynamic non–covalent interactions to yield stimuli-dependent surfaces. The current chapter summarizes the salient aspects of each of the previous chapters, and presents the author's opinion on various future prospects of the work.

Chapter 2

As explained in **chapter 1**, click functionalization of surfaces –especially by metal–free click reactions– has garnered increasing interest.[1] In **chapter 2**, we described SuFEx[2] as a click reaction for surfaces. Although the click nature of SuFEx was well known especially for polymer synthesis,[3] hardly any literature on its application to surface modification was available.[4] Moreover, the most well-known SuFEx reaction involves a reaction between silylated alcohols and sulfonyl fluorides,[5] which limits the interfacial application to a large degree. We therefore developed two distinct changes in the reaction to make the reaction surface facile.

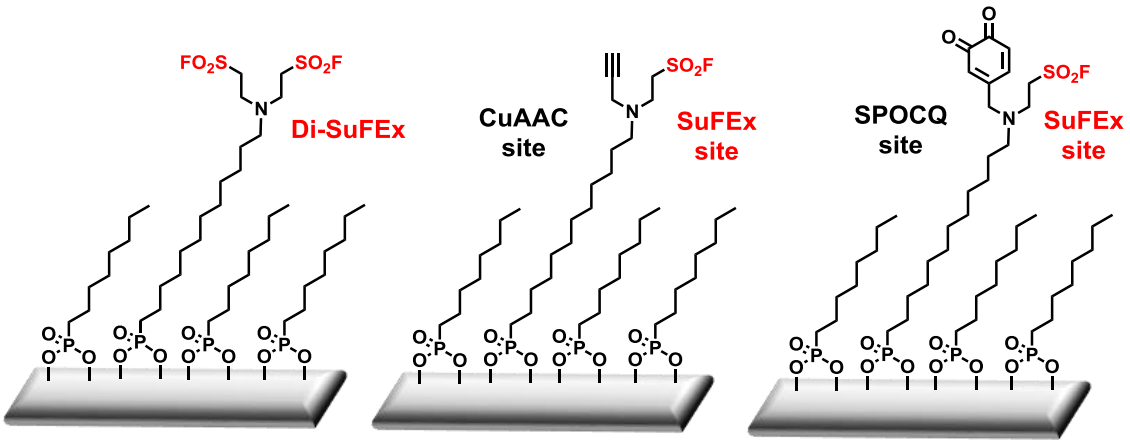

Figure 1. Different click platforms studied in **chapter 2**.

Firstly, we envisioned that a Michael addition with an amine-terminated surface and ethene sulfonyl fluoride (ESF)[3] should allow for an easy access to a SuFExable substrate. Interestingly, we found that Michael addition to a 1° and 2° amine-terminated surface happened quantitatively as evidenced by XPS results. Moreover, this approach further allowed us to design a route allowing multiple

clicks (SuFEx–CuAAC and SuFEx–SPOCQ) sequentially on the same chip. Secondly, we realized that using an amine nucleophile, instead of silylated alcohols, would significantly widen the scope of the reaction given the abundance of available natural and synthetic amines. Moreover, since the resulting sulfonamide bond is typically more stable than the corresponding ester bond, this presents an extra advantage in terms of surface stability. Upon 'SuFExing' the ESF-terminated surfaces with 4–iodobenzylamine, we observed by XPS that the reaction achieved quantitative conversion. We further elucidated the interfacial reaction kinetics of such an interfacial SuFEx reaction (k_2 = 0.18 ± 0.02 $M^{-1}s^{-1}$) using DART–HRMS.[6] The major novelties of our approach were the cleavage of the newly formed sulfonamide bond under DART conditions and the use of the ionized amine species as internal tag for kinetics measurements instead of external tags as were used previously for other reactions.[7] Even for sterically challenged environments such as dual–click platforms, SuFEx achieved quantitative conversions, which establishes it as a real click reaction, also for surfaces. Moreover, we showed the applicability of our strategy by quantitatively functionalizing CuAAC-clicked surfaces with aminoferrocene using SuFEx. As shown in this thesis, DART–HRMS can be effectively used for both quantitative and qualitative surface analysis. A major area of improvement achieved in this respect, as addressed in this chapter is the use of an internal tag, i.e. cleavage, ionization and detection of a bond formed in the

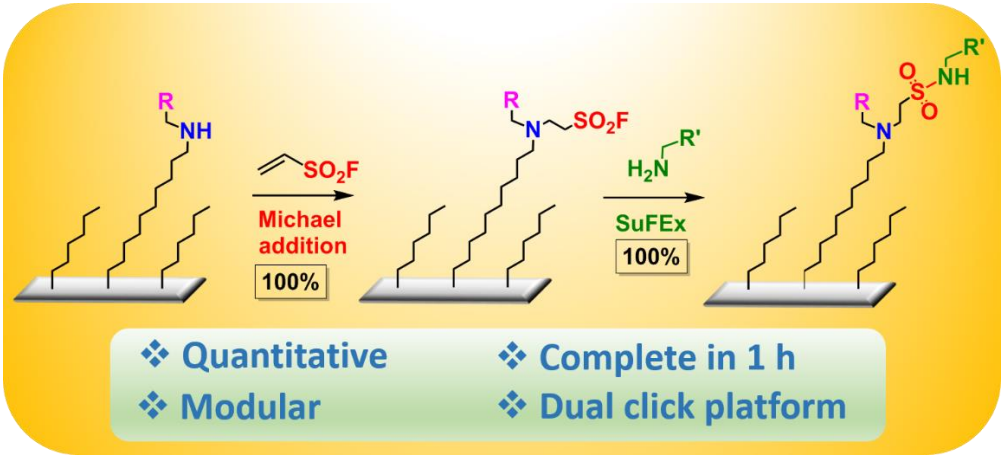

Figure 2. TOC image for chapter 2.

reaction process. While we demonstrate this concept using a sulfonamide bond, it can also be used for other functionalities such as amides, esters, sulfonates etc. Also the different fragmentation patterns in the MS data have to be fully understood and explored further.

A major takeaway from our results is that SuFEx is a true click reaction on surfaces. We demonstrated this for modified Al surfaces, but the substrate itself does likely not play a significant role in the reaction. Therefore, I envision the use of this chemistry for easy attachment of amine-containing biomolecules such as an antibodies, nucleic acids, cells, etc. on all kinds of platforms, such as hard/inorganic surfaces, soft/organic surfaces, but also thereby being used in variety of applications. Another avenue could be the use of SuFEx for easy on–resin assembly of repeating or random molecular units. Currently the most successful example of solid phase synthesis for growing long chains include peptide synthesis by amide coupling. However, with the increasing need for more efficient reactions, the possibility of SuFEx type reactions as an alternative for on–resin conjugations becomes realistic, which I am currently developing as a spin-off of the work in this chapter.

Chapter 3

In **chapter 3**, we went a step further and reported a novel click strategy for both solution and surface functionalization. Our approach builds on the SPOCQ reaction reported by Van Delft and co–workers,[8] which involves a cycloaddition between a quinone and a strained cyclooctyne, BCN.[9] A great feature of this reaction is that it can be ‘turned on’, by the oxidation of catechols to ortho-quinones, which can be induced electrochemically, enzymatically or by the oxidation of soluble oxidants. While high-yielding, fast enough to outcompete many reactions in vitro, and (partially because of this) also bio-orthogonal, a major drawback of this reaction is the inherent hydrophobicity and bulk of cyclooctynes. This moiety itself is rarely essential for bio–conjugations, and is definitely not favorable in sterically hindered environments, such as relevant for

bioconjugations, polymer functionalization or surface modifications. Thus, we aimed to conserve this inducible character, yet with a much smaller reactive

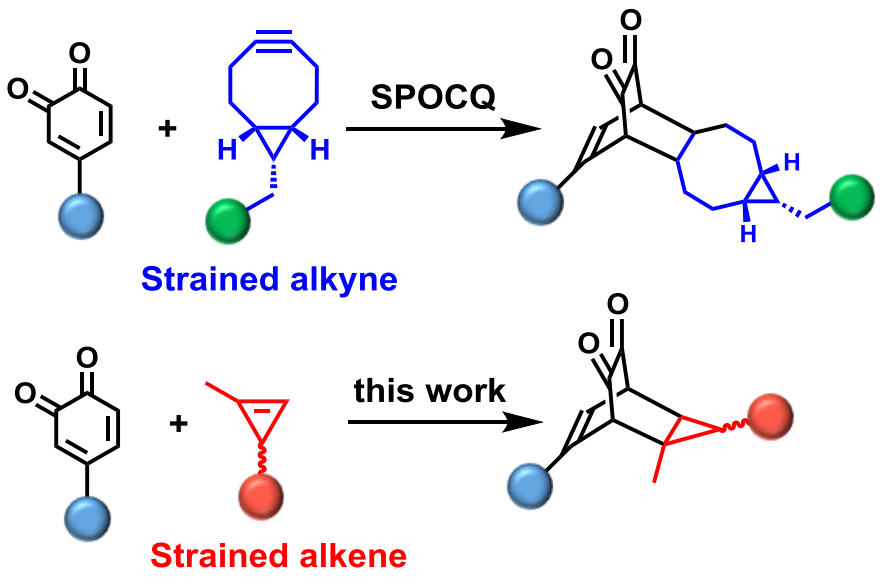

Figure 3. Inspiration for use of cyclopropenes as a dienophile.

species. Therefore a novel reaction was aimed for, and the use of cyclopropenes as a smaller dienophile was investigated, both in solution and on surfaces.

Based on studies of Devaraj and co–workers,[10] we synthesized a cyclopropene analogue that could be diversified easily as an ester or a carbamate. The reaction proceeded rapidly in solution (k_2 = 1.95 ± 0.2 $M^{-1}s^{-1}$) as shown by UV kinetics and afforded a 75% yield. Since the ^{1}H NMR spectra (including NOESY and COSY) were not conclusively interpretable, we postulated two tentative structures, both with an *endo* configuration of the formed cyclopropane ring. DFT calculations to study the reaction mechanism further confirmed that the *endo* transition states were energetically more favorable than the *exo* (7.5 vs. 9.1 kcal/mol, respectively). The reaction also was facile on surfaces (k_2 = 0.50 ± 0.01 $M^{-1}s^{-1}$) and achieved completion in 20 min as compared to 4 h for SPOCQ.[7]

We further demonstrated the applicability of this click reaction for sterically hindered environments by using surface-grafted polymer brushes as an example.

We compared the click effciency of BCN versus cyclopropene with quinones generated onto poly(MeOEGMA) brushes that have been shown to possess good anti-fouling properties by Kuzmyn *et al*.[11] Whereas the SPOCQ reaction with a BCN analogue yielded a ~30% yield, the sterically advantageous cyclopropene provided ~50% conversion. This further substantiated our hypothesis regarding the effect of the reactant's steric bulk on click reactivities in constrained environments.

Scheme 1. Reaction scheme for SPOCQ and cyclopropene-quinone click on polymer brushes.

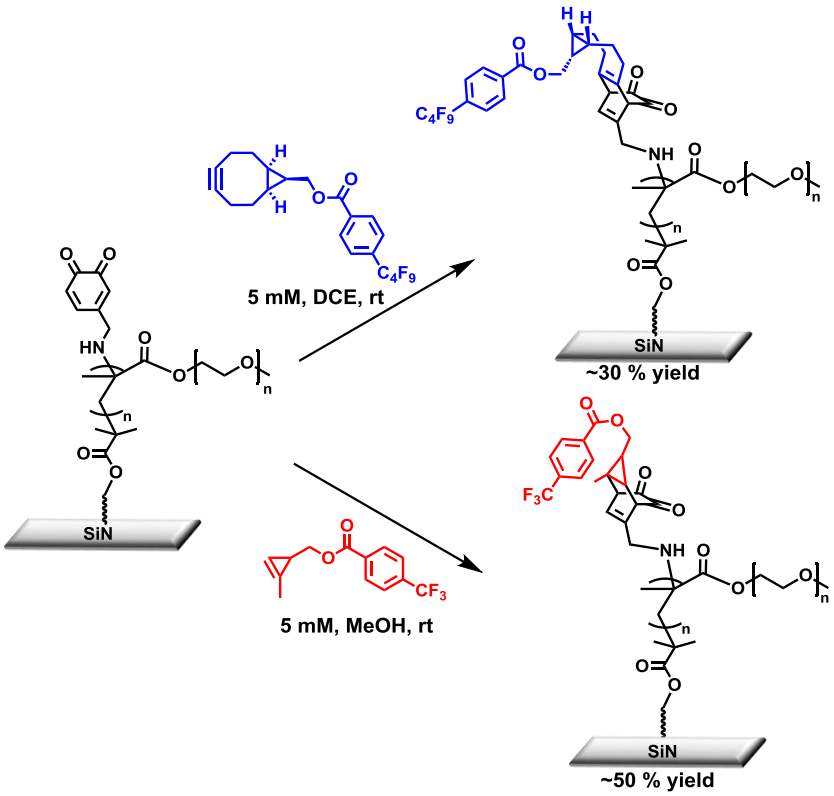

The data in this chapter also pointed to another, actually much further reaching point. Typically, the efficiency of bio-conjugation click reactions is directly coupled to the reaction rate of the two reagents in a dilute solution. As a point in case, Houk gives colors (red = not suitable; green = suitable for *in vivo* bioconjugations) to quickly evaluate the usefulness of a reaction based on such a reaction rate. The unexpressed, but underlying hypothesis is that the reaction rate is indicative for this reaction in sterically congested environments, as e.g. the *in vivo* modification of an extremely bulky polymer like an antibody. The data in this

chapter basically show that this hypothesis is wrong: while the SPOCQ in solution is much faster than the cyclopropene–quinone click (two orders of magnitude), the same reactions in the sterically confined environments of a covalently modified surface are roughly equal in rate. In other words: while dilute-solution reactions can be mimicked with increasing efficiency by e.g. high-level quantum chemical calculations, the transposition of such conclusions to sterically confined environments is not straight-forward. Or phrased more explicitly: the efficiency of surface-modifying or bio-conjugating reactions cannot be derived with high precision based on dilute-solution data. As a result, I think that the cyclopropene-quinone click reaction should have considerable scope for biological modifications, such as site–specific protein conjugation, and antibody–drug conjugate synthesis.

Another area of further research should be an investigation into the effect of different substitutents at the cyclopropene ring on the kinetics and efficiency of our click reaction. Of course, one can think of *trans*-cyclooctene derivatives with extra ring strain for an increased reactivity, but there again a eight-membered ring with even more attached groups is then required. More daunting and speculative, but potentially more rewarding in the long run would be the use of other three-membered rings, that could combine a high-ring strain with a small steric demand, such as bicyclic cyclopropenes. The critical feature here will primarily not be a higher reactivity, but a high reactivity with a manageable stability: without a significant shelf-life, such a reagent will not become sufficiently often used to find the optimal conditions for a wide range of circumstances relevant for bioconjugations or polymer or surface modifications; and yet: only in eating lots of puddings, a good taste for the best ones can be obtained, so such a managable stability is not ‘just another’ reagent property. The quinone moiety can also be optimized by introduction of electron withdrawing nitro groups[12] that should allow facile IEDDA with dienophiles. This in combination with TCO or other rapidly reactive species can lead to a superfast click reaction.

Alternatively, an area of improvement is the inducibility of such click reactions. While the inducible nature of SPOCQ type reactions using enzymatic oxidation is well reported for proteins,[13] similar techniques on surfaces are still to be explored. Similarly, enzymatic oxidation using horseradish peroxidase (HRP) has previously been used for inducing tetrazine click reactions based on oxidation of inactive dihydroanalogues into reactive aromatized tetrazines.[14] In the same vein, DNAzyme[15] or electrochemical oxidation[16] based methods can be envisioned for interfacial quinone generation.

Chapter 4

While most surface attachment functionalization strategies focus on covalent attachment of a molecule to a mono-/multilayer, an alternative approach is the use of non–covalent supramolecular interactions.[17] While providing a robust attachment similar to covalent interactions upon use of multiple interactions, this approach allows easy control over interfacial chemical composition, architecture, topology, etc.

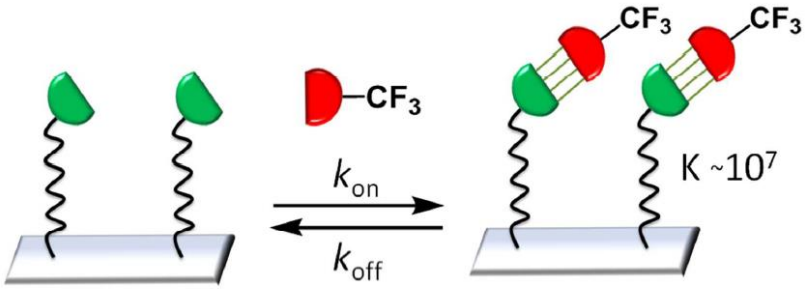

Figure 4. TOC image for chapter 4.

Probably, the most useful advantage of any supramolecular interfacial attachment strategy is the strong yet dynamic character of the culminating interaction. Thus the resulting bonds can be manipulated based on solvent, light, temperature, pH and chemical stimuli, hereby providing possibility of an ON/OFF control. **Chapter 4** describes the development of dynamic and exchangeable surfaces based on the quadruple hydrogen-bonded ureidopyrimidinone (UPy)

motif. Although the utility of multiple hydrogen bonds for surface applications is widely reported,[18] interestingly the use of the UPy motif was not studied in detail.

Moreover, no mechanistic investigation of these interfacially H–bonded UPy motifs was known until our report. Our study involved preparation of UPy-terminated surfaces using isocyanate chemistry that could subsequently serve as receptor molecules for incoming UPy molecules in solution. Using a combination of XPS and DART–HRMS we determined the reaction kinetics of interfacial UPy dimer formation (k_2 = 2.2 ± 0.1 $M^{-1}s^{-1}$) and calculated the reaction efficiency of dimer formation to be about 40% after sonication. Use of sonication was deemed necessary to avoid any non–specific interactions such as with the amine monolayer, which were mostly overlooked in previous reports.[19] To get a better understanding of the orientation of the interfacial UPy dimers, we performed molecular dynamics experiments which revealed that crowding at the surface by surface-bound UPy can hamper further binding.

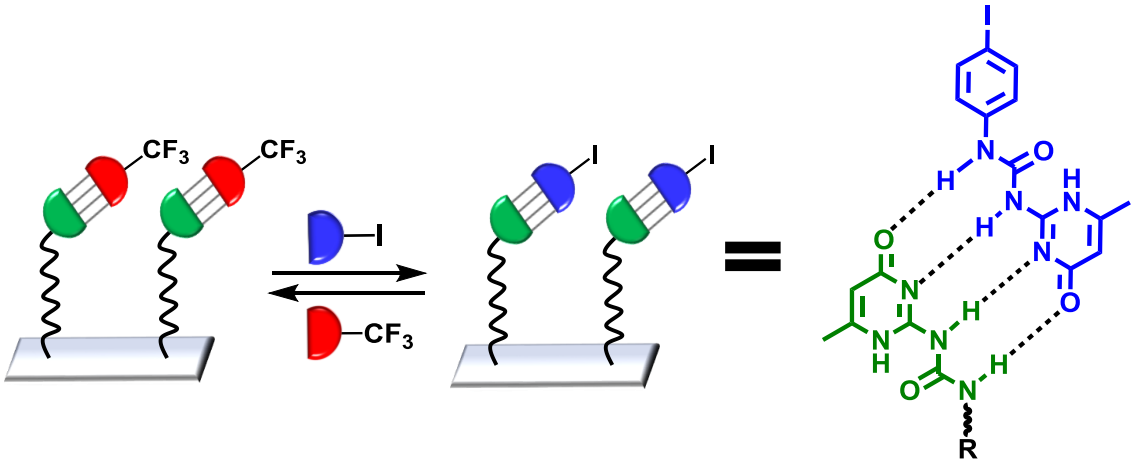

Figure 5. A cartoon representation of interfacial UPy dimer exchange.

Furthermore, we demonstrated that using a solvent stimulus we could easily disassemble the formed dimers followed by reassembly in presence of a UPy moiety in solution. This process could be easily repeated and monitored by XPS. In addition, we explored the exchangeability of the interfacial dimers with a competing UPy motif and elucidated the kinetics of the process (k_2 = 0.4 ± 0.1 $M^{-1}s^{-1}$) [Figure 5]. The process was about 4 times slower than dimer formation and

could be repeated with two distinct UPy dimers. To complete the mechanistic study, we calculated the equilibrium constant ($K = k_{on}/k_{off}$) for interfacial dimer formation to be in the order of 10^7 M^{-1} in toluene, which was similar to the value in solution (6×10^8 M^{-1}).[20]

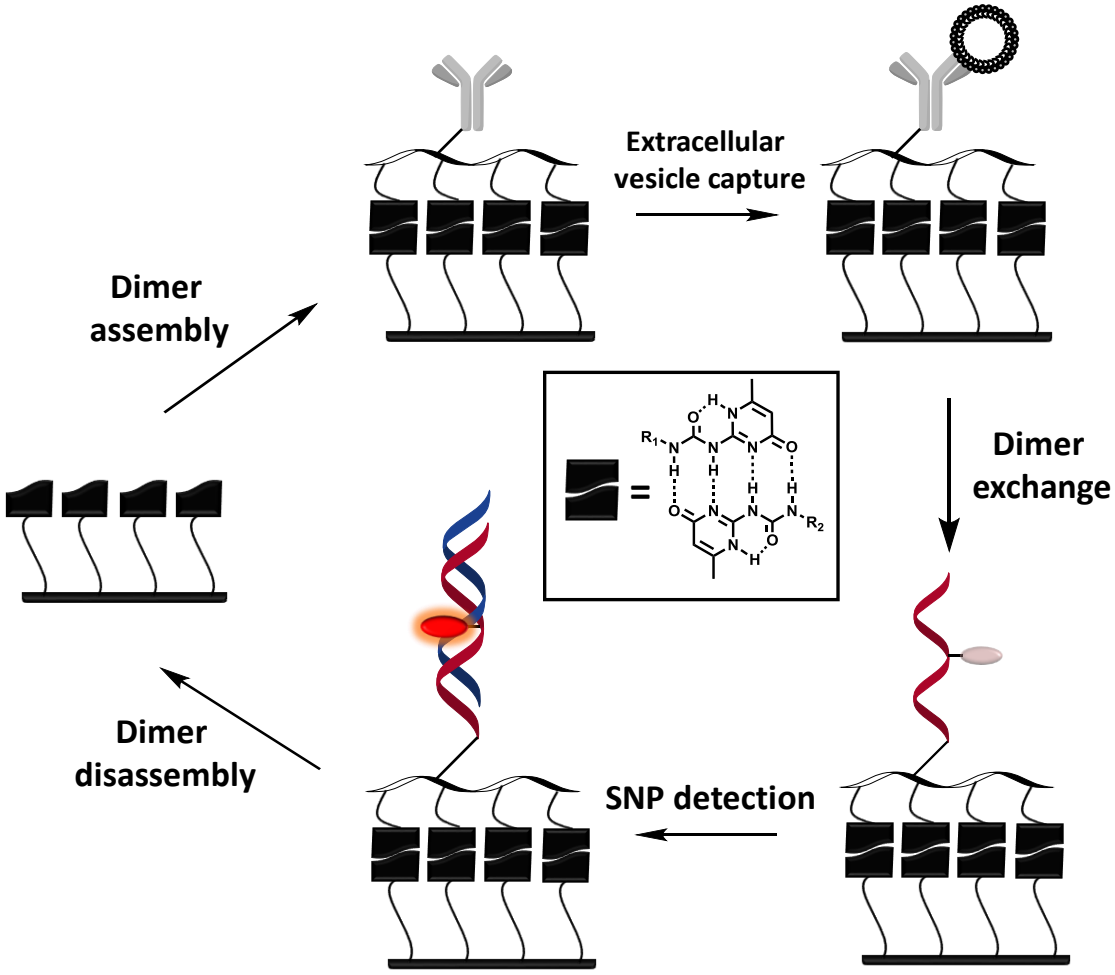

Figure 6. Representation of a dynamic bio-sensing system based on UPy dimer exchange that can allow use of the same chip for two distinct detection modes.

In our study, we focussed on the exchange of individual UPy dimers on surfaces. While individual dimers are quite strong, they will likely not suffice for binding materials onto a surface that is mechanically perturbed, e.g. by being in flow in a microchannel. Yet, under such circumstances the dynamic, replaceable aspect of the attached species could be highly beneficial. Here, I would propose to use multivalency as the road forward, with di-, tri- or multi-UPy components onto a surface (see image below – one could think of UPy oligomers or polymers). These

more strongly bound yet reversible and functionalizable oliomers can provide a handle for altering surface properties such as self-healing, wettability, anti-fouling and development of regeneratable bio–sensors such as for flow-based systems.

For example, I envision a flow system incorporating two distinct biosensing mechanisms that can be utilized on the same chip. One bio–sensing mode can involve capture of extracellular vesicles for cancer detection onto a oligomeric UPy dimer system containing a capturing antibody. Following the capture and detection, the chip can be cleared of the attached UPy oligomers by exchange with another UPy system with a different bio-sensing element such as a SNP detection platform (discussed in the next chapter).

Chapter 5

Peptide nucleic acids (PNAs) were first introduced by Nielsen and co–workers[21] as nucleic acid mimics with increased enzymatic stability[22] and stronger binding.[23] Their structure usually consists of a repeating *N*-(2-aminoethyl)glycine (Aeg) backbone with nucleobases linked via an amide linkage.[24] While the current synthesis strategies for PNA synthesis are well–optimized, a major drawback is lack of modularity in case of internal modification.[25] For example, replacement of a nucleobase with another molecule such as a fluorophore is not straightforward.[26] We tried to tackle this challenge in **chapter 5** wherein we described a novel click strategy for internal modification of PNAs by incorporating α-azido D-ornithine (Orn) during standard solid-phase PNA synthesis. We envisioned that the azido group could serve as an isostere for amide bonds, thereby allowing facile PNA–DNA hybridization.

To this end, we clicked a thiazole orange (TO) analogue using CuAAC onto an internal position in a growing PNA chain in high yields. As shown previously by the group of Seitz,[26] internally amide-linked PNA–TO hybrids, so–called forced intercalation–PNA (FIT–PNA) possess excellent single nucleotide polymorphism (SNP) detection ability. Our triazole-linked PNA–TO hybrid showed a 3.5–fold

match/mismatch discrimination when used for a sequence reported by Seitz and co–workers, thus proving our hypothesis.[25] We were further interested in studying these PNA constructs for antisense delivery applications given the higher enzymatic stability of PNA–DNA duplexes as compared to DNA–DNA duplexes.

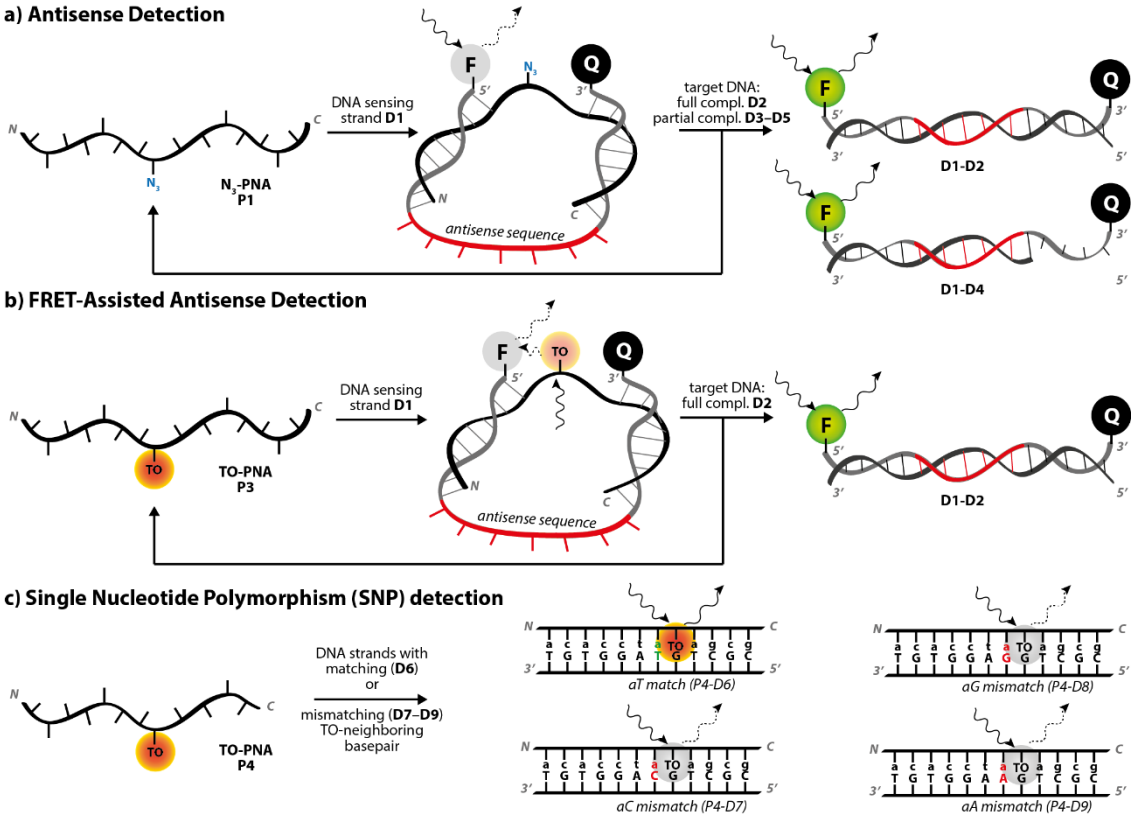

Figure 7. Different applications of internally triazole-linked PNA–TO constructs studied in chapter 5.

Thus, we designed a PNA–TO sequence that hybridized with a ssDNA sequence containing an internal antisense stretch to form a circular construct with the TO label directly opposite to the sensing portion. Using a FRET signal of TO with a fluorophore attached to one of the DNA arms and melting curve analysis, we confirmed formation of the PNA–DNA hybrid. To demonstrate antisense sequence release we tested the PNA–DNA duplex against a competing DNA strand. As expected addition of the competing strand triggered disassembly of the PNA–DNA heterodimer in favor of dsDNA formation as further confirmed by the higher melting temperature values for the dsDNA (ΔT_M = 10 °C).

Although we only demonstrated the click of a simple fluorophore onto the internal azide, this paves the way for more complex conjugate synthesis. One avenue for further research is synthesis of cell penetrating peptide (CPP)–PNA delivery vectors that will allow easy cellular uptake and delivery of a targeting DNA sequence with incresed stability towards exonucleases. Such conjugates open a new domain of research such as in gene suppression and targeted delivery. Alternatively, a different area of exploration is application of newer metal-free click strategies such as SPAAC, SPOCQ, IEDDA for PNA modification using an internally modified D–Orn/Aeg analogue or a modified nucleobase.

Another important conclusion to be drawn based on my work is that while successful for some cases as reported by Seitz *et al.*, the applicability of forced intercalation–PNA probes is not as universal as advertized. In our hands, the probes did not provide a good match/mismatch SNP discrimination when used in the context of *P. falciparum* genes for identifying drug resistance. Thus in my opinion, further research in this regard is necessary to make such probes universally useful for SNP detection instead of being sequence specific.

Chapter 6

Chapter 6 concerns with the application of a click-type approach to a completely different and difficult target substrate. Mica is a substrate widely used for AFM visualization of biological structures[27] and investigation of the fundamental principles linked with adhesion,[28] friction[29] and surface forces,[30] etc. However, its modification is rather difficult to achieve, with none to little literature precedent.[31] Inspired by reports from the goups of Butler[32] and Hwang,[33] we tackled the challenge using a mussel-mimetic surface anchor.[34] We designed a catechol-based molecule with an amine handle, that could be synthesized in only two steps (66% overall yield) and allowed easy functionalization of mica substrates via the freed-up amine handle.

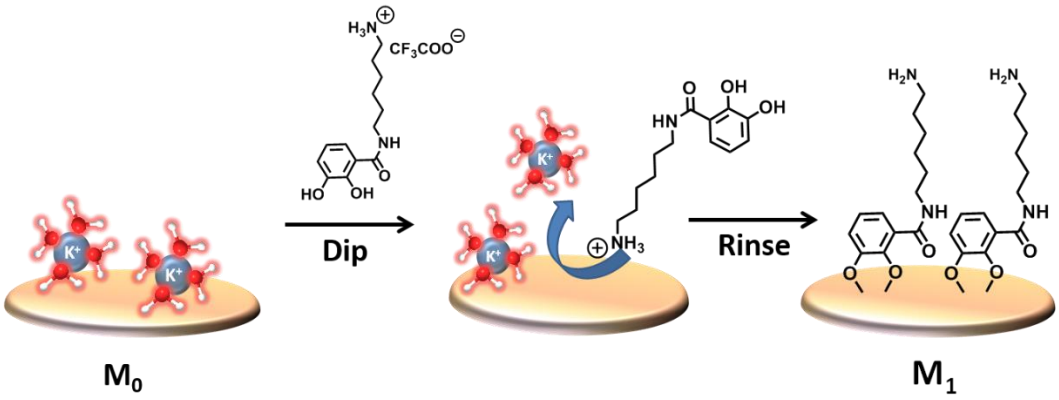

Figure 9. Tentative mechanism of mica modification by surface anchor.

Interestingly, surface modification with the our compound provided ultrasmooth layers (roughness = 0.4 nm) with layer thickness of about 2.5 ± 0.5 nm, thereby confirming formation of well defined thin layers, instead of rough polymeric layers as had been shown before.[33] The layers could be extensively characterized by AFM analysis and were stable under sonication conditions and under–water storage for 7 days, thus demonstrating good adhesive strength. Subsequently, we could perform easy diversification of the surfacial amines to different clickable modules that provided excellent surface yields for SPAAC (83%) and SPOCQ (91%). Thereafter we demonstrated the applicability of our coatings for step–wise microscopic visualization of biological nanostructures using DNA minicircles[35] as an example. To this end, we covalently immobilized a receptor DNA strand onto amine-modified mica substrates, which in turn allowed the self-assembly of a minicircle upon placing in a solution of appropriate complementary strands. Such circles could be easily visualized upon AFM analysis. Similarly, we explored immobilization of a catalytic DNA strand,[36] which allowed the chips to perform an HRP-mimicking oxidation.[37]

While we could show easy preparation and diverse applicability of our ultrasmooth layers, a thorn in the flesh remains. The length of our surface anchor in stretched–out fashion is ca. 1.3 nm, which means that the slowed auto–oxidation of surface anchor leads to formation of di–/trimeric layers (2.5 nm).

Scheme 2. Examples of 2nd generation surface anchors with electron–withdrawing substituents.

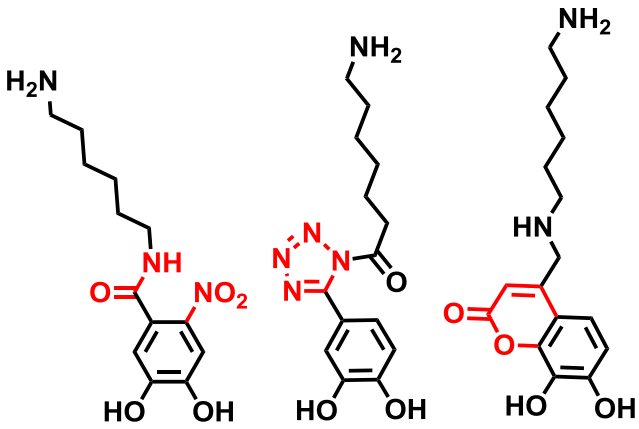

Although this in itself is a step forward, the ideal situation would be formation of completely defined monolayers onto mica substrates. This can be achieved by incorporating strong electron–withdrawing groups such as in nitrocatechols as shown by group of Spencer.[12] Combining the nitrocatechol head group with the amine chain could prove to be the ideal surface anchor for mica modification (Scheme 2). Another point of further research is the mode of attachment of our surface anchor to the hydrophilic aluminosilicate structure of mica. An in–depth AFM adhesion analysis could provide insights into this question and promote further structural modifications for the surface anchor. Finally, a field of further research that can stem from this chapter is an investigation of the material-independent adhesive nature[38] of our catechol-based adhesive and tailoring of thus formed layers towards different substrate-dependent demands.

Chapter 7

Usually for most interfacial reactions, one reactant is immobilized on surfaces while the other is in solution. However, a simple yet important aspect is often overlooked, namely that reactions on a surface are more restricted in terms of reactant approach than in solution. We thus hypothesized that looking carefully at the approach of both the reactants towards a surface should provide an indication as to which component is better to be surface–bound or better to be in solution. Thus in **chapter 7**, we investigated in detail the effects of reactant

approach on reaction kinetics for an interfacial inverse electron demand Diels–Alder (IEDDA) reaction, specifically the norbornene–tetrazine click reaction, using XPS and DART–HRMS as analytical tools. In addition, we also studied the effect of reactant stereochemistry and surface microenvironment on the reaction efficiency and kinetics.

Interestingly, we found a discernible reaction rate difference for the different reaction combinations, i.e. norbornene$_{(surf.)}$ + tetrazine$_{(soln.)}$ versus tetrazine$_{(surf.)}$ + norbornene$_{(soln.)}$. While the differences were relatively small, the important features were that this was the first example that any accurate kinetic data had been obtained for any reactive pairs at all, and that secondly these differences now also demanded an explanation: good scientific answers lead to even more questions. Using a combination of DFT calculations and molecular dynamics, we elucidated that surface-bound tetrazines tend to aggregate together due to π–π interactions, hereby rendering the reactant species less accesible to the incoming soluble counterpart. In contrast, the norbornene groups are oriented with the double bond facing upwards, thus being more easily accessible to the incoming tetrazine, leading to a faster reaction rate.

In addition, the rate difference for the *exo*– vs. *endo*– diastereomers for this IEDDA reaction in solution (2 times) was also observed for the surface reaction. While unfortunately not considered by the reviewers of our manuscript, in my opinion, the determination of this small difference with high precision speaks volumes about our analysis methodology, and could be of vital importance in closely related reactions that differ ever so slightly kinetically. Importantly, we found that for all the possible combinations, the reaction achieved quantitative conversion within 15 min with the *exo*–norbornene$_{(surf.)}$ + tetrazine$_{(soln.)}$ system outcompeting all others (k_2 = 3.6 ± 0.2 $M^{-1}s^{-1}$). This is relevant in its own accord, as quantitative conversions in short reaction times are highly desirable for surface applications as discussed in **chapter 1**.

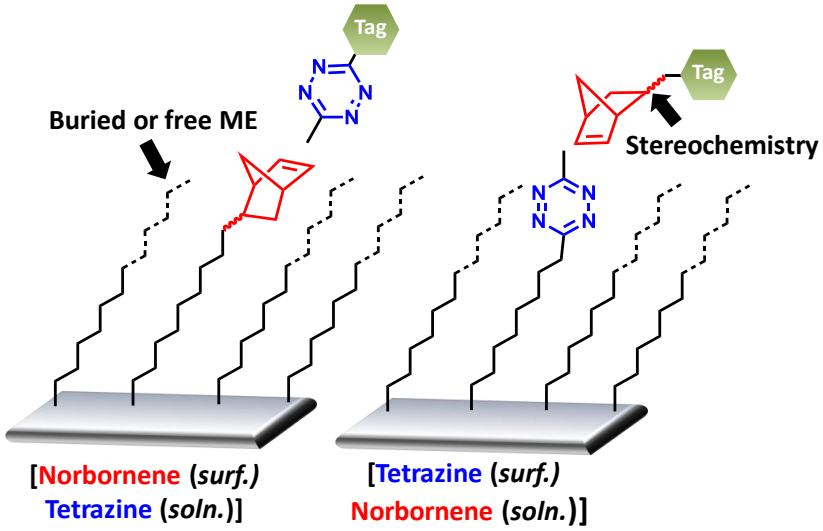

Figure 8. Factors affecting an interfacial IEDDA reaction studied in chapter 7.

These observations provide a precedent for further click reactions and the role that orientation plays during their interfacial applications. Similarly, other phenomena dependent on the orientation of a reactant group in space can be studied, for example, marrying UV-based change in surface disposition such as in molecular motors (azobenzene or overcrowded alkene based) to click reactions, thus leading to inducible click reactivity. A different class of IEDDA reactions yet unexplored for surface applications is the tetrazine–cyclopropene ligation as shown in **chapter 3**. This reaction offers advantages of faster kinetics as compared to norbornene and higher stability as compared to TCO. Thus, further research towards development of a reaction methodology for tailoring this facile click reaction for surface applications is an exciting challenge.

FINAL REMARKS

Taking a step back and wondering what future prospects can be envisioned pertaining interfacial click methodologies, reveals three major areas of exploration. Firstly, the improvement of reactions themselves is of primary interest. Taking the cyclopropene–quinone click described in **chapter 3** as an example, careful computational analysis and imaginative thinking can lead to substitution patterns that would help alleviate the remaining steric or electronic

burden on the reactants and hence enhance reaction rate and efficiency. A second area of exploration is the field of analytical tools used for interfacial reaction characterization. Traditionally, XPS and IRRAS have been widely used for gaining insight into interfacial reactions. I propose that ambient mass spectrometry presents an interesting and accurate alternative to intricately study the effect of several parameters involved in an interfacial reaction both qualitatively and quantitatively. Other MS techniques that are also gaining foothold in interfacial analysis involve laser ablation electrospray ionization (LAESI)[39] and time of flight–secondary ion mass spectrometry (TOF-SIMS).[40] Finally, broadening the scope of the applicability of the click methodologies explained in this thesis is the ultimate frontier of future exploration. As shown in chapter **3** in a proof-of-concept study, newer click strategies for anti–fouling polymer brush modifications with interesting biomolecules form the next area to focus on for a range of biomedical applications.[41]

To summarize, a helicopter view of all our endeavours suggests that while we have come a long way towards efficient surface functionalization, in the spirit of science, our answers both invoke and demand further inquiries in the future.

REFERENCES

(1) Escorihuela, J.; Marcelis, A. T. M.; Zuilhof, H. *Adv. Mater. Interfaces* **2015**, *2*, 1500135.

(2) Dong, J.; Krasnova, L.; Finn, M. G.; Sharpless, K. B. *Angew. Chem. Int. Ed.* **2014**, *53*, 9430.

(3) Wang, H.; Zhou, F.; Ren, G.; Zheng, Q.; Chen, H.; Gao, B.; Klivansky, L.; Liu, Y.; Wu, B.; Xu, Q.; Lu, J.; Sharpless, K. B.; Wu, P. *Angew. Chem. Int. Ed.* **2017**, *56*, 11203.

(4) Yatvin, J.; Brooks, K.; Locklin, J. *Angew. Chem. Int. Ed.* **2015**, *54*, 13370.

(5) Li, S.; Wu, P.; Moses, J. E.; Sharpless, K. B. *Angew. Chem. Int. Ed.* **2017**, *56*, 2903.

(6) Sen, R.; Escorihuela, J.; Smulders, M. M. J.; Zuilhof, H. *Langmuir* **2016**, *32*, 3412.

(7) Sen, R.; Escorihuela, J.; van Delft, F.; Zuilhof, H. *Angew. Chem. Int. Ed.* **2017**, *56*, 3299.

(8) Borrmann, A.; Fatunsin, O.; Dommerholt, J.; Jonker, A. M.; Löwik, D. W. P. M.; van Hest, J. C. M.; van Delft, F. L. *Bioconjugate Chem.* **2015**, *26*, 257.

(9) Dommerholt, J.; van Rooijen, O.; Borrmann, A.; Guerra, C. F.; Bickelhaupt, F. M.; van Delft, F. L. *Nat. Commun.* **2014**, *5*, 5378.

(10) Yang, J.; Liang, Y.; Šečkutė, J.; Houk, K. N.; Devaraj, N. K. *Chem. Eur. J.* **2014**, *20*, 3365.

(11) Kuzmyn, A. R.; de los Santos Pereira, A.; Pop-Georgievski, O.; Bruns, M.; Brynda, E.; Rodriguez-Emmenegger, C. *Polym. Chem.* **2014**, *5*, 4124.

(12) Rodenstein, M.; Zürcher, S.; Tosatti, S. G. P.; Spencer, N. D. *Langmuir* **2010**, *26*, 16211.

(13) Bruins, J. J.; Westphal, A. H.; Albada, B.; Wagner, K.; Bartels, L.; Spits, H.; van Berkel, W. J. H.; van Delft, F. L. *Bioconjugate Chem.* **2017**, *28*, 1189.

(14) Zhang, H.; Trout, W. S.; Liu, S.; Andrade, G. A.; Hudson, D. A.; Scinto, S. L.; Dicker, K. T.; Li, Y.; Lazouski, N.; Rosenthal, J.; Thorpe, C.; Jia, X.; Fox, J. M. *J. Am. Chem. Soc.* **2016**, *138*, 5978.

(15) Golub, E.; Albada, H. B.; Liao, W.-C.; Biniuri, Y.; Willner, I. *J. Am. Chem. Soc.* **2016**, *138*, 164.

(16) Lee, P. T.; Lowinsohn, D.; Compton, R. G. *Analyst* **2014**, *139*, 3755.

(17) della Sala, F.; Kay, E. R. *Angew. Chem. Int. Ed.* **2015**, *54*, 4187.

(18) Liang, C.-K.; Dubacheva, G. V.; Buffeteau, T.; Cavagnat, D.; Hapiot, P.; Fabre, B.; Tucker, J. H. R.; Bassani, D. M. *Chem. Eur. J.* **2013**, *19*, 12748.

(19) Sanyal, A.; Norsten, T. B.; Uzun, O.; Rotello, V. M. *Langmuir* **2004**, *20*, 5958.

(20) Scherman, O. A.; Ligthart, G. B. W. L.; Sijbesma, R. P.; Meijer, E. W. *Angew. Chem. Int. Ed.* **2006**, *45*, 2072.

(21) Nielsen, P.; Egholm, M.; Berg, R.; Buchardt, O. *Science* **1991**, *254*, 1497.

(22) Demidov, V. V.; Potaman, V. N.; Frank-Kamenetskii, M. D.; Egholm, M.; Buchard, O.; Sonnichsen, S. H.; Nielsen, P. E. *Biochem. Pharmacol.* **1994**, *48*, 1310.

(23) Egholm, M.; Buchardt, O.; Christensen, L.; Behrens, C.; Freier, S. M.; Driver, D. A.; Berg, R. H.; Kim, S. K.; Norden, B.; Nielsen, P. E. **1993**, *365*, 566.

(24) Egholm, M.; Buchardt, O.; Nielsen, P. E.; Berg, R. H. *J. Am. Chem. Soc.* **1992**, *114*, 1895.

(25) Kohler, O.; Seitz, O. *Chem. Commun.* **2003**, 2938.

(26) Socher, E.; Jarikote, D. V.; Knoll, A.; Röglin, L.; Burmeister, J.; Seitz, O. *Anal. Biochem.* **2008**, *375*, 318.

(27) Rothemund, P. W. K. *Nature* **2006**, *440*, 297.

(28) Horn, R. G.; Israelachvili, J. N.; Pribac, F. *J. Colloid Interface Sci.* **1987**, *115*, 480.

(29) Homola, A. M.; Israelachvili, J. N.; Gee, M. L.; McGuiggan, P. M. *J. Tribol.* **1989**, *111*, 675.

(30) Christenson, H. K. *J. Dispersion Sci. Technol.* **1988**, *9*, 171.

(31) Liu, Z.-H.; Brown, N. M. D.; McKinley, A. *Appl. Surf. Sci.* **1997**, *108*, 319.

(32) Maier, G. P.; Rapp, M. V.; Waite, J. H.; Israelachvili, J. N.; Butler, A. *Science* **2015**, *349*, 628.

(33) Lim, C.; Huang, J.; Kim, S.; Lee, H.; Zeng, H.; Hwang, D. S. *Angew. Chem. Int. Ed.* **2016**, *55*, 3342.

(34) Lee, H.; Scherer, N. F.; Messersmith, P. B. *Proc. Natl. Acad. Sci. USA* **2006**, *103*, 12999.

(35) Rasched, G.; Ackermann, D.; Schmidt, T. L.; Broekmann, P.; Heckel, A.; Famulok, M. *Angew. Chem. Int. Ed.* **2008**, *47*, 967.

(36) Li, Y.; Sen, D. *Nat. Struct. Biol.* **1996**, *3*, 743.

(37) Carvalho, R. R.; Pujari, S. P.; Gahtory, D.; Vrouwe, E. X.; Albada, B.; Zuilhof, H. *Langmuir* **2017**, *33*, 8624.

(38) Lee, H.; Dellatore, S. M.; Miller, W. M.; Messersmith, P. B. *Science* **2007**, *318*, 426.

(39) van Geenen, F. A. M. G.; Franssen, M. C. R.; Schotman, A. H. M.; Zuilhof, H.; Nielen, M. W. F. *Anal. Chem.* **2017**, *89*, 4031.

(40) Stepien, M.; Saarinen, J. J.; Teisala, H.; Tuominen, M.; Aromaa, M.; Haapanen, J.; Kuusipalo, J.; Mäkelä, J. M.; Toivakka, M. *Langmuir* **2013**, *29*, 3780.

(41) Lange, S. C.; van Andel, E.; Smulders, M. M. J.; Zuilhof, H. *Langmuir* **2016**, *32*, 10199.

APPENDIX 1

SuFEx click chemistry delivers a quantitative and orthogonal platform for surface modification

1. MATERIAL AND METHODS.

Materials. Unless otherwise specified, all chemicals were used as received without further purification. Ethenesulfonylfluoride (ESF), 4–iodobenzylamine (IBZ), propargylamine, triazabicyclodecene (TBD), 3,4 dihydroxybenzylamine hydrobromide, sodium metaperiodate ($NaIO_4$), triethylamine, copper(I) iodide, aminoferrocene, hydrochloric acid, methanol, hexane, acetone, dichloromethane, 2-propanol were purchased from Sigma-Aldrich. 12-Aminododecylphosphonic acid hydrochloride salt, 12-bromododecylphosphonic acid and octylphosphonicacid was purchased from SiKÉMIA. Aluminum pieces (99.5% purity, mirror polished, Staalmarkt Beuningen BV) were cut using mechanical cutter into exactly 2×1 cm dimensions. For surface modification reactions, the samples were loaded onto a specially constructed PTFE wafer holder able to hold up to 16 samples at a time thus ensuring rigorous reproducibility between samples.

X-ray photoelectron spectroscopy (XPS) measurements. The XPS analysis of surfaces was performed using a JPS–9200 photoelectron spectrometer (JEOL, Japan). Survey and high-resolution spectra were obtained under UHV conditions using monochromatic Al Kα X-ray radiation at 12 kV and 20 mA and an analyzer pass energy of 50 eV for wide scans and 10 eV for narrow scans. The emitted electrons were collected at 10° from the surface normal (take-off angle relative to the surface normal 10°). All XPS spectra were evaluated by using Casa XPS software (version 2.3.15). Survey spectra were corrected with linear background before fitting, whereas high-resolution spectra were corrected with linear background. Atomic area ratios were determined after a baseline correction and normalizing the peak area ratios by the corresponding atomic sensitivity factors (1.00 for C1s, 1.80 for N1s, 2.93 for O1s, 4.43 for F1s, 1.18 for P2s, and 0.54 for Al2p).

DART-HRMS measurements. Analysis of the modified aluminum surfaces was performed using a DART-SVP ion source (Ion-Sense, Saugus, MA) coupled to a Q–Exactive orbitrap high-resolution mass spectrometer (Thermo Fisher Scientific, San Jose, CA, USA), mounted on a motorized rail travelling at 0.2 mm/s. Thermo Scientific Xcalibur software (V2.1.0.1139) was used for data acquisition and processing.[1] The measurements were performed in positive and negative mode at 450 °C using a mass resolution of 70,000 (FWHM) at a scan rate of 1 Hz. The DART source was positioned 6.1 cm on the horizontal scale, 7 cm on the vertical scale with an angle of 45°, such that it is around 1 mm above the surface (Fig. S5). The distance from the surface to the ceramic tube is minimized by placing them at the edge of the moving rail so that maximum of the ionized species would enter the MS.

Scanning electron microscopy (SEM) measurements. (SEM). Morphologies of ferrocene micro patterns were analyzed by SEM. Measurements were performed at room temperature with a scanning Auger electron spectroscope system (JEOL Ltd. JAMP-9500F field emission scanning Auger microprobe), with an acceleration voltage of 0.8 kV.

Preparation of phosphonic acid monolayers. 2×1 cm Al slides were sonicated in hexane for 15 min followed by wiping with lint–free cotton swabs (Texwipe, NC, USA) to remove the polymer protection layer on top and remove any residual glue. The surfaces were chemically activated by immersion in 1:1 (v/v) 37% HCl–MeOH mixture for 5 min, followed by washing with copious amounts of water and 2–propanol. The activated surfaces were then immersed into N_2 filled vials of a mixture of 1.5 and 0.5 mM solution of 3:1 ratio of phosphonic acid derivatives (octylphosphonic acid:12–aminododecylphosphonic acid hydrochloride salt for M_1 and octylphosphonic acid:12–bromododecylphosphonic acid for M_4 surfaces) in 2–propanol, heated to 50 °C for 5 min, and then left undisturbed for 5 h at room temperature to obtain self–assembled mixed monolayers.[2] The surfaces were taken out and sonicated successively for 5 min with 2–propanol, acetone and

dichloromethane. The surfaces were finally cleaned with dichloromethane, air dried and used immediately for further reactions.

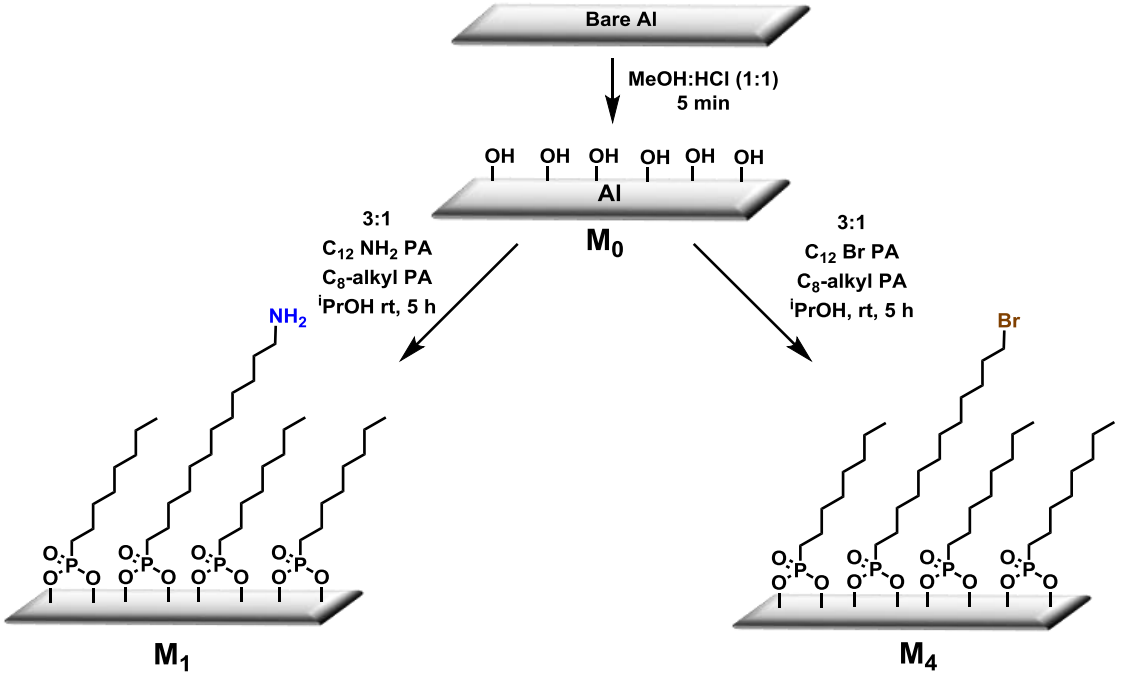

Preparation of di–ESF terminated monolayers (M_2). Amine–terminated surfaces (M_1) were stirred with 50 mM ethenesulfonylfluoride (ESF) solution in MeOH for 16 h at 50 °C h to yield M_2 surfaces. The samples were sonicated and washed with copious amounts of methanol, dried and stored under nitrogen atmosphere.

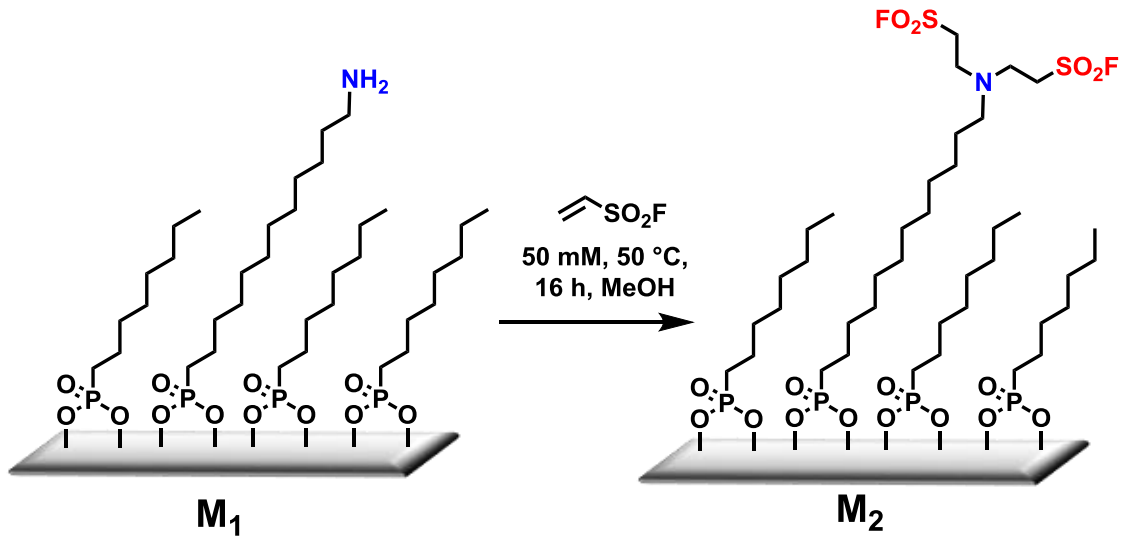

Preparation of propargyl-terminated monolayers (M_5). Bromo–terminated surfaces (M_4) were stirred with 50 mM of propargylamine in methanol for 16 h at 60 °C to yield propargyl surfaces (M_5). The samples were sonicated and washed with copious amounts of methanol, dried and stored under nitrogen atmosphere.

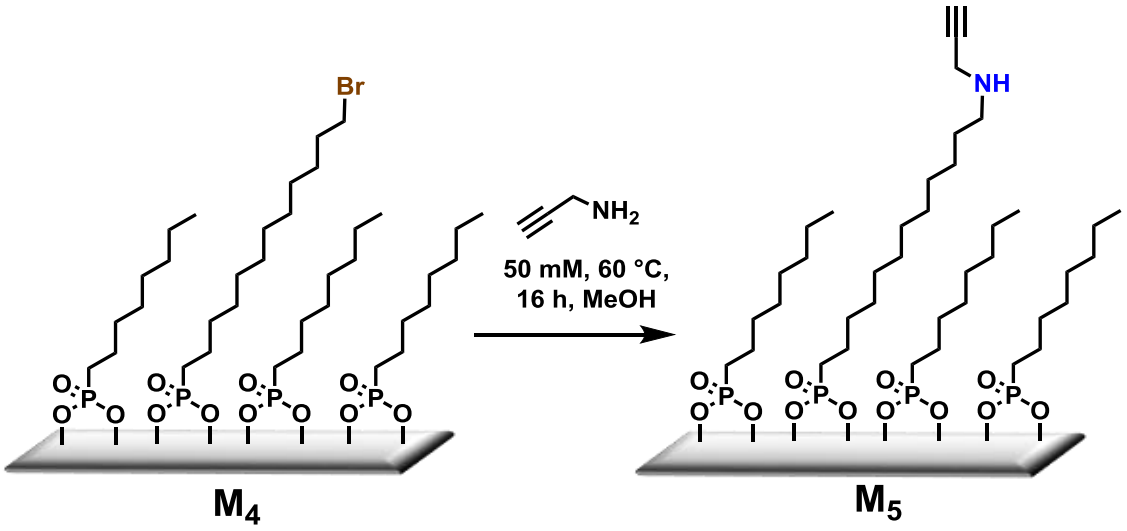

Preparation of mono–ESF-terminated monolayers (M_6). Propargyl–terminated surfaces (M_5) were stirred with 50 mM ethenesulfonylfluoride (ESF) solution in MeOH for 16 h at 50 °C h to yield M_6 surfaces. The samples were sonicated and washed with copious amounts of methanol, dried and stored under nitrogen atmosphere.

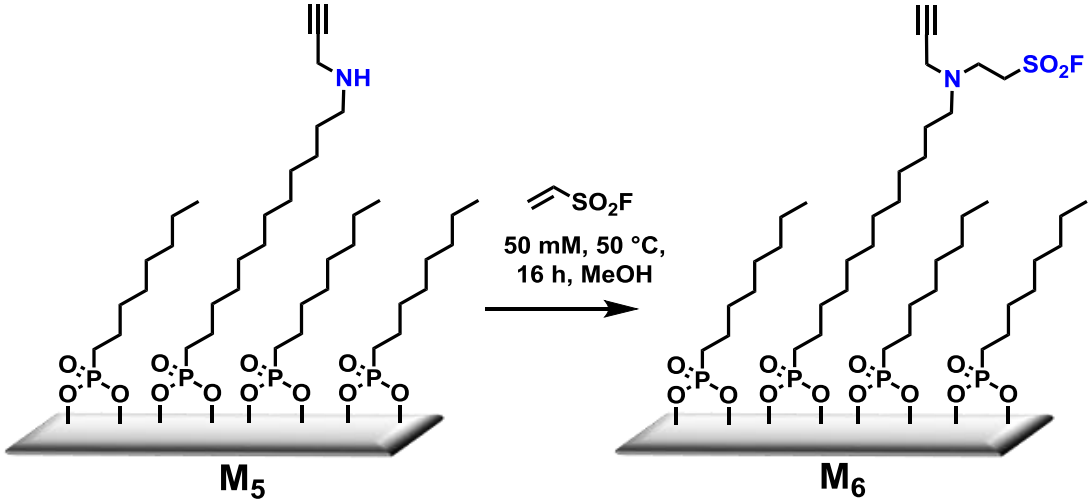

General method for SuFEx reaction on surface: The R-SO_2F terminated surfaces (M_2 and M_6) were reacted with a 5 mM solution of 4–iodobenzylamine (IBZ) and 0.5 mM triazabicyclodecene (TBD) in methanol at 30 °C for 2 h and 6 h, respectively. The reaction was stirred at a constant speed using a magnetic bead and stirrer and all samples were loaded in a specially constructed Teflon holder to ensure rigorous reproducibility between samples. Samples were immersed into the solution for a set period of reaction time and immediately taken out and washed with copious amounts of methanol. The samples were further sonicated in methanol to remove any physisorbed species for 15 min, dried under a dry nitrogen stream and stored for further analysis in a sealed vial.

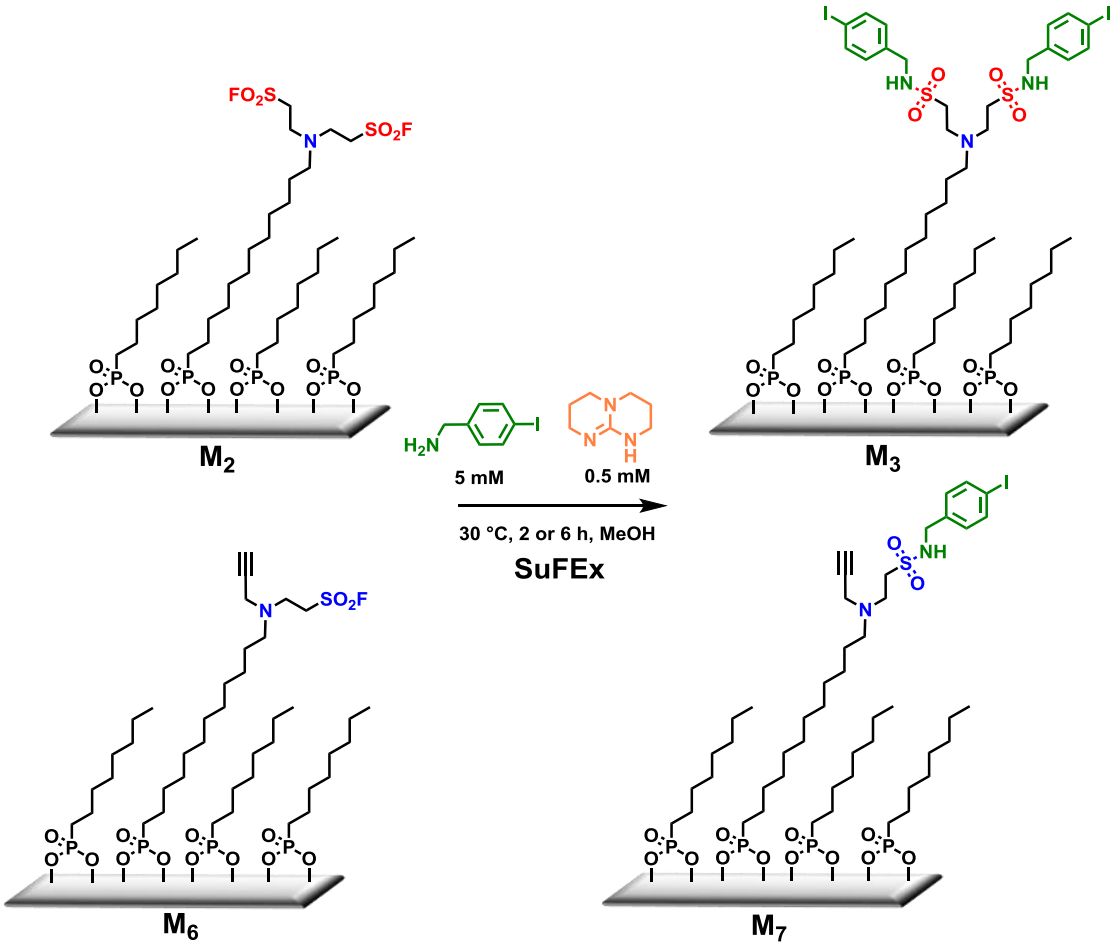

General method for CuAAC reaction on M_6 surfaces with 4: Mono–ESF-terminated surfaces (M_6) were reacted with a 5 mM solution of 4 and 50 µM copper(I) iodide in DMF at 30 C for 16 h.. The samples were sonicated for 15

min and washed with copious amounts of DMF, followed by MQ water, dried and stored under nitrogen atmosphere.

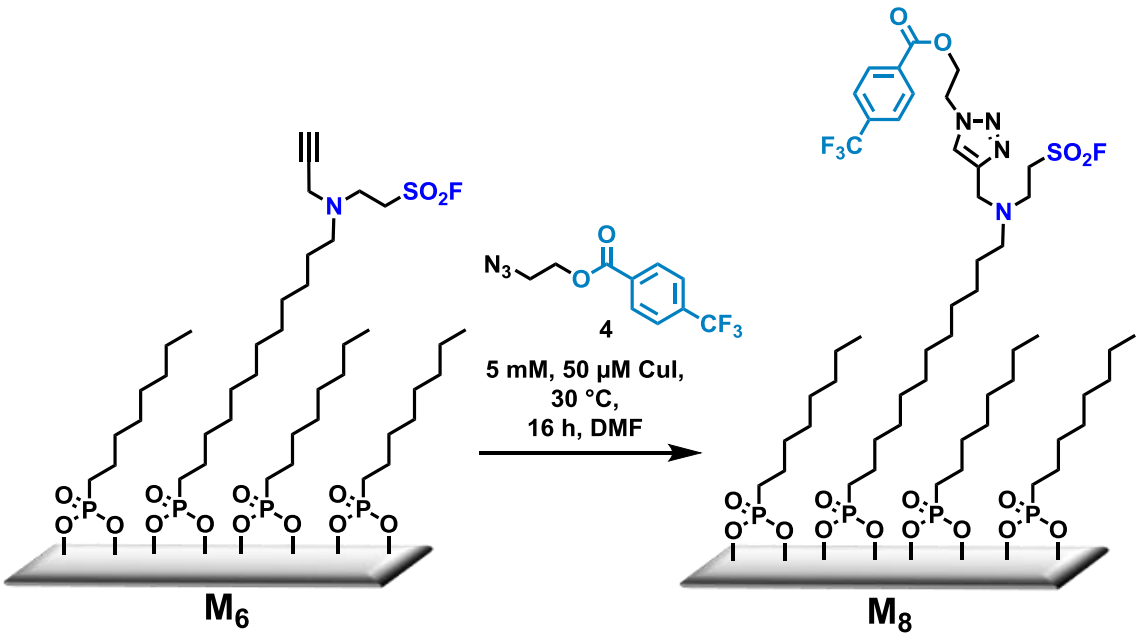

Preparation of ferrocene terminated surfaces (M_{12}). For aminoferrocene attachment, M_8 surfaces were reacted with a 5 mM solution of aminoferrocene and 0.5 mM triazabicyclodecene (TBD) in methanol at 30 °C for 16 h. The reaction was stirred at a constant speed using a magnetic bead and stirrer. Samples were immediately taken out after 16 h and washed with copious amounts of methanol. The samples were further sonicated in methanol to remove any physisorbed species for 15 min, dried under a dry nitrogen stream and stored for further analysis in a sealed vial. For microarray preparation, the reactant solution was adsorbed onto a PDMS stamp and placed onto M_8 surfaces for 5 h. The surfaces were gently rinsed with methanol and dried under argon followed by SEM analysis.

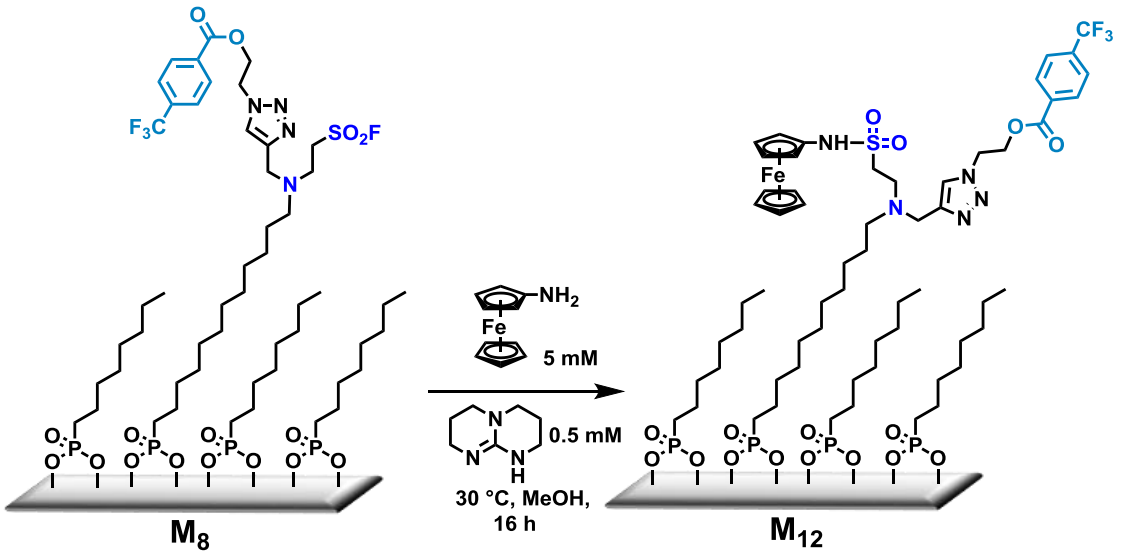

Preparation of quinone-terminated monolayers (M_9). Bromo–terminated surfaces (M_4) were stirred with 50 mM solution of 3,4 dihydroxybenzylamine hydrobromide and 50 mM triethylamine in methanol for 1 h at 30 °C to yield catechol terminated surfaces. The samples were sonicated and washed with copious amounts of methanol and then stirred with a 50 mM solution of sodium metaperiodate in MQ water for 30 min followed by sonication in water for 20 min to yield quinone terminated surfaces (M_9). The samples were then dried and stored under nitrogen atmosphere.

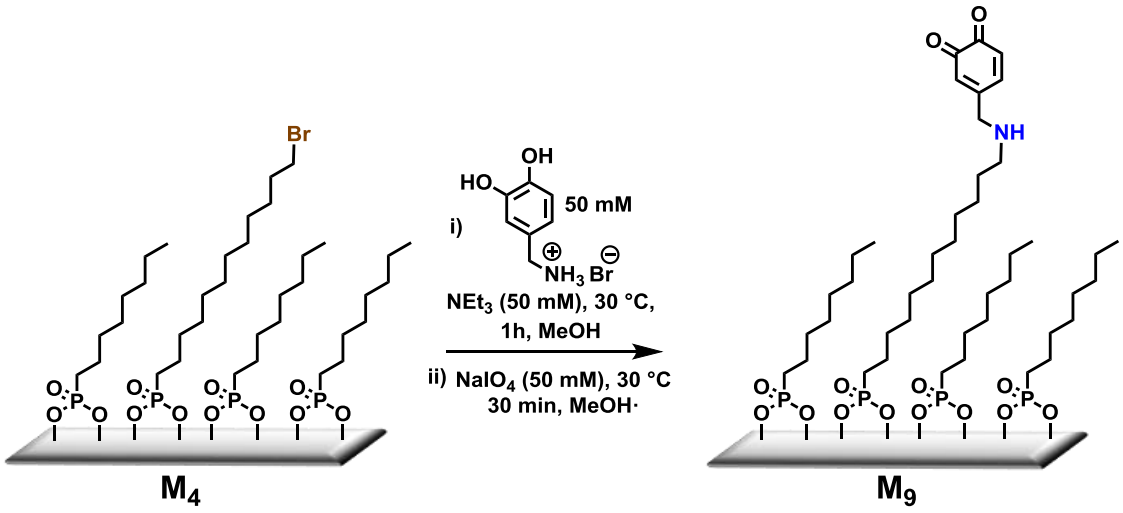

Preparation of quinone–ESF-terminated monolayers (M_{10}). Quinone-terminated surfaces (M_9) were stirred with 50 mM ethenesulfonylfluoride (ESF) solution in MeOH for 16 h at 50 °C to yield M_{10} surfaces. The samples were

sonicated and washed with copious amounts of methanol, dried and stored under nitrogen atmosphere.

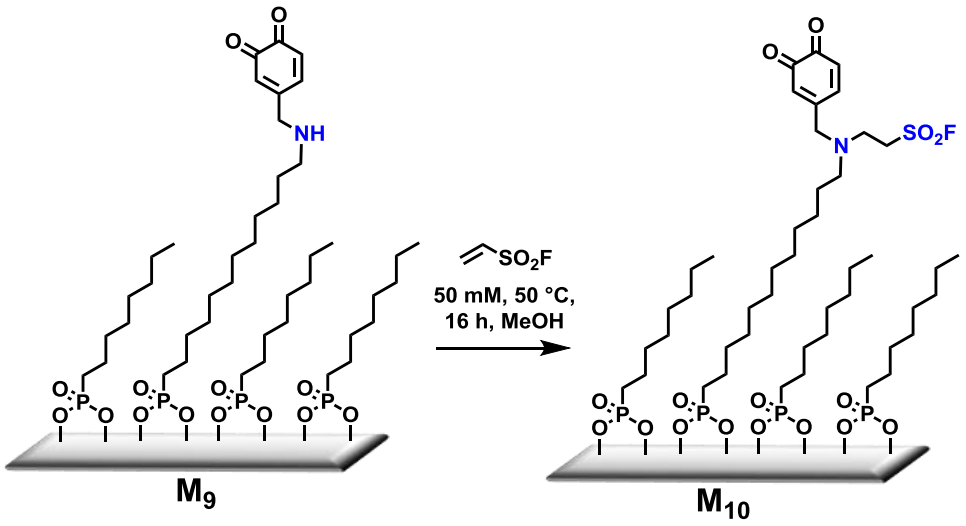

General method for SPOCQ reaction on M_{10} surfaces with 5: Quinone–ESF terminated surfaces (M_{10}) were reacted with a 3 mM solution of 5 in DCE at 30 °C for 5 h. The samples were sonicated for 15 min and washed with copious amounts of DCM, dried and stored under nitrogen atmosphere.

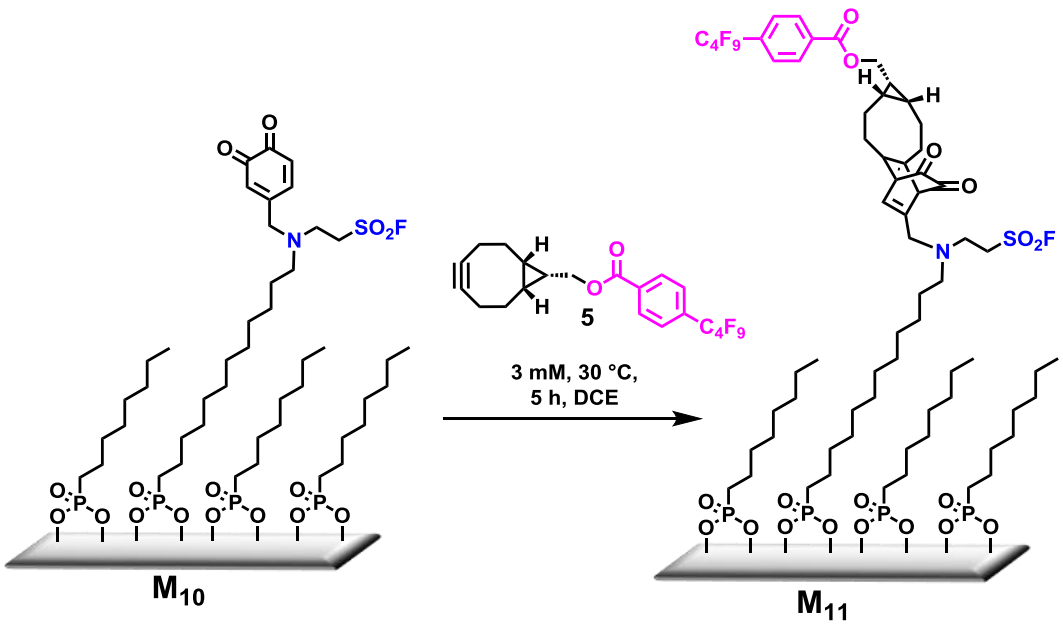

Rate constant determination. Equation S1 describes the second–order kinetics for the studied reaction (mol·cm^{-2}·s^{-1}), where Γ_S is the density of SO_2F groups on the surface (mol·cm^{-2}) and k_2 is the second–order rate constant (M^{-1}s^{-1}). Since, the amount of 4–iodobenzylamine (IBZ, 5 mM) is in very large excess compared to the amount of surficial SO_2F (Γ_S = ~ 6 pmol·cm^{-2}), it can be assumed to be essentially constant throughout the entire kinetics experiment. Thus, the interfacial SuFEx reaction can be reduced to pseudo–first order kinetics, with rate constant, k′. Therefore, the resulting pseudo first–order rate constant (k′) can be obtained from the slope of the plots of ln [($I_\infty - I_t$)/($I_\infty - I_0$)] versus time, as shown in equation S3. Based on this pseudo–first order rate constant, the corresponding second–order rate constant k_2 can subsequently be calculated from equations S4, S5 and S6.

$$v = k_2\left[IBZ_{(soln)}\right]\Gamma_S = \frac{d\Gamma_S}{dt} \quad \text{(S1)}$$

$$v = k'\Gamma_S \ (\text{since}, \left[IBZ_{(soln)}\right] \gg \Gamma_S) \quad \text{(S2)}$$

$$\ln\left(\frac{I_\infty - I_t}{I_\infty - I_0}\right) = k't \quad \text{(S3)}$$

$$k'(s^{-1}) = k_2(M^{-1}s^{-1})\left[IBZ_{(soln)}\ (M)\right] \quad \text{(S4)}$$

$$k_2(M^{-1}s^{-1}) = k'/\left[IBZ_{(soln)}\right] \quad \text{(S5)}$$

$$k_2(M^{-1}s^{-1}) = \frac{k'}{5*10^{-3}} \quad \text{(S6)}$$

2. CHEMICAL SYNTHESIS

2.1 General Remarks. Unless stated otherwise, solvents like dichloromethane, methanol, acetonitrile and 2–propanol were purchased from Sigma–Aldrich. Unless stated otherwise all of these chemicals were used without further purification.

2.2. Reaction Handling. Unless stated otherwise all non–aqueous reactions were performed in dried glassware under an atmosphere of argon. All flasks were equipped with rubber septa and reactants were handled using standard Schlenk techniques. Temperatures above the room temperature refer to oil bath temperatures which were controlled by a thermostat. Reactions were magnetically stirred.

2.3. ^{1}H–NMR spectra were recorded at room temperature on a Bruker–400 spectrometer and Bruker–600 spectrometer with ^{1}H operating frequency of 400 MHz and 600 MHz respectively. Unless stated otherwise all spectra were recorded at room temperature in $CDCl_3$ and all chemical shifts are given in δ units relative to the residual solvent [central line of singlet: δ_H = 7.27 ppm ($CDCl_3$)]. Analysis followed first order and the following abbreviations were used throughout: s = singlet, br. s. = broad singlet, d = doublet, t = triplet, q = quartet, quin = quintet, sxt = sextet, sept = spt, dd = doublet of doublet, dt = doublet of triplet, ddd = doblet of doublet of doublet, ddt = doblet of doublet of triplet, m = multiplet, mc = centred multiplet. Coupling constants (J) are given in Hertz (Hz).

2.4. ^{13}C–NMR spectra were recorded at room temperature on a Bruker–400 spectrometer and Bruker–600 spectrometer with ^{13}C operating frequency of 101 MHz and 151 MHz, respectively. Unless stated otherwise all spectra were recorded at room temperature in $CDCl_3$ and all chemical shifts are given in δ units relative to the residual solvent [central line of triplet: δ_C = 77.2 ppm ($CDCl_3$)]. The following abbreviation was used throughout: s = singlet, d = doublet, dd = doublet

of doublet. If no coupling constants are given, the multiplicity refers to ^{1}H–decoupled spectra.

2.5 Synthesis of 1 and 2. Compounds 1 and 2 were prepared according to previously published work.[3]

2.6 Synthesis of phenyl 2-((4-(trifluoromethyl)phenyl)amino)ethane-1-sulfonate, 3.

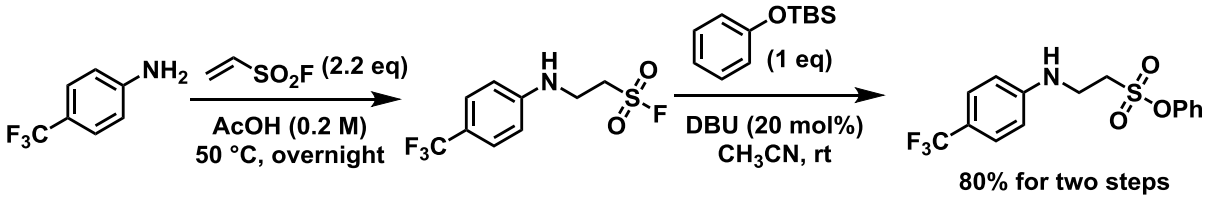

Step 1: A 20-mL vial equipped with a stir bar was charged with 4-trifluoromethylaniline (161.1 mg, 1.000 mmol), and ethenesulfonyl fluoride (242.2 mg, 2.2 mmol, 2.2 equiv). Into the vial, glacial acetic acid (5 mL, 0.2 M for aniline) was added. The mixture was stirred as a yellow solution in an external oil bath (50 °C) overnight, then concentrated *in vacuo* to give a yellow solid. The crude product was virtually pure (>90% purity, containing ca. 8% bis-ESF adduct), and it was used in the second step without purification. For the major product (mono-ESF adduct): ^{1}H NMR (600 MHz, $CDCl_3$) δ 7.47 (d, J = 8.4 Hz, 2H), 6.66 (d, J = 8.5 Hz, 2H), 4.43 (s, 1H), 3.87 (m, 2H), 3.65 (m, 2H). ^{13}C NMR (151 MHz, $CDCl_3$) δ 148.4, 127.2 (q, J = 3.8 Hz), 124.7 (q, J = 270.6 Hz), 120.9 (q, J = 32.8 Hz), 49.9 (d, J = 14.5 Hz), 37.8. ^{19}F NMR (376 MHz, $CDCl_3$) 56.8, -61.9. Thin-layer chromatography R_f = 0.28 (25% ethyl acetate in hexanes, UV and $KMnO_4$ stain). Mass spectroscopy (ESI-Q) Calc'd for $C_9H_{10}F_4NO_2S$ $[M + H]^+$ 272.04, found 272.0.

Step 2: A 20-mL vial equipped with a stir bar was charged the crude sulfonyl fluoride, and phenyl silyl ether (208.4 mg, 1.000 mmol, 1.0 equiv). Anhydrous CH_3CN (5.0 mL, 0.2 M for substrate), and 1,8-diazabicyclo(5.4.0)undec-7-ene (DBU, 30.4 mg, 0.200 mmol, 20 mol%) were added. The mixture was stirred at

room temperature overnight until the completion of the reaction (HPLC). Volatiles were removed under reduced pressure and the crude product was purified by flash column chromatography on silica gel (eluted by 10% to 25% ethyl acetate in hexanes) to give the title compound as a white crystalline (283.1 mg, 0.7990 mmol, 80% yield for two steps). ^{1}H NMR (600 MHz, $CDCl_3$) δ 7.45 (d, J = 8.5 Hz, 2H), 7.43 – 7.38 (m, 2H), 7.36 – 7.31 (m, 1H), 7.25 – 7.19 (m, 2H), 6.65 (d, J = 8.5 Hz, 2H), 4.56 (t, J = 6.1 Hz, 1H), 3.85 (q, J = 6.4 Hz, 2H), 3.52 (m , 2H). ^{13}C NMR (151 MHz, $CDCl_3$) δ 149.0, 130.3, 127.7, 127.1 (q, J = 3.8 Hz), 124.8 (q, J = 270.6 Hz), 122.0, 120.4 (q, J = 32.7 Hz), 112.4, 49.3, 38.1. ^{19}F NMR (376 MHz, $CDCl_3$) δ -61.8. Thin-layer chromatography R_f = 0.30 (25% ethyl acetate in hexanes, UV and $KMnO_4$ stain). Mass-spectroscopy (ESI-Q) Calc'd for $C_{15}H_{15}F_3NO_3S$ $[M + H]^+$ 346.07, found 346.0. Melting point 92 – 94 °C.

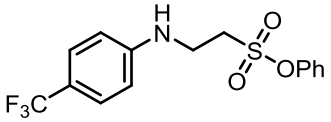

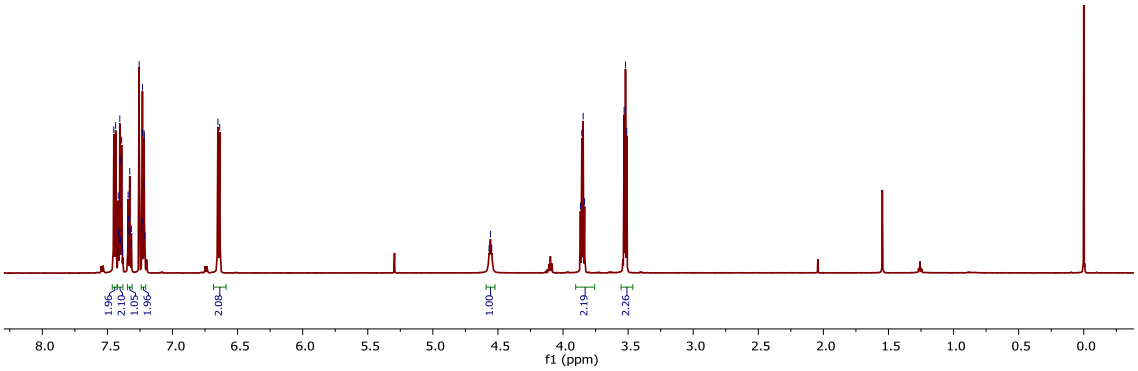

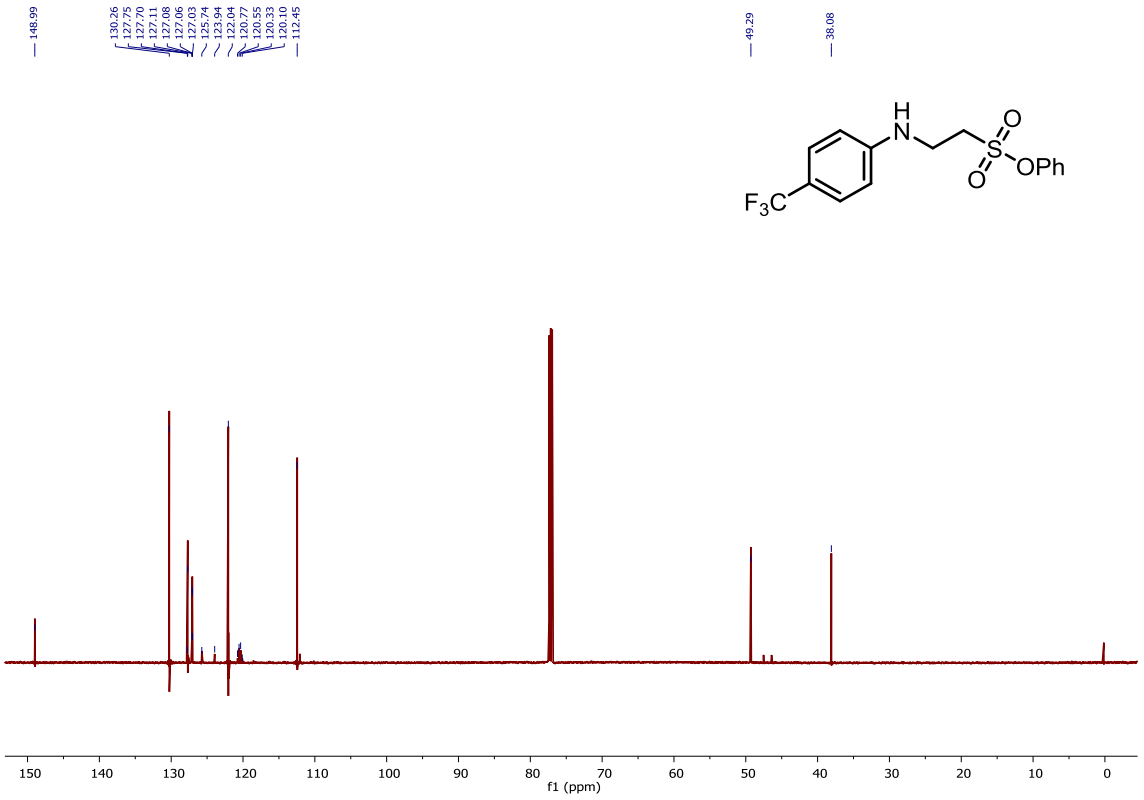
148.99
130.26
127.75
127.70
127.11
127.08
127.06
127.03
125.74
123.94
122.04
120.77
120.55
120.33
120.10
112.45
49.29
38.08
H
N
O
S
O
OPh
F3C
150
140
130
120
110
100
90
80
70
60
50
40
30
20
10
0
f1 (ppm)

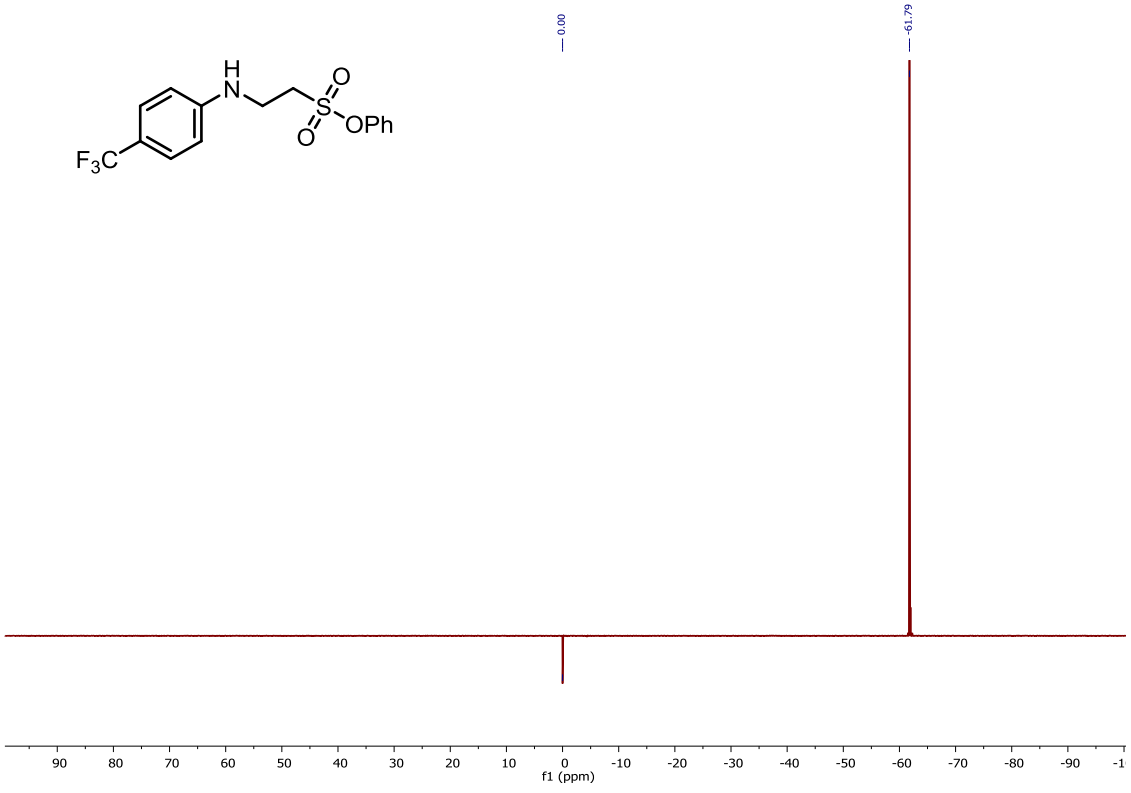
0.00
-61.79
H
N
O
S
O
OPh
F3C
90
80
70
60
50
40
30
20
10
0
-10
-20
-30
-40
-50
-60
-70
-80
-90
f1 (ppm)

2.7 Synthesis of 2–azidoethanol from 2–bromoethanol.

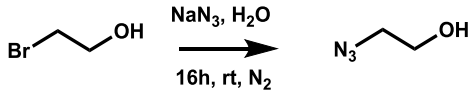

Sodium azide (15.6 g, 0.24 mol) was dissolved in 100mL milliQ water, followed by the addition of 5.67 mL of 2–bromoethanol (10 g, 0.08 mol). The mixture was heated at 80 °C overnight under N_2 flow, during which the color changed from yellow to orange. The product was extracted four times with 75 mL diethyl ether. The combined organic fractions were dried and evaporated under reduced pressure. The product was obtained as a clear oil. Yield: 54 %. The ^{1}H–NMR spectrum was in accordance with literature values (Giorgio *et al*. Molecular Pharmaceutics 2013, *10* (3), 975–978). ^{1}H–NMR (400 MHz, $CDCl_3$) δ 3.75 (m, 2H), 3.42 (t, J = 5.0 Hz, 2H), 2.66 (s, 1H).

2.8. Synthesis of 2–azidoethyl 4–(trifluoromethyl)benzoate, 4.

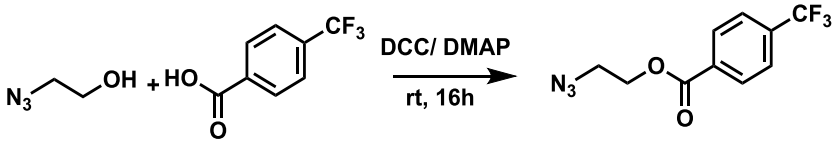

4–(Trifluoromethyl)benzoic acid (13.0 g, 68.8 mmol) was transferred to a three-necked round bottom flask (100 mL) dicyclohexylcarbodiimide (DCC) (13.60 g, 66.02 mmol) and 4–dimethylaminopyridine (DMAP) (4.00 g, 33.33 mmol) dissolved in 100 mL DCM were added to the flask. The reaction mixture was stirred for 30 min before adding 2–azidoethanol (6.66 g, 65.55 mmol). The final reaction mixture was left stirring overnight at room temperature. The reaction mixture was then filtered and evaporated under reduced pressure, forming a yellow oil. The crude product was purified by column chromatography 10:90 ethyl acetate : hexane as solvent. Yield: 35%. ^{1}H–NMR (400 Hz, $CDCl_3$) δ 8.19 (d, J = 8.4 Hz, 2H), 7.74 (d, J = 8.0 Hz, 2H), 4.54 (t, J = 5.2 Hz, 2H), 3.63 (t, J = 5.2 Hz, 2H). ^{13}C–NMR (101 Hz, $CDCl_3$) δ 165.02, 135.27, 132.74, 130.15, 127.64, 125.47, 64.09, 49.85.

3. SUPPLEMENTARY KINETICS DATA.

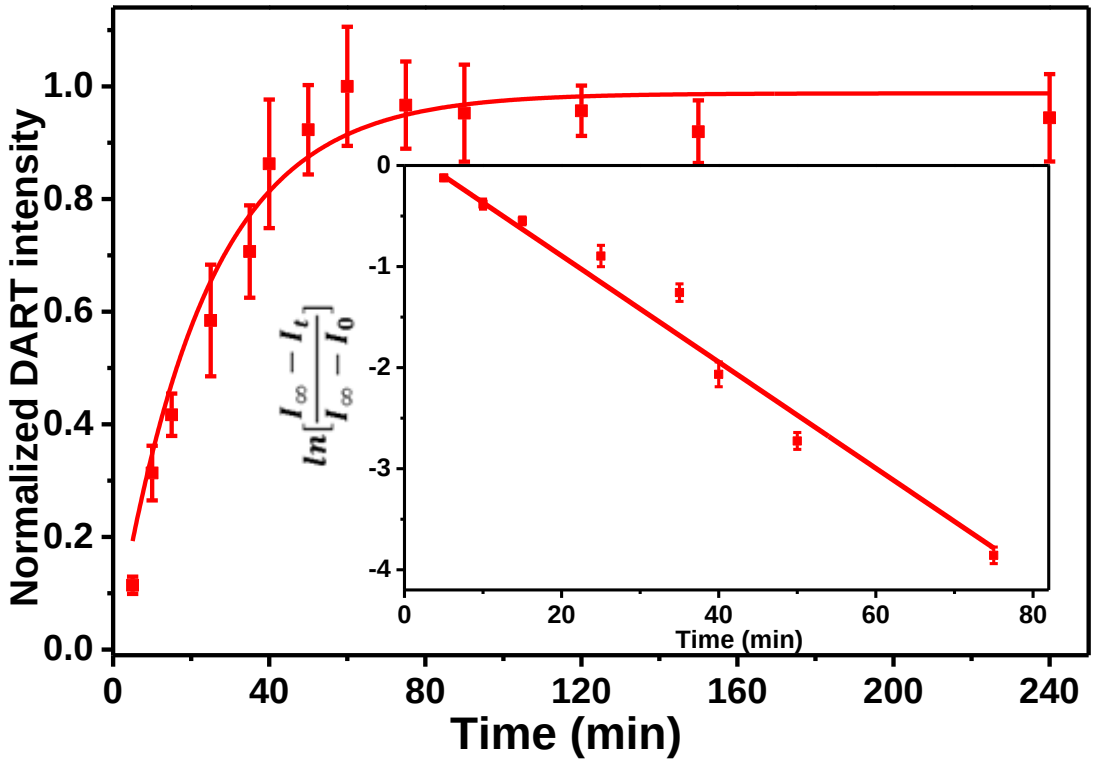

Figure S3.1. Sigmoidal plot of normalized integrated DART–HRMS intensity *vs* time (min) for di–ESF-terminated surfaces (M_2) reacting with 4–iodobenzylamine at 30 °C. Inset: Linear plot of $ln\,|(I_\infty - I_t)\,/\,(I_\infty - I_0)|$ *vs* time (min), the slope of which is the pseudo—first order reaction rate (k′) obtained by a least–squares fit ($R^2 > 0.95$). (Each time point is an average of hexaplet samples.) The second-order rate constant is derived from here using the concentration of the other agent (typically ~ 5 mM, but precisely determined to 2 digits precision (e.g. 5.0 mM) in each case).

4. SUPPLEMENTARY FIGURES.

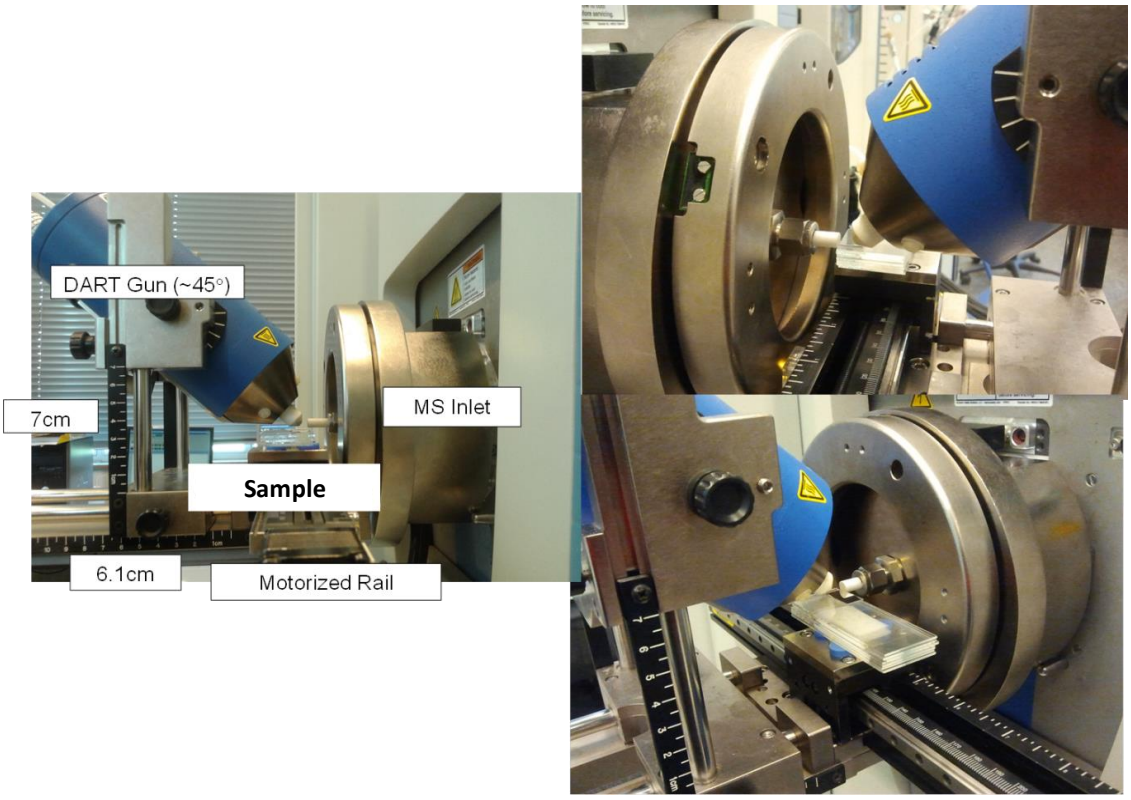

Figure S4.1. Pictures of DART setup for the kinetic analysis of organic surface reactions.

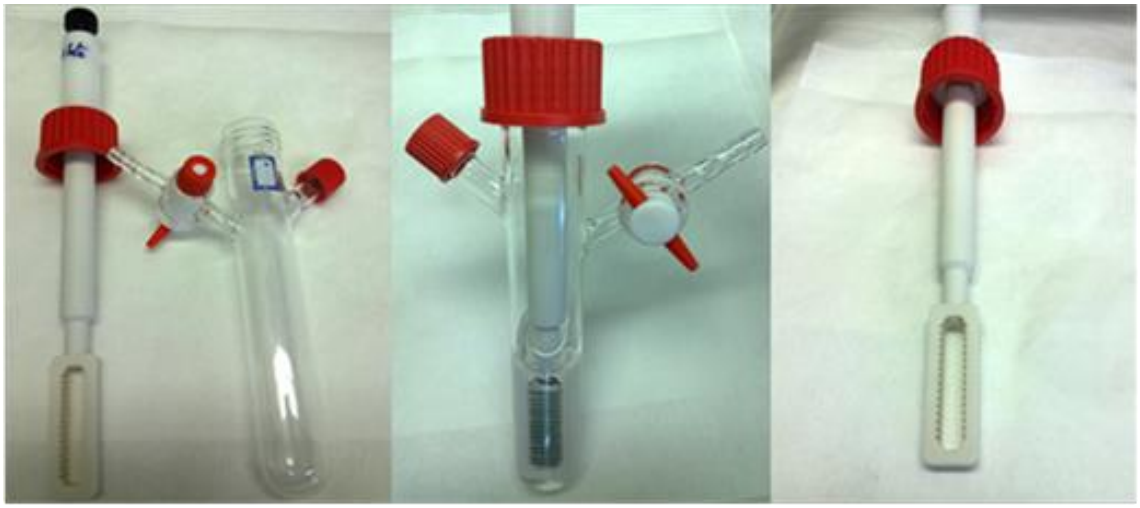

Figure S4.2. Image of the sample holder (16 slots).

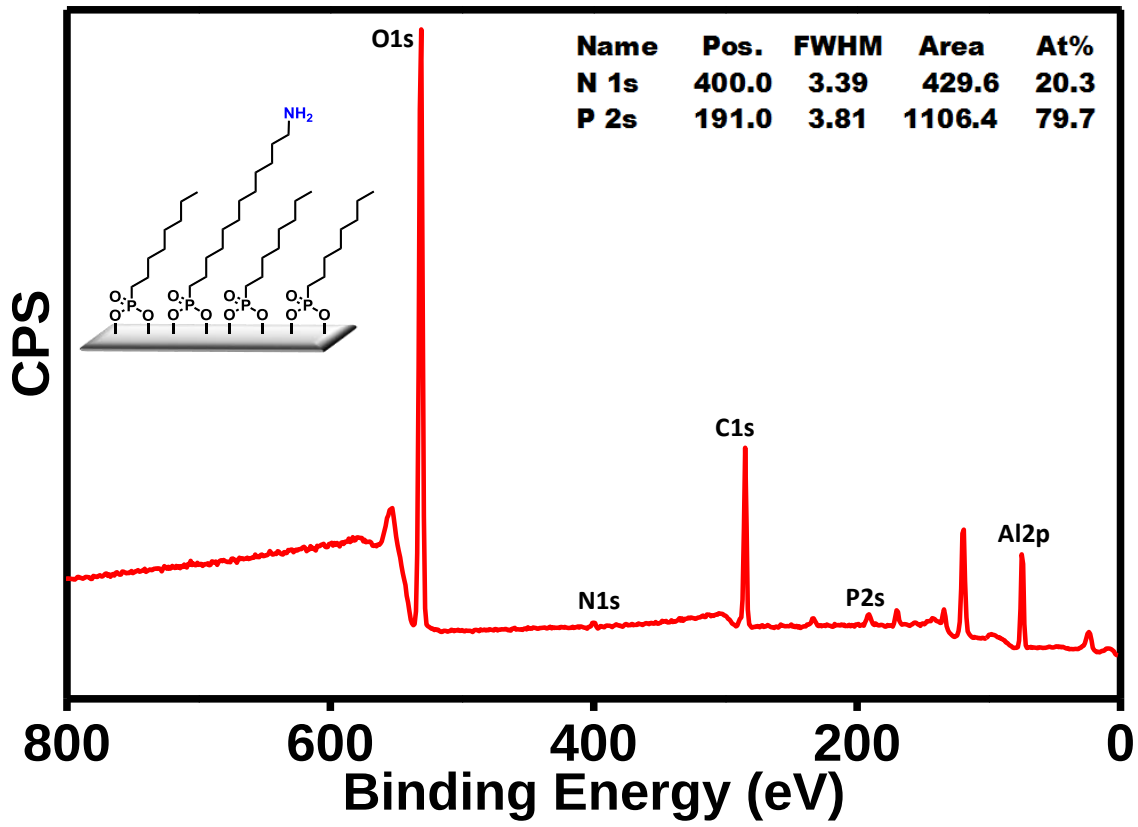

Figure S4.3. XPS wide scan of M_1 modified Al surfaces.

Theoretical N/P ratio = 1/4 = 0.25

Experimental N/P = 0.25 ± 0.02 ⇒ 3:1 monolayers.

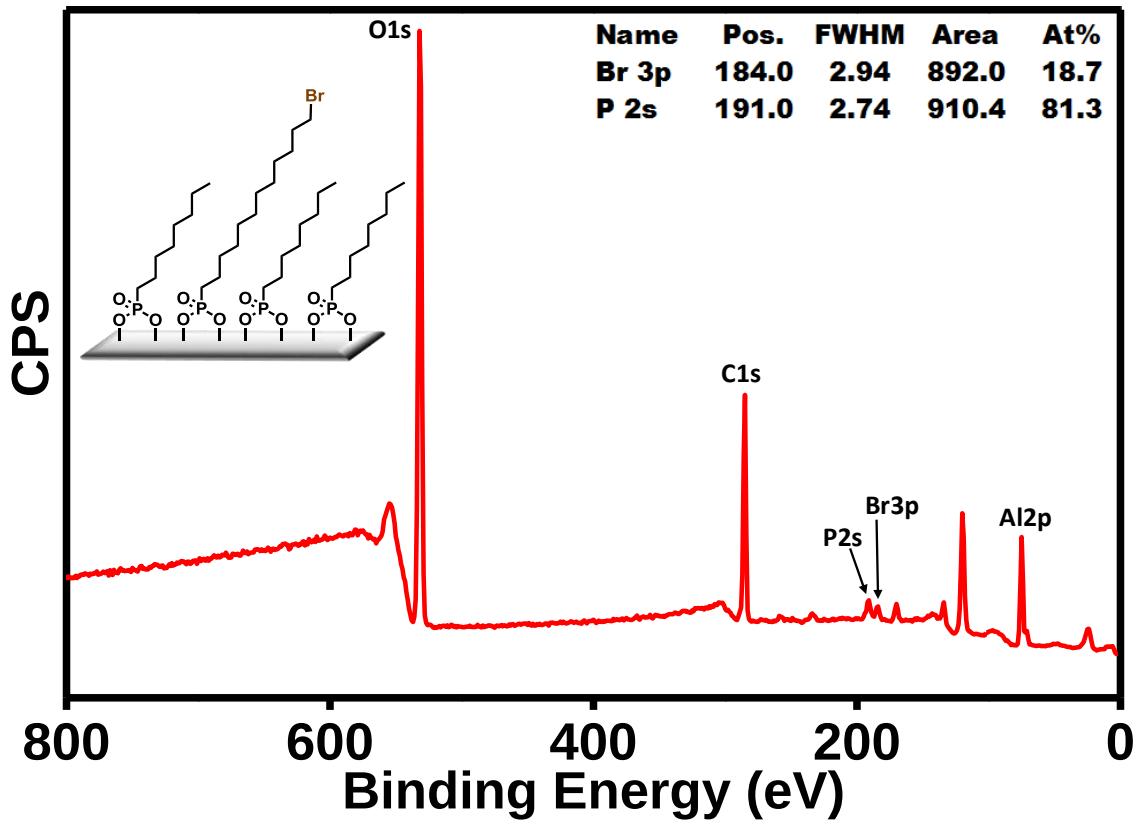

Figure S4.4. XPS wide scan of M_4 modified Al surfaces.

Theoretical Br/P ratio = 1/4 = 0.25

Experimental N/P = 0.23 ± 0.01 ⇒ 3:1 monolayers.

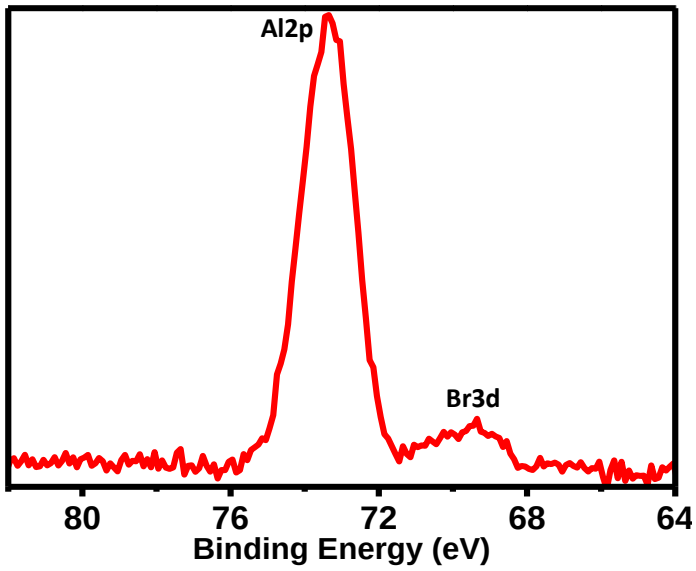

Figure S4.5. XPS Br3d narrow scan of M_4 modified Al surfaces.

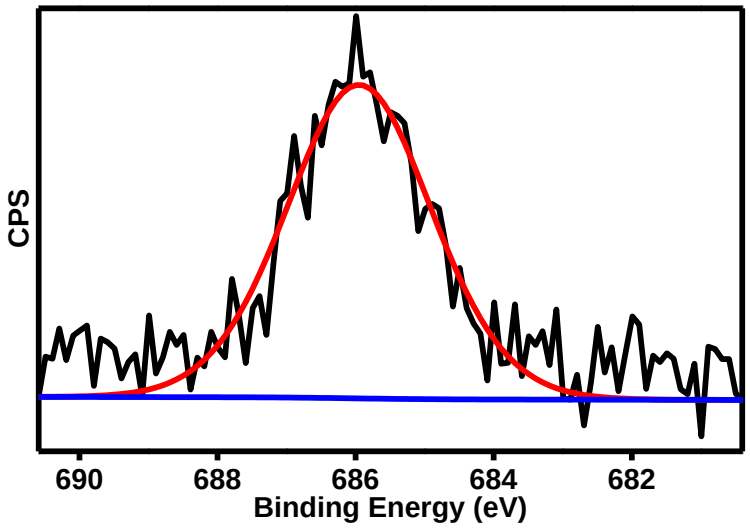

Figure S4.6. XPS F1s narrow scan of M_2 modified Al surfaces.

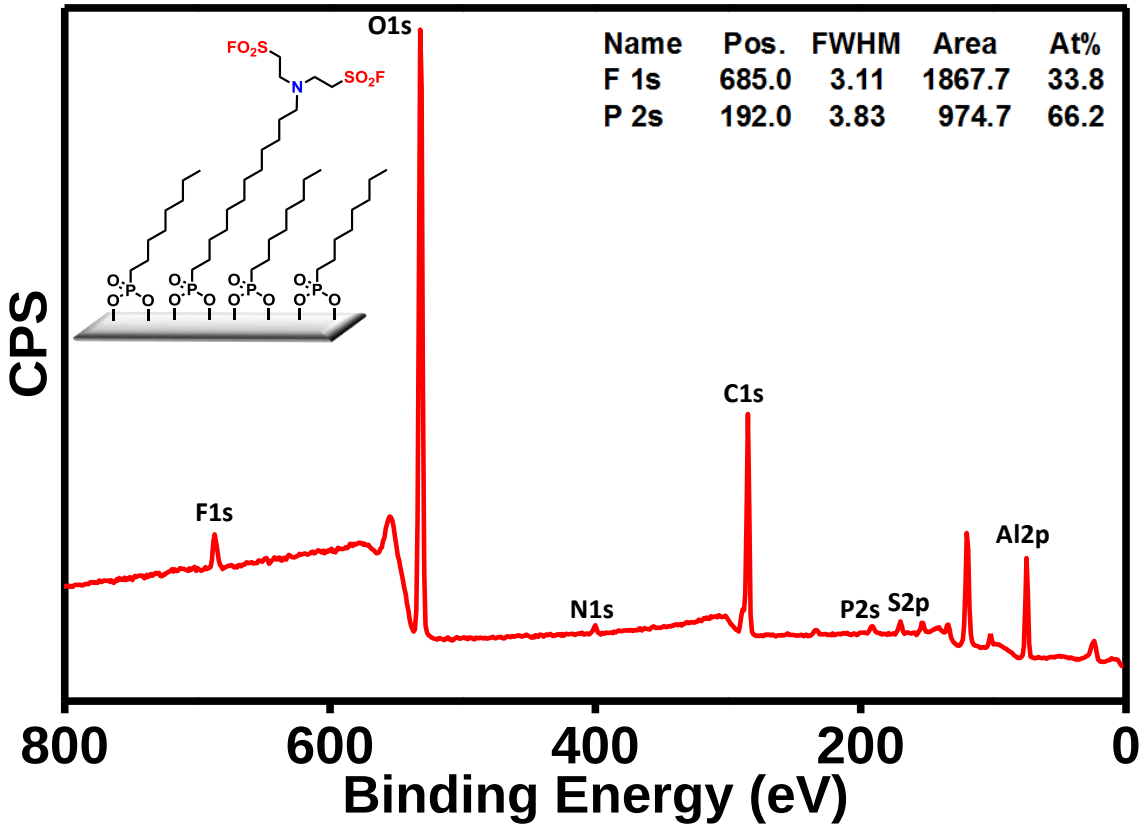

Figure S4.7. XPS wide scan of M_2 modified Al surfaces.

Theoretical F/P ratio = 2/4 = 0.50

Experimental F/P = 0.51 ± 0.02 ⇒ Quantitative surface yield.

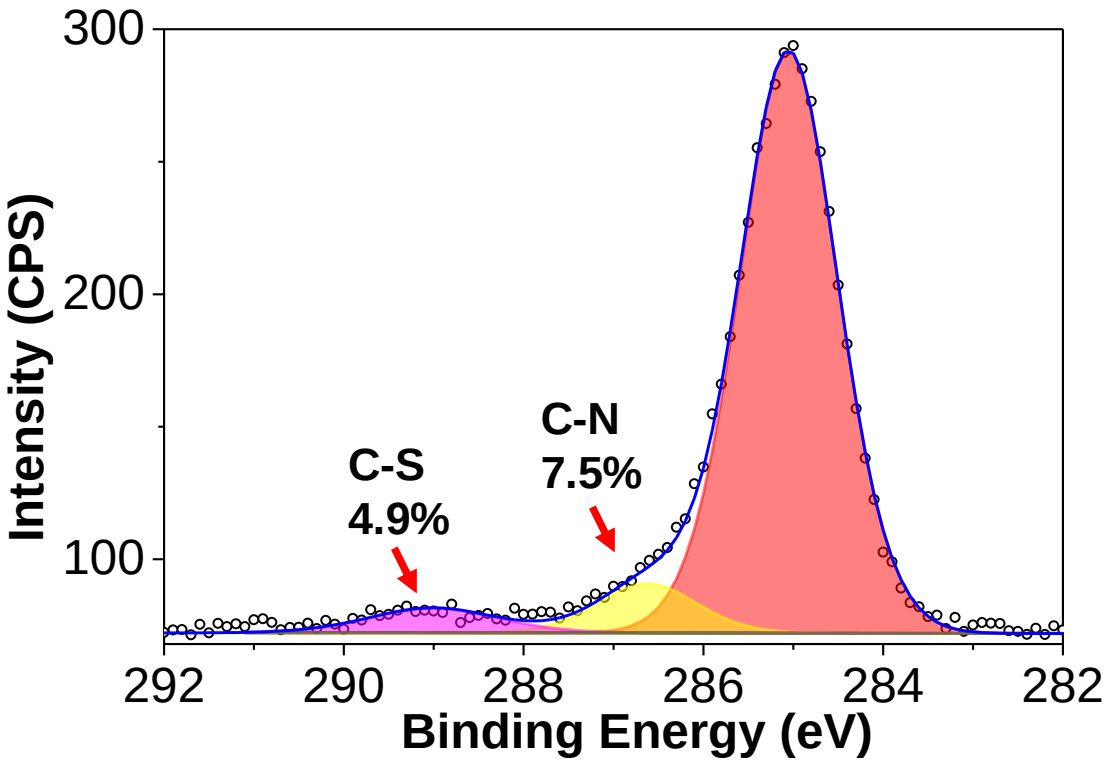

Figure S4.8. XPS C1s narrow scan of M_2 surfaces.

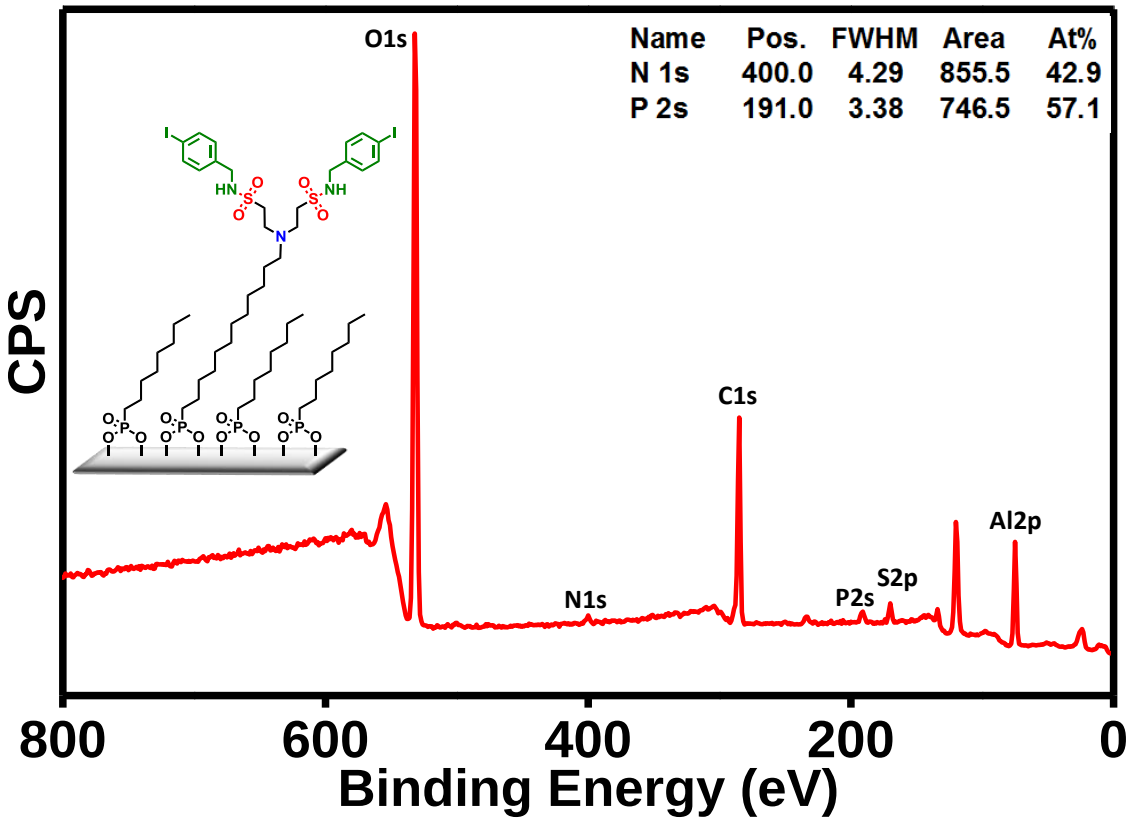

Figure S4.9. XPS wide scan of M_3 modified Al surfaces.

Theoretical N/P ratio = 3/4 = 0.75

Experimental N/P = 0.75 ± 0.01 ⇒ Quantitative surface yield.

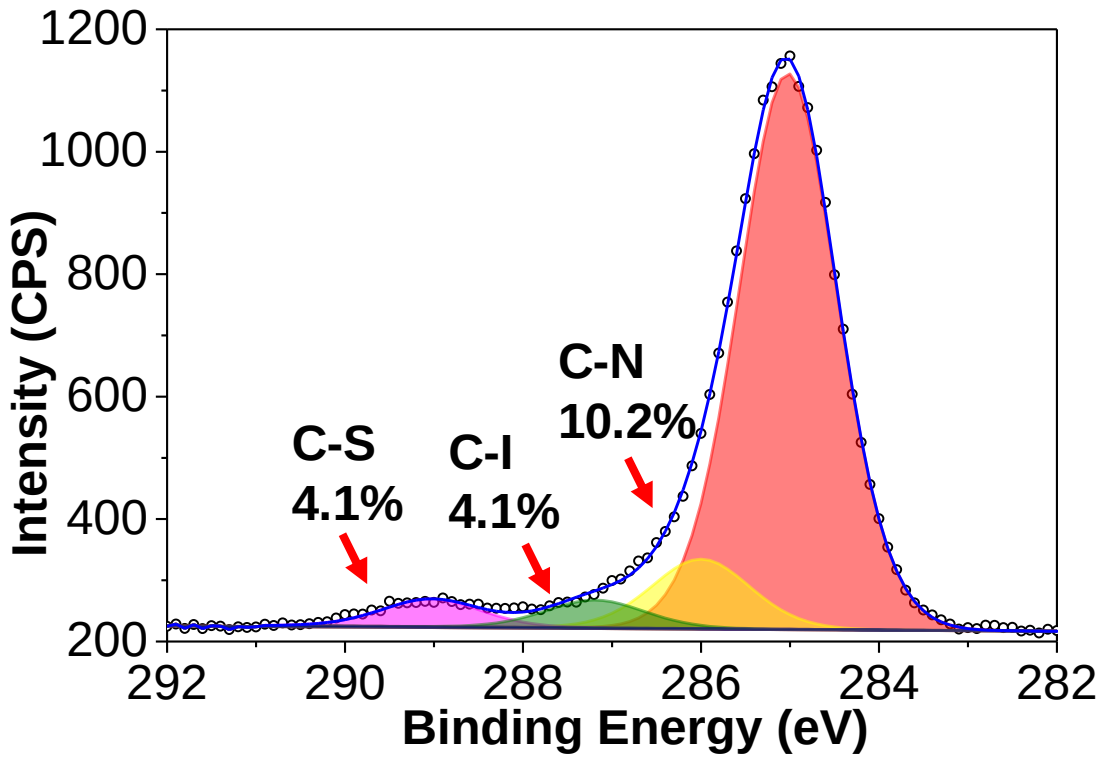

Figure S4.10. XPS C1s narrow scan of M_3 surfaces.

a)

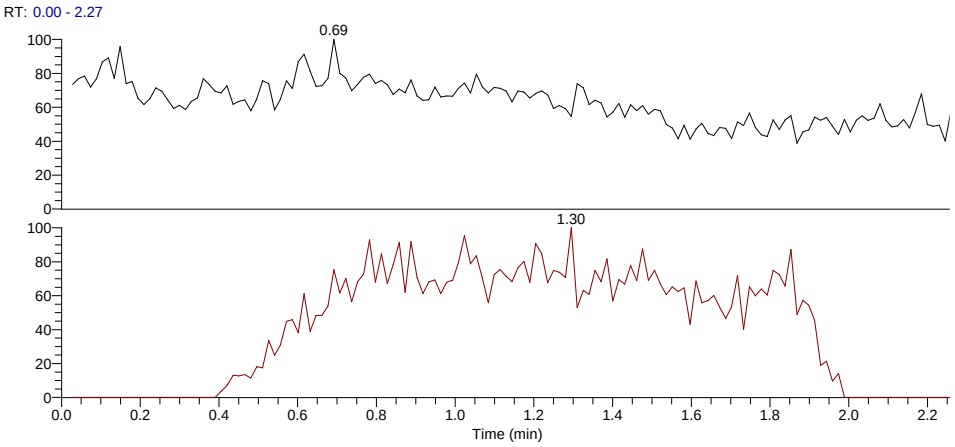

b)

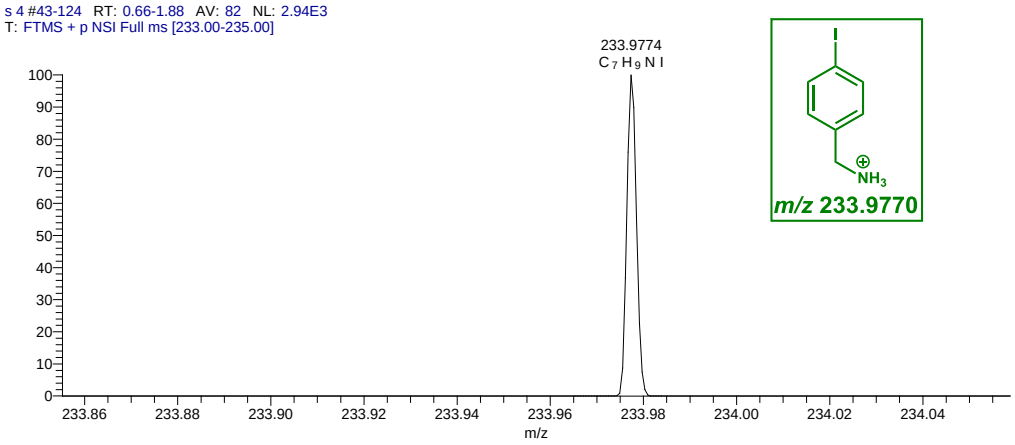

c)

Elemental composition search on mass 233.9774

m/z= 228.9774-238.9774

m/z	Theo. Mass	Delta (mmu)	RDB equiv.	Composition
233.9774	233.9774	0.02	3.5	C_7H_9NI
	233.9782	-0.72	10.5	$C_8O_6N_3$
	233.9755	1.96	6.0	$C_5H_2O_9N_2$
	233.9795	-2.06	10.0	$C_{10}H_2O_7$
	233.9747	2.70	-1.0	$C_4H_{11}O_3I$
	233.9741	3.30	6.5	$C_3O_8N_5$
	233.9734	4.04	-0.5	$C_2H_9O_2N_3I$
	233.9822	-4.74	14.5	$C_{13}O_4N$
	233.9721	5.39	0.0	H_7ON_6I
	233.9846	-7.19	-0.5	CH_9ON_5I

Figure S4.11. Representative DART ion intensity EIC of protonated 4–iodobenzylamine (IBZ). a) Top panel represents total ion current (TIC); bottom panel represents extracted ion chromatogram (EIC) (*m/z* window 10 mmu around

ion of interest). b) peak of ion of interest (*m/z* 233.9774) c) relative error between obtained *m/z* and theoretical *m/z* of ion of interest.

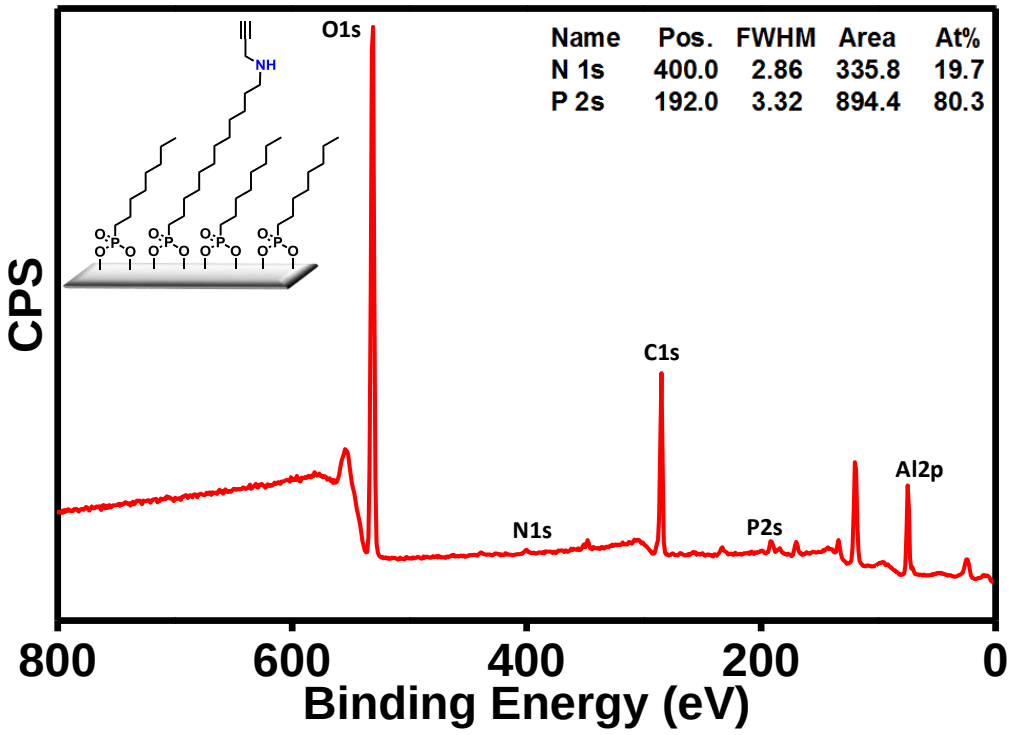

Figure S4.12. XPS wide scan of M_5 modified Al surfaces.

Theoretical N/P ratio = 1/4 = 0.25

Experimental N/P = 0.25 ± 0.02 ⇒ Quantitative surface yield.

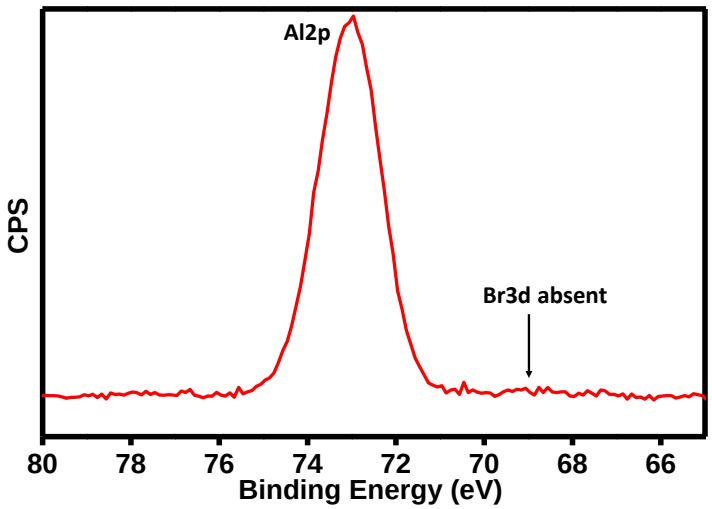

Figure S4.13. XPS Br3d narrow scan of M_5 modified Al surfaces.

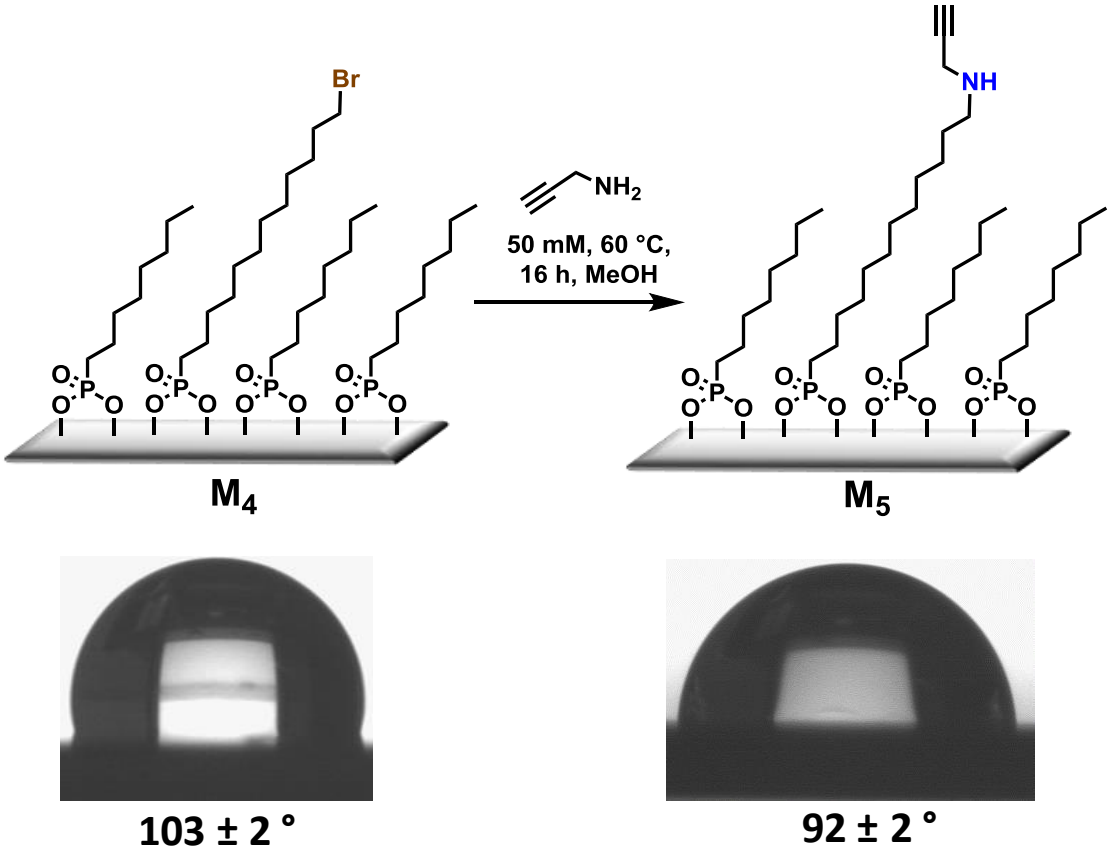

Figure S4.14. Water static contact angle (SCA) clearly shows drop of contact angle upon functionalization with propargylamine starting from M_4 surfaces.

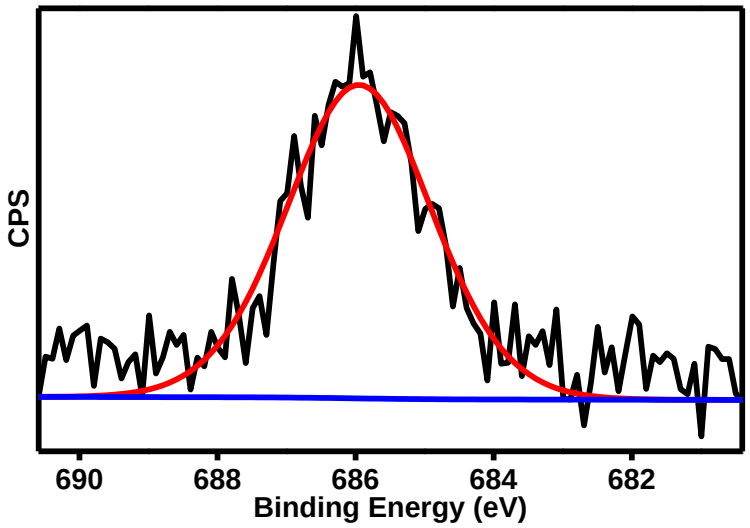

Figure S4.15. XPS F1s narrow scan of M_8 modified Al surfaces.

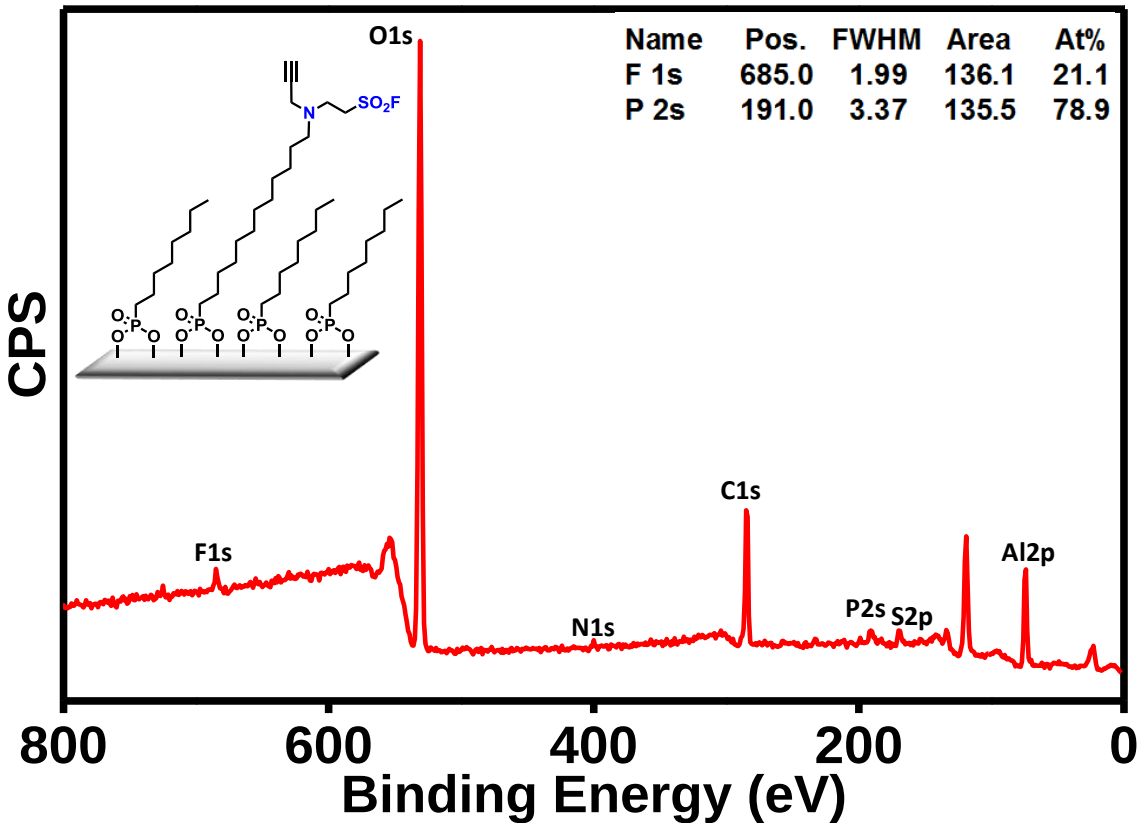

Figure S4.16. XPS wide scan of M_6 modified Al surfaces.

Theoretical F/P ratio = 1/4 = 0.25

Experimental F/P = 0.27 ± 0.02 ⇒ Quantitative surface yield.

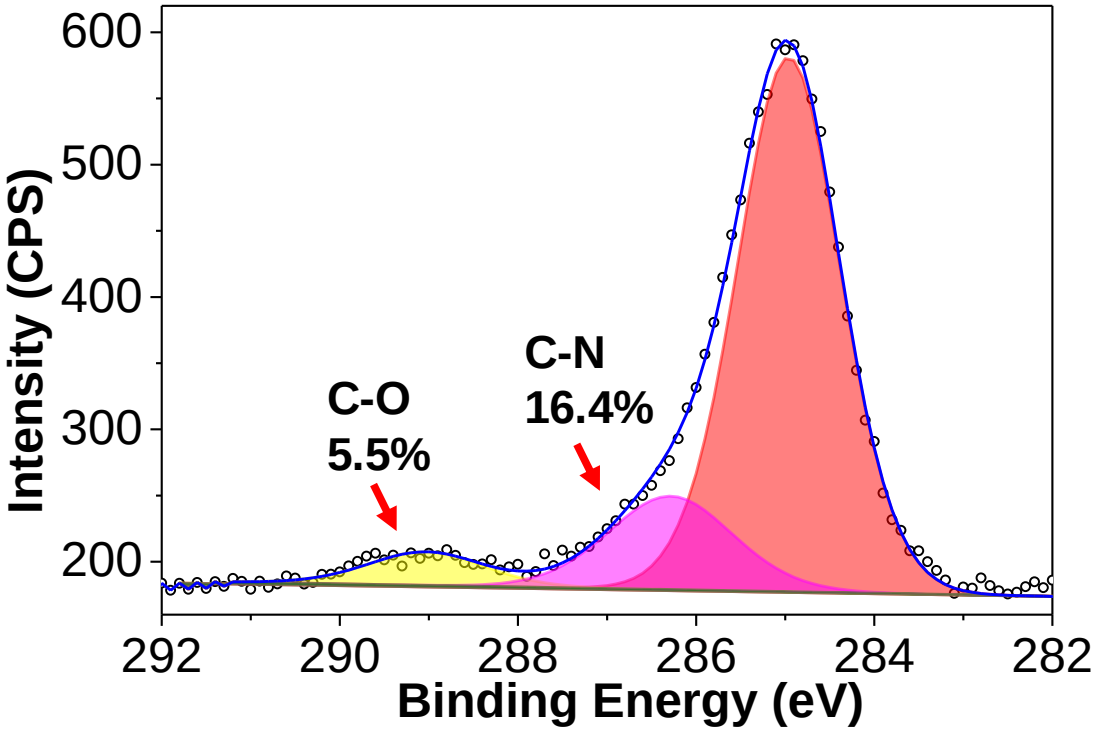

Figure S4.17. XPS C1s narrow scan of M_6 surfaces.

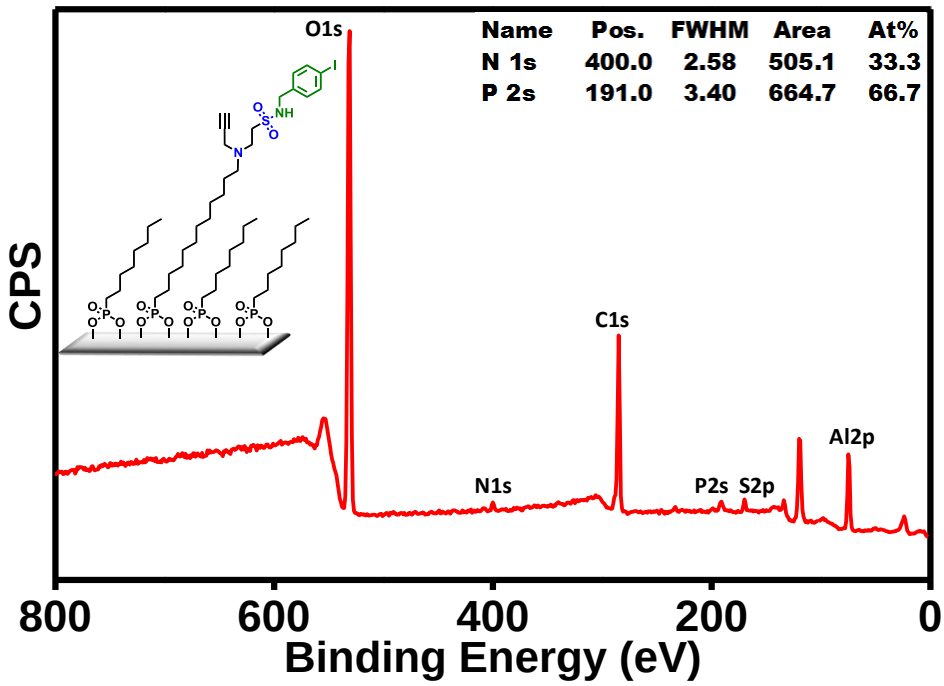

Figure S4.18. XPS wide scan of M_7 modified Al surfaces.

Theoretical N/P ratio = 2/4 = 0.50

Experimental N/P = 0.50 ± 0.01 ⇒ Quantitative surface yield.

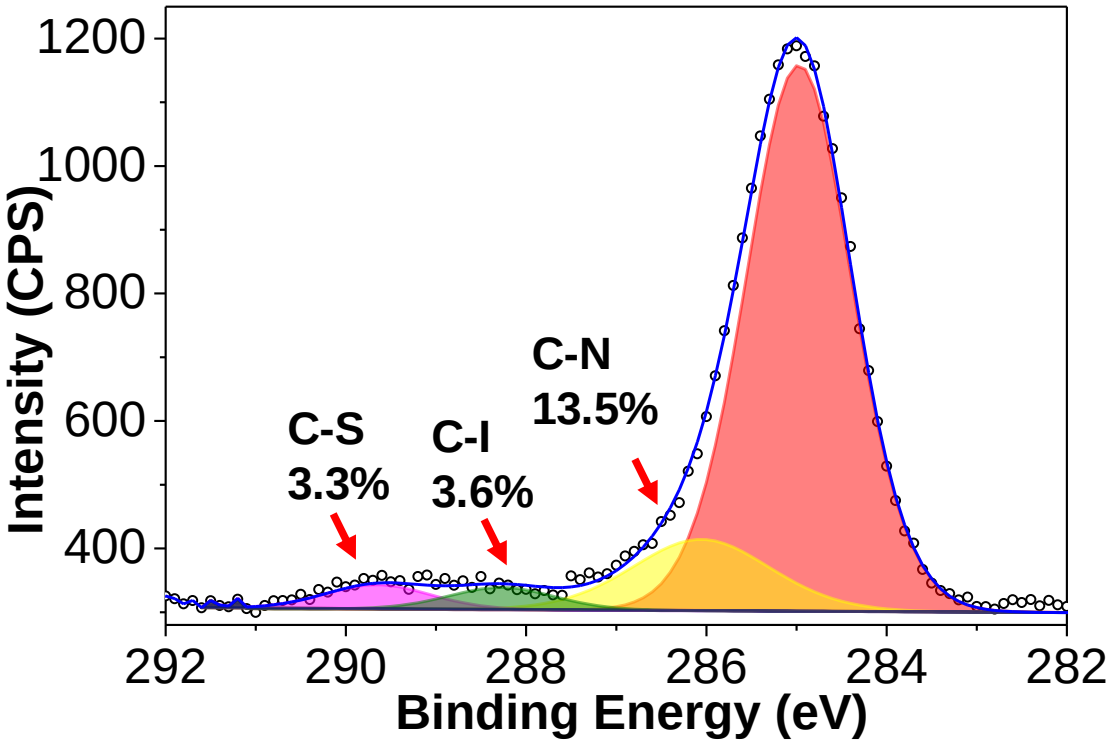

Figure S4.19. XPS C1s narrow scan of M_7 surfaces.

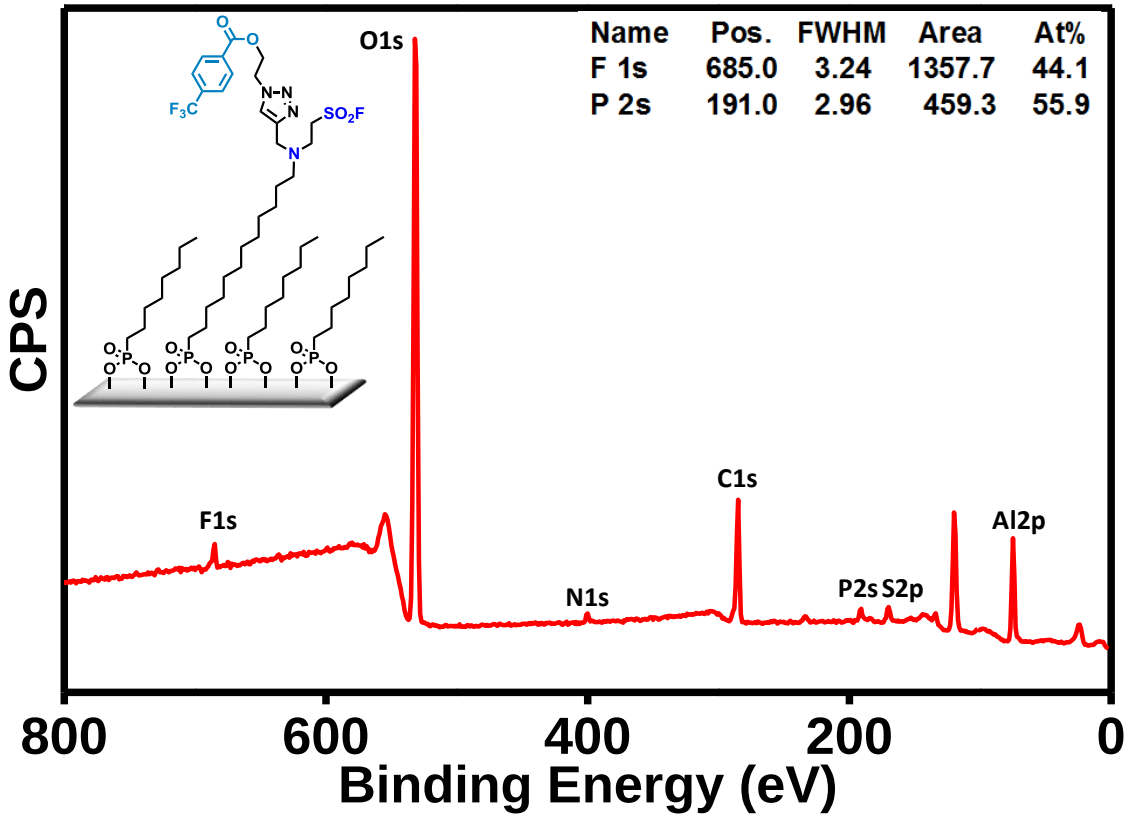

Figure S4.20. XPS wide scan of M_8 modified Al surfaces.

Theoretical F/P ratio = 4/4 = 1.00

Experimental F/P = 0.79 ± 0.02 ⇒ 80 ± 2% surface yield.

a)

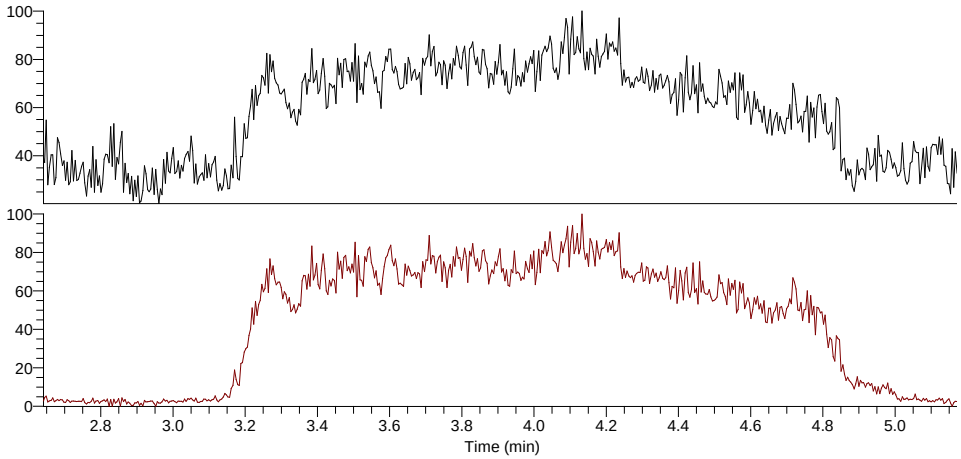

b)

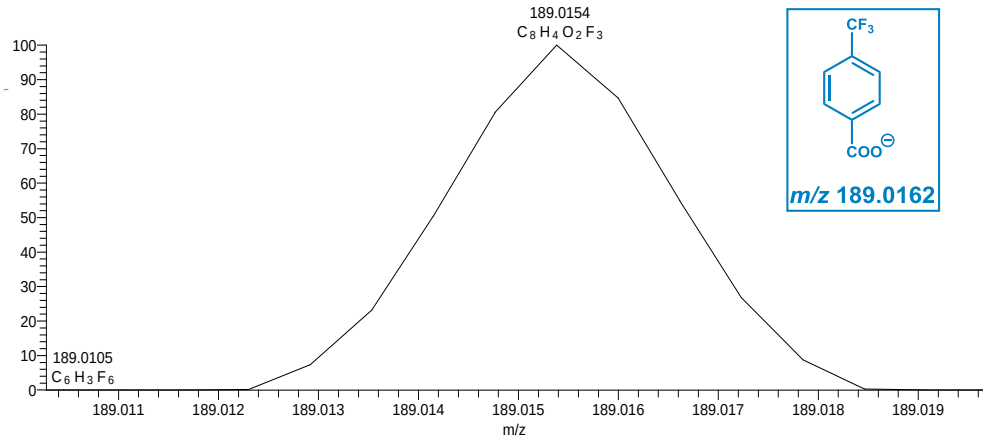

c)

Elemental composition search on mass 189.0154

m/z= 184.0154-194.0154

m/z	Theo. Mass	Delta (mmu)	RDB equiv.	Composition
189.0154	189.0158	-0.37	5.5	$C_8H_4O_2F_3$
	189.0146	0.77	9.5	$C_{11}H_3OF_2$
	189.0169	-1.51	1.5	$C_5H_5O_3F_4$
	189.0135	1.92	13.5	$C_{14}H_2F$
	189.0133	2.07	2.5	$C_6H_3F_6$
	189.0182	-2.82	8.5	$C_{10}H_5O_4$
	189.0194	-3.96	4.5	$C_7H_6O_5F$
	189.0205	-5.10	0.5	$C_4H_7O_6F_2$
	189.0241	-8.69	-0.5	$C_3H_9O_9$
	189.0041	11.30	0.5	$C_3H_6O_8F$

Figure S4.21. Rep s. a) Top panel represents total ion current (TIC); bottom panel represents extracted ion chromatogram (EIC) (*m/z* window 10 mmu around ion of interest). b) peak of ion of interest (*m/z* 189.0154) c) relative error between obtained *m/z* and theoretical *m/z* of ion of interest.

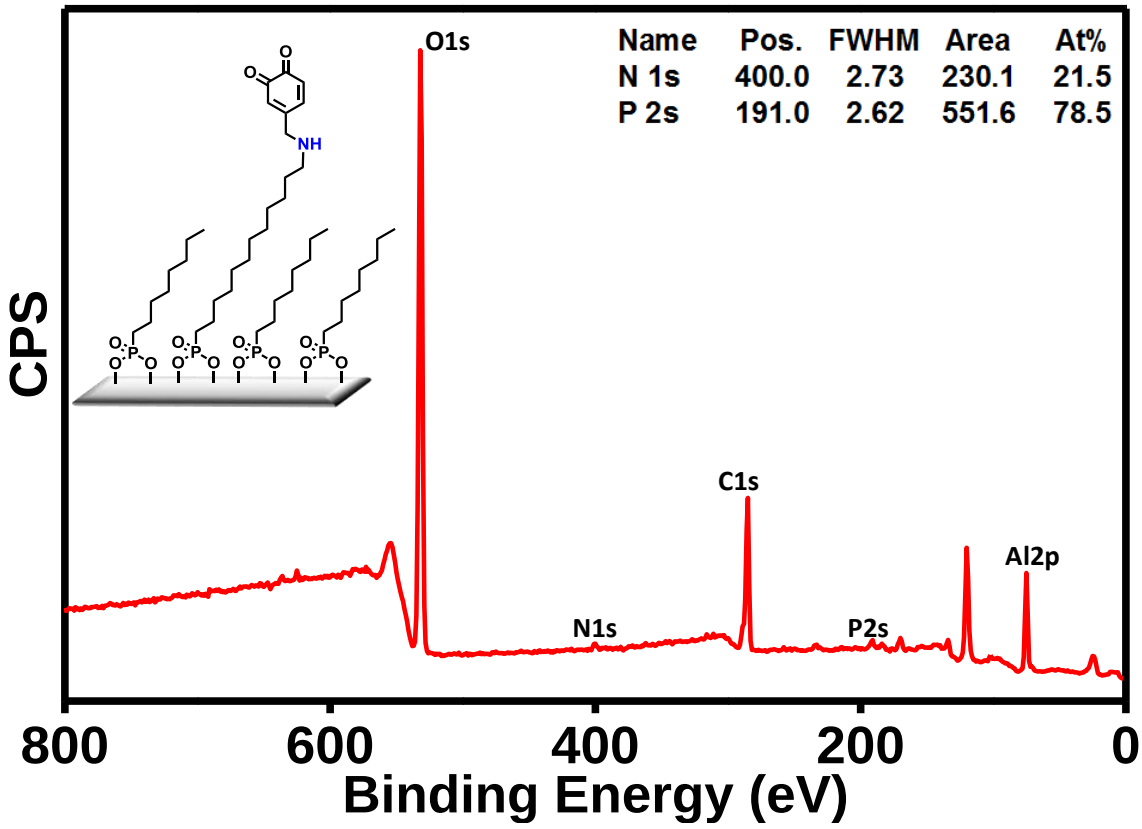

Figure S4.22. XPS wide scan of catechol terminated Al surfaces.

Theoretical N/P ratio = 1/4 = 0.25

Experimental N/P = 0.27 ± 0.02 ⇒ Quantitative surface yield

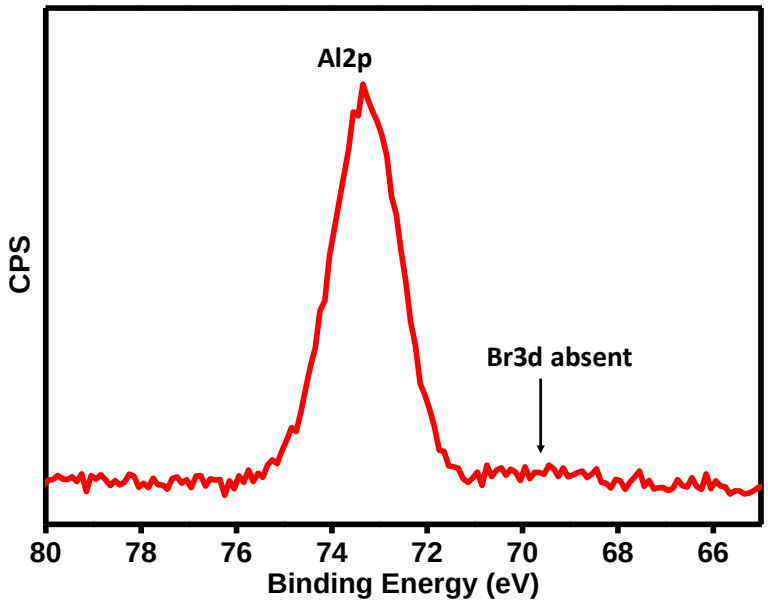

Figure S4.23. XPS Br3d narrow scan of catechol terminated Al surfaces.

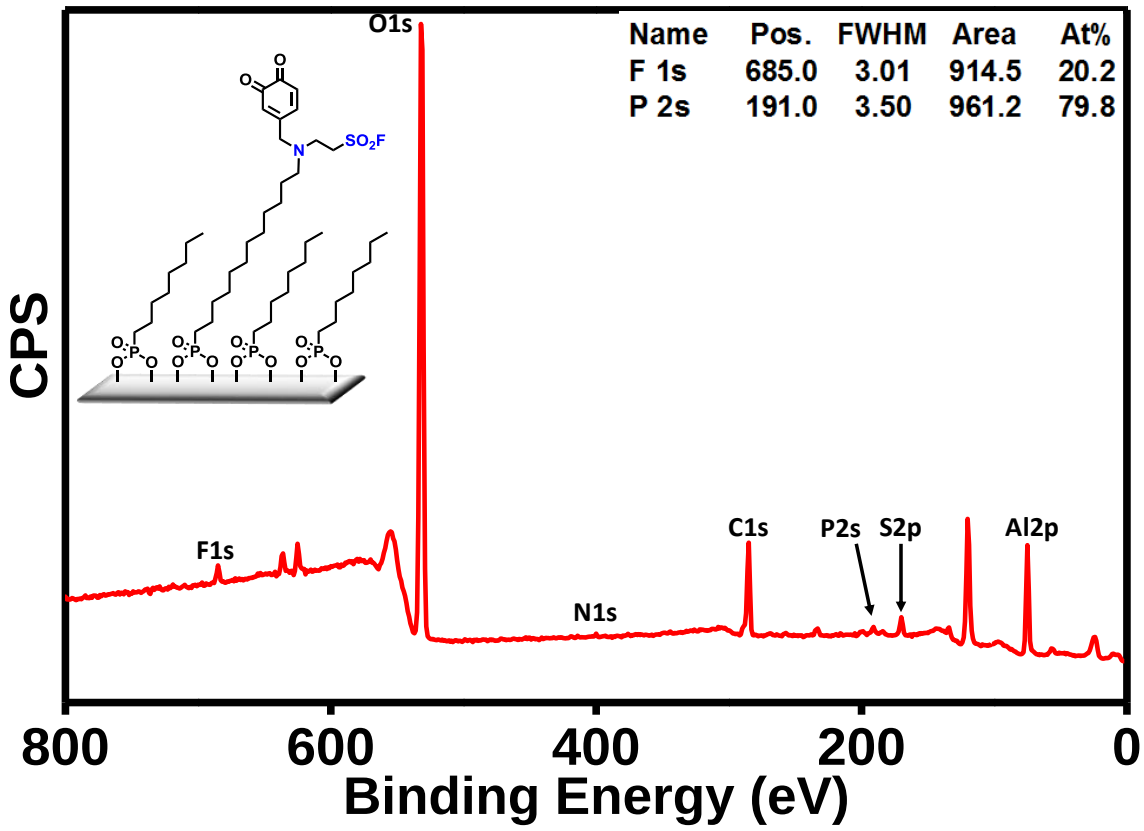

Figure S4.24. XPS wide scan of M_{10} modified Al surfaces.

Theoretical F/P ratio = 1/4 = 0.25

Experimental F/P = 0.25 ± 0.01 ⇒ Quantitative surface yield.

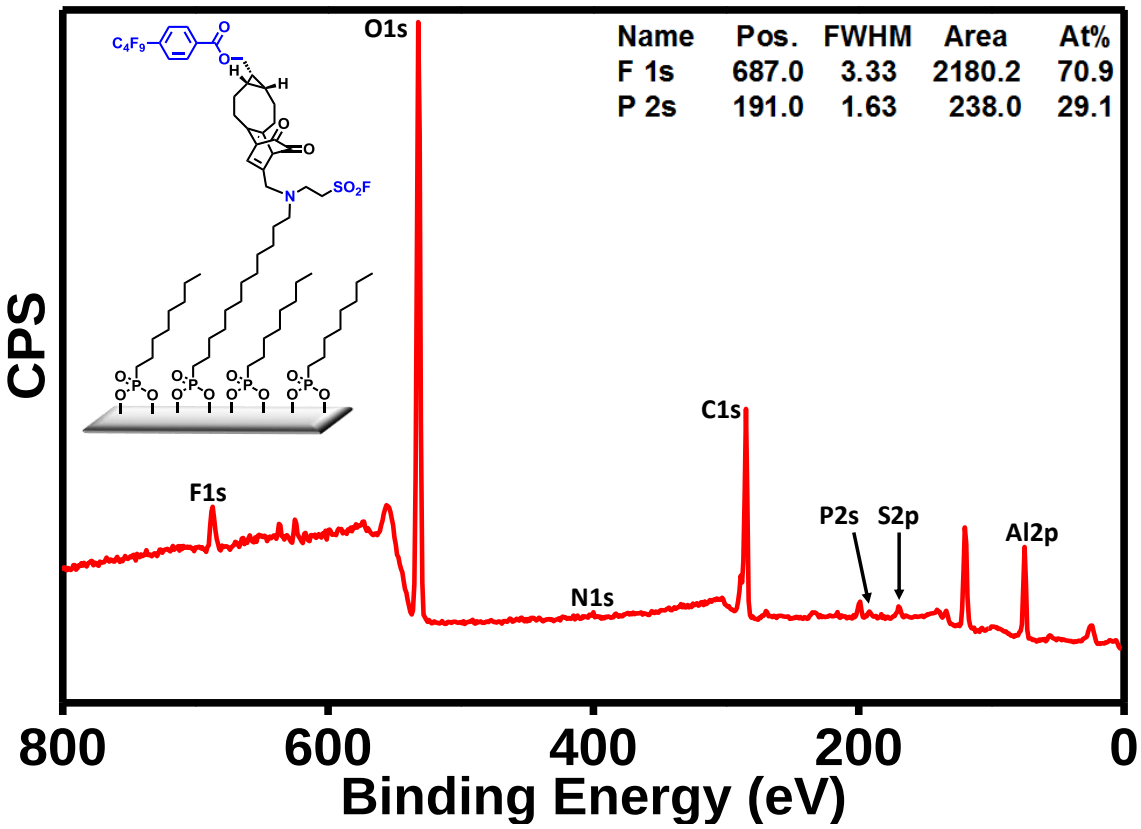

Figure S4.25. XPS wide scan of M_{11} modified Al surfaces.

Theoretical F/P ratio = 10/4 = 2.5

Experimental F/P = 2.4 ± 0.03 ⇒ 95 ± 3% surface yield.

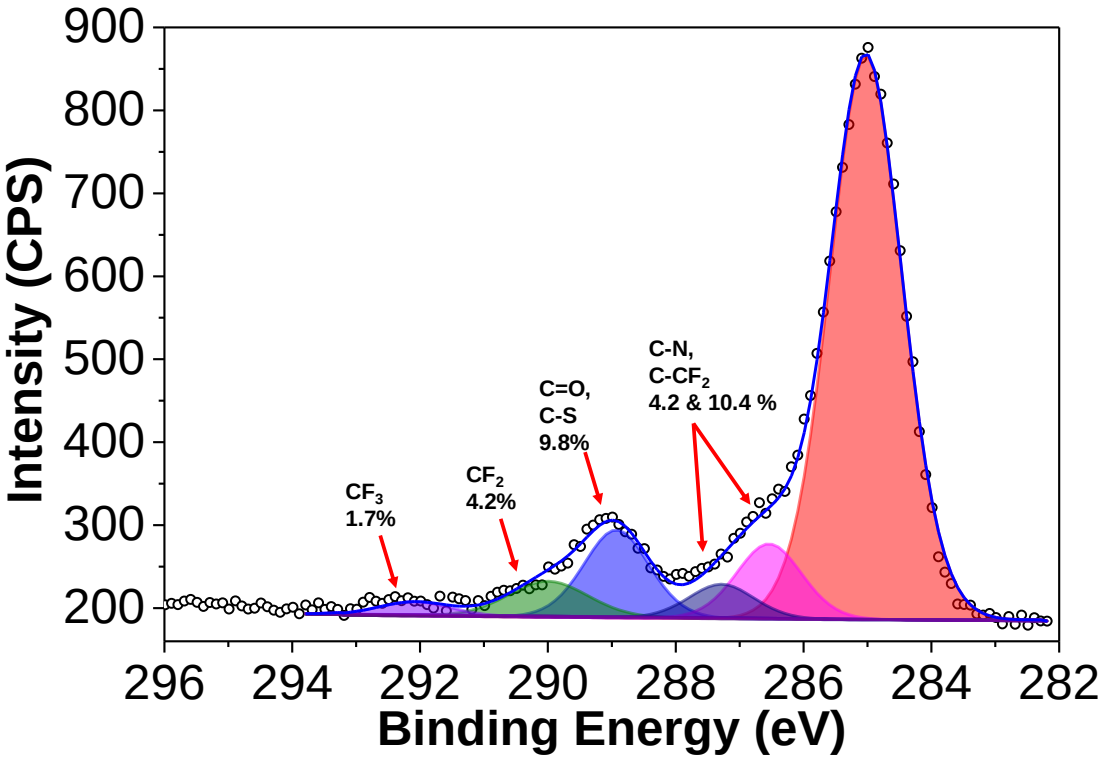

Figure S4.26. XPS C1s narrow scan of M_{11} surfaces.

a)

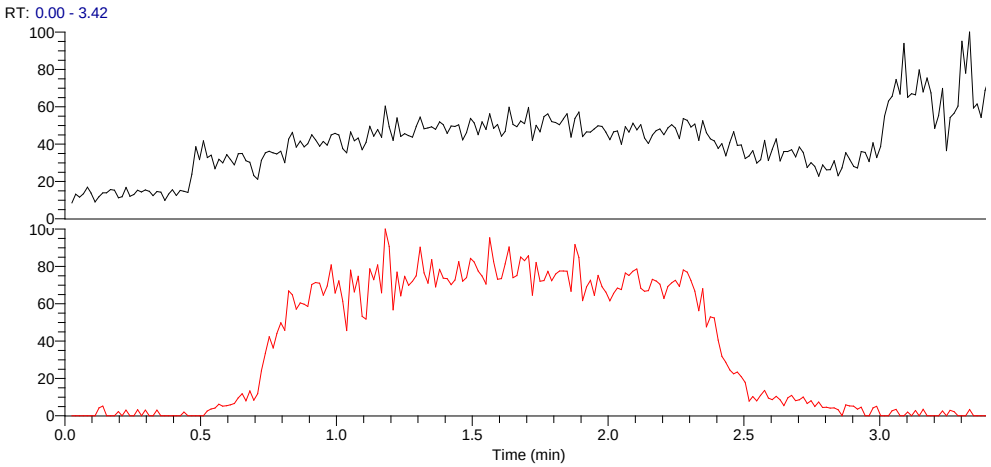

b)

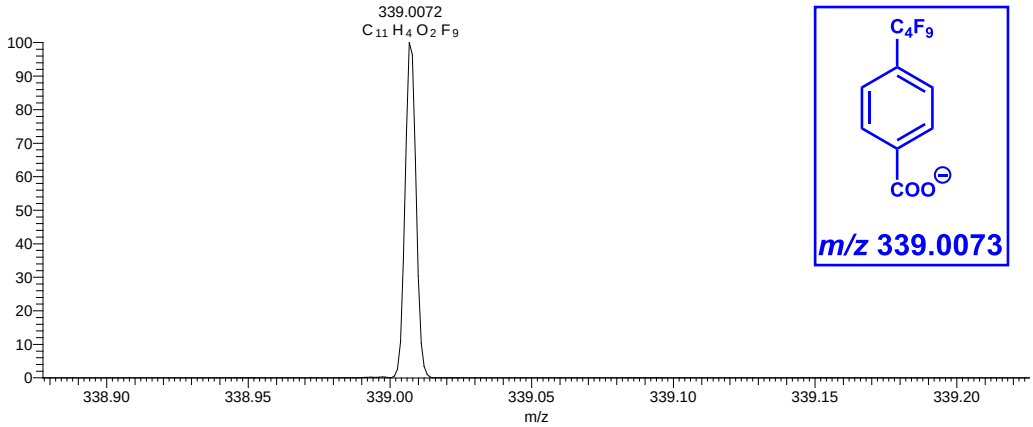

c)

Elemental composition search on mass 339.0072

m/z= 334.0072-344.0072

m/z	Theo. Mass	Delta (mmu)	RDB equiv.	Composition
339.0072	339.0062	1.02	5.5	$C_{11}H_4O_2F_9$
	339.0098	-2.57	4.5	$C_{10}H_6O_5F_7$
	339.0109	-3.71	0.5	$C_7H_7O_6F_8$
	339.0134	-6.15	3.5	$C_9H_8O_8F_5$
	339.0145	-7.30	-0.5	$C_6H_9O_9F_6$
	339.0158	-8.60	6.5	$C_{11}H_9O_{10}F_2$
	338.9970	10.24	3.5	$C_8H_7O_{10}F_4$
	338.9958	11.39	7.5	$C_{11}H_6O_9F_3$
	338.9945	12.69	0.5	$C_6H_6O_8F_7$
	338.9934	13.83	4.5	$C_9H_5O_7F_6$

Figure S4.27. Representative DART ion intensity EIC of M_{11} surfaces. a) Top panel represents total ion current (TIC); bottom panel represents extracted ion chromatogram (EIC) (*m/z* window 10 mmu around ion of interest). b) peak of ion of interest (*m/z* 339.0072) c) relative error between obtained *m/z* and theoretical *m/z* of ion of interest.

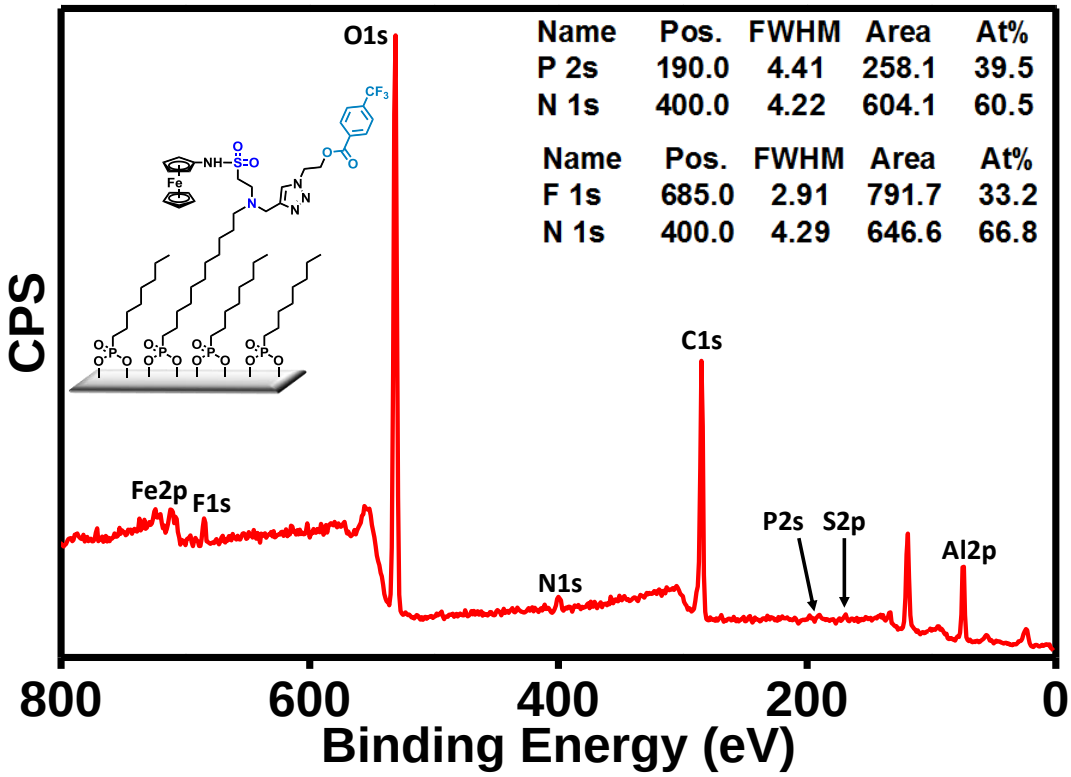

Figure S4.28. XPS wide scan of M_{12} modified Al surfaces.

Theoretical N/P ratio = 5/4 = 1.25

Experimental N/P = 1.5 ± 0.1 ⇒ Quantitative surface yield.

Theoretical F/P ratio = 2.4/5 = 0.48

Experimental F/P = 0.49 ± 0.01 ⇒ Quantitative surface yield.

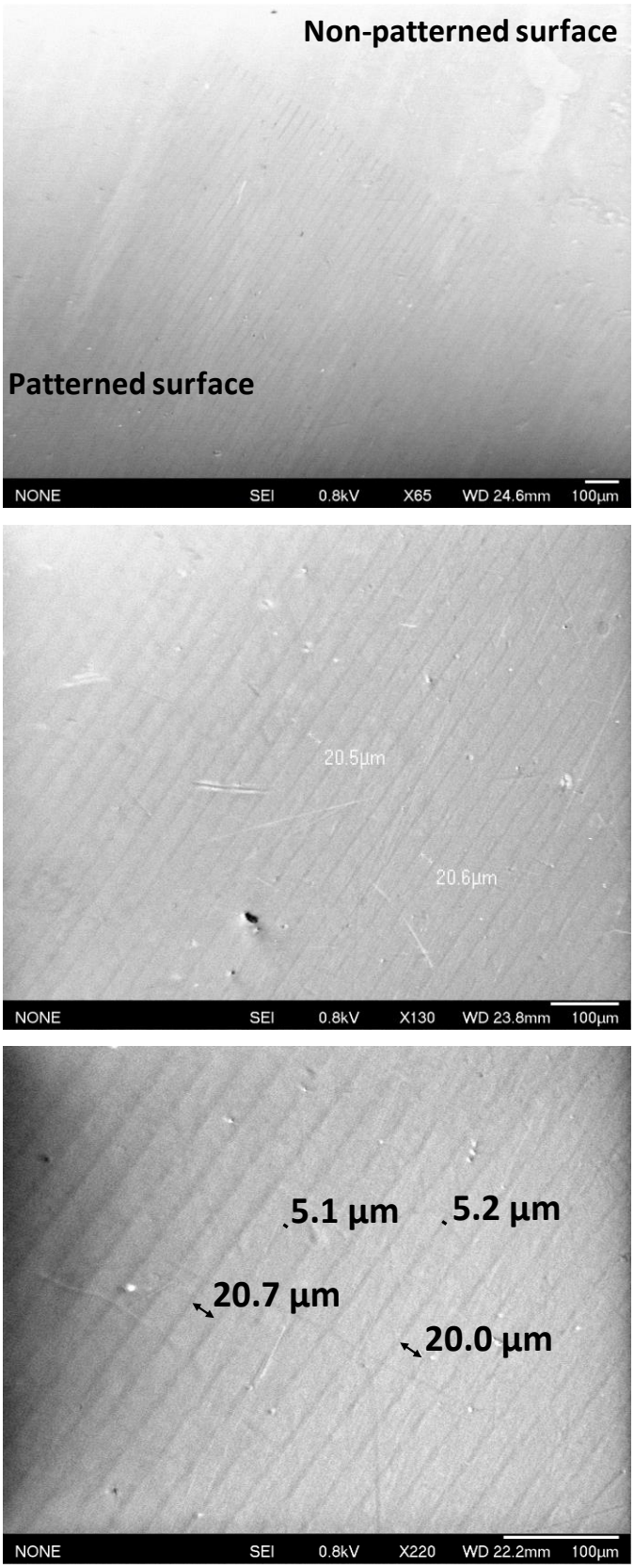

Figure S4.29. SEM images of non-patterned & patterned aminoferrocene on M_{12} surfaces (images processed by ImageJ).

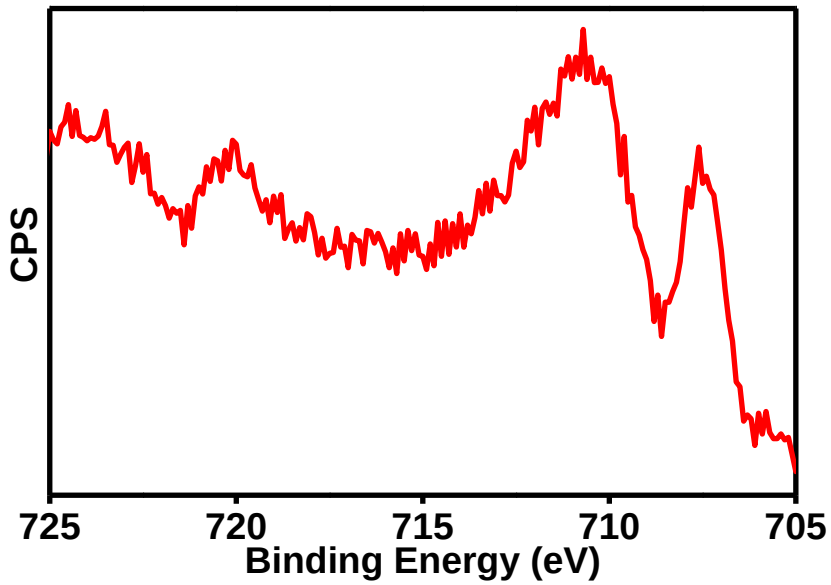

Figure S4.30. XPS Fe2p narrow scan of M_{12} surfaces.

5. SOLUTION DART–HRMS FRAGMENTATION DATA.

5.1 Fragmentation products for compound 1 in positive mode (top panel: total ion current (TIC), middle panel: extracted ion chromatogram (EIC) (*m/z* window 10 mmu around ion of interest) and bottom panel: peak of ion of interest).

a)

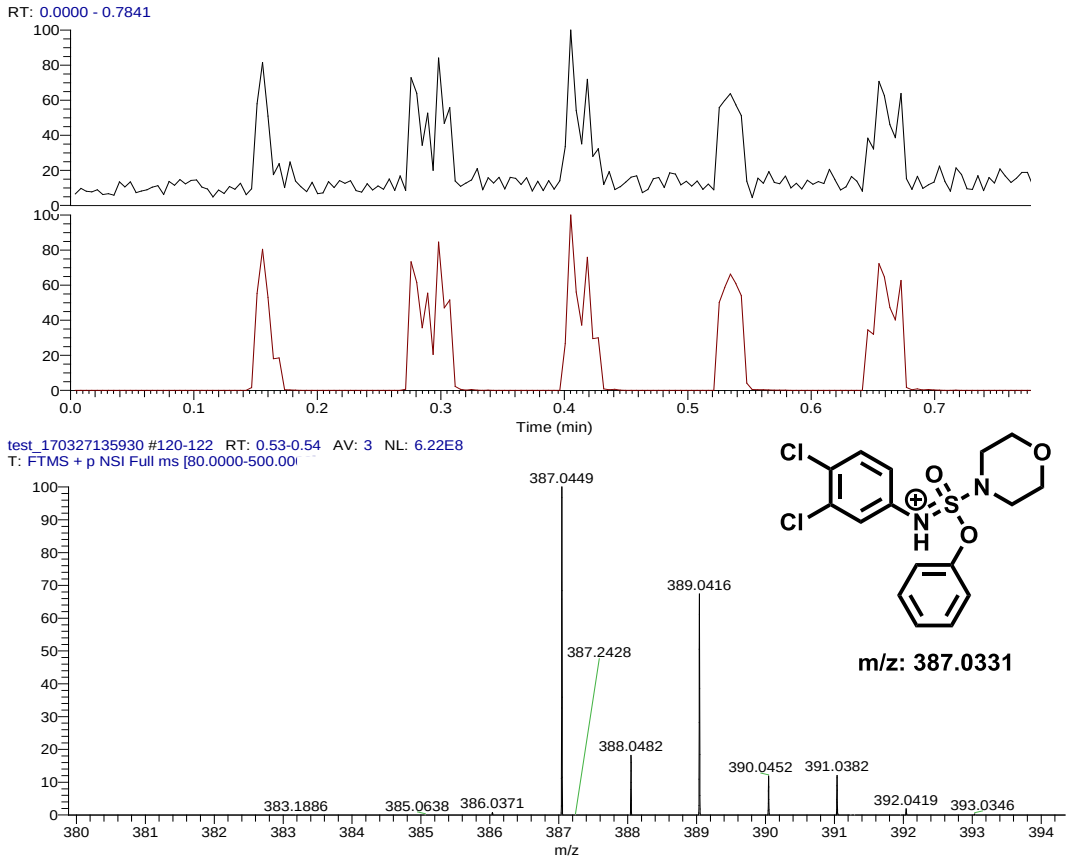

b) RT: 0.0000 - 0.7841

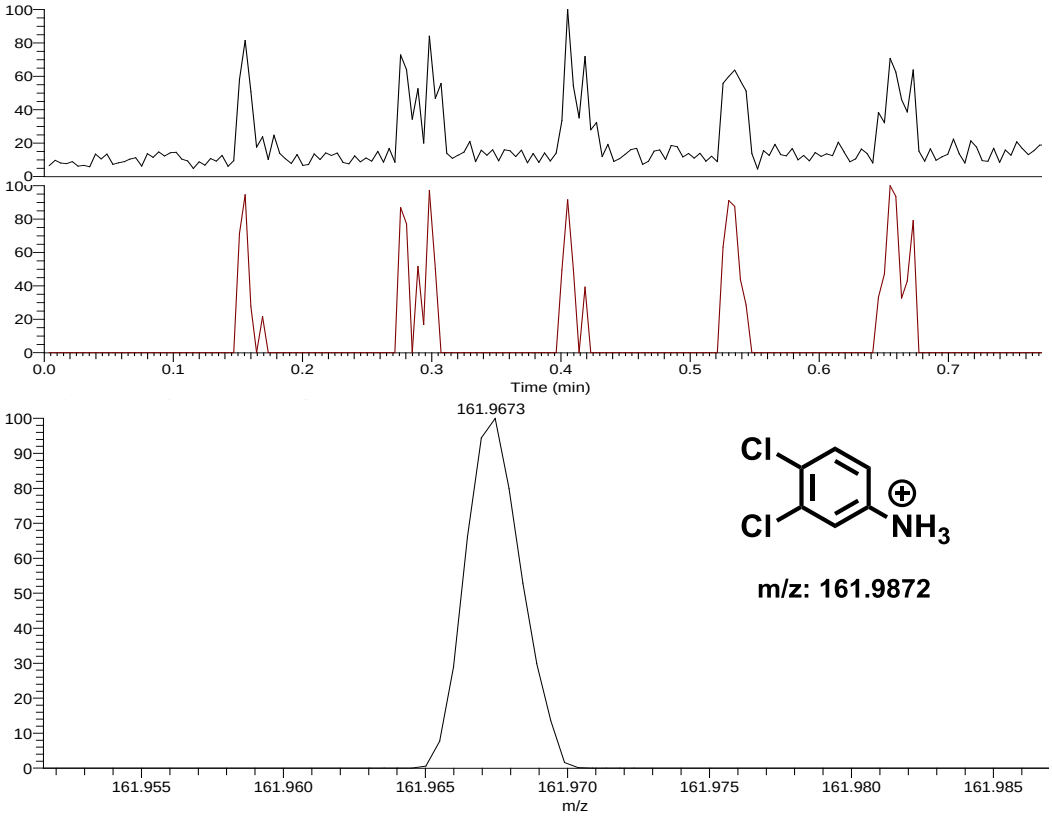

5.2 Fragmentation products for compound 1 in negative mode (top panel: total ion current (TIC), middle panel: extracted ion chromatogram (EIC) (*m/z* window 10 mmu around ion of interest) and bottom panel: peak of ion of interest).

a)

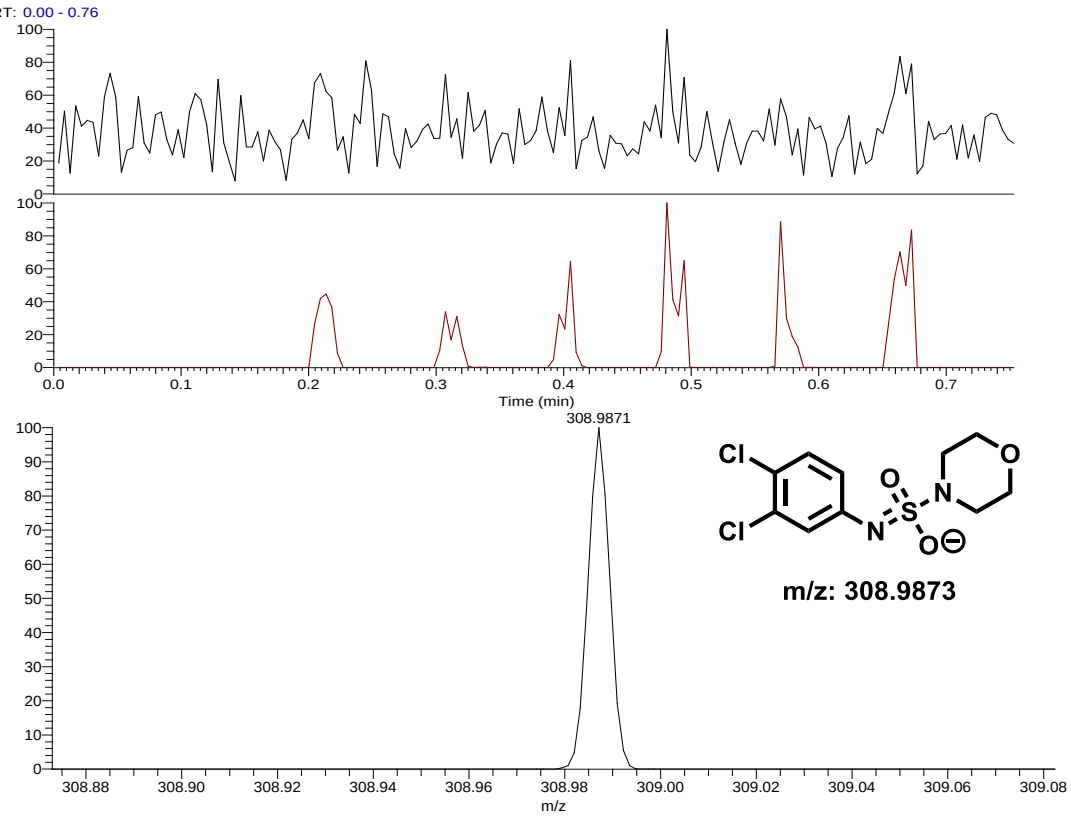

b)

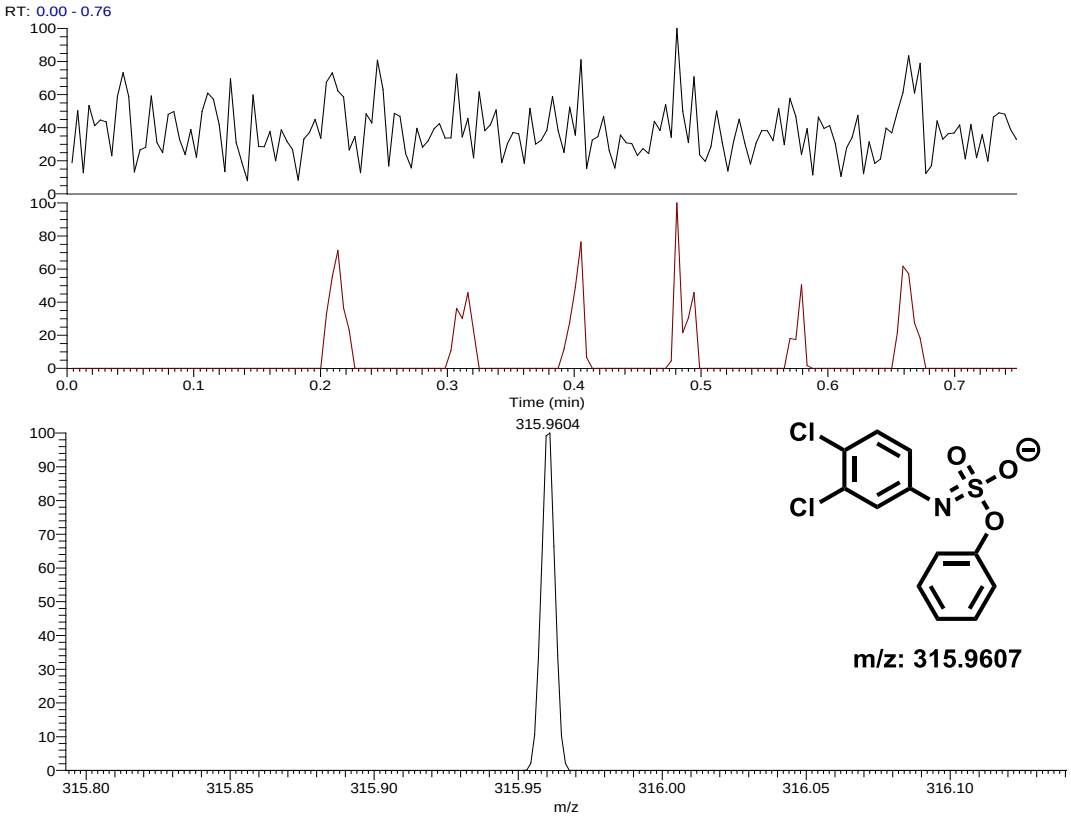
RT: 0.00 - 0.76
Time (min)
315.9604
m/z
Cl
Cl
N
S
O
O
O
m/z: 315.9607

c)

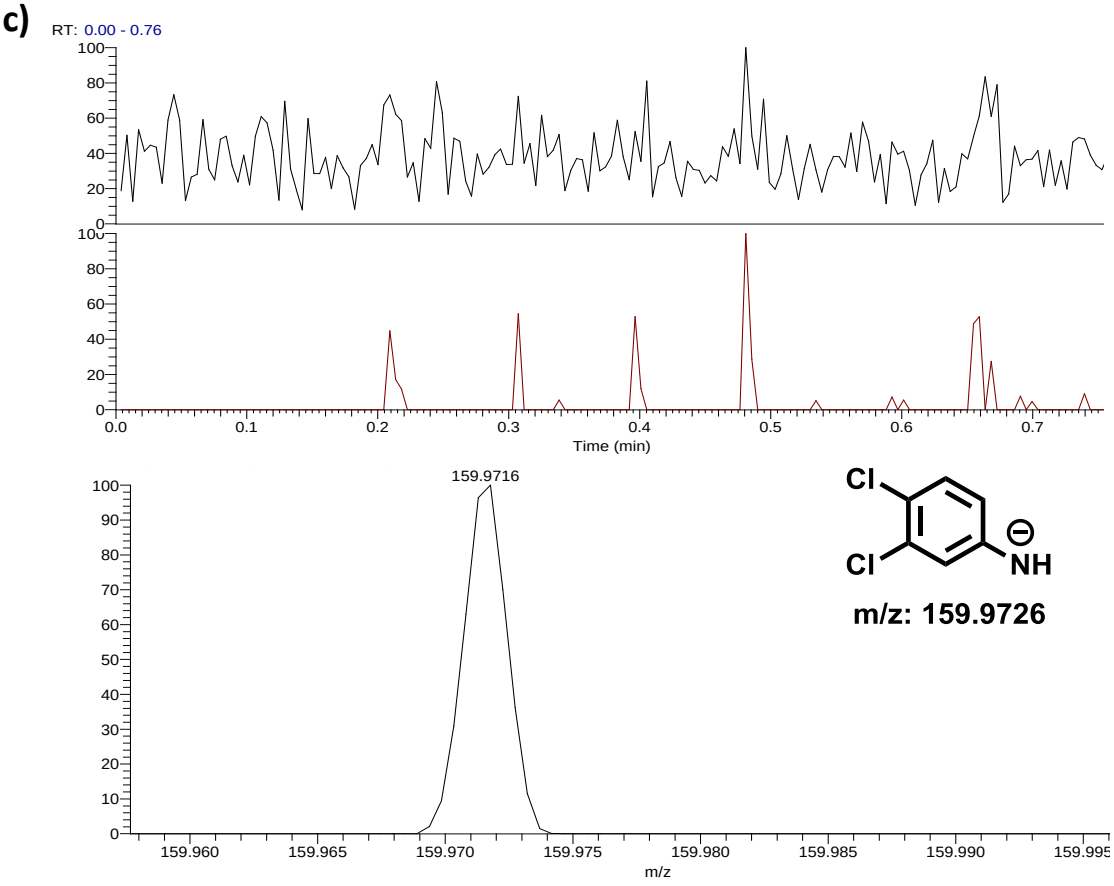
RT: 0.00 - 0.76
Time (min)
159.9716
m/z
Cl
Cl
NH
m/z: 159.9726

5.3 Fragmentation products for compound 2 in positive mode (top panel: total ion current (TIC), middle panel: extracted ion chromatogram (EIC) (*m/z* window 10 mmu around ion of interest) and bottom panel: peak of ion of interest).

a)

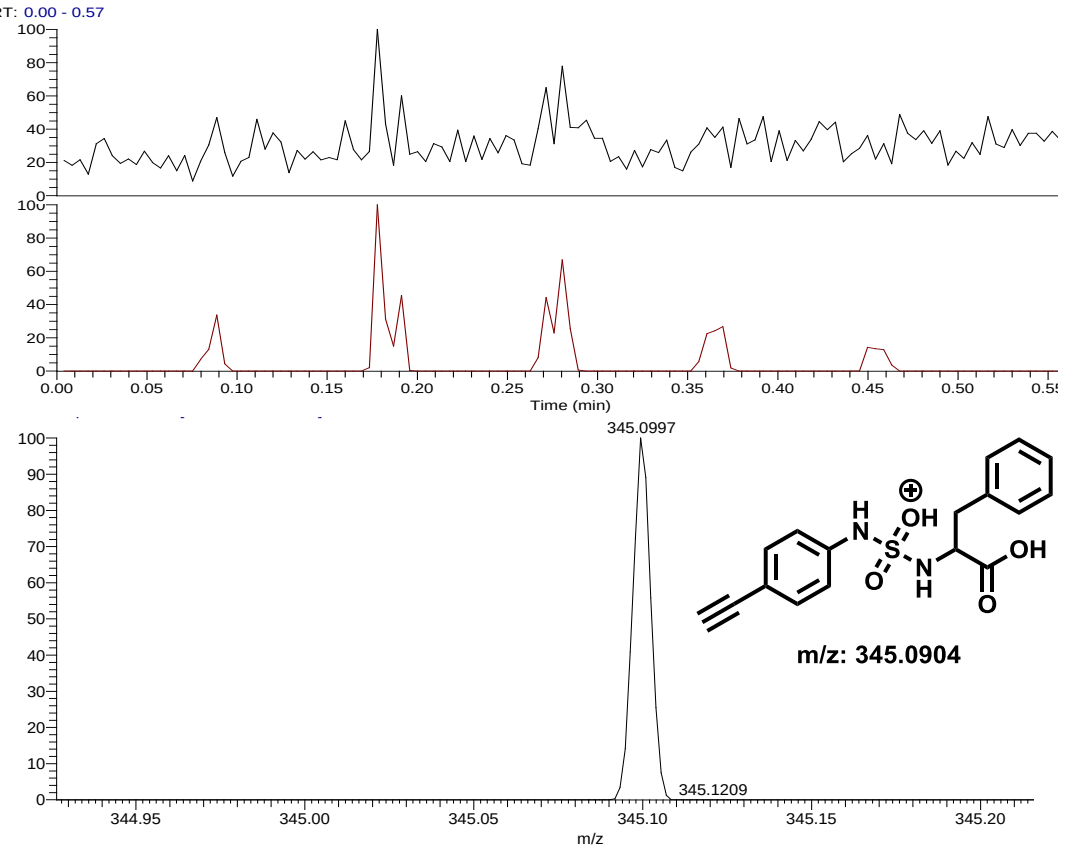

b)

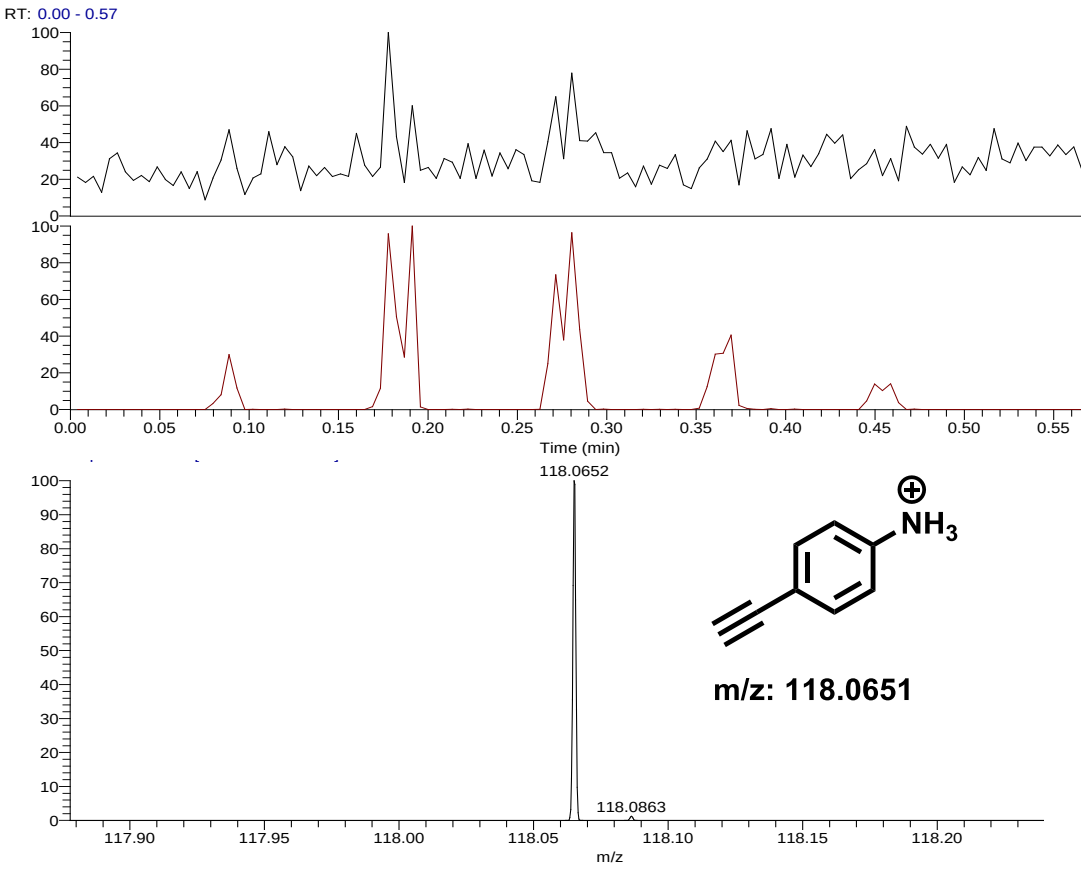
RT: 0.00 - 0.57
Time (min)
118.0652
118.0863
m/z
NH3
m/z: 118.0651

c)

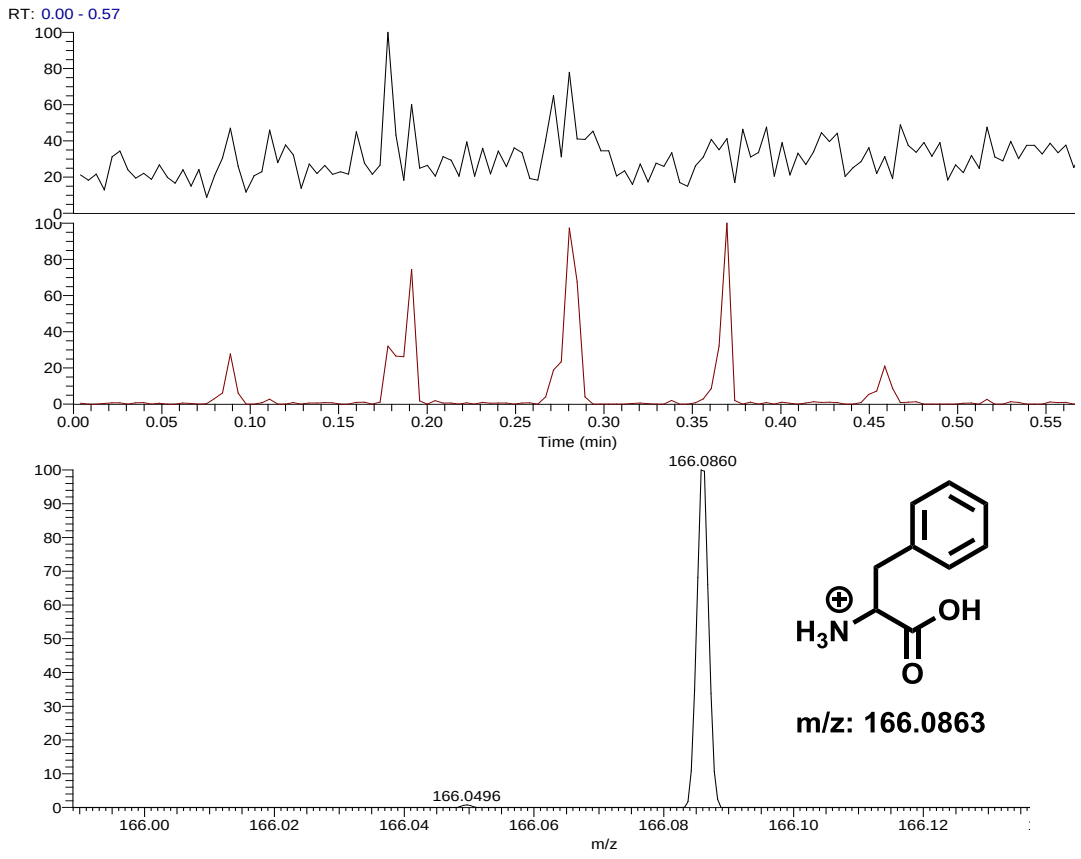
RT: 0.00 - 0.57
Time (min)
166.0860
166.0496
m/z
H3N
OH
O
m/z: 166.0863

5.4 Fragmentation products for compound 2 in negative mode (top panel: total ion current (TIC), middle panel: extracted ion chromatogram (EIC) (*m/z* window 10 mmu around ion of interest) and bottom panel: peak of ion of interest).

a)

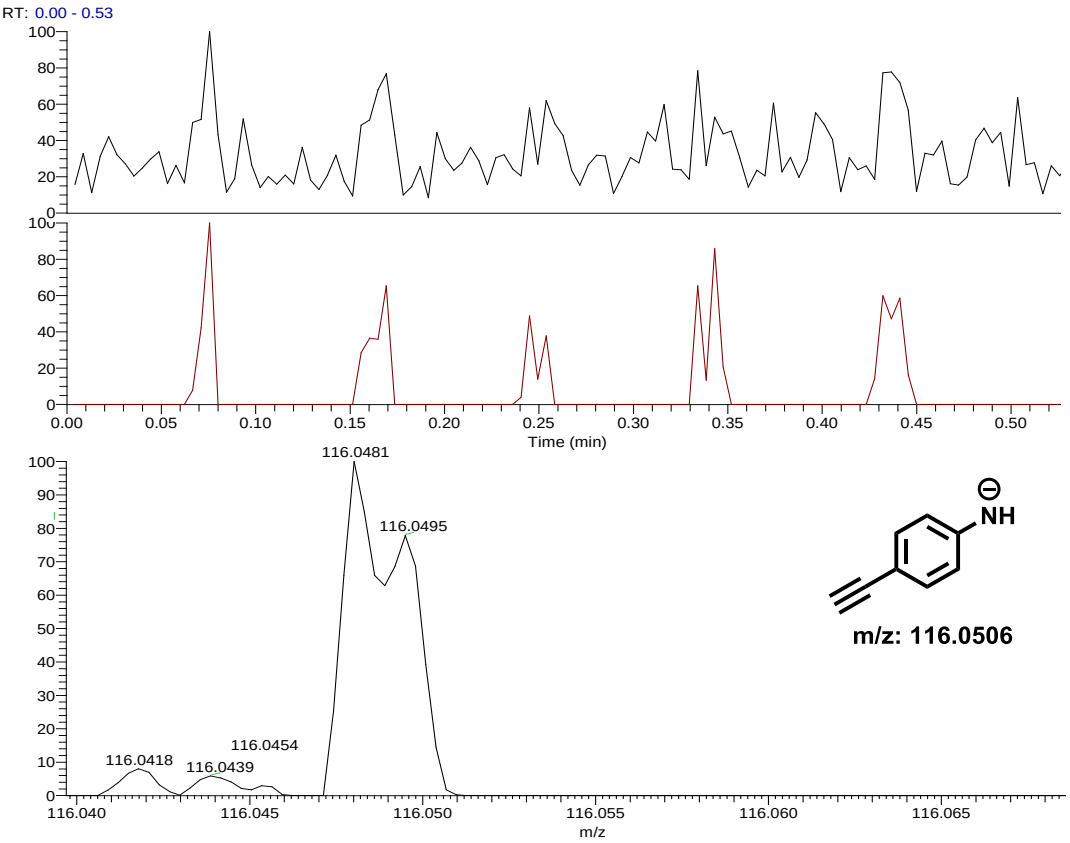

b)

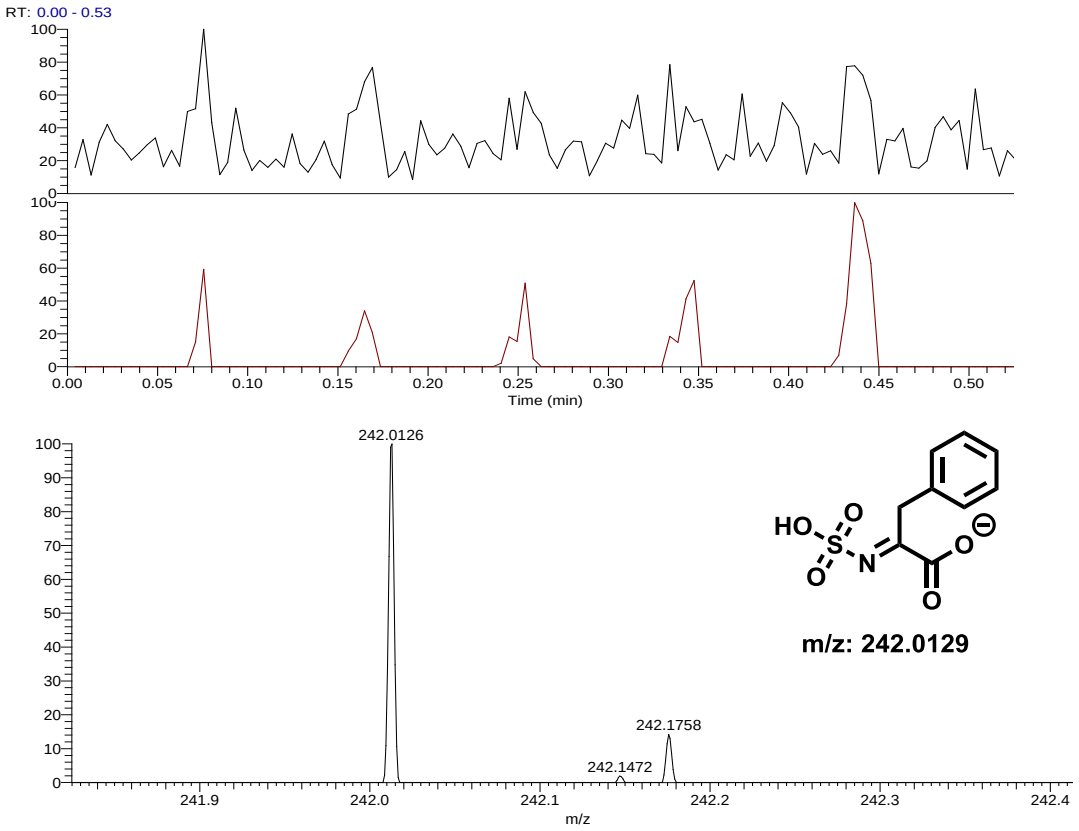
RT: 0.00 - 0.53
Time (min)
242.0126
242.1758
242.1472
m/z
HO
S
N
O
O
O
O
m/z: 242.0129

c)

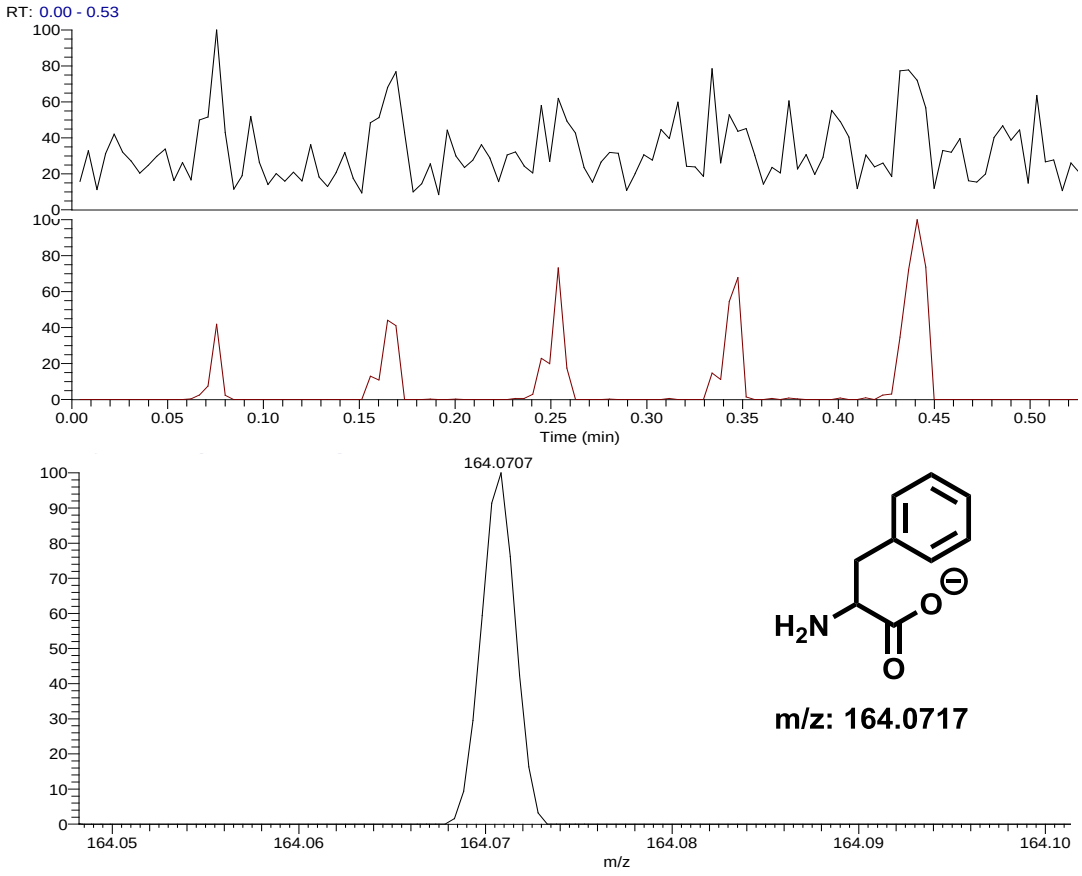
RT: 0.00 - 0.53
Time (min)
164.0707
m/z
H_2N
O
O
m/z: 164.0717

d)

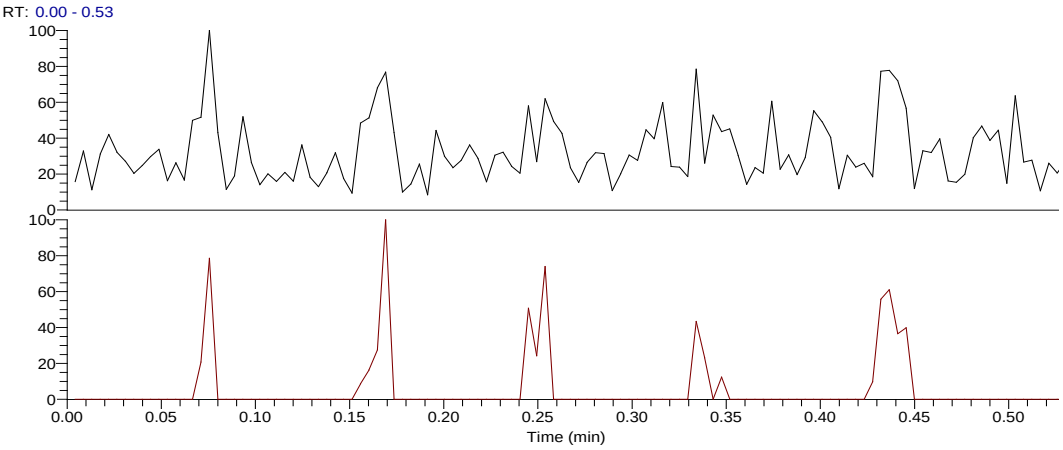
RT: 0.00 - 0.53
Time (min)

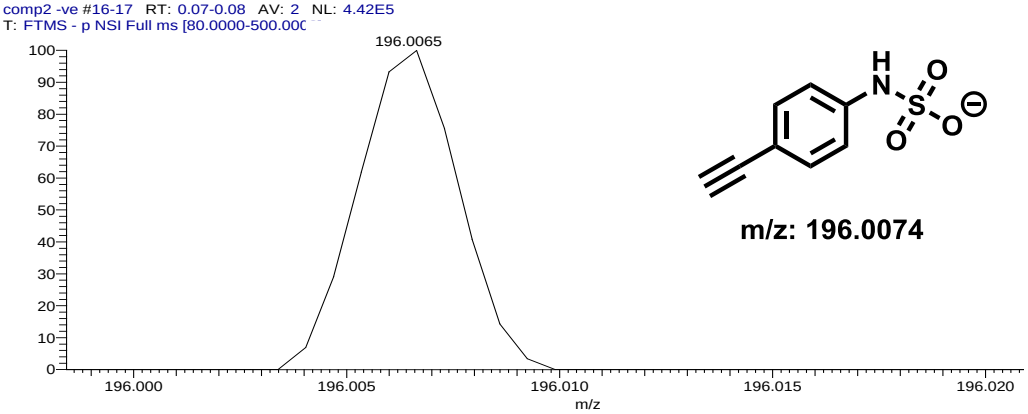
comp2 -ve #16-17 RT: 0.07-0.08 AV: 2 NL: 4.42E5
T: FTMS - p NSI Full ms [80.0000-500.000
196.0065
m/z

m/z: 196.0074

5.5 Fragmentation products for compound 3 in positive mode (top panel: total ion current (TIC), middle panel: extracted ion chromatogram (EIC) (*m/z* window 10 mmu around ion of interest) and bottom panel: peak of ion of interest).

a)

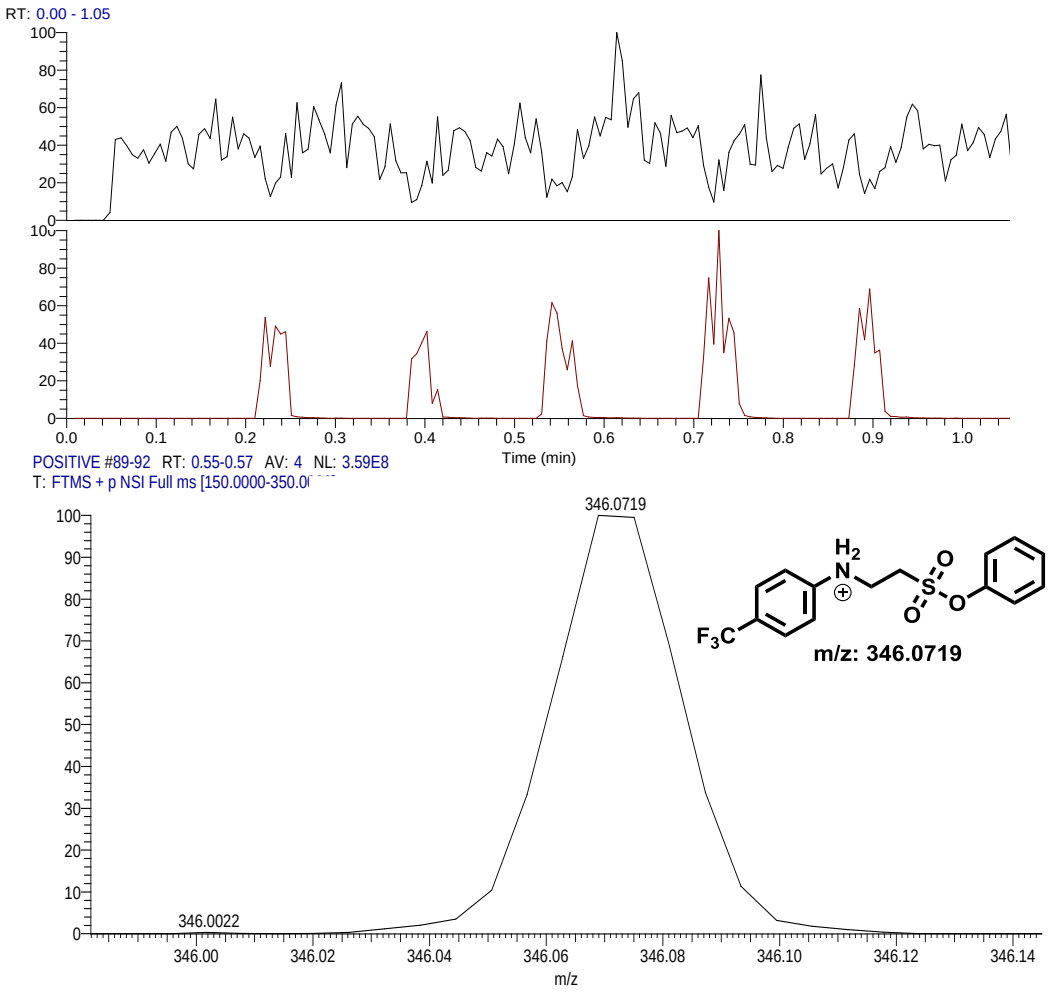

b)

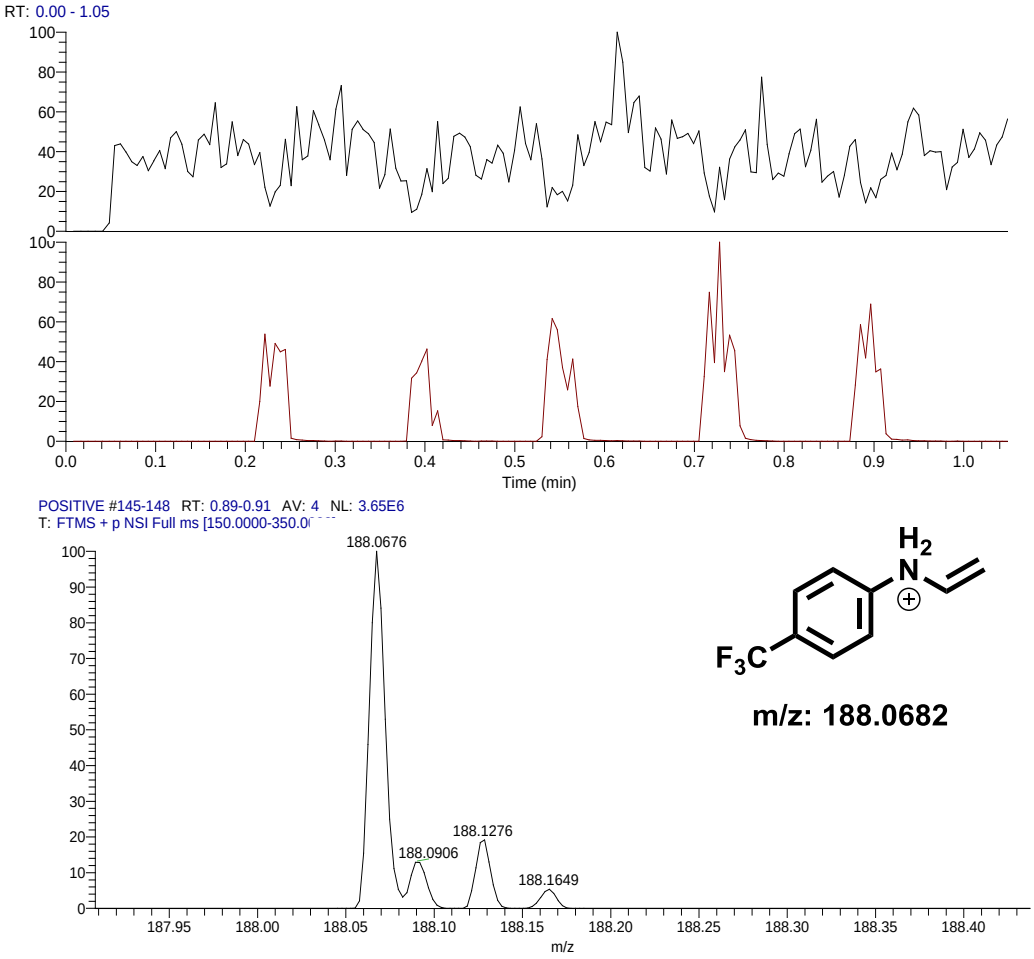
RT: 0.00 - 1.05
Time (min)
POSITIVE #145-148 RT: 0.89-0.91 AV: 4 NL: 3.65E6
188.0676
188.1276
188.0906
188.1649
m/z
m/z: 188.0682

c)

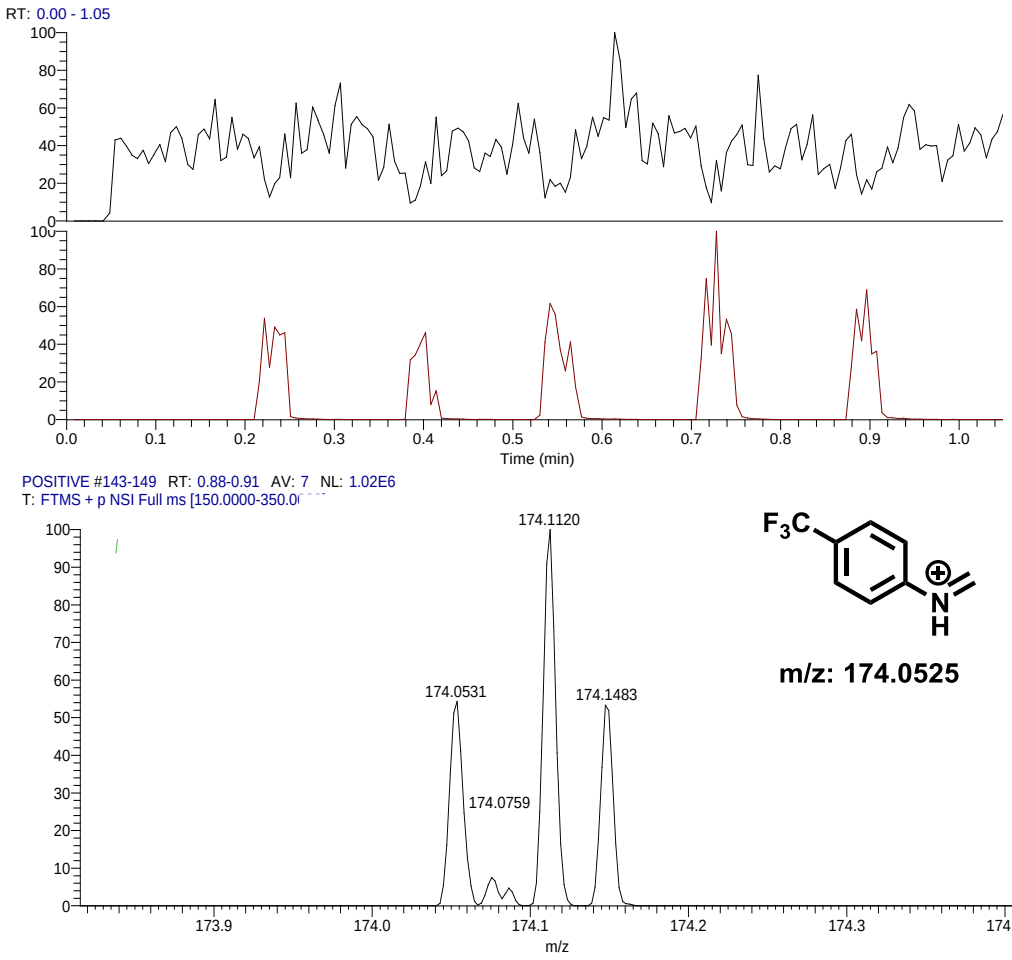
RT: 0.00 - 1.05
Time (min)
POSITIVE #143-149 RT: 0.88-0.91 AV: 7 NL: 1.02E6
T: FTMS + p NSI Full ms [150.0000-350.0
174.1120
174.0531
174.1483
174.0759
m/z
F3C
N
H
m/z: 174.0525

5.6 Fragmentation products for compound 3 in negative mode (top panel: total ion current (TIC), middle panel: extracted ion chromatogram (EIC) (*m/z* window 10 mmu around ion of interest) and bottom panel: peak of ion of interest).

a)

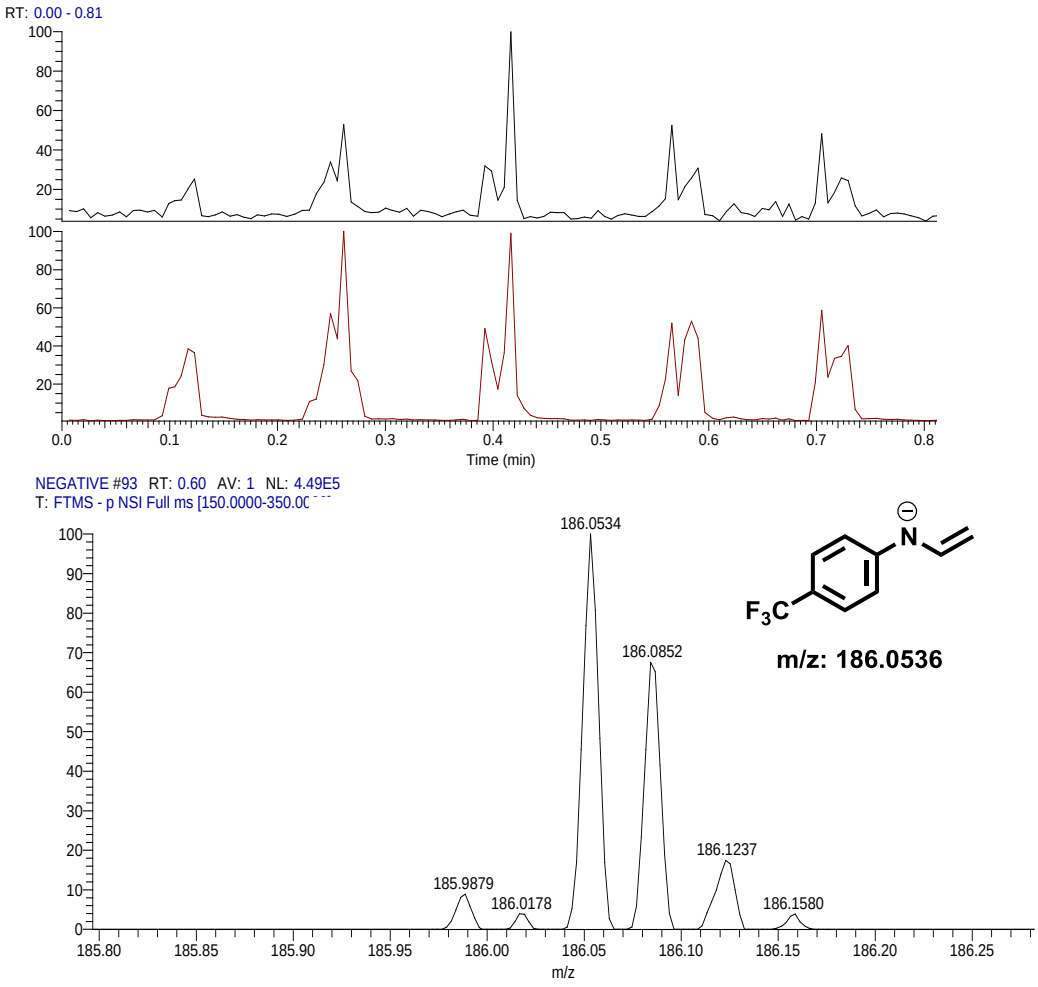

b)

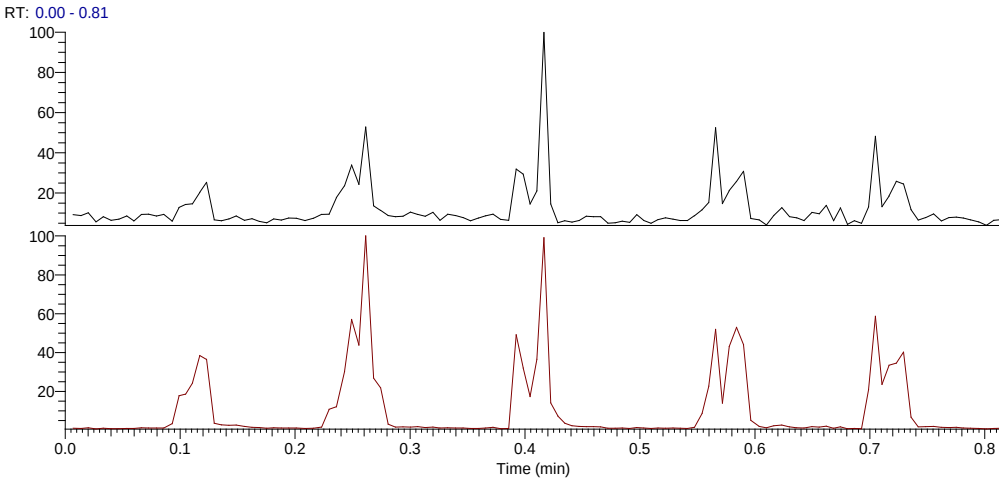
RT: 0.00 - 0.81
Time (min)

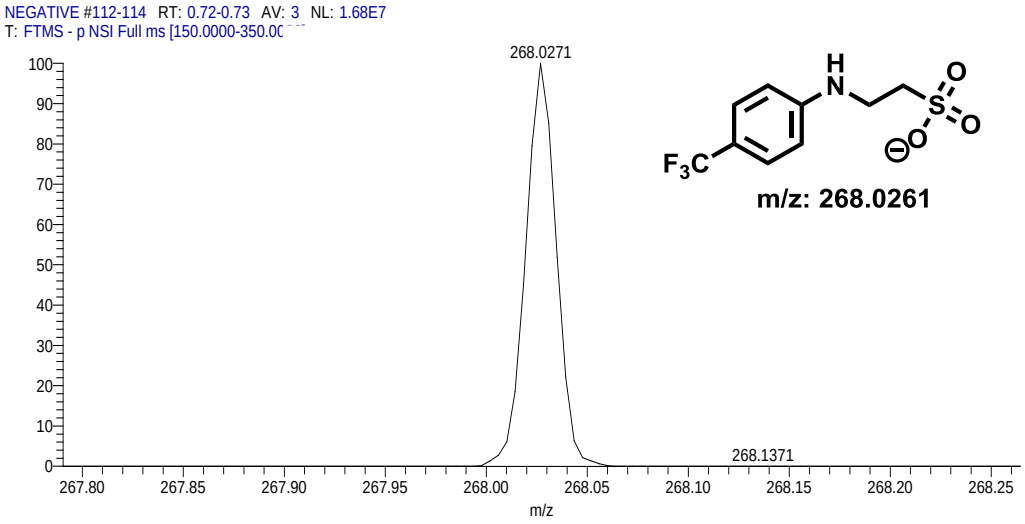
NEGATIVE #112-114 RT: 0.72-0.73 AV: 3 NL: 1.68E7
T: FTMS - p NSI Full ms [150.0000-350.0
268.0271
268.1371
m/z

m/z: 268.0261

6. DENSITY FUNCTIONAL THEORY (DFT) FOR XPS C1S CALCULATION.

Electronic core level calculations (ECC) were used to simulate core levels of C 1s XPS spectra. All ECC were done with the GAUSSIAN09 program. The effect of the bulk substrate on Al–O–P bound monolayers was mimicked by attaching the organic species to a $(OH_2)_2Al–$ moiety. The geometries of the different systems were optimized at the B3LYP/6-311G(d,p) and using B3LYP/LanL2DZ level of theory for iodine containing molecules. Natural bond orbital (NBO) analysis (Glendening, E. D.; Reed, A. E.; Carpenter, J. E.; Weinhold, F. NBO, Version 3.1) was employed to obtain the core orbital energies.[4,5] The simulated XPS spectra were used to facilitate the peak fitting procedure for overlapping contributions in the experimental XPS data.

a)

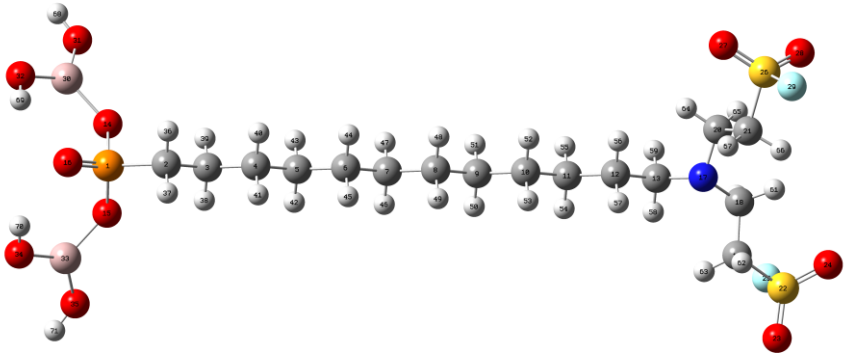

b)

Carbon Number (3D picture)	2-12,	13,18,20	19, 21
Functional group	C-C	C-N	C-S
Number of Functional group	11	3	2
Theory Binding Energy (eV)	285.0	287.4	288.4
Expt. Binding Energy (eV)	285.0	286.6	289.0
Theory ratio	-	3	2
Expt. ratio (%)	-	7.5	5

c)

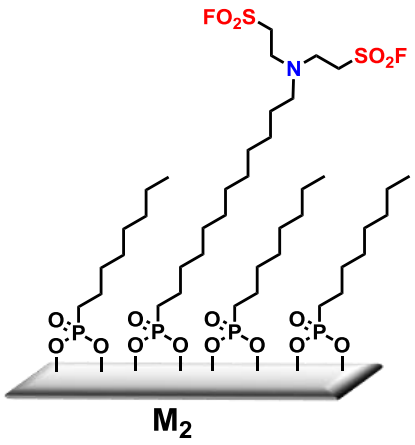

d)

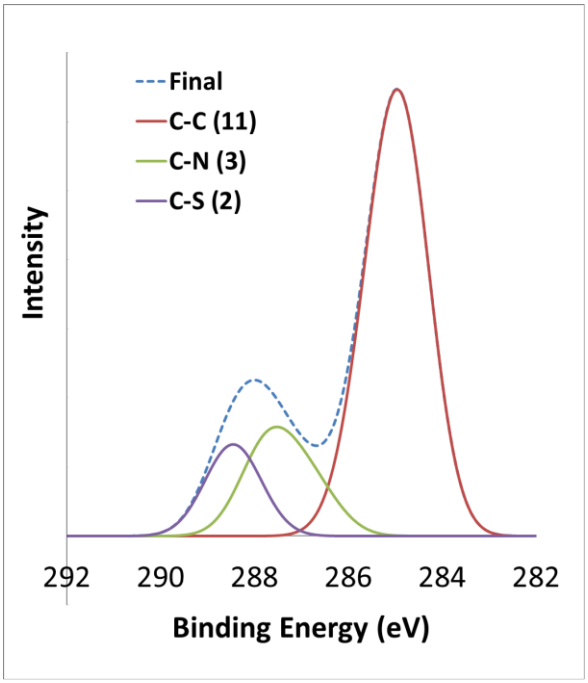

Figure S6.1. a) Gaussview structure of model compound used for the calculation of binding energies b) table showing C1s energies for the different functional group binding energy c) ChemDraw model of M_2 surfaces and d) C1s XPS spectra simulation based on DFT calculations.

a)

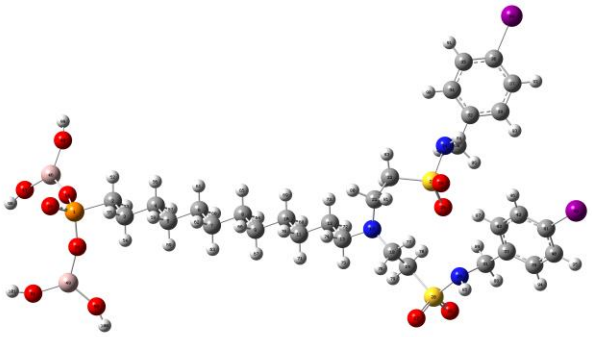

b)

Carbon Number (3D picture 100% reaction)	2-12,32-35, 37-40, 42-43,	13, 18, 21, 30, 31	36, 41	19, 21	
Functional group	C-C	C-N	C-S and C-I		C-N/(C-S + C-I)
Number of Functional group	21	5	4		
Theory Binding Energy (eV)	285.0	286.4	287.9		
Expt. Binding Energy (eV)	285.0	286.0	287.2	289.0	
Theory (%) for 80 % reaction	-	16.9	13.2		0.78
Theory (%) for 90 % reaction		16.7	13.2		0.79
Theory (%) for 95 % reaction		18.0	14.3		0.79
Theory (%) for 100 % reaction		16.6	13.3		**0.80**
Expt. ratio (%)	-	10.2	8.2		**0.80**

c)

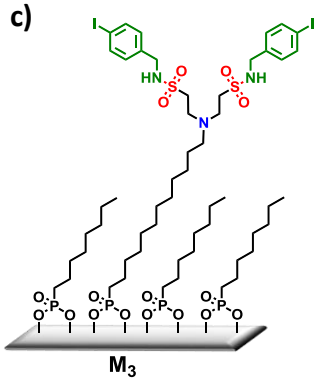

d)

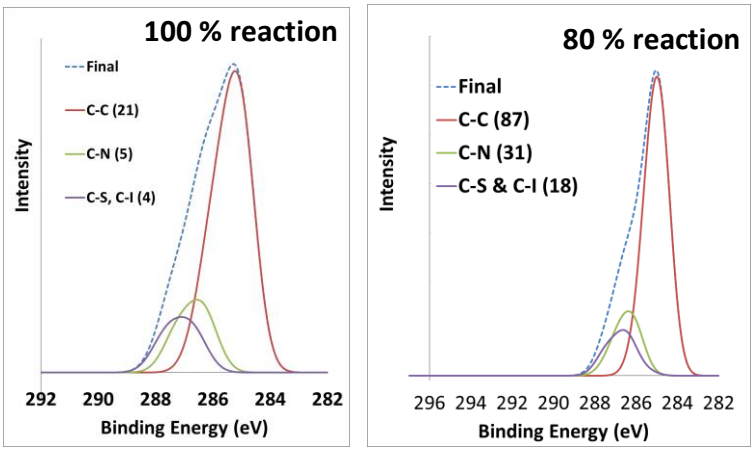

Figure S6.2. a) Gaussview structure of model compound used for the calculation of binding energies b) table showing C1s energies for the different functional group binding energy (for varying degrees of SuFEx reaction) c) ChemDraw model of M_3 surfaces and d) C1s XPS spectra simulation based on DFT calculations for 100 % and 80 % surface reaction .

a)

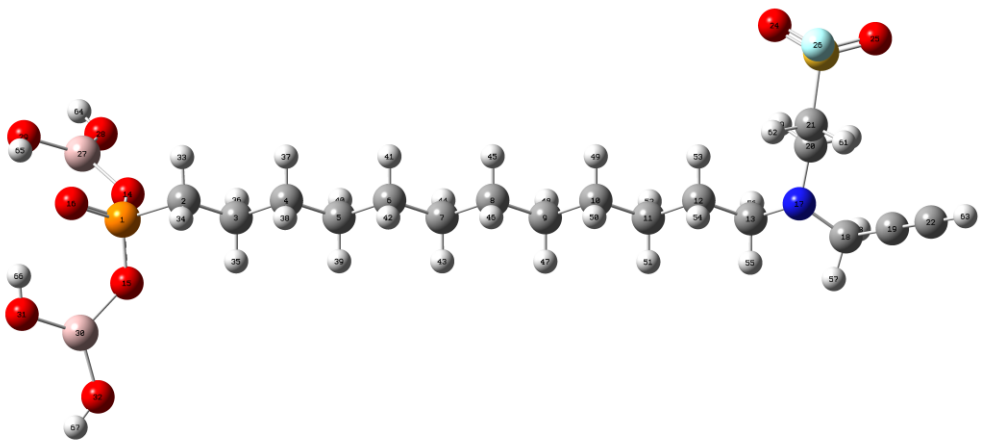

b)

Carbon Number (3D picture)	2-12, 19, 22	13,18,20	21
Functional group	C-C	C-N	C-S
Number of Functional group	13	3	1
Theory Binding Energy (eV)	285.0	286.6	287.1
Expt. Binding Energy (eV)	285.0	286.3	289.0
Theory ratio	-	5	2
Expt. ratio (%)	-	6.6	16.4

c)

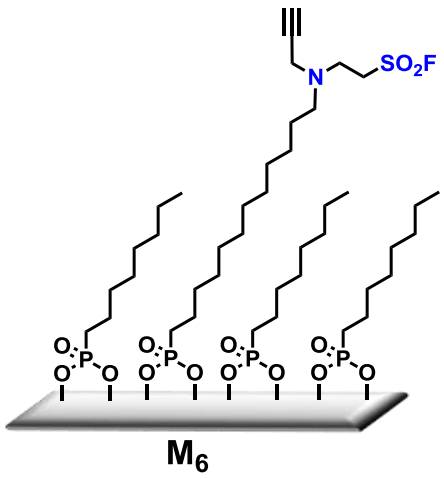

d)

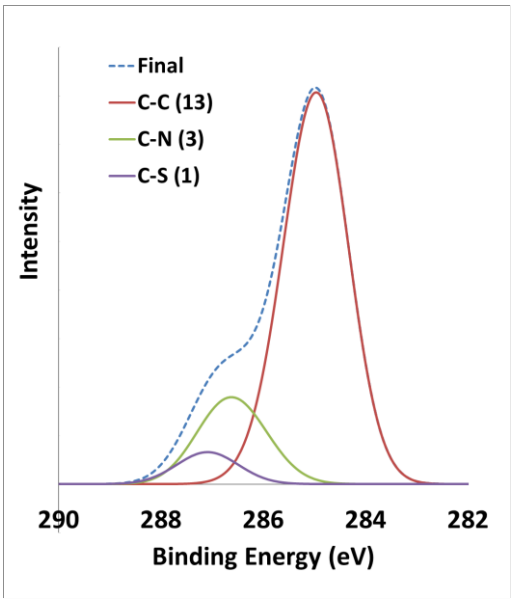

Figure S6.3. a) Gaussview structure of model compound used for the calculation of binding energies b) table showing C1s energies for the different functional group binding energy c) ChemDraw model of M_6 surfaces and d) C1s XPS spectra simulation based on DFT calculations.

a)

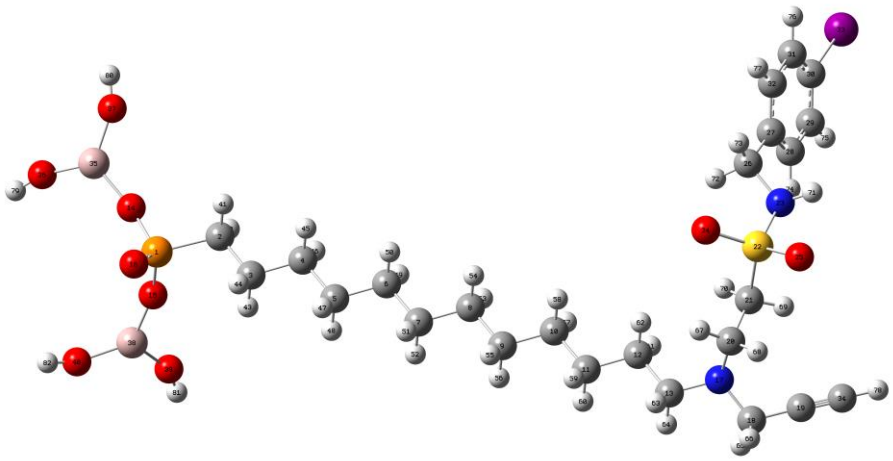

b)

Carbon Number (3D picture)	2-12,19, 34, 27-29, 31-32	13, 18, 20, 26	30	21
Functional group	C-C	C-N	C-I	C-S
Number of Functional group	18	4	1	1
Theory Binding Energy (eV)	285.0	286.4	288.3	289.7
Expt. Binding Energy (eV)	285.0	286.1	287.2	289.0
Theory ratio	-	4	1	1
Expt. ratio (%)	-	13.5	3.3	3.6

c)

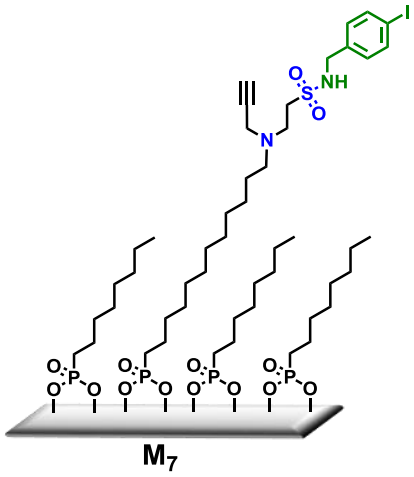

d)

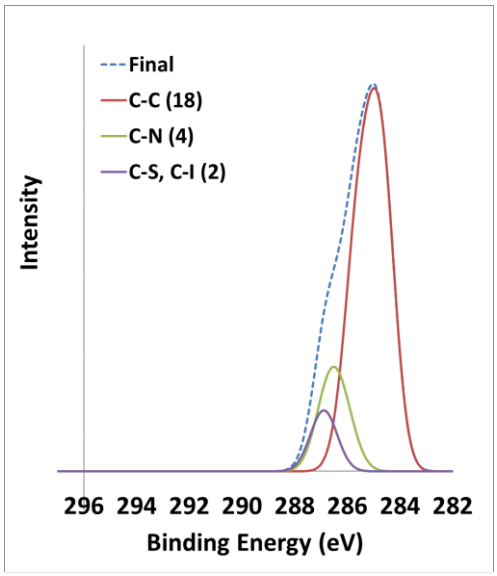

Figure S6.4. a) Gaussview structure of model compound used for the calculation of binding energies b) table showing C1s energies for the different functional group binding energy c) ChemDraw model of M_7 surfaces and d) C1s XPS spectra simulation based on DFT calculations.

a)

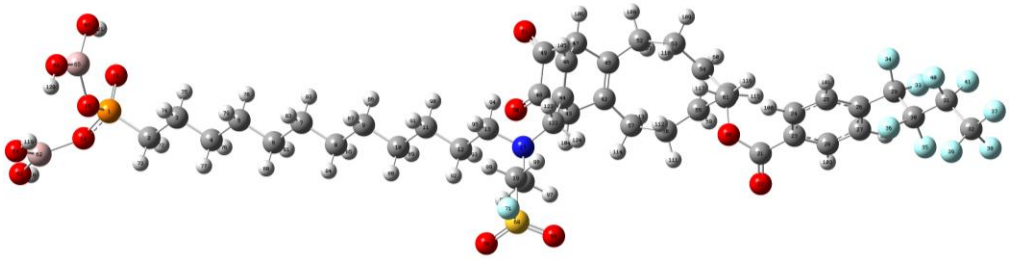

b)

Carbon Number (3D picture)	2-12, 24-25, 27-28, 42-43, 45-47, 52-58	13, 18, 23, 26, 44, 122	19,48, 49,61	21	CF2	CF3
Functional group	C-C	C-N, ArCO-, CF2-C, N-C-C=	C=O, C-S, C-O	ArC=O-O	29,30, 31	32
Number of Functional group	26	6	4	1	3	1
Theory Binding Energy (eV)	285.0	286.0	287.4	289.2	292.1	294.3
Expt. Binding Energy (eV)	285.0	286.5, 287.5	298.0		290.1	292.1
Theory ratio	-	6	4	1	3	1
Expt. ratio (%)	-	10.4, 4.2	9.8		4.2	1.7

c)

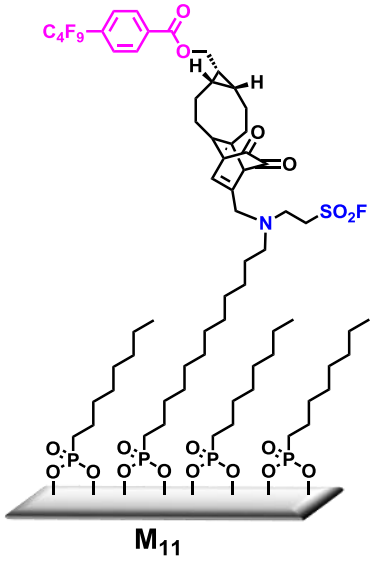

d)

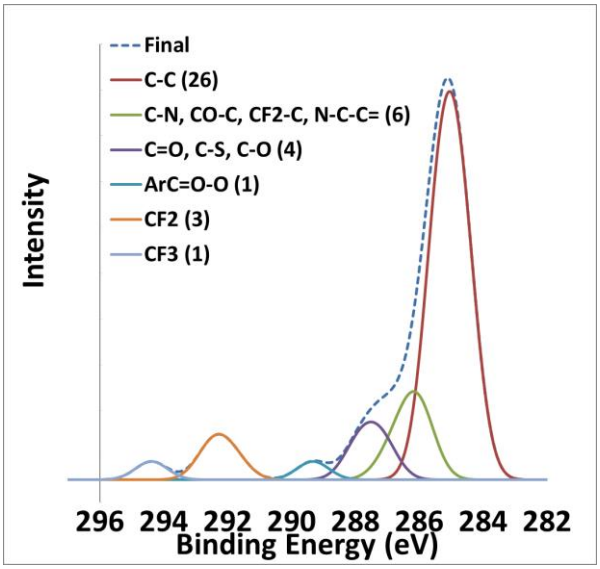

Figure S6.5. a) Gaussview structure of model compound used for the calculation of binding energies b) table showing C1s energies for the different functional group binding energy c) ChemDraw model of M_{11} surfaces and d) C1s XPS spectra simulation based on DFT calculations.

7. REFERENCES.

(1) Sen, R.; Escorihuela, J.; Smulders, M. M. J.; Zuilhof, H. *Langmuir* **2016**, *32*, 3412.

(2) Gahtory, D.; Sen, R.; Smulders, M. J.; Zuilhof, H. *Faraday Discuss.* **2017**, *204*, 383.

(3) Li, S.; Wu, P.; Moses, J. E.; Sharpless, K. B. *Angew. Chem. Int. Ed.* **2017**, *56*, 2903.

(4) Frisch, M. J.; Trucks, G. W.; Schlegel, H. B.; Scuseria, G. E.; Robb, M. A.; Cheeseman, J. R.; Scalmani, G.; Barone, V.; Mennucci, B.; Petersson, G. A.; Nakatsuji, H.; Caricato, M.; Li, X.; Hratchian, H. P.; Izmaylov, A. F.; Bloino, J.; Zheng, G.; Sonnenberg, J. L.; Hada, M.; Ehara, M.; Toyota, K.; Fukuda, R.; Hasegawa, J.; Ishida, M.; Nakajima, T.; Honda, Y.; Kitao, O.; Nakai, H.; Vreven, T.; Montgomery Jr., J. A.; Peralta, J. E.; Ogliaro, F.; Bearpark, M. J.; Heyd, J.; Brothers, E. N.; Kudin, K. N.; Staroverov, V. N.; Kobayashi, R.; Normand, J.; Raghavachari, K.; Rendell, A. P.; Burant, J. C.; Iyengar, S. S.; Tomasi, J.; Cossi, M.; Rega, N.; Millam, N. J.; Klene, M.; Knox, J. E.; Cross, J. B.; Bakken, V.; Adamo, C.; Jaramillo, J.; Gomperts, R.; Stratmann, R. E.; Yazyev, O.; Austin, A. J.; Cammi, R.; Pomelli, C.; Ochterski, J. W.; Martin, R. L.; Morokuma, K.; Zakrzewski, V. G.; Voth, G. A.; Salvador, P.; Dannenberg, J. J.; Dapprich, S.; Daniels, A. D.; Farkas, Ö.; Foresman, J. B.; Ortiz, J. V.; Cioslowski, J.; Fox, D. J.; Gaussian, Inc.: Wallingford, CT, USA, **2009**.

(5) Zhao, Y.; Truhlar, D. G. *Theor. Chem. Acc.* **2008**, *120*, 215.

APPENDIX 2

Strain-promoted cycloaddition of cyclopropenes with o–quinones: a rapid click reaction

1. MATERIAL AND METHODS.

Materials. Unless otherwise specified, all chemicals were used as received without further purification. Trimethyl(prop–1–yn–1–yl)silane, ethyl 2–diazoacetate, rhodium acetate, 4–(trifluoromethyl)benzoyl chloride, 1–isocyanato–4–(trifluoromethyl)benzene, 3,4–dihydroxybenzylamine hydrobromide, diisobutylaluminium hydride (DIBAL–H), potassium hydroxide, triethylamine, dibutyltin dilaurate (DBTDL), tetrabutylammonium fluoride (TBAF), octylphosphonic acid, hydrochloric acid, tetrahydrofuran (THF), 3,4–dihydroxybenzylamine hydrobromide, 4–(tert–butyl)benzene–1,2–diol, sodium periodate, oligo(ethylene glycol)methyl ether methacrylate (M_n 300 g M^{-1}, MeOEGMA), CuBr (99.999%), $CuBr_2$ (99.999%), 2,2–dipyridyl (BiPy), 2–bromoisobutyryl bromide methanol, hexane, acetone, dichloromethane (CH_2Cl_2) and 2–propanol were purchased from Sigma–Aldrich. ATRP initiator 11-(trichlorosilyl)undecyl-2-bromo-2-methylpropanoate was purchased from Gelest, Inc. 12–Bromododecylphosphonic acid hydrochloride salt was purchased from SiKÉMIA. Aluminium (Al) pieces (99.5% purity, mirror polished, Staalmarkt Beuningen BV) were cut using a mechanical cutter into 2 × 1 cm pieces. Silicon substrates coated with 50 nm of silicon nitride (SiN) were purchased from Synchrotonix. For surface modification reactions, the samples were loaded onto a specially constructed PTFE wafer holder able to hold up to 16 samples at a time thus ensuring rigorous reproducibility between samples.

X–ray Photoelectron Spectroscopy (XPS) Measurements. The XPS analysis of surfaces was performed using a JPS–9200 photoelectron spectrometer (JEOL, Japan). Survey and high–resolution spectra were obtained under UHV conditions using monochromatic Al Kα X–ray radiation at 12 kV and 20 mA, and an analyzer pass energy of 50 eV for wide scans and 10 eV for narrow scans. The emitted electrons were collected at 10° from the surface normal (take–off angle relative to the surface normal 10°). All XPS spectra were evaluated by using Casa XPS software (version 2.3.15). Survey spectra were corrected with linear background

before fitting, whereas high–resolution spectra were corrected with linear background. Atomic area ratios were determined after a baseline correction and normalizing the peak area ratios by the corresponding atomic sensitivity factors (1.00 for C1s, 1.80 for N1s, 2.93 for O1s, 4.43 for F1s, 1.18 for P2s, 5.03 for Br3p and 0.75 for Al2s).

DART–HRMS Measurements. Analysis of the modified mica surfaces were performed using a DART–SVP ion source (Ion–Sense, Saugus, MA, USA) coupled to a Q–Exactive orbitrap high–resolution mass spectrometer (Thermo Fisher Scientific, San Jose, CA, USA), mounted on a motorized rail travelling at 0.2 mm/s. Thermo Scientific Xcalibur software (V2.1.0.1139) was used for data acquisition and processing. The measurements were performed in negative mode at 450 °C using a scan range of *m/z* 188.6–189.4, a mass resolution of 70000 (FWHM) at a scan rate of 1 Hz. The ion trap was tuned with 0.1 mg/mL methanol solution of quinine (*m/z* 323.41 in negative mode) and optimized. The DART source was positioned 6.1 cm on the horizontal scale, 7 cm on the vertical scale with an angle of 45°, such that it is around 1 mm above the surface. The distance from the surface to the ceramic tube is minimized by placing them at the edge of the moving rail so that maximum of the (4–trifluoro)methyl benzoate ion (*m/z* 189.016) would enter the MS.[1]

Computational Procedures. All of the DFT calculations reported herein were carried out using Gaussian16.[2] All geometries were fully optimized using the dispersion-corrected density functional B97D,[3] which has been found to give relatively accurate energetics for cycloadditions.[4] Analytical frequencies were calculated at this level in all cases, and the nature of the stationary points was determined in each case according to the proper number of imaginary frequencies. The intrinsic reaction coordinate (IRC) path was traced to check the energy profiles connecting each transition state to the two associated minima of the proposed mechanism.[5] Initially, a Monte Carlo conformational search using conformer distribution option available in Spartan'14 was used (Wavefunction,

Inc., Irvine, CA, USA, 2014.). With this option, a search without constraints was performed for every structure. The torsion angles were randomly varied and the obtained structures were fully optimized using the MMFF force field. Thus, different minima of energy within an energy gap of 10 kcal·mol^{-1} were generated. These structures were analyzed and ordered considering the relative energy, being the repeated geometries eliminated. In all cases, molecules with the lowest energy and an energy gap of 4.0 kcal·mol^{-1} were selected and studied quantum chemically.

Preparation of bromo–terminated phosphonic acid monolayers (M_1). 2×1 cm Al slides were sonicated in hexane for 15 min followed by wiping with lint–free cotton swabs (Texwipe, NC, USA) to remove the polymer protection layer on top and remove any residual glue. The surfaces were chemically activated by immersion in 1:1 (v/v) 37% HCl–MeOH mixture for 5 min, followed by washing with copious amounts of water and 2–propanol. The activated surfaces were then immersed into N_2-filled vials of 5 mM solution of 3:1 ratio of phosphonic acid derivatives (octylphosphonic acid and 12–bromododecylphosphonic acid hydrochloride salt. The solution was heated to 50 °C for 5 min, and then left undisturbed for 5 h at room temperature to obtain self–assembled mixed monolayers.

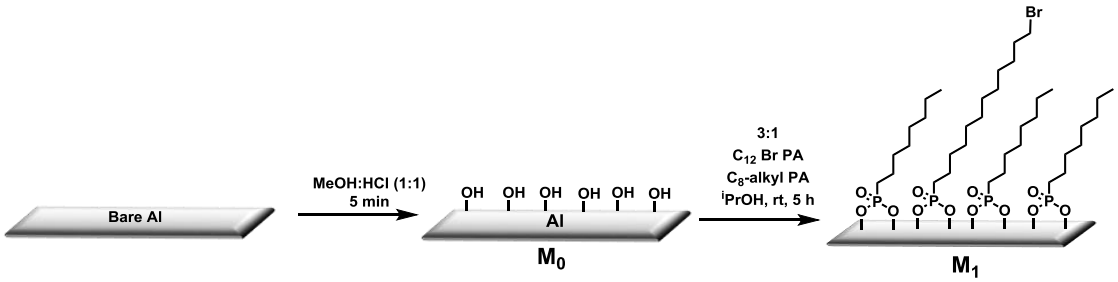

Then surfaces were taken out and sonicated successively for 5 min with 2–propanol, acetone and CH_2Cl_2. The surfaces were finally cleaned with CH_2Cl_2, air dried and stored under N_2 atmosphere. From static water contact angle (SCA) measurements, it was found that the reaction was complete after 5 h, yielding monolayers with 28–30% C as determined by XPS. Substantially longer reaction

times (16 h) contributed to the formation of undesirable multilayers (42–44% C1s).[1]

Preparation of *o*–quinone terminated monolayers (M_2). Bromo–terminated monolayers (M_1) were stirred with 50 mM 3,4–dihydroxybenzyl amine hydrobromide solution neutralized with triethylamine (Et_3N) in MeOH for 1 h, at 30 °C, to yield catechol-terminated surfaces. These surfaces were immediately oxidized by stirring in 50 mM aq. $NaIO_4$ solution at 30 °C. The samples were sonicated and washed with copious amounts of water and MeOH, dried and stored under nitrogen atmosphere. This resulted in *o*–quinone-terminated Al samples (M_3).[6]

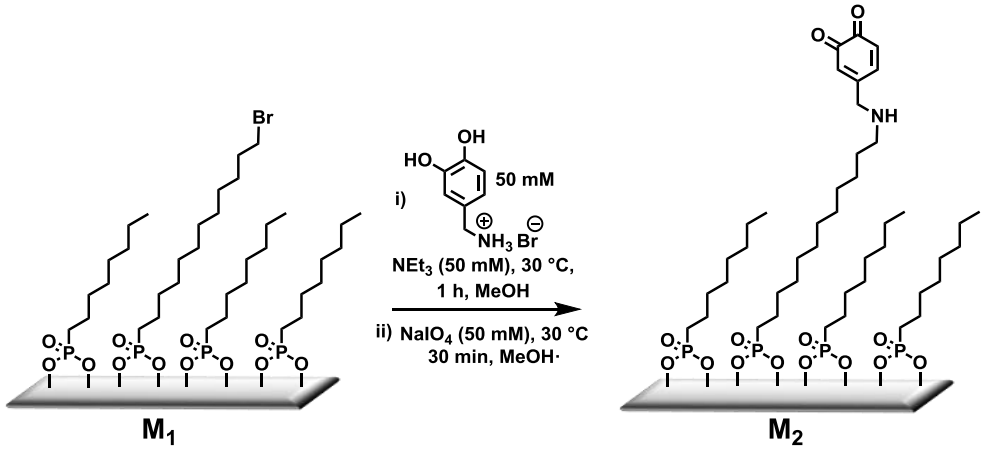

Method for reaction of *o*–quinone terminated surfaces (M_3) and cyclopropene MS–ionizable tag, 5 in solution. M_3 surfaces were reacted 5 mM solution of 5 in MeOH (HPLC grade purity) at 30 °C. The reaction was stirred at a constant speed using a magnetic bead and stirrer and all samples were loaded in a specially constructed Teflon holder to ensure rigorous reproducibility between samples.[1,6–7] Samples were immersed into the solution for a set period of reaction time and immediately taken out and washed with copious amounts of MeOH. The samples were further sonicated in MeOH for 15 min, to remove any physisorbed species, dried under a dry nitrogen stream and stored for further analysis in a sealed vial.

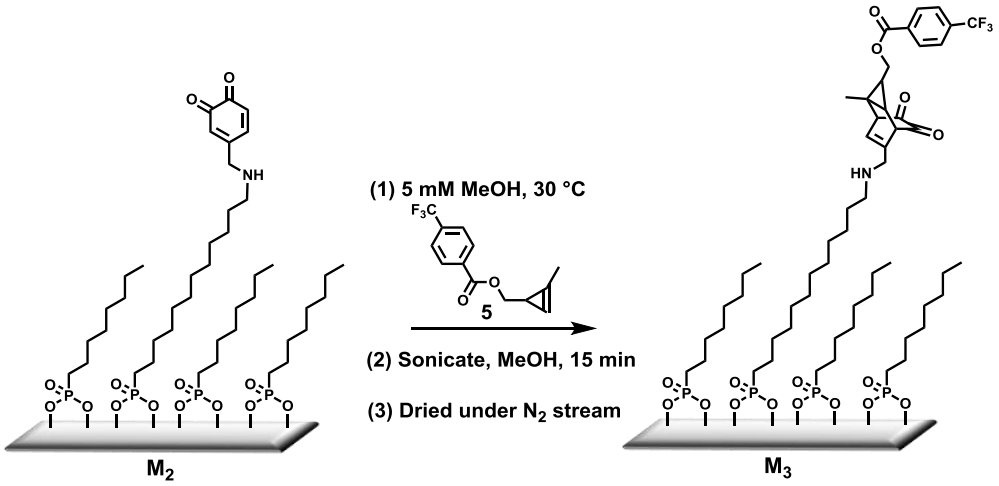

Preparation of self–assembled monolayers of initiator on SiN surfaces. The SiN substrates were rinsed with, acetone, absolute EtOH and MilliQ water, followed by exposure to air plasma for 5 min to generate hydroxyl groups at the surface. The freshly activated surfaces were subsequently immersed in a freshly prepared 1 mg/mL solution of 11-(trichlorosilyl)undecyl 2-bromo-2-methylpropanoate in dry toluene. The silanization of the substrates to form the self-assembled monolayer proceeded overnight at room temperature in a dry environment. The substrates were subsequently rinsed with toluene, acetone, EtOH and MilliQ water and dried with argon.

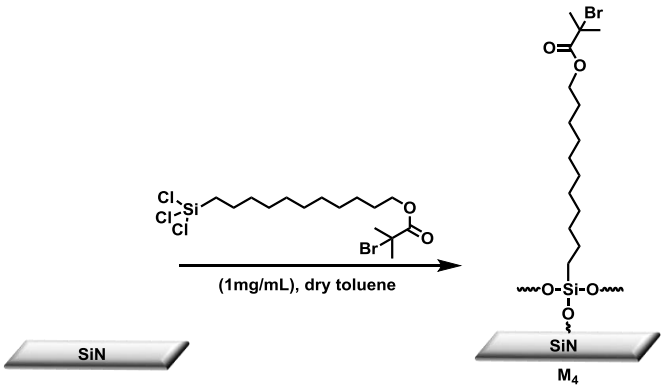

Preparation of bromine–terminated MeOEGMA polymer brushes (M_5) by SI-ATRP. Polymerization was carried out according to our modified procedure published previously.[8] The solution of MeOEGMA (2.85 g, 9.48 mmol) in water (2.5 mL) was degassed by bubbling Ar for 1h, separately from solid compounds, $CuBr_2$(8.4 mg, 3.8 µmol), CuBr(26.9 mg 188 µmol) and and 2,2- dipyridyl (77.4

mg 49.5 µmol) and methanol (2.5 mL). The methanol and the monomer solutions were transferred under argon protection to the flask containing the degassed solid components and the polymerization mixture was stirred under an inert atmosphere until full dissolution. The polymerization solution was transferred under an Ar atmosphere to the degassed reactors containing the initiator-SAM-coated substrates. The polymerization was allowed to proceed at 30 ˚C and was stopped by removing the substrates and rinsing them with copious amounts of ethanol and water to yield M_5 brushes.

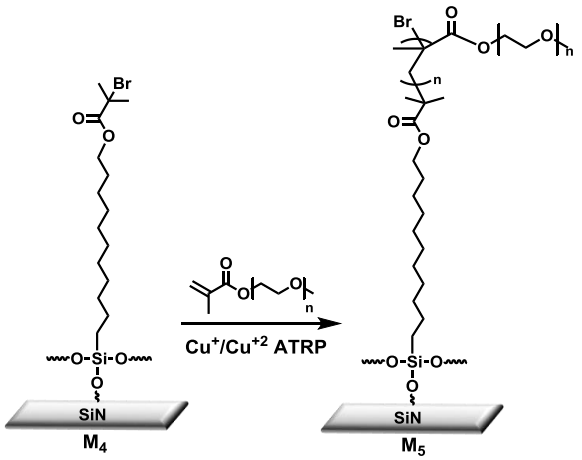

Preparation of *o*–quinone-terminated brushes (M_6). Bromo–terminated brushes (M_6) were stirred with 50 mM 3,4–dihydroxybenzyl amine hydrobromide solution neutralized with triethylamine (Et_3N) in MeOH for 3 h, at 30 °C, to yield catechol-terminated surfaces. These surfaces were immediately oxidized by stirring in 50 mM aq. $NaIO_4$ solution at 30 °C. The samples were sonicated and washed with copious amounts of water and MeOH, dried and stored under nitrogen atmosphere. This resulted in *o*–quinone-terminated brushes (M_7).

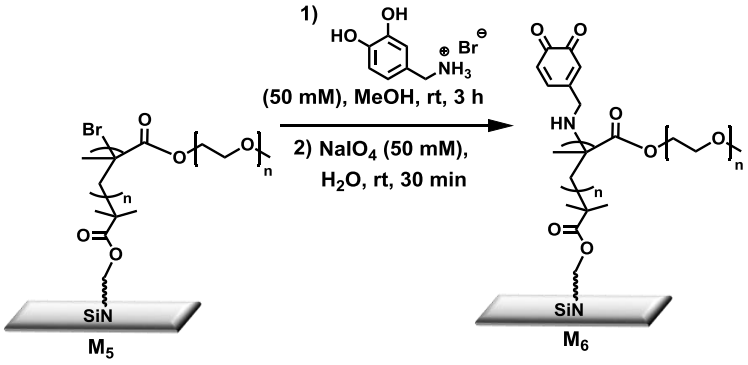

Method for SPOCQ reaction of *o*–quinone-terminated brushes (M_6) with cyclopropene tag, 5 and BCN tag, 10 in solution. M_6 surfaces were reacted with a 5 mM solution of 5 in MeOH or 10 in DCE at 30 °C. Samples were immersed into the solution for 16 h and washed with copious amounts of MeOH. The samples were further sonicated in MeOH for 15 min, to remove any physisorbed species, dried under a dry nitrogen stream and stored for further analysis in a sealed vial.

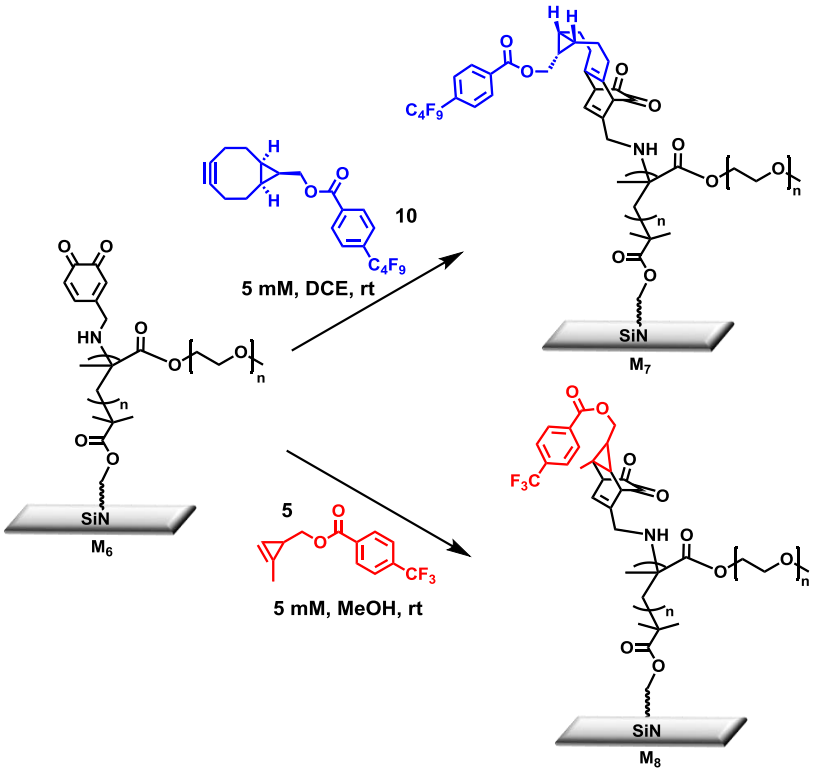

2. GENERAL SYNTHESIS

2.1 General Remarks. Unless stated otherwise, solvents and dry solvents like dichloromethane, methanol and isopropanol were purchased from Sigma–Aldrich. Unless stated otherwise all of these chemicals were used without further purification.

2.2. Reaction Handling. Unless stated otherwise all non–aqueous reactions were performed in dried glassware under an atmosphere of argon. All flasks were equipped with rubber septa and reactants were handled using standard Schlenk techniques. Temperatures above the room temperature refer to oil bath temperatures which were controlled by a thermostat. Reactions were magnetically stirred.

2.3. ^{1}H–NMR spectra were recorded at room temperature on a Bruker–400 spectrometer with ^{1}H operating frequency of 400 MHz. Unless stated otherwise all spectra were recorded at room temperature in $CDCl_3$ and all chemical shifts are given in δ units relative to the residual solvent [central line of singlet: δ_H = 7.27 ppm ($CDCl_3$)]. Analysis followed first order and the following abbreviations were used throughout: s = singlet, br. s. = broad singlet, d = doublet, t = triplet, q = quartet, quin = quintet, sxt = sextet, sept = spt, dd = doublet of doublet, dt = doublet of triplet, ddd = doblet of doublet of doublet, ddt = doblet of doublet of triplet, m = multiplet, mc = centred multiplet. Coupling constants (J) are given in Hertz (Hz).

2.4. ^{13}C–NMR spectra were recorded at room temperature on a Bruker–400 spectrometer with ^{13}C operating frequency of 101 MHz. Unless stated otherwise all spectra were recorded at room temperature in $CDCl_3$ and all chemical shifts are given in δ units relative to the residual solvent [central line of triplet: δ_C = 77.2 ppm ($CDCl_3$)]. The following abbreviation was used throughout: s = singlet, d = doublet, dd = doublet of doublet. If no coupling constants are given, the multiplicity refers to ^{1}H–decoupled spectra.

2.5 Synthesis and characterization of cyclopropene probes:

2.5.1. Synthesis of 2–methylcycloprop–2–ene–1–carboxylic acid, 2.

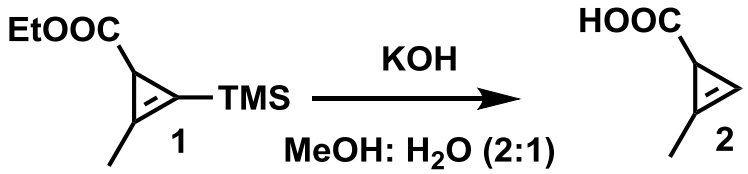

Compound **1** was synthesized according to a literature protocol.[9] The NMR spectra were in accordance with the literature values.[10] ^{1}H–NMR (400 MHz, $CDCl_3$), δ 4.10 (qq, J = 7.4, 3.7 Hz, 2H), 2.19 (s, 3H), 1.98 (s, 1H), 1.23 (t, J = 7.1 Hz, 3H), 0.19 (s, 9H). ^{13}C–NMR (101 MHz, $CDCl_3$), δ 178.57, 124.19, 105.74, 61.35, 22.84, 16.02, 13.42.

Compound **2** was synthesized from 1 according to a literature protocol.[11] ^{1}H–NMR (400 MHz, $CDCl_3$), δ 6.36 (q, J = 1.3 Hz, 1H), 2.20 (d, J = 1.3 Hz, 3H), 2.14 (d, J = 1.5 Hz, 1H). ^{13}C–NMR (101 MHz, $CDCl_3$), δ 182.96, 111.27, 94.21, 19.83, 10.40.

2.5.2. Synthesis of (2–methyl–3–(trimethylsilyl)cycloprop–2–en–1–yl)methanol, 3.

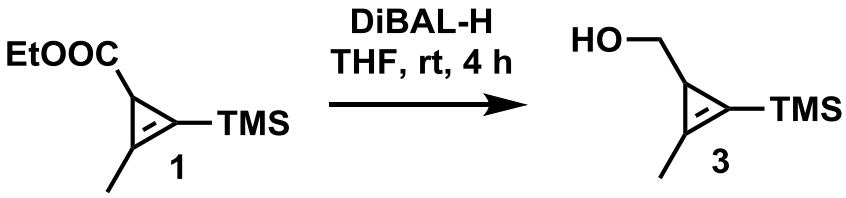

Compound 3 was synthesized according to a literature protocol.[12] The NMR spectra were in accordance with the literature values. ^{1}H–NMR (400 MHz, $CDCl_3$), δ 3.49 (d, J = 4.6 Hz, 2H), 2.22 (s, 3H), 1.57 (t, J = 4.6 Hz, 1H), 0.18 (s, 10H). ^{13}C–NMR (101 MHz, $CDCl_3$), δ 136.60, 112.40, 70.41, 23.32, 14.57, 0.01.

2.5.3. Synthesis of (2–methyl–3–(trimethylsilyl)cycloprop–2–en–1–yl)methyl4–(trifluoro- methyl)benzoate, 4.

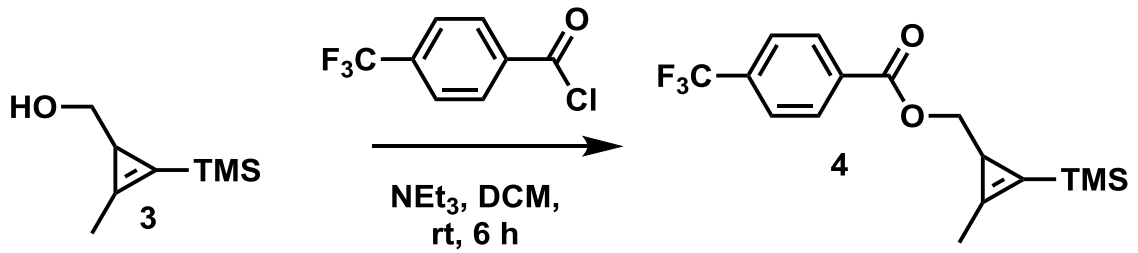

To a stirred solution of compound 3 (0.5 g, 3.20 mmol) in DCM (10 mL) at 0 °C was added triethylamine (0.5 mL, 3.52 mmol) followed by dropwise addition of 4–(trifluoromethyl)benzoylchloride (0.5 mL, 3.52 mmol). The reaction was allowed to run at room temperature until completion as shown by TLC. After completion, the reaction was carefully diluted with water (20 mL) and extracted with DCM (3 × 20 mL), the combined organic layer was dried over Na_2SO_4 and evaporated to afford a crude yellowish residue. The crude residue was purified by silica gel column chromatography using 2% EtOAc in hexane to afford 0.77 g of 4 in 74 % yield as a colourless oil. ^{1}H–NMR (400 MHz, $CDCl_3$), δ 8.18 (d, J = 8.1 Hz, 2H), 7.71 (d, J = 8.2 Hz, 2H), 4.29 – 4.08 (m, 2H), 2.22 (s, 3H), 1.69 (t, J = 5.5 Hz, 1H), 0.17 (s, 9H). ^{13}C–NMR (101 MHz, $CDCl_3$), δ 166.78, 135.54, 135.26, 131.13, 126.55, 126.30, 123.59, 112.44, 75.55, 19.55, 14.48, 0.01.

2.5.4. Synthesis of (2–methylcycloprop–2–en–1–yl)methyl 4–(trifluoromethyl) benzoate, 5.

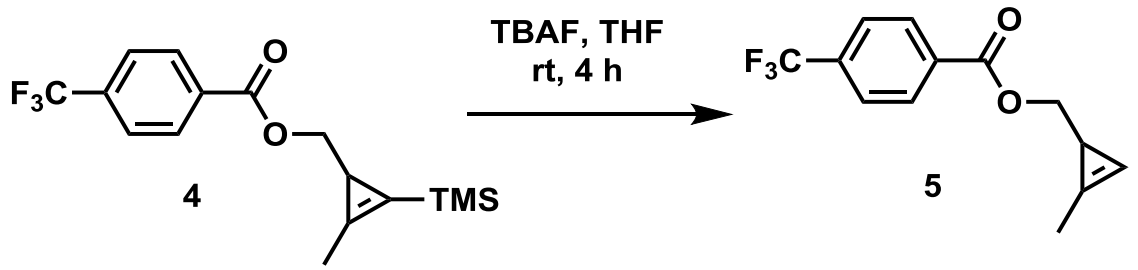

To a stirred solution of compound 4 (0.1 g, 0.304 mmol) in THF (2 mL) was added a 1 M solution of TBAF in THF (0.36 mL, 0.365 mmol). The reaction was allowed to run at room temperature until completion as shown by TLC. After completion, the solvent was evaporated using compressed air and the crude residue was purified by silica gel column chromatography using 0.7 % EtOAc in hexane to

afford 0.061 g of 5 in 76 % yield as a colorless oil. ^{1}H–NMR (400 MHz, $CDCl_3$), δ 8.17 (d, J = 8.3 Hz, 2H), 7.69 (d, J = 8.3 Hz, 2H), 6.60 (s, 1H), 4.29 (dd, J = 11.1, 4.9 Hz, 1H), 4.20 (dd, J = 11.0, 5.3 Hz, 1H), 2.16 (s, 3H), 1.86 – 1.72 (m, 1H).. ^{13}C–NMR (101 MHz, $CDCl_3$), δ 165.68, 134.28, 130.15, 128.00, 125.50, 122.58, 120.69, 102.21, 73.12, 17.19, 11.77. Calculated *m/z*: $[M + Na]^+$ = 279.0603, obtained *m/z*: $[M + Na]^+$ = 279.0590.

2.5.5. Synthesis of (2–methyl–3–(trimethylsilyl)cycloprop–2–en–1–yl)methyl(4–(trifluoro- methyl)phenyl)carbamate, 6.

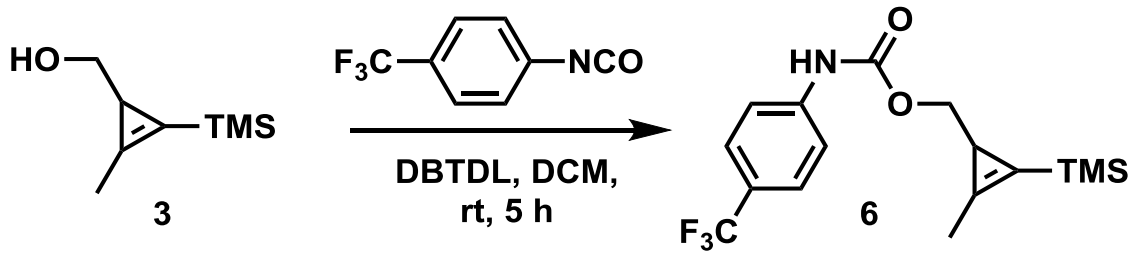

To a stirred solution of compound 3 (0.5 g, 3.20 mmol mmol) in DCM (6 mL) at 0 °C was added dibutyltindilaurate (DBTDL) (0.19 mL, 0.320 mmol) followed by dropwise addition of 4–(trifluoromethyl)phenyl isocyanate (0.46 mL, 3.20 mmol). The reaction was allowed to run at room temperature until completion as shown by TLC. After completion, the reaction was carefully diluted with water (20 mL) and extracted with DCM (20 mL × 3), the combined organic layer was dried over Na_2SO_4 and evaporated to afford a crude residue. The crude residue was purified by silica gel column chromatography using 2 % EtOAc in hexane to afford 0.89 g of 6 in 81 % yield as a colorless oil which solidified upon cooling. ^{1}H–NMR (400 MHz, $CDCl_3$), δ 7.54 (t, J = 6.7 Hz, 4H), 6.90 (s, 1H), 4.08 (dd, J = 10.9, 5.4 Hz, 1H), 3.98 (dd, J = 10.9, 5.7 Hz, 1H), 2.21 (s, 3H), 1.60 (s, 1H), 0.17 (s, 9H). ^{13}C–NMR (101 MHz, $CDCl_3$), δ 154.73, 142.51, 135.39, 127.41, 126.22, 123.98, 119.13, 112.06, 75.57, 19.54, 14.33, 0.15.

2.5.6. Synthesis of (2–methylcycloprop–2–en–1–yl)methyl(4–(trifluoromethyl)phenyl) carbamate, 7

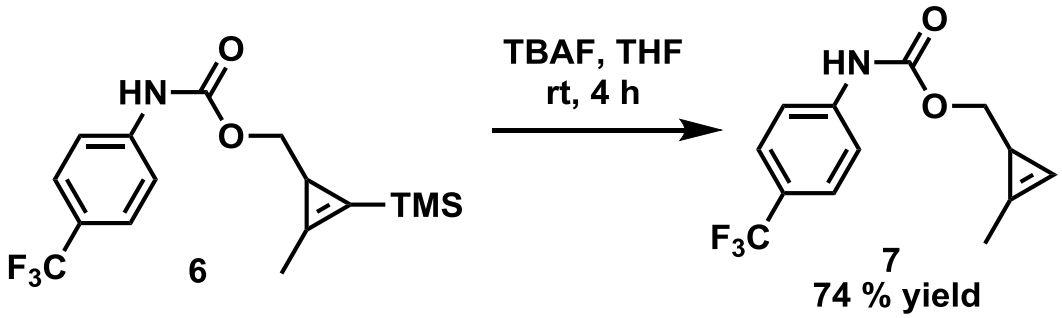

To a stirred solution of compound 6 (0.21 g, 0.611 mmol) in THF (2 mL) was added a 1 M solution of TBAF in THF (0.67 mL, 0.672 mmol). The reaction was allowed to run at room temperature until completion as shown by TLC. After completion, the solvent was evaporated using compressed air and the crude residue was purified by silica gel column chromatography using 0.7 % EtOAc in hexane to afford 0.196 g of 7 in 74 % yield as a colorless oil. ^{1}H–NMR (400 MHz, $CDCl_3$), δ 7.59 – 7.54 (m, 2H), 7.50 (d, J = 8.8 Hz, 2H), 6.77 (s, 1H), 6.59 (s, 1H), 4.15 – 3.99 (m, 2H), 2.16 (s, 3H), 1.70 (t, J = 6.0 Hz, 1H). ^{13}C–NMR (101 MHz, $CDCl_3$), δ 154.52, 142.39, 127.46, 126.29, 125.96, 123.95, 121.67, 119.03, 103.11, 74.31, 18.18, 12.79. Calculated *m/z*: $[M - H]^-$ = 270.0747, obtained *m/z*: $[M - H]^-$ = 270.0744.

2.5.7. Synthesis of 4-(tert-butyl)cyclohexa-3,5-diene-1,2-dione, 8.

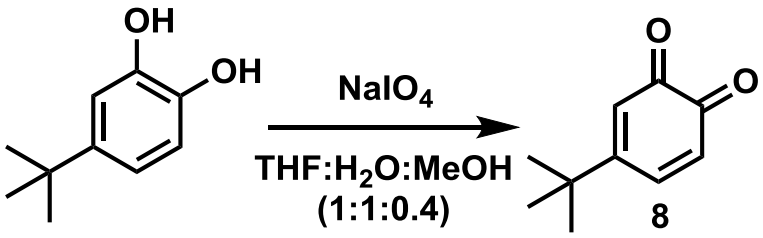

Compound 8 was synthesized according to a literature protocol.[13] The NMR spectra was in accordance with the literature values. ^{1}H–NMR (400 MHz, $CDCl_3$), δ 7.19 (d, J = 12.7 Hz, 1H), 6.39 (d, J = 10.4 Hz, 1H), 6.27 (d, J = 2.1 Hz, 1H), 1.23 (s, 9H).

2.5.8. General scheme for reaction for the reaction between 5 and 8 to yield, 6–(tert–butyl)–2–methyl–8,9–dioxotricyclo[3.2.2.0]non–6–en–3–yl)methyl 4–(trifluoromethyl)benzoate, 9.

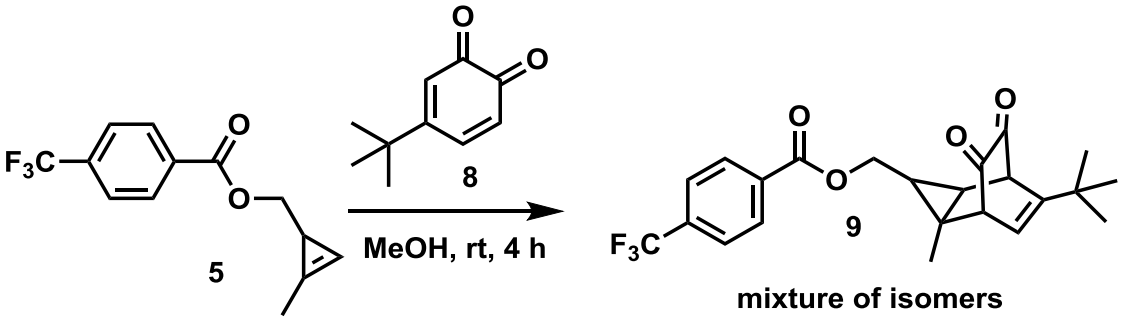

To a stirred compound 5 (0.042 g, 0.164 mmol) in MeOH (2 mL) was added compound 8 (0.027 g, 0.164 mmol). The reaction was allowed to run at room temperature until completion as shown by TLC. After 4 h, the solvent was evaporated and the crude residue was purified by silica gel column chromatography using 10 % EtOAc in hexane to afford 0.052 g of **9** (two isomers : **9a** [0.024 g] and **9b** [0.028 g]) in 75.3 % total yield as yellow sticky solids. Although the determination of structures by NMR proved to be difficult, we assigned following plausible structures of the isomers (only one enantiomer depicted for simplicity) based on NOESY correlations and DFT calculations:

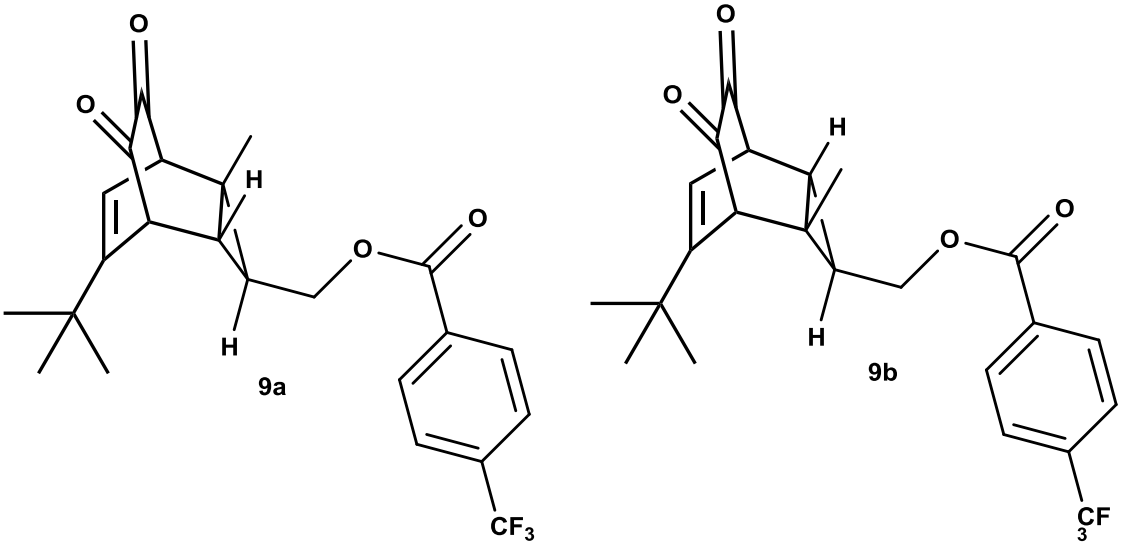

9a: ^{1}H–NMR (400 MHz, $CDCl_3$), δ 8.14 (d, J = 8.2 Hz, 2H), 7.73 (d, J = 8.3 Hz, 2H), 5.74 (dd, J = 7.0, 2.6 Hz, 1H), 4.54 (dd, J = 11.7, 7.5 Hz, 1H), 4.45 – 4.32

(m, 1H), 3.77 (dd, J = 4.8, 2.6 Hz, 1H), 3.31 (d, J = 6.9 Hz, 1H), 1.73 (td, J = 7.6, 3.5 Hz, 2H), 1.31 (s, 3H), 1.27 (d, J = 6.3 Hz, 1H), 1.25 – 1.21 (m, 1H), 1.07 (s, 9H). ^{13}C–NMR (101 MHz, $CDCl_3$), δ 188.46, 188.21, 165.19, 150.45, 134.85, 133.10, 129.96, 125.54, 122.20, 117.03, 64.02, 53.46, 49.69, 35.34, 27.52, 19.85, 19.52, 18.07, 15.87. Calculated *m/z*: $[M + Na]^+$ = 443.1441, obtained *m/z*: $[M + Na]^+$ = 443.1415.

9b: ^{1}H–NMR (400 MHz, $CDCl_3$), δ 8.13 (d, J = 8.2 Hz, 2H), 7.73 (d, J = 8.2 Hz, 2H), 5.73 (dd, J = 6.9, 2.4 Hz, 1H), 4.67 (dd, J = 11.7, 6.5 Hz, 1H), 4.26 (dd, J = 11.7, 8.9 Hz, 1H), 3.56 (dd, J = 7.0, 4.5 Hz, 1H), 3.48 (d, J = 2.2 Hz, 1H), 1.76 (ddd, J = 9.5, 6.6, 3.5 Hz, 1H), 1.32 (s, 3H), 1.23 (t, J = 3.9 Hz, 1H), 1.07 (s, 10H). ^{13}C–NMR (101 MHz, $CDCl_3$), δ 189.08, 187.61, 165.13, 151.12, 134.85, 133.11, 129.33, 125.60, 125.53, 122.20, 116.47, 63.88, 56.42, 46.82, 35.41, 27.63, 26.97, 20.93, 18.10, 17.92, 15.99. Calculated *m/z*: $[M + Na]^+$ = 443.1441, obtained *m/z*: $[M + Na]^+$ = 443.1418.

3. SUPPLEMENTARY KINETICS DATA.

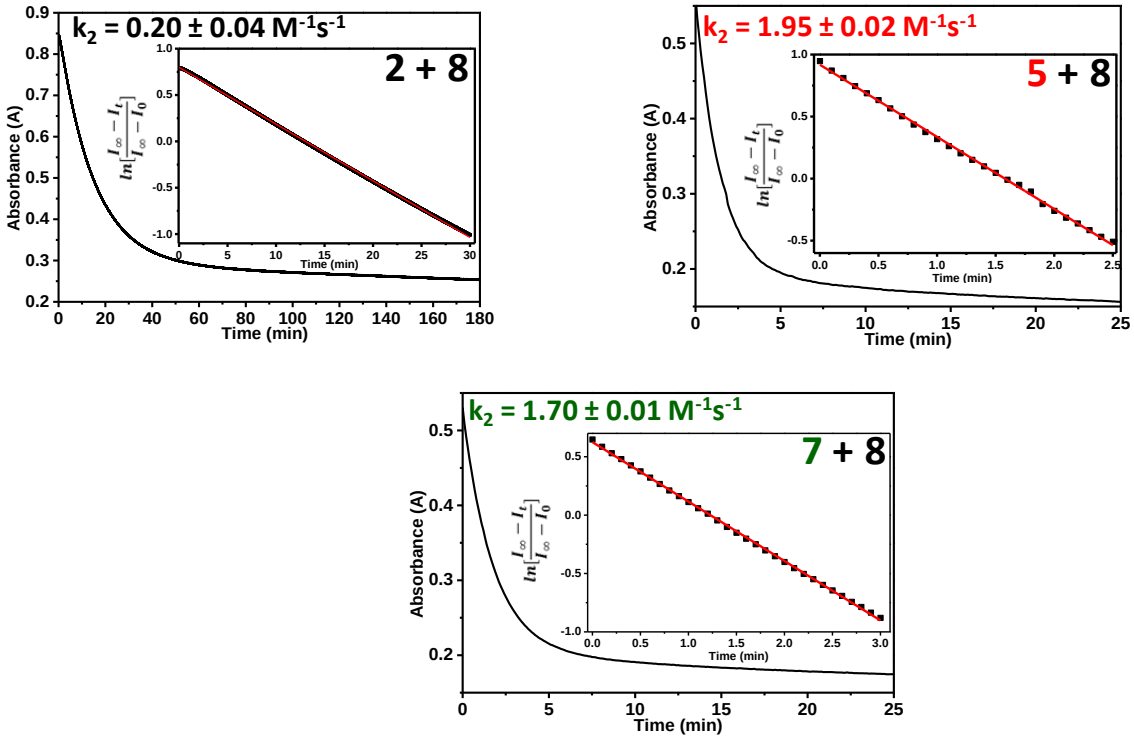

Figure S3.1. Sigmoidal plot of decay of UV absorbance of charecteristic *o*–quinone (**8**) peak at 385 nm. The experiments were carried out in triplicate with 1:10 excess of cyclopropene **2**, **5** or **7** (5.0 mM MeOH solution, at 30 °C was used) with respect to **8**, to ensure pseudo–first order kinetics. Inset: Linear plot of $ln|(A_\infty - A_t)/(A_\infty - A_0)|$ *vs* time (min), the slope of which is the pseudo—first order reaction rate (k′) obtained by a least–squares fit ($R^2 > 0.95$). The second–order rate constant (k_2) is derived from here using the concentration of cyclopropene (5.0 mM).

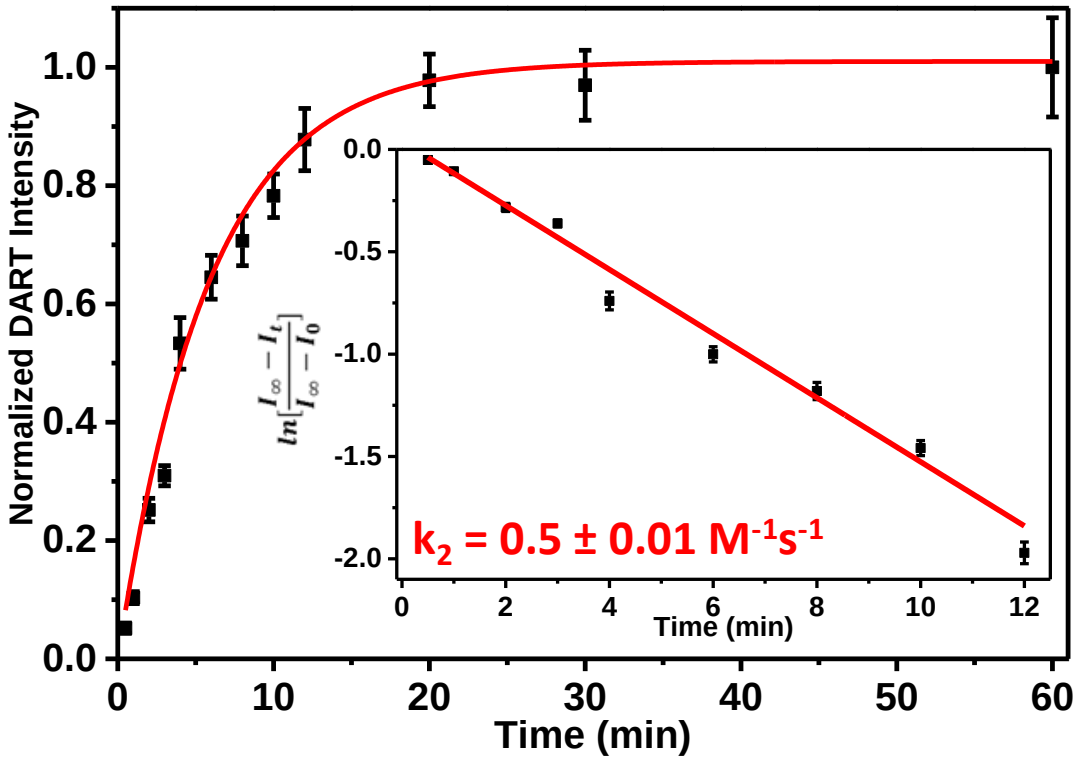

Figure S3.2. Sigmoidal plot of normalized integrated DART–HRMS intensity vs time (min) for an *o*–quinone-terminated surface (M_4) reacting with cyclopropene **5** in MeOH solution at 30 °C. Inset: Linear plot of $ln\ |(I_\infty - I_t)\ /\ (I_\infty - I_0)|$ *vs* time (min), the slope of which is the pseudo—first order reaction rate (k′) obtained by a least–squares fit ($R^2 > 0.95$). (Each time point is an average of hexaplet samples.) The second–order rate constant is derived using the solution concentration of cyclopropene tag **5** (5.0 mM).

4. SUPPLEMENTARY FIGURES.

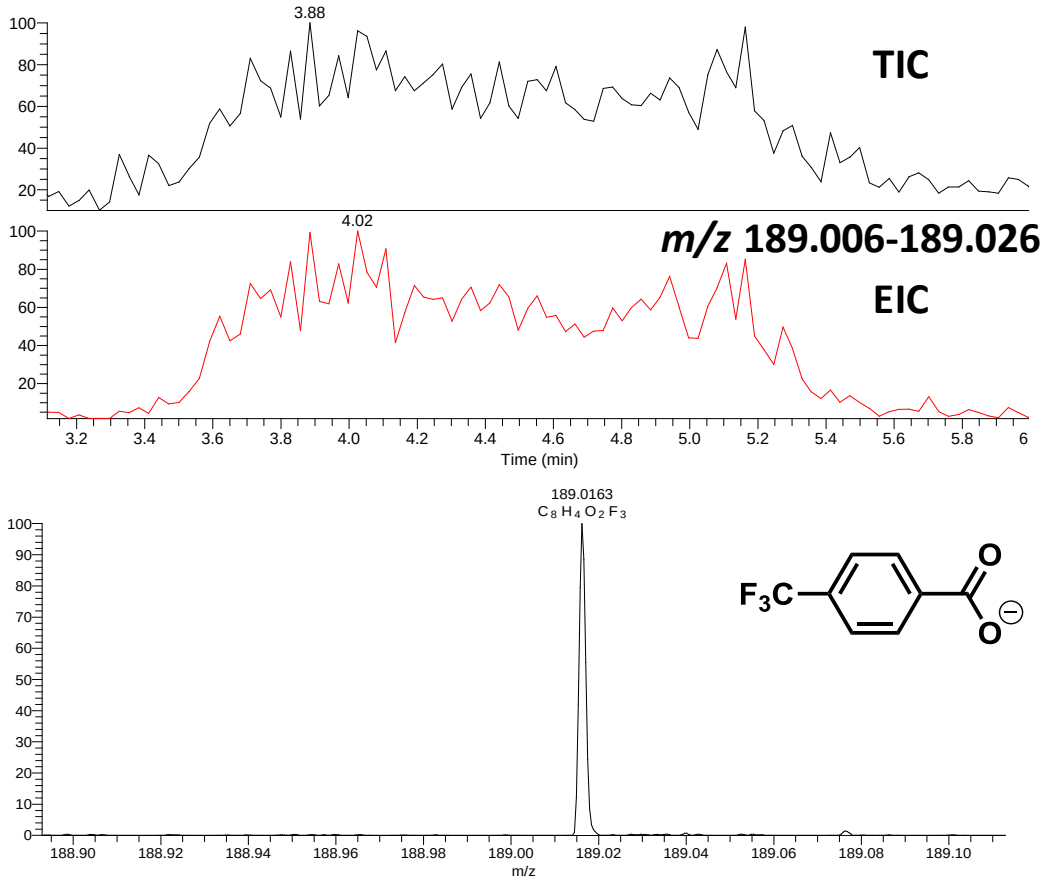

Elemental composition search on mass 189.0163

m/z= 184.0163-194.0163

m/z	Theo. Mass	Delta (mmu)	RDB equiv.	Composition
189.0163	189.0158	0.47	5.5	$C_8H_4O_2F_3$
	189.0169	-0.67	1.5	$C_5H_5O_3F_4$
	189.0146	1.61	9.5	$C_{11}H_3OF_2$
	189.0182	-1.98	8.5	$C_{10}H_5O_4$
	189.0135	2.76	13.5	$C_{14}H_2F$
	189.0133	2.91	2.5	$C_6H_3F_6$
	189.0194	-3.12	4.5	$C_7H_6O_5F$
	189.0205	-4.26	0.5	$C_4H_7O_6F_2$
	189.0241	-7.85	-0.5	$C_3H_9O_9$
	189.0041	12.14	0.5	$C_3H_6O_8F$

Figure S4.1. Representative spectra of a typical DART–HRMS measurement for SPOCQ samples. Top: Total Ion Current (TIC); middle: Extracted ion chromatogram (EIC) of 10 mmu window around the theoretical *m/z* of the ion (189.016) of interest; bottom: error between obtained mass and predicted mass fragments (an error of <1 mmu indicates match between our MS–tag and that predicted by Xcalibur software). All statistics (average, standard deviation) of the XPS data are derived from six independent samples in each case.

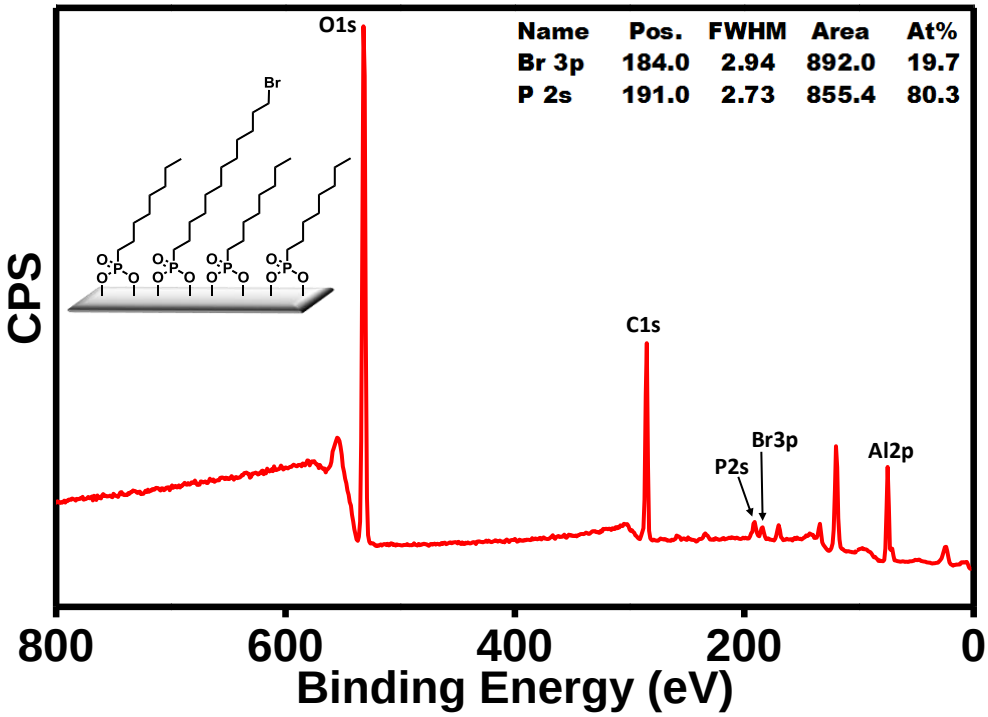

Figure S4.2. XPS wide scan of Br–terminated **M_1** surfaces.

Theoretical Br/P ratio = 1/ 4 = 0.25

Experimental Br/P = 0.25 ± 0.02

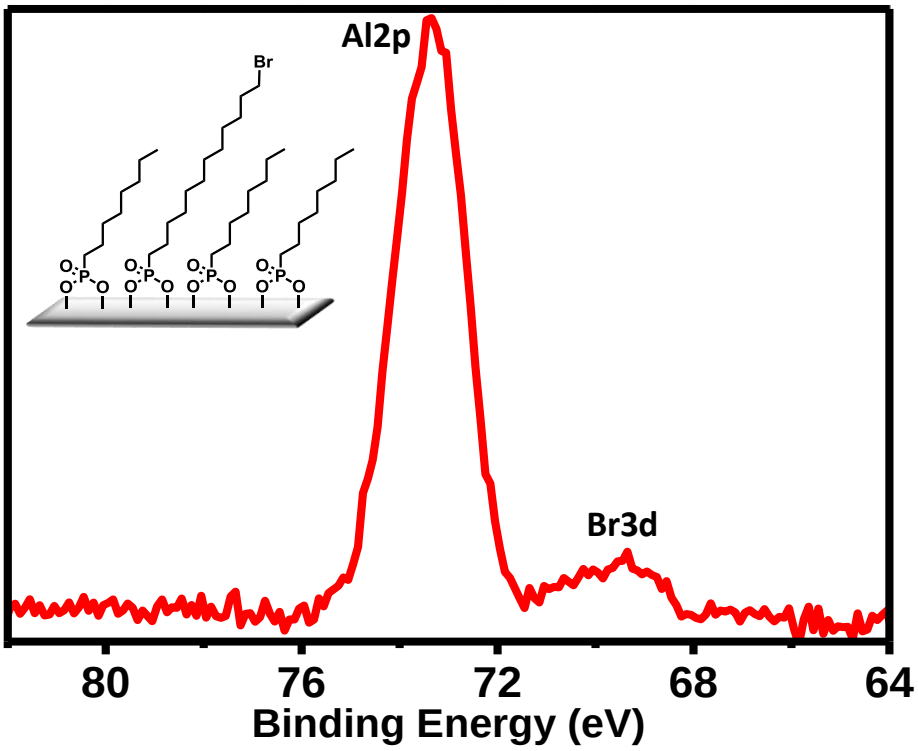

Figure S4.3. XPS Br3d narrow scan of **M_1** surfaces.

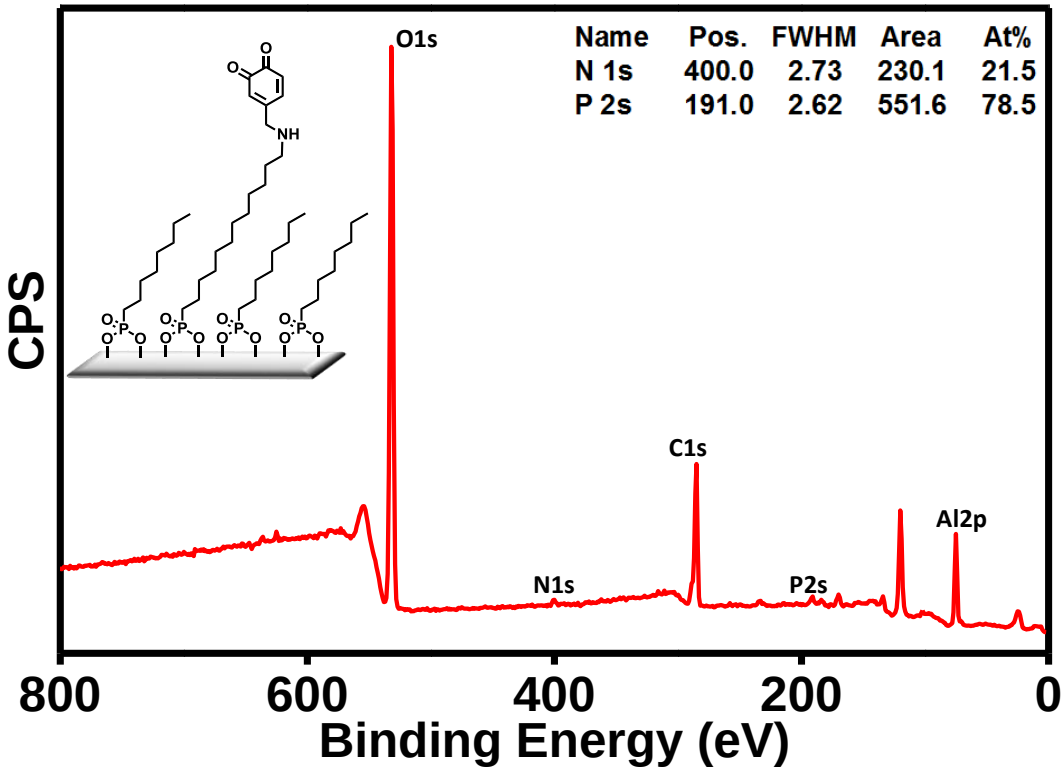

Figure S4.4. XPS wide scan of quinone-terminated **M₂** surfaces.

Theoretical N/P ratio = 1/4 = 0.25

Experimental N/P = 0.25 ± 0.02

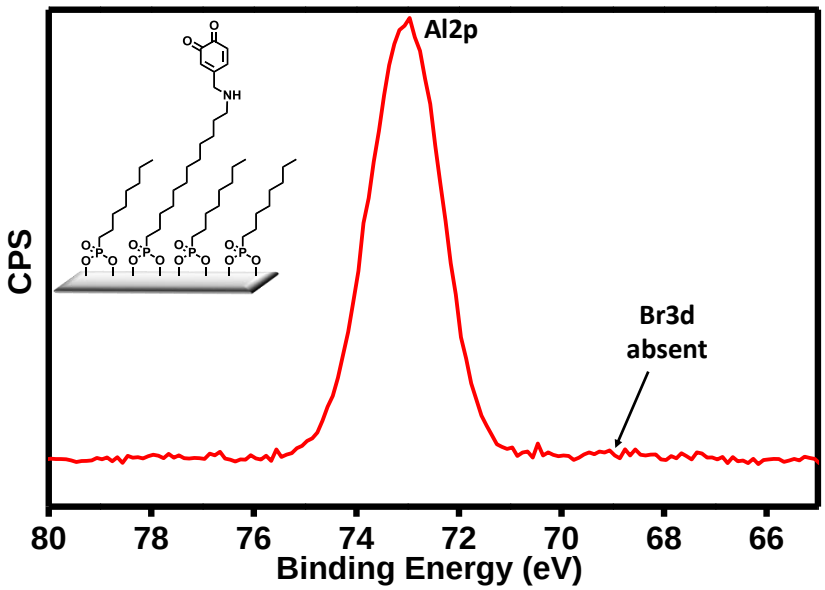

Figure S4.5. XPS Br3d narrow scan of **M₂** surfaces showing absence of a Br signal.

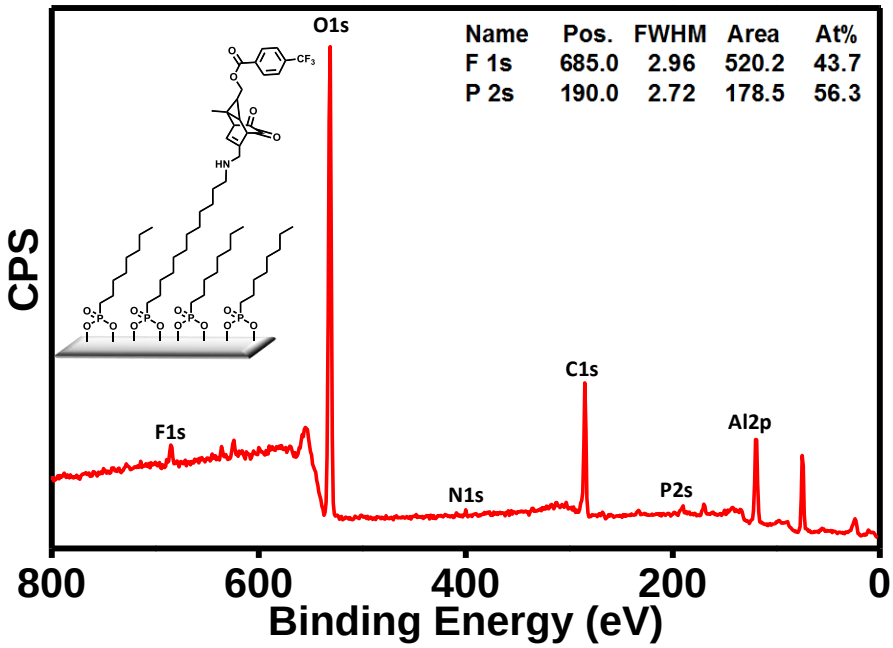

Figure S4.6. XPS wide scan of **M₃** surfaces (**M₂** surfaces reacted with 5).

Th. F/P = 3/4 = 0.75

Expt. F/P = 0.78 ± 0.03

Surface yield = 100 ± 3 %

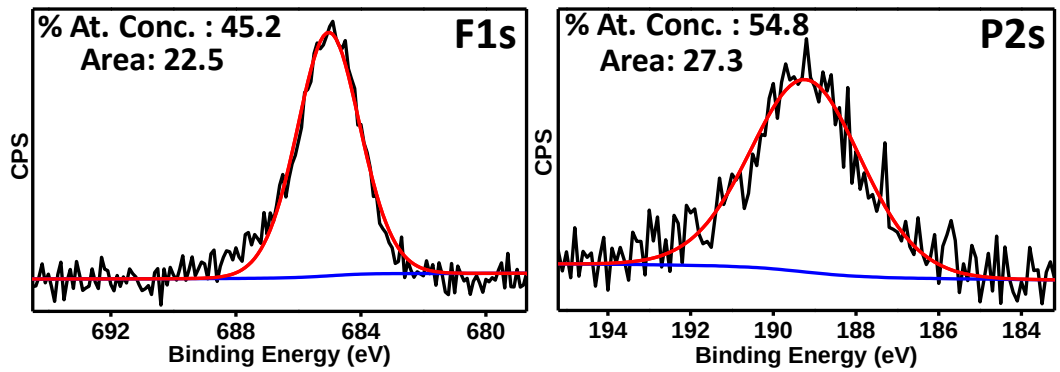

Figure S4.7. F1s and P2s narrow scans (centered on 686.0 eV and 187.0 eV, respectively) of **M₃** surfaces for establishing conversion.

Th. F/P = 3/4 = 0.75

Expt. F/P = 45.2/54.8 = 0.82 ± 0.02

Surface yield = 109 ± 3 % ⇒ quantitative conversion, even when taking attenuation of the P2s signal by the overlaying monolayer into account.

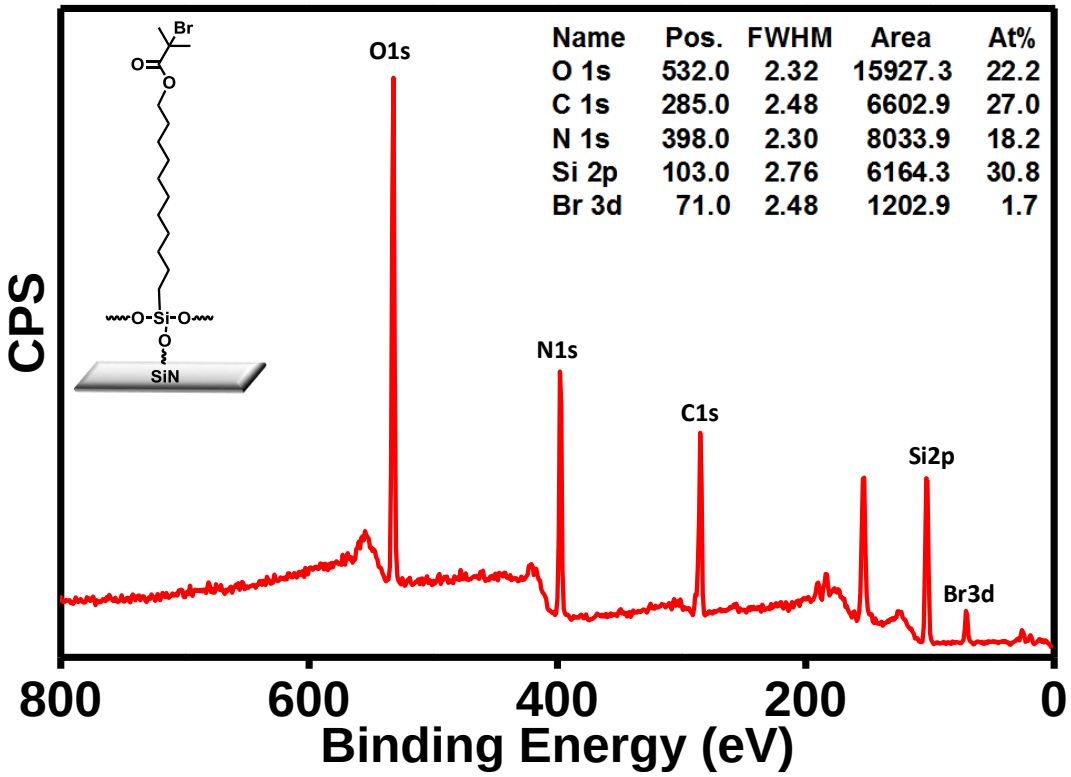

Figure S4.8. XPS wide scan of **M**$_4$ surfaces.

Th. C/Br = 15/1 = 15

Expt. C/Br = 27.0/1.7 = 16 ± 1

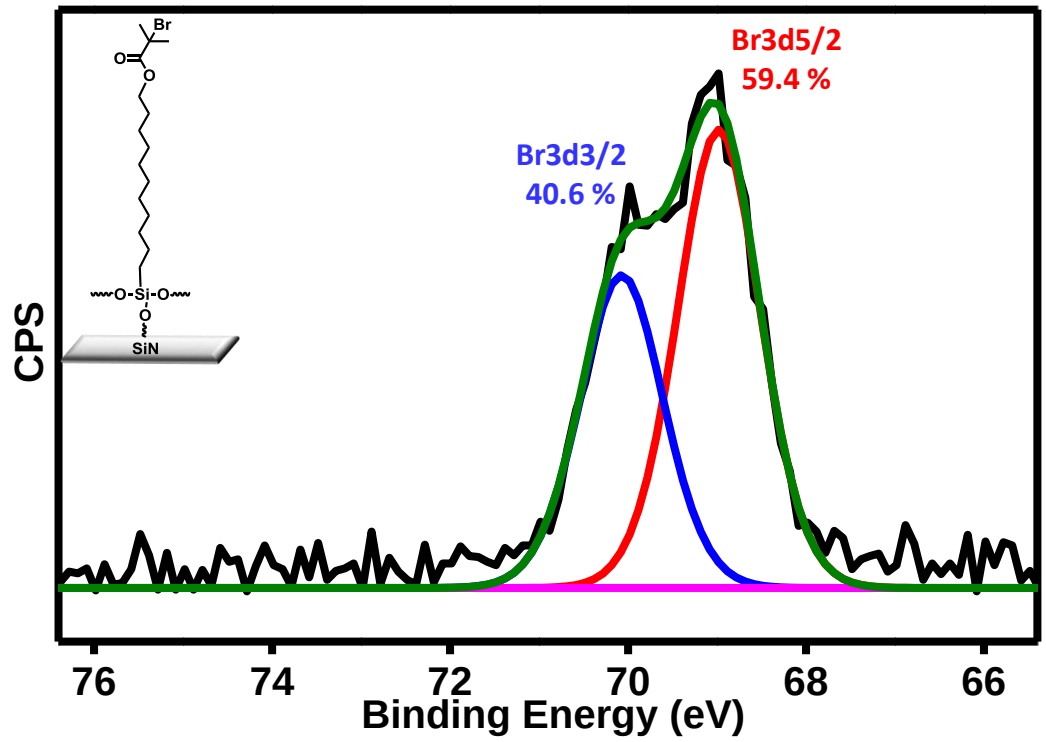

Figure S4.9. XPS Br3d narrow scan of **M₄** surfaces.

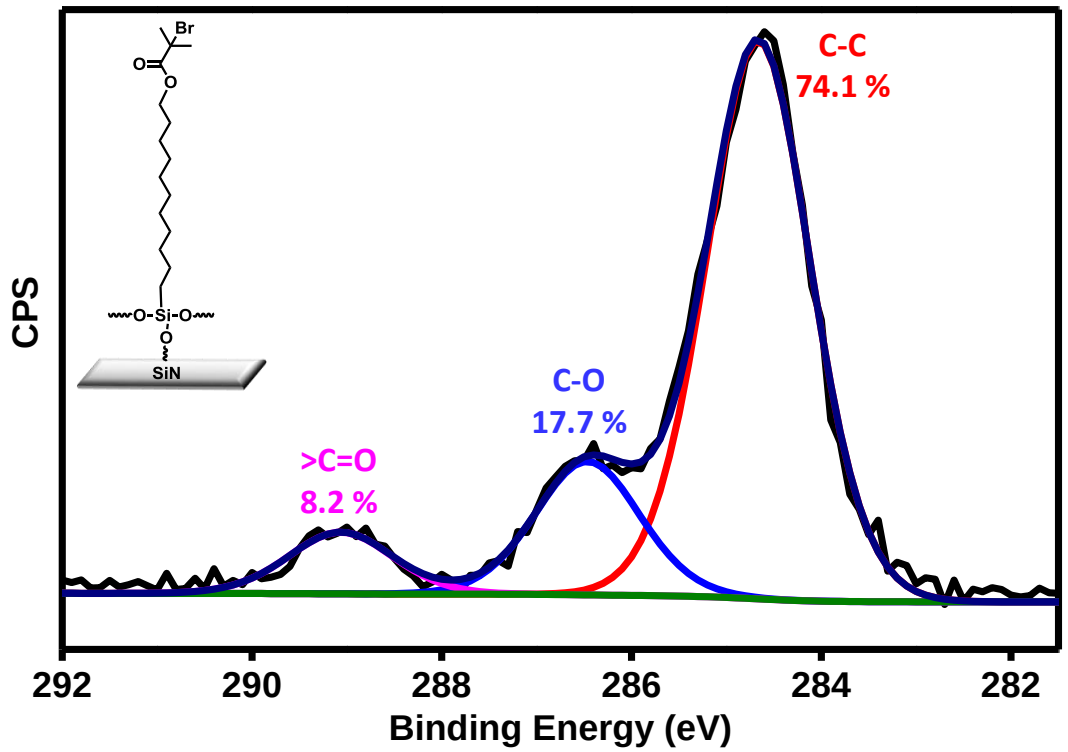

Figure S4.10. XPS C1s narrow scan of **M₄** surfaces.

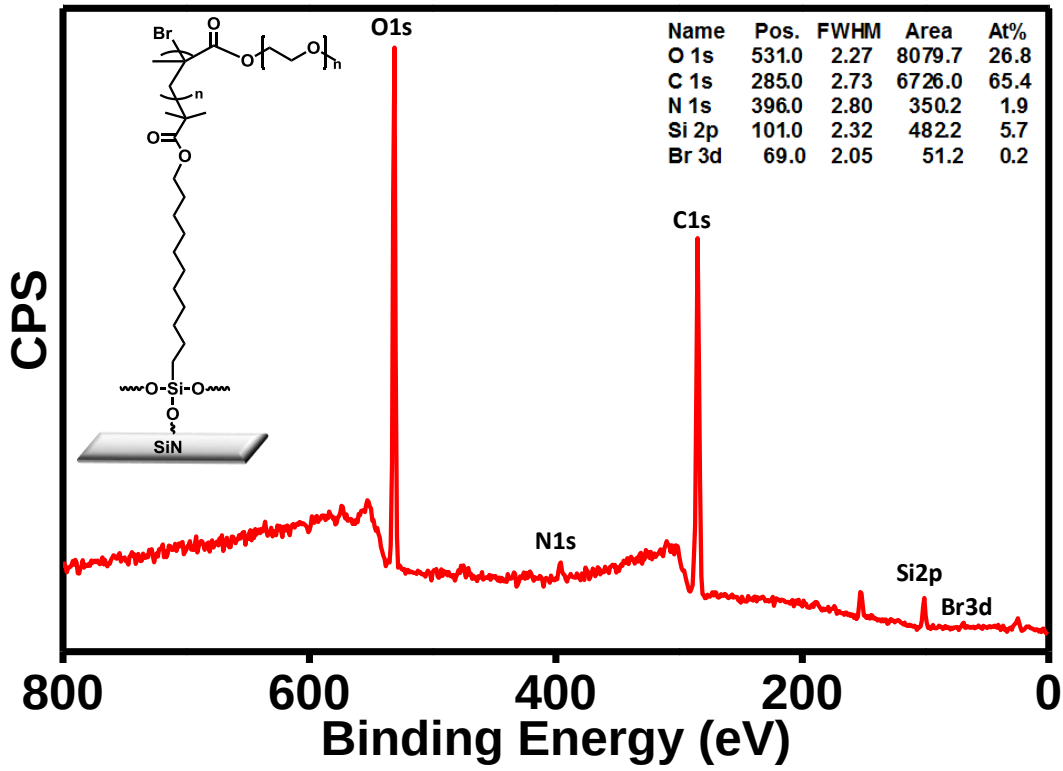

Figure S4.11. XPS wide scan of **M5** surfaces.

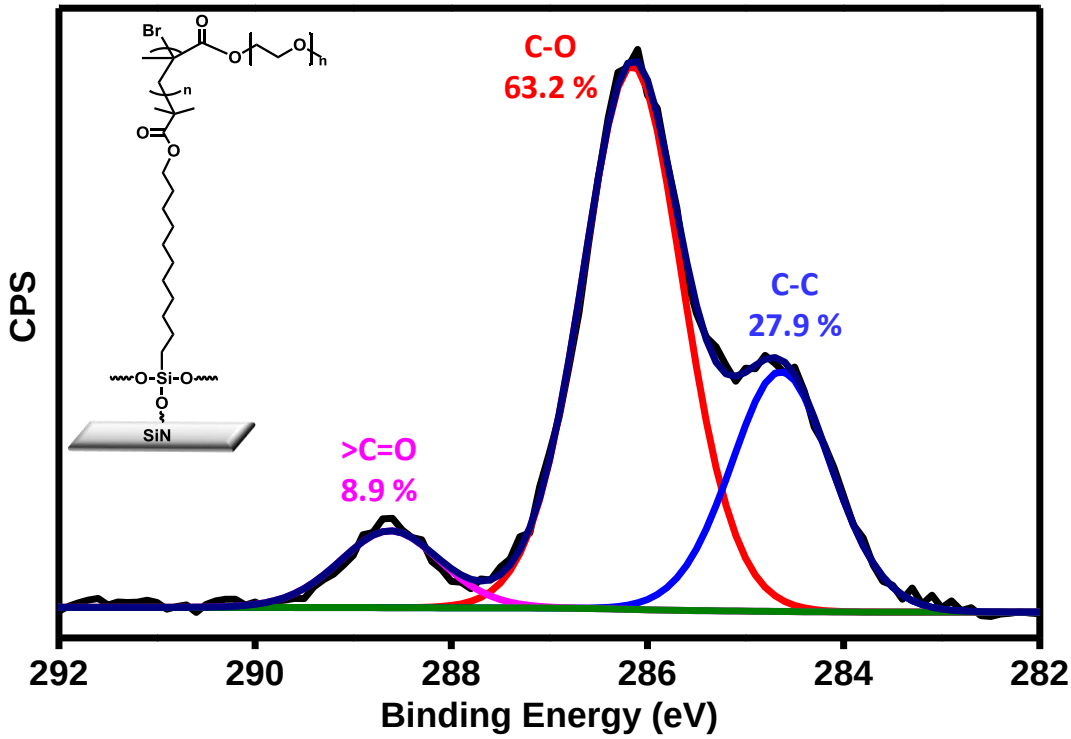

Figure S4.12. XPS C1s narrow scan of **M5** surfaces.

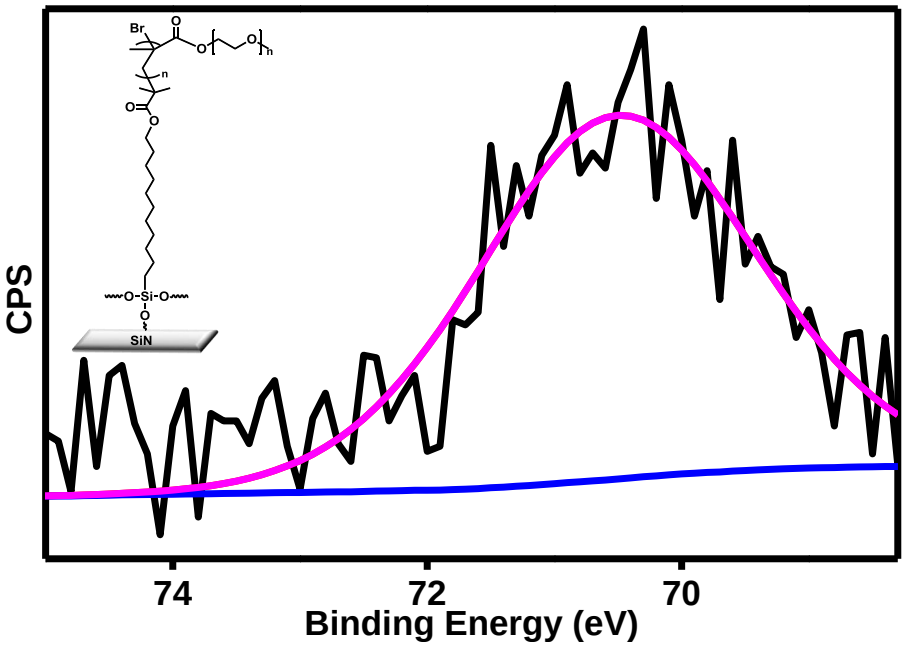

Figure S4.13. XPS Br3d narrow scan of **M_5** surfaces.

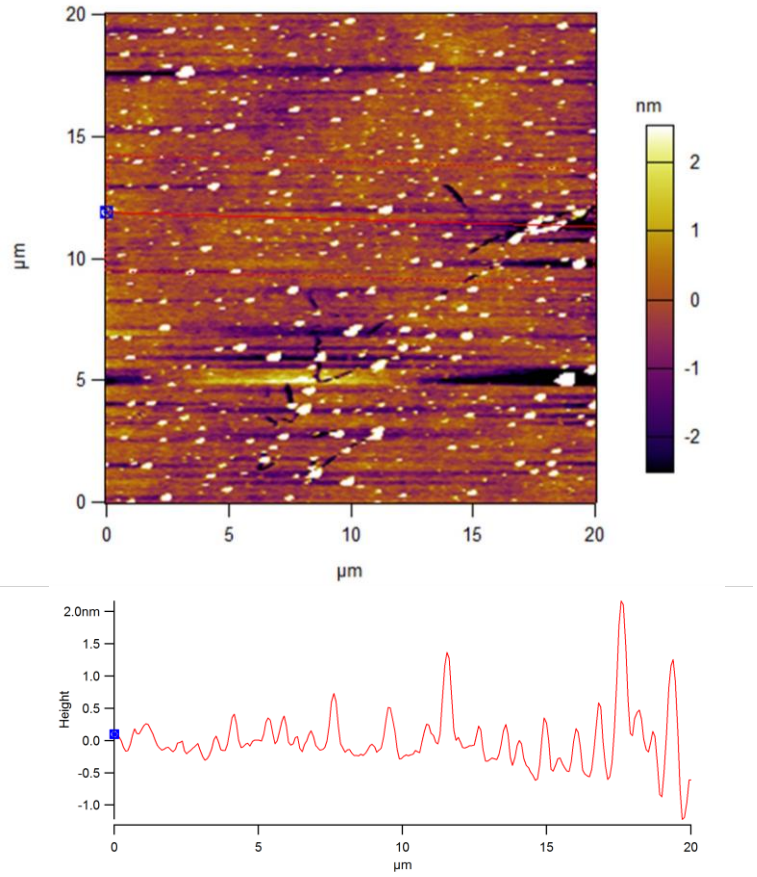

Figure S4.14. AFM image of **M_5** surfaces along with a cross section (roughness = 2.2 nm).

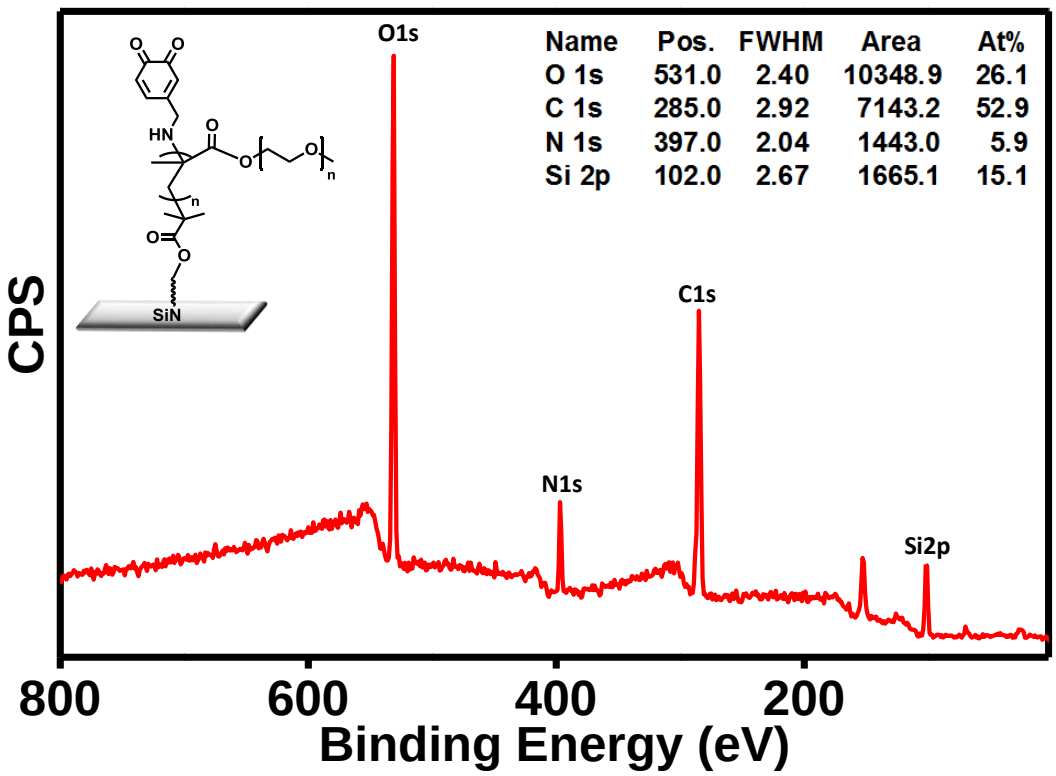

Figure S4.15. XPS wide scan of **M6** surfaces.

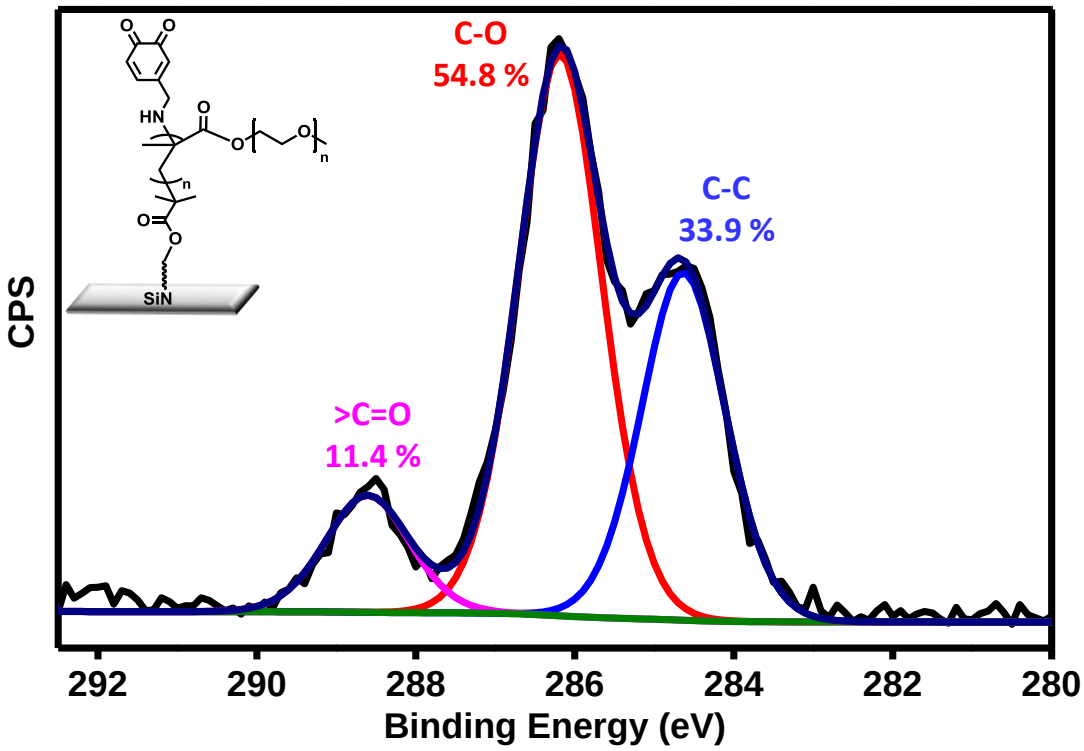

Figure S4.16. XPS C1s narrow scan of **M6** surfaces.

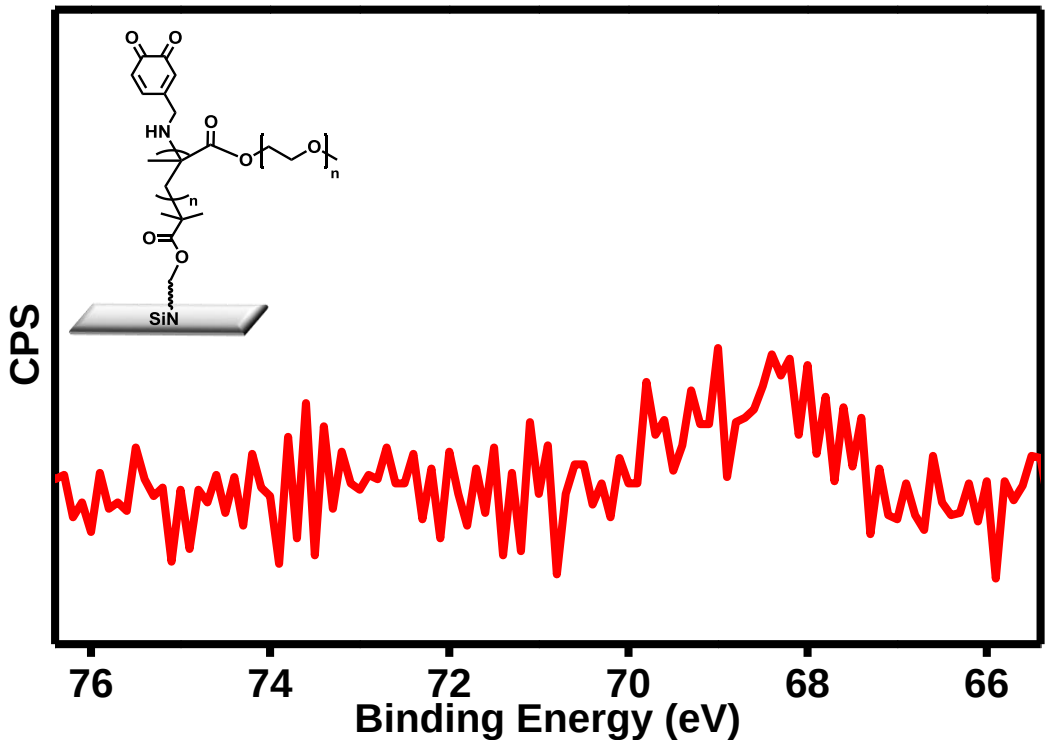

Figure S4.17. XPS Br3d narrow scan of **M_6** surfaces.

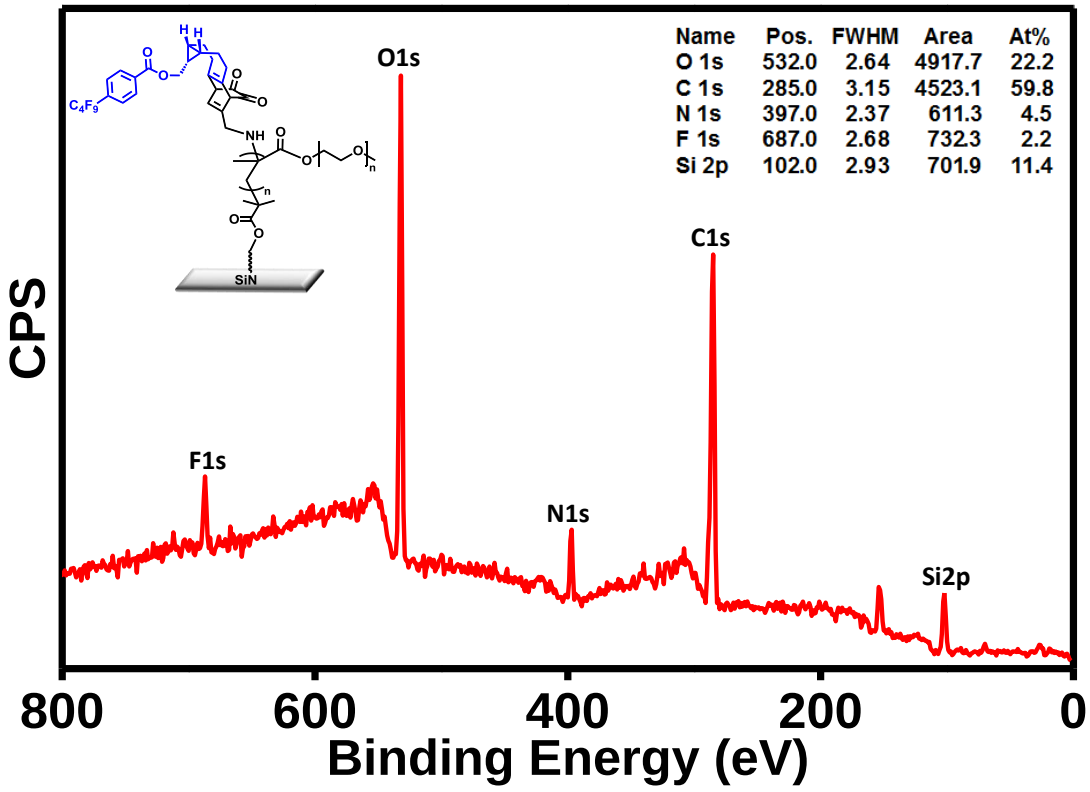

Figure S4.18. XPS wide scan of **M_7** surfaces.

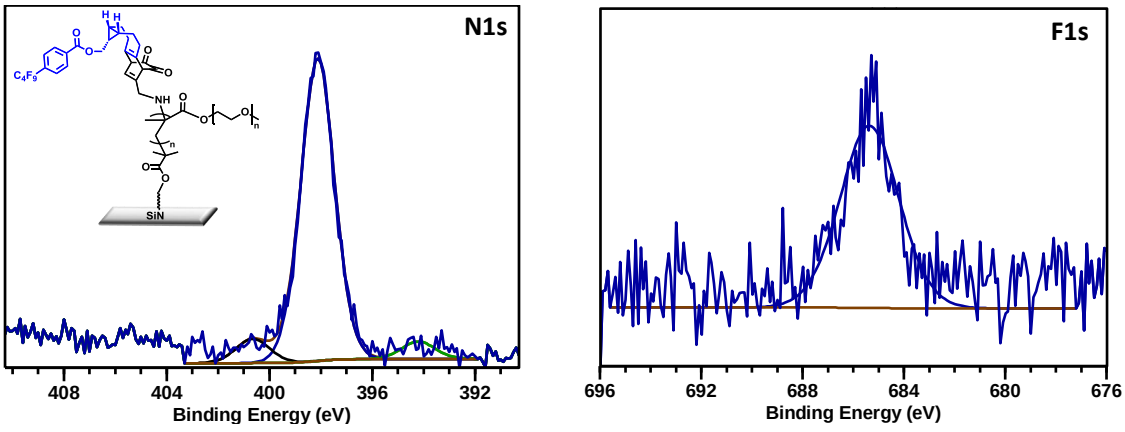

Name	Position	Area/(RSF*T*MFP)	%At Conc
N 1s	398.1	120.153	74.2
N 1s	400.7	9.65246	6.0
N 1s	394.2	6.9665	4.3
F 1s	685.4	25.1232	15.5

Figure S4.19. F1s and N1s narrow scans (centered on 686.0 eV and 400.7 eV; respectively) of **M7** surfaces for establishing conversion. NB: only organic N (~400.7 eV) is relevant.

Th. F/N = 9/1 = 9

Expt. F/N = 15.5 / 6.0 = 2.9 ± 0.1 ⇒ conversion: 2.9/9.0 = 0.32; this was measured over five more samples, yielding an average over 6 samples: ~30 % conversion.

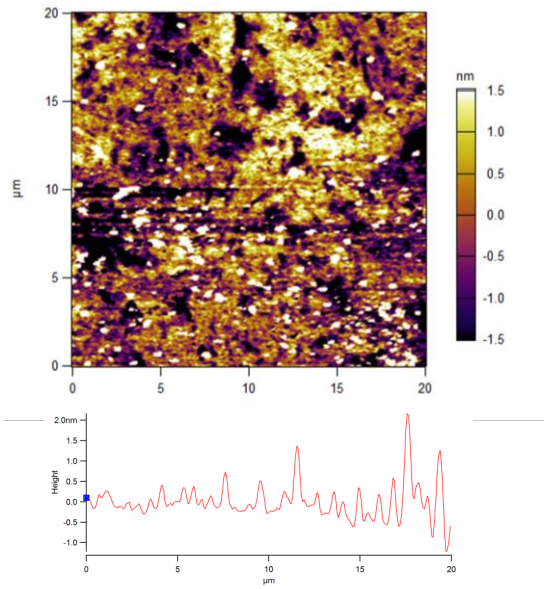

Figure S4.20. AFM image of **M7** surfaces along with a cross section (roughness = 1.9 nm).

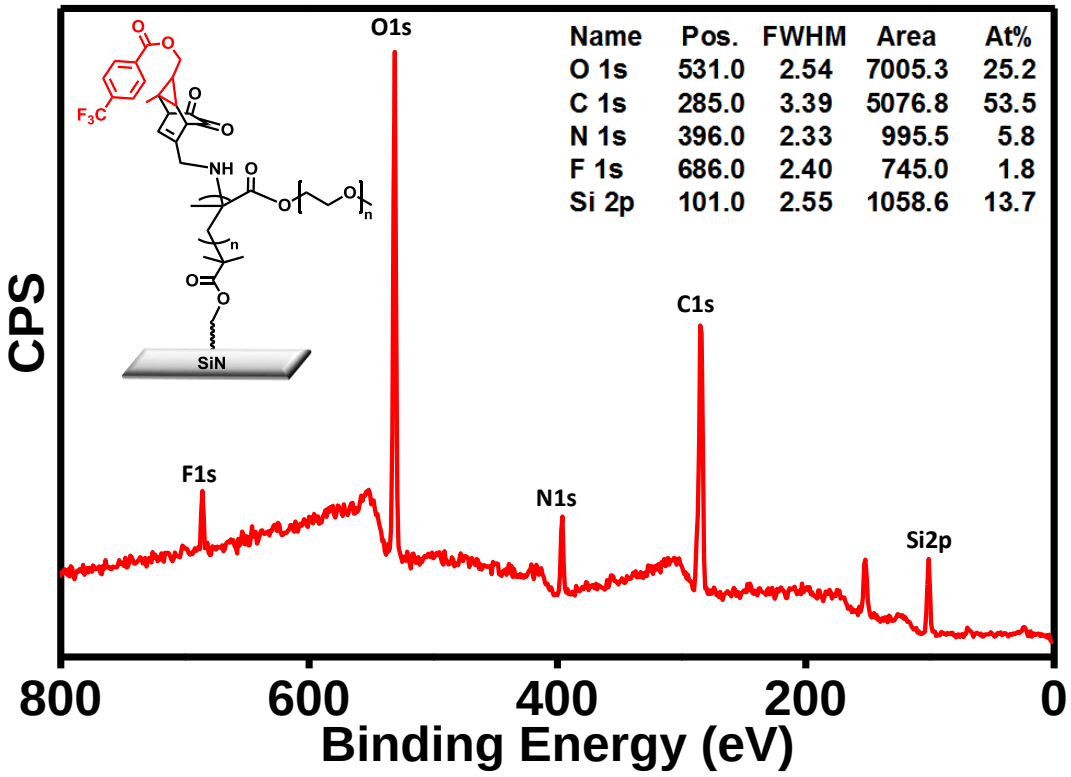

Figure S4.21. XPS wide scan of **M8** surfaces.

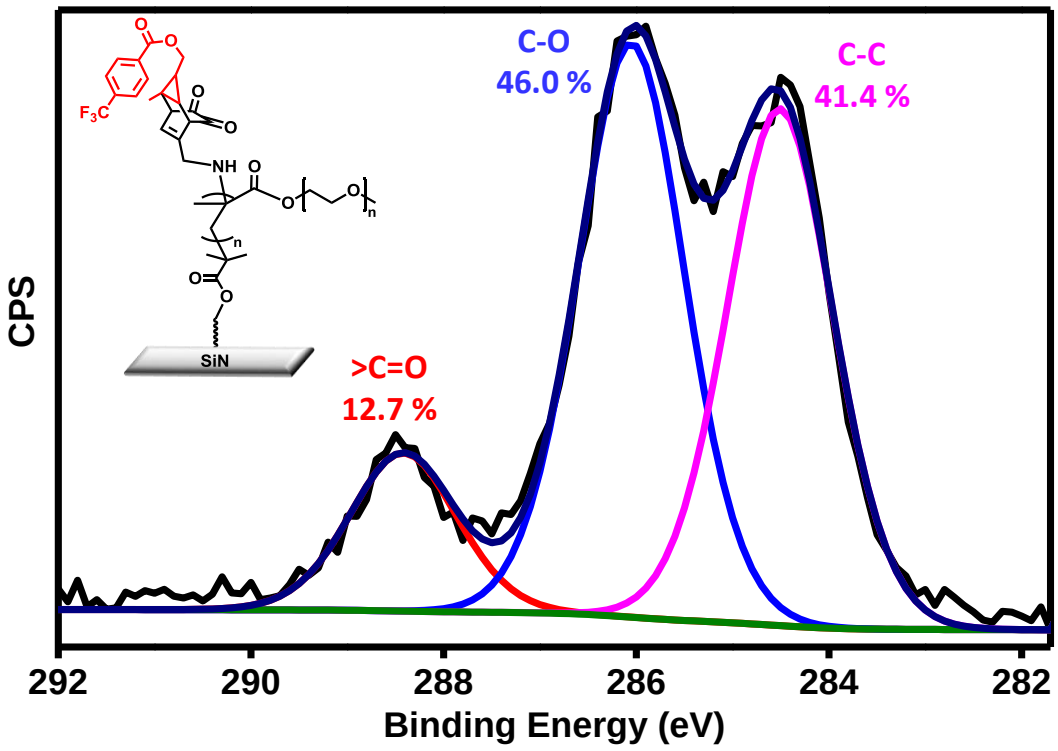

Figure S4.22. XPS C1s narrow scan of **M8** surfaces.

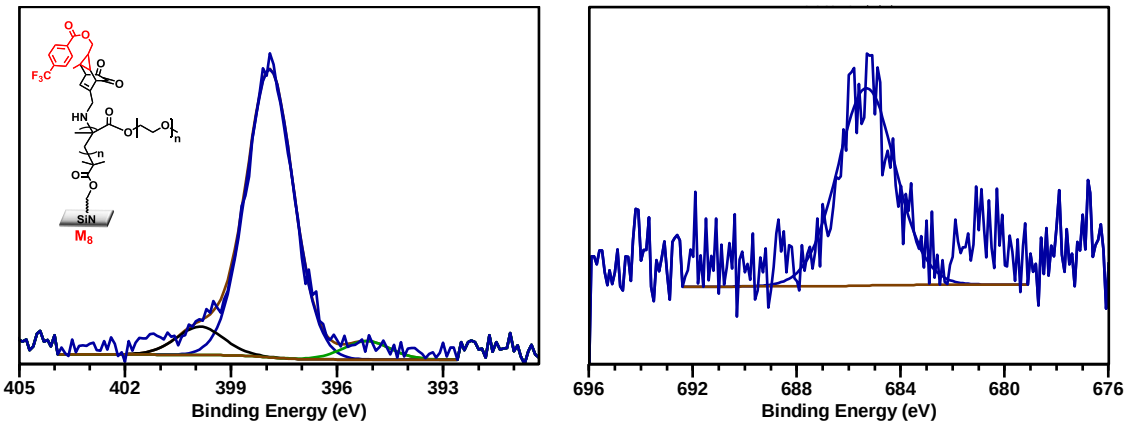

Name	Position	Area/(RSF*T*MFP)	%At Conc
N 1s	397.9	110.145	73.0
N 1s	400.1	11.2757	7.5
N 1s	395.2	7.0463	4.7
F 1s	685.3	22.3211	14.8

Figure S4.23. F1s and N1s narrow scans (centered on 686.0 eV and 400 eV; respectively) of **M8** surfaces for establishing conversion. NB: only organic N (~400.1 eV) is relevant.

Th. F/N = 3/1 = 3

Expt. F/N = 14.8 / 7.5 = 1.9 ± 0.1 ⇒ conversion: 1.9/3 = 0.63; this was measured over five more samples, yielding an average over six samples: ~60 % conversion.

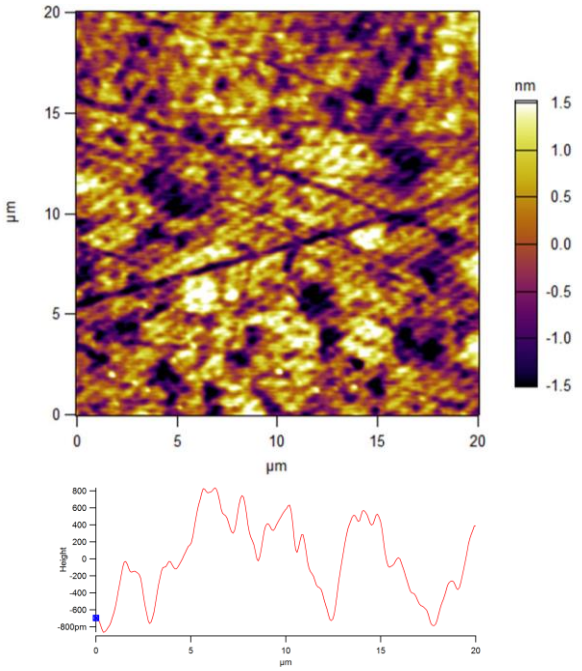

Figure S4.24. AFM image of M8 surfaces along with a cross section (roughness = 0.7 nm).

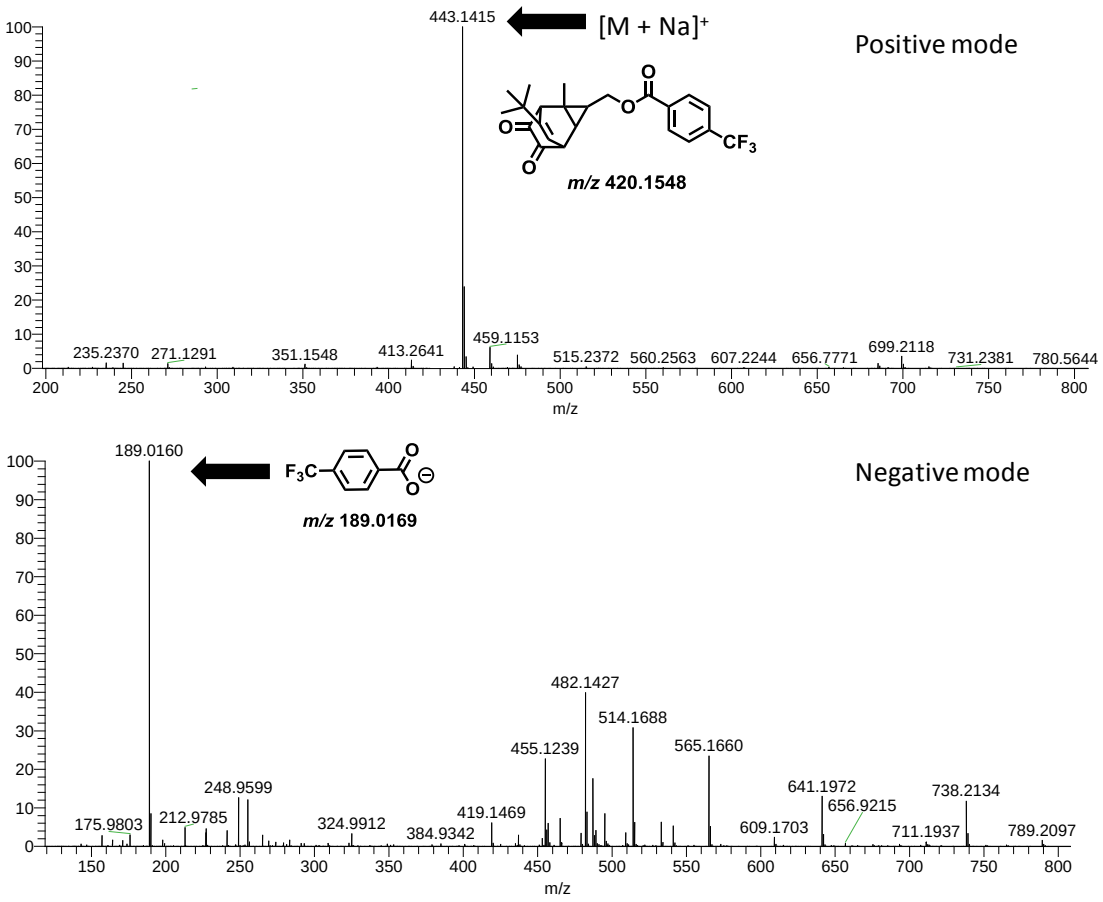

Figure S4.25. Positive and negative mode MS spectrum of compound **9**.

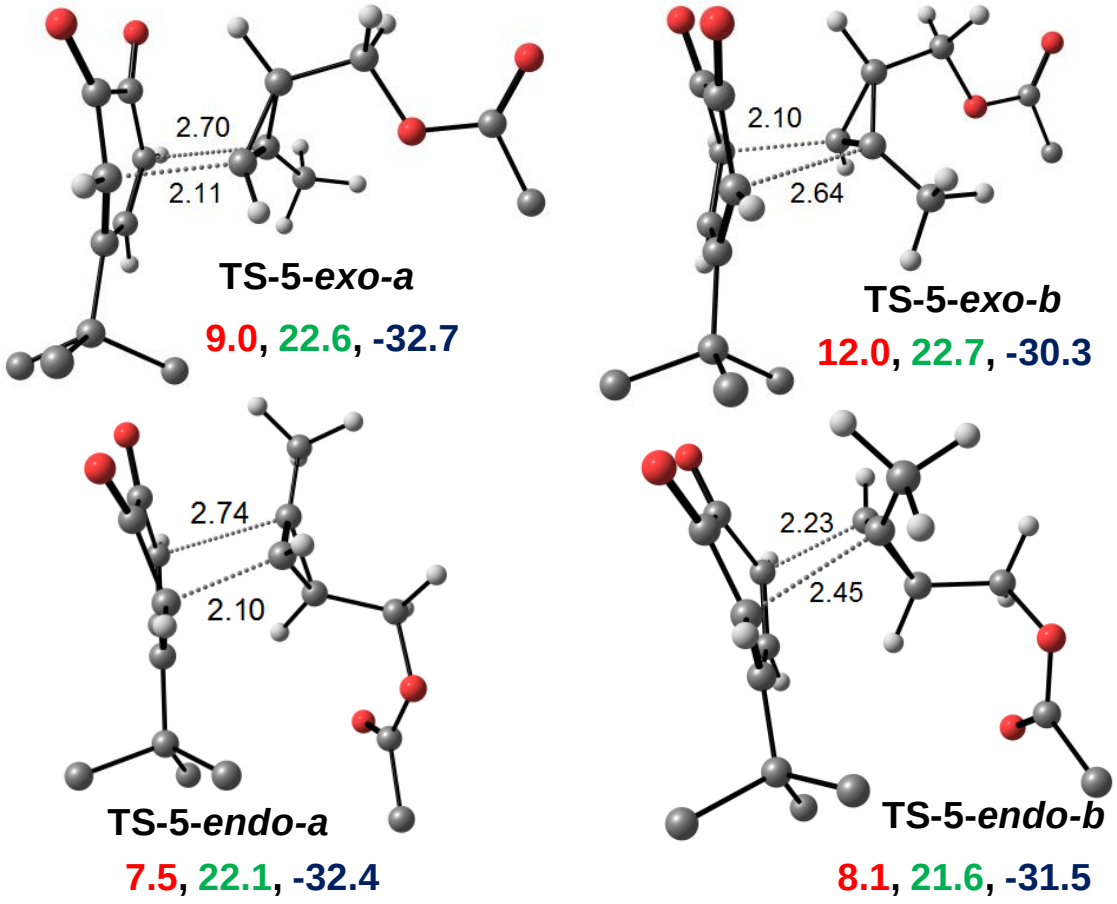

Figure S4.26. B97D/6-311+G(d,p) transition state geometries for the *exo* and *endo* attack of **5** + **8**. In TSs labeled with "a" the methyl group in the cyclopropene is at the opposite side of the *t*-butyl group in the *o*-quinone, whereas TSs labeled with "b", both groups are in the same side. Bond lengths reported in Å. Solution-phase activation free energies (red), distortion energies (green) and reaction free energies (blue) are in kcal/mol.

5. NMR DATA.

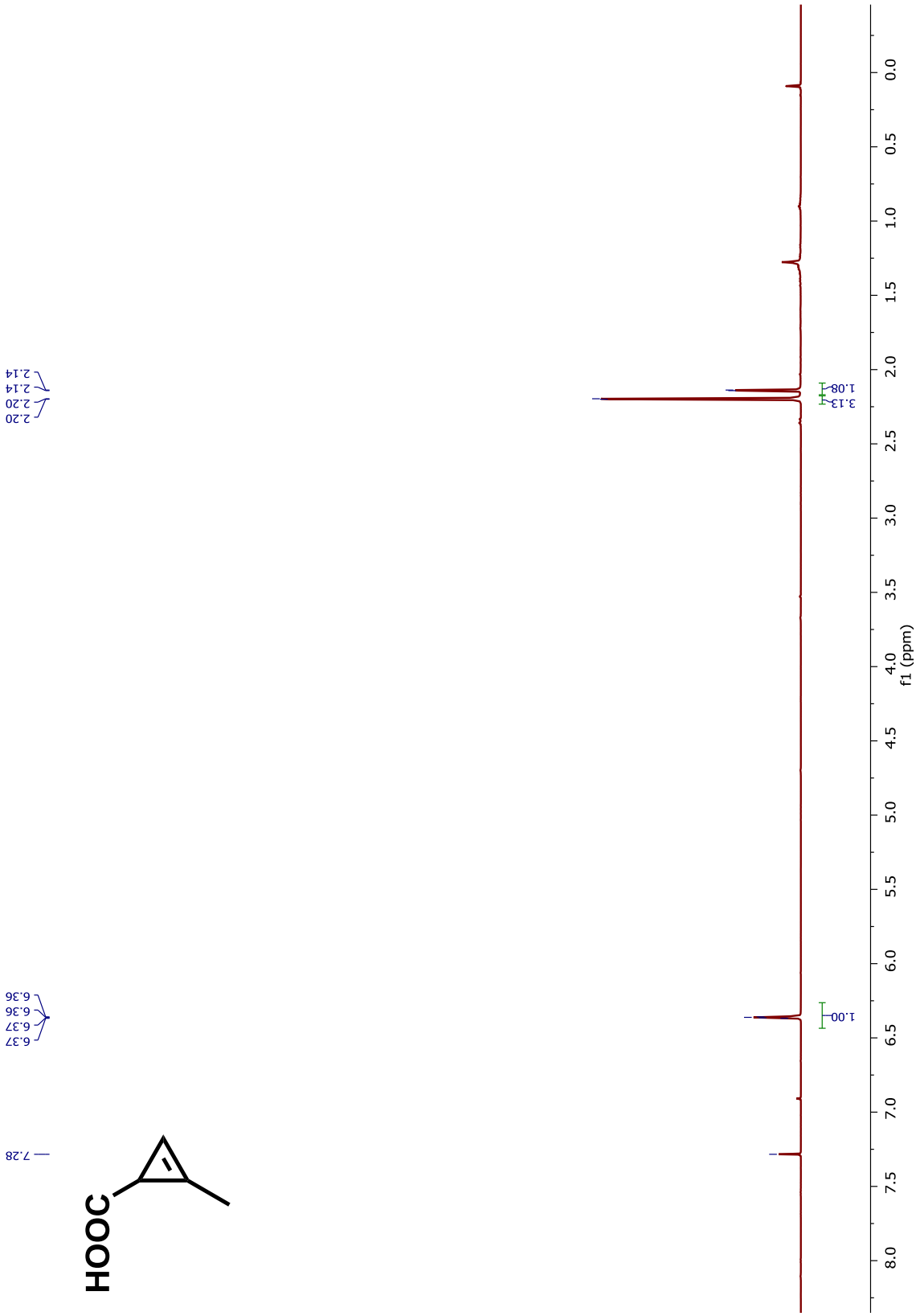

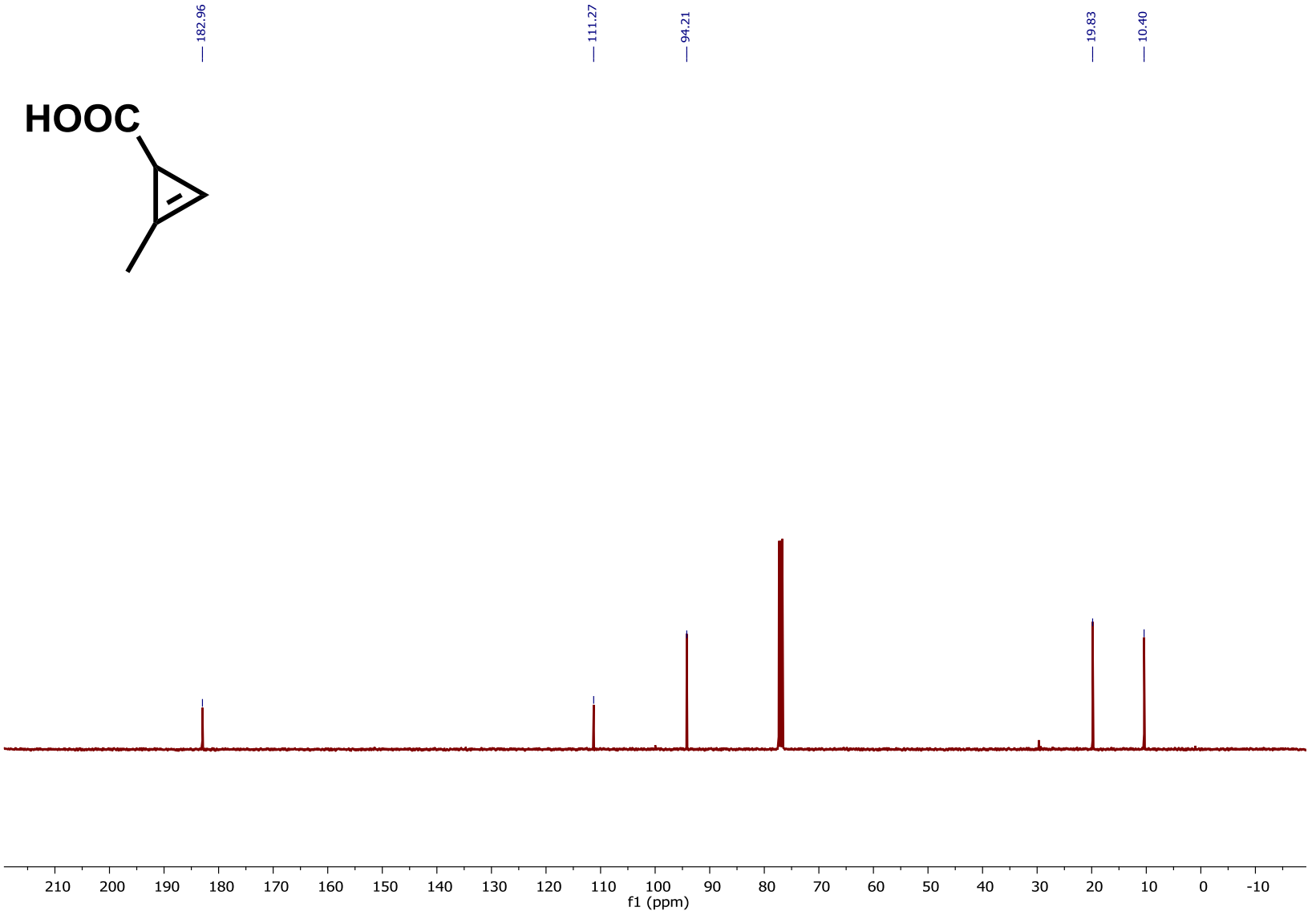
182.96
111.27
94.21
19.83
10.40
HOOC
210
200
190
180
170
160
150
140
130
120
110
100
90
80
70
60
50
40
30
20
10
0
-10
f1 (ppm)

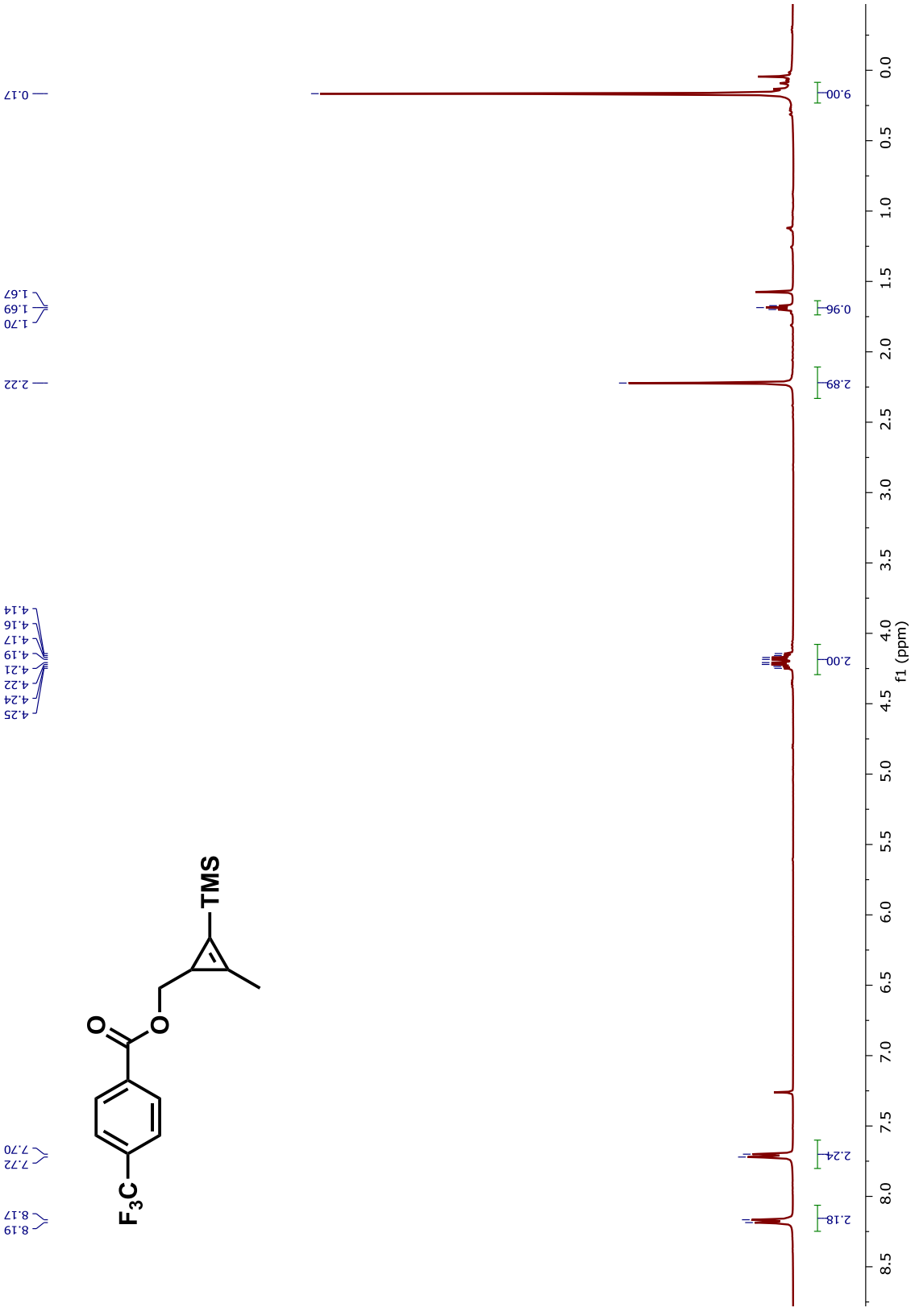
TMS
O
O
F3C
0.17
1.67
1.69
1.70
2.22
4.14
4.16
4.17
4.19
4.21
4.22
4.24
4.25
7.70
7.72
8.17
8.19
9.00
0.96
2.89
2.00
2.24
2.18
f1 (ppm)

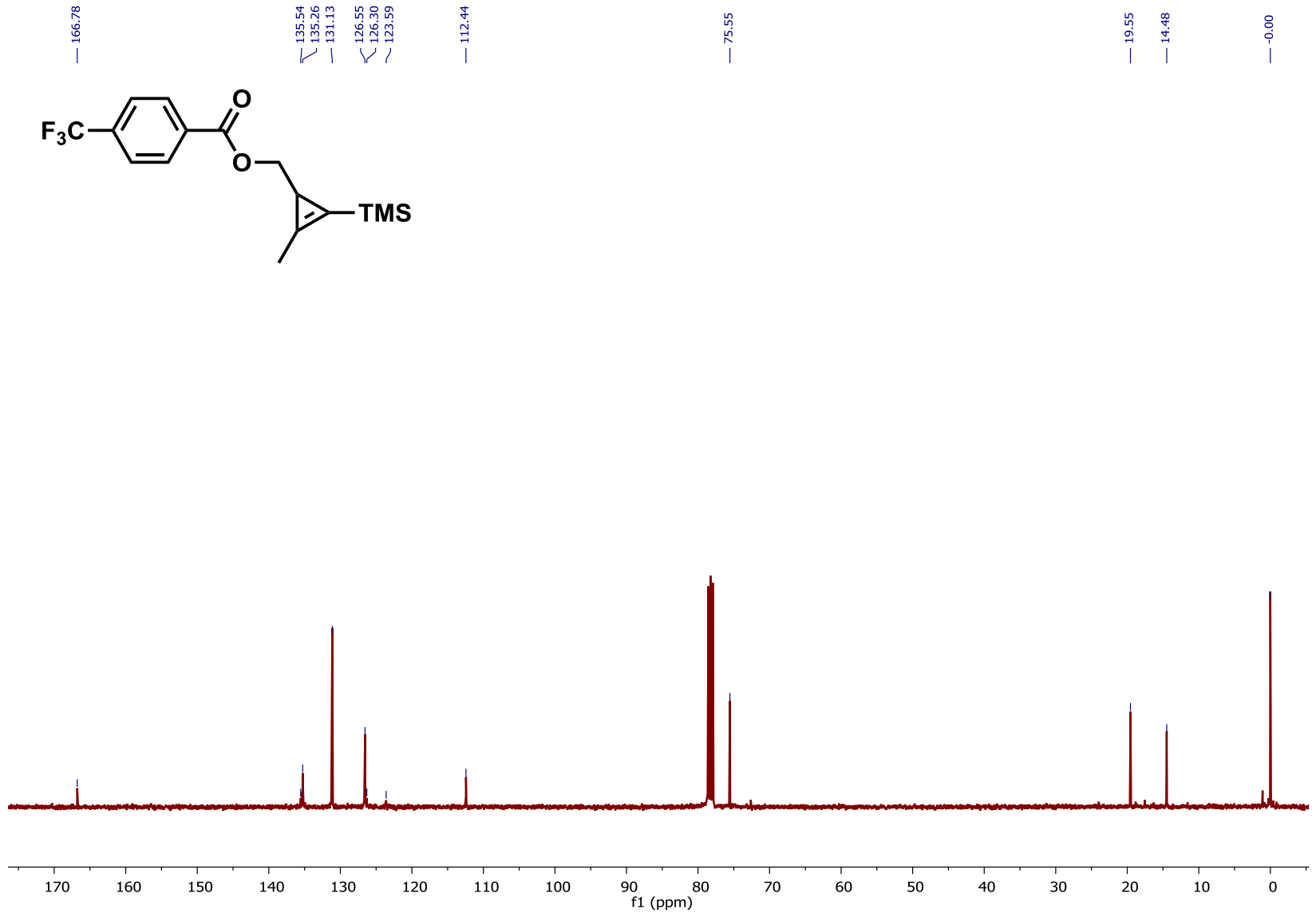
166.78
135.54
135.26
131.13
126.55
126.30
123.59
112.44
75.55
19.55
14.48
-0.00
F3C
O
O
TMS
170
160
150
140
130
120
110
100
90
80
70
60
50
40
30
20
10
0
f1 (ppm)

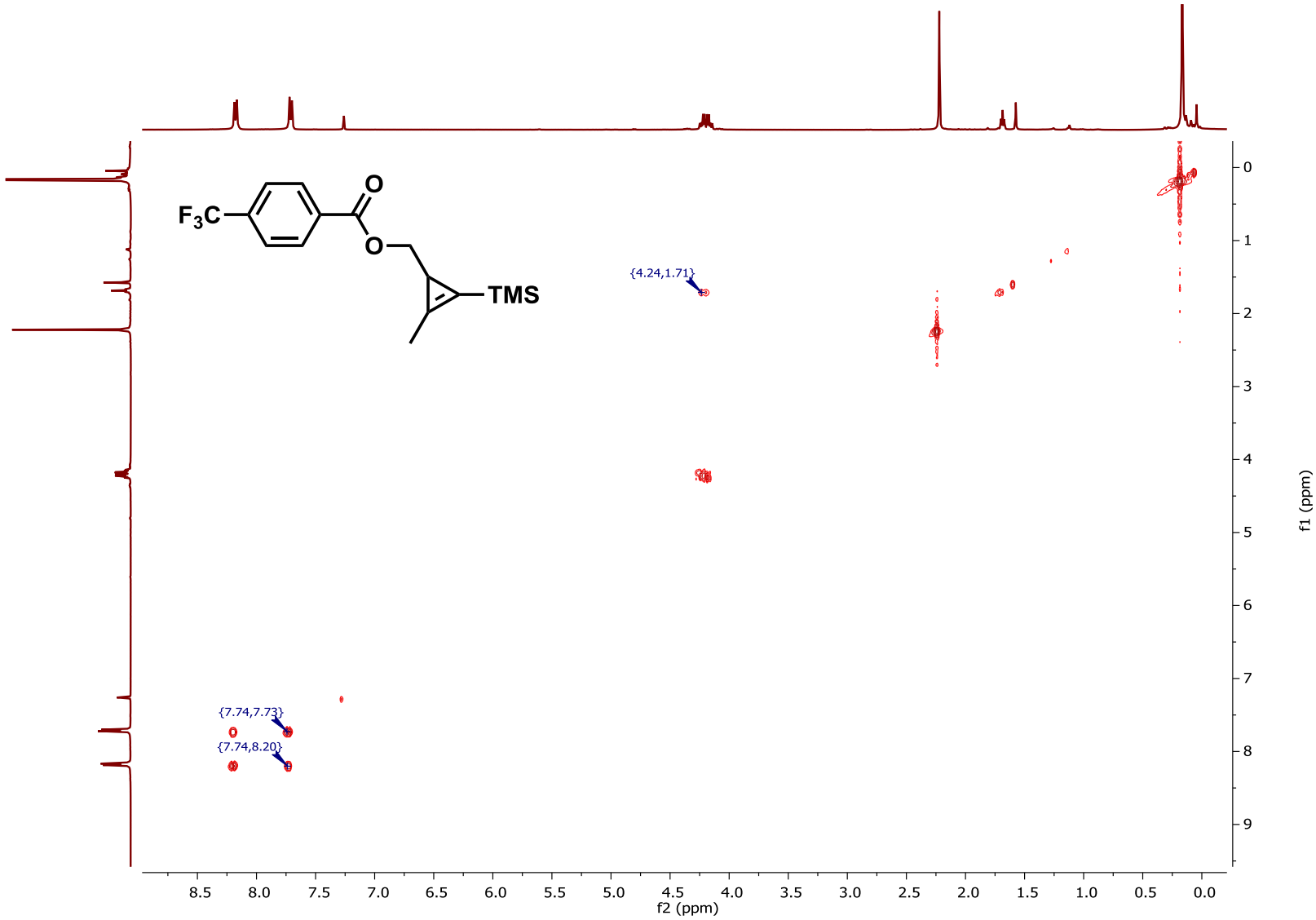
F3C
O
O
TMS
{4.24,1.71}
{7.74,7.73}
{7.74,8.20}
f2 (ppm)
f1 (ppm)

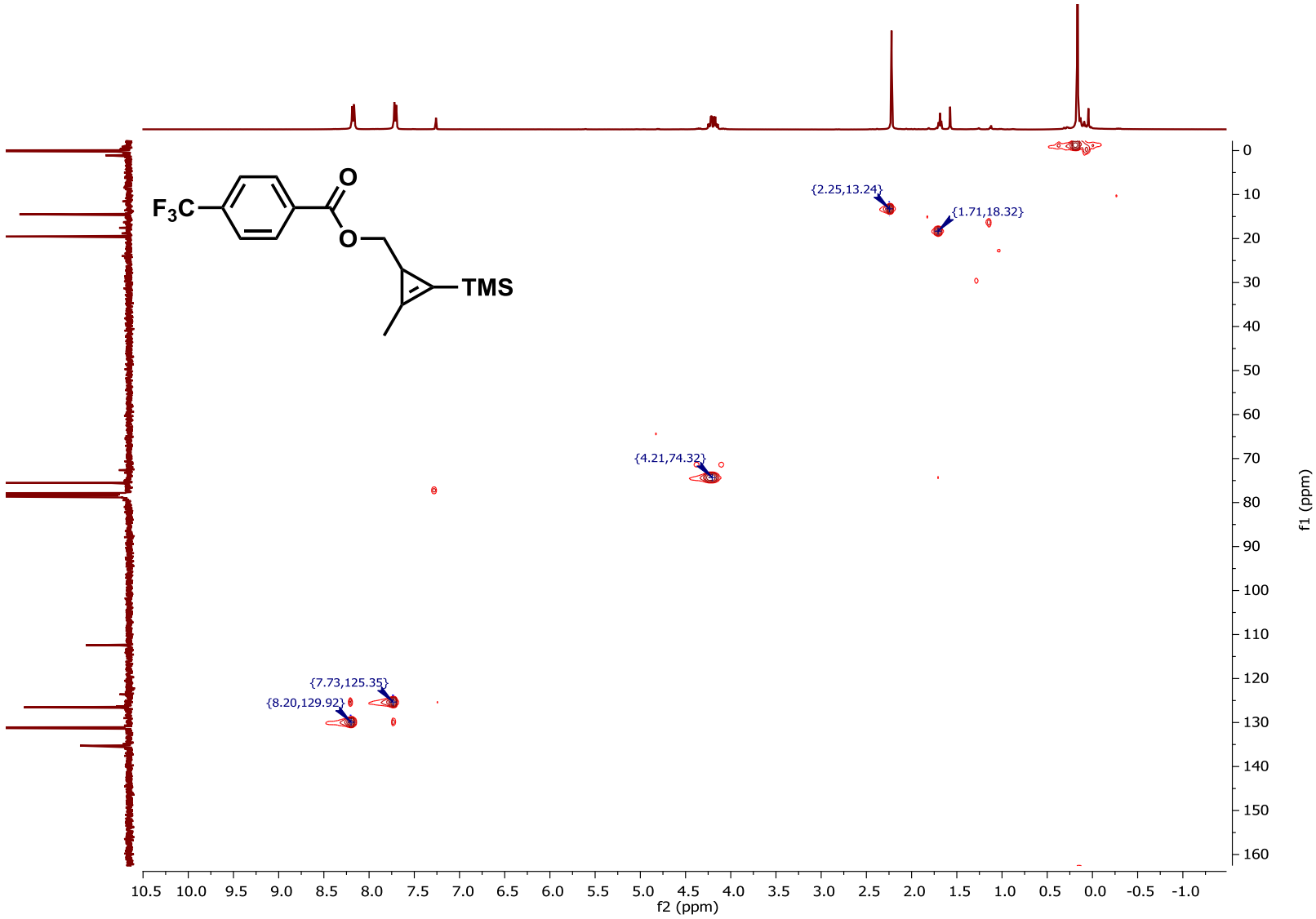
F3C
O
O
TMS
{2.25,13.24}
{1.71,18.32}
{4.21,74.32}
{7.73,125.35}
{8.20,129.92}
f2 (ppm)
f1 (ppm)

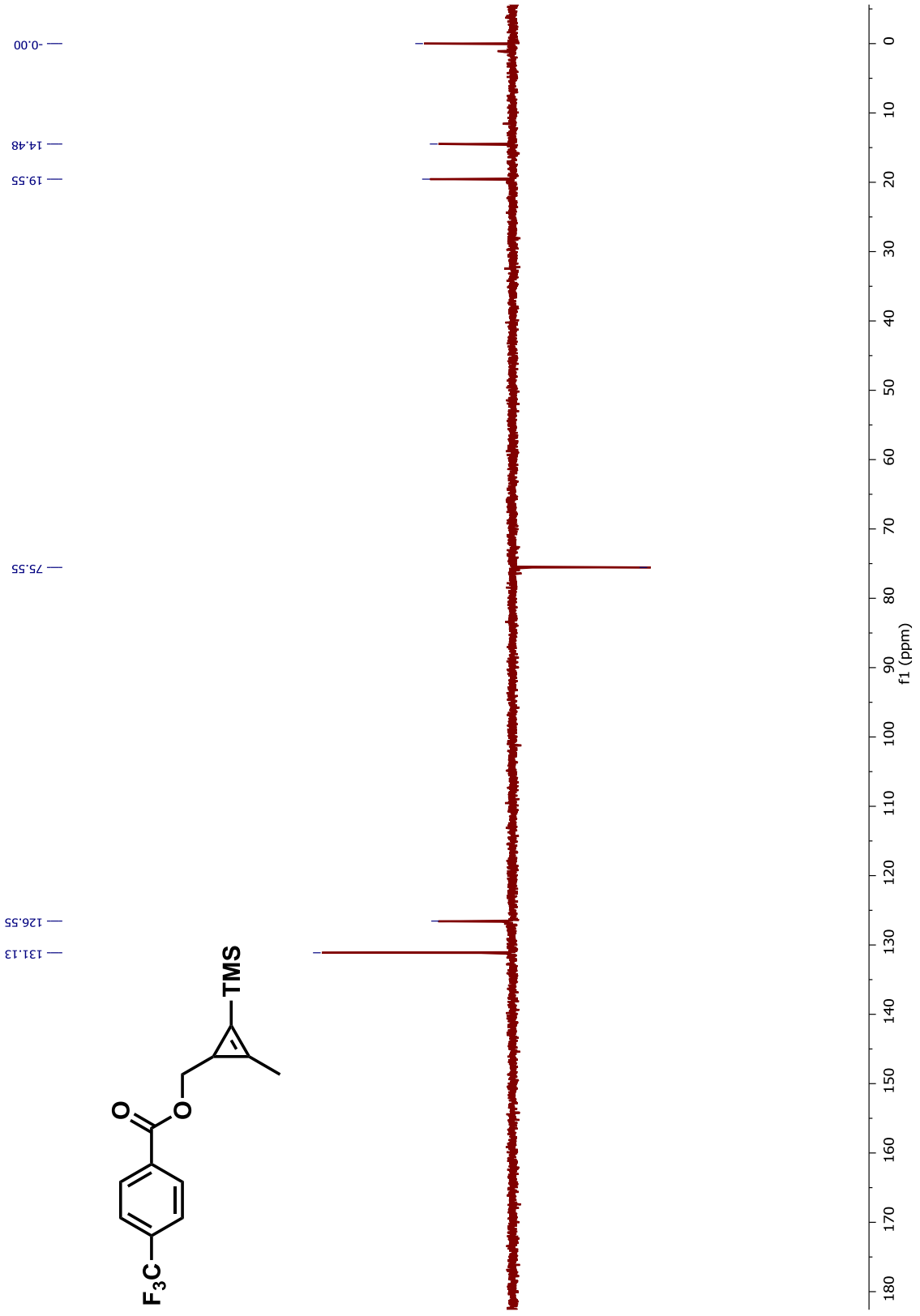
-0.00
14.48
19.55
75.55
126.55
131.13
TMS
O
O
F3C
0
10
20
30
40
50
60
70
80
90
100
110
120
130
140
150
160
170
180
f1 (ppm)

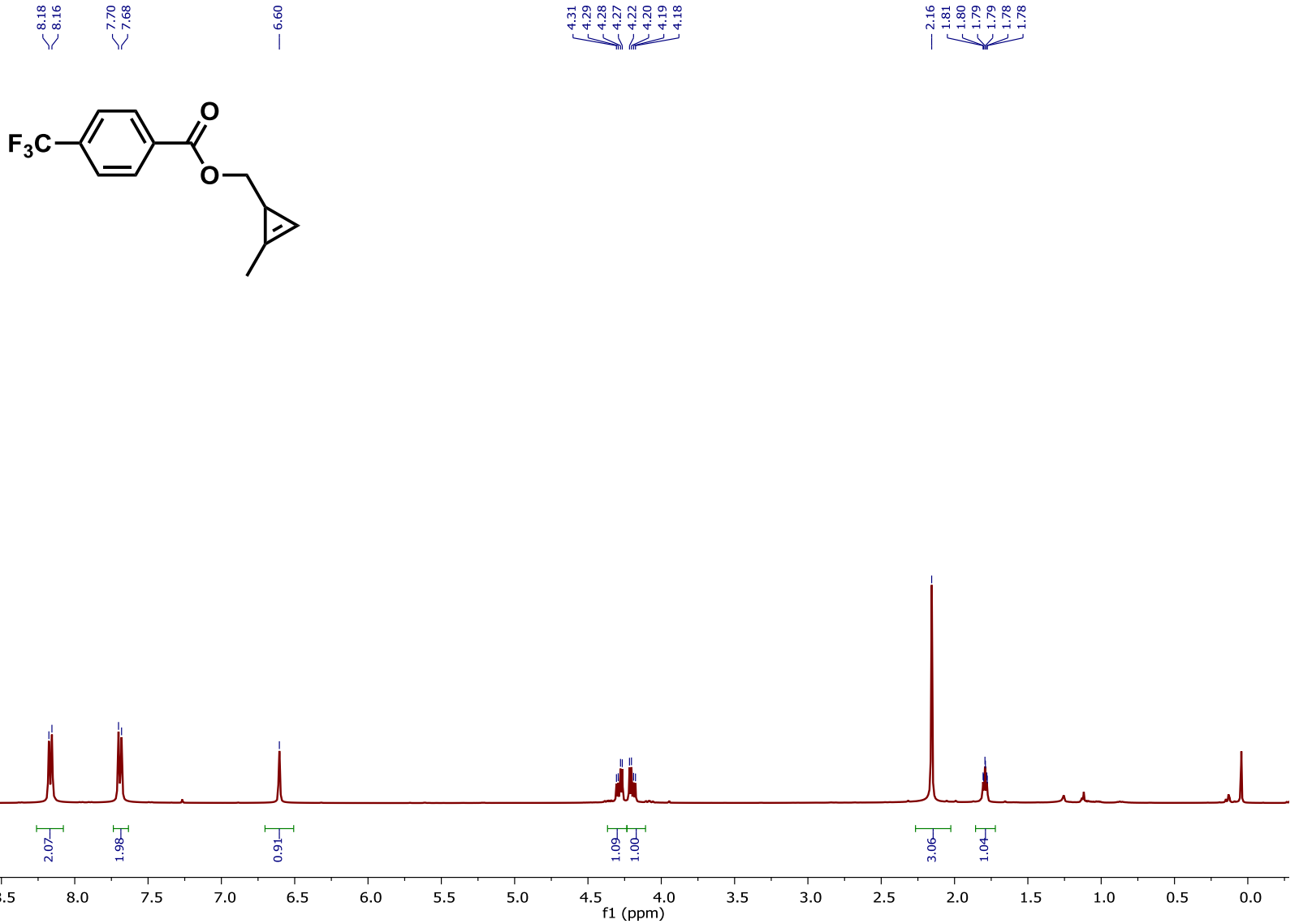
8.18
8.16
7.70
7.68
6.60
4.31
4.29
4.28
4.27
4.22
4.20
4.19
4.18
2.16
1.81
1.80
1.79
1.79
1.78
1.78
F3C
O
O
2.07
1.98
0.91
1.09
1.00
3.06
1.04
8.5
8.0
7.5
7.0
6.5
6.0
5.5
5.0
4.5
4.0
3.5
3.0
2.5
2.0
1.5
1.0
0.5
0.0
f1 (ppm)

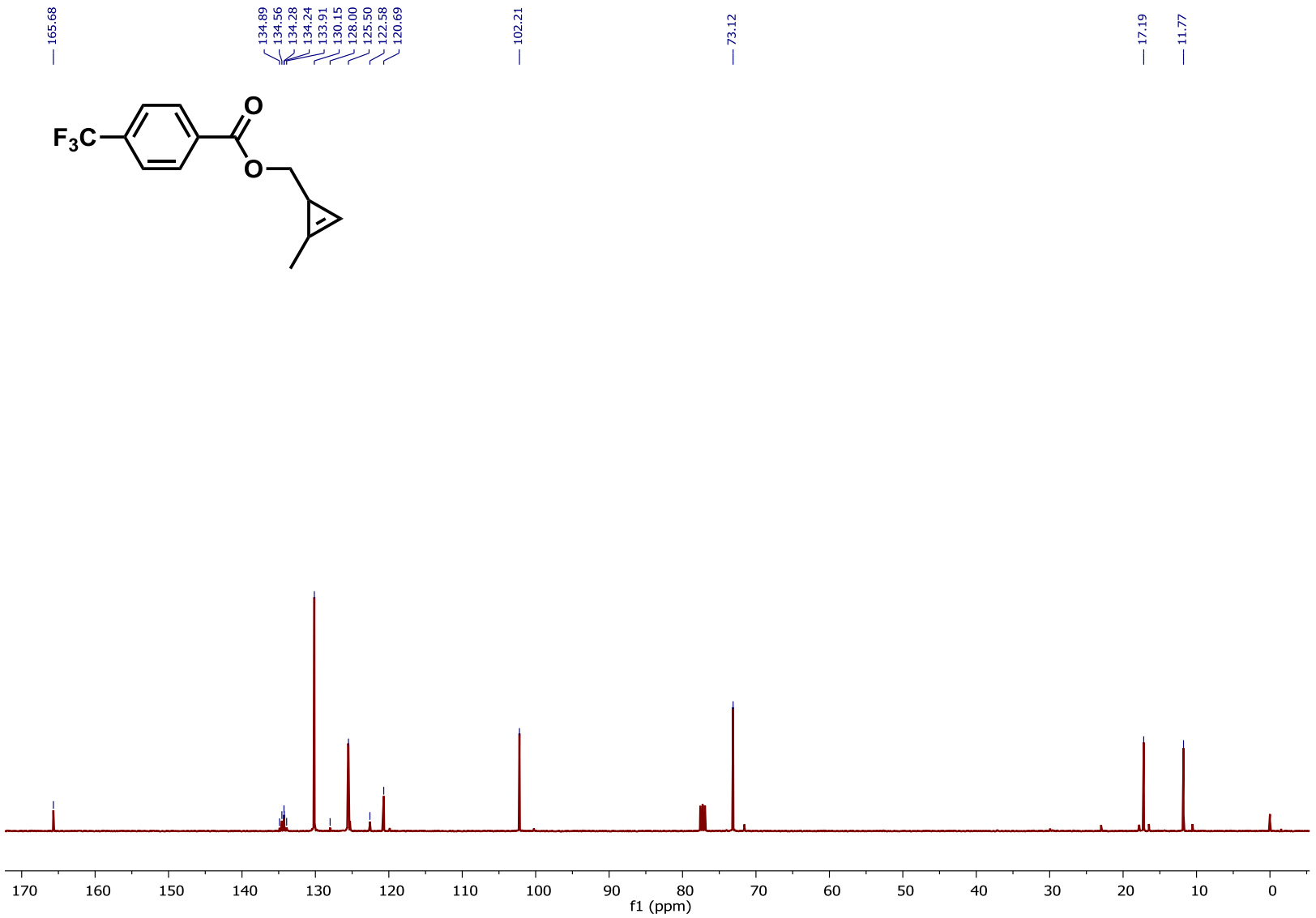
165.68
134.89
134.56
134.28
134.24
133.91
130.15
128.00
125.50
122.58
120.69
102.21
73.12
17.19
11.77
F3C
O
O
170
160
150
140
130
120
110
100
90
80
70
60
50
40
30
20
10
0
f1 (ppm)

f1 (ppm)
f2 (ppm)
{1.82,4.25}
{4.22,1.81}
{4.28,1.81}
{6.61,2.17}
{8.18,7.71}
O
O
F3C

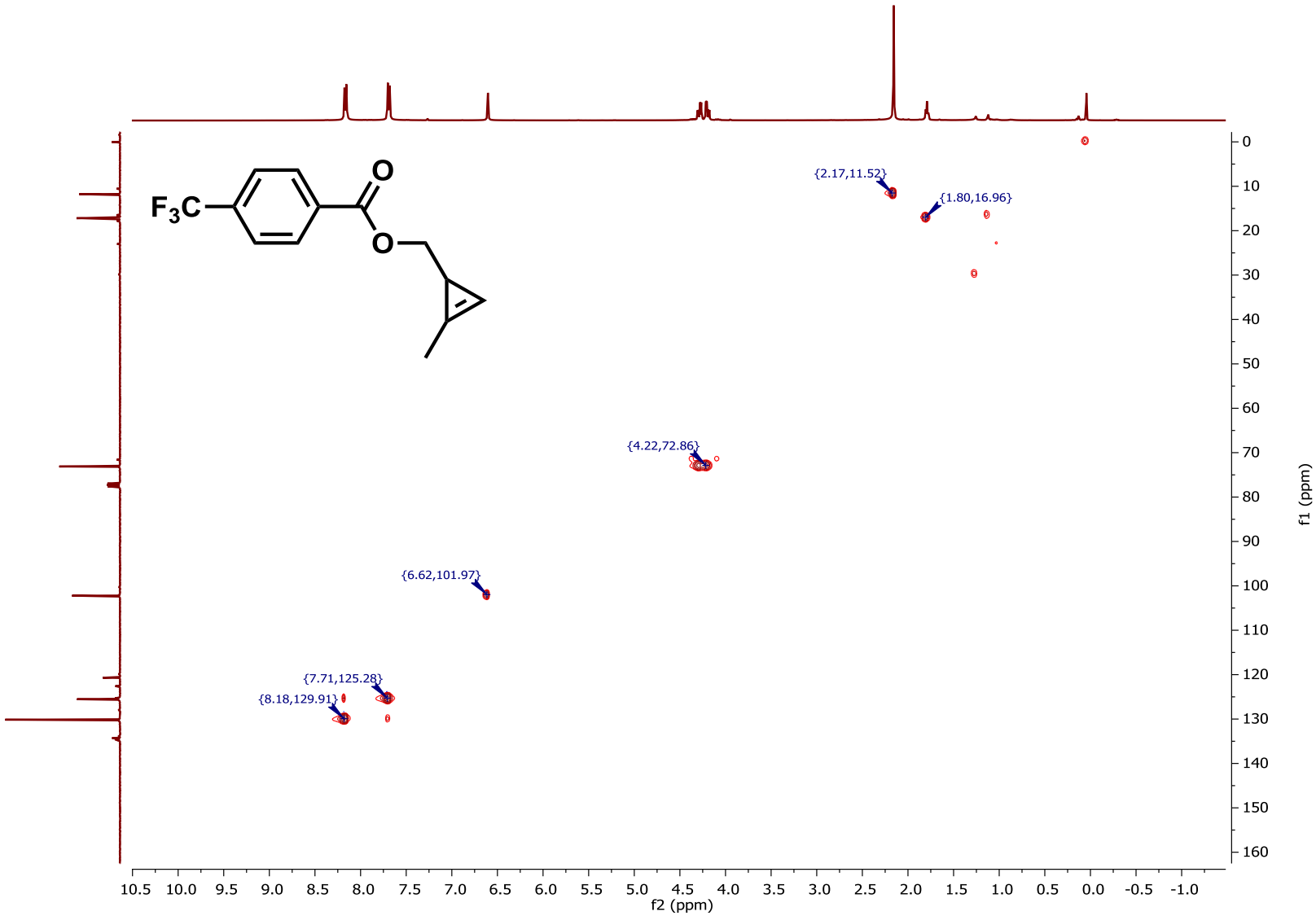
F3C
O
O
{2.17,11.52}
{1.80,16.96}
{4.22,72.86}
{6.62,101.97}
{7.71,125.28}
{8.18,129.91}
f2 (ppm)
f1 (ppm)

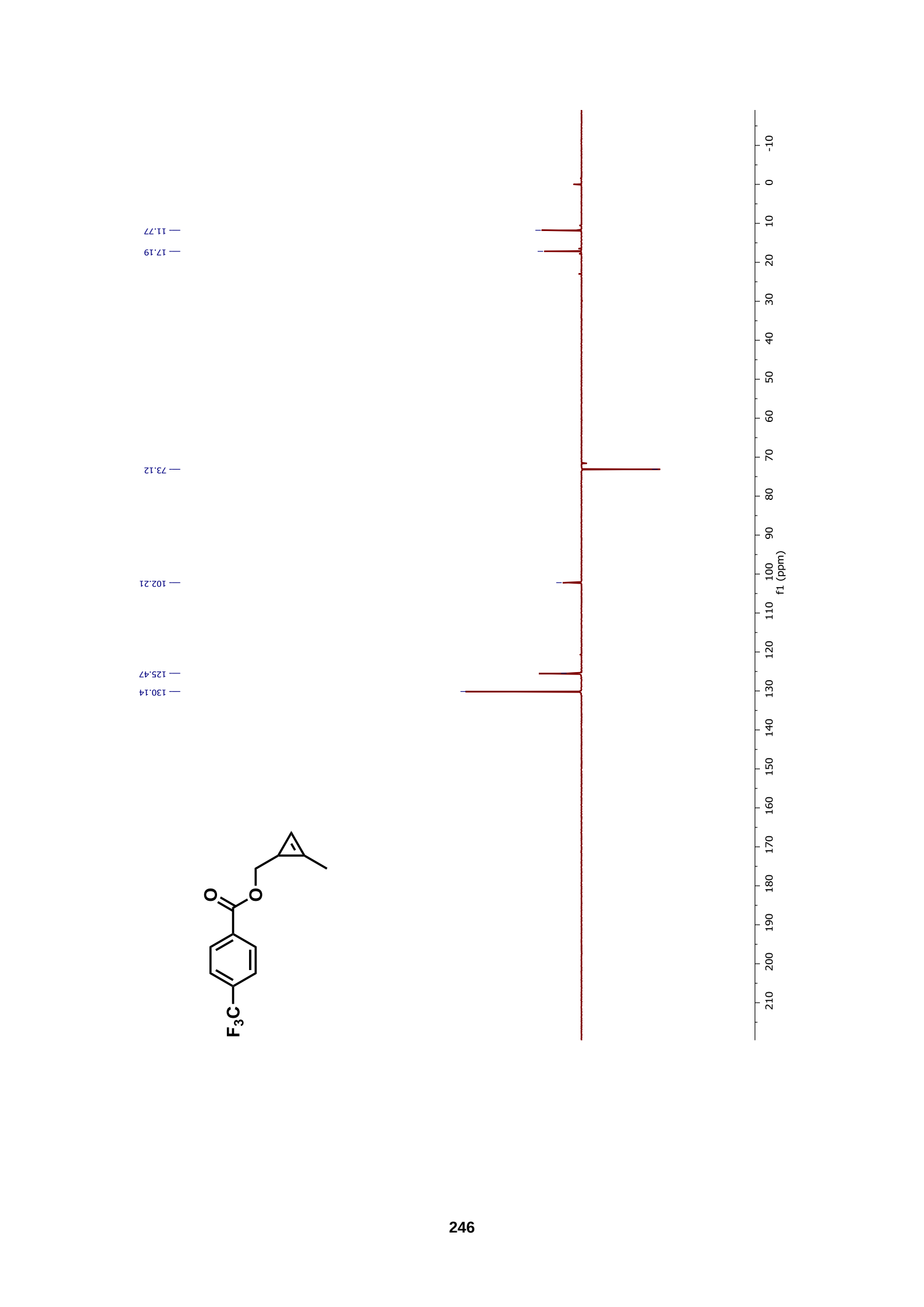
11.77
17.19
73.12
102.21
125.47
130.14
f1 (ppm)

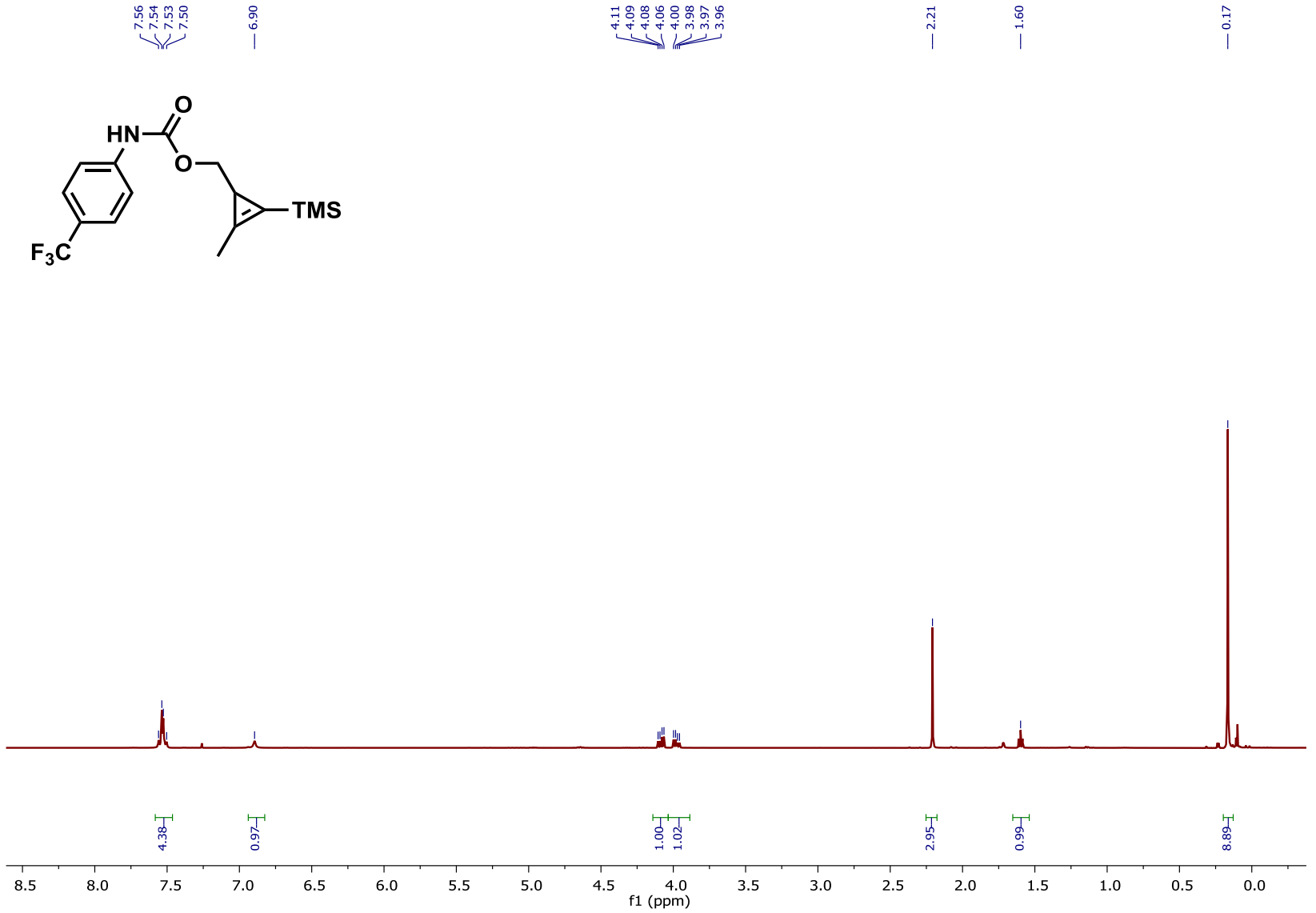
7.56
7.54
7.53
7.50
6.90
4.11
4.09
4.08
4.06
4.00
3.98
3.97
3.96
2.21
1.60
0.17
HN
O
O
TMS
F3C
4.38
0.97
1.00
1.02
2.95
0.99
8.89
8.5
8.0
7.5
7.0
6.5
6.0
5.5
5.0
4.5
4.0
3.5
3.0
2.5
2.0
1.5
1.0
0.5
0.0
f1 (ppm)

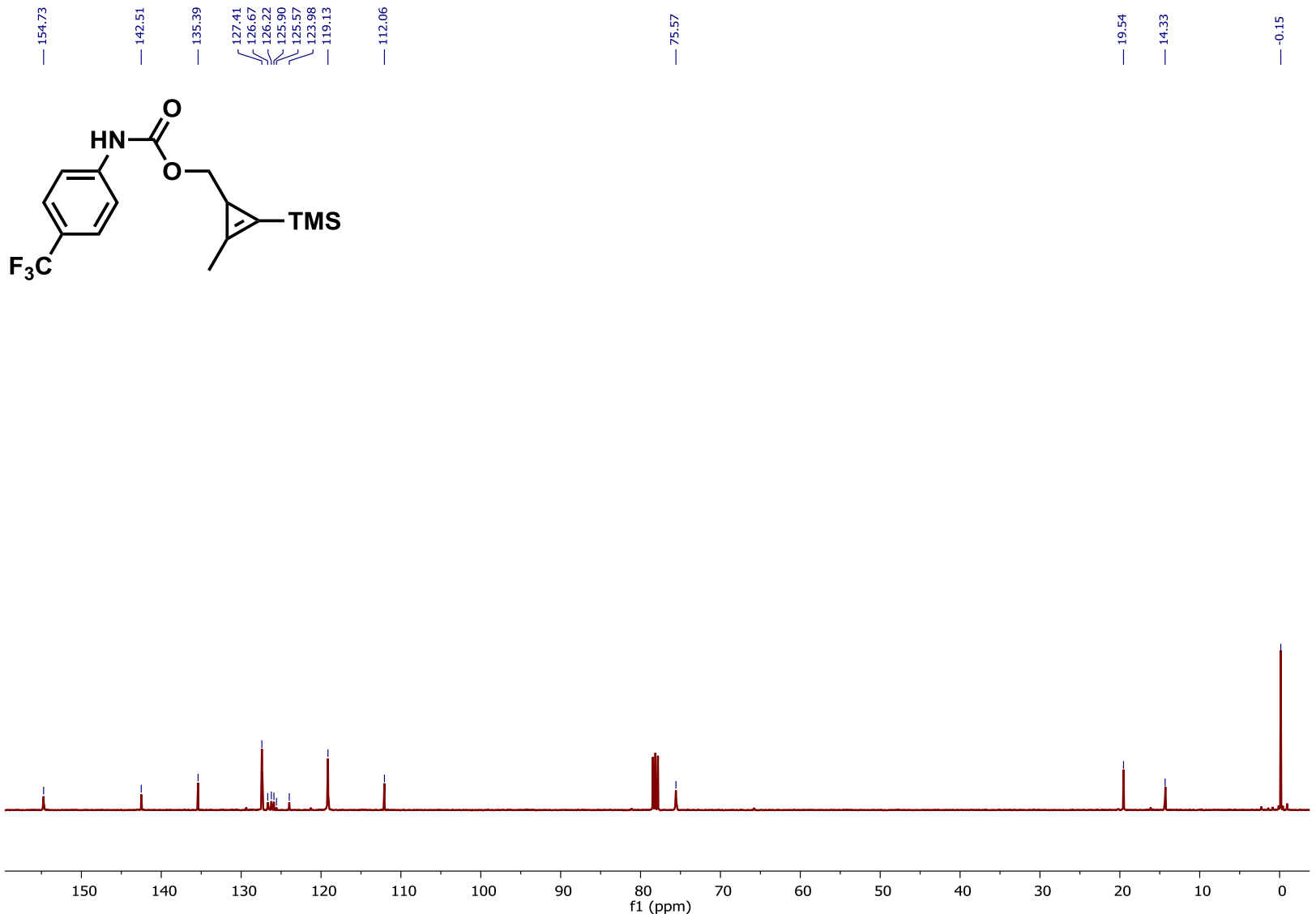
154.73
142.51
135.39
127.41
126.67
126.22
125.90
125.57
123.98
119.13
112.06
75.57
19.54
14.33
-0.15
HN
O
O
TMS
F3C
150
140
130
120
110
100
90
80
70
60
50
40
30
20
10
0
f1 (ppm)

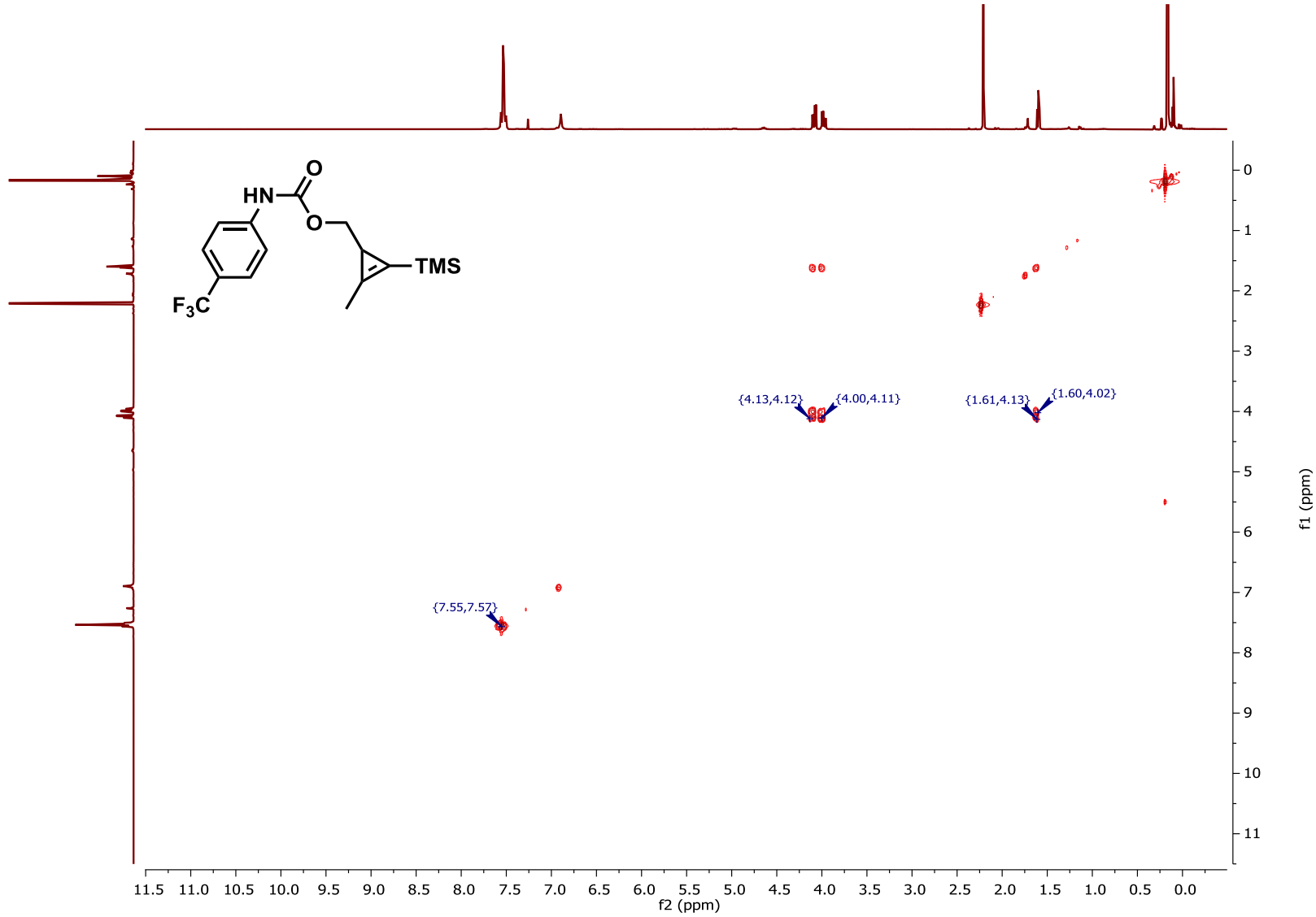
HN
O
O
TMS
F3C
{4.13,4.12}
{4.00,4.11}
{1.61,4.13}
{1.60,4.02}
{7.55,7.57}
f2 (ppm)
f1 (ppm)

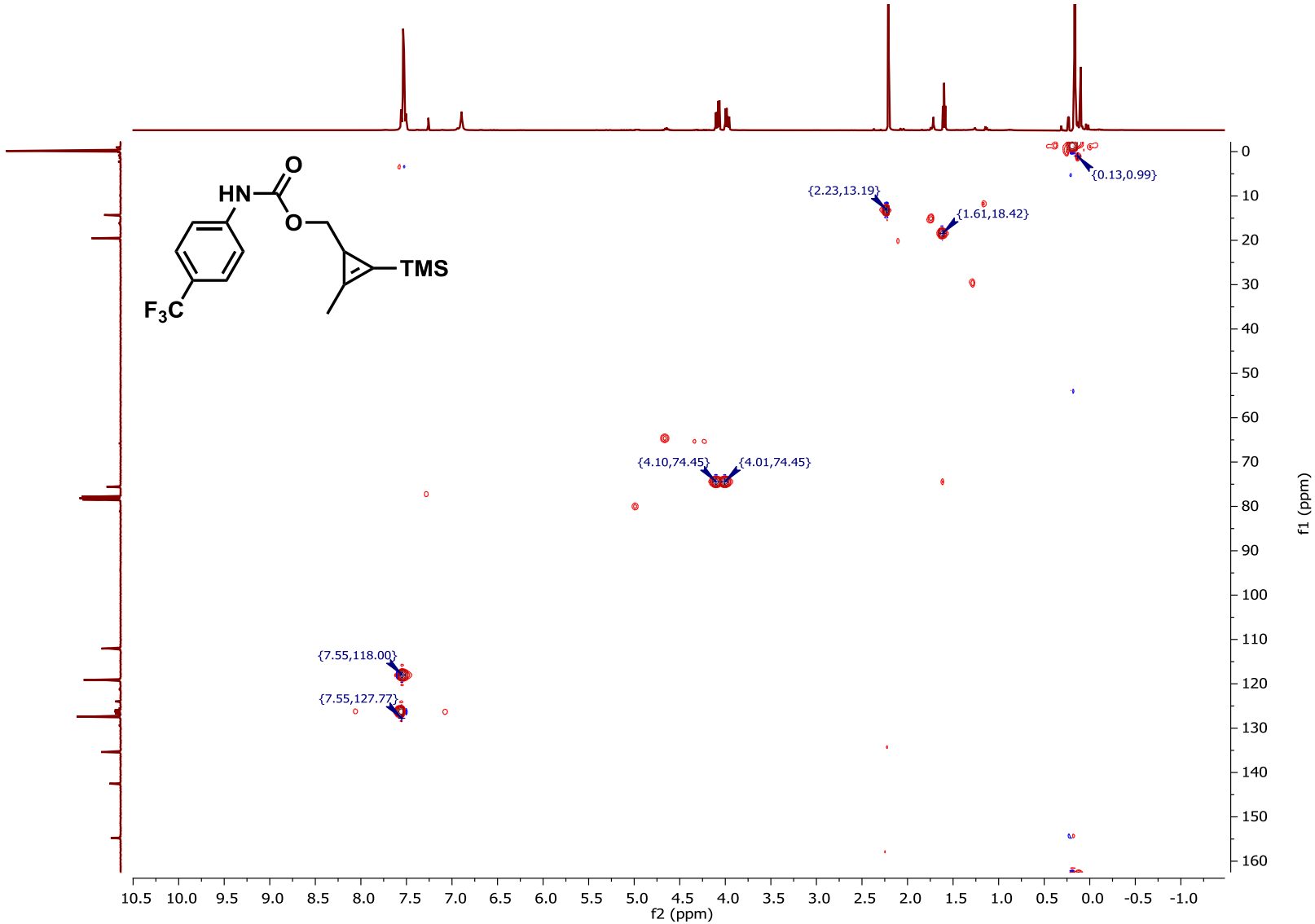
HN
O
O
TMS
F3C
{0.13,0.99}
{2.23,13.19}
{1.61,18.42}
{4.10,74.45}
{4.01,74.45}
{7.55,118.00}
{7.55,127.77}
f2 (ppm)
f1 (ppm)

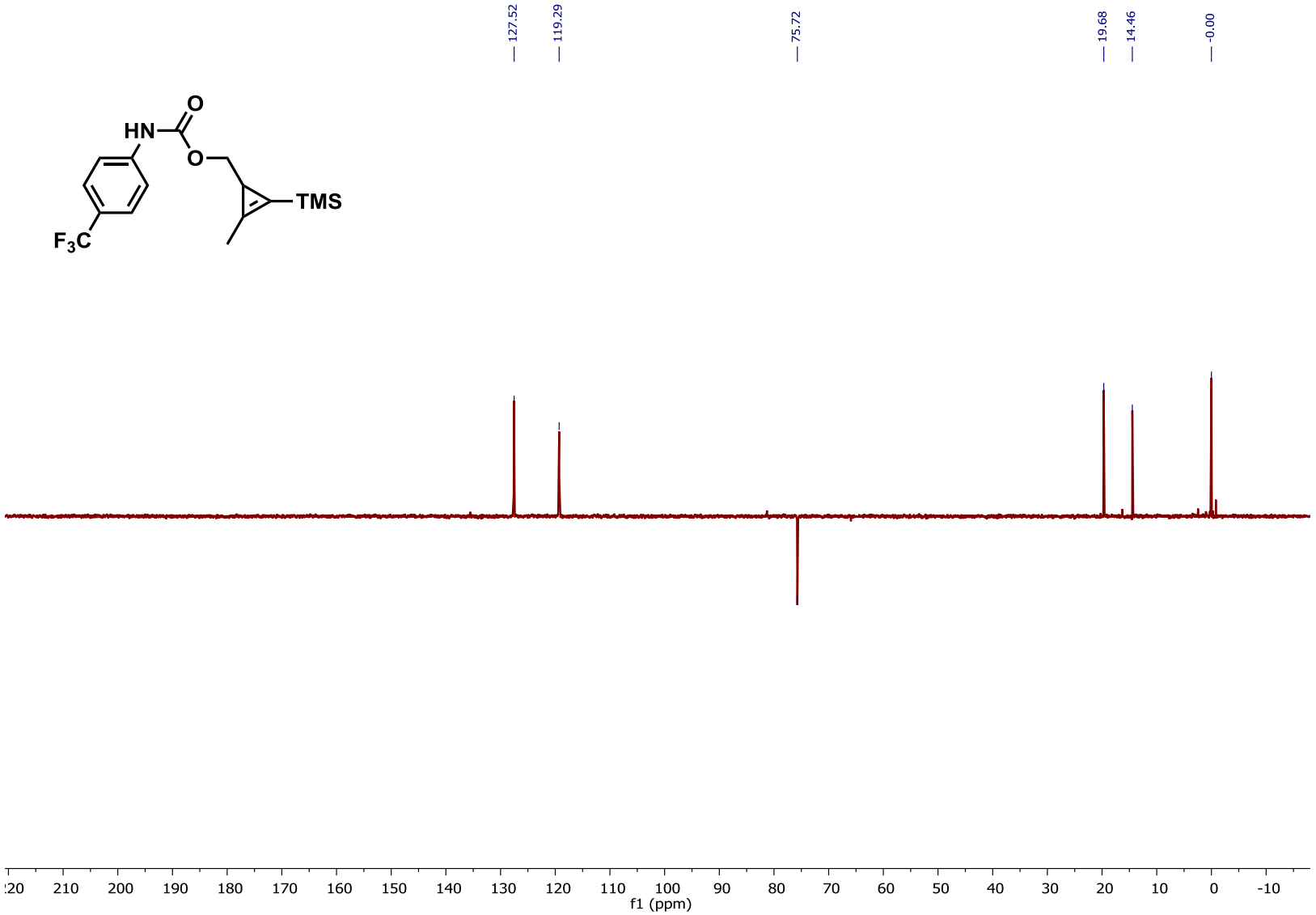
127.52
119.29
75.72
19.68
14.46
-0.00
HN
O
O
TMS
F3C
f1 (ppm)

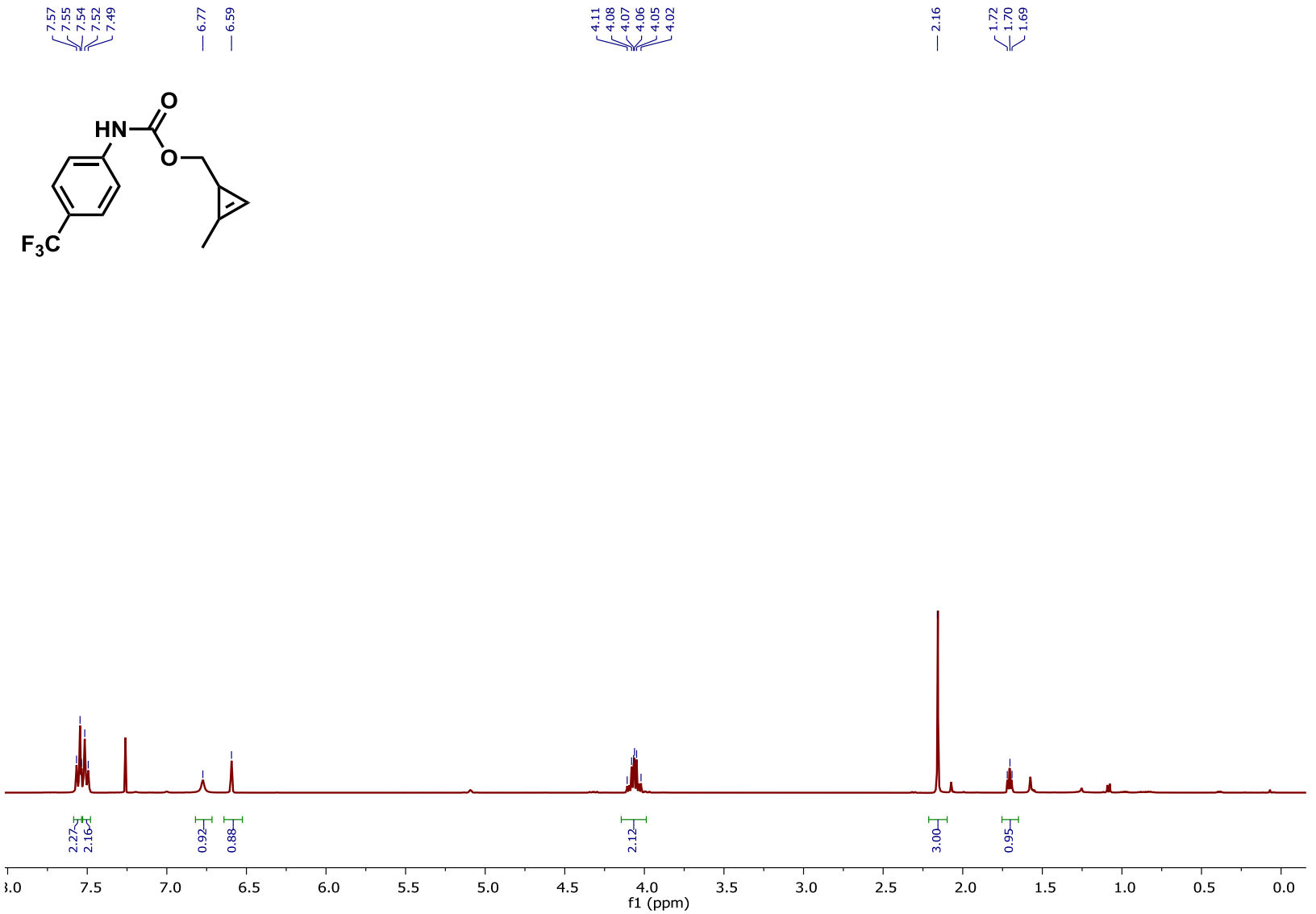
7.57
7.55
7.54
7.52
7.49
6.77
6.59
4.11
4.08
4.07
4.06
4.05
4.02
2.16
1.72
1.70
1.69
HN
O
O
F3C
2.27
2.16
0.92
0.88
2.12
3.00
0.95
f1 (ppm)

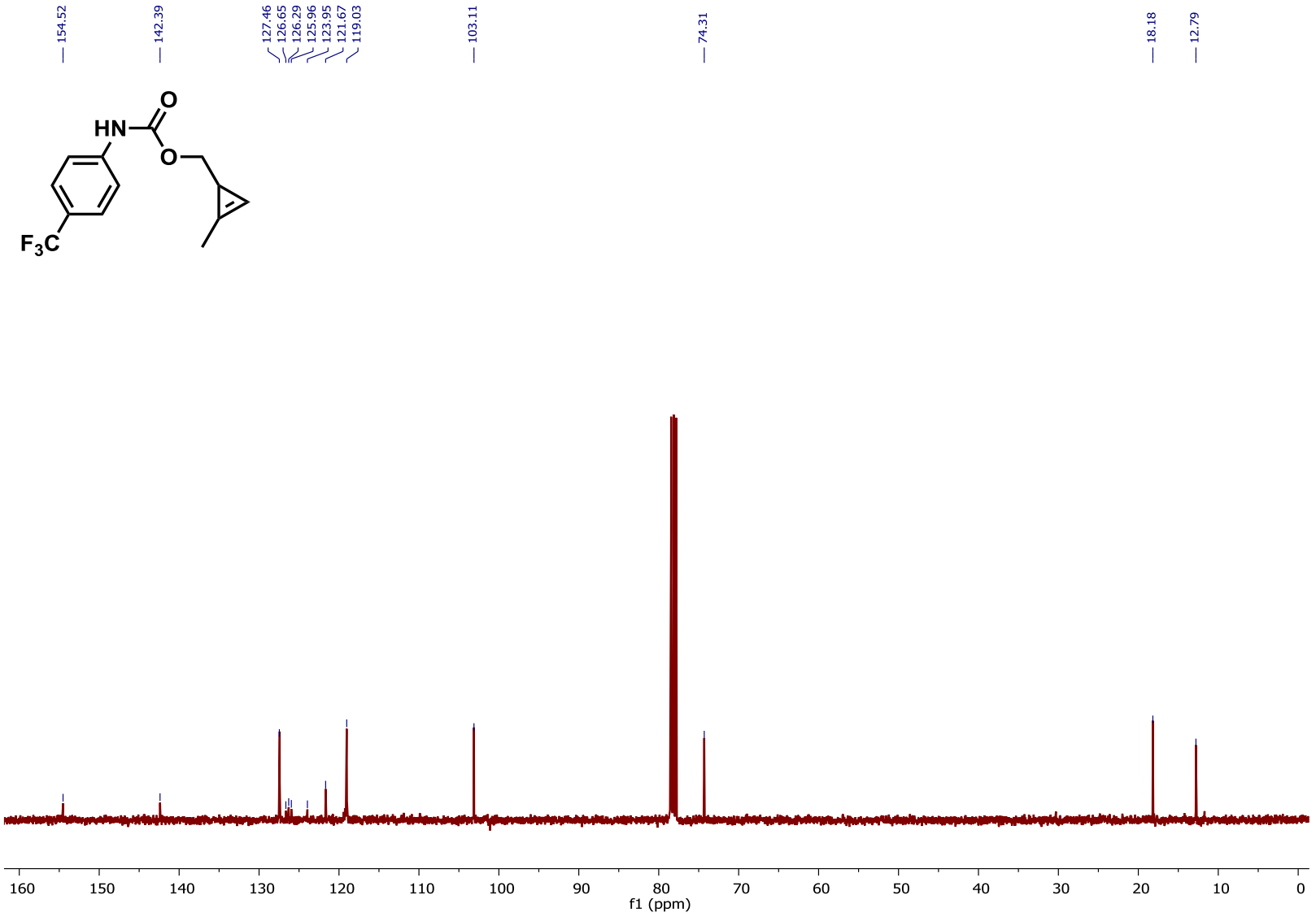
154.52
142.39
127.46
126.65
126.29
125.96
123.95
121.67
119.03
103.11
74.31
18.18
12.79
HN
O
O
F3C
160
150
140
130
120
110
100
90
80
70
60
50
40
30
20
10
0
f1 (ppm)

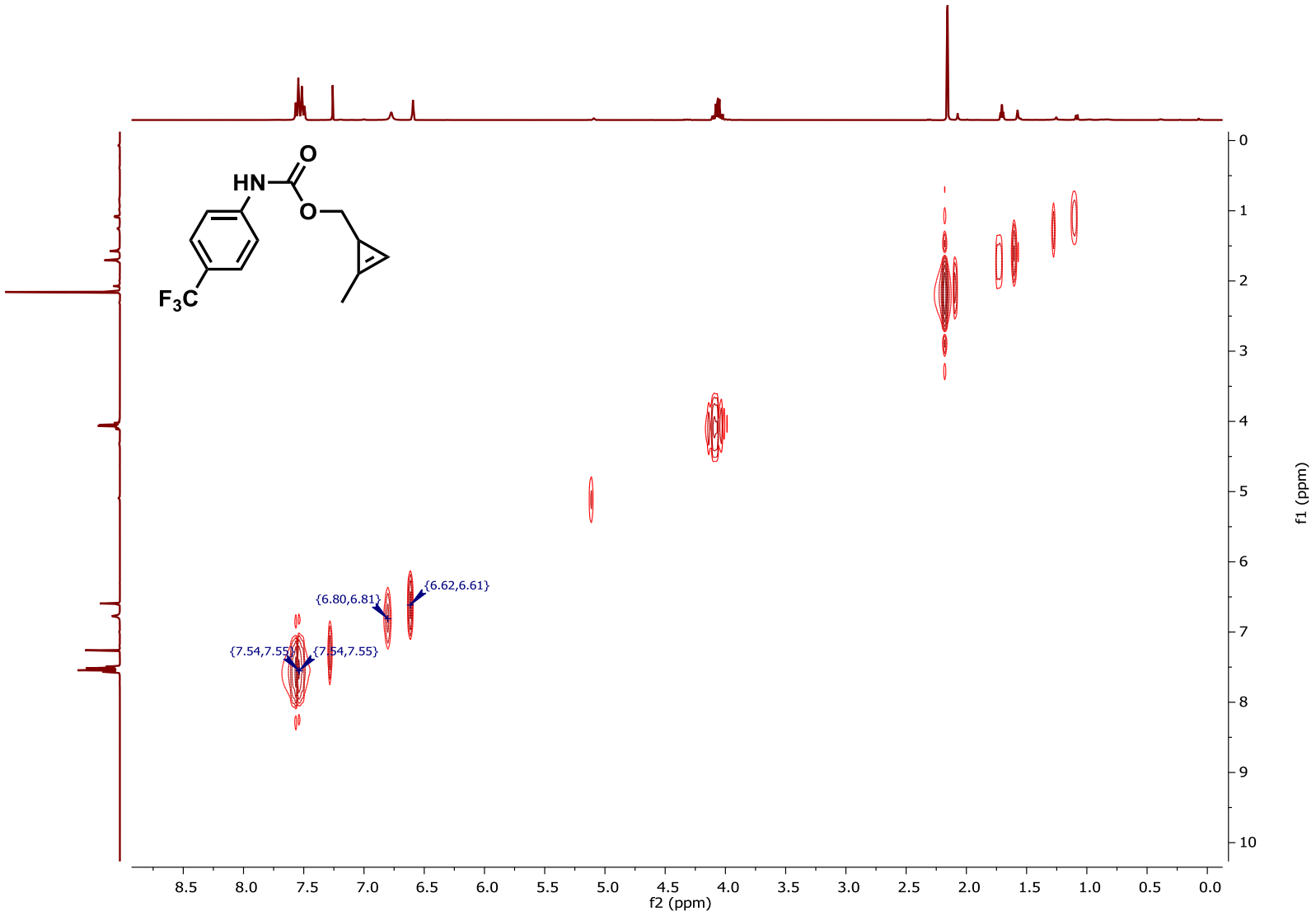
HN
O
O
F3C
{6.80,6.81}
{6.62,6.61}
{7.54,7.55}
{7.54,7.55}
f2 (ppm)
f1 (ppm)

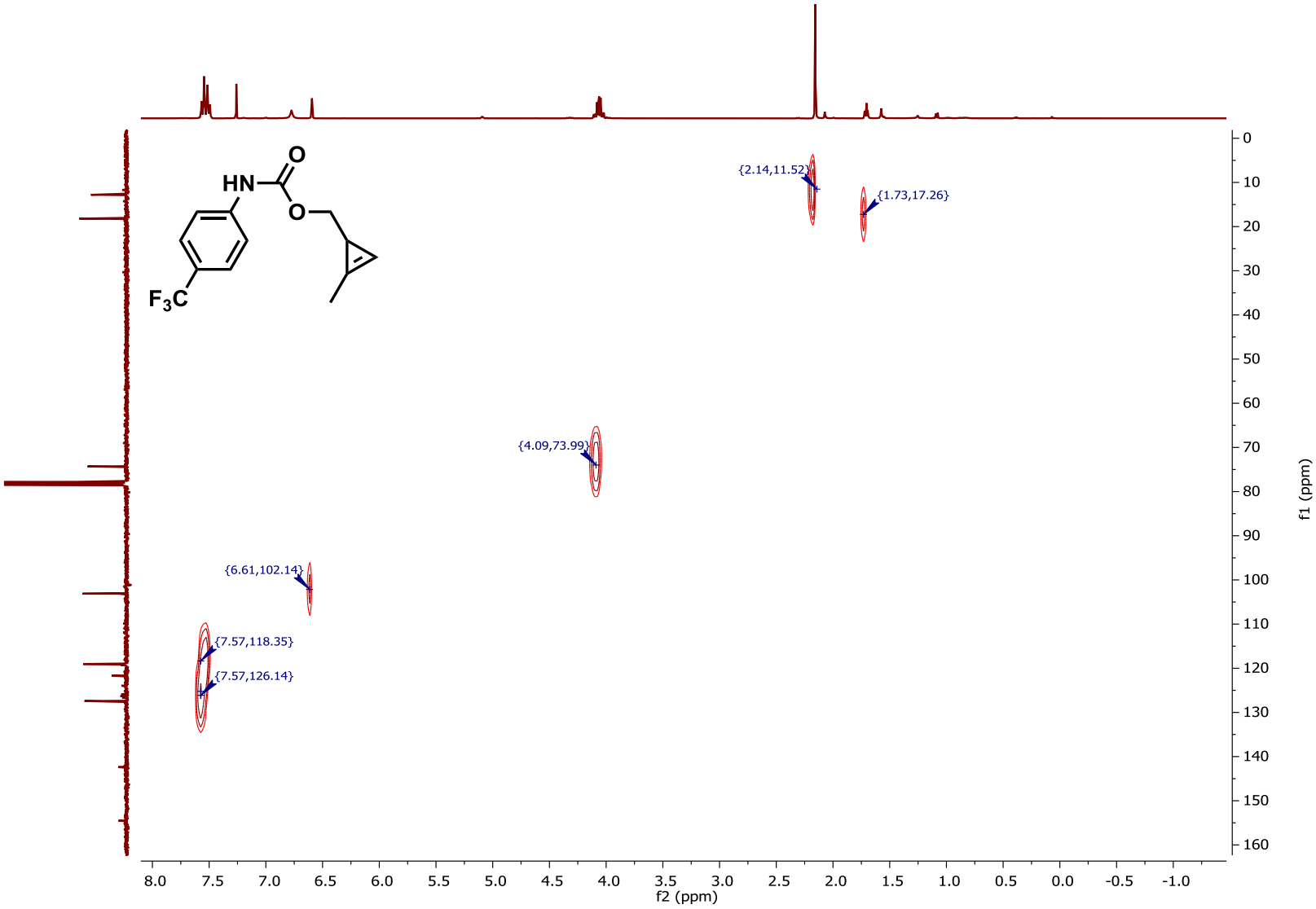
HN
O
O
F3C
{2.14,11.52}
{1.73,17.26}
{4.09,73.99}
{6.61,102.14}
{7.57,118.35}
{7.57,126.14}
f2 (ppm)
f1 (ppm)

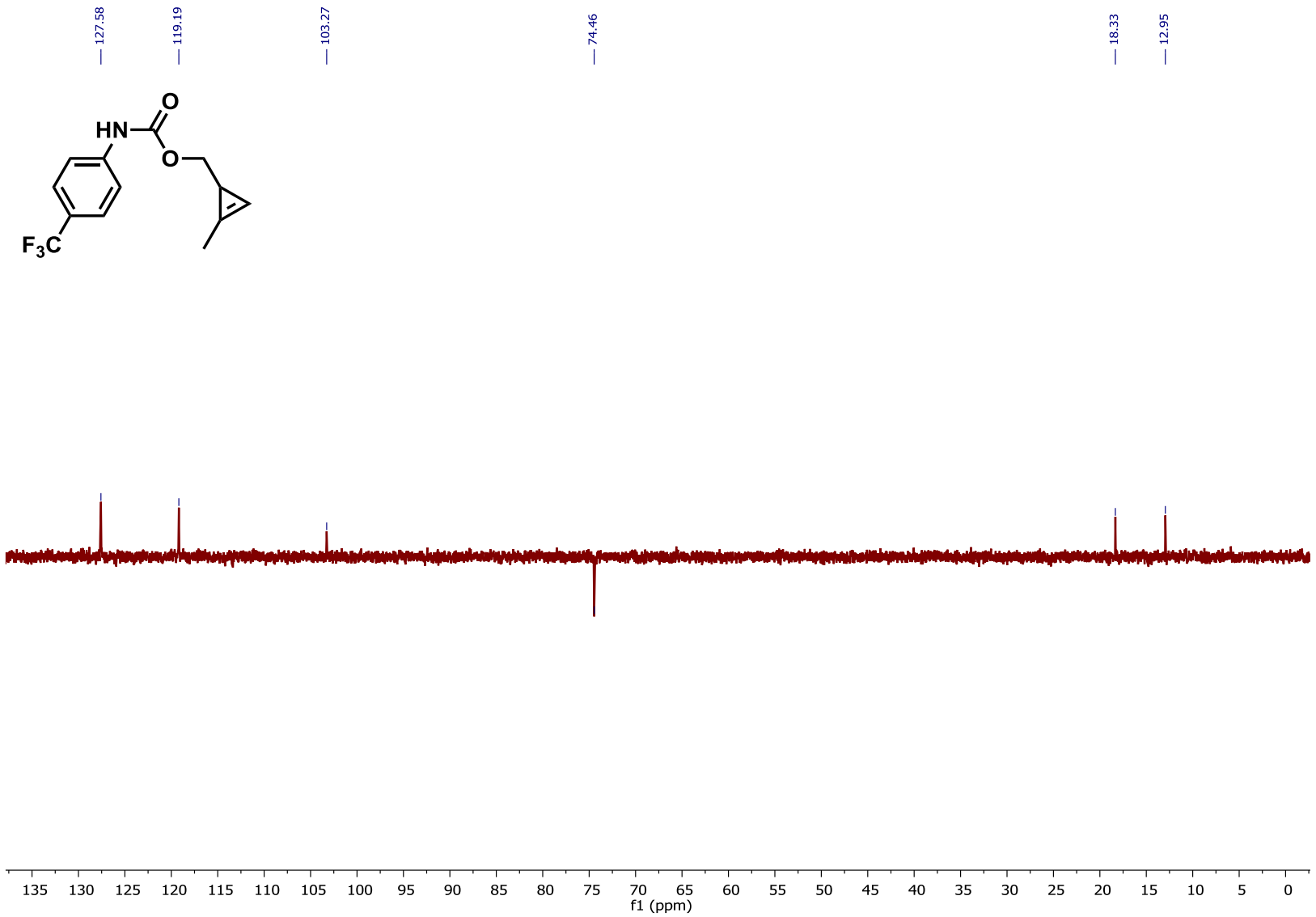
127.58
119.19
103.27
74.46
18.33
12.95
HN
O
O
F3C
135 130 125 120 115 110 105 100 95 90 85 80 75 70 65 60 55 50 45 40 35 30 25 20 15 10 5 0
f1 (ppm)

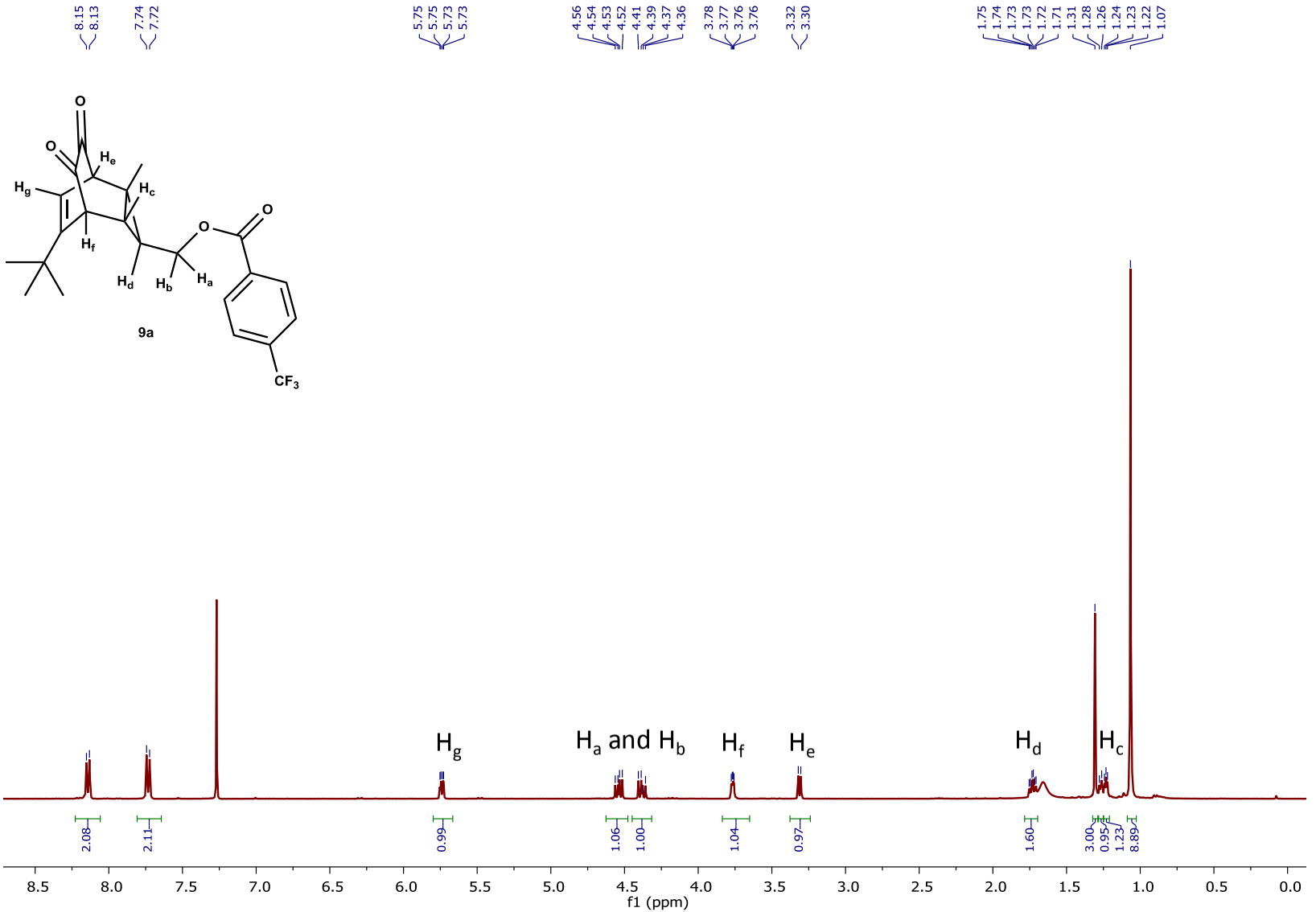
8.15
8.13
7.74
7.72
5.75
5.75
5.73
5.73
4.56
4.54
4.53
4.52
4.41
4.39
4.37
4.36
3.78
3.77
3.76
3.76
3.32
3.30
1.75
1.74
1.73
1.73
1.72
1.71
1.31
1.28
1.26
1.24
1.23
1.22
1.07
O
O
O
O
H_e
H_g
H_c
H_f
H_d
H_b
H_a
CF_3
9a
H_g
H_a and H_b
H_f
H_e
H_d
H_c
2.08
2.11
0.99
1.06
1.00
1.04
0.97
1.60
3.00
0.95
1.23
8.89
8.5
8.0
7.5
7.0
6.5
6.0
5.5
5.0
4.5
4.0
3.5
3.0
2.5
2.0
1.5
1.0
0.5
0.0
f1 (ppm)

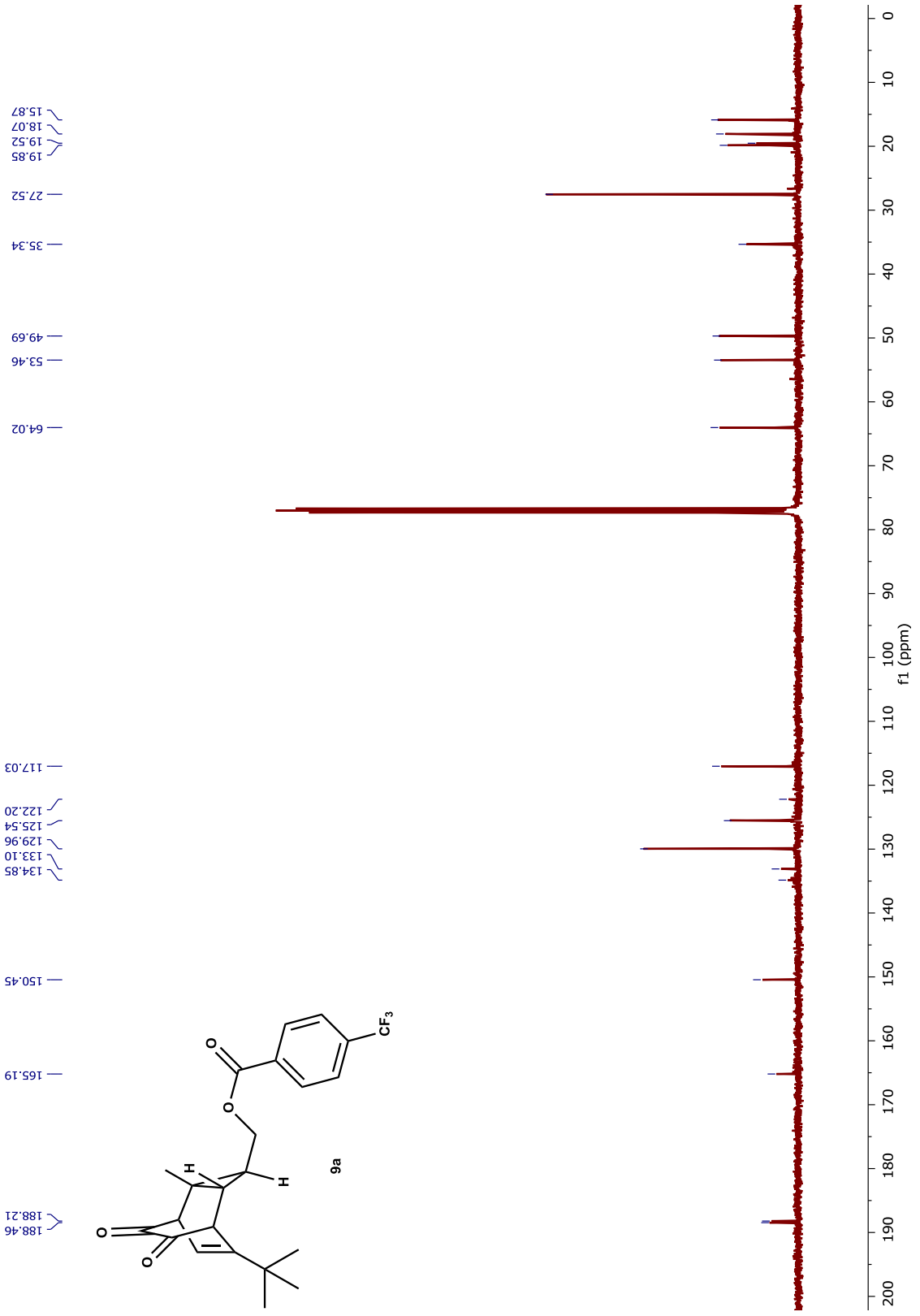
15.87
18.07
19.52
19.85
27.52
35.34
49.69
53.46
64.02
117.03
122.20
125.54
129.96
133.10
134.85
150.45
165.19
188.21
188.46
f1 (ppm)
9a

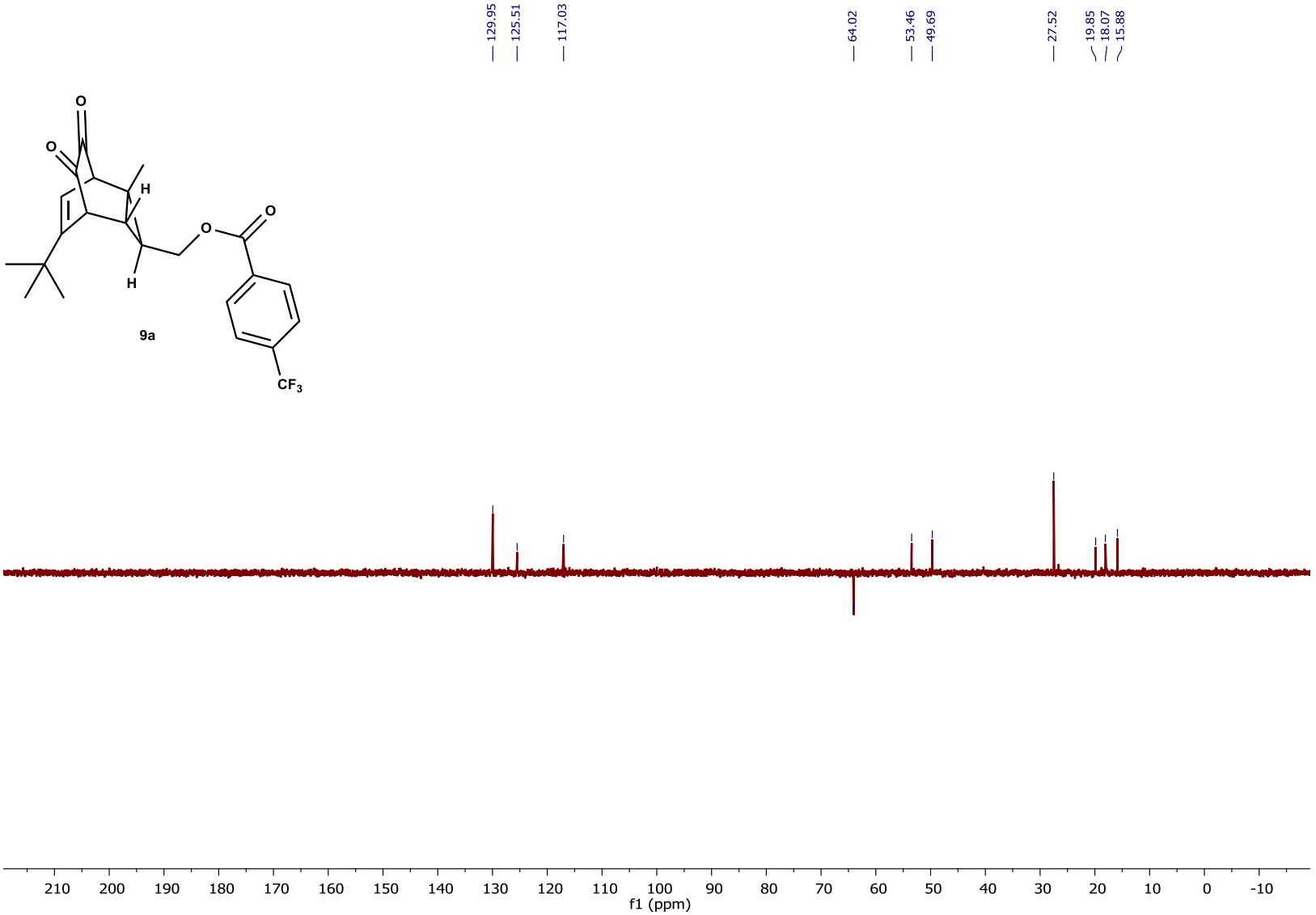
129.95
125.51
117.03
64.02
53.46
49.69
27.52
19.85
18.07
15.88
O
O
H
O
O
H
CF3
9a
210
200
190
180
170
160
150
140
130
120
110
100
90
80
70
60
50
40
30
20
10
0
-10
f1 (ppm)

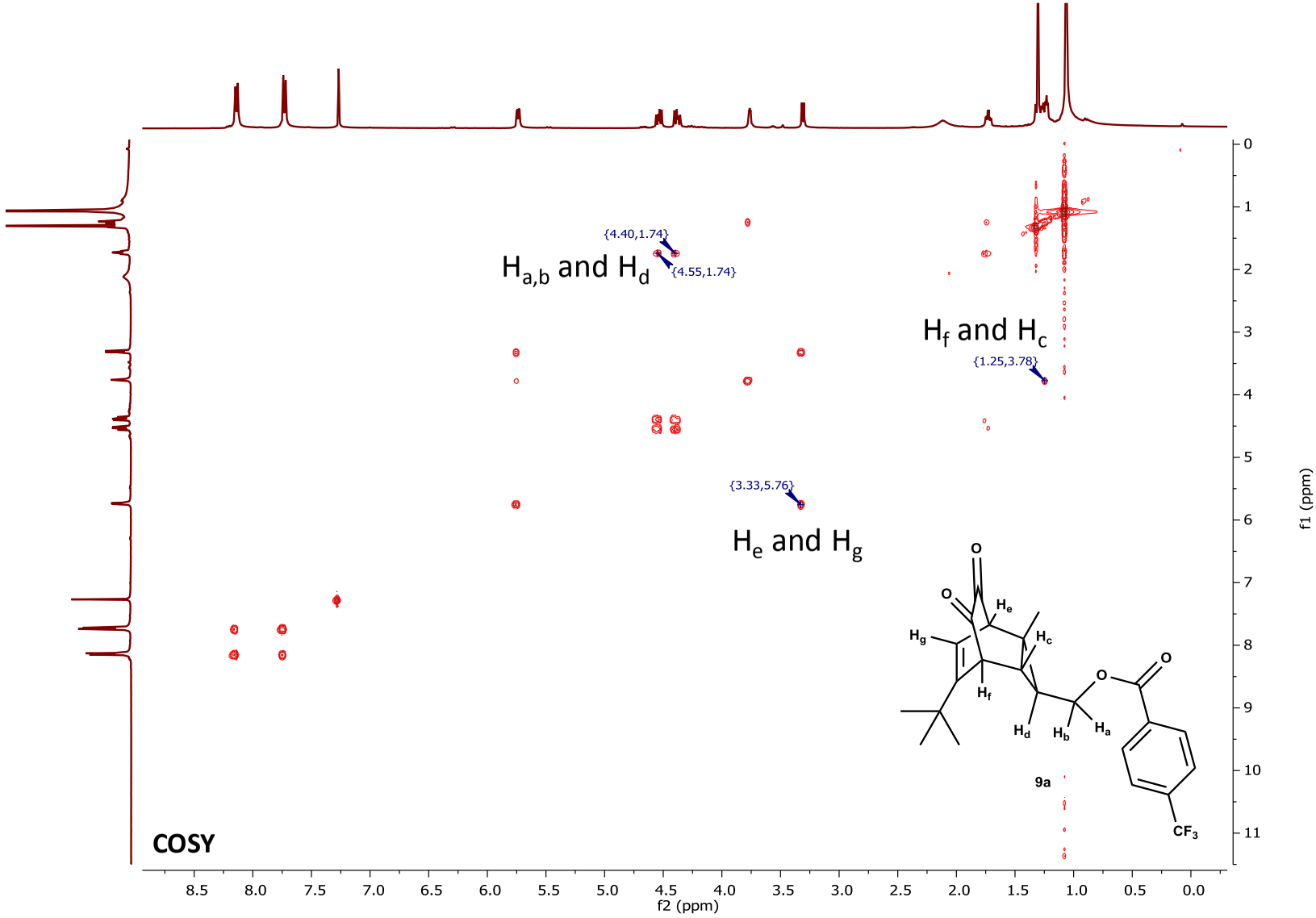
{4.40,1.74}
{4.55,1.74}
Ha,b and Hd
Hf and Hc
{1.25,3.78}
{3.33,5.76}
He and Hg
COSY
9a
f2 (ppm)
f1 (ppm)

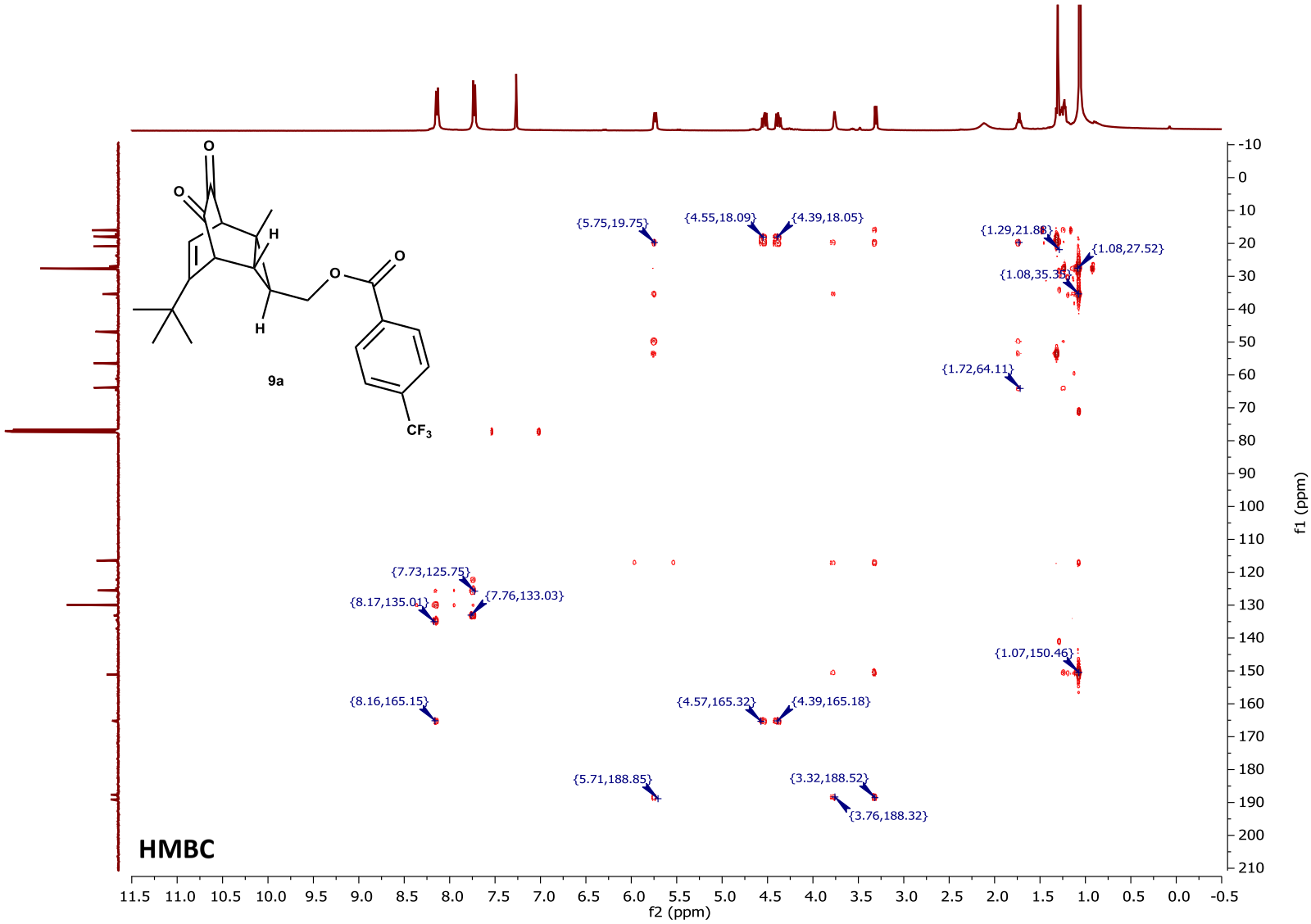
HMBC
9a
{5.75,19.75}
{4.55,18.09}
{4.39,18.05}
{1.29,21.88}
{1.08,27.52}
{1.08,35.35}
{1.72,64.11}
{7.73,125.75}
{8.17,135.01}
{7.76,133.03}
{1.07,150.46}
{8.16,165.15}
{4.57,165.32}
{4.39,165.18}
{5.71,188.85}
{3.32,188.52}
{3.76,188.32}
f2 (ppm)
f1 (ppm)

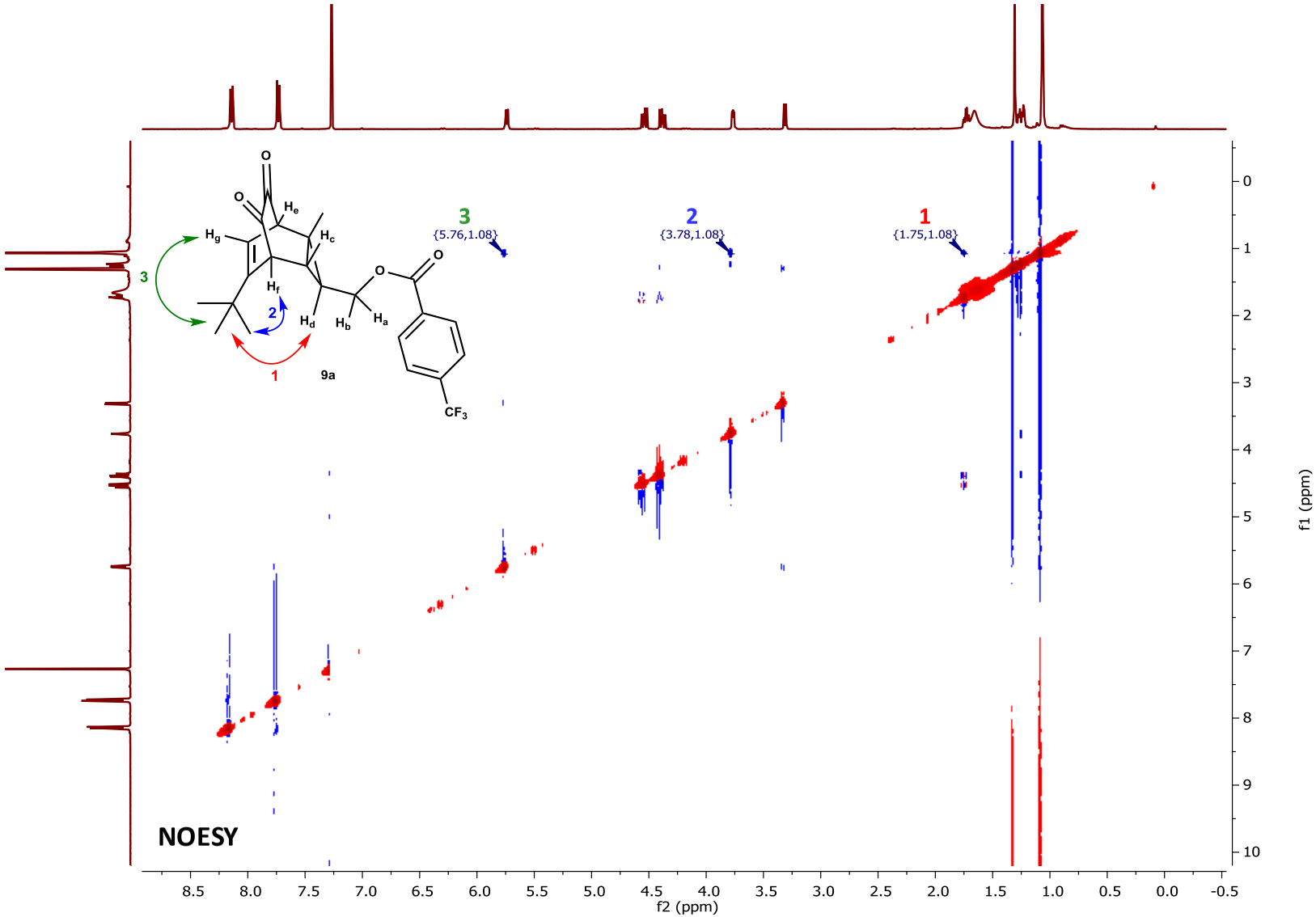
NOESY
3
{5.76,1.08}
2
{3.78,1.08}
1
{1.75,1.08}
9a
f2 (ppm)
f1 (ppm)

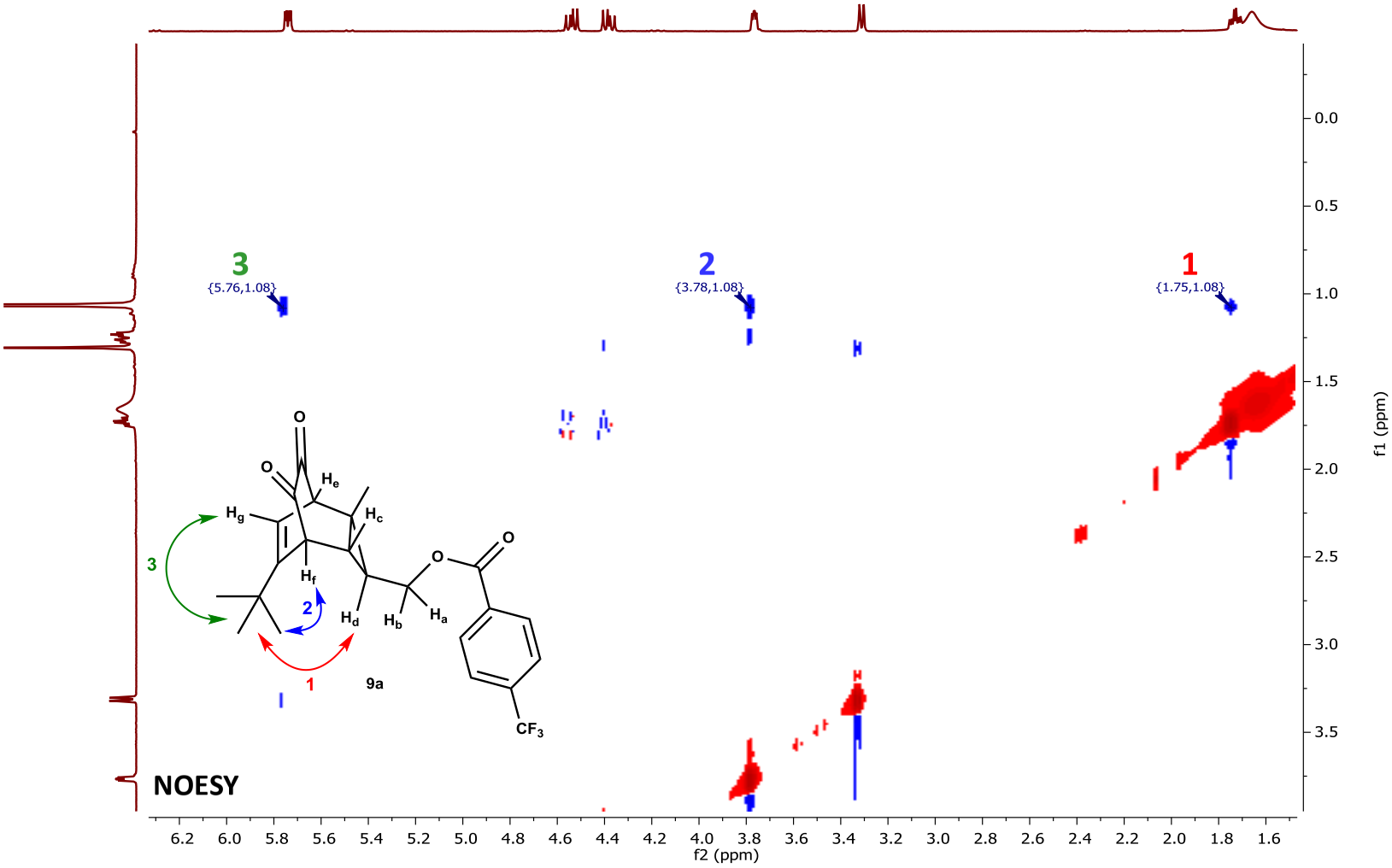
3
{5.76,1.08}
2
{3.78,1.08}
1
{1.75,1.08}
O
O
He
Hg
Hc
Hf
Hd
Hb
Ha
O
O
CF3
3
2
1
9a
NOESY
6.2 6.0 5.8 5.6 5.4 5.2 5.0 4.8 4.6 4.4 4.2 4.0 3.8 3.6 3.4 3.2 3.0 2.8 2.6 2.4 2.2 2.0 1.8 1.6
f2 (ppm)
0.0 0.5 1.0 1.5 2.0 2.5 3.0 3.5
f1 (ppm)

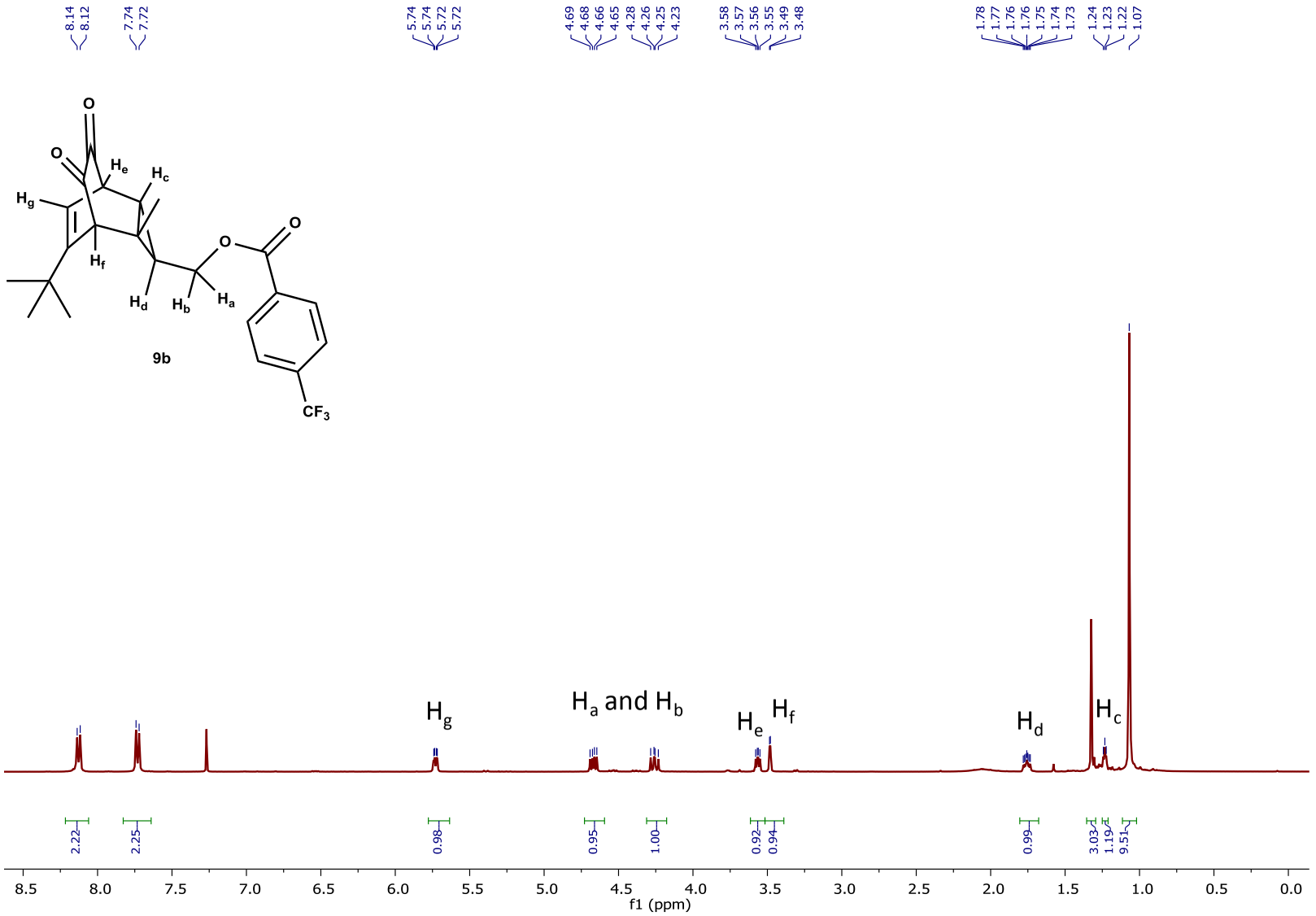
8.14
8.12
7.74
7.72
5.74
5.74
5.72
5.72
4.69
4.68
4.66
4.65
4.28
4.26
4.25
4.23
3.58
3.57
3.56
3.55
3.49
3.48
1.78
1.77
1.76
1.76
1.75
1.74
1.73
1.24
1.23
1.22
1.07
O
O
He
Hc
Hg
Hf
Hd
Hb
Ha
O
O
CF3
9b
Hg
Ha and Hb
He
Hf
Hd
Hc
2.22
2.25
0.98
0.95
1.00
0.92
0.94
0.99
3.03
1.19
9.51
8.5
8.0
7.5
7.0
6.5
6.0
5.5
5.0
4.5
4.0
3.5
3.0
2.5
2.0
1.5
1.0
0.5
0.0
f1 (ppm)

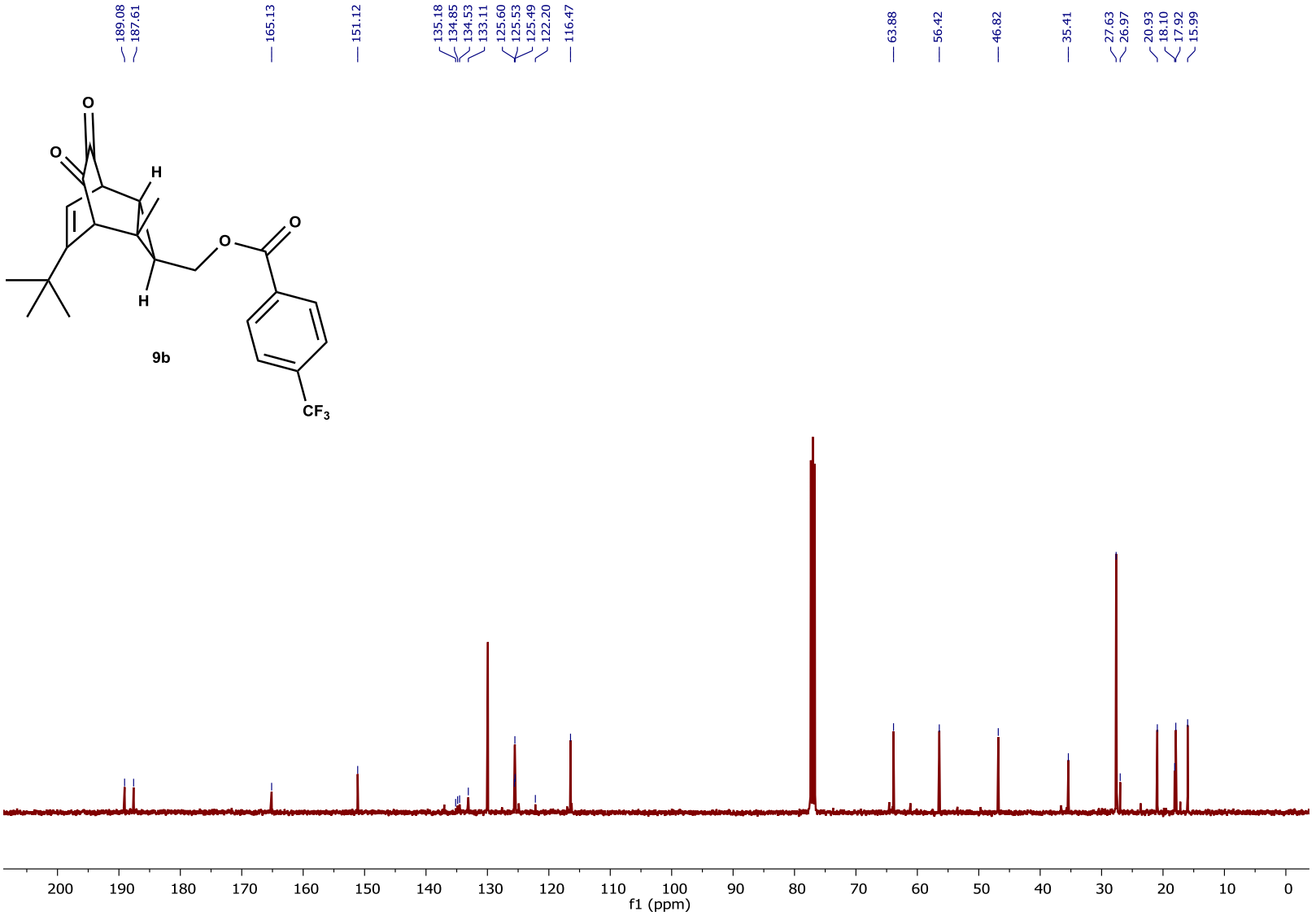
189.08
187.61
165.13
151.12
135.18
134.85
134.53
133.11
125.60
125.53
125.49
122.20
116.47
63.88
56.42
46.82
35.41
27.63
26.97
20.93
18.10
17.92
15.99
O
O
H
O
O
H
9b
CF3
200
190
180
170
160
150
140
130
120
110
100
90
80
70
60
50
40
30
20
10
0
f1 (ppm)

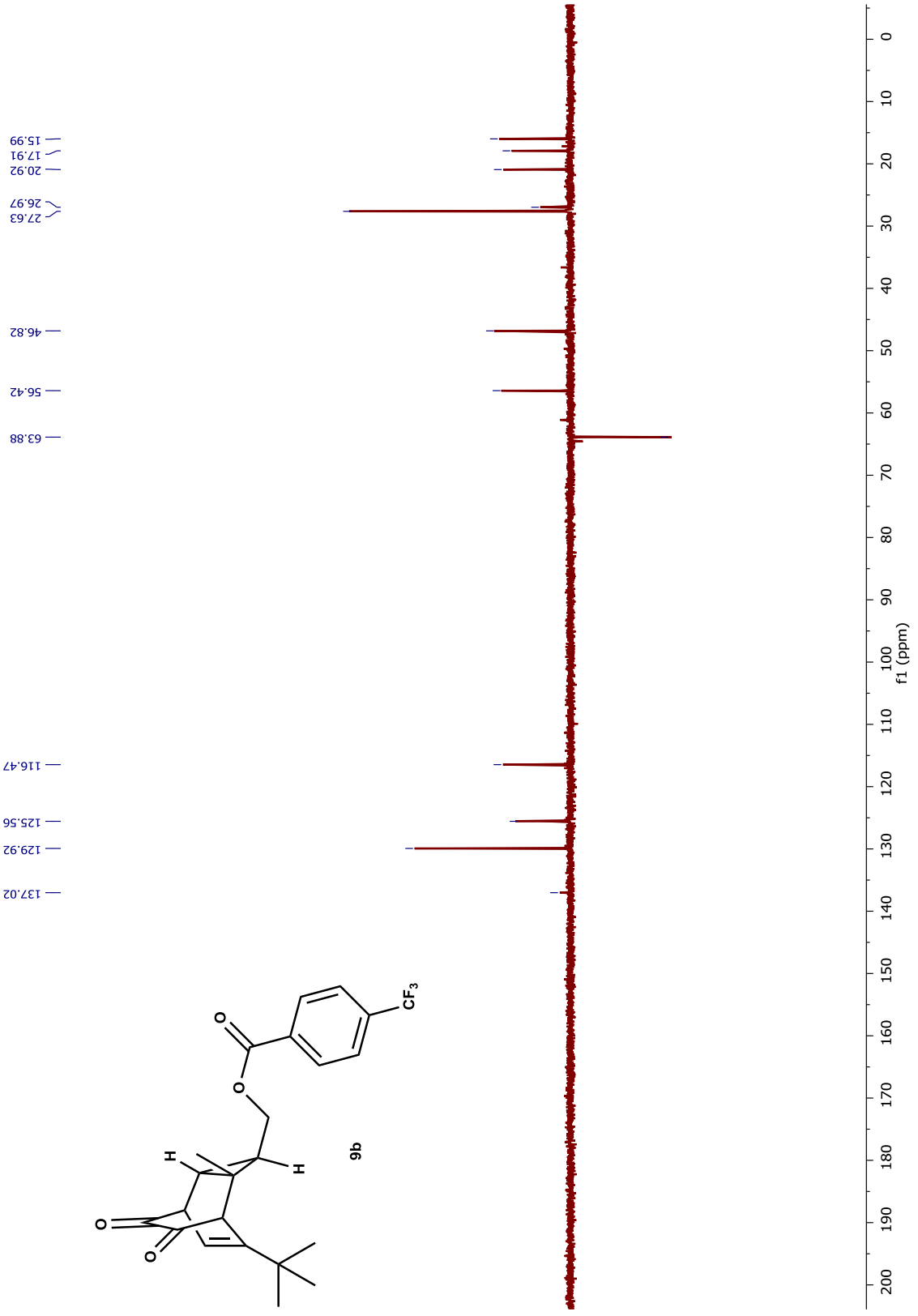
15.99
17.91
20.92
26.97
27.63
46.82
56.42
63.88
116.47
125.56
129.92
137.02
O
O
O
H
H
O
CF3
9b
f1 (ppm)

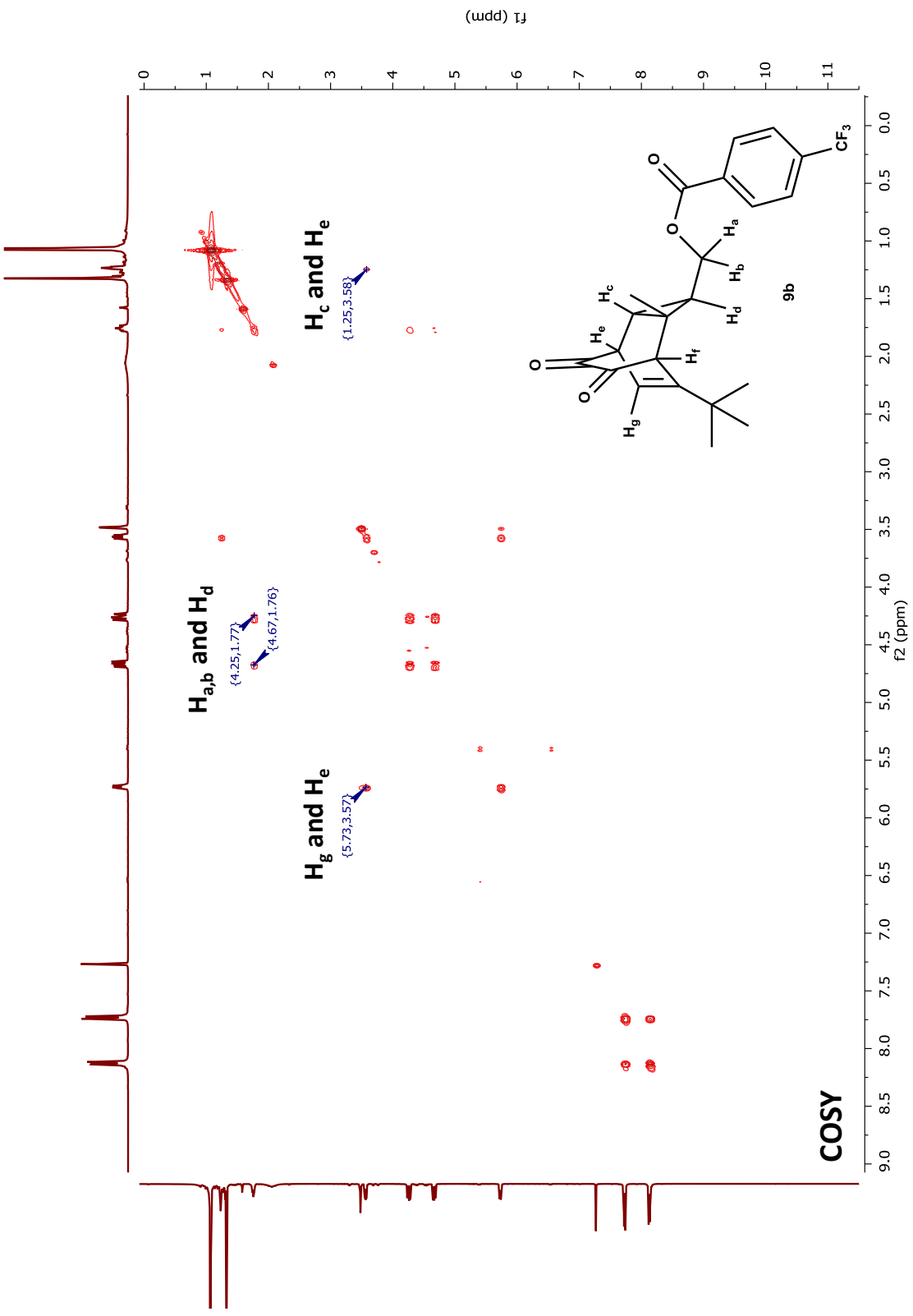
COSY
$H_{a,b}$ and H_d
{4.25,1.77}
{4.67,1.76}
H_c and H_e
{1.25,3.58}
H_g and H_e
{5.73,3.57}
9b
f2 (ppm)
f1 (ppm)

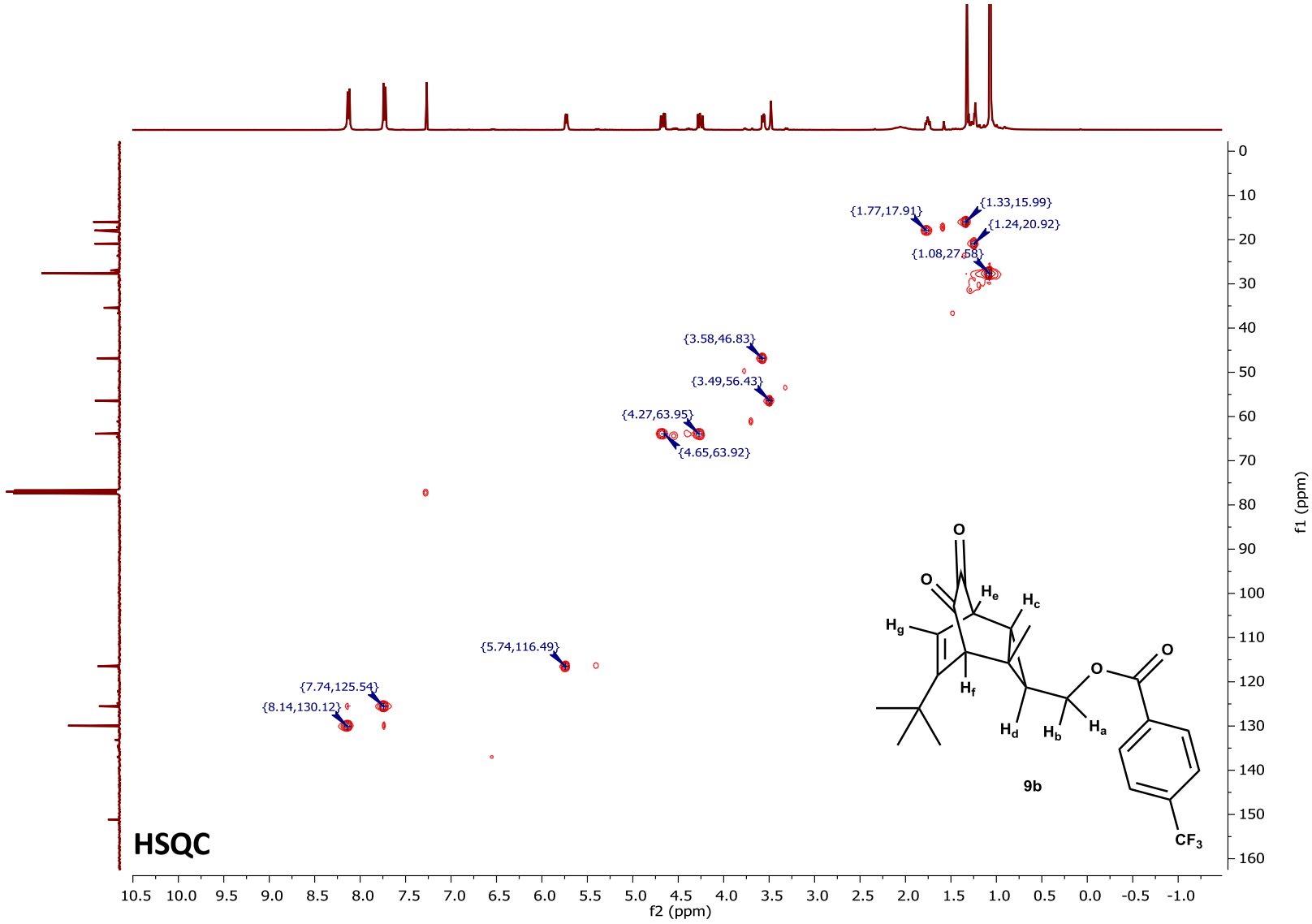
{1.77,17.91}
{1.33,15.99}
{1.24,20.92}
{1.08,27.58}
{3.58,46.83}
{3.49,56.43}
{4.27,63.95}
{4.65,63.92}
{5.74,116.49}
{7.74,125.54}
{8.14,130.12}
HSQC
f2 (ppm)
f1 (ppm)
9b

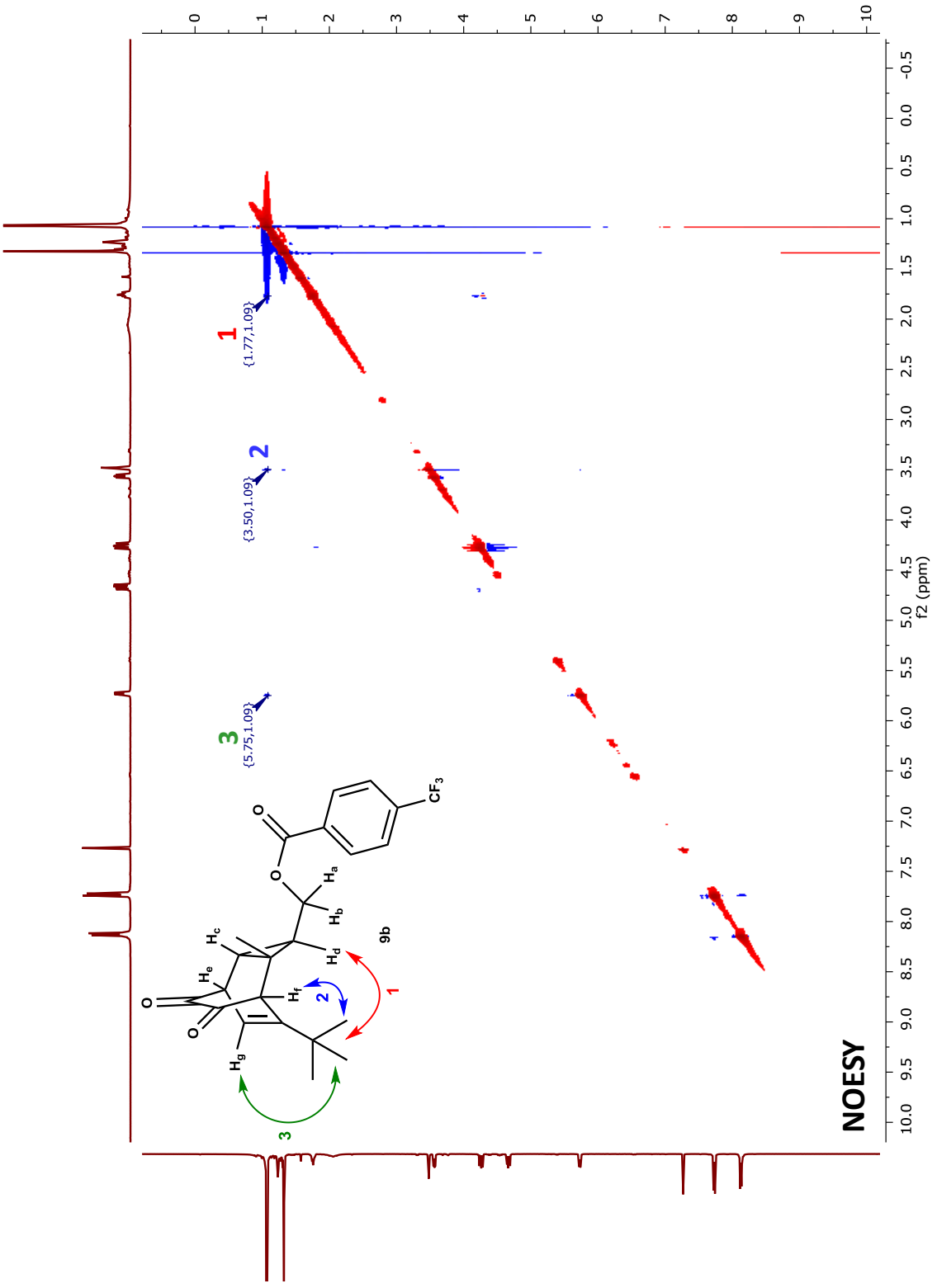
NOESY
f2 (ppm)
f1 (ppm)
1
{1.77,1.09}
2
{3.50,1.09}
3
{5.75,1.09}
O
O
O
CF_3
H_a
H_b
H_c
H_d
H_e
H_f
H_g
9b
1
2
3

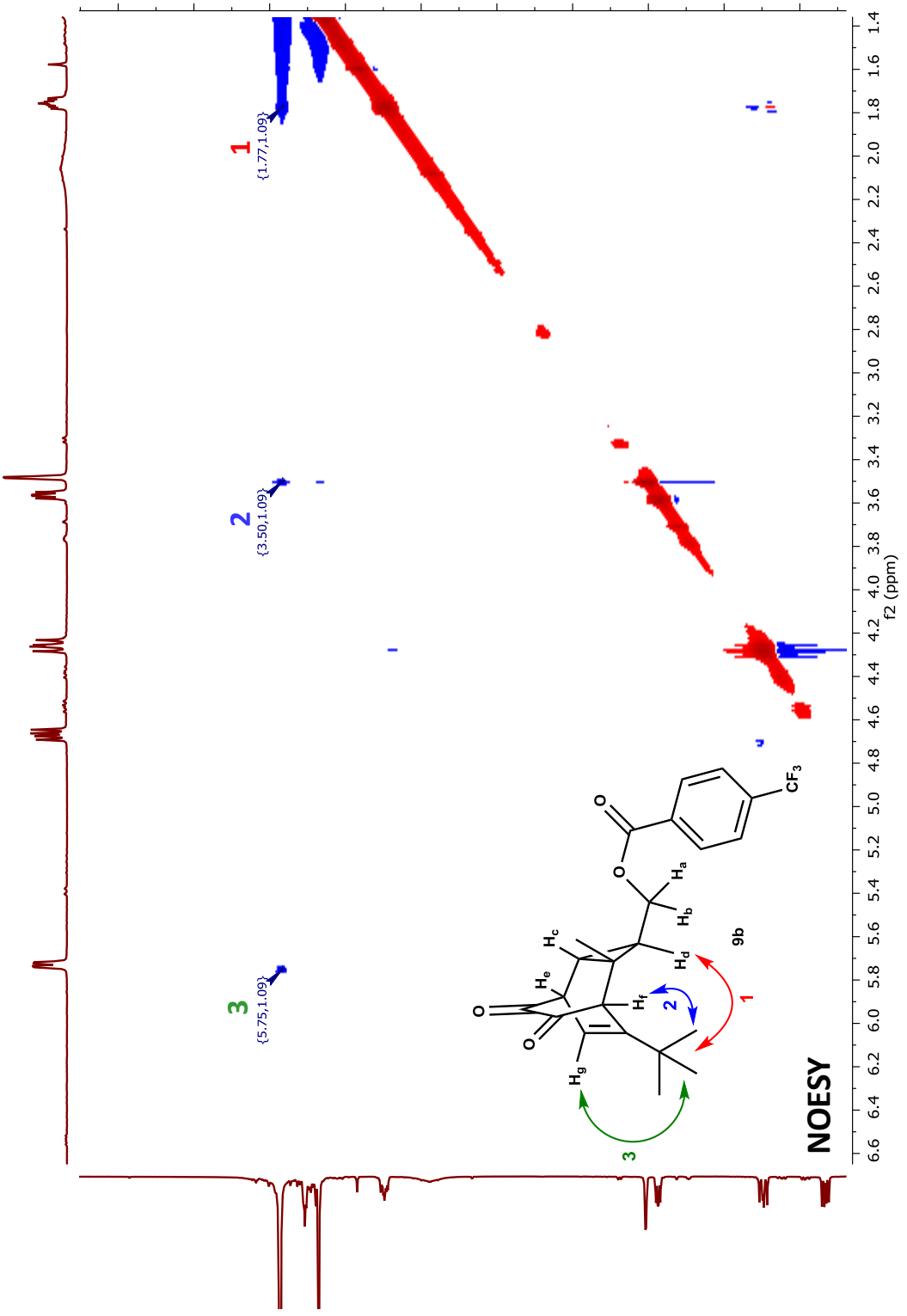
f1 (ppm)
f2 (ppm)
1
{1.77,1.09}
2
{3.50,1.09}
3
{5.75,1.09}
NOESY
9b
CF3
O
Ha
Hb
Hc
Hd
He
Hf
Hg
1
2
3

6. CARTESIAN COORDINATES OF DFT–OPTIMIZED STRUCTURES.

RC-5-*endo*-a

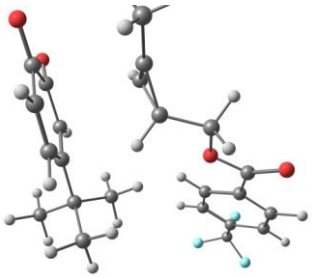

6	-2.566232000	-1.336489000	1.185795000
6	-3.344049000	-2.085833000	0.439921000
6	-2.080737000	-1.590569000	-0.210248000
6	-3.111558000	1.654063000	0.832899000
1	-2.404413000	2.170032000	1.479490000
6	-4.999755000	0.259945000	-0.842100000
1	-5.697926000	-0.267723000	-1.489851000
6	-2.920066000	1.594996000	-0.522138000
6	-3.909515000	0.897073000	-1.350496000
6	-4.285088000	1.087144000	1.491985000
6	-5.299975000	0.296106000	0.589919000
8	-4.514379000	1.223820000	2.694534000
8	-6.300361000	-0.218791000	1.085796000
6	-0.923394000	-2.525729000	-0.494467000
1	-0.909392000	-2.857738000	-1.540266000
1	-0.934452000	-3.401590000	0.166914000
8	0.310651000	-1.768814000	-0.238115000
6	1.477396000	-2.364416000	-0.561879000
8	1.561548000	-3.483248000	-1.046659000
6	2.659111000	-1.487764000	-0.261853000
6	2.530829000	-0.251550000	0.399858000
6	3.932679000	-1.932274000	-0.663143000
6	3.660165000	0.530578000	0.653475000
1	1.553090000	0.098555000	0.714331000
6	5.063540000	-1.152807000	-0.414163000
1	4.026024000	-2.888034000	-1.172590000
6	4.923688000	0.081805000	0.240011000
1	3.557439000	1.484953000	1.163229000
1	6.044885000	-1.497120000	-0.730364000
6	6.153292000	0.897565000	0.561641000
9	6.704465000	0.521268000	1.761387000
9	5.891473000	2.231319000	0.660681000
9	7.136423000	0.755432000	-0.372865000
6	-1.695125000	2.272944000	-1.159084000
6	-1.519823000	1.928888000	-2.654270000
1	-0.604525000	2.411884000	-3.020109000
1	-1.420486000	0.845290000	-2.808889000
1	-2.359665000	2.297089000	-3.258897000
6	-1.874702000	3.809024000	-1.023817000
1	-2.785608000	4.141571000	-1.541014000
1	-1.943656000	4.101203000	0.032149000
1	-1.010075000	4.315952000	-1.475278000
6	-0.405181000	1.839776000	-0.417258000
1	-0.268920000	0.754104000	-0.487461000
1	0.458707000	2.334752000	-0.881747000
1	-0.429188000	2.122710000	0.642539000
1	-3.749744000	0.867078000	-2.424723000
1	-2.151902000	-0.777353000	-0.951907000
1	-2.318399000	-0.889961000	2.139038000
6	-4.513535000	-2.974336000	0.252605000
1	-5.259784000	-2.815639000	1.040502000
1	-4.975685000	-2.811576000	-0.729609000
1	-4.179058000	-4.023187000	0.288074000

RC-5-*endo*-b

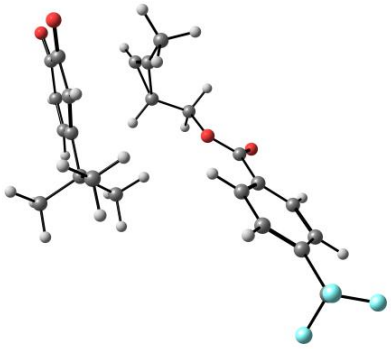

6	2.622143000	-1.657523000	1.084259000
6	3.398255000	-2.216501000	0.184724000
6	2.078715000	-1.708510000	-0.316159000
6	4.873262000	0.147233000	-1.323542000
1	5.409013000	-0.305654000	-2.156531000
6	3.409321000	1.356178000	0.857518000
1	2.869438000	1.794084000	1.692857000
6	3.751468000	0.888991000	-1.521366000
1	3.387667000	1.028303000	-2.537115000
6	2.983738000	1.512761000	-0.432215000
6	5.439664000	-0.019497000	0.018778000
6	4.633284000	0.633120000	1.199034000
8	6.508036000	-0.587321000	0.236991000
8	5.060499000	0.548016000	2.350956000
1	2.067192000	-0.788439000	-0.917781000
1	4.301327000	-2.750398000	-0.080859000
6	2.272573000	-1.329874000	2.485146000
1	3.168316000	-1.279818000	3.116429000
1	1.728333000	-0.379193000	2.541411000
1	1.607429000	-2.114529000	2.879231000
6	1.755731000	2.340063000	-0.815661000
6	0.998089000	2.877135000	0.413919000
1	0.127209000	3.451792000	0.073050000
1	0.642335000	2.055559000	1.050788000
1	1.632666000	3.539863000	1.017742000
6	0.767110000	1.492161000	-1.660312000
1	-0.078826000	2.129184000	-1.952763000
1	1.230905000	1.104600000	-2.576381000
1	0.383846000	0.645304000	-1.078698000
6	2.243300000	3.545541000	-1.666876000
1	2.928272000	4.176459000	-1.084168000
1	2.759170000	3.215919000	-2.578364000
1	1.373126000	4.147647000	-1.963029000
6	0.928070000	-2.625939000	-0.675515000
1	0.943445000	-3.557234000	-0.094824000
1	0.899702000	-2.862691000	-1.747120000
8	-0.293404000	-1.880267000	-0.340286000
6	-1.474680000	-2.418935000	-0.702947000
8	-1.591822000	-3.504309000	-1.252529000
6	-2.627201000	-1.519975000	-0.357019000
6	-2.444557000	-0.266684000	0.259860000
6	-3.926757000	-1.954456000	-0.675291000
6	-3.546307000	0.540648000	0.550236000
1	-1.445644000	0.076435000	0.510444000
6	-5.031495000	-1.150870000	-0.385866000
1	-4.061963000	-2.922835000	-1.150379000
6	-4.838651000	0.095134000	0.230749000
1	-3.402214000	1.507431000	1.025877000
1	-6.033724000	-1.490882000	-0.632896000
6	-6.019842000	1.000453000	0.487993000
9	-7.186586000	0.315595000	0.649226000
9	-6.221124000	1.868750000	-0.556233000
9	-5.856166000	1.771901000	1.600935000

RC-5-*exo*-a

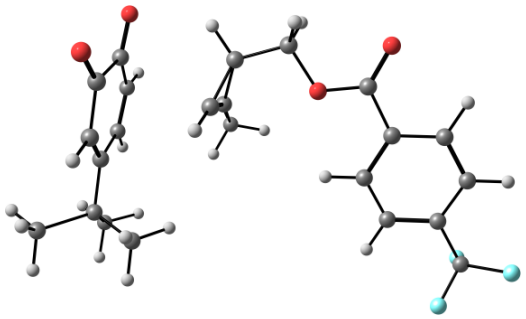

6	-1.465399000	-0.995002000	0.740410000
6	-1.642239000	-1.009080000	-0.560468000
6	-1.356909000	-2.340840000	0.075476000
6	-4.546360000	-0.655466000	1.541552000
1	-4.577171000	-1.063336000	2.550698000
6	-4.449929000	0.463520000	-1.116545000
1	-4.395535000	0.873056000	-2.123671000
6	-4.512672000	0.685392000	1.319174000
1	-4.521760000	1.351332000	2.177459000
6	-4.428490000	1.280540000	-0.018458000
6	-4.548941000	-1.605734000	0.427184000
6	-4.566397000	-0.988684000	-1.016445000
8	-4.567281000	-2.826442000	0.578884000
8	-4.695855000	-1.726301000	-1.994940000
1	-2.175802000	-3.068084000	0.195005000
1	-1.759289000	-0.465007000	-1.488550000
6	-1.261933000	-0.260967000	2.008857000
1	-1.570848000	0.787700000	1.916465000
1	-1.815314000	-0.734098000	2.831317000
1	-0.192851000	-0.293110000	2.272524000
6	-4.274068000	2.800466000	-0.198043000
6	-2.901362000	3.069135000	-0.872143000
1	-2.771241000	4.151969000	-1.008801000
1	-2.081199000	2.693056000	-0.245046000
1	-2.841753000	2.581999000	-1.853911000
6	-4.321399000	3.579704000	1.133473000
1	-4.213930000	4.650690000	0.918029000
1	-5.277022000	3.429898000	1.654942000
1	-3.502814000	3.284502000	1.804293000
6	-5.407487000	3.332314000	-1.112892000
1	-5.383973000	2.853693000	-2.099967000
1	-6.390236000	3.147802000	-0.657140000
1	-5.282001000	4.415446000	-1.249853000
6	-0.024528000	-3.070677000	-0.082016000
1	0.014150000	-3.642977000	-1.019597000
1	0.149650000	-3.759921000	0.755673000
8	1.044809000	-2.079383000	-0.098642000
6	2.312774000	-2.531180000	-0.171189000
8	2.615348000	-3.712782000	-0.244751000
6	3.306945000	-1.406239000	-0.146015000
6	2.913312000	-0.057831000	-0.039735000
6	4.674431000	-1.726981000	-0.227686000
6	3.875618000	0.954341000	-0.014232000
1	1.859586000	0.197632000	0.022608000
6	5.639379000	-0.718268000	-0.201978000
1	4.971803000	-2.769310000	-0.310553000
6	5.236806000	0.622672000	-0.099736000
1	3.569791000	1.994240000	0.066455000
1	6.694707000	-0.969996000	-0.266138000
6	6.278098000	1.712663000	-0.006668000
9	6.627504000	1.960759000	1.297626000
9	5.845063000	2.899285000	-0.519883000
9	7.432033000	1.396544000	-0.659735000

RC-5-*exo*-b

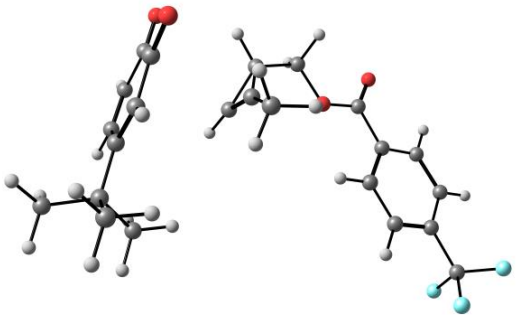

6	1.615427000	-0.994781000	-0.625892000
6	1.416145000	-1.014029000	0.671022000
6	1.298424000	-2.338802000	-0.032124000
6	4.668371000	-0.837298000	-1.548538000
1	4.771464000	-1.336456000	-2.510955000
6	4.385569000	0.525034000	0.990986000
1	4.265031000	1.017897000	1.952019000
6	4.688140000	0.515835000	-1.441190000
1	4.808889000	1.111538000	-2.343328000
6	4.519565000	1.234035000	-0.168923000
6	4.525672000	-1.681870000	-0.356273000
6	4.418698000	-0.935649000	1.020409000
8	4.523271000	-2.910989000	-0.394652000
8	4.390234000	-1.586192000	2.066612000
1	2.109071000	-3.078969000	0.066328000
6	4.475469000	2.759799000	-0.228470000
6	4.293629000	3.402806000	1.159802000
1	4.266883000	4.494330000	1.046665000
1	3.352969000	3.081638000	1.627551000
1	5.125187000	3.145106000	1.829971000
6	3.279463000	3.181151000	-1.126433000
1	3.245183000	4.278087000	-1.181369000
1	3.376446000	2.790721000	-2.147785000
1	2.333401000	2.819336000	-0.700961000
6	5.797251000	3.287652000	-0.847542000
1	6.654752000	3.005019000	-0.221590000
1	5.960733000	2.900319000	-1.861408000
1	5.750190000	4.383951000	-0.905145000
6	-0.040767000	-3.048078000	-0.220671000
1	-0.213855000	-3.782337000	0.578143000
1	-0.091067000	-3.566365000	-1.188547000
8	-1.103852000	-2.050962000	-0.170902000
6	-2.372269000	-2.487393000	-0.304224000
8	-2.678142000	-3.656005000	-0.488953000
6	-3.363012000	-1.364517000	-0.194469000
6	-2.970063000	-0.038988000	0.073804000
6	-4.727900000	-1.665661000	-0.358199000
6	-3.930216000	0.970818000	0.178169000
1	-1.918808000	0.200706000	0.203962000
6	-5.690017000	-0.659659000	-0.256068000
1	-5.024981000	-2.690966000	-0.563676000
6	-5.288703000	0.657710000	0.018509000
1	-3.624831000	1.992376000	0.388581000
1	-6.743497000	-0.896525000	-0.381377000
6	-6.327294000	1.752961000	0.072247000
9	-6.600503000	2.246229000	-1.179412000
9	-5.936508000	2.816919000	0.828266000
9	-7.517027000	1.321200000	0.581293000
6	1.259563000	-0.340317000	1.976634000
1	1.399865000	0.744371000	1.888122000
1	0.258070000	-0.547948000	2.381934000
1	1.992407000	-0.742531000	2.692960000
1	1.793885000	-0.433794000	-1.533663000

TS-5-*endo*-a

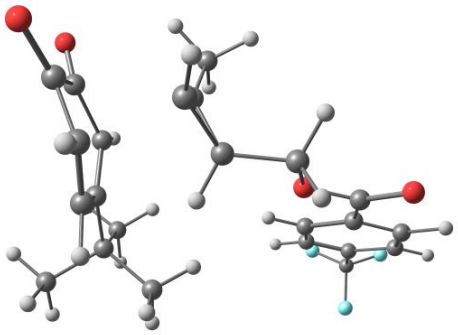

Frequency -329.4162

6	2.552211000	1.336151000	0.779641000		1	-3.564304000	-1.651749000	0.828272000
6	3.360012000	1.869236000	-0.199668000		1	-6.124522000	1.597785000	-0.416628000
6	1.994118000	1.411981000	-0.589578000		6	-6.184637000	-0.952319000	0.539507000
6	3.295514000	-0.994159000	0.954127000		9	-5.964196000	-1.871799000	1.521088000
1	2.657666000	-1.428803000	1.719097000		9	-6.584883000	-1.657452000	-0.568215000
6	4.761788000	0.387749000	-0.984556000		9	-7.258007000	-0.207070000	0.928418000
1	5.302379000	0.941892000	-1.750732000		6	2.221982000	-2.506182000	-0.838450000
6	3.186680000	-1.397569000	-0.386381000		6	3.076203000	-3.646547000	-1.452860000
6	3.954487000	-0.701403000	-1.349793000		1	2.414142000	-4.458511000	-1.785470000
6	4.484908000	-0.312601000	1.453887000		1	3.650080000	-3.288862000	-2.318152000
6	5.347481000	0.416036000	0.371762000		1	3.778521000	-4.047260000	-0.708654000
8	4.805022000	-0.265474000	2.642878000		6	1.394808000	-3.081949000	0.328508000
8	6.395527000	0.980177000	0.659511000		1	2.041502000	-3.518598000	1.101858000
6	0.859974000	2.361778000	-0.913630000		1	0.767163000	-2.307537000	0.791448000
1	0.824231000	2.602303000	-1.983611000		1	0.737047000	-3.872144000	-0.056843000
1	0.912853000	3.290468000	-0.332776000		6	1.234843000	-1.982249000	-1.912748000
8	-0.364542000	1.644217000	-0.555584000		1	1.761307000	-1.572545000	-2.784102000
6	-1.538059000	2.266351000	-0.800981000		1	0.602171000	-2.813460000	-2.254159000
8	-1.626709000	3.387967000	-1.276345000		1	0.585525000	-1.201322000	-1.495428000
6	-2.712010000	1.411585000	-0.422630000		1	3.820194000	-0.924495000	-2.405546000
6	-2.559643000	0.111253000	0.097071000		1	3.984488000	2.745083000	-0.334538000
6	-4.002797000	1.941112000	-0.605341000		1	1.958039000	0.488822000	-1.191724000
6	-3.684253000	-0.648826000	0.427049000		6	2.093379000	1.556866000	2.178166000
1	-1.567172000	-0.304987000	0.241903000		1	1.665507000	2.569871000	2.251436000
6	-5.129007000	1.185000000	-0.275871000		1	1.318114000	0.834933000	2.461871000
1	-4.113458000	2.945601000	-1.005899000		1	2.930374000	1.491229000	2.884385000
6	-4.966727000	-0.108949000	0.244216000					

TS-5-*endo*-b

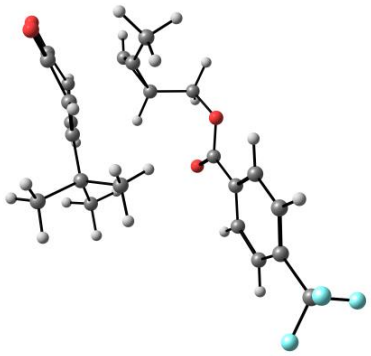

Frequency -308.7444

6	-2.662060000	1.383075000	0.837373000	1	-1.908321000	-2.781345000	-2.692898000
6	-3.504125000	1.758262000	-0.181344000	1	-0.898141000	-1.315936000	-2.541303000
6	-2.060968000	1.575527000	-0.502917000	6	-1.674000000	-3.678656000	-0.095504000
6	-4.553294000	-0.007263000	-1.056115000	1	-1.879677000	-3.669157000	0.983290000
1	-5.138380000	0.429973000	-1.864051000	1	-2.531418000	-4.132651000	-0.611927000
6	-2.966954000	-1.042751000	0.996556000	1	-0.785049000	-4.299112000	-0.278522000
1	-2.308800000	-1.347777000	1.807049000	6	-1.121134000	2.741104000	-0.781220000
6	-3.501937000	-0.886946000	-1.352751000	1	-1.343340000	3.602166000	-0.145094000
1	-3.246201000	-1.053955000	-2.394823000	1	-1.148758000	3.028841000	-1.838215000
6	-2.670483000	-1.399853000	-0.328701000	8	0.242863000	2.355330000	-0.418013000
6	-5.213561000	-0.076998000	0.260455000	6	0.931864000	1.607021000	-1.314948000
6	-4.301510000	-0.624126000	1.406392000	8	0.533562000	1.353829000	-2.441159000
8	-6.365801000	0.282268000	0.474800000	6	2.227999000	1.108230000	-0.752290000
8	-4.705114000	-0.649432000	2.570531000	6	2.577424000	1.281977000	0.600238000
1	-1.810622000	0.681949000	-1.103282000	6	3.091104000	0.401092000	-1.610146000
1	-4.292784000	2.478440000	-0.364858000	6	3.776471000	0.756413000	1.088268000
6	-2.326664000	1.661275000	2.260875000	1	1.910733000	1.816234000	1.270472000
1	-3.168356000	1.415166000	2.920193000	6	4.290726000	-0.122488000	-1.127289000
1	-1.438504000	1.101119000	2.576913000	1	2.810366000	0.262564000	-2.651040000
1	-2.114175000	2.737204000	2.368513000	6	4.627888000	0.050828000	0.225034000
6	-1.418442000	-2.241402000	-0.620067000	1	4.041938000	0.886722000	2.133942000
6	-0.189920000	-1.646695000	0.114101000	1	4.955223000	-0.669173000	-1.791501000
1	0.703909000	-2.227900000	-0.149741000	6	5.952549000	-0.472609000	0.728394000
1	-0.026999000	-0.604775000	-0.182664000	9	5.959951000	-0.692743000	2.072392000
1	-0.305435000	-1.680220000	1.204360000	9	6.969215000	0.413625000	0.473986000
6	-1.091419000	-2.314455000	-2.125891000	9	6.309831000	-1.646713000	0.132402000
1	-0.189580000	-2.925225000	-2.264104000				

TS-5-*exo*-a

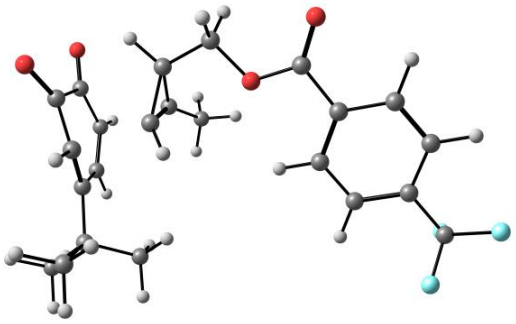

Frequency -307.0926

6	-1.860596000	-1.031521000	0.839841000	1	-4.151210000	4.878506000	-0.351706000
6	-1.929036000	-0.573971000	-0.453694000	6	-0.566520000	-2.866793000	-0.535273000
6	-1.830437000	-2.074069000	-0.225365000	1	-0.584548000	-3.249920000	-1.564451000
6	-4.221662000	-0.115202000	1.770391000	1	-0.450194000	-3.713145000	0.154626000
1	-4.282913000	-0.289364000	2.844052000	8	0.573496000	-1.972298000	-0.389337000
6	-3.753671000	0.343209000	-0.975729000	6	1.806962000	-2.506972000	-0.524042000
1	-3.620037000	0.500074000	-2.043747000	8	2.013855000	-3.685636000	-0.765483000
6	-4.001588000	1.165129000	1.278384000	6	2.881423000	-1.477010000	-0.337832000
1	-3.901811000	1.978019000	1.995319000	6	2.589100000	-0.123497000	-0.076445000
6	-3.774342000	1.440679000	-0.091921000	6	4.221573000	-1.894059000	-0.430487000
6	-4.568517000	-1.222850000	0.902349000	6	3.625155000	0.797654000	0.088734000
6	-4.482695000	-0.902536000	-0.624776000	1	1.557499000	0.207891000	-0.005187000
8	-4.957942000	-2.334978000	1.279542000	6	5.260670000	-0.975985000	-0.263139000
8	-4.942081000	-1.665860000	-1.461829000	1	4.440299000	-2.939366000	-0.633502000
1	-2.719977000	-2.689628000	-0.416038000	6	4.959250000	0.370537000	-0.008537000
6	-3.366765000	2.855651000	-0.518182000	1	3.398202000	1.842283000	0.286560000
6	-3.184831000	2.982859000	-2.044163000	1	6.294572000	-1.302417000	-0.335279000
1	-2.918652000	4.019859000	-2.287642000	6	6.068275000	1.367583000	0.232083000
1	-2.379576000	2.331161000	-2.410540000	9	7.256394000	0.983383000	-0.310341000
1	-4.111221000	2.728145000	-2.577707000	9	6.293608000	1.550867000	1.573528000
6	-2.021620000	3.215816000	0.169768000	9	5.779001000	2.599969000	-0.278365000
1	-1.720344000	4.230625000	-0.126858000	1	-1.324251000	0.112777000	-1.037025000
1	-2.114343000	3.187097000	1.263282000	6	-1.175295000	-0.751481000	2.128193000
1	-1.230225000	2.515130000	-0.130225000	1	-1.551394000	-1.393148000	2.935932000
6	-4.455884000	3.861172000	-0.067909000	1	-0.101903000	-0.971420000	2.000512000
1	-5.415093000	3.633460000	-0.553429000	1	-1.284725000	0.301507000	2.413009000
1	-4.601498000	3.838016000	1.019986000				

TS-5-*exo*-b

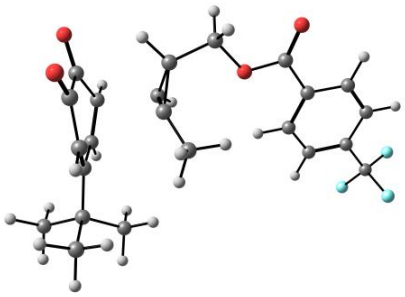

Frequency -313.1427

6	1.735746000	-0.908571000	-0.829448000
6	1.802326000	-0.788913000	0.539945000
6	1.634712000	-2.172787000	0.010756000
6	3.518383000	-0.418526000	-1.835913000
1	3.279568000	-0.667404000	-2.869505000
6	4.211619000	0.258539000	0.806829000
1	4.354047000	0.490892000	1.859337000
6	3.697553000	0.923230000	-1.464755000
1	3.456128000	1.700924000	-2.185151000
6	4.007282000	1.277678000	-0.131295000
6	4.245150000	-1.462683000	-1.072642000
6	4.480623000	-1.116510000	0.432995000
8	4.596507000	-2.532073000	-1.547847000
8	4.895206000	-1.990534000	1.204360000
1	2.485024000	-2.867630000	0.007767000
6	4.027084000	2.766103000	0.253489000
6	4.289832000	2.988648000	1.756166000
1	4.303667000	4.067317000	1.960315000
1	3.502451000	2.533236000	2.372927000
1	5.258283000	2.567627000	2.059352000
6	2.671269000	3.427987000	-0.106708000
1	2.707185000	4.492847000	0.162816000
1	2.455068000	3.353126000	-1.179854000
1	1.846145000	2.959021000	0.446249000
6	5.156568000	3.458052000	-0.553254000
1	6.132790000	3.018896000	-0.304623000
1	4.992843000	3.356298000	-1.634243000
1	5.178655000	4.528735000	-0.304861000
6	0.334181000	-2.946168000	0.187675000
1	0.290574000	-3.424897000	1.174985000
1	0.230391000	-3.720187000	-0.584525000
8	-0.774416000	-2.010189000	0.063137000
6	-2.019429000	-2.491906000	0.274426000
8	-2.258507000	-3.656288000	0.552523000
6	-3.061663000	-1.423512000	0.127460000
6	-2.734073000	-0.092325000	-0.194900000
6	-4.408796000	-1.781403000	0.322254000
6	-3.741264000	0.867864000	-0.320700000
1	-1.697421000	0.192016000	-0.348881000
6	-5.417581000	-0.825129000	0.197519000
1	-4.655066000	-2.810847000	0.569888000
6	-5.081182000	0.498692000	-0.129066000
1	-3.486044000	1.894069000	-0.571141000
1	-6.457257000	-1.105236000	0.346724000
6	-6.171299000	1.541819000	-0.203532000
9	-5.833686000	2.607021000	-0.982341000
9	-6.465992000	2.046470000	1.038383000
9	-7.339208000	1.041762000	-0.700555000
6	1.249241000	0.012511000	1.662944000
1	1.384828000	1.086030000	1.492680000
1	0.169352000	-0.198600000	1.734844000
1	1.706648000	-0.266721000	2.621197000
1	1.084113000	-0.480263000	-1.584511000

PROD-5-*endo*-a

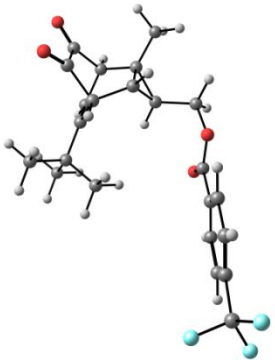

6	-2.300628000	-0.884606000	-0.896286000
6	-3.350332000	-1.608535000	-0.072490000
6	-1.904880000	-1.588996000	0.386107000
6	-4.331601000	-0.566098000	0.559448000
1	-5.071140000	-1.037148000	1.214597000
6	-2.518875000	0.648415000	-0.941166000
1	-1.764334000	1.160893000	-1.542636000
6	-3.616447000	0.606765000	1.210291000
1	-3.870148000	0.900637000	2.224564000
6	-2.676222000	1.234938000	0.462534000
6	-5.001397000	0.119718000	-0.635753000
6	-3.916853000	0.836715000	-1.533536000
8	-6.188972000	0.150416000	-0.894344000
8	-4.202991000	1.437473000	-2.550915000
1	-1.675679000	-0.962952000	1.244799000
6	-1.788942000	2.385676000	0.895637000
6	-0.311591000	1.915131000	0.823379000
1	0.347939000	2.749332000	1.100679000
1	-0.135588000	1.084200000	1.519405000
1	-0.041302000	1.585837000	-0.188518000
6	-2.102226000	2.832715000	2.336248000
1	-1.434751000	3.659912000	2.612317000
1	-3.140992000	3.180014000	2.424277000
1	-1.945872000	2.009638000	3.047211000
6	-1.994932000	3.585777000	-0.062851000
1	-1.756688000	3.319572000	-1.100998000
1	-3.035044000	3.937825000	-0.021434000
1	-1.332542000	4.408804000	0.239867000
6	-1.015245000	-2.803959000	0.294587000
1	-1.269288000	-3.454102000	-0.545380000
1	-1.014049000	-3.377209000	1.228483000
8	0.359613000	-2.373683000	-0.002458000
6	1.060632000	-1.815009000	1.010515000
8	0.674669000	-1.774821000	2.169135000
6	2.362927000	-1.236144000	0.543769000
6	2.693617000	-1.130514000	-0.820835000
6	3.259078000	-0.755601000	1.516457000
6	3.905544000	-0.552440000	-1.206284000
1	2.003370000	-1.492760000	-1.576918000
6	4.472937000	-0.181342000	1.135842000
1	2.995195000	-0.835843000	2.567909000
6	4.795482000	-0.084465000	-0.227130000
1	4.158307000	-0.469223000	-2.260124000
1	5.164741000	0.184664000	1.889948000
6	6.076912000	0.596524000	-0.646244000
9	7.070885000	0.462249000	0.276825000
9	5.892034000	1.945467000	-0.822021000
9	6.565033000	0.119194000	-1.826213000
6	-4.036245000	-2.871630000	-0.564746000
1	-4.407907000	-3.464030000	0.283900000
1	-4.892702000	-2.616255000	-1.204887000
1	-3.353905000	-3.495549000	-1.153510000
1	-1.982012000	-1.331746000	-1.837166000

PROD -5-*endo*-b

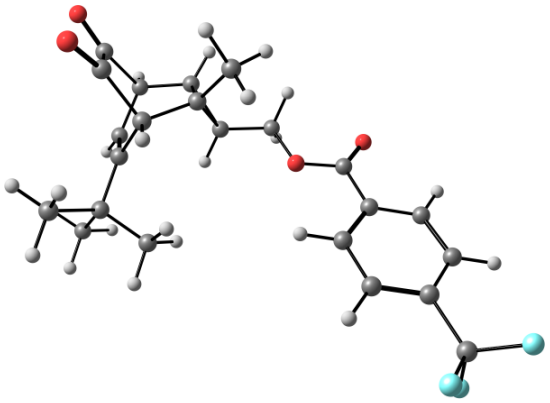

6	2.287214000	-0.945103000	0.603842000
6	3.137495000	-1.831671000	-0.290231000
6	1.803635000	-1.308601000	-0.786880000
6	4.468497000	-1.147609000	-0.704424000
1	5.082285000	-1.766110000	-1.365666000
6	2.986486000	0.432245000	0.817753000
1	2.377055000	1.101759000	1.430650000
6	4.238496000	0.256984000	-1.240914000
1	4.685545000	0.558070000	-2.183736000
6	3.468492000	1.074655000	-0.481946000
6	5.189534000	-0.851629000	0.614560000
6	4.307300000	0.099540000	1.516579000
8	6.283812000	-1.252225000	0.960504000
8	4.669450000	0.483243000	2.611683000
1	1.832321000	-0.525611000	-1.542386000
1	3.218577000	-2.890177000	-0.045648000
6	1.609656000	-1.474062000	1.856749000
1	2.314558000	-1.475648000	2.700250000
1	0.752962000	-0.839579000	2.124991000
1	1.252125000	-2.500578000	1.718018000
6	3.060392000	2.498965000	-0.806495000
6	3.554551000	3.444310000	0.317986000
1	3.237747000	4.472089000	0.092157000
1	3.136435000	3.164354000	1.293751000
1	4.650973000	3.421044000	0.386969000
6	1.511990000	2.559473000	-0.884828000
1	1.199907000	3.593764000	-1.086148000
1	1.139653000	1.917574000	-1.694987000
1	1.047579000	2.237279000	0.056592000
6	3.650395000	2.965774000	-2.150842000
1	4.748775000	2.947284000	-2.126743000
1	3.306986000	2.326341000	-2.975837000
1	3.324909000	3.995141000	-2.351894000
6	0.662629000	-2.271332000	-0.964525000
1	0.707535000	-3.122245000	-0.276499000
1	0.612142000	-2.651188000	-1.992558000
8	-0.561887000	-1.511694000	-0.691221000
6	-1.727606000	-2.190022000	-0.724876000
8	-1.815844000	-3.381761000	-0.980439000
6	-2.898561000	-1.305976000	-0.406849000
6	-2.746956000	0.057051000	-0.086698000
6	-4.184824000	-1.876642000	-0.428509000
6	-3.867540000	0.838297000	0.207391000
1	-1.757660000	0.504796000	-0.065785000
6	-5.306535000	-1.099870000	-0.134820000
1	-4.294715000	-2.929661000	-0.675024000
6	-5.144483000	0.257156000	0.188370000
1	-3.747734000	1.889406000	0.456026000
1	-6.298425000	-1.544338000	-0.150201000
6	-6.366427000	1.105791000	0.449698000
9	-7.356406000	0.414155000	1.084548000
9	-6.912111000	1.571698000	-0.720600000
9	-6.097792000	2.201856000	1.212600000

PROD -5-*exo*-a

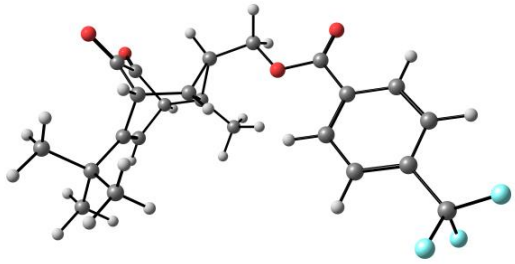

6	-2.101426000	-1.088773000	1.023393000
6	-1.834934000	-0.457239000	-0.321069000
6	-1.783098000	-1.971855000	-0.172145000
6	-3.592648000	-0.864380000	1.421496000
1	-3.830451000	-1.311758000	2.390953000
6	-3.070516000	0.274491000	-0.895413000
1	-2.863414000	0.754470000	-1.854150000
6	-3.873659000	0.636290000	1.359133000
1	-4.302087000	1.152984000	2.212997000
6	-3.599427000	1.243747000	0.175056000
6	-4.572217000	-1.355248000	0.356494000
6	-4.266114000	-0.669349000	-1.023714000
8	-5.489879000	-2.137833000	0.518802000
8	-4.919965000	-0.875888000	-2.028093000
1	-2.603529000	-2.552906000	-0.599639000
1	-0.893115000	0.064690000	-0.473405000
6	-1.145243000	-0.935501000	2.192677000
1	-1.338054000	0.017289000	2.707037000
1	-1.285301000	-1.752377000	2.915943000
1	-0.103054000	-0.941731000	1.857376000
6	-3.786967000	2.709549000	-0.160715000
6	-2.410164000	3.298374000	-0.565007000
1	-2.532436000	4.357076000	-0.833347000
1	-1.699662000	3.226707000	0.270150000
1	-1.987348000	2.771628000	-1.430871000
6	-4.341374000	3.502285000	1.038485000
1	-4.449572000	4.558154000	0.756403000
1	-5.326314000	3.120983000	1.341394000
1	-3.661717000	3.441351000	1.899752000
6	-4.770246000	2.839833000	-1.352001000
1	-4.403511000	2.306184000	-2.238572000
1	-5.756617000	2.436790000	-1.083861000
1	-4.882797000	3.901433000	-1.612804000
6	-0.492786000	-2.759582000	-0.303544000
1	-0.468464000	-3.293537000	-1.261619000
1	-0.386252000	-3.491397000	0.508075000
8	0.651565000	-1.855619000	-0.260890000
6	1.879172000	-2.418657000	-0.311336000
8	2.071980000	-3.620257000	-0.411055000
6	2.968955000	-1.391180000	-0.229106000
6	2.700553000	-0.019111000	-0.060283000
6	4.302048000	-1.832774000	-0.321916000
6	3.751565000	0.898267000	0.014219000
1	1.675614000	0.331429000	0.013366000
6	5.354840000	-0.919396000	-0.249463000
1	4.502788000	-2.893136000	-0.452125000
6	5.076399000	0.447145000	-0.086112000
1	3.541863000	1.956678000	0.144071000
1	6.383059000	-1.263726000	-0.324597000
6	6.218013000	1.426416000	0.053684000
9	6.644193000	1.515422000	1.355423000
9	5.880400000	2.690002000	-0.328022000
9	7.308343000	1.067840000	-0.682903000

PROD -5-*exo*-b

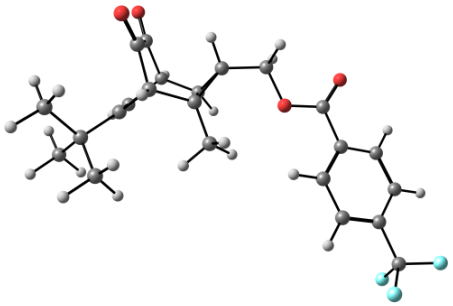

6	-1.597215000	-0.599376000	0.808876000	1	-6.558851000	2.561343000	-1.414076000
6	-2.053128000	-0.511756000	-0.627386000	6	-0.348534000	-2.569419000	-0.484026000
6	-1.614751000	-1.851780000	-0.055429000	1	-0.374891000	-2.824256000	-1.551784000
6	-2.730877000	-0.275377000	1.810959000	1	-0.223527000	-3.494089000	0.092934000
1	-2.395951000	-0.286710000	2.851396000	8	0.816383000	-1.724553000	-0.242774000
6	-3.575900000	-0.184296000	-0.683588000	6	2.017798000	-2.222879000	-0.611153000
1	-3.941157000	-0.140200000	-1.712740000	8	2.172652000	-3.332688000	-1.096247000
6	-3.386063000	1.040320000	1.395194000	6	3.130354000	-1.250308000	-0.353677000
1	-3.531118000	1.834392000	2.121967000	6	2.897498000	0.050658000	0.133365000
6	-3.833917000	1.105914000	0.113336000	6	4.447179000	-1.666271000	-0.623369000
6	-3.924277000	-1.214983000	1.622016000	6	3.967780000	0.922069000	0.346991000
6	-4.418370000	-1.165304000	0.131133000	1	1.884716000	0.382520000	0.340305000
8	-4.459250000	-1.895761000	2.476278000	6	5.520187000	-0.799450000	-0.407865000
8	-5.358550000	-1.820819000	-0.276840000	1	4.620412000	-2.670501000	-1.001662000
1	-2.393089000	-2.592830000	0.139983000	6	5.277017000	0.496814000	0.072423000
6	-4.600324000	2.252800000	-0.519239000	1	3.785514000	1.927109000	0.718602000
6	-3.845239000	2.744923000	-1.779260000	1	6.535656000	-1.124967000	-0.617275000
1	-4.426233000	3.544810000	-2.258990000	6	6.434824000	1.421667000	0.365941000
1	-2.858398000	3.144363000	-1.508351000	9	6.842634000	1.313323000	1.672059000
1	-3.707485000	1.935976000	-2.508135000	9	6.119237000	2.734022000	0.170711000
6	-4.766961000	3.432896000	0.457567000	9	7.529004000	1.158821000	-0.402111000
1	-5.315807000	4.242082000	-0.042439000	6	-1.244141000	0.207656000	-1.691492000
1	-5.332260000	3.130159000	1.349663000	1	-0.171422000	0.039421000	-1.553476000
1	-3.789946000	3.821756000	0.776589000	1	-1.527479000	-0.144631000	-2.694340000
6	-6.003748000	1.741368000	-0.937398000	1	-1.434374000	1.287849000	-1.641100000
1	-5.933264000	0.912363000	-1.653541000	1	-0.626950000	-0.184489000	1.072338000
1	-6.567005000	1.398277000	-0.058662000				

Reacting complex (7+8)

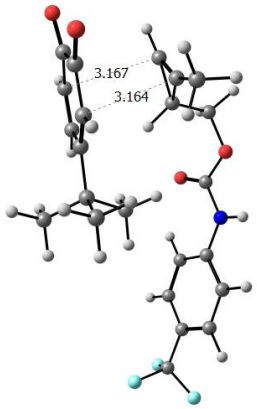

6	-3.631326000	1.549873000	0.834761000	1	-1.210475000	-1.596440000	2.516799000
6	-4.170907000	1.753391000	-0.344075000	1	-1.593597000	-3.290825000	2.106070000
6	-2.670898000	1.815263000	-0.290828000	6	-0.067388000	-0.875713000	0.117943000
6	-3.892783000	-0.962326000	-1.949468000	1	0.954700000	-1.186368000	0.372794000
1	-4.019165000	-0.711064000	-3.001517000	1	-0.073934000	-0.556396000	-0.930675000
6	-3.501708000	-1.611207000	0.842269000	1	-0.337970000	-0.017908000	0.745522000
1	-3.378047000	-1.849480000	1.895367000	6	-0.598488000	-3.277953000	-0.474161000
6	-2.677376000	-1.298539000	-1.441737000	1	-1.269598000	-4.130609000	-0.302156000
1	-1.815721000	-1.310776000	-2.105848000	1	-0.591986000	-3.047442000	-1.547229000
6	-2.452207000	-1.652213000	-0.031173000	1	0.420386000	-3.566856000	-0.181550000
6	-5.090320000	-0.974554000	-1.105020000	6	-1.921499000	3.137740000	-0.390507000
6	-4.862278000	-1.278606000	0.420111000	1	-2.454612000	3.938226000	0.132554000
8	-6.228700000	-0.804688000	-1.538534000	1	-1.738641000	3.425613000	-1.433034000
8	-5.817868000	-1.265052000	1.195777000	8	-0.634550000	3.037241000	0.305225000
1	-2.094432000	0.979550000	-0.715031000	6	0.372364000	2.428288000	-0.382421000
1	-5.043303000	1.886494000	-0.970081000	8	0.341194000	2.138530000	-1.567754000
6	-3.724018000	1.363868000	2.300038000	6	2.597947000	1.475283000	0.263720000
1	-4.723244000	1.020619000	2.595647000	6	3.378882000	1.156446000	1.396780000
1	-2.968663000	0.648892000	2.649906000	6	3.028602000	1.056031000	-1.011725000
1	-3.519609000	2.325458000	2.797180000	6	4.557017000	0.426793000	1.263063000
6	-1.036543000	-2.056733000	0.379756000	1	3.051849000	1.478779000	2.384215000
6	-0.939099000	-2.440998000	1.868690000	6	4.209346000	0.320969000	-1.136419000
1	0.096124000	-2.727466000	2.094865000	1	2.442471000	1.296365000	-1.889710000

6	4.981501000	0.005277000	-0.008426000	9	7.159393000	-0.562465000	0.797284000
1	5.144517000	0.187119000	2.145841000	9	6.815302000	-0.717239000	-1.363280000
1	4.531204000	-0.000522000	-2.123982000	7	1.419011000	2.202588000	0.489213000
6	6.210900000	-0.845788000	-0.145299000	1	1.235753000	2.460968000	1.452511000
9	5.930193000	-2.188056000	-0.003546000				

Transition state (7+8)

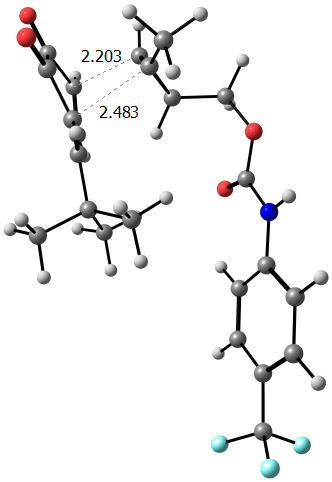

Frequency -313.2986

6	3.481037000	-1.247120000	0.631979000	1	2.018531000	-0.716549000	-0.963260000
6	4.103815000	-1.325386000	-0.591291000	1	4.974040000	-1.803851000	-1.025650000
6	2.628430000	-1.536270000	-0.541429000	6	3.607260000	-1.652258000	2.057722000
6	4.413421000	0.663837000	-1.485107000	1	4.494561000	-1.201377000	2.519403000
1	4.878983000	0.428809000	-2.441390000	1	2.714889000	-1.374092000	2.631187000
6	3.164859000	1.193691000	0.957363000	1	3.720381000	-2.747681000	2.103432000
1	2.667912000	1.289001000	1.920081000	6	1.018097000	1.976148000	-0.157695000
6	3.133154000	1.239393000	-1.456939000	6	1.036509000	3.445101000	0.340680000
1	2.599464000	1.357484000	-2.395107000	1	0.005217000	3.818224000	0.419513000
6	2.473160000	1.485696000	-0.229644000	1	1.512421000	3.515051000	1.328201000
6	5.333781000	0.884903000	-0.352538000	1	1.588659000	4.085777000	-0.361234000
6	4.617870000	1.130095000	1.014881000	6	0.204492000	1.115584000	0.842081000
8	6.555647000	0.853372000	-0.440700000	1	-0.847792000	1.427809000	0.812063000
8	5.273516000	1.224007000	2.055489000	1	0.258847000	0.053742000	0.577811000

1	0.562228000	1.233703000	1.872360000	6	-4.644301000	-0.765876000	1.255345000
6	0.306559000	1.925023000	-1.526255000	1	-3.210011000	-2.115859000	2.122168000
1	0.800494000	2.574889000	-2.261414000	6	-4.077855000	0.117373000	-0.933071000
1	0.273427000	0.900375000	-1.919345000	1	-2.205623000	-0.536926000	-1.772931000
1	-0.725588000	2.278116000	-1.401632000	6	-4.959068000	0.051093000	0.156586000
6	1.970176000	-2.897255000	-0.734234000	1	-5.319748000	-0.828724000	2.104713000
1	2.556395000	-3.700852000	-0.280291000	1	-4.314791000	0.746793000	-1.787464000
1	1.802610000	-3.102977000	-1.797922000	6	-6.266714000	0.788480000	0.113904000
8	0.692485000	-2.933205000	-0.027790000	9	-6.727030000	1.125490000	1.355186000
6	-0.325257000	-2.231433000	-0.610979000	9	-7.265965000	0.038409000	-0.467749000
8	-0.287656000	-1.750203000	-1.732045000	9	-6.199761000	1.945825000	-0.609306000
6	-2.563009000	-1.421248000	0.172822000	7	-1.373451000	-2.160868000	0.279633000
6	-3.456501000	-1.492438000	1.264004000	1	-1.218573000	-2.627845000	1.166430000
6	-2.884899000	-0.608172000	-0.933179000				

Product (5+8)

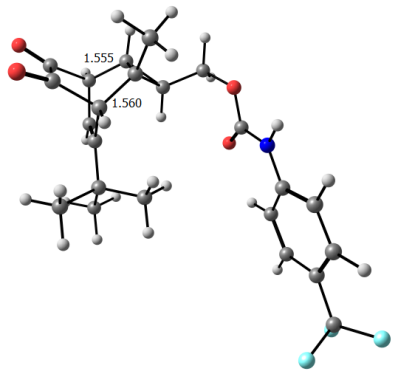

6	3.020080000	1.073541000	-0.583583000	1	3.636865000	-1.536453000	2.337340000
6	3.911189000	1.393640000	0.604259000	6	2.820512000	-1.314604000	0.355376000
6	2.407268000	1.539725000	0.722101000	6	5.454226000	-0.404143000	-0.015347000
6	4.627272000	0.129279000	1.157803000	6	4.509730000	-0.762673000	-1.229943000
1	5.256189000	0.337345000	2.028301000	8	6.659322000	-0.560266000	-0.055028000
6	3.050377000	-0.456282000	-0.887059000	8	4.933309000	-1.211450000	-2.277437000
1	2.390253000	-0.714619000	-1.719380000	1	1.894166000	0.790568000	1.319035000
6	3.649983000	-1.014782000	1.384855000	1	4.522464000	2.294611000	0.566249000

6	3.009812000	1.936245000	-1.833929000
1	3.834392000	1.649832000	-2.502250000
1	2.064073000	1.808913000	-2.379498000
1	3.129875000	2.997594000	-1.588941000
6	1.717319000	-2.355503000	0.348874000
6	1.981338000	-3.379696000	-0.783783000
1	1.166548000	-4.116986000	-0.803096000
1	2.024656000	-2.892081000	-1.766573000
1	2.929821000	-3.907612000	-0.612709000
6	0.367356000	-1.635267000	0.087772000
1	-0.439330000	-2.380909000	0.055458000
1	0.147464000	-0.916150000	0.887558000
1	0.375571000	-1.098200000	-0.869947000
6	1.635084000	-3.102071000	1.693839000
1	2.572651000	-3.633658000	1.907845000
1	1.430447000	-2.405861000	2.518958000
1	0.820696000	-3.837585000	1.651274000
6	1.769899000	2.903692000	0.825598000
1	2.355828000	3.685802000	0.337299000
1	1.590944000	3.174449000	1.872654000
8	0.492922000	2.919632000	0.102867000
6	-0.510710000	2.179239000	0.654118000
8	-0.497008000	1.708825000	1.780917000
6	-2.730637000	1.348909000	-0.169536000
6	-3.583065000	1.372063000	-1.296146000
6	-3.118551000	0.621043000	0.974692000
6	-4.792313000	0.682321000	-1.284538000
1	-3.289521000	1.933346000	-2.182022000
6	-4.333441000	-0.067928000	0.977238000
1	-2.475809000	0.593536000	1.845506000
6	-5.178635000	-0.038940000	-0.142097000
1	-5.435911000	0.710297000	-2.160198000
1	-4.622808000	-0.627272000	1.863637000
6	-6.448961000	-0.839506000	-0.152608000
9	-6.255018000	-2.113225000	-0.642660000
9	-7.420240000	-0.282707000	-0.936577000
9	-6.989448000	-0.996573000	1.091966000
7	-1.524335000	2.059227000	-0.273304000
1	-1.345971000	2.505308000	-1.166222000

7. REFERENCES

(1) R. Sen, J. Escorihuela, M. M. J. Smulders, H. Zuilhof, *Langmuir* **2016**, *32*, 3412–3419.

(2) M. J. Frisch, G. W. Trucks, H. B. Schlegel, G. E. Scuseria, M. A. Robb, J. R. Cheeseman, G. Scalmani, V. Barone, G. A. Petersson, H. Nakatsuji, X. Li, M. Caricato, A. V. Marenich, J. Bloino, B. G. Janesko, R. Gomperts, B. Mennucci, H. P. Hratchian, J. V. Ortiz, A. F. Izmaylov, J. L. Sonnenberg, Williams, F. Ding, F. Lipparini, F. Egidi, J. Goings, B. Peng, A. Petrone, T. Henderson, D. Ranasinghe, V. G. Zakrzewski, J. Gao, N. Rega, G. Zheng, W. Liang, M. Hada, M. Ehara, K. Toyota, R. Fukuda, J. Hasegawa, M. Ishida, T. Nakajima, Y. Honda, O. Kitao, H. Nakai, T. Vreven, K. Throssell, J. A. Montgomery Jr., J. E. Peralta, F. Ogliaro, M. J. Bearpark, J. J. Heyd, E. N. Brothers, K. N. Kudin, V. N. Staroverov, T. A. Keith, R. Kobayashi, J. Normand, K. Raghavachari, A. P. Rendell, J. C. Burant, S. S. Iyengar, J. Tomasi, M. Cossi, J. M. Millam, M. Klene, C. Adamo, R. Cammi, J. W. Ochterski, R. L. Martin, K. Morokuma, O. Farkas, J. B. Foresman, D. J. Fox, Wallingford, CT, **2016**. Revison A. 03.

(3) Y. Zhao, D. G. Truhlar, *Theor. Chem. Acc.* **2008**, *120*, 215–241.

(4) a) L. Törk, G. Jiménez–Osés, C. Doubleday, F. Liu, K. N. Houk, *J. Am. Chem. Soc.* **2015**, *137*, 4749–4758; b) F. Liu, R. S. Paton, S. Kim, Y. Liang, K. N. Houk, *J. Am. Chem. Soc.* **2013**, *135*, 15642–15649.

(5) C. Gonzalez, H. B. Schlegel, *J. Phys. Chem.* **1990**, *94*, 5523–5527.

(6) R. Sen, J. Escorihuela, F. van Delft, H. Zuilhof, *Angew. Chem. Int. Ed.* **2017**, *56*, 3299–3303.

(7) a) D. Gahtory, R. Sen, M. J. Smulders, H. Zuilhof, *Faraday Discuss.* **2017**, *204*, 383–394; b) R. Sen, D. Gahtory, J. Escorihuela, J. Firet, S. P. Pujari, H. Zuilhof, *Chem. Eur. J.* **2017**, *23*, 13015–13022.

(8) A. R. Kuzmyn, A. S. Pereira, O. P. Georgievski, M. Bruns, E. Brynda, C. R. Emmenegger, *Polym. Chem.* **2014**, *5*, 4124–4131.

(9) L. Liao, F. Zhang, N. Yan, J. A. golen, J. M. Fox, *Tetrahedron* **2004**, *60*, 1803–1816.

(10) M. K. Pallerla, J. M. Fox, *Org. Lett.* **2005**, *7*, 3593–3595.

(11) J. Yang, J. Šečkutė, C. M. Cole, N. K. Devaraj, *Angew. Chem. Int. Ed.* **2012**, *51*, 7476–7479.

(12) J. Yang, Y. Liang, J. Šečkutė, K. N. Houk, N. K. Devaraj *Chem. Eur. J.* **2014**, *20*, 3365–3375.

(13) A. Borrmann, O. fatunsin, J. Dommerholt, A. M. Jonker, D. W. P. M. Löwik, J. C. M. van Hest, F. L. van Delft *Bioconjugate Chem.* **2015**, *26*, 257–261.

APPENDIX 3

Surface-Bound Quadruple H–bonded Dimers: Formation and Exchange Kinetics

1. MATERIAL AND METHODS

Materials. Unless otherwise specified, all chemicals were used as received without further purification. 6-Methylisocytosine, 1,6-hexamethylene diisocyanate, 4-iodophenyl isocyanate, 4-(trifluoromethyl)phenyl isocyanate, hydrochloric acid, methanol, hexane, acetone, dichloromethane, and 2-propanol were purchased from Sigma-Aldrich. 12-Aminododecylphosphonic acid hydrochloride salt was purchased from SiKÉMIA. Aluminium pieces (99.5% purity, mirror polished, Staalmarkt Beuningen BV) were cut using mechanical cutter into exactly 2×1 cm or 1×1 cm dimensions. For surface modification reactions, the samples were loaded onto a specially constructed PTFE wafer holder able to hold up to 16 samples at a time thus ensuring rigorous reproducibility between samples.

Grazing Angle Total Reflection Fourier Transform Infrared Spectroscopy (GATR–FTIR). GATR–FTIR spectra were recorded with a Bruker Tensor 27 FT–IR spectrometer using a commercial variable-angle reflection unit (Auto Seagull, Harrick Scientific). A Harrick grid polarizer was installed in front of the detector and was used for measuring spectra with p-polarized radiation with respect to the plane of incidence at the sample surface. Single channel transmittance spectra were collected at an angle of 35° using a spectral resolution of 2 cm^{-1} and 2048 scans while flushing with dry N_2. Obtained spectra were referenced with a freshly cleaned and etched aluminium sample.

X-ray Photoelectron Spectroscopy (XPS) Measurements. The XPS analysis of surfaces was performed using a JPS–9200 photoelectron spectrometer (JEOL, Japan). Survey and high-resolution spectra were obtained under UHV conditions using monochromatic Al Kα X-ray radiation at 12 kV and 20 mA and an analyzer pass energy of 50 eV for wide scans and 10 eV for narrow scans. The emitted electrons were collected at 10° from the surface normal (take-off angle relative to the surface normal 10°). All XPS spectra were evaluated by using Casa XPS software (version 2.3.15). Survey spectra were corrected with linear background before fitting, whereas high-

resolution spectra were corrected with linear background. Atomic area ratios were determined after a baseline correction and normalizing the peak area ratios by the corresponding atomic sensitivity factors (1.00 for C1s, 1.80 for N1s, 2.93 for O1s, 4.43 for F1s, 1.18 for P2s, 33.64 for I3d and 0.54 for Al2p).

DART-HRMS Measurements. Analysis of the modified aluminium surfaces was performed using a DART-SVP ion source (Ion-Sense, Saugus, MA) coupled to a Q-Exactive orbitrap high-resolution mass spectrometer (Thermo Fisher Scientific, San Jose, CA, USA), mounted on a motorized rail travelling at 0.2 mm/s. Thermo Scientific Xcalibur software (V2.1.0.1139) was used for data acquisition and processing. The measurements were performed in negative mode at 550°C using a scan range of *m/z* 312.0 – 372.0, a mass resolution of 70,000 (FWHM) at a scan rate of 1 Hz. The DART source was positioned 6.1 cm on the horizontal scale, 7 cm on the vertical scale with an angle of 45°, such that it is around 1 mm above the surface (Fig. S5). The distance from the surface to the ceramic tube is minimized by placing them at the edge of the moving rail so that maximum of the singly protonated UPy–CF_3 and UPy–I ions (*m/z* 313.09029 and 370.99859 respectively) would enter the MS.

2. SYNTHESIS

2.1 General Remarks. Unless stated otherwise, solvents and dry solvents like 2-propanol, dichloromethane, chloroform, DMSO, *N*-methylpyrrolidone and toluene were purchased from Sigma-Aldrich. Unless stated otherwise all of these chemicals were used without further purification.

2.2. Reaction Handling. Unless stated otherwise all non-aqueous reactions were performed in dried glassware under an atmosphere of argon. All flasks were equipped with rubber septa and reactants were handled using standard Schlenk techniques. Temperatures above the room temperature refer to oil bath temperatures which were controlled by a thermostat. Reactions were magnetically stirred.

2.3. ^{1}H-NMR spectra were recorded at room temperature on a Bruker AVB-400 spectrometer with ^{1}H operating frequency of 400 MHz. Unless stated otherwise all

spectra were recorded at room temperature in $CDCl_3$ and DMSO-d_6 and all chemical shifts are given in δ units relative to the residual solvent [central line of singlet: δ_H = 7.27 ppm ($CDCl_3$) and 2.50, 3.33 ppm (DMSO-d_6)]. Analysis followed first order and the following abbreviations were used throughout: s = singlet, br. s. = broad singlet, d = doublet, t = triplet, q = quartet, quin = quintet, sxt = sextet, sept = spt, dd = doublet of doublet, dt = doublet of triplet, m = multiplet, mc = centred multiplet. Coupling constants (J) are given in Hertz (Hz).

2.4. ^{13}C-NMR spectra were recorded at room temperature on a Bruker AVB-400 spectrometer with ^{13}C operating frequency of 101 MHz. Unless stated otherwise all spectra were recorded at room temperature in $CDCl_3$ and DMSO-d_6 and all chemical shifts are given in δ units relative to the residual solvent [central line of triplet: δ_C = 77.0 ppm ($CDCl_3$) and heptet δ_C = 77.0 ppm (DMSO-d_6)]. The following abbreviation was used throughout: s = singlet, d = doublet, dd = doublet of doublet. If no coupling constants are given, the multiplicity refers to ^{1}H-decoupled spectra.

2.5. Synthesis of UPy–Link, 1.

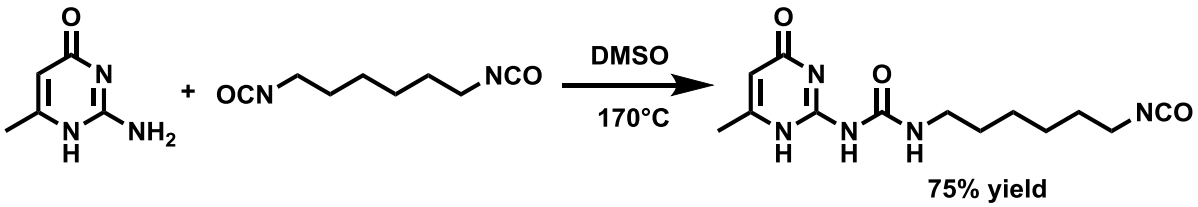

The synthesis of above was carried out according to a literature procedure.[S1] Briefly, 6-methylisocytosine (2.0 g, 16.0 mmol) was added to 15 mL of DMSO and heated up to 170 °C for 10 min. Once the solid dissolved, the oil bath was removed. 1,6-Hexamethylene diisocyanate (2.68 mL, 17.6 mmol) was added immediately to the flask under vigorous stirring. The mixture was quickly cooled using a water bath. A fine white solid precipitated upon cooling. The precipitate was collected and washed with excess acetone and dried under vacuum to obtain 3.50 g of a white solid (yield 75%). The ^{1}H-NMR spectrum was in accordance to literature values.[S2] The ^{13}C NMR could not be obtained due to low solubility in NMR solvents even at high temperatures.

2.6. Synthesis of UPy–CF_3, 2.

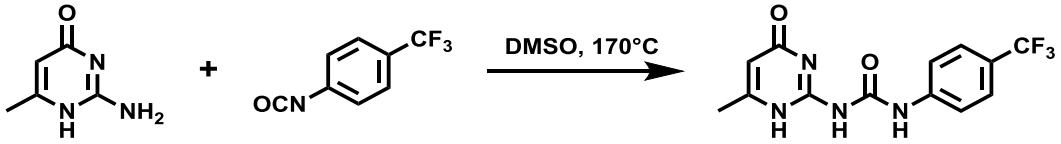

The synthesis of above was carried out according to a literature procedure.[S1] 6-Methylisocytosine (1.0 g, 8.0 mmol) was added to 15 mL of DMSO and heated up to 170 °C for 10 min. Once the solid dissolved, the oil bath was removed. 4-(Trifluoromethyl)phenyl isocyanate (1.3 mL, 8.8 mmol) was added immediately to the flask under vigorous stirring. The mixture was quickly cooled using a water bath. A fine white solid precipitated upon cooling. The precipitate was collected and washed with excess acetone and dried under vacuum to obtain 1.50 g of a white solid (yield 72%). The ^{1}H-NMR spectrum was in accordance to literature values.[S3] ^{13}C NMR (600 MHz NMR, DMSO-d_6, 70 °C) δ = 162.0, 155.1, 151.5, 142.0, 125.7, 125.0, 118.9, 112.87, 103.34, 100.09 21.6.

2.7. Synthesis of UPy–I, 3.

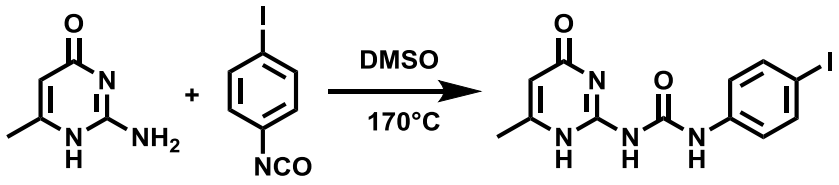

The synthesis of above was carried by modification of a literature procedure.[SS1] 6-Methylisocytosine (1.0 g, 8.0 mmol) was added to 15 mL of DMSO and heated up to 170 °C for 10 min. Once the solid dissolved, the oil bath was removed. 4-Iodophenyl isocyanate (2.1 g, 8.8 mmol) was added immediately to the flask under vigorous stirring. The mixture was quickly cooled using a water bath. A fine white solid precipitated upon cooling. The precipitate was collected and washed with excess acetone and dried under vacuum to obtain 1.80 g of a white solid (yield 61%). ^{1}H NMR (400 MHz, DMSO-d_6) δ = 11.04 (s, 1H), 10.05 (s, 1H), 7.62 (d, J = 8.6 Hz, 2H), 7.36 (d, J = 8.6 Hz, 2H), 5.80 (s, 1H), 2.16 (s, 3H) ^{13}C NMR (600 MHz NMR, DMSO-d_6, 70 °C) δ = 162.0, 155.1, 151.8, 137.2, 121.3, 116.37, 103.5, 100.1, 86.1, 21.7.

3. NMR DATA

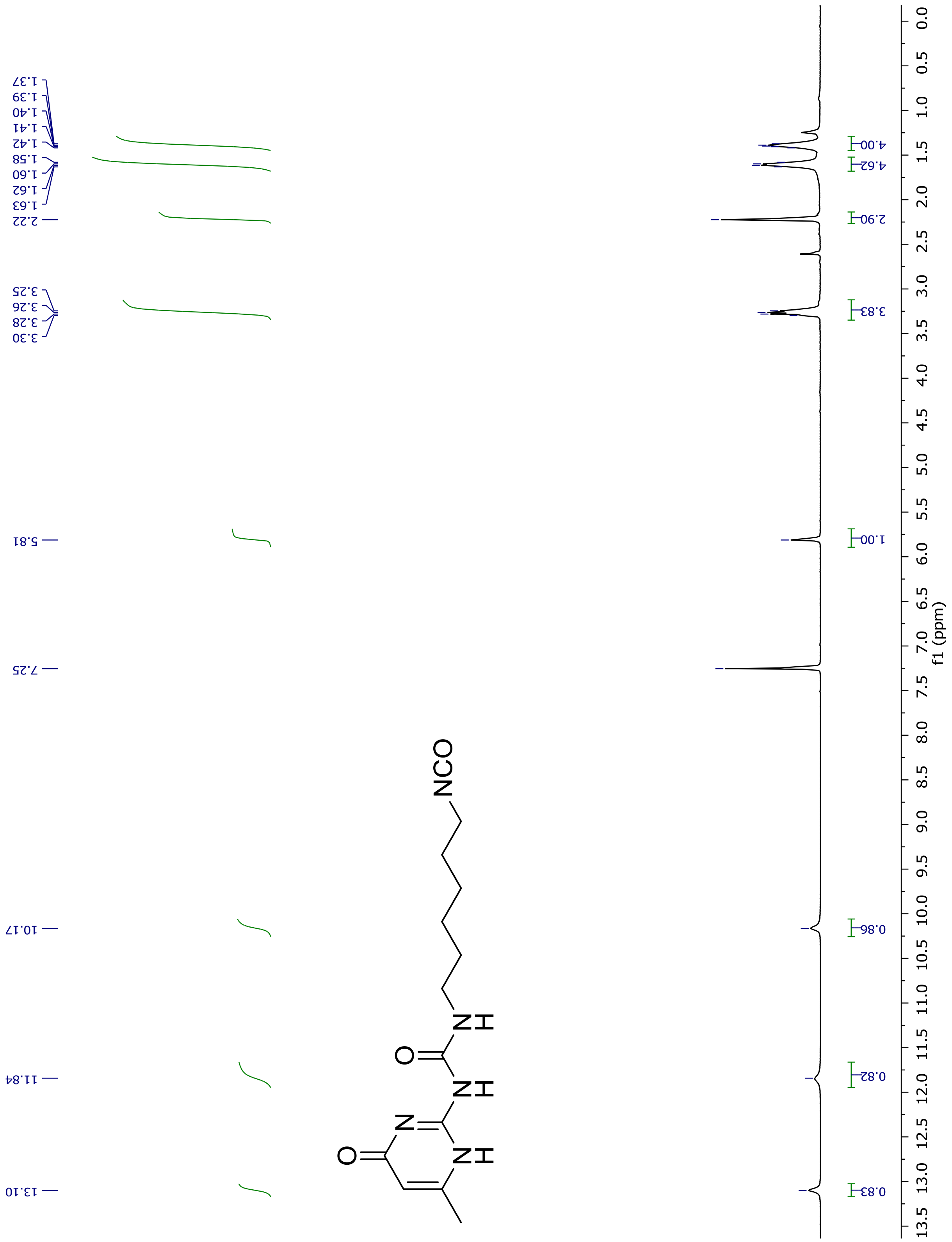

1.37
1.39
1.40
1.41
1.42
1.58
1.60
1.62
1.63
2.22
3.25
3.26
3.28
3.30
5.81
7.25
10.17
11.84
13.10
NCO
4.00
4.62
2.90
3.83
1.00
0.86
0.82
0.83
f1 (ppm)

11.12
10.02
7.63
7.60
7.37
7.35
5.80
3.28
2.51
2.47
2.16
1.22
1.05
2.18
2.18
1.00
3.19
f1 (ppm)

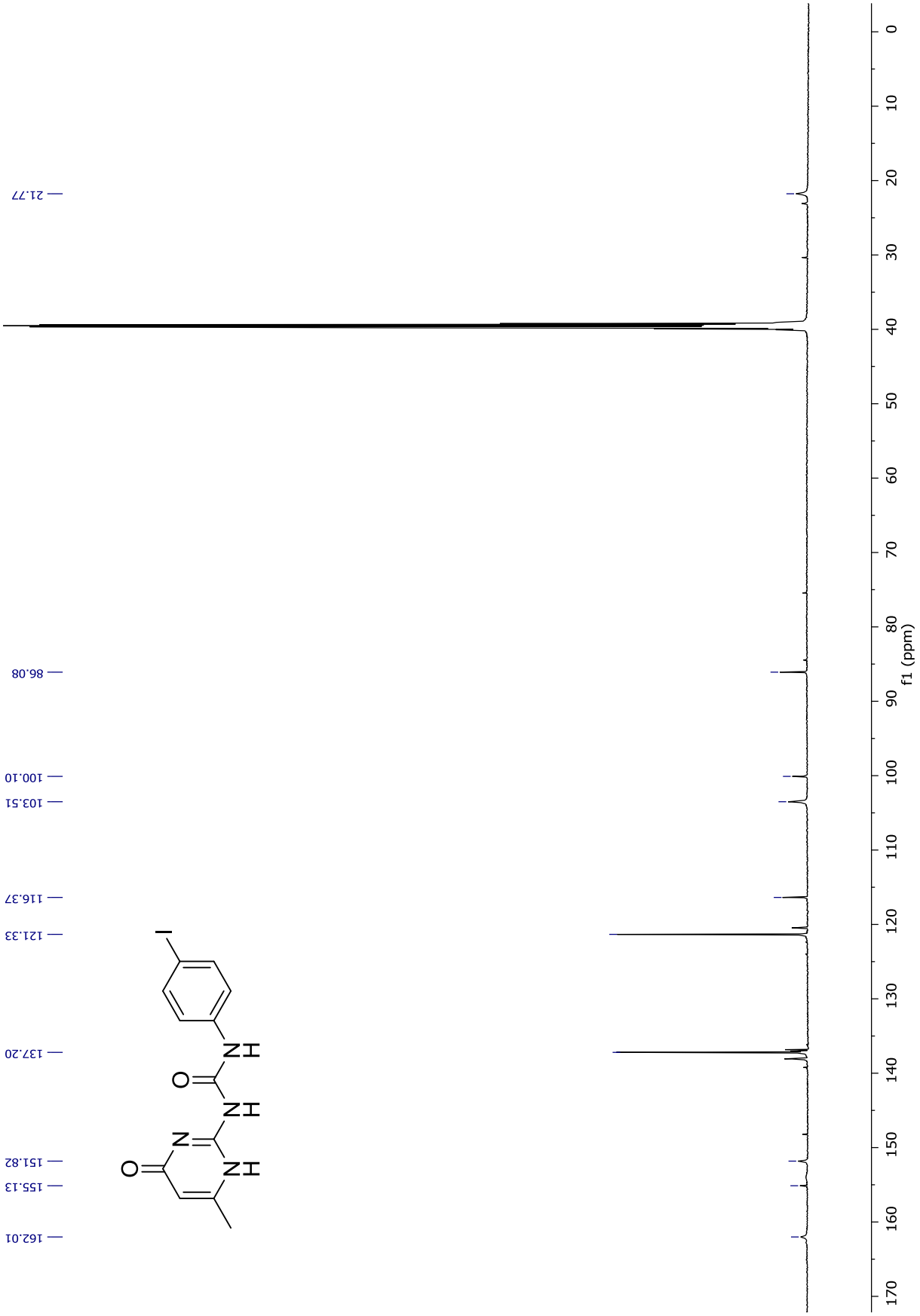
21.77
86.08
100.10
103.51
116.37
121.33
137.20
151.82
155.13
162.01
f1 (ppm)

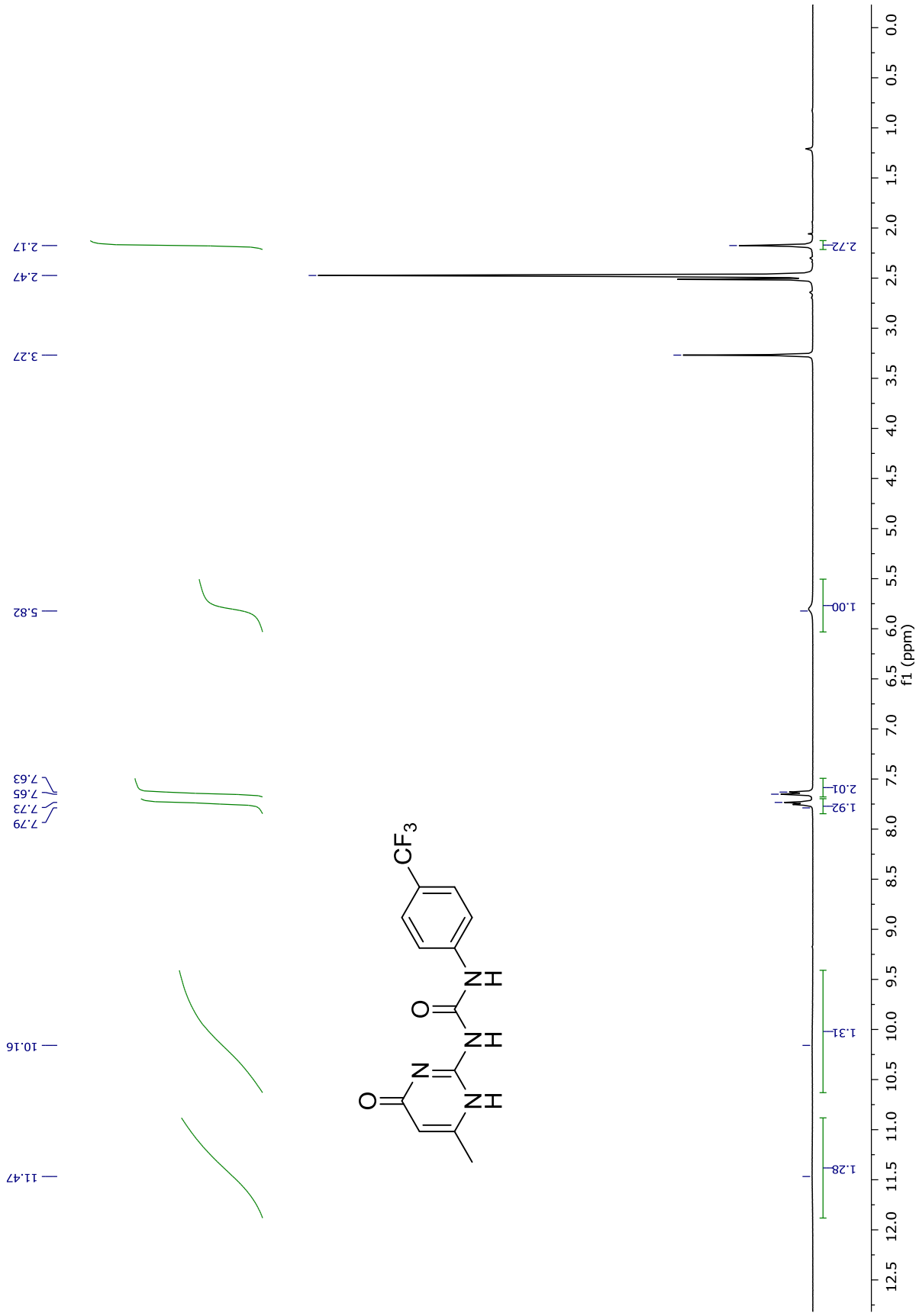
11.47
10.16
7.79
7.73
7.65
7.63
5.82
3.27
2.47
2.17
2.72
1.00
2.01
1.92
1.31
1.28
f1 (ppm)

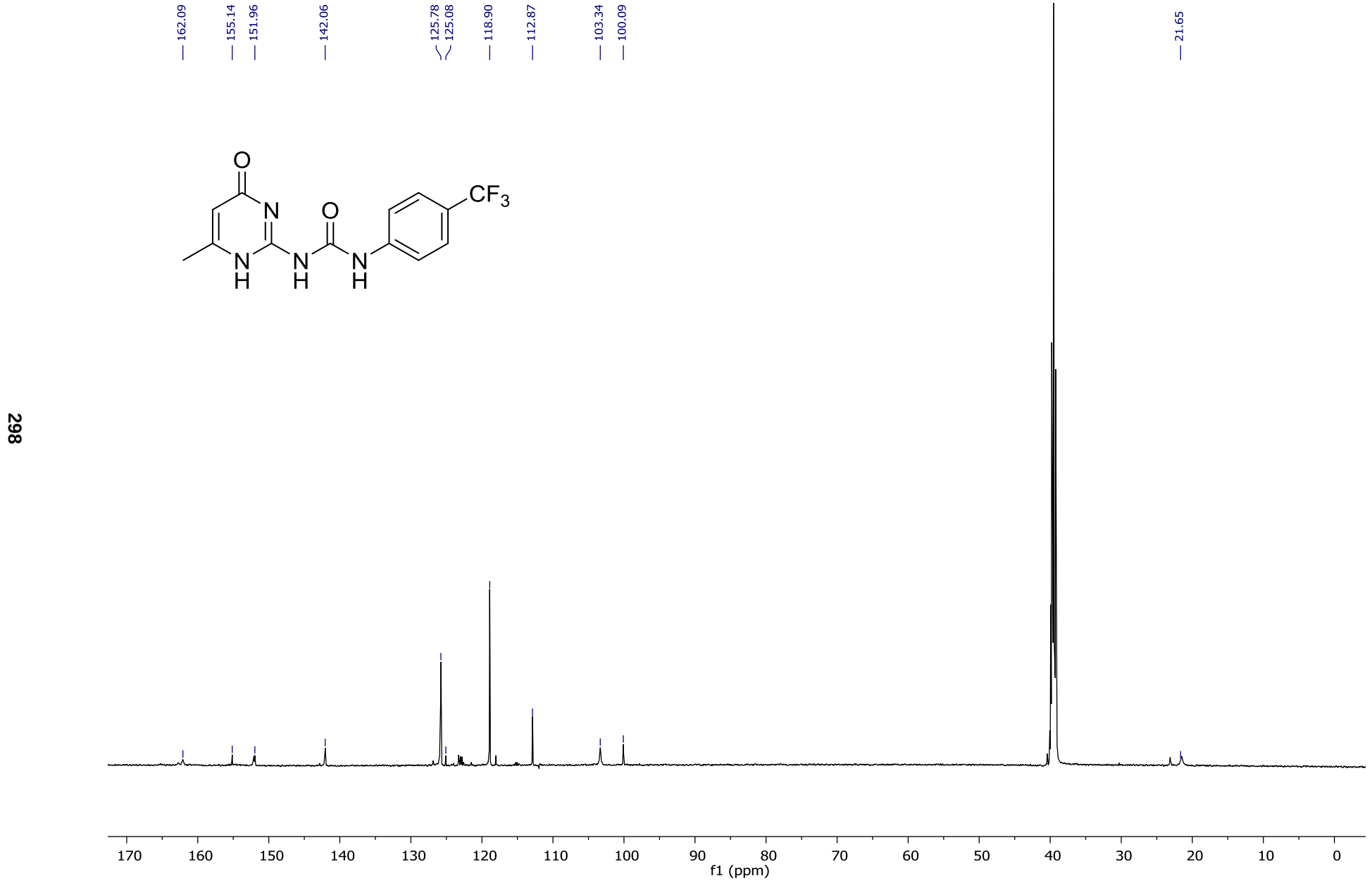
162.09
155.14
151.96
142.06
125.78
125.08
118.90
112.87
103.34
100.09
21.65
O
N
O
N
H
N
H
N
H
CF3
170
160
150
140
130
120
110
100
90
80
70
60
50
40
30
20
10
0
f1 (ppm)

4. SURFACE PREPARATION AND KINETICS DETERMINATION

4.1 Preparation of phosphonic acid monolayers. 2×1 cm Al slides were sonicated in DCM for 15 min followed by wiping with lint-free cotton swabs (Texwipe, NC, USA) to remove the polymer protection layer on top and remove any residual glue. The surfaces were chemically activated by immersing in 1:1 (v/v) 37% HCl/MeOH mixture for 5 min, followed by washing with water and 2-propanol. The activated surfaces were then immersed into N_2 filled vials of 5 mM solution of 12-aminododecylphosphonic acid hydrochloride salt (C_{12}–NH_2 PA HCl salt) in 2-propanol, heated to 50 °C for 5 min, and then left undisturbed for 5 h at room temperature to obtain self-assembled monolayers. Thereafter, surfaces were taken out and sonicated successively for 5 min with 2-propanol, acetone and dichloromethane. The surfaces were then cleaned with dichloromethane, air dried and stored under argon atmosphere.

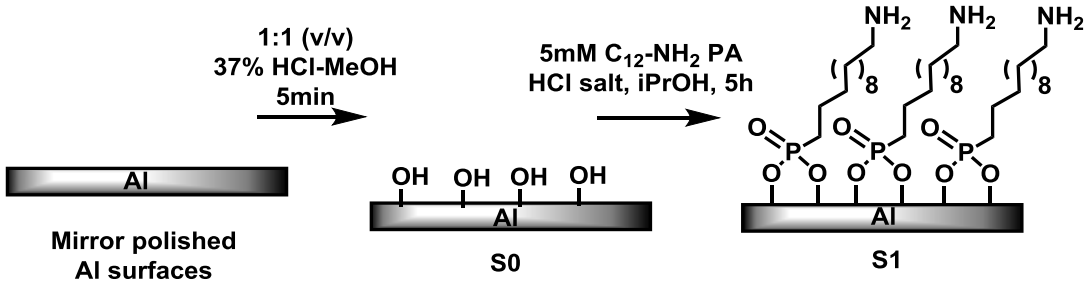

Scheme S1. Preparation of C_{12}–NH_2-terminated self-assembled monolayer on Al. (**S1**)

4.2 Preparation of UPy-terminated monolayers. UPy–Link (300 mg, 40 mM) was dissolved in 25 mL *N*-methylpyrrolidone (NMP) by sonication and heating followed by addition of DBTDL (45 µl, 0.4 mM). Amine-terminated Al chips were loaded onto a PTFE holder and stirred in this solution at 60 °C for 6 h. The N1s/P2s ratio in XPS was used to optimize the stirring time and temperature. The samples were sonicated for 10 min successively with NMP, water, 2-propanol and acetone followed by drying under N_2 stream and storage under argon atmosphere.

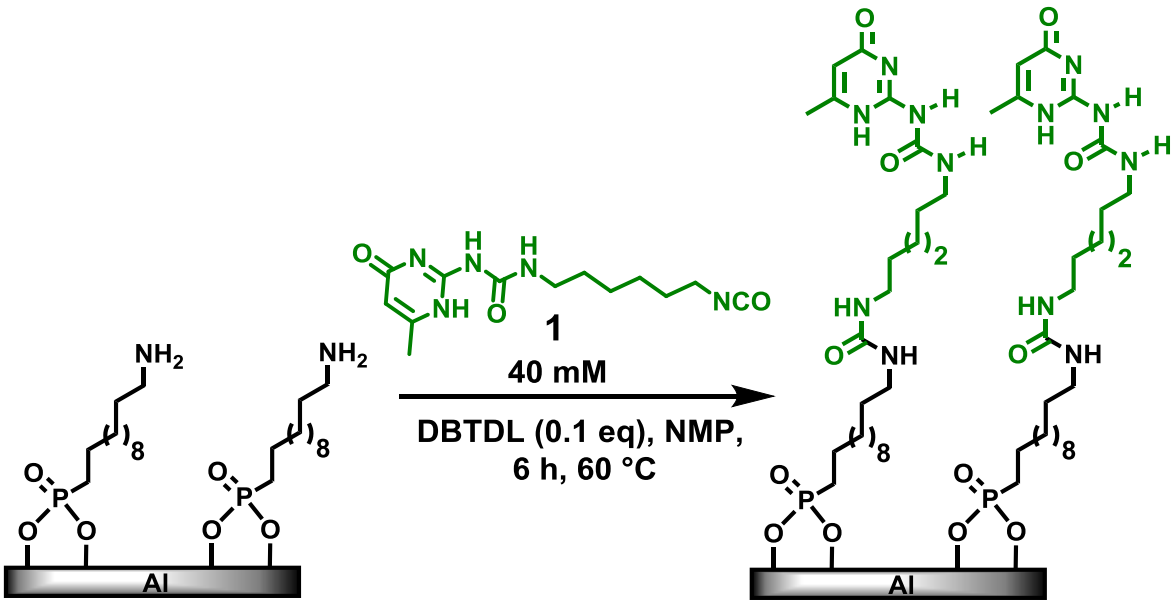

Scheme S2. Preparation of UPy–Link terminated surfaces from C_{12}–NH_2-terminated monolayers. (**S2**)

4.3 Preparation of H-bonded dimers on the surface. UPy–CF_3 (7.8 mg, 1 mM) or UPy–I (9.2 mg, 1mM) was dissolved in 25 mL toluene by sonication. UPy–Link terminated samples were loaded onto a PTFE holder and stirred in this solution at 25 °C. To commence the kinetic studies, samples were taken out of the solution at different time points, sonicated in toluene for 5 min and dried under nitrogen stream. The samples were then directly used for different analysis or exchange experiments.

Scheme S3. Preparation of Link–UPy···UPy–CF_3 (**S3**) from UPy–Link termination (**S2**).

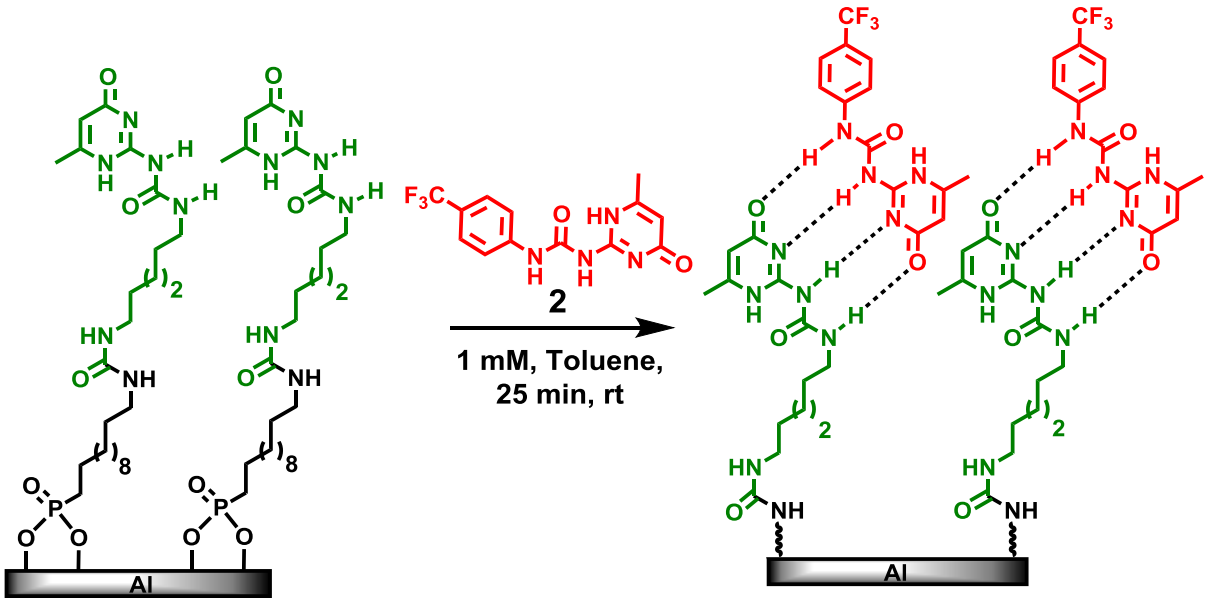

Scheme S4. Preparation of Link–UPy···UPy–I (**S4**) from UPy–Link termination (**S2**).

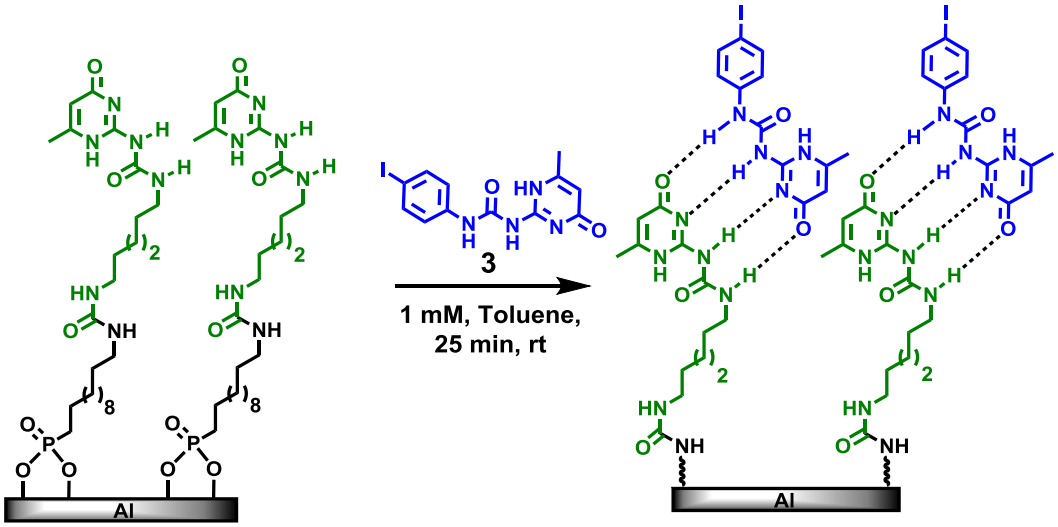

4.4 Functionality-independent UPy exchange. For exchange experiments, H-bonded dimer containing samples were allowed to react with a 1 mM solution of the incoming UPy in toluene at 25 °C or 50 °C followed by sonication for 1 min in toluene and drying under argon. The samples were then directly used for DART or XPS analysis.

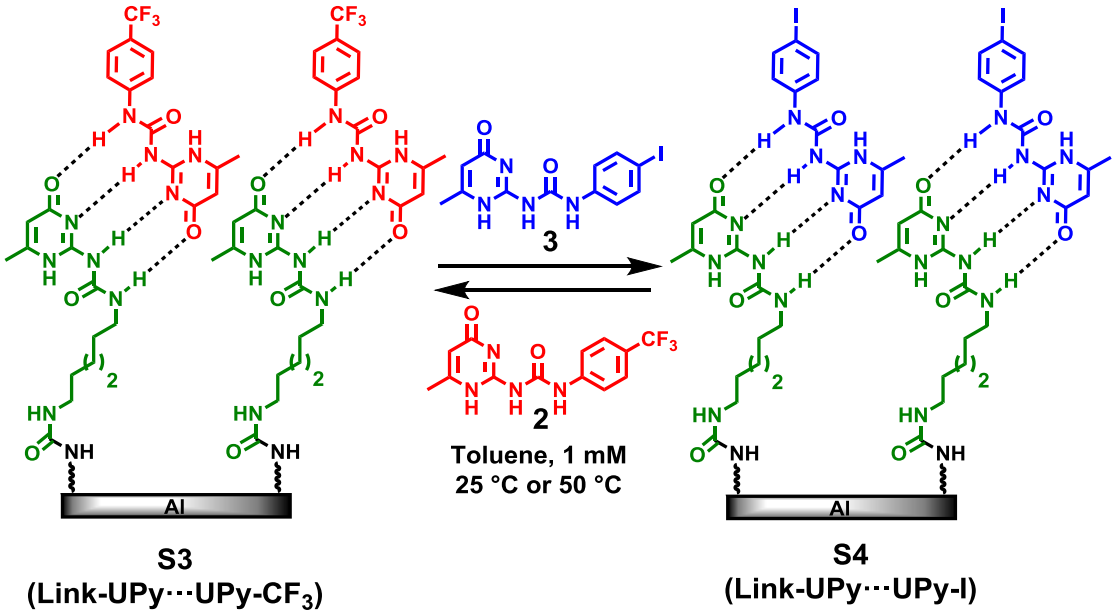

Scheme S5. Functionality independent exchange of UPy on Al surface. (**S3** to **S4** and vice versa)

4.5 Kinetics of UPy–CF_3 attachment on surface. Equations S1–S3 describe the rate $\frac{d\Gamma_{UPy}}{dt}$ for the studied reaction (mol·cm^{-2}·s^{-1}), where Γ_{UPy} is the density of surfacial UPy groups on the surface (mol·cm^{-2}) available to undergo H-bonding with its UPy counterpart in solution, and k_2 is the second-order rate constant (M^{-1}·s^{-1}). Since the amount of UPy in solution ($[\mathrm{UPy}\ (soln)]$ = 1 mM) is in very large excess compared to the amount of surfacial UPy (Γ_{UPy} = ~18 pmol·cm^{-2}) it can be assumed to be essentially constant throughout the entire kinetic regime. Thus, the self-complementary UPy···UPy quadruple hydrogen bonding on a surface can be reduced to pseudo-first order kinetics, with rate constant, k', where, $k' = k_2 \cdot$ [UPy (soln)]. Therefore, using the MS intensity data, from plots of ln $|(I_t - I_\infty)/(I_0 - I_\infty)|$ versus time (where I corresponds to the integrated EIC intensity at t = 0, t or ∞ (completed reaction)), the resulting

pseudo-first order rate constant (k') can be obtained directly from the slope, as shown in equation (S3). Based on this pseudo-first order rate constant, the corresponding second-order rate constant k_2 can subsequently be calculated from equation (S5).

$$v = k_2 \left[\text{UPy}\ (soln)\right]\Gamma_{UPy} = \frac{d\Gamma_{UPy}}{dt} \quad \text{(S1)}$$

$$v = k'\Gamma_{UPy} \qquad (\ \because \left[\text{UPy}\ (soln)\right] \gg \Gamma_{UPy}) \quad \text{(S2)}$$

$$ln\left(\left|\frac{I_t - I_\infty}{I_0 - I_\infty}\right|\right) = -k't \quad \text{(S3)}$$

$$k'(s^{-1}) = k_2 \left[\text{UPy}\ (soln)\right] \quad \text{(S4)}$$

$$k_2(M^{-1}s^{-1}) = k'/\left[\text{UPy}\ (soln)\right] \quad \text{(S5)}$$

5. SUPPLEMENTARY FIGURES

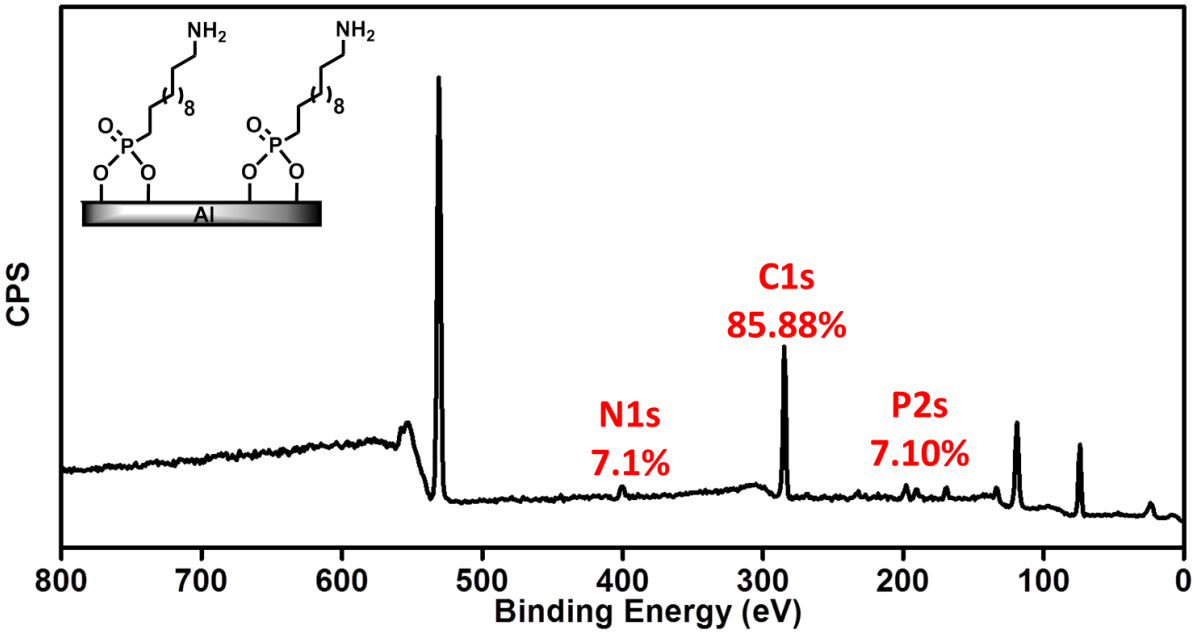

Supplementary Figure S1. XPS wide scan of C_{12}–NH_2 monolayers.

Calculation of atomic percentages:

Theoretical N/P = 1

Observed N/P = 0.98 ± 0.3

Theoretical C/P = 12

Observed C/P = 13 ± 0.5

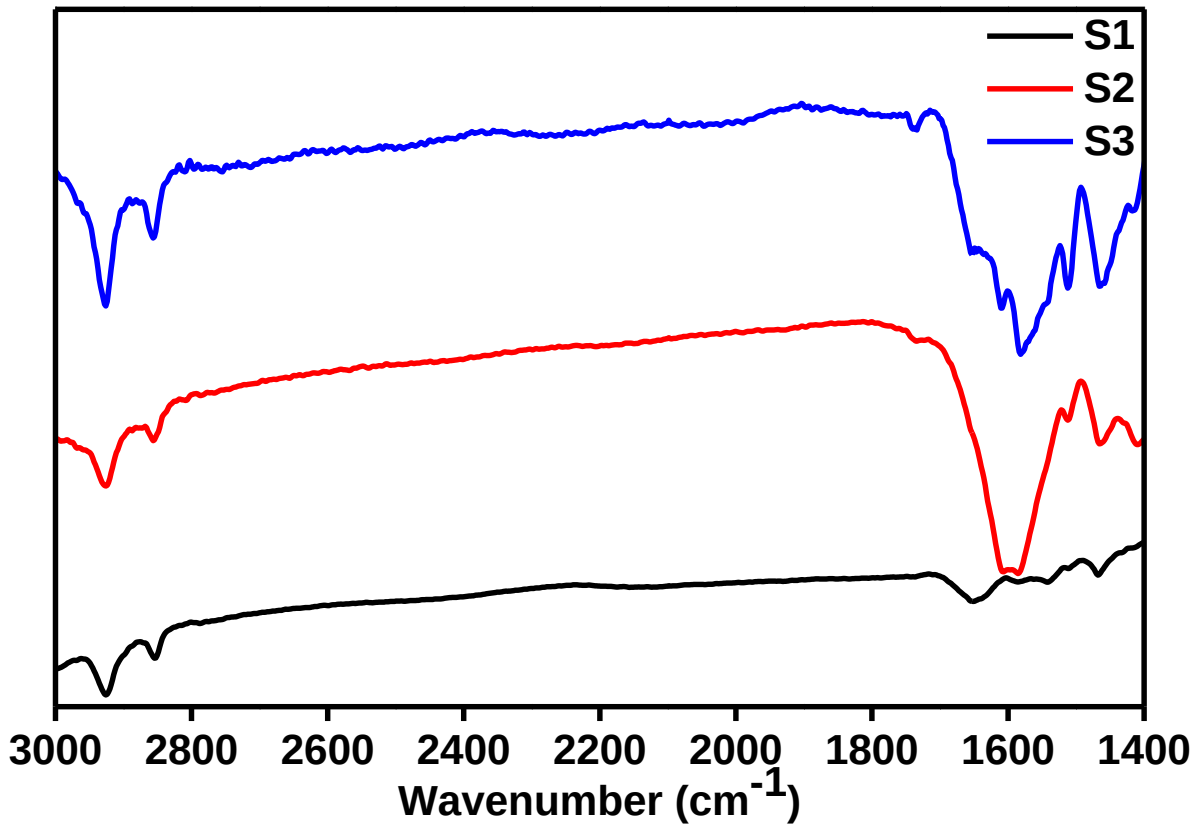

Supplementary Figure S2. GATR–FTIR spectra of Al surface terminated with C_{12}–NH_2 (S1), UPy–Link (S2) and Link–UPy···UPy–CF_3 (S3) dimers.

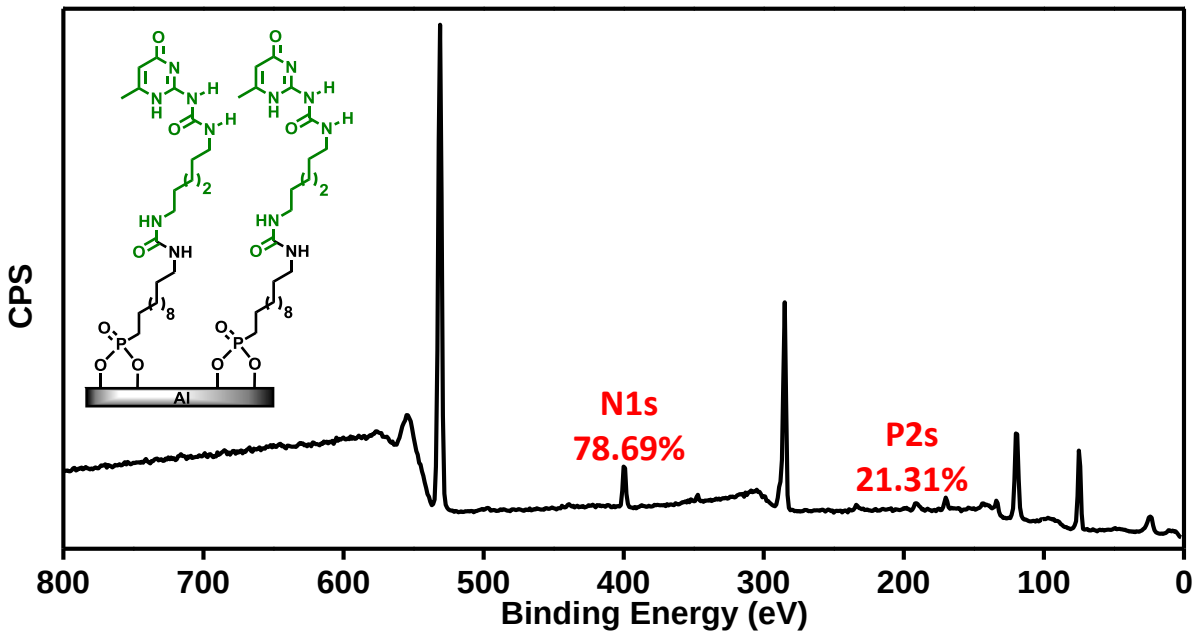

Supplementary Figure S3. XPS wide scan of UPy–Link attachment.

Calculation of Surface Attachment from Atomic percentages:

For surface S1 the N/P ratio is equal to 1.

For surface S2 the N/P ratio at 100% covalent UPy binding is equal to 6.

Hence, if the degree of UPy binding is not 100%, the degree can be calculated from the experimentally determined N/P ratio, according to:

$$Conversion\ S1 \rightarrow S2 = \frac{\left(\frac{N}{P}\right)_{exp} - 1}{6 - 1}$$

Inserting an experimentally determined N/P ratio of 3.6 for surface S2 in the above equation leads to a conversion of 52%.

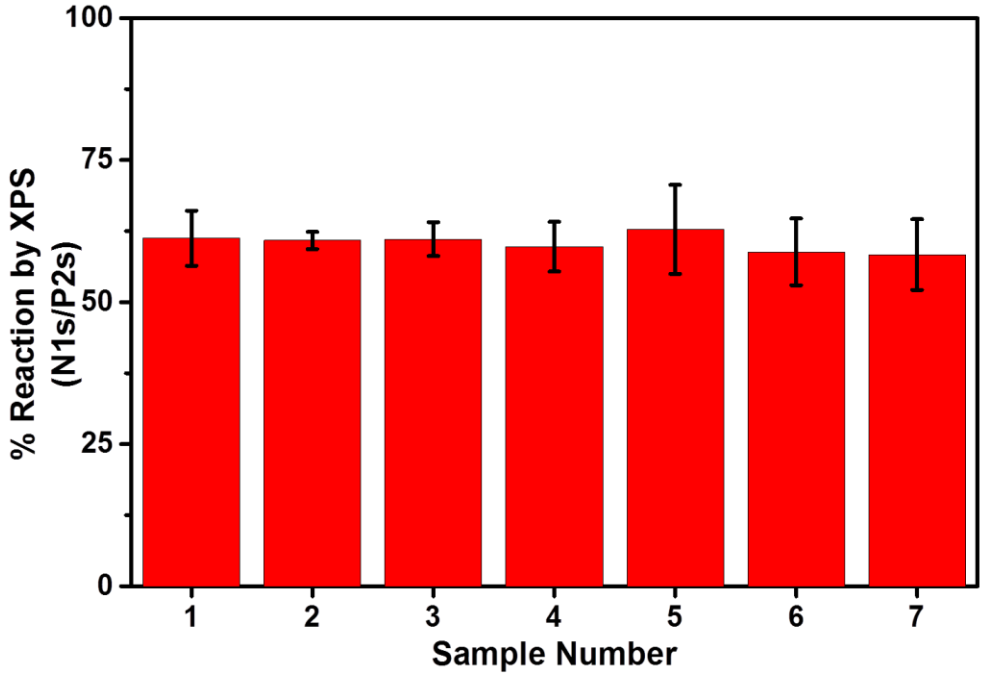

Supplementary Figure S4. Percentage completion for UPy–Link formation across several samples as determined by XPS.

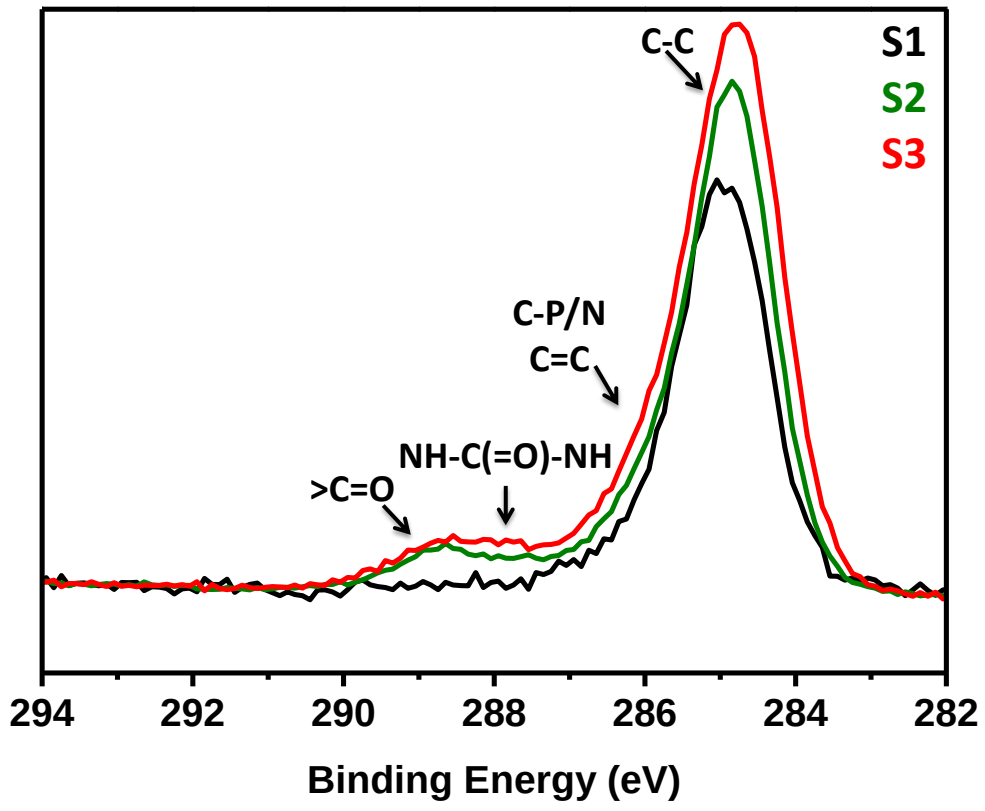

Supplementary Figure S5. Stacked XPS C1s narrow scan of surfaces S1, S2 and S3.

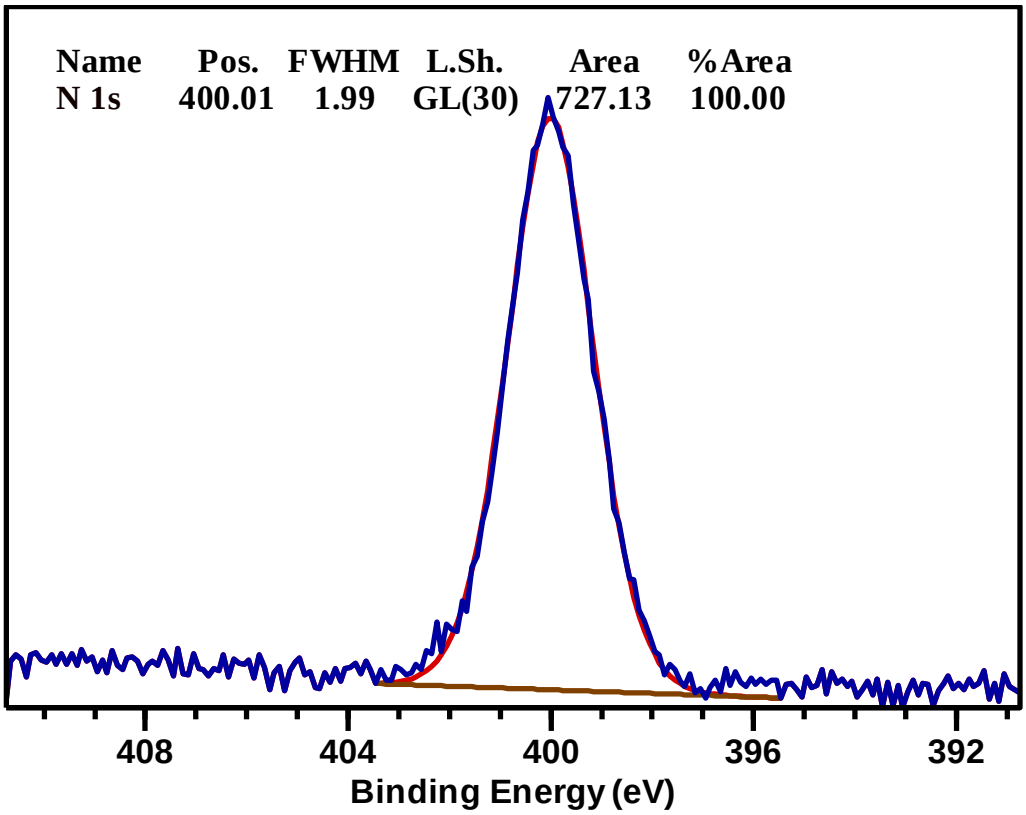

Supplementary Figure S6. XPS N1s narrow scan of UPy–Link attachment.

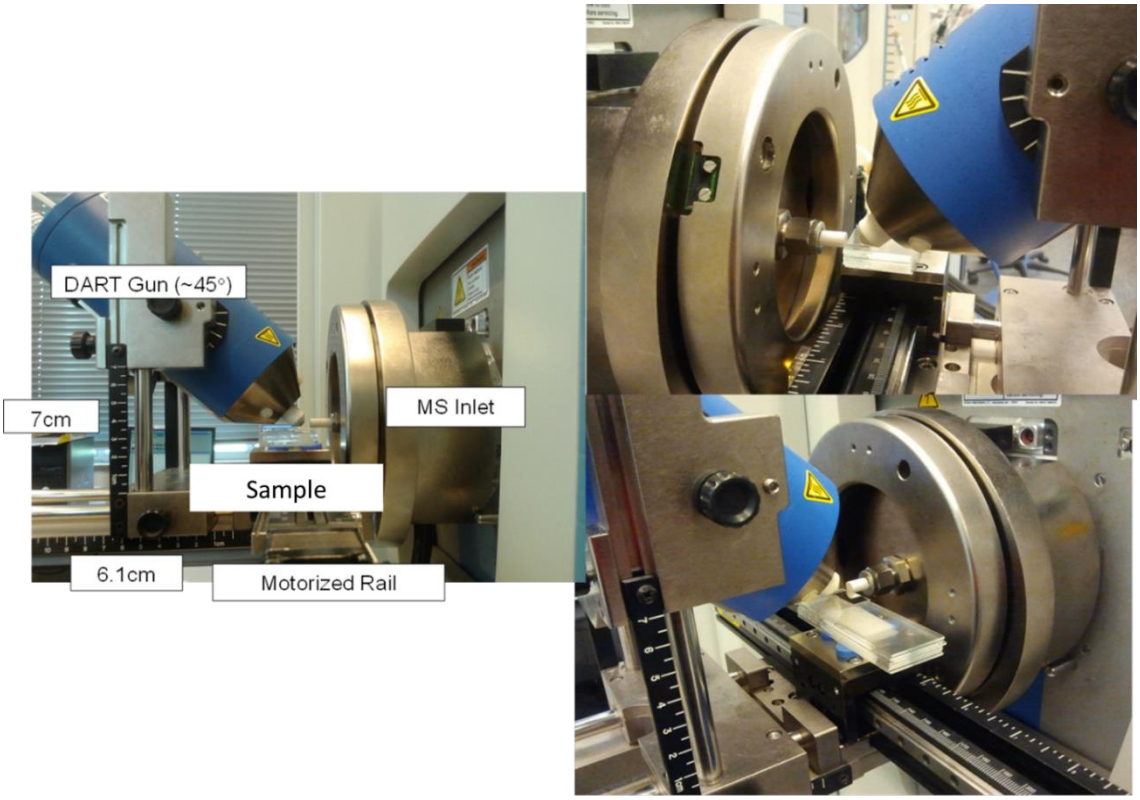

Supplementary Figure S7. Typical DART setup.

a)

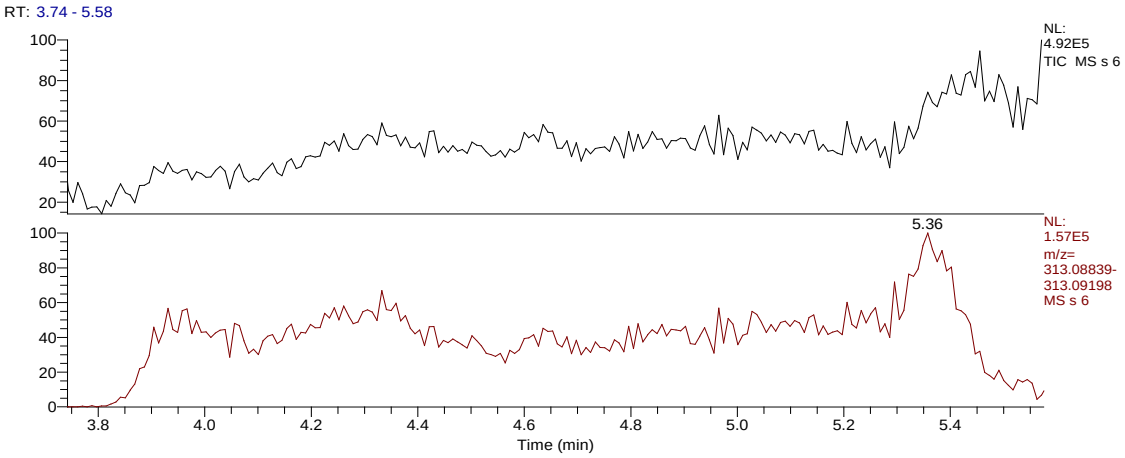

b) Elemental composition search on mass 313.09027

m/z= 308.09027-318.09027

m/z	Theo. Mass	Delta (mmu)	RDB equiv.	Composition
313.09027	313.09069	-0.42	8.5	$C_{13}H_{12}O_2N_4F_3$
	313.08974	0.53	16.0	$C_{21}H_{12}ONF$
	313.09089	-0.62	12.0	$C_{18}H_{13}O_2NF_2$
	313.08954	0.73	12.5	$C_{16}H_{11}ON_4F_2$
	313.08860	1.67	20.0	$C_{24}H_{11}N$
	313.08840	1.87	16.5	$C_{19}H_{10}N_4F$
	313.09471	-4.44	12.5	$C_{18}H_{12}N_2F_3$
	313.08458	5.69	16.0	$C_{19}H_{11}O_2N_3$
	313.08348	6.79	12.5	$C_{19}H_{12}OF_3$
	313.09715	-6.88	15.5	$C_{20}H_{13}O_2N_2$

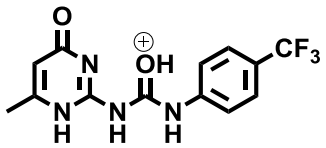

m/z: 313.09069 (100.0%)

c)

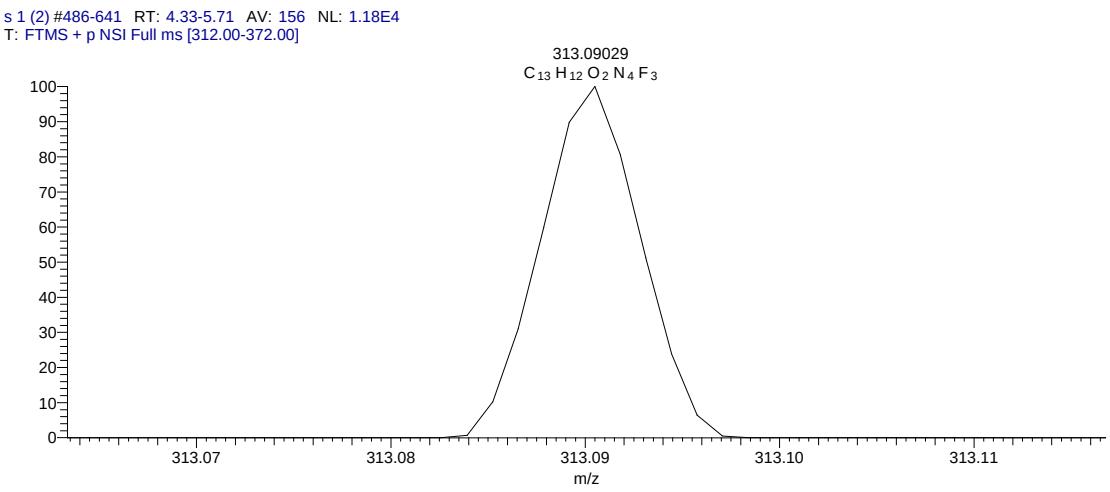

Supplementary Figure S8. Representative DART ion intensity EIC for Link–UPy···UPy–CF_3 dimers (S3). a) Top panel represents total ion current (TIC); bottom panel represents extracted ion chromatogram (EIC) (*m/z* window 10 mmu around ion of interest). b) relative error between obtained *m/z* and theoretical *m/z* of ion of interest c) peak of ion of interest. (UPy–CF_3).

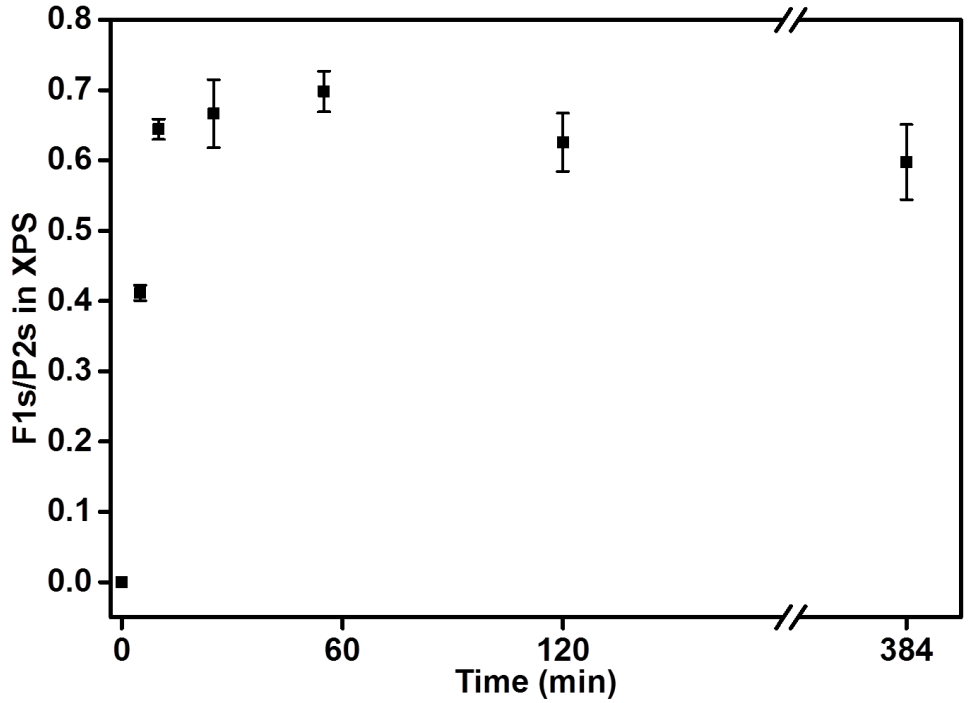

Supplementary Figure S9. F/P ratio in XPS for Link–UPy···UPy–CF_3 formation over time (min).

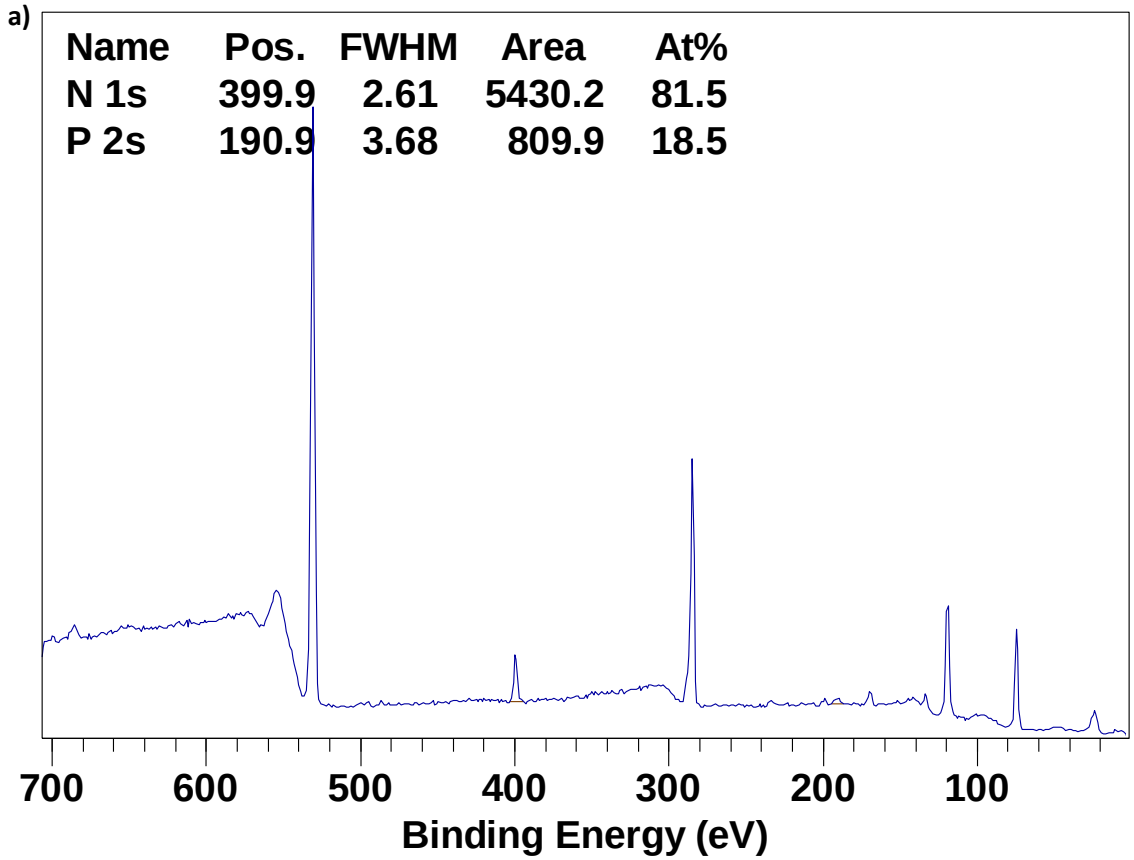

b)

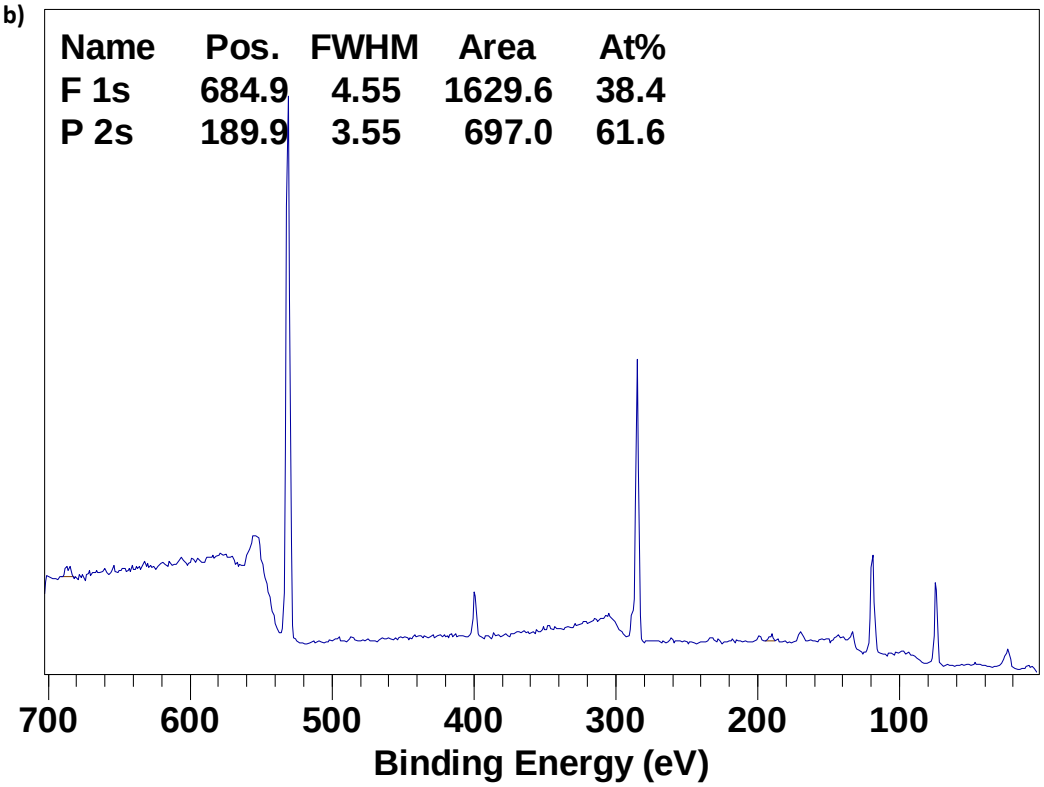

Supplementary Figure S10. XPS wide scan of Link–UPy···UPy–CF_3 on surface with a) N/P and b) F/P ratios.

Calculation of Atomic percentages:

To calculate the maximum N/P ratio for surface S3, one should consider that 48% of the surface sites are amine-terminated, with N/P ratio of 1 (see Figure S3, page S19). If all UPy sites on the surfaces, which make up 52% of the surface, will dimerize, their N/P becomes 10. Hence, the maximum N/P ratio for surface S3 is: 0.48 × 1 + 0.52 × 10 = 5.68.

Consequently, the actual degree of surface UPy dimerization is calculated by:

$$Conversion\ S2 \rightarrow S3 = \frac{\left(\frac{N}{P}\right)_{exp} - 3.6}{5.68 - 3.6}$$

Inserting an experimentally determined N/P ratio of 4.3 for surface S3 in the above equation leads to a degree of UPy dimerization of 34%.

Similarly, based on the F/P ratio, also a degree a UPy dimerization can be calculated. As explained above, only 52% of the surface sites are capable of binding UPy–CF_3. Hence, the maximum F/P ratio (at 100% dimerization) is equal to 0.52 × 3 = 1.56. Consequently, the actual degree of surface UPy dimerization is calculated by:

$$Conversion\ S2 \rightarrow S3 = \frac{\left(\frac{F}{P}\right)_{exp}}{1.56}$$

Inserting an experimentally determined F/P ratio of 0.6 for surface S3 in the above equation leads to a degree of UPy dimerization of 38%.

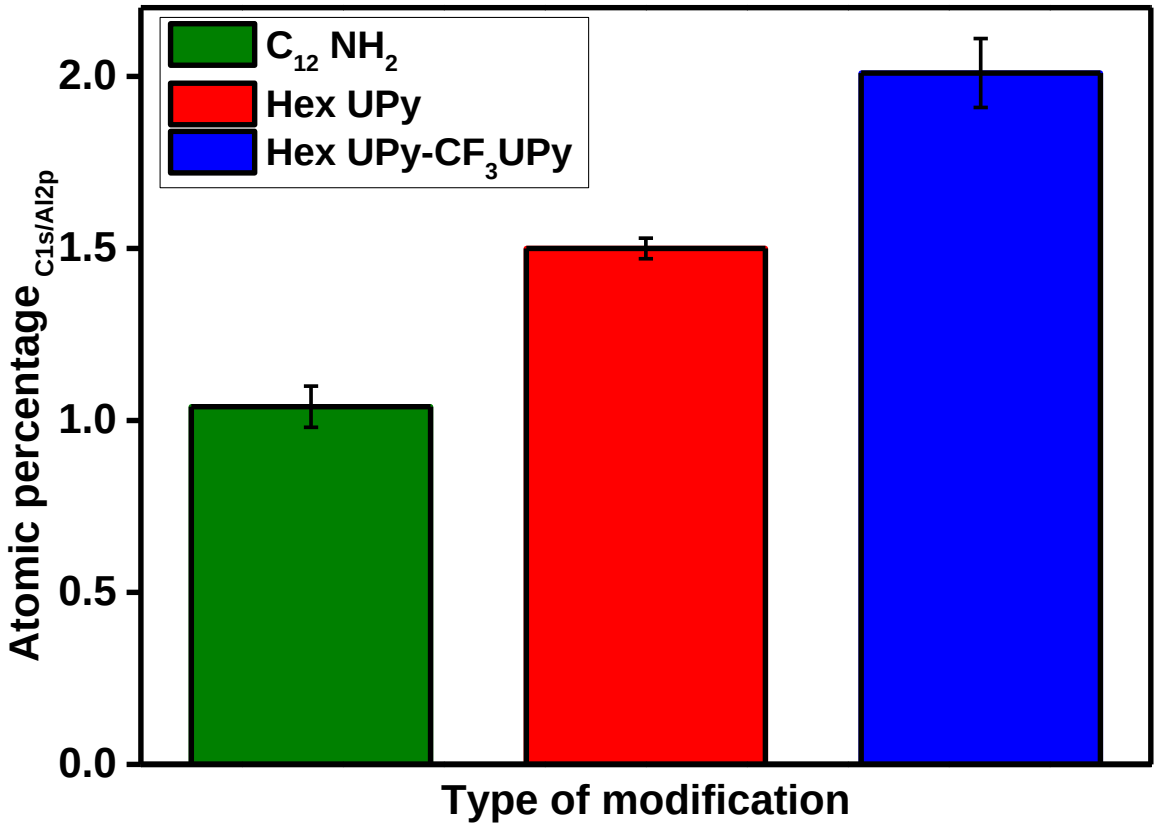

Supplementary Figure S11. Attenuation of Al2p intensity in XPS on formation of C_{12}–NH_2, UPy–Link and Link–UPy···UPy–CF_3 dimers.

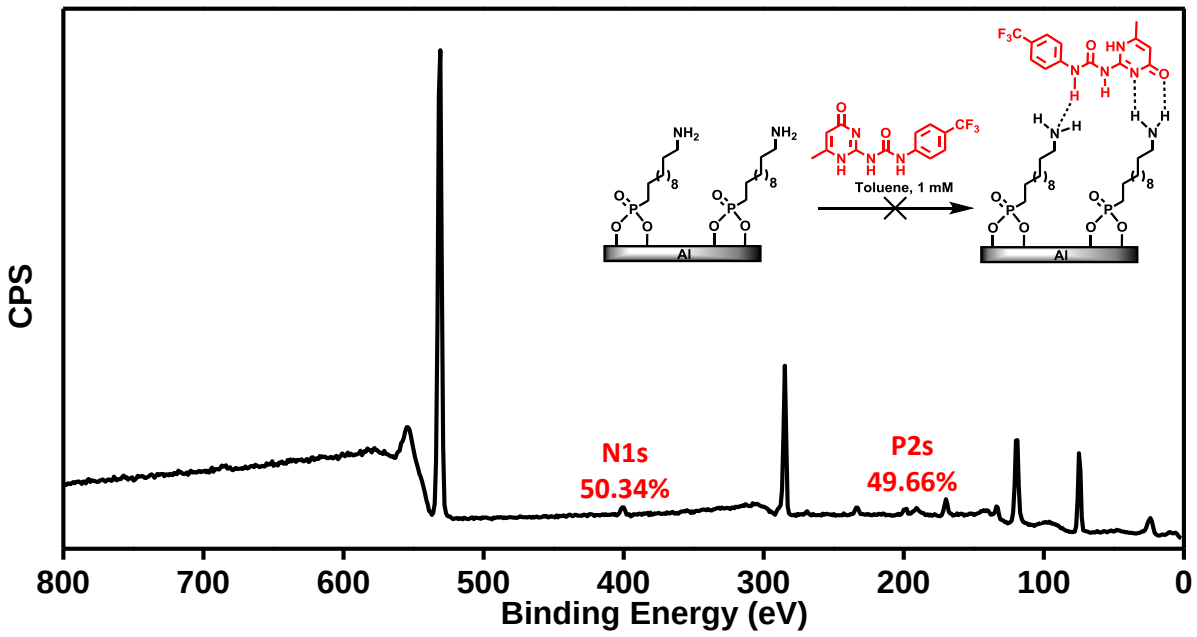

Supplementary Figure S12. XPS wide scan of control samples reacted with UPy–CF_3.

Calculation of Atomic percentages:

Theoretical N/P ratio ≤ 4

Observed N/P ratio = 1 ± 0.1

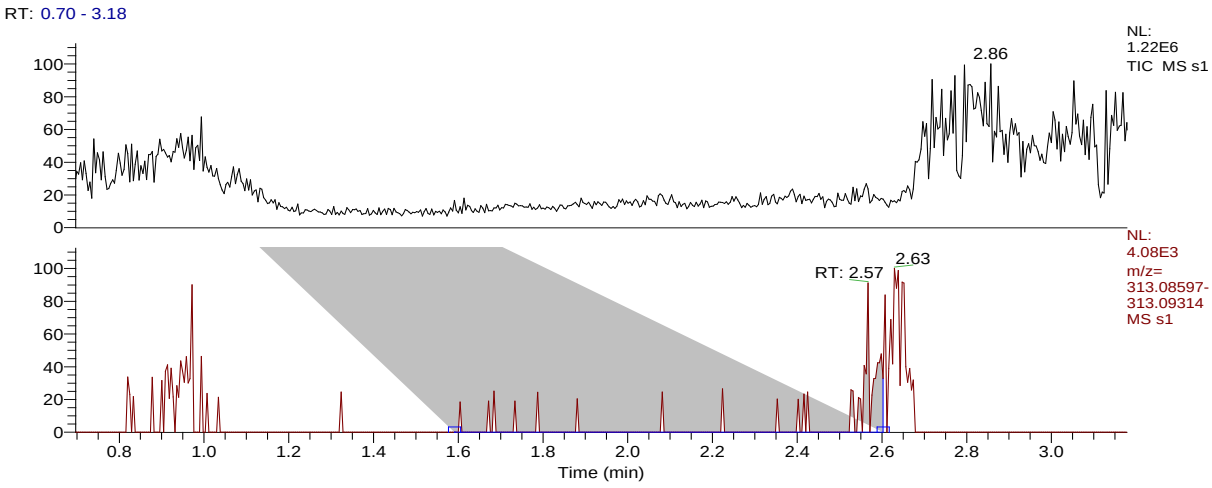

Supplementary Figure S13. DART measurement of control samples reacted with UPy–CF_3.

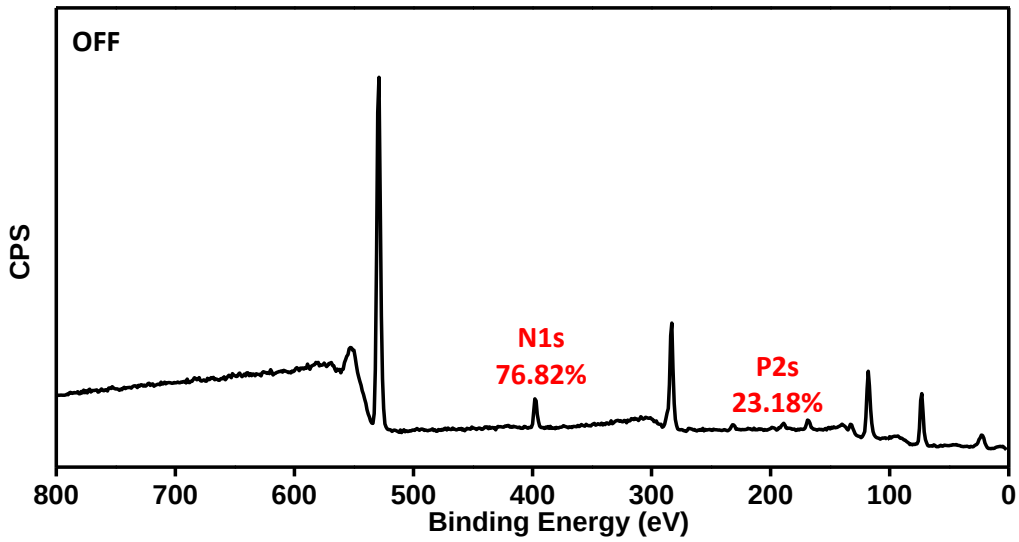

Calculation of Atomic percentages:

Theoretical N/P (100% recovery) = 3.6

Observed N/P = 3.3 ± 0.2

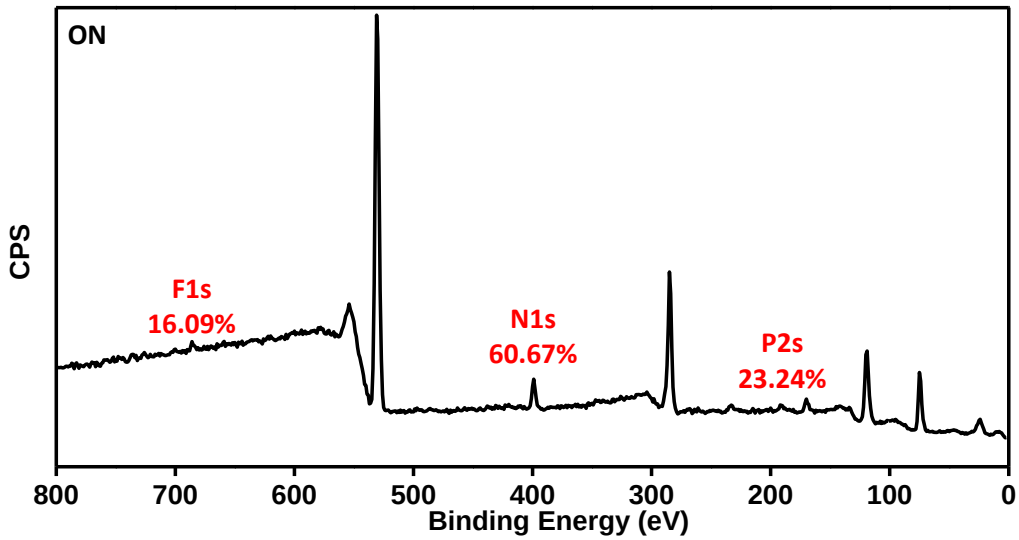

Calculation of Atomic percentages:

Theoretical F/P = 1.6

Observed F/P = 0.7 ± 0.03, Fraction of H-bonded surface-bound UPy–CF_3 (F/P) = 43 ± 2%

Supplementary Figure S14. XPS wide scan of UPy–CF_3 removal by sonication in acetone and subsequent reassembly.

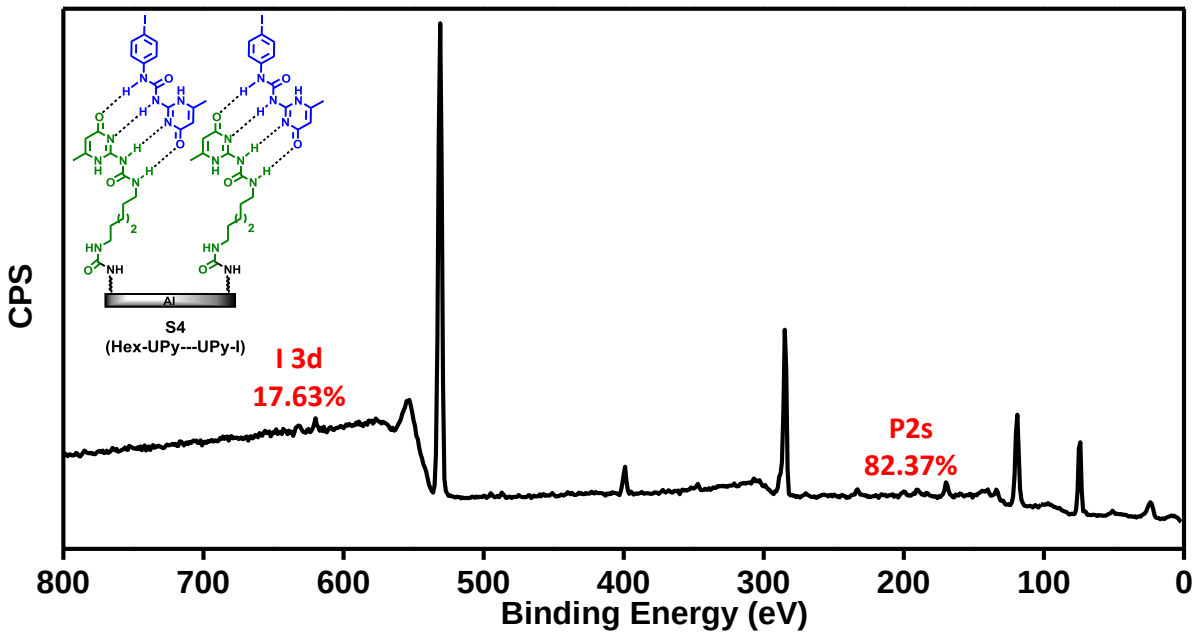

Supplementary Figure S15. XPS wide scan of Link–UPy···UPy–I on surface.

Calculation of Atomic percentages:

Theoretical I/P = 0.6

Observed I/P = 0.2 ± 0.03

Fraction of H-bonded surface-bound UPy–I = 35 ± 5%

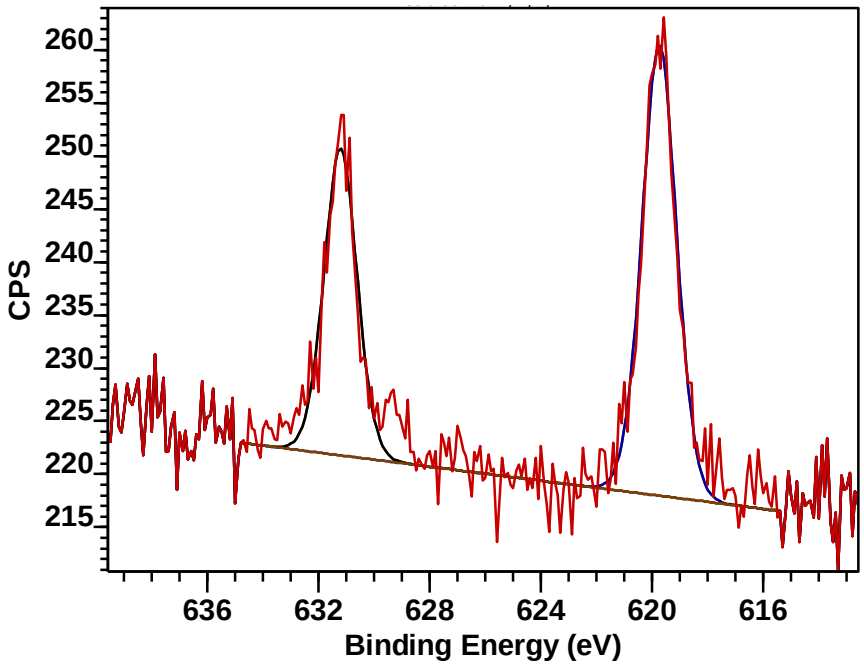

Supplementary Figure S16. XPS I3d narrow scan of Link–UPy···UPy–I on surface.

a)

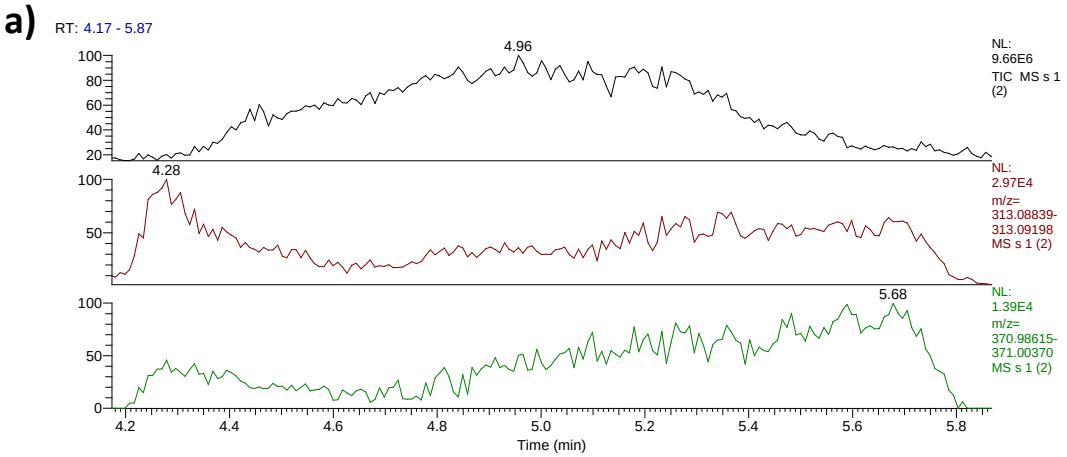

b)

Elemental composition search on mass 370.99835

m/z= 365.99835-375.99835

m/z	Theo. Mass	Delta (mmu)	RDB equiv.	Composition
370.99835	370.99995	-1.60	8.5	$C_{12}H_{12}O_2N_4I$
	371.00018	-1.83	28.0	$C_{27}HO_2N$
	370.99273	5.62	12.5	$C_{18}H_{12}OI$
	371.00397	-5.62	12.5	$C_{17}H_{12}N_2I$
	370.99139	6.96	13.0	$C_{16}H_{10}N_3I$
	371.01141	-13.06	28.0	$C_{26}HON_3$
	371.01252	-14.17	8.0	$C_{13}H_{14}O_2N_3I$
	371.01276	-14.41	27.5	$C_{28}H_3O_2$
	370.98016	18.19	13.0	$C_{17}H_{10}ONI$
	371.01654	-18.19	12.0	$C_{18}H_{14}NI$

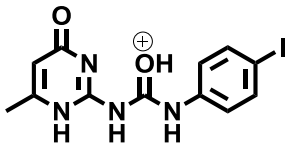

m/z: 370.9995 (100.0%)

c)

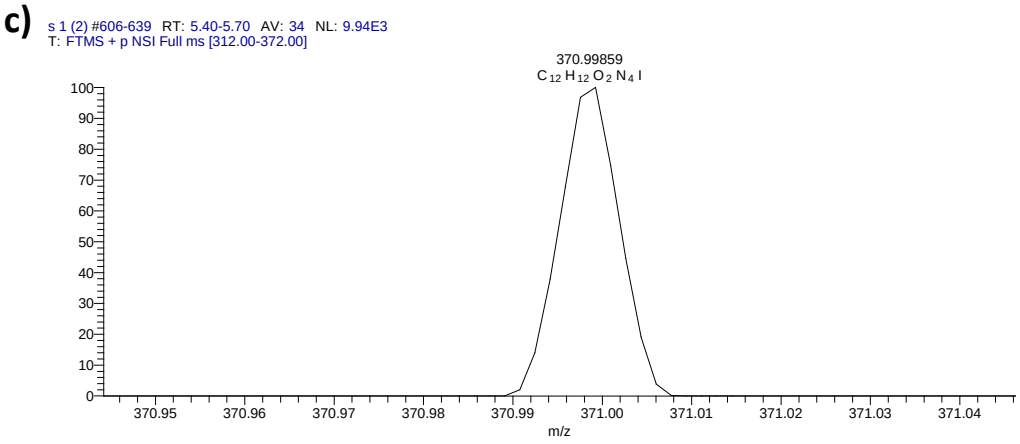

Supplementary Figure S17. DART measurement of UPy–CF_3 displacement with UPy–I showing both ionized species. a) Top: total ion current (TIC); middle: extracted ion chromatogram (EIC) of UPy–CF_3; bottom: extracted ion chromatogram (EIC) of UPy–I. b) relative error between obtained *m/* and theoretical *m/z*. c) peak of ion of interest. (UPy–I).

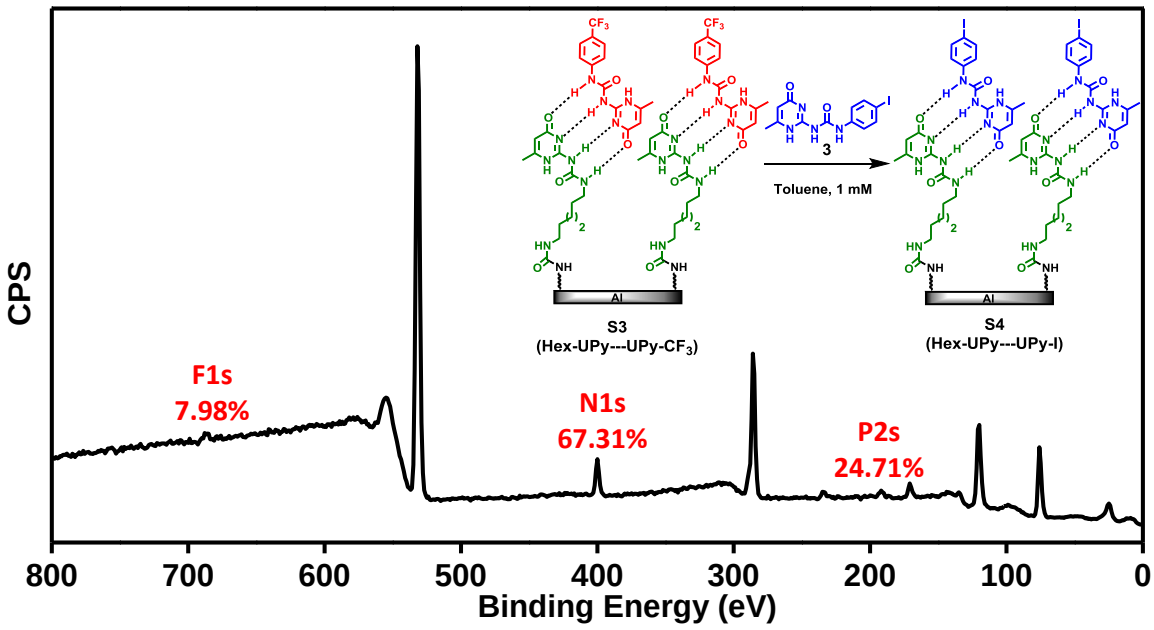

Supplementary Figure S18. XPS wide scan of UPy–CF_3 displacement by UPy–I.

Calculation of atomic percentages after exchange:

Theoretical F/P = 0

Observed F/P = 0.30 ± 0.04

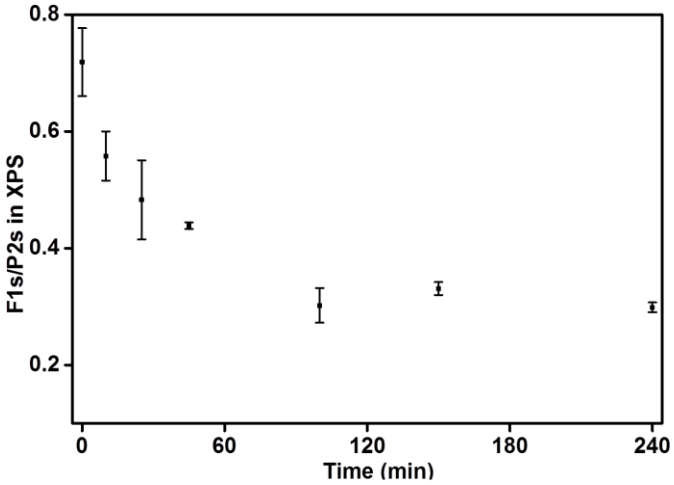

Supplementary Figure S19. F/P ratio in XPS for UPy–CF_3 displacement by UPy–I.

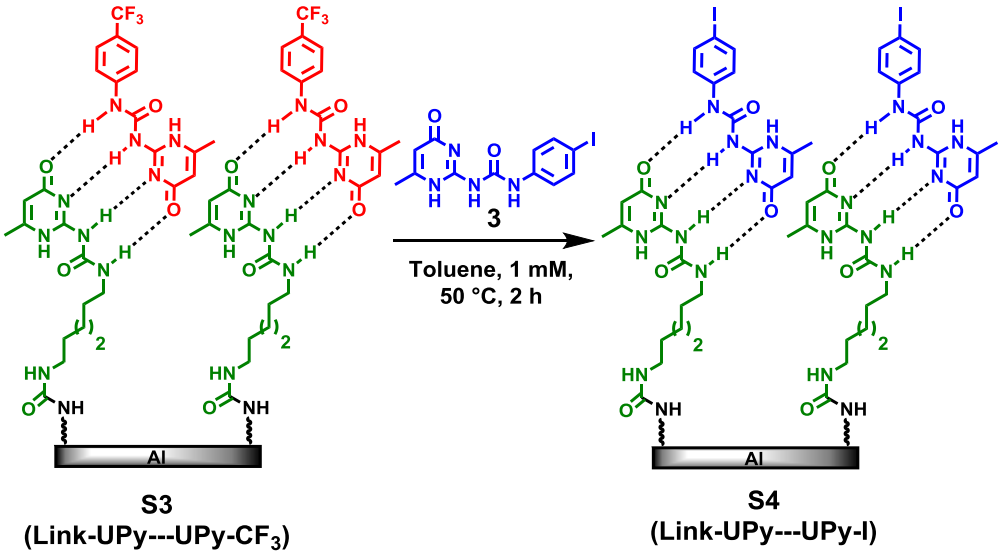

S3
(Link-UPy---UPy-CF_3)

S4
(Link-UPy---UPy-I)

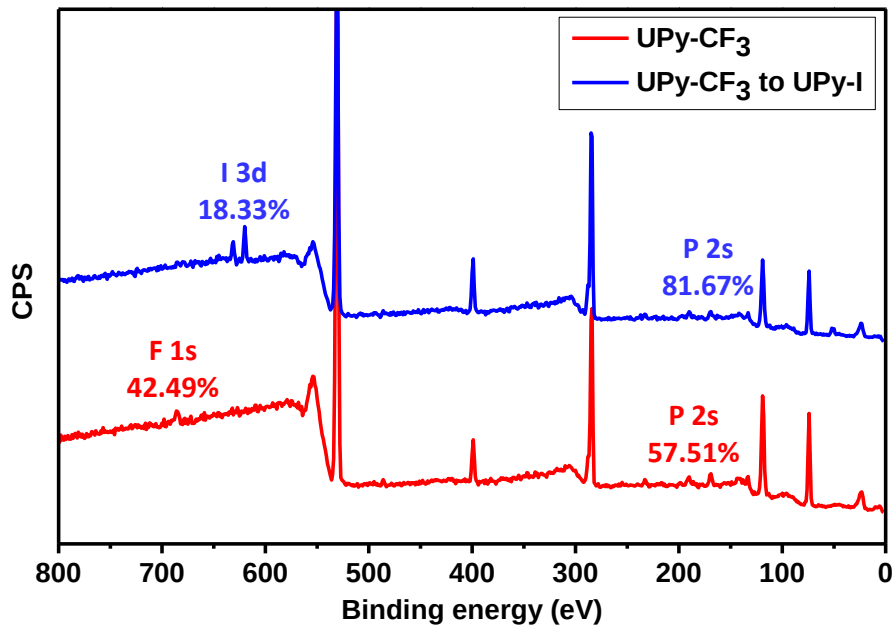

Supplementary Figure S20. XPS wide scan of UPy–CF_3 displacement by UPy–I at 50 °C.Calculation of Atomic percentages after exchange:

Theoretical I/P = 0.6

Observed I/P = 0.21 ± 0.04

% UPy–I on surface = 35 ± 5%

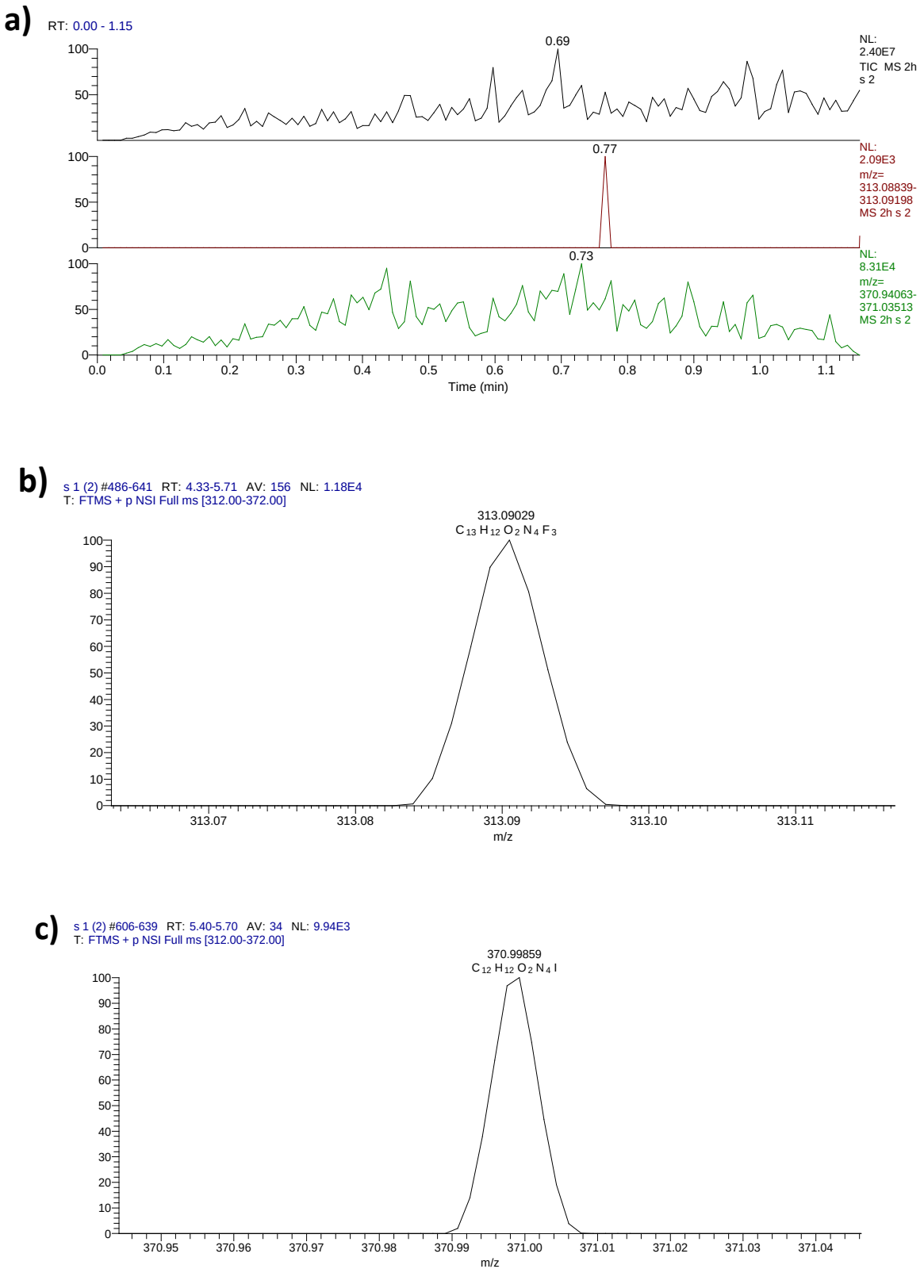

Supplementary Figure S21. DART–HRMS Scan of UPy–CF_3 displacement by UPy–I at 50 °C. a) top: total ion current (TIC) middle: EIC of UPy–CF_3 bottom: EIC of UPy–I. b) peak of ion of interest (UPy–CF_3) c) peak of ion of interest (UPy–I).

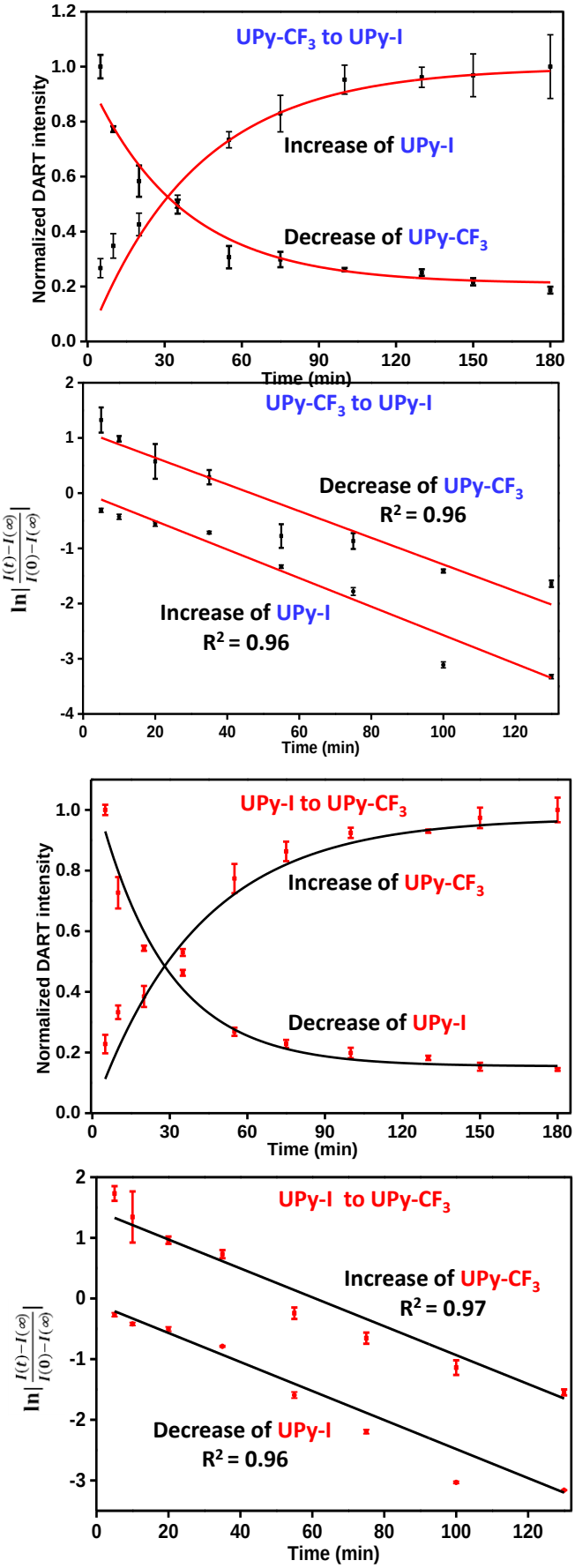

Supplementary Figure S22. DART kinetics of UPy exchange at a surface.

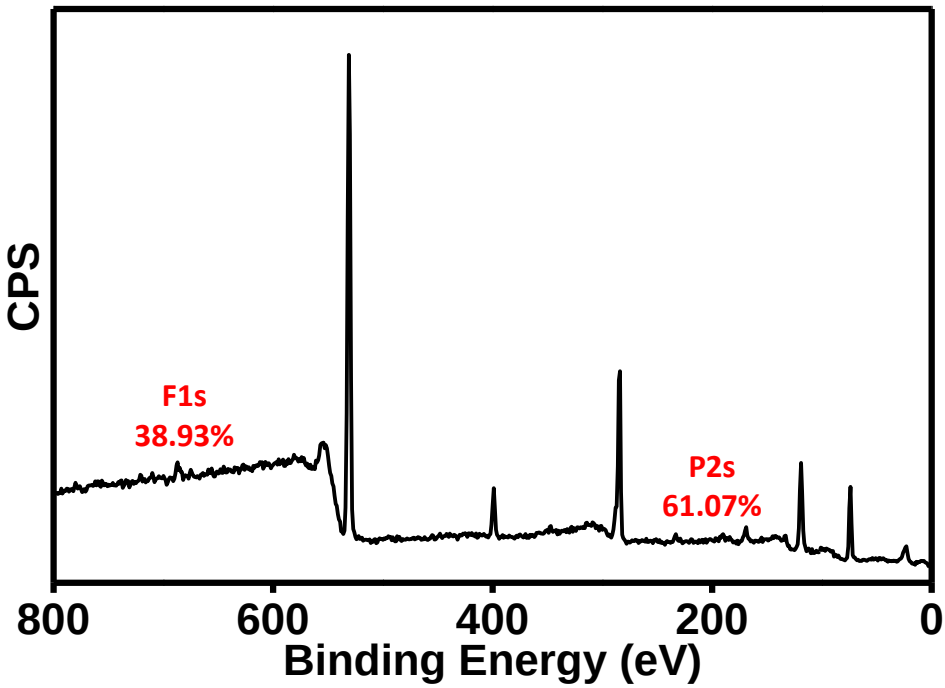

Supplementary Figure S23. XPS wide scan of Link–UPy···UPy–CF_3 (S3) surfaces after stirring in toluene at 80 °C for 24 h.

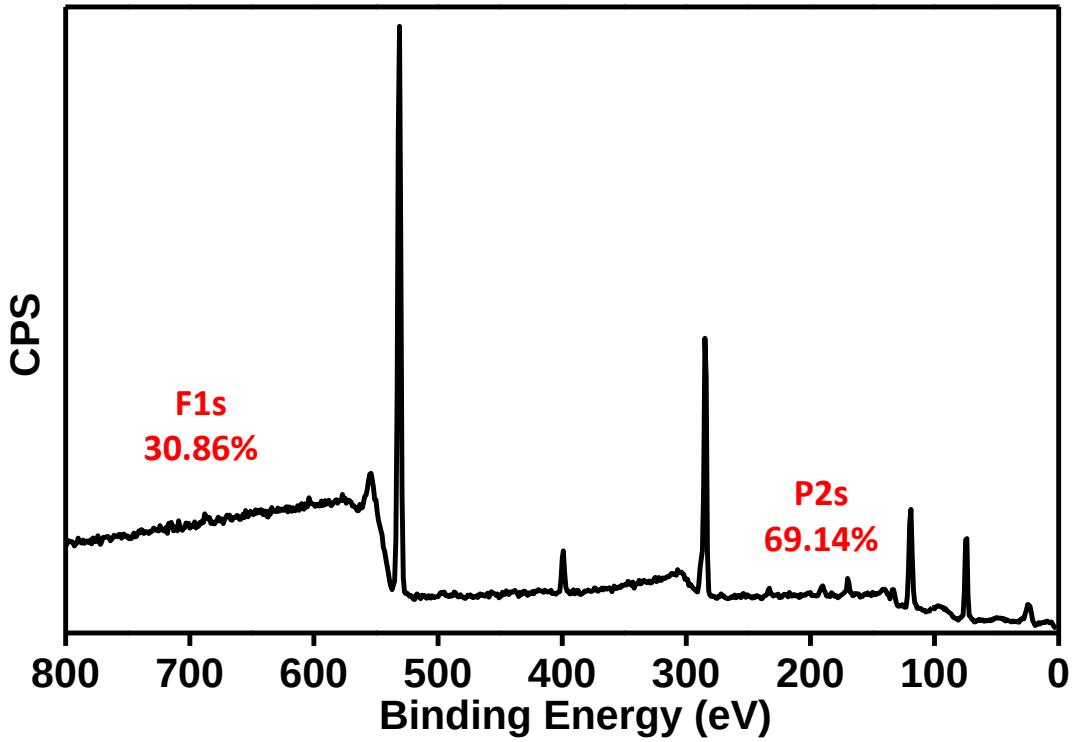

Supplementary Figure S24. XPS wide scan of Link–UPy···UPy–CF_3 (S3) surfaces after stirring in toluene at 80 °C for 48 h.

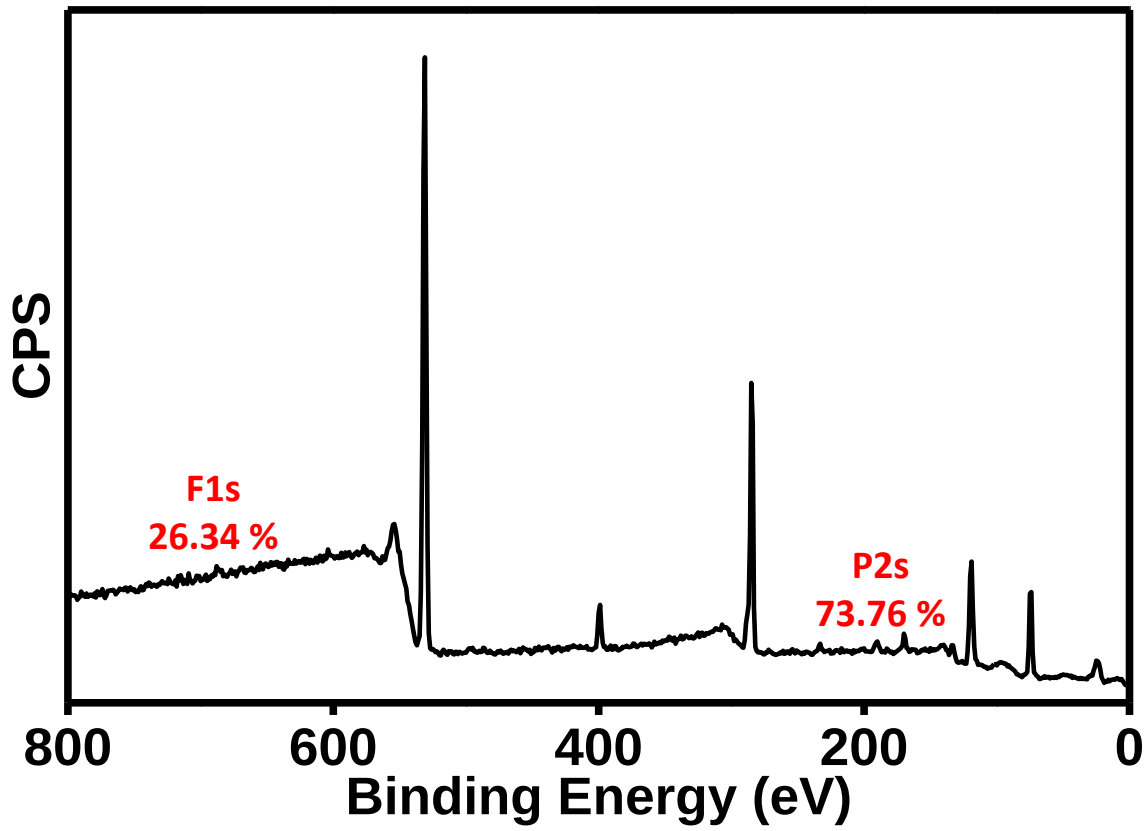

Supplementary Figure S25. XPS wide scan of Link–UPy···UPy–CF_3 (S3) surfaces after stirring in toluene at 80 °C for 120 h.

Calculation of atomic percentages

Initial F/P = 0.7

Observed F/P (after 120 h) = 26.34/73.76 = 0.36

% UPy remaining on surface = 0.36/0.7 = 52%

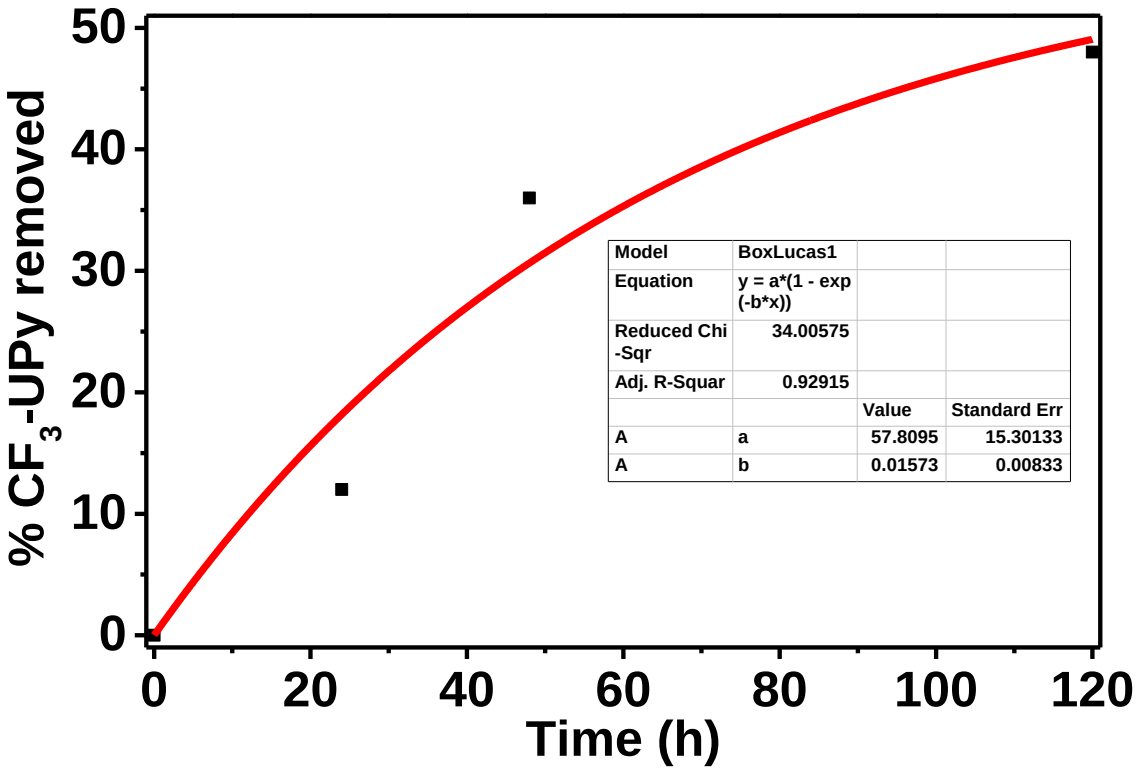

Supplementary Figure S26. Plot of % CF_3–UPy removed (F/P in XPS) from S3 surfaces after stirring in toluene at 80 °C vs time (h).

Rate Constant (80 °C) = 0.016 h^{-1} = 4.4 × 10^{-6} s^{-1}

Rate (25 °C) = k_{off} ~ 10^{-7} s^{-1}

k_{on} (pseudo-first order) = 22 × 10^{-4} s^{-1}

k_{on} (second order for 1 mM UPy in solution) = 22 × 10^{-4} s^{-1} / 10^{-3} M = 2.2 $M^{-1}s^{-1}$

K = k_{on} (second order) / k_{off} = 2.2 × 10^{7} M^{-1}

6. SUPPLEMENTARY TABLES

Table S1. Rate constants for UPy exchange (25 °C in toluene) at the surface.

UPy displacement	Increasing/ Decreasing signal	Rate ($\times 10^{-4}$ s^{-1})
CF_3–UPy to **UPy–I**	Decrease in CF_3–UPy	4.0 ± 0.4
	Increase in UPy–I	4.3 ± 0.3
UPy–I to **CF_3–UPy**	Decrease in UPy–I	3.8 ± 0.3
	Increase in CF_3–UPy	3.9 ± 0.2

7. MATERIAL STUDIO DATA

7.1 Surface preparation. Al oxide (Al_2O_3) surface in bulk. All colors used are standard throughout (Grey = C, purple = P, white = H, pink = Al, red = O, blue = N)

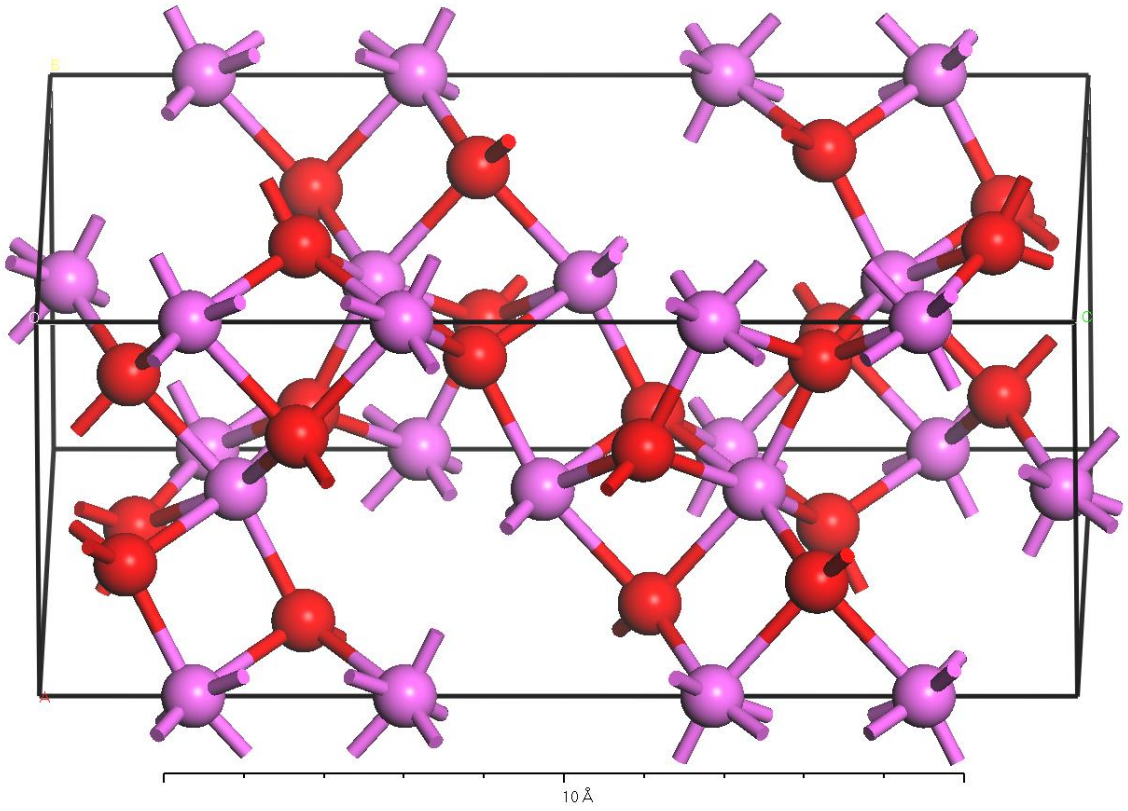

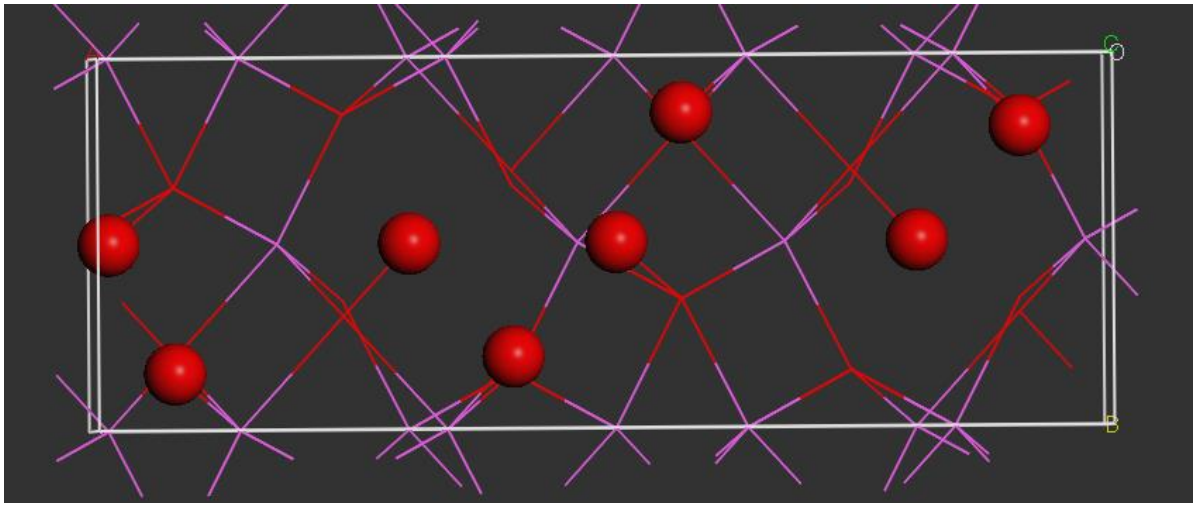

Al_2O_3 were cleaved along (h k l) = (–1 0 0) to build oxidic aluminium surfaces.

Thickness fractional = 1

Thickness (Å) = 4.121

Cap bonds on Top = O(oxygen)

Vacuum Slab Build Dimensions

Vacuum orientation C (axis)

Vacuum thickness = 74.5048 Å

Crystal thickness = 80.00 Å

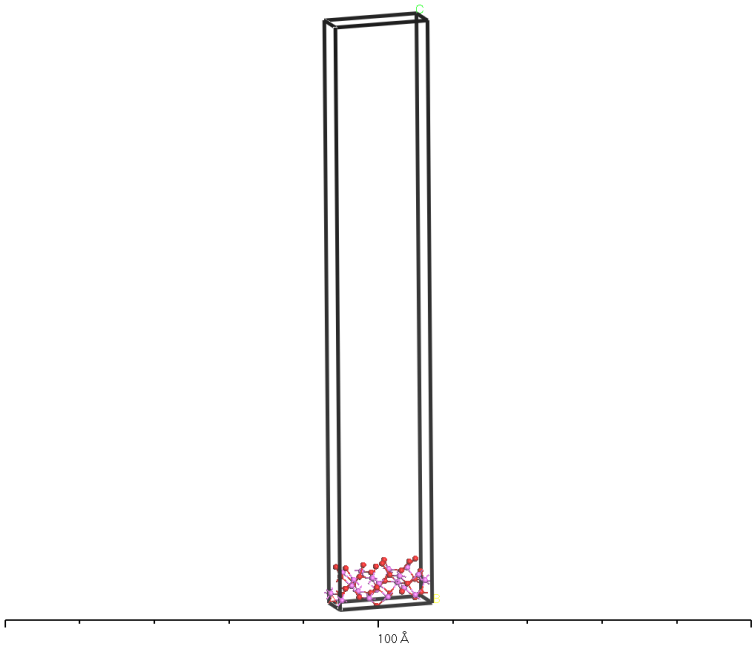
100 Å

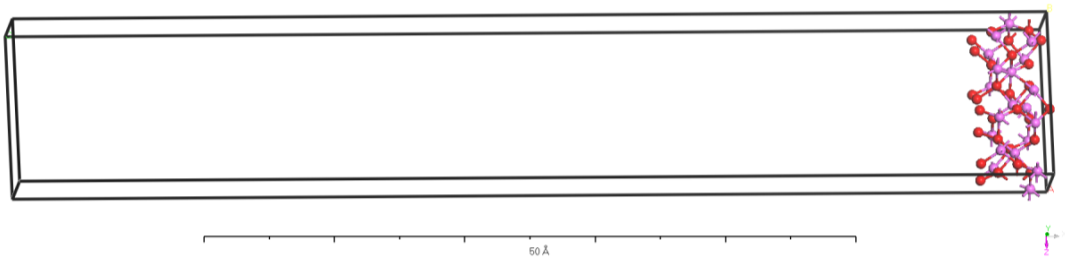
50 Å

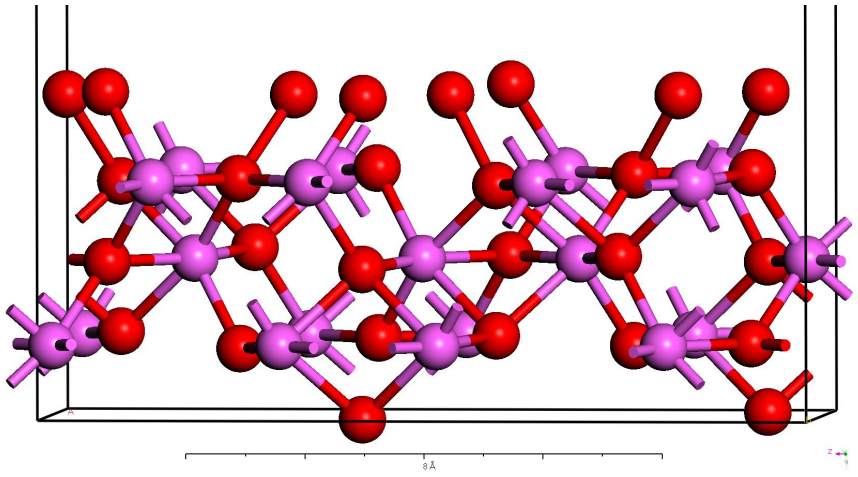
8 Å

7.2 Scheme for monolayer attachment (2×4).

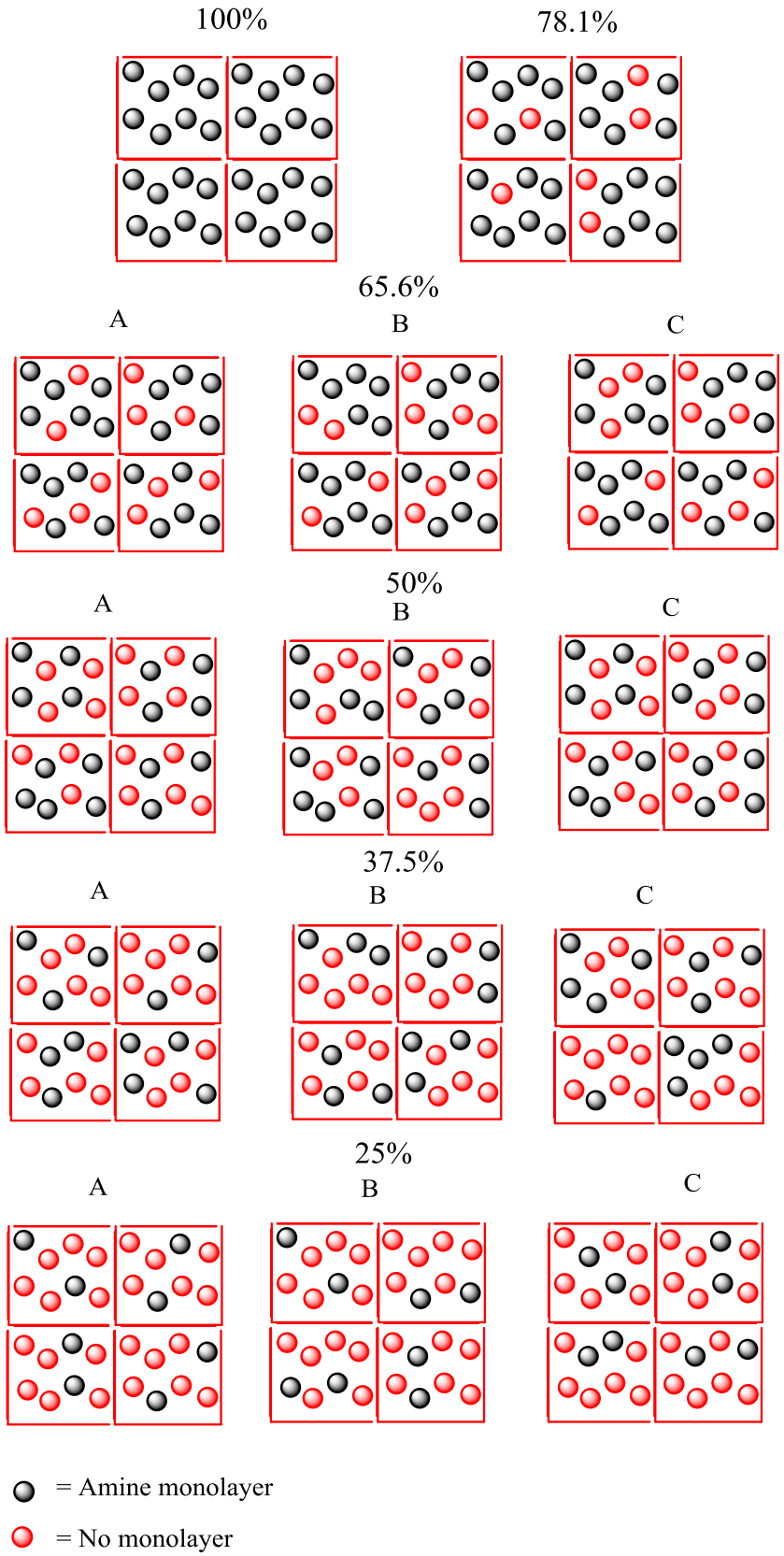

7.3 Example of 8×16 cell used for packing energy calculation (50% coverage).

7.4 Example of 8×16 cell used for packing energy calculation (50% coverage).

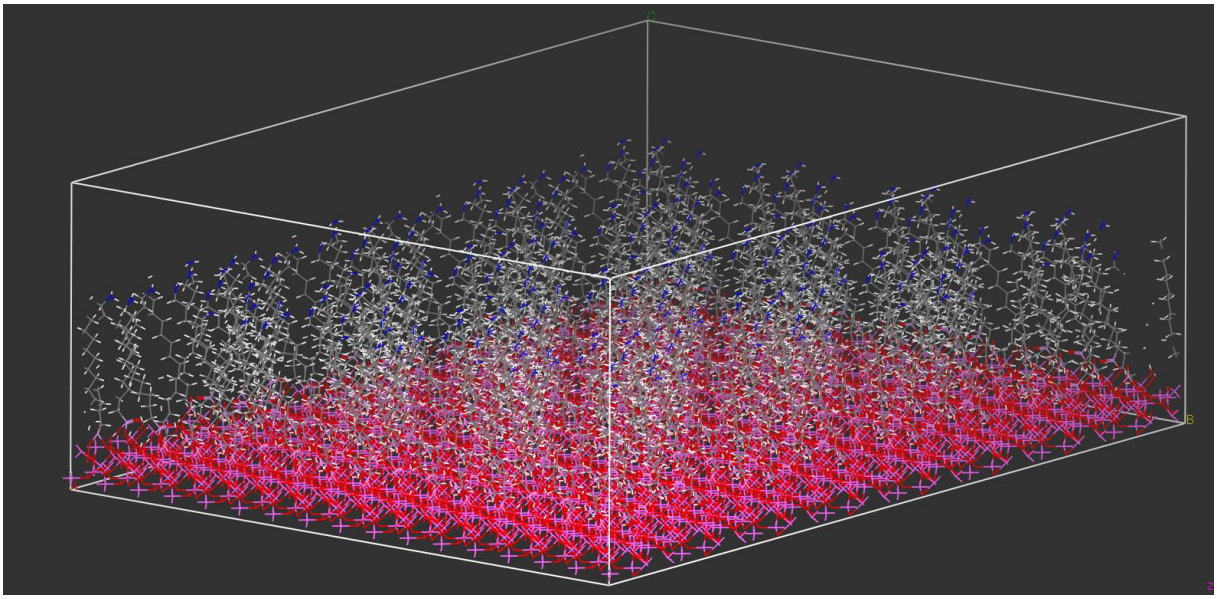

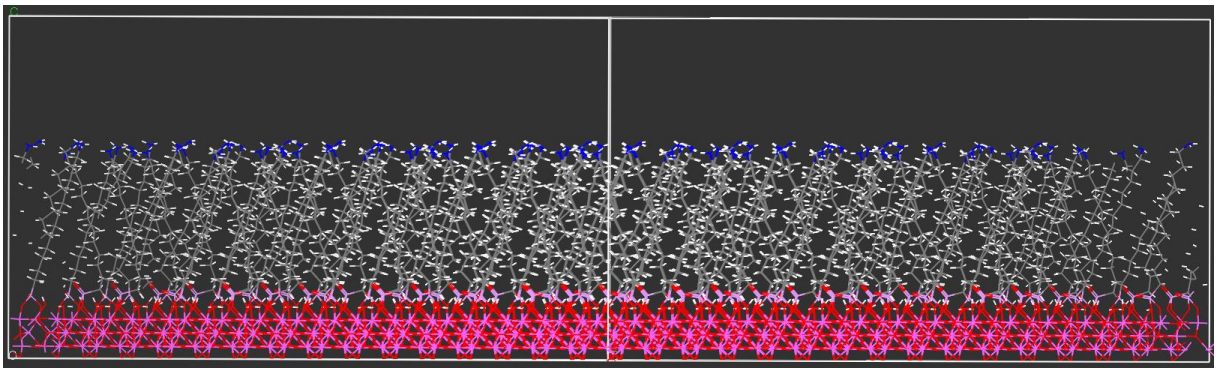

7.5 Plot of energies of various coverages plotted (kcal/mol) vs percentage monolayer coverage (%).

% Coverage	Packing energy (kcal/mol)
78.1	23.61
65.6	-3.34
50.0	-7.75
37.5	-4.81
25.0	-4.78

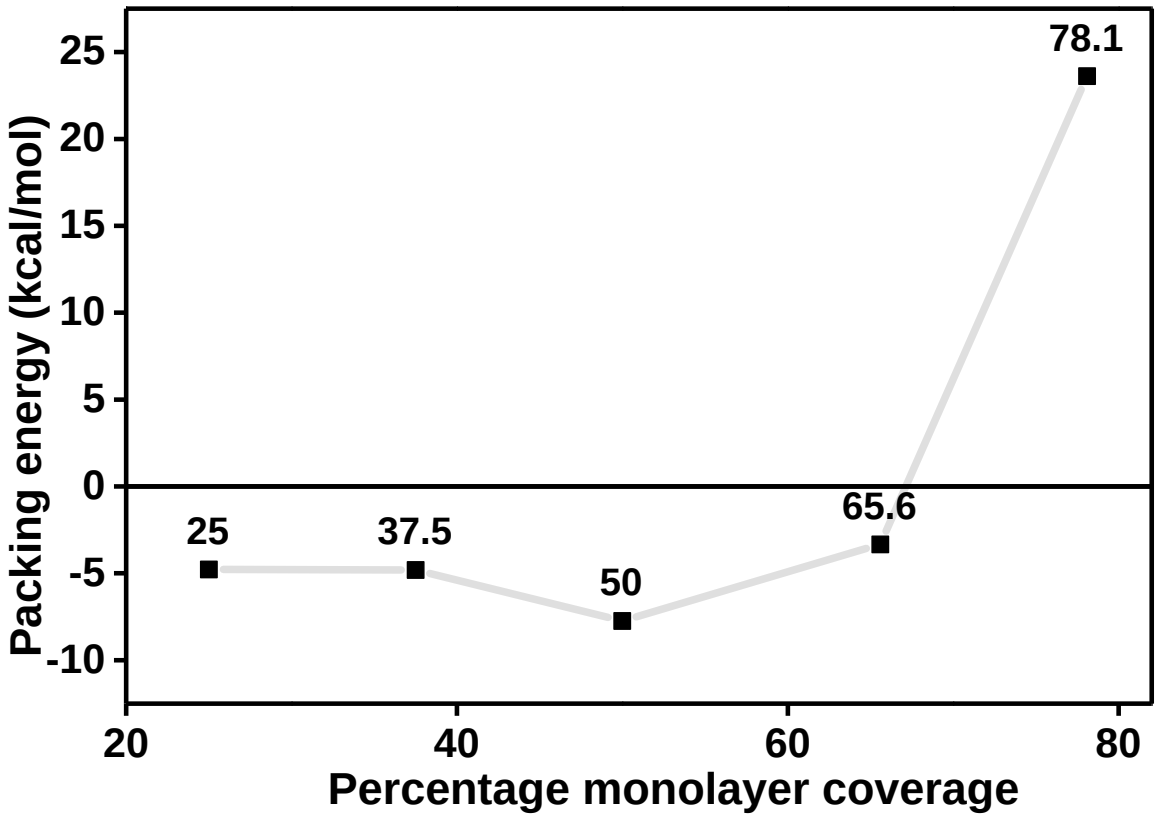

7.6 Scheme for Link–UPy attachment in a 8×16 cell (on 50% monolayer coverage).

37.5%

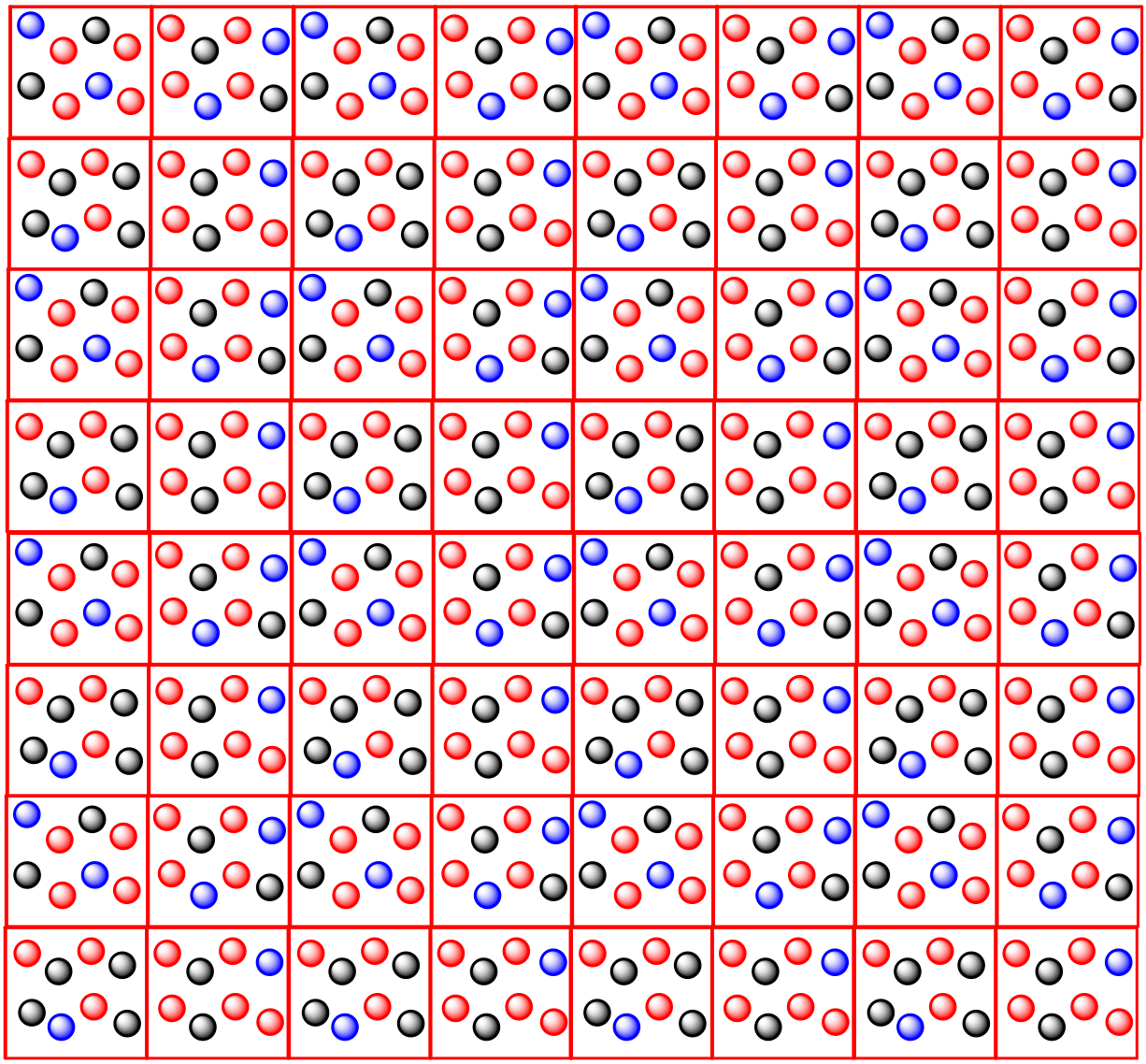

62.5%

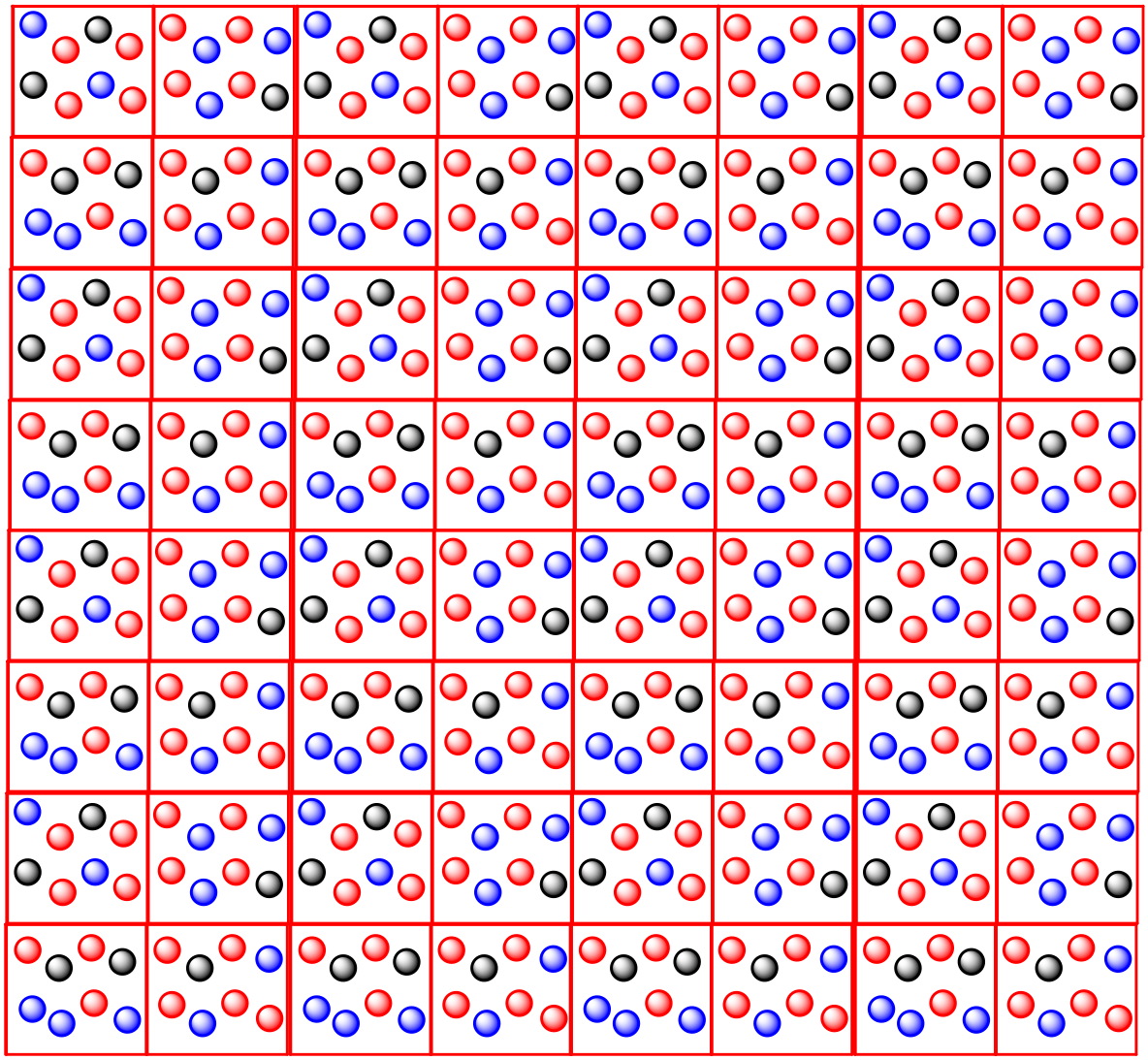

= Amine termination

= No monolayer

= Hex UPy

7.7 Representative images for initial 62% Link–UPy attachment in a 8×16 cell (on 50% monolayer coverage).

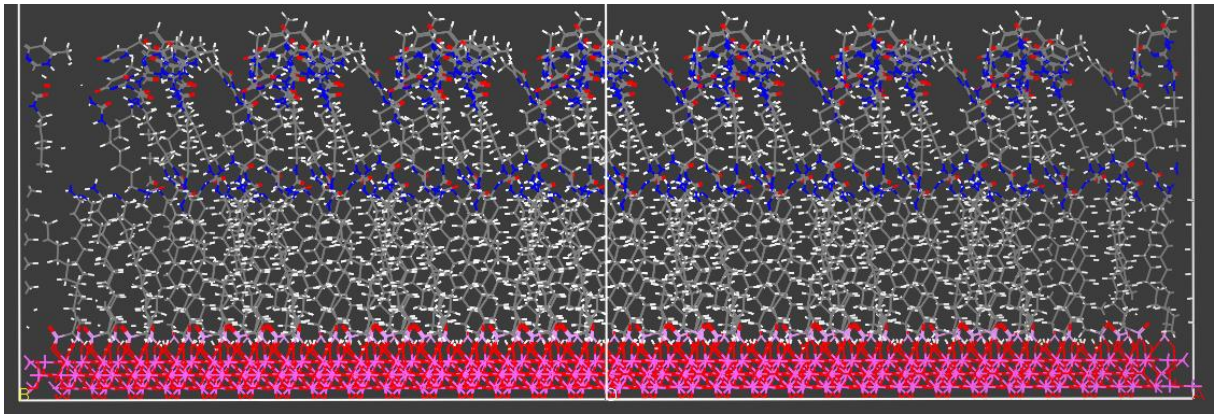

7.8 Molecular modelling (MM) results using Forcite module (NVT ensemble, PCFF) on Link–UPy attachment on aluminum surface (62% coverage). Extensive H-bonding between adjacent surface-bound UPy moieties can be seen.

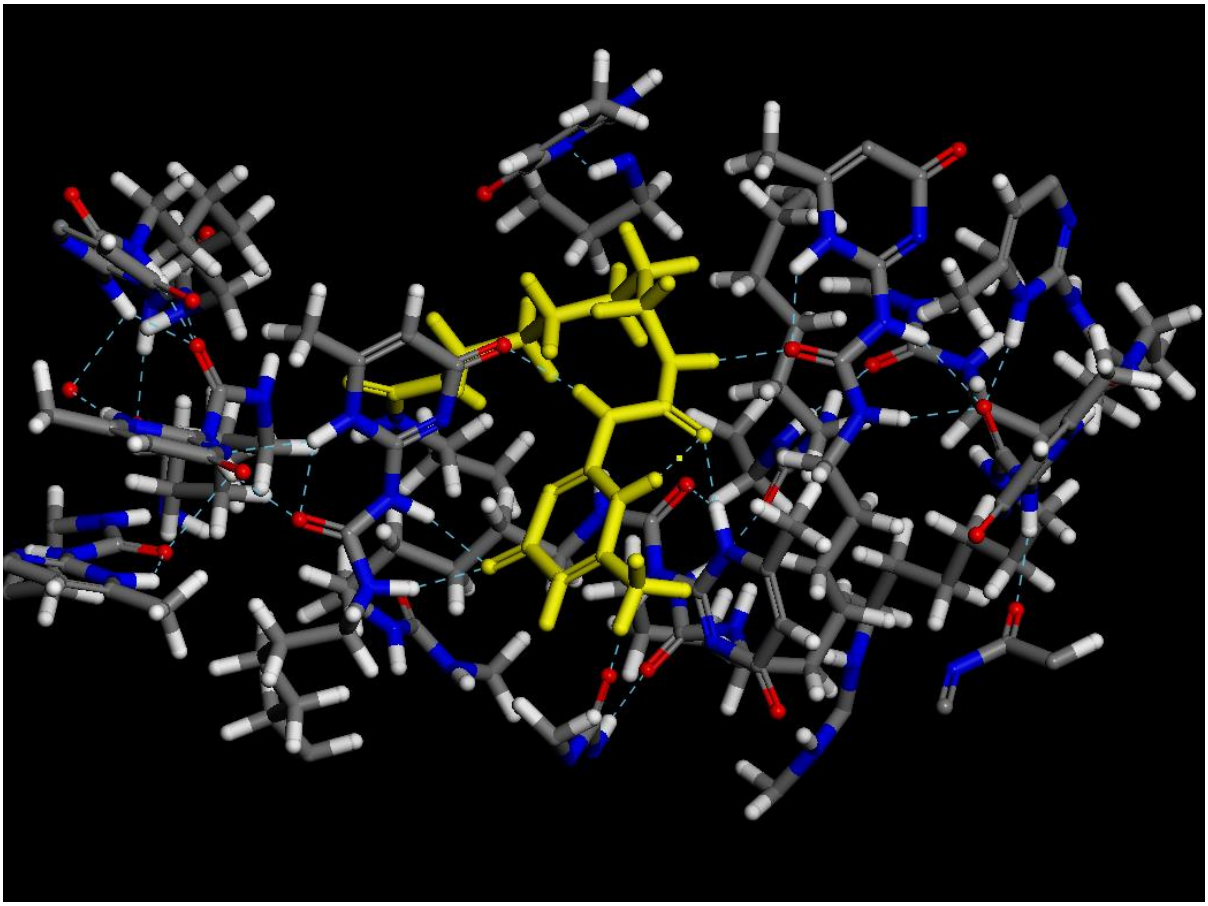

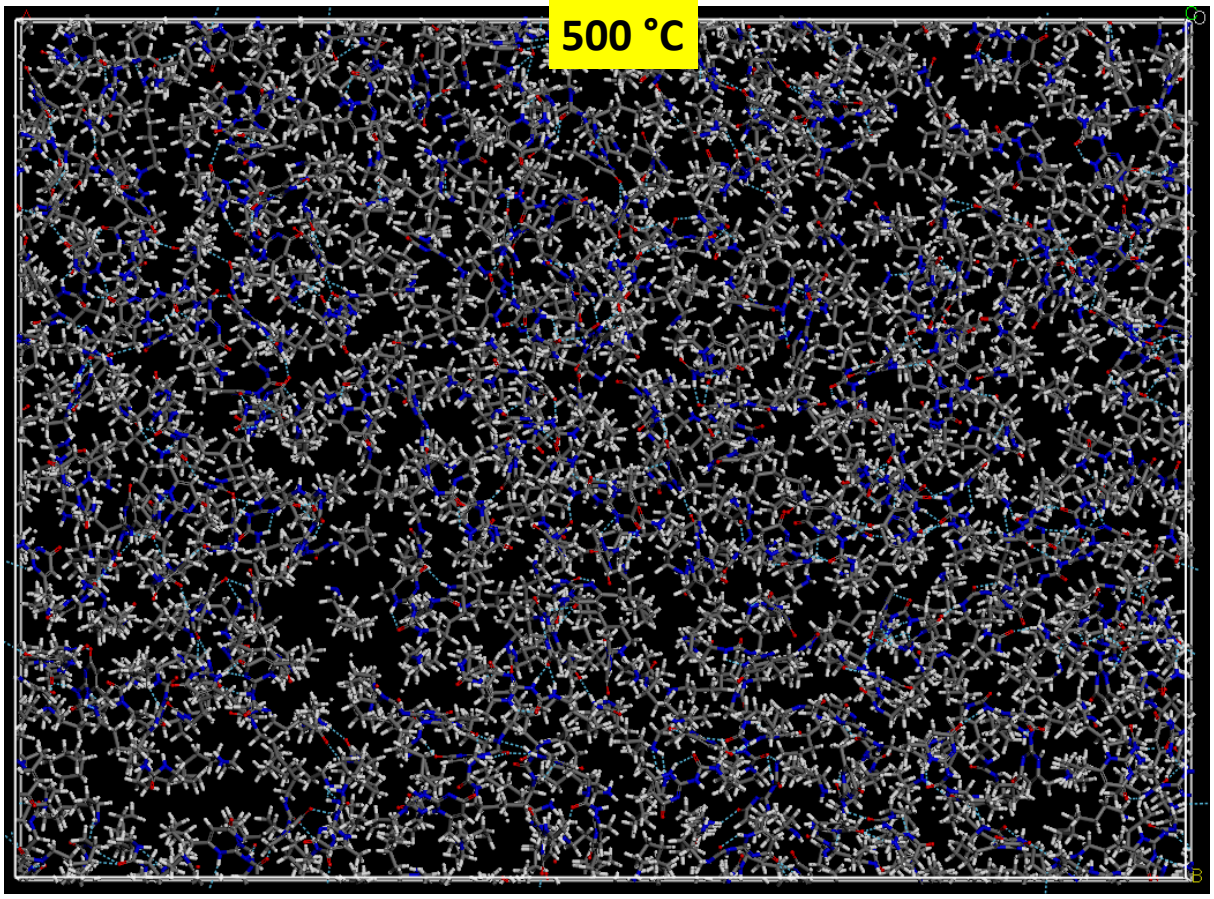
500 °C

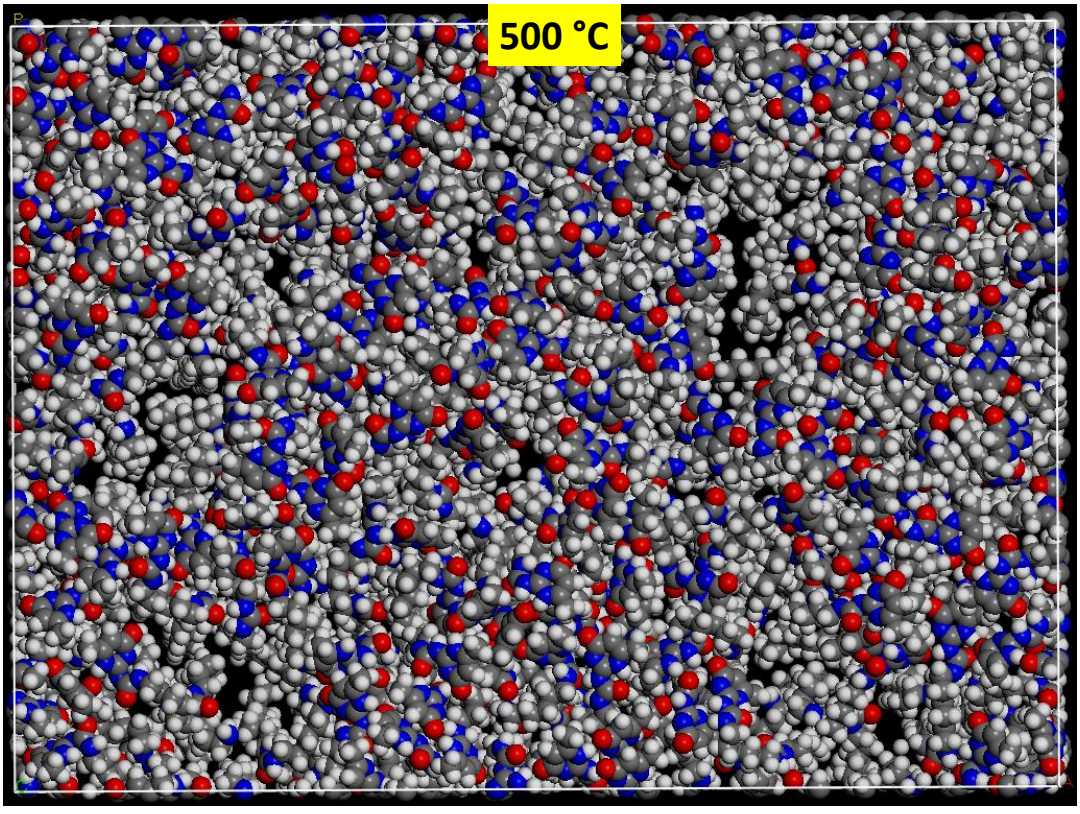
500 °C

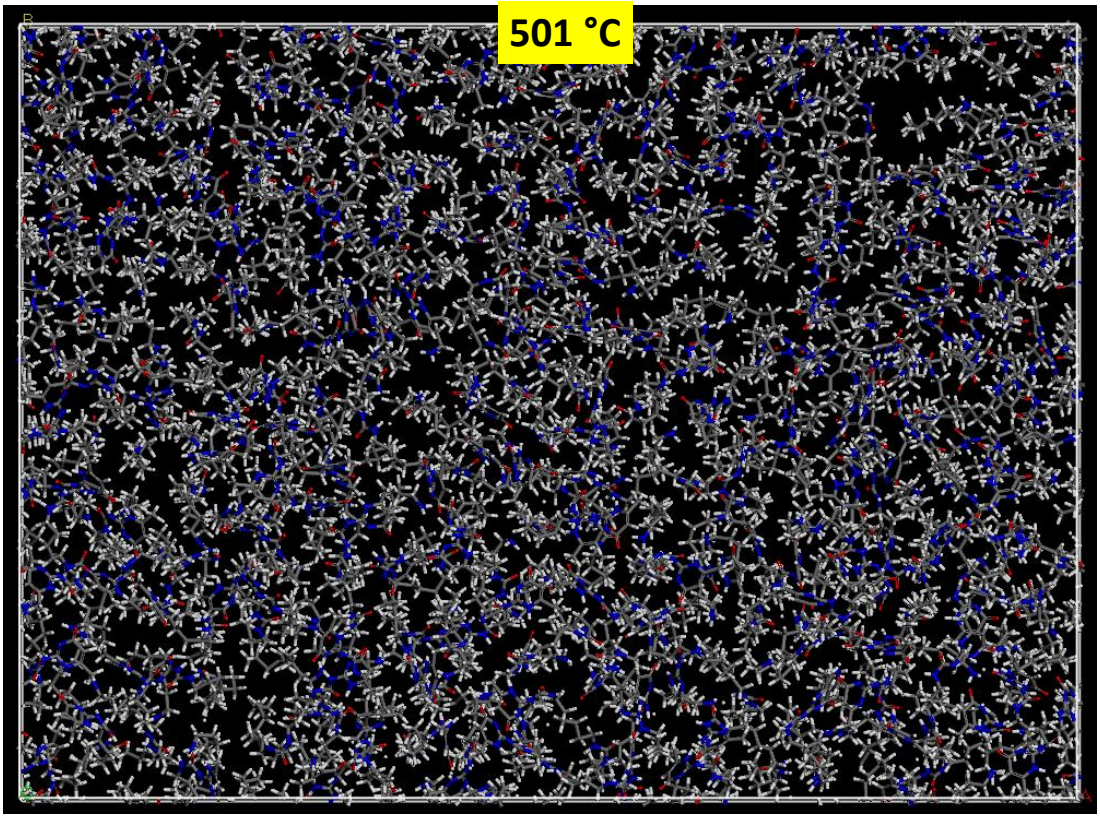
501 °C

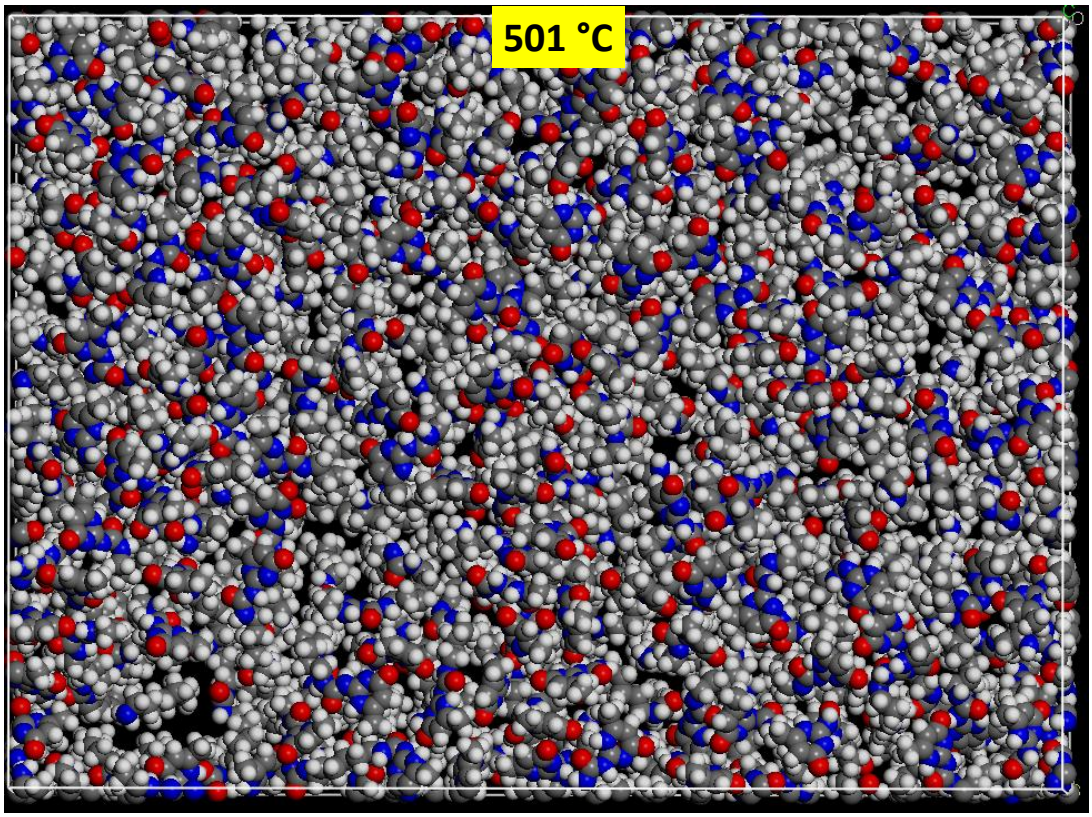
501 °C

8. REFERENCES

S1. J. Cui and A. d. Campo, *Chem. Commun.*, **2012**, *48*, 9302.

S2. P. A. Delgado and M. A. Hillmyer, *RSC Advances*, **2014**, *4*, 13266.

S3. X.-L. Yue, H. Li, S.-S. Liu, Q.-Y. Zhang, J.-J. Yao and F.-Y. Wang, *Chin. Chem. Lett.*, **2014**, *25*, 1069.

APPENDIX 4

Facile functionalization of peptide nucleic acids (PNAs) for antisense and single nucleotide polymorphism detection

1. MATERIAL AND METHODS

Materials. Unless otherwise specified, all chemicals were used as received without further purification. 2-Mercaptobenzothiazole, methyl iodide (MeI), propargyl bromide, lepidine, sodium hydride (NaH), tris[(1-benzyl-1H-1,2,3-triazol-4-yl)methyl]amine (TBTA), dimethylformamide (DMF), ethanol (EtOH), acetonitrile (MeCN), copper(I) iodide (CuI), diisopropylethylamine (DIPEA), trifluoroacetic acid (TFA), triisopropylsilane (TIS), dichloromethane (DCM), *N*-methylpyrrolidone (NMP) piperidine, lutidine and acetic anhydride were purchased from Sigma-Aldrich. Peptide nucleic acid monomers (Fmoc-PNA-A(Bhoc)-OH, Fmoc-PNA-G(Bhoc)-OH, Fmoc-PNA-C(Bhoc)-OH and Fmoc-PNA-T-OH) were purchased from Link Technologies. Azido D-Orn (N_3-D-Orn(Fmoc)-OH) Iris Biotech GmbH. Fmoc–glycine (Fmoc-Gly-OH) Cambridge Research Biochemicals. Ethyl cyano(hydroxyimino) acetate (Oxyma) and *N*,*N*'-diisopropylcarbodiimide (DIC)) were purchased from Merck-Millipore. Rink Amide ChemMatrix® resin, 0.47 mmol/g was purchased from Biotage. Unless stated otherwise, all non–aqueous reactions were performed in dried glassware under an atmosphere of argon. All flasks were equipped with rubber septa and reactants were handled using standard Schlenk techniques. Temperatures above the room temperature refer to oil bath temperatures which were controlled by a thermostat. Reactions were magnetically stirred. Water was purified with a Milli-Q® Ultra Pure Water Purification System (Millipore Corp.).

Methods. ^{1}H-NMR spectra were recorded at room temperature on a Bruker AVB-400 spectrometer with ^{1}H operating frequency of 400 MHz. Unless stated otherwise all spectra were recorded at room temperature in $CDCl_3$, DMSO-d_6 and D_2O and all chemical shifts are given in δ units relative to the residual solvent [central line of singlet: δ_H = 7.27 ppm ($CDCl_3$), 4.79 ppm (D_2O) and 2.50ppm (DMSO-d_6)]. Analysis followed first order and the following abbreviations were used throughout: s = singlet, br. s. = broad singlet, d = doublet, t = triplet, q = quartet, quin = quintet, sxt = sextet, sept = spt, dd = doublet of doublet, dt = doublet of triplet, m = multiplet, mc = centred multiplet.

Coupling constants (*J*) are given in Hertz (Hz). ^{13}C-NMR spectra were recorded at room temperature on a Bruker AVB-400 spectrometer with ^{13}C operating frequency of 101 MHz. Unless stated otherwise all spectra were recorded at room temperature in $CDCl_3$, D_2O, and DMSO-d_6 and all chemical shifts are given in δ units relative to the residual solvent [central line of triplet: δ_C = 77.0 ppm ($CDCl_3$) and heptet δ_C = 39.52 ppm (DMSO-d_6)]. The following abbreviation was used throughout: s = singlet, d = doublet, dd = doublet of doublet. If no coupling constants are given, the multiplicity refers to ^{1}H-decoupled spectra.

HPLC was performed with an Agilent 1220 series instrument using a Reprosil gold 300-C_{18} column (5 µm, 250 × 3 mm) for analytical runs and a XTerra prep MS-C_{18} column (5 µm, 100 × 7.8 mm) for semi-preparative runs at 55 °C. Eluents analytical: A (0.1% TFA in water) and B (0.1% TFA in MeCN) were used in a linear gradient with a flow rate of 0.5 mL/min for analytical and 2 mL/min for semi preparative HPLC. Gradient A: 5% B for 5 min, 5→70% B in 25 min. High resolution mass spectra were measured with a Exactive orbitrap high-resolution mass spectrometer (Thermo Fisher Scientific, San Jose, CA, USA), using Thermo Scientific Xcalibur software (V2.1.0.1139) for data acquisition and processing (ESI+). Determination of yields: Purified PNA was dissolved in 500 µL of water. An aliquot of 5 µL was diluted to 1 mL and the optical density was measured at 260 nm by using a quartz cuvette with a 10–mm path length. The sample concentration was calculated by using oligo calculation at www.idtdna.com and approximating ε = 9400 L.mol^{-1} for thiazole orange, *i.e.* ε_{260}(TO) ≈ ε_{260}(thymine).[S1]

2. GENERAL SYNTHESIS

2.1 Synthesis of 1

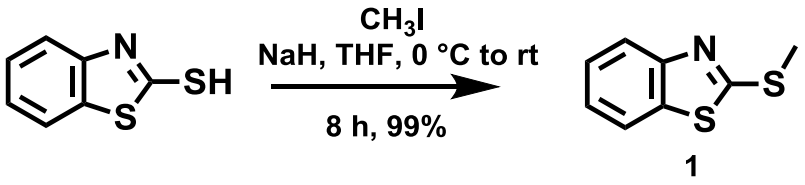

A solution of 2–mercaptobenzothiazole (2 g, 12 mmol, 1.0 equiv) in THF (5 mL) was cooled to 0 °C and NaH (60% in min. oil) (0.53 g, 13.2 mmol, 1.1 equiv) was added in portions. The resulting solution was stirred at 0 °C for 30 min, following which methyl iodide (0.9 mL, 14.4 mmol, 1.2 equiv) was added dropwise. The cooling bath was removed and the resulting mixture was allowed to warm to room temperature and stirred for a further 8 h. Saturated aqueous NH_4Cl (20 mL) was added and resulting layers were separated. The aqueous layer was extracted with ethyl acetate (3 × 20 mL) and the combined organic layers were washed with brine (50 mL), dried over $MgSO_4$, filtered and the solvents were removed under reduced pressure. The residue was purified by flash column chromatography yielding the desired sulfide 1 as a white solid (2.14 g, 99% yield). ^1H NMR spectrum was found to be in accordance with literature values.[S2]

2.2 Synthesis of 2

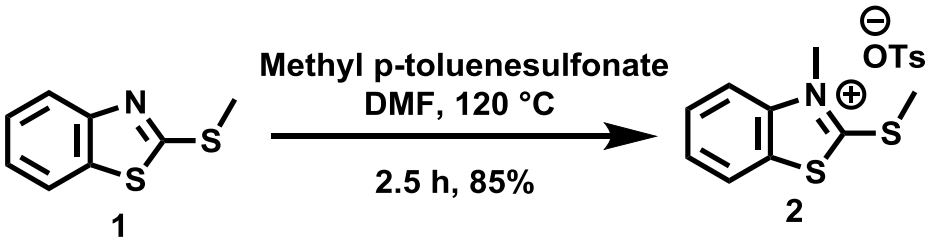

To a stirred solution of 1 (1 g, 5.5 mmol, 1 equiv) in DMF (5 mL) was added methyl *p*-toluenesulfonate (1.2 mL, 8.25 mmol, 1.5 equiv) followed by stirring at 120 °C for 2.5 h. After cooling to room temperature, acetone (10 mL) was added which led to

formation of a white precipitate. The precipitate was washed with acetone and dried overnight to yield a white solid 1 (1.7 g, 85% yield). ^{1}H NMR spectrum was found to be in accordance with literature values.[S3]

2.3 Synthesis of 3

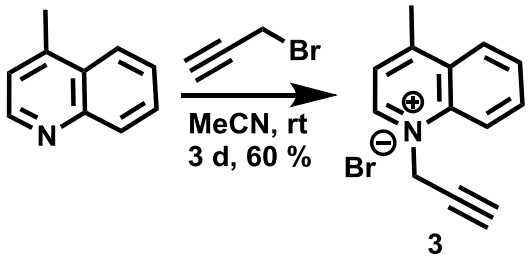

A solution of lepidine (1 g, 7.0 mmol, 1 equiv) and propargyl bromide (80 wt% in toluene) (1.1 mL, 3.75 mmol, 10.5 equiv) in MeCN (8 mL) was stirred for 3 days at room temperature. The resulting light-gray precipitate was collected by filtration, washed with acetone and dried to afford the desired product as a solid 3 (1.1 mg, 60%). ^{1}H NMR spectrum was found to be in accordance with literature values.[S4]

2.4 Synthesis of alkyne–TO, 4

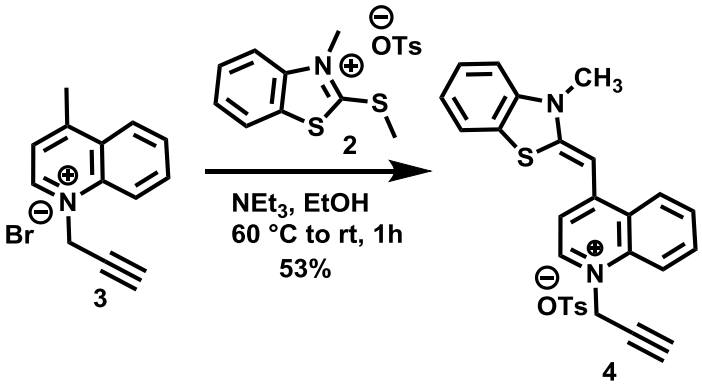

Compound 3 (0.5 g, 1.9 mmol, 1 equiv) and compound 4 (0.7 g, 1.9 mmol, 1 equiv) were suspended in anhydrous ethanol (5 mL) and dissolved by heating at 60 °C for 10 min. Following this, triethylamine (0.3 mL, mmol, 2.09 mmol, 1.1 equiv) was added and the reaction was allowed to stir at room temperature for 1 h during which a red precipitate appeared. The precipitate was filtered off, washed with cold ethanol and

dried under vacuum to yield 4 as a red solid (0.5 g, 53% yield). ^{1}H NMR (400 MHz, DMSO-d_6) δ 8.74 (d, J = 8.3 Hz, 1H), 8.56 (d, J = 7.4 Hz, 1H), 8.08 – 7.90 (m, 3H), 7.75 (d, J = 8.3 Hz, 1H), 7.69 (t, J = 7.7 Hz, 1H), 7.57 (t, J = 7.4 Hz, 1H), 7.50 (d, J = 8.1 Hz, 2H), 7.38 (t, J = 7.6 Hz, 1H), 7.31 (d, J = 7.3 Hz, 1H), 7.11 (d, J = 7.9 Hz, 2H), 6.92 (s, 1H), 5.44 (s, 2H), 4.00 (s, 3H), 3.64 (s, 1H), 2.26 (s, 3H); ^{13}C NMR (101 MHz, DMSO-d_6) δ 161.53, 149.08, 146.33, 143.98, 140.89, 137.97, 137.17, 133.68, 128.76, 128.47, 127.34, 126.23, 125.96, 125.33, 124.65, 124.49, 123.42, 118.57, 113.84, 108.15, 89.49, 79.42, 77.59, 44.09, 34.54, 21.24.

2.5 PNA synthesis

The PNA sequences were prepared on a Biotage® Initiator+ Alstra™ microwave peptide synthesizer. The sequences were assembled automatically on Rink Amide ChemMatrix® resin (supplier Biotage, 0.47 mmol/g) on a 10 µmol scale in a 5 mL reactor vial using Fmoc chemistry under inert gas (N_2). Resin swelling 20 min at 70 °C. Fmoc deprotection was performed at room temperature (RT) in two stages by treating the resin with piperidine–NMP (1:4) for 3 min followed by piperidine–NMP (1:4) for 10 minutes. The resin was then washed with NMP (×4). PNA couplings were performed using 4 eq. of PNA monomer, 4 eq. oxyma and 4 eq. DIC in NMP. A coupling time of 6 min at 75 °C (microwave) was employed and the resin was washed with NMP (×4). This was followed by a capping step using NMP-lutidine-acetic anhydride (89:6:5) for 2 min and then washing with NMP (×4). After the synthesis was completed, the resin was washed with NMP (×5), DCM (×6) and thoroughly dried. The azido–PNA P1 was cleaved off the dried resin by reacting with TFA/TIS/H_2O (95:2.5:2.5, 1 mL) for 30 min and the cleavage solution was added to cold diethylether. The precipitate was collected by centrifugation and disposal of the supernatant followed by HPLC purification.

2.6 Click modification of azido-PNA on resin

The synthesis was performed by using a 5 mL polyethylene syringe reactor equipped with a fritted disc. The resin supported, azido-PNAs obtained as above were treated

with 4 (10 mM) in the presence of tris[(1-benzyl-1H-1,2,3-triazol-4-yl)methyl]amine (TBTA, 100 µM), copper(I) iodide (100 µM) in 3:1 (v/v) DMF:H_2O at room temperature overnight. The progress of the reaction was monitored by HPLC and ESI–HRMS after cleavage of a small portion of the PNA from the solid support. Upon reaction completion, the resin was washed with DMF (×3) and H_2O (×3) and thoroughly dried. The TO-PNA P3 was cleaved off the dried resin by reacting with TFA/TIS/H_2O (95:2.5:2.5, 1 mL) for 30 min and the cleavage solution was added to cold diethylether. The red precipitate was collected by centrifugation and disposal of the supernatant followed by HPLC purification.

2.7 Melting temperature determination: Melting experiments, fluorescence *vs*. temperature profiles, were measured on a Cary Eclipse fluorescence spectrophotometer (Varian). Melting temperatures were measured with 1:1 molar mixtures of PNA and the corresponding target DNA, each at a concentration of 4 µM, in a phosphate buffer (10 mM NaH_2PO_4, 100 mM NaCl, pH = 7.0), λ_{ex} = 650 nm and λ_{em} = 670 nm. The samples were heated to rapidly to 90 °C, left for 5 min and then allowed to cool to 20 °C. After equilibration for 10 min at the starting temperature, the dissociation was recorded by heating to 90 °C at a rate of 0.2 °C min^{-1}.

3. NMR SPECTRA

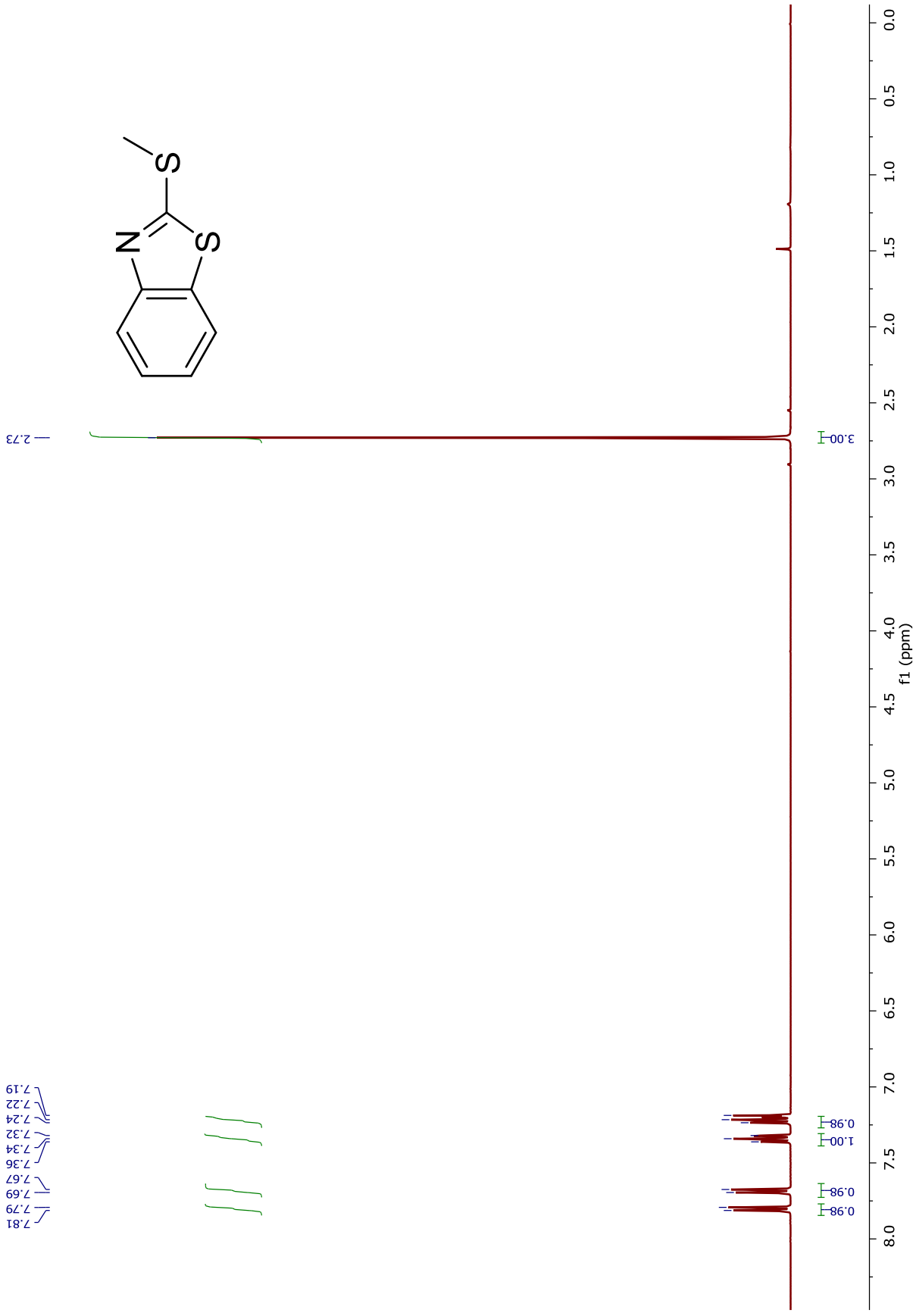

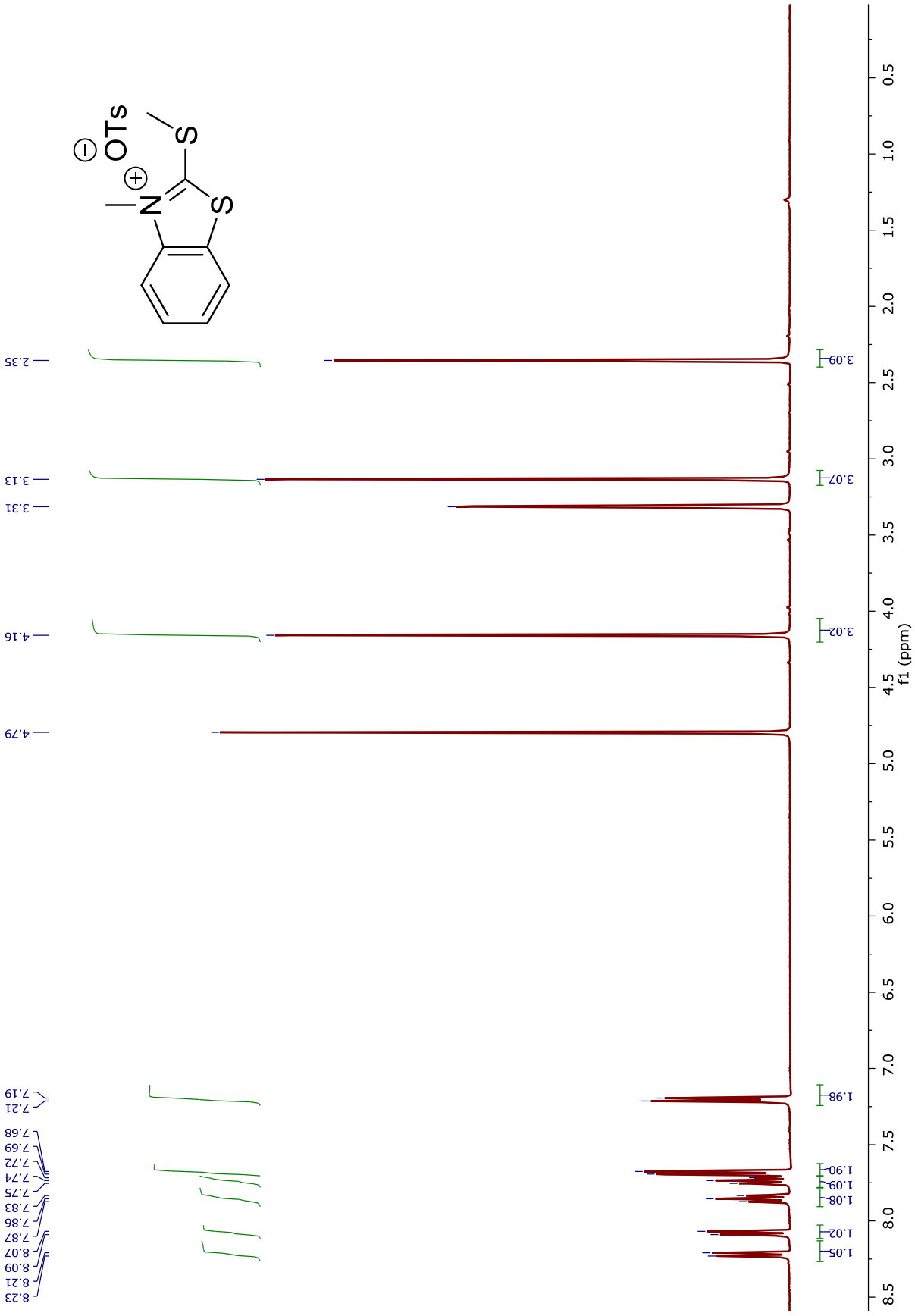
OTs
S
N
S
8.23
8.21
8.09
8.07
7.87
7.86
7.83
7.75
7.74
7.72
7.69
7.68
7.21
7.19
4.79
4.16
3.31
3.13
2.35
1.98
1.90
1.09
1.08
1.02
1.05
3.09
3.07
3.02
8.5
8.0
7.5
7.0
6.5
6.0
5.5
5.0
4.5
4.0
3.5
3.0
2.5
2.0
1.5
1.0
0.5
f1 (ppm)

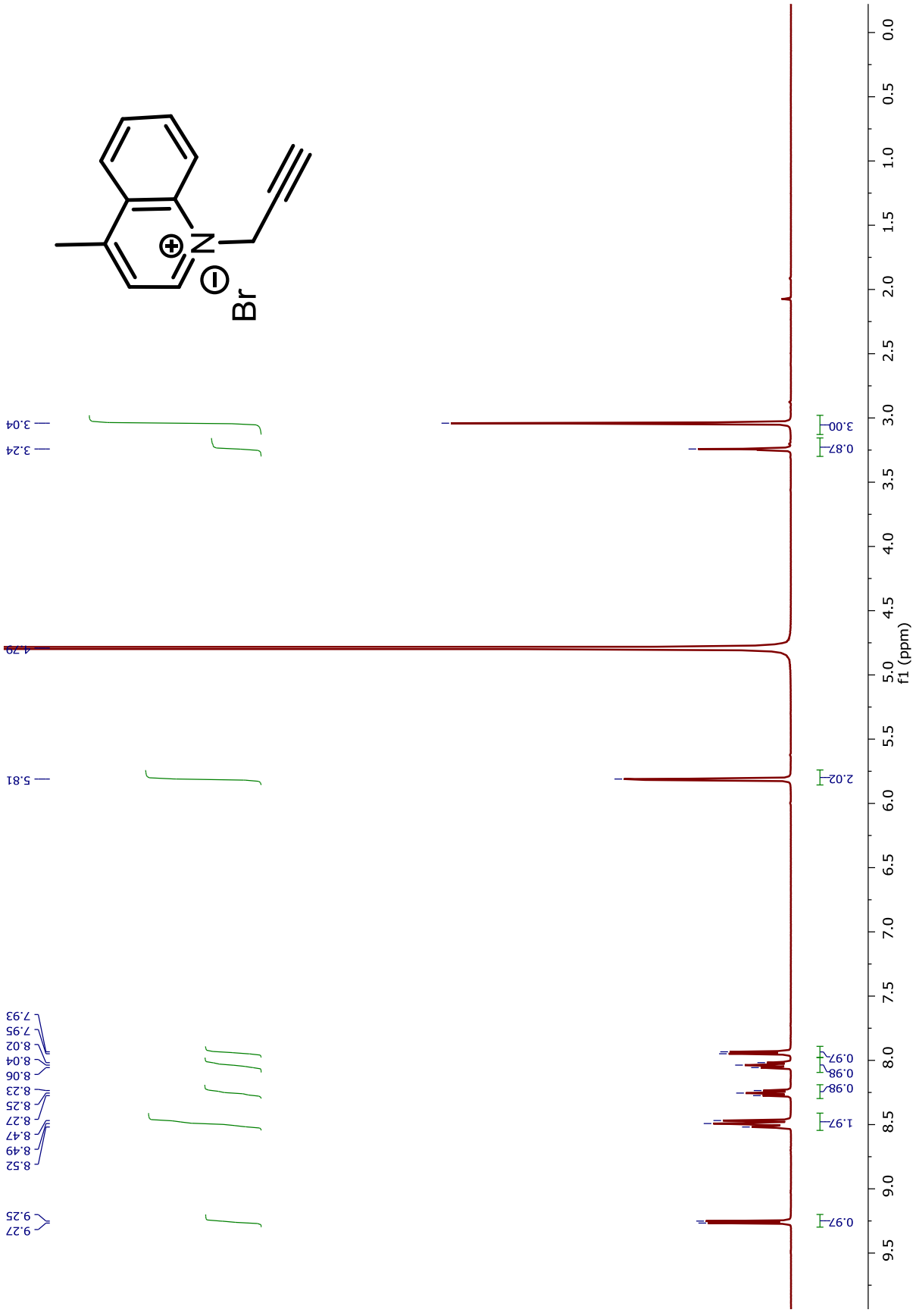
Br
f1 (ppm)

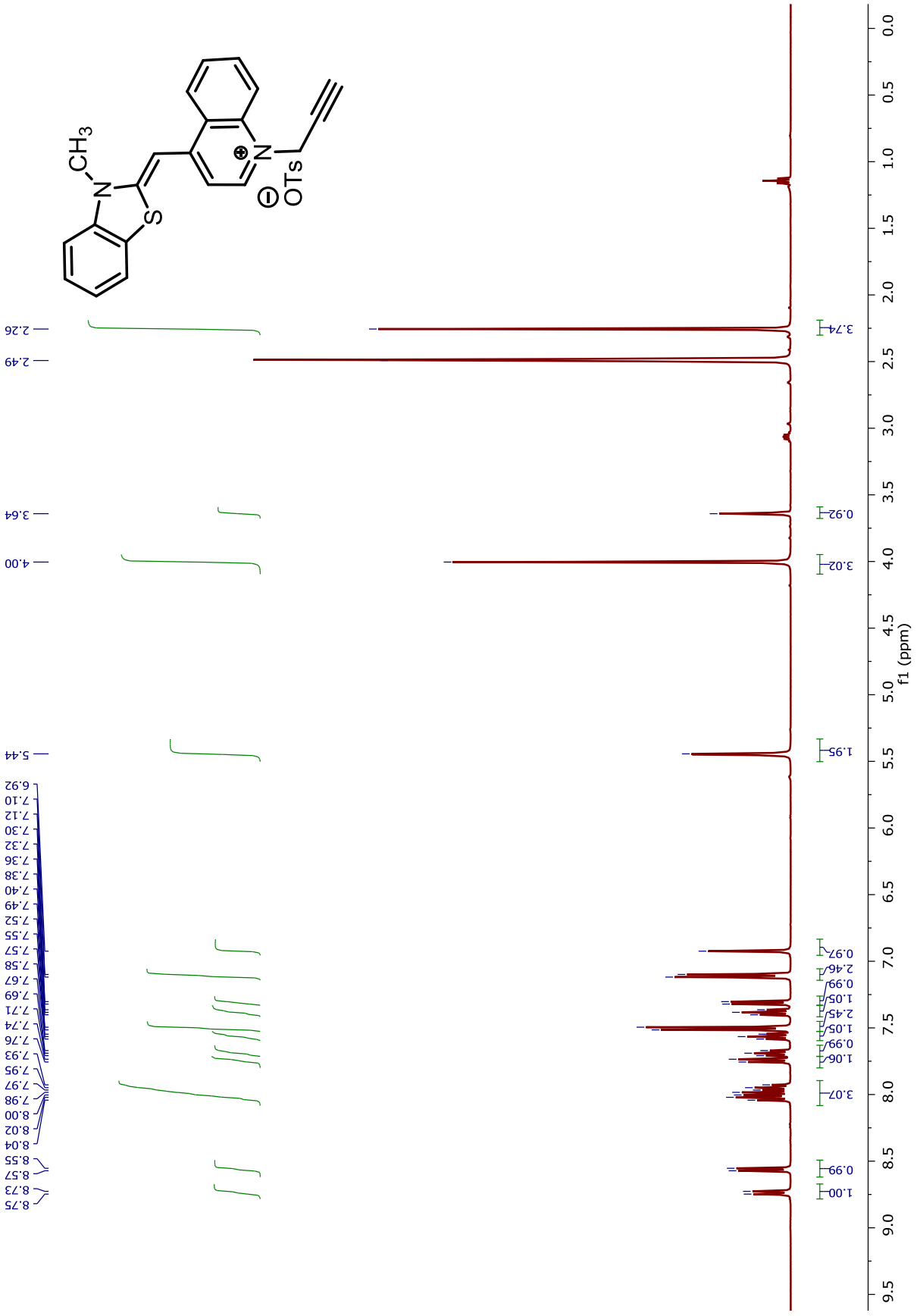
CH3
N
S
N
OTs
f1 (ppm)

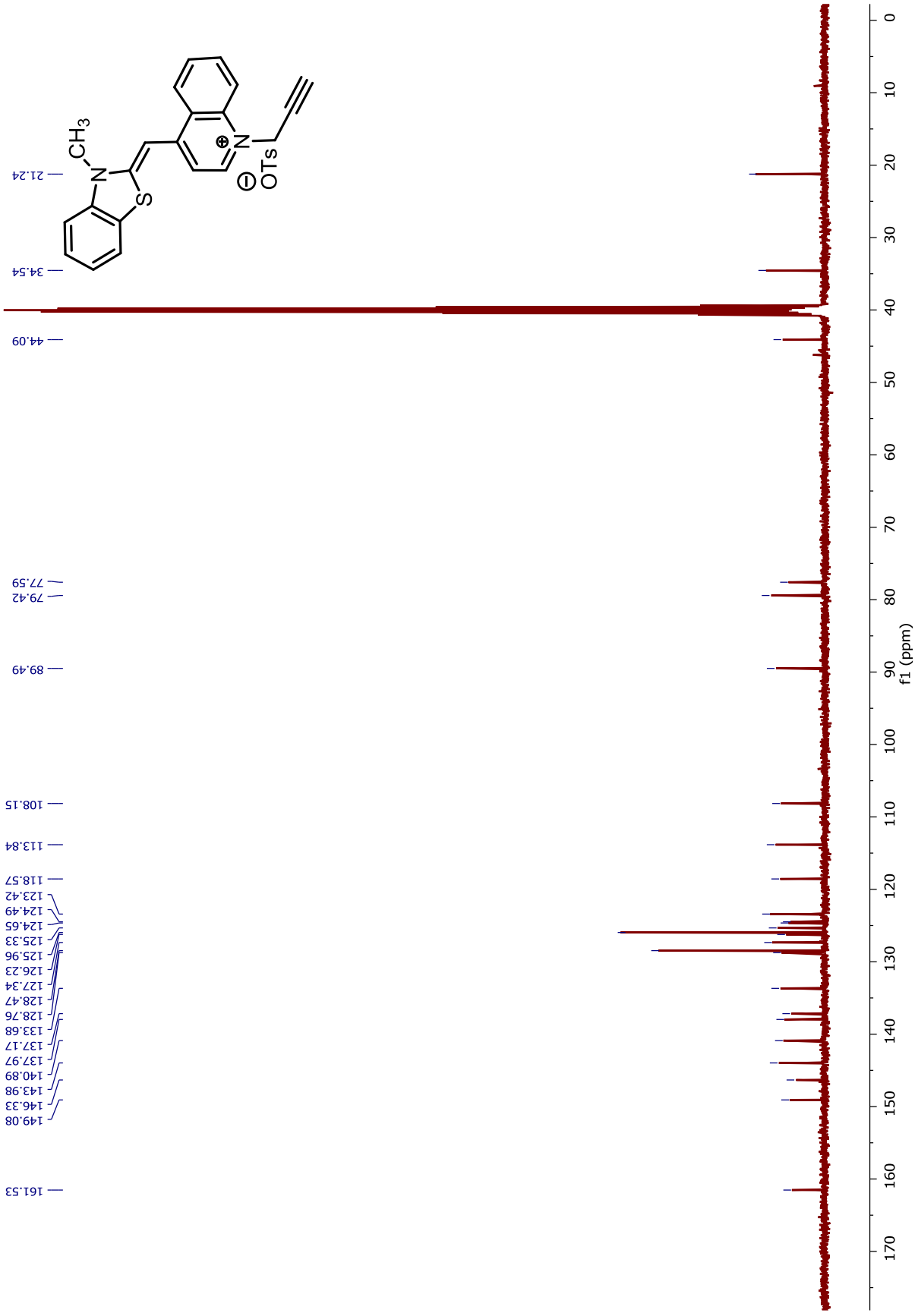
21.24
34.54
44.09
77.59
79.42
89.49
108.15
113.84
118.57
123.42
124.49
124.65
125.33
125.96
126.23
127.34
128.47
128.76
133.68
137.17
137.97
140.89
143.98
146.33
149.08
161.53
f1 (ppm)

4. SUPPORTING TABLE

Supplementary Table S1. Different PNA and DNA sequences used in the study.

PNA/DNA	Sequence
P1	Ac-Lys-taaagaaN_3agacgcc-Lys-NH_2
P3	Ac-Lys-taaagaaTOagacgcc-Lys-NH_2
P4	Ac-acacctaTOagcg-Gly-NH_2
D1	5′-Cy5-TTCTTTATGTTTTTGGCGTCT-3IAbRQSp-3′
D2	5′-AGACGCCAAAAACATAAAGAA-3′
D3	5′-AGACGCCAAAAACA-3′
D4	5′-AAAAACATAAAGAA-3′
D5	5′-CGCCAAAAACATAAA-3′
D6	5′-CGCTGTAGGTGT-3′
D7	5′-CGCTGCAGGTGT-3′
D8	5′-CGCTGGAGGTGT-3′
D9	5′-CGCTGAAGGTGT-3′

5. SUPPLEMENTARY FIGURES

Ac-Lys-taaagaaN_3agacgcc-Lys-NH_2

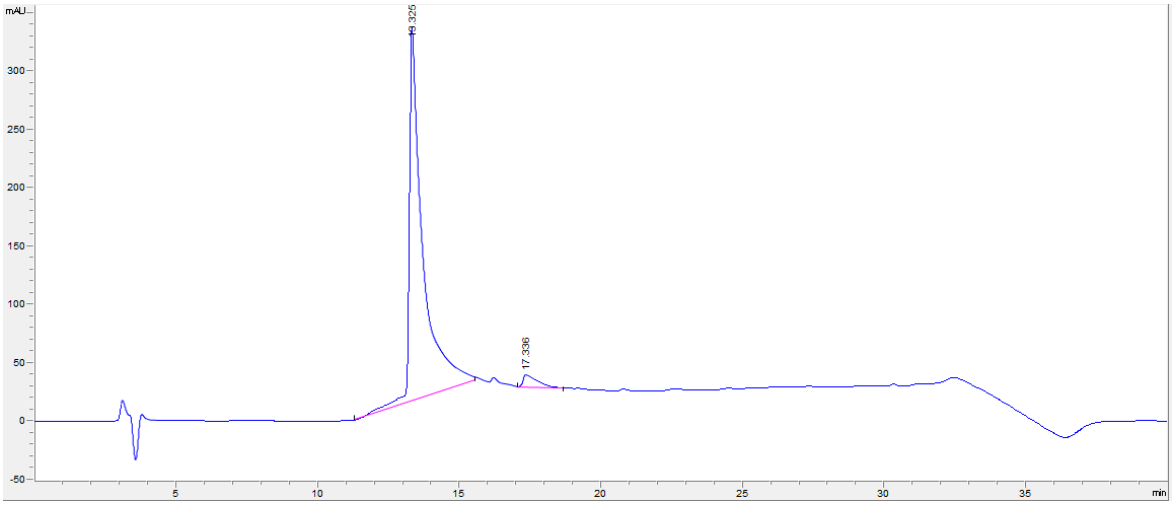

Figure S1. HPLC trace (Gradient A) of P1.

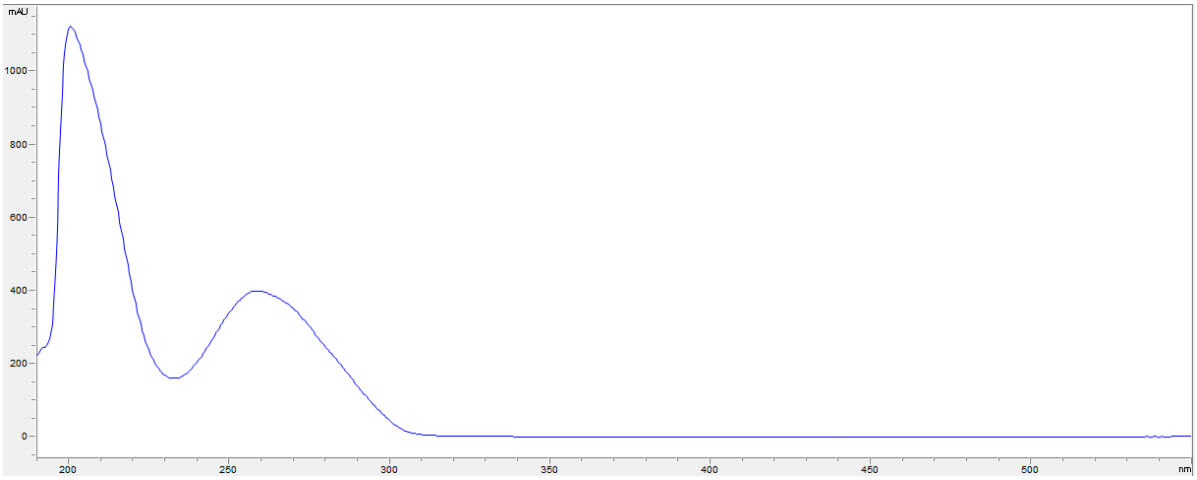

Figure S2. UV spectrum of peak at 13.3 min in the HPLC trace of P1.

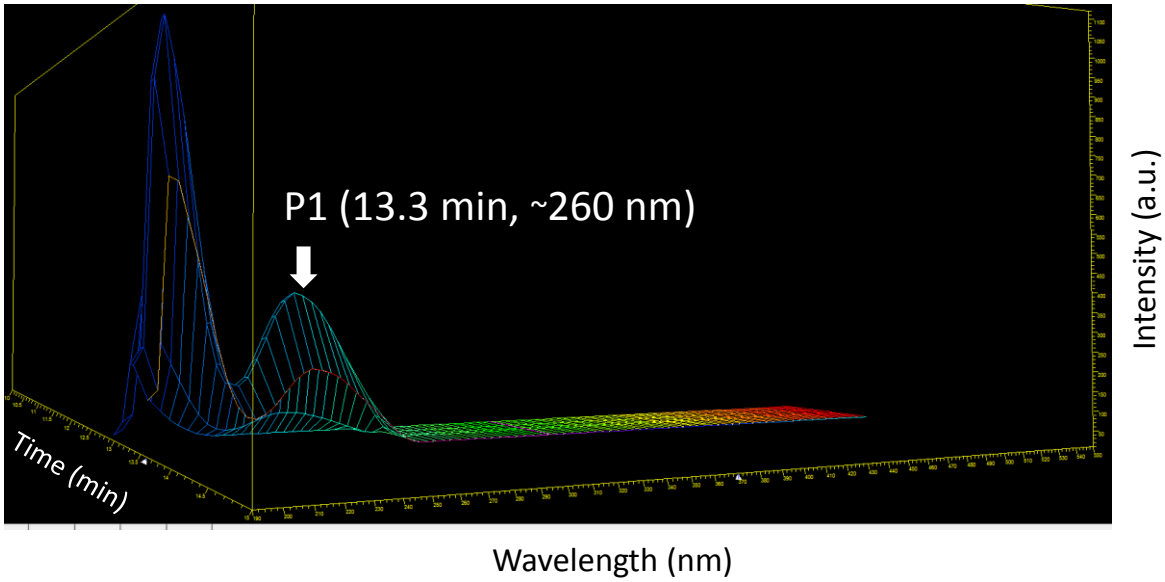

Figure S3. 3D plot (intensity *vs* retention time *vs* wavelength) of HPLC trace of P1.

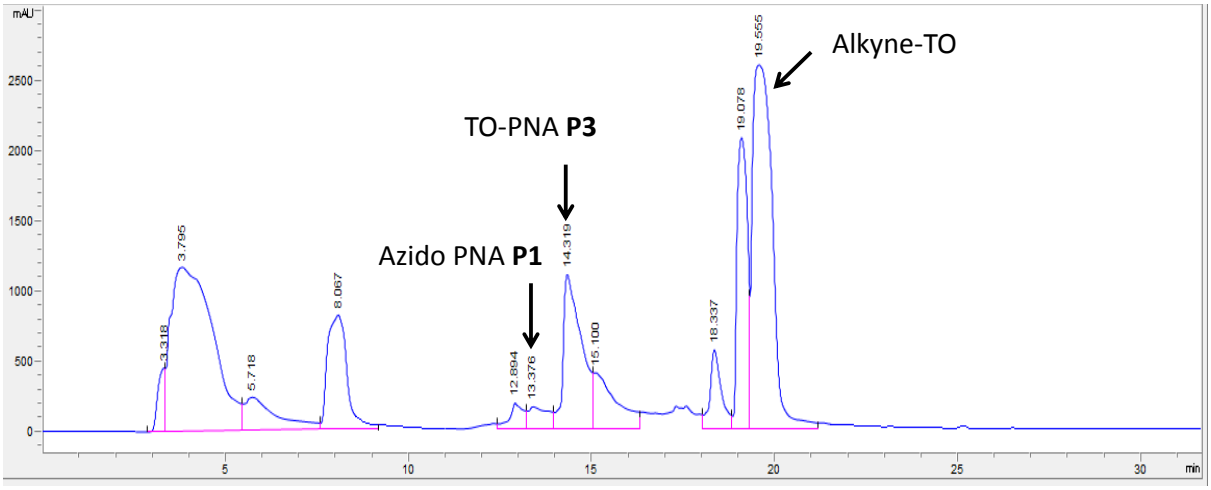

Figure S4. HPLC trace (Gradient A) of crude P3.

Ac-Lys-taaagaaTOagacgcc-Lys-NH_2

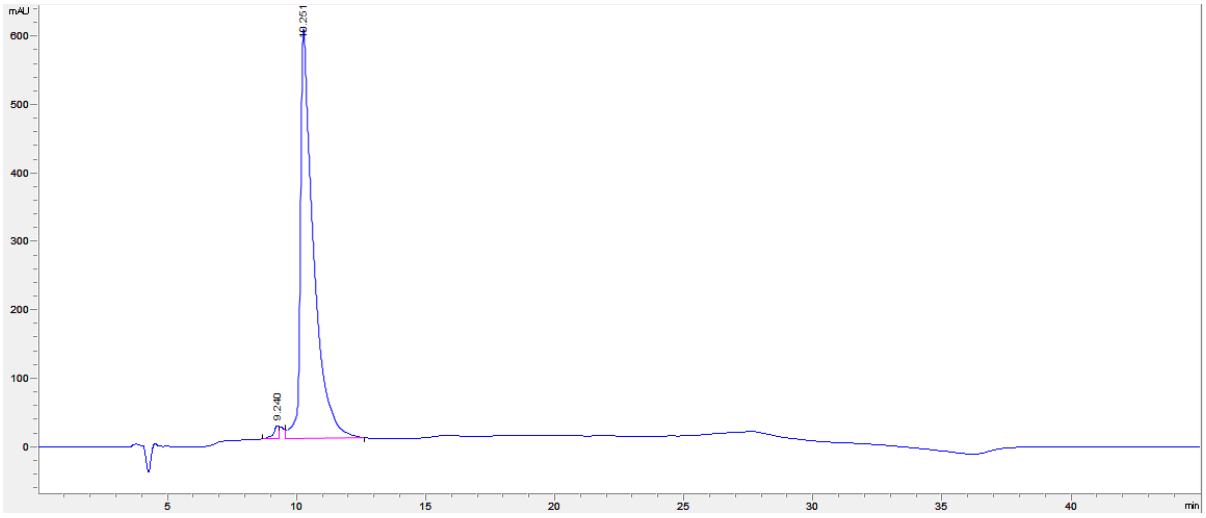

Figure S5. HPLC trace (Gradient A) of purified P3 during a semi-preparative run.

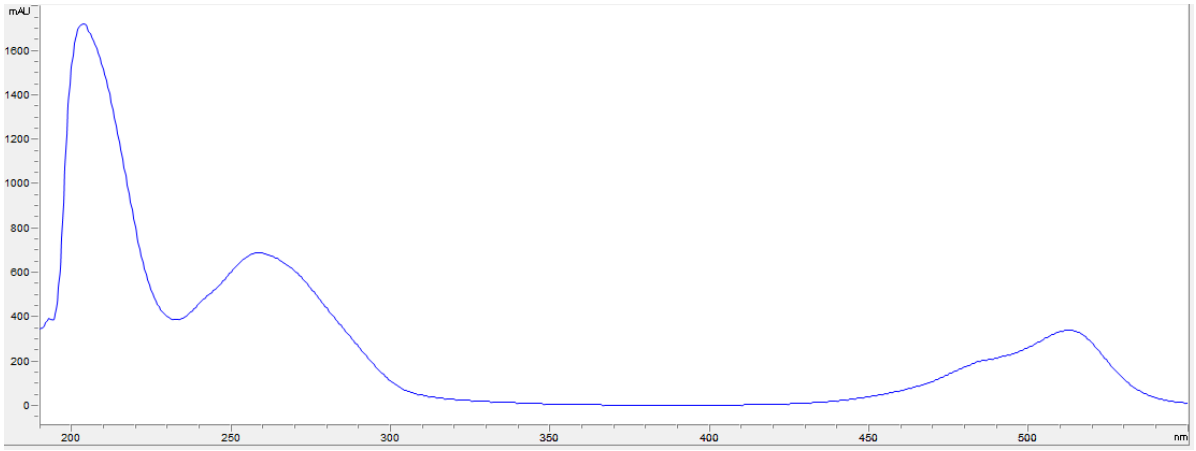

Figure S6. UV spectrum of the peak at 10.2 min in the HPLC trace of P3.

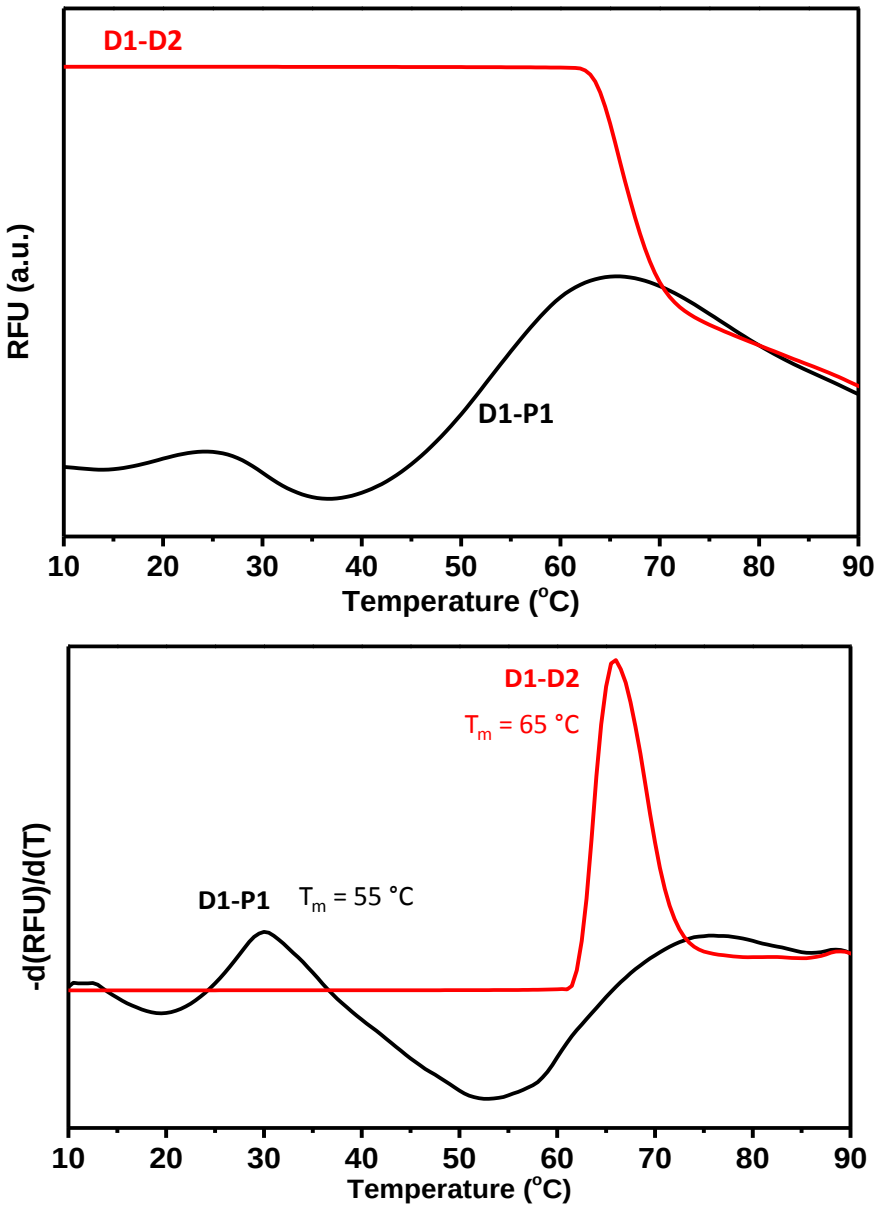

Figure S7. Melting temperature and derivative curves for D1-D2 and P1-D2 strands.

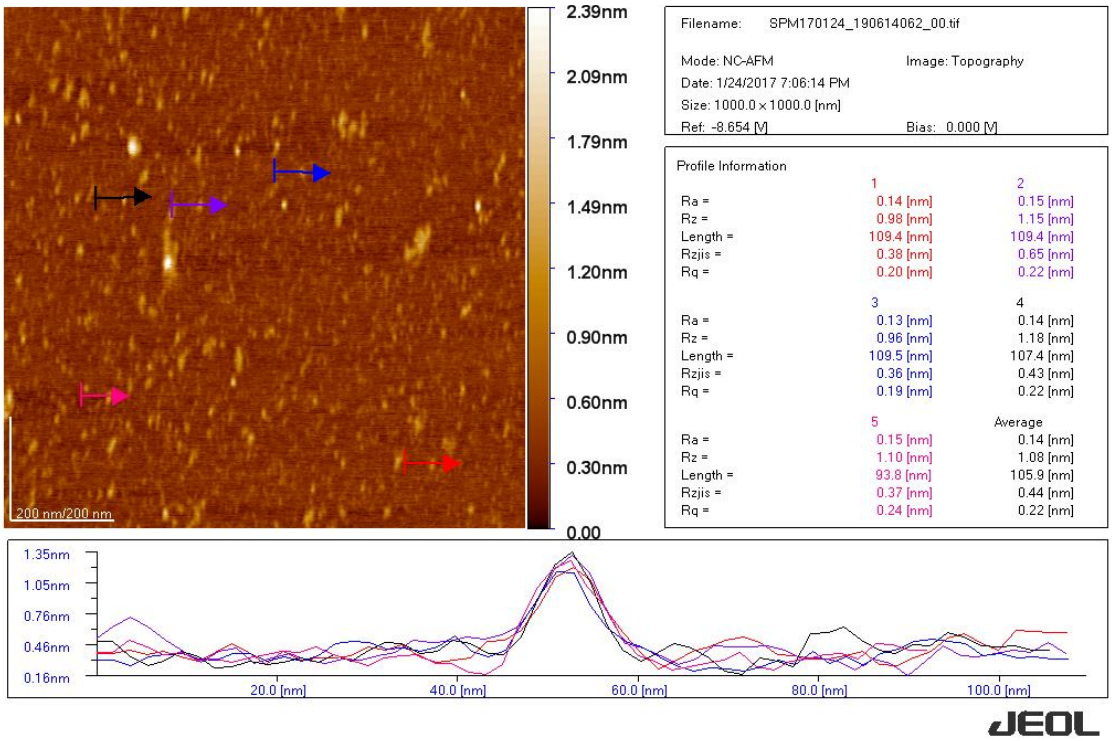

Figure S8. AFM height image of P1-D1 hybrid adsorbed on a mica surface.

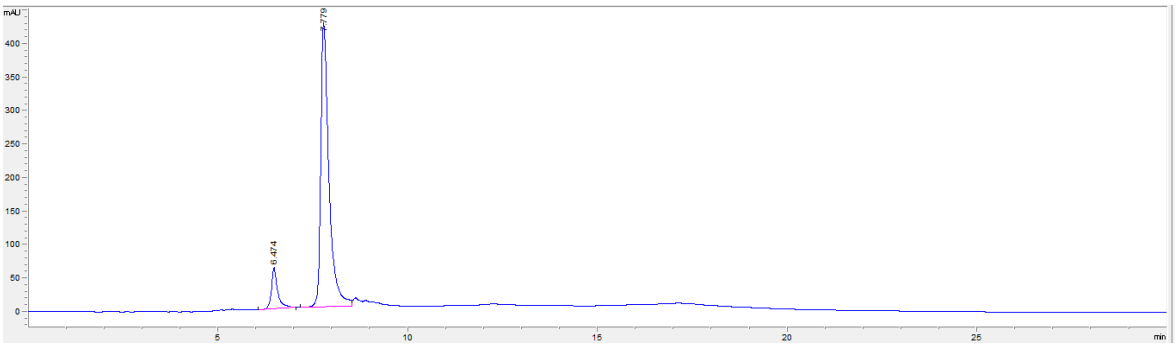

Figure S9. HPLC trace (Gradient A) of P4.

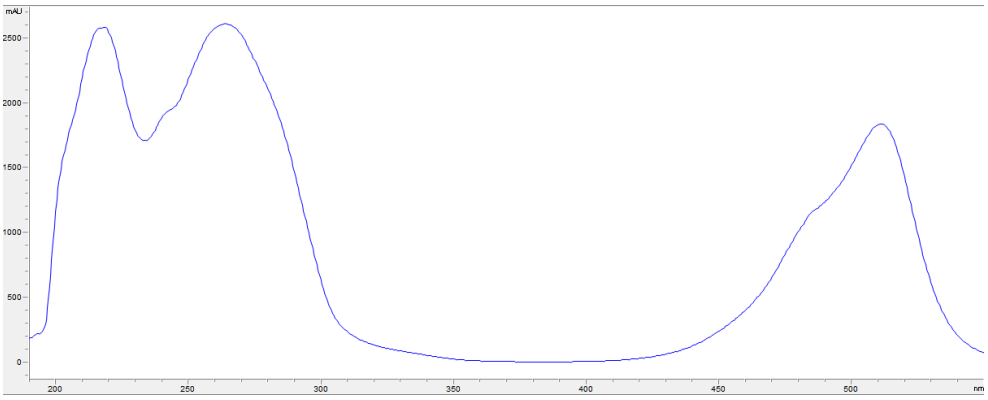

Figure S10. UV spectrum of the peak at 7.7 min in the HPLC trace of P4.

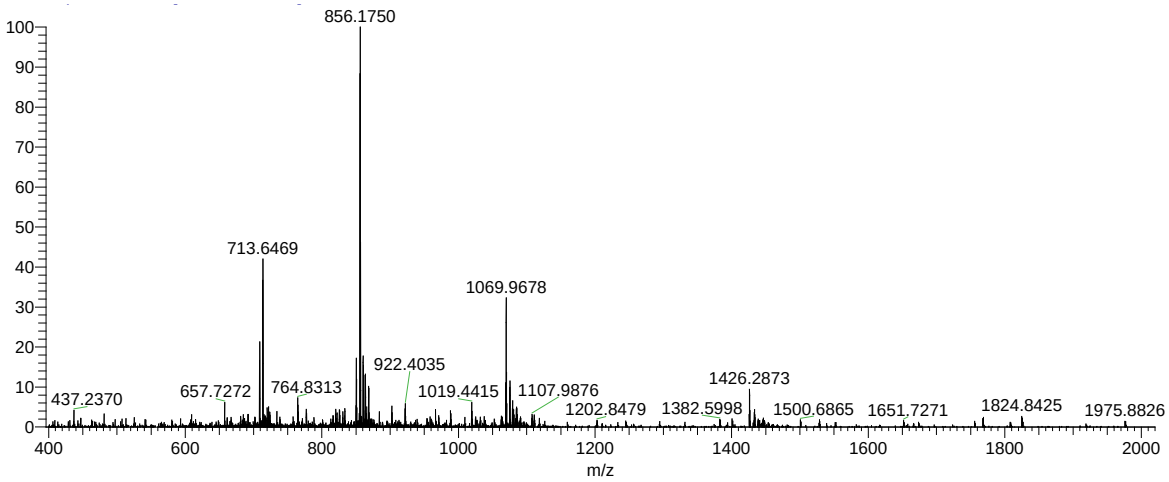

Figure S11. ESI–HRMS spectrum of P1 (*m/z* = 4276.20). Calculated *m/z*-values: for $[P1+4H]^{4+}$ = 1070.05, for $[P1+5H]^{5+}$ = 856.24, and for $[P1+6H]^{6+}$ = 713.70.

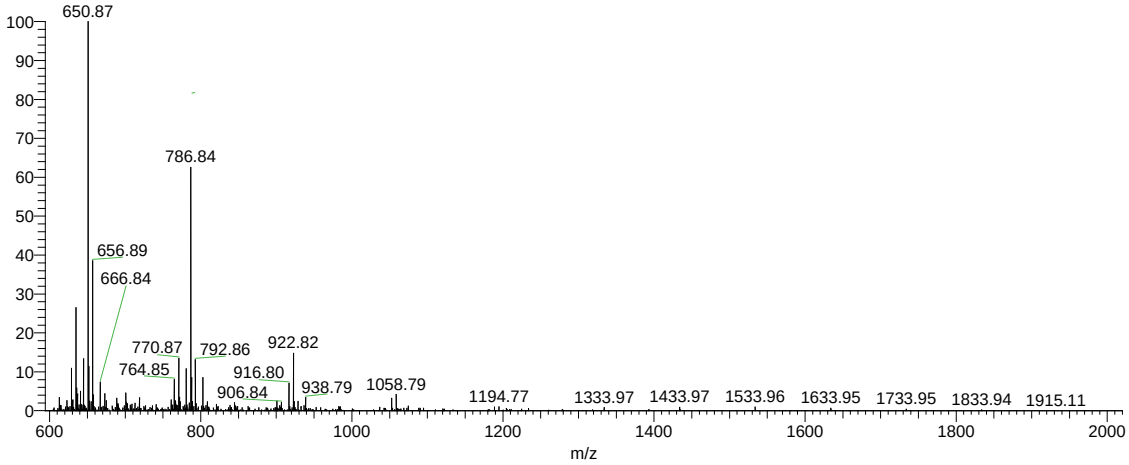

Figure S12. ESI–HRMS spectrum of P3 (*m/z* = 4605.64). Calculated *m/z*-values: for $[P3+5H]^{5+}$ = 922.13, and for $[P3+5Na+H]^{6+}$ = 786.94.

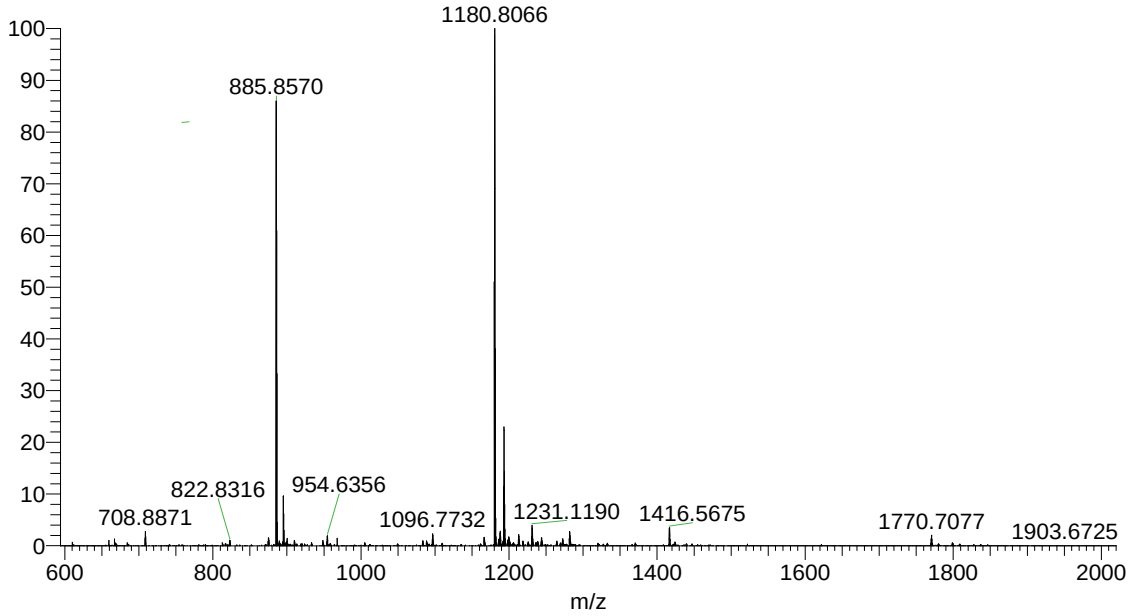

Figure S13. ESI–HRMS spectrum of P4 (*m/z* = 3540.19), Calculated *m/z*-values: for $[P4+3H]^{3+}$ = 1181.06, for $[P4+4H]^{4+}$ = 886.04 and for $[P4+5H]^{5+}$ = 709.038.

D1: 5’-Cy5-TTCTTTATGTTTTTGGCGTCT-3IAbRQSp-3’
D2: 5’-AGACGCCAAAAACATAAAGAA-3’

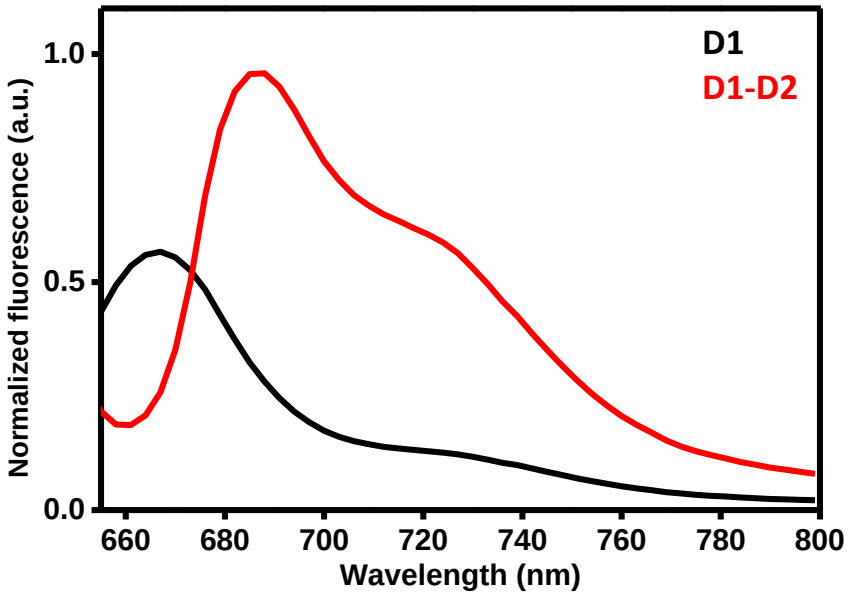

Figure S14: Fluorescence spectra of D1 before (black) and after addition of D2 (red). Measurement conditions: 1 µM PNA and DNA in 10 mM NaH_2PO_4, 100 mM NaCl buffer at pH = 7.0, 25 °C, λ_{ex} = 650 nm.

PNA

P3: Ac-acacctaTOagcg-Gly-NH_2

DNA

D(6-9): 5'-CGCTGXAGGTGT-3'

X= T, C, G, A

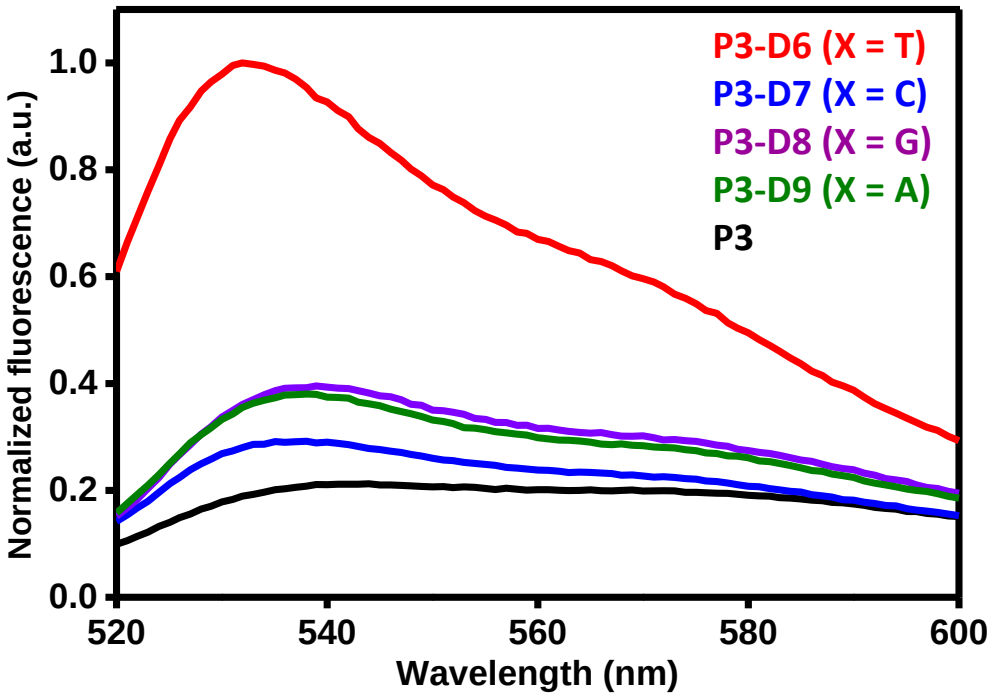

Figure S15: Fluorescence spectra of P4 (black), after addition of DNA strands D6 (red), D7 (blue), D8 (purple) and D9 (green).

8. REFERENCES

S1 D. V. Jarikote, O. Köhler, E. Socher and O. Seitz, *Eur. J. Org. Chem.*, **2005**, *2005*, 3187.

S2 J. Pospíšil and H. Sato, *J. Org. Chem.*, **2011**, *76*, 2269.

S3 R. Brown, J. Plumb, W. G. Aherne, E. McDonald, K. Jones and S. Hilton, WO, 096618, **2007**.

S4 B. Ditmangklo, C. Boonlua, C. Suparpprom and T. Vilaivan, *Bioconjugate Chem.*, **2013**, *24*, 614.

APPENDIX 5

Ultrathin covalently bound organic layers on mica: Formation of atomically flat bio–functionalizable surfaces

1. METHODS

Materials. Unless otherwise specified, all chemicals were used as received without further purification. Muscovite mica surfaces (Grade V–1, 12 mm diameter × 0.15 mm thick) were purchased from SPI supplies. 2,3–dihydroxy benzoic acid (DHBA), N–Boc–1,6–hexanediamine, trifluoroacetic acid (TFA), 1H–imidazole–1–sulfonyl azide–HCl salt, copper sulphate pentahydrate, 1,1′–carbonyldiimidazole, 2,3–dihydroxyl benzylamine hydrobromide, sodium periodate, 2,2′–azino–bis(3–ethylbenzothiazoline–6–sulfonic acid) diammonium salt ($ABTS^{2-}$), Fe(III)–protoporphyrin IX chloride, hydrogen peroxide, potassium carbonate, PBS buffer, ethyl acetate, methanol, hexane, acetone, dichloromethane (DCM) and 2–propanol were purchased from Sigma–Aldrich. For rinsing, solution preparation and contact angle measurements, Milli–Q water (resistivity 18.3 MΩ cm) was used. Oligonucleotides were purchased from Integrated DNA Technologies (IDT), Belgium.

Static Water Contact Angle (SCA) Measurements. The wettability of the modified surfaces was determined by automated static water contact angle measurements with a Krüss DSA 100 goniometer (volume of the drop of deionized water was 3.0 μL). The reported values are the average of at least six droplets, and the relative error is less than ± 1°.

X–ray Photoelectron Spectroscopy (XPS) Measurements. The XPS analysis of surfaces was performed using a JPS–9200 photoelectron spectrometer (JEOL, Japan). Survey and narrow scan spectra were obtained under UHV conditions using monochromatic Al Kα X–ray radiation at 12 kV and 20 mA, and an analyser pass energy of 50 eV for wide scans and 10 eV for narrow scans. The emitted electrons were collected at 10° from the surface normal (take–off angle relative to the surface normal 10°). All XPS spectra were evaluated by using Casa XPS software (version 2.3.15). Survey spectra were corrected with linear background before fitting, whereas high–resolution spectra were corrected with linear background. Atomic area ratios were determined after a baseline correction and normalizing the peak area ratios by

the corresponding atomic sensitivity factors (1.00 for C1s, 1.80 for N1s, 2.93 for O1s, 4.43 for F1s, 1.18 for P2s and 0.75 for Al2s, 5.03 for Br3p, 2.27 for K2s).

DART–HRMS Measurements. Analysis of the modified mica surfaces were performed using a DART–SVP ion source (Ion–Sense, Saugus, MA, USA) coupled to a Q–Exactive orbitrap high–resolution mass spectrometer (Thermo Fisher Scientific, San Jose, CA), mounted on a motorized rail travelling at 0.2 mm/s. Thermo Scientific Xcalibur software (V2.1.0.1139) was used for data acquisition and processing. The measurements were performed in negative mode at 450 °C using a scan range of m/z 180.0 – 345.0, a mass resolution of 70,000 (FWHM) at a scan rate of 1 Hz. The ion trap was tuned with 0.1 mg/mL methanol solution of quinine (*m/z* 323.41 in negative mode) and optimized. The DART source was positioned 6.1 cm on the horizontal scale, 7 cm on the vertical scale with an angle of 45°, such that it is around 1 mm above the surface (Fig. S1). The distance from the surface to the ceramic tube is minimized by placing them at the edge of the moving rail so that maximum of the *p*–CF_3 benzoate ion and *p*–C_4F_9 benzoate ions (*m/z* 189.016 and 339.0062, respectively) would enter the MS.

Atomic Force Microscopy (AFM) Imaging. AFM imaging was performed under air using a Digital Instruments NanoScope V Multimode Scanning Probe Microscopy with a noncontact silicon nitride cantilever with a stiffness of 0.58 N/m (Veeco Metrology, CA) at a scan speed of 1 μm/s, in the Scan–assist imaging mode. Images were flattened with a third–order flattening procedure using Nanoscope Analysis software (v1.5).

Preparation of modified mica samples [M_0–M_1]. Mica samples were washed with copious amounts of acetone, methanol and dichloromethane and dried under a stream of nitrogen gas. Samples were then left undisturbed for 16 h in 5 mM solution of 1 in PBS buffer (pH 7.4) in sealed vials under nitrogen atmosphere. Both sides of the mica were found to be identically modified without preference. Multiple samples (up to 25) could be simultaneously modified in this manner. The samples were sonicated in water for 15 min after the modification and stored for future applications.

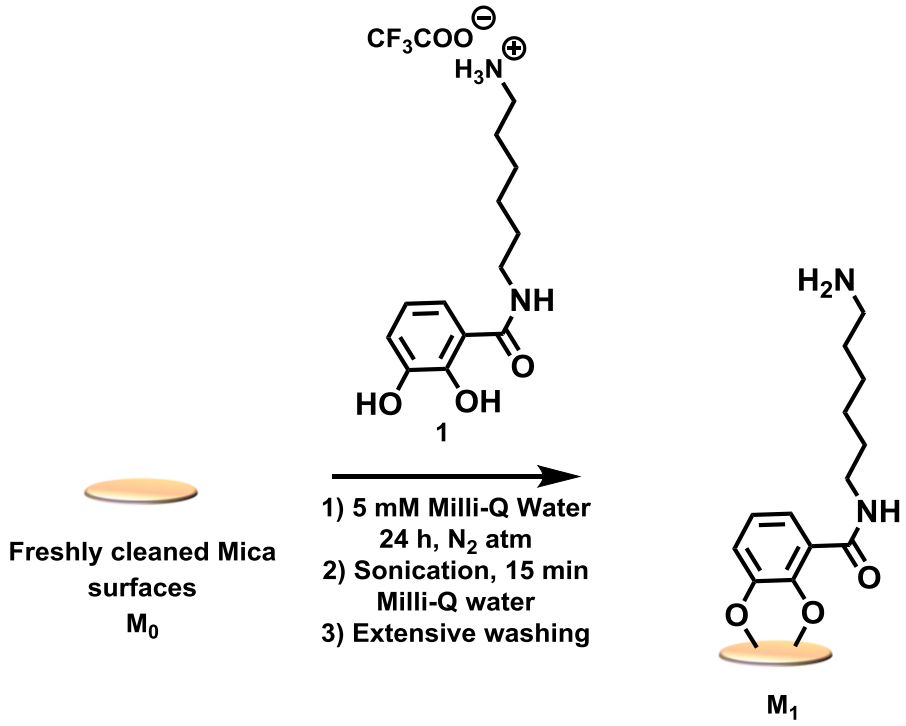

Scheme 1. Attachment of surface anchor 1 to a freshly cleaned mica sample.

Preparation of azide-terminated surface. M_1 samples were stirred with a 50 mM solution of 1H–imidazole–1–sulfonyl azide–HCl salt, $CuSO_4.5H_2O$ and K_2CO_3 in water for 2 h, followed by sonication in water for 15 min, to afford azide-terminated samples M_2. The samples were stored under nitrogen atmosphere for further use.

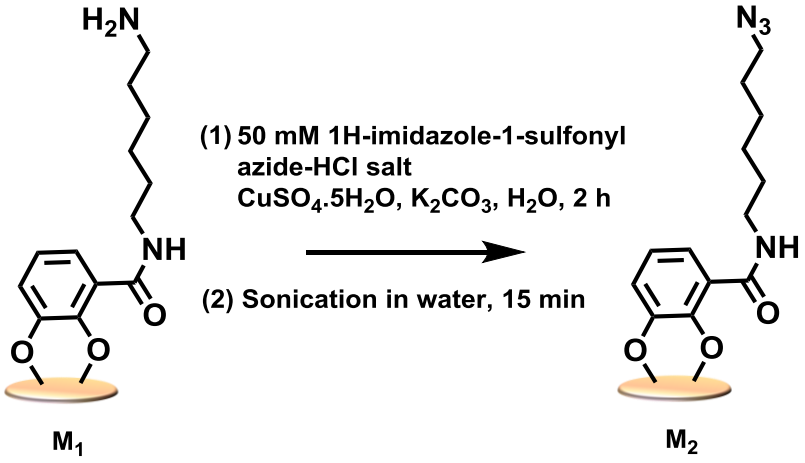

Scheme 2. Conversion of amine-terminated surface anchor 1 to azide-terminated layers.

Interfacial SPAAC on azide-terminated surface. Azide-terminated samples M_2 were stirred 16 h with *endo*–BCN–C_4F_9 MS tag, 2, in DCE solvent at 22 °C, followed by sonication in dichloromethane for 15 min. The samples were dried under a stream of nitrogen and used for XPS and DART–HRMS measurements. The blue tag connected by aromatic ester linkage with *endo*–BCN, 2, is used to determine the yield on the surface of the SPAAC reaction independently by XPS (F1s signal at 686.0 eV) and DART–HRMS (*m/z* 339.0062).

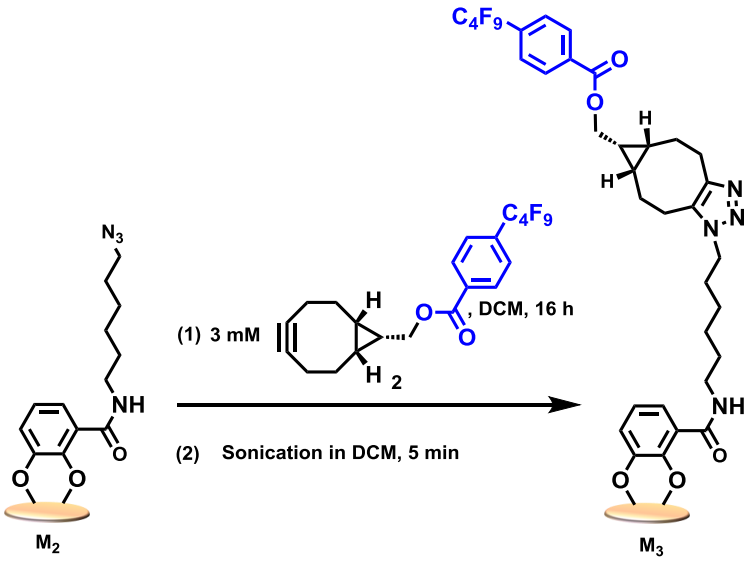

Scheme 3. Interfacial SPAAC reaction between an azide-terminated mica surface and *endo*–BCN 2 in solution.

Preparation of *endo*–BCN terminated surfaces Amine-terminated mica was activated using 1,1'–carbonyldiimidazole (50 mM) in water for 1 h. The activated surfaces were linked with *endo*–BCN–OH, 3, via carbamate linkage.

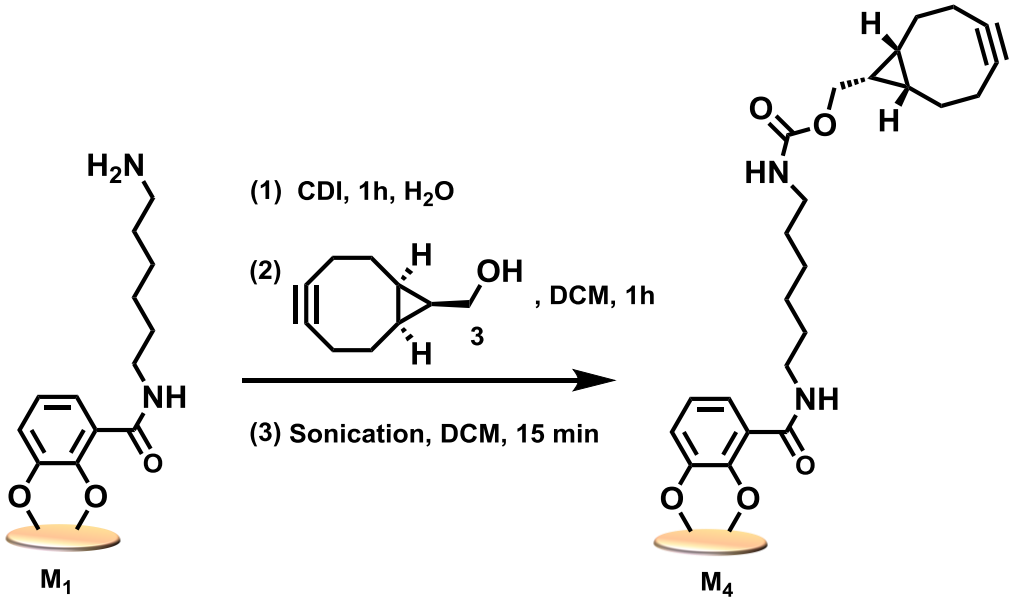

Scheme 4. Preparation of *endo*–BCN-terminated layers on mica.

Interfacial SPAAC on *endo*–BCN-terminated surface. Freshly prepared *endo*–BCN-terminated samples were stirred 16 h with 3 mM azide-terminated counterpart in dichloromethane solution. The azide moiety was coupled with fluorinated tag *via* aromatic ester bond, which allowed for independent verification of surface yield by XPS (F1s signal at 686.0 eV) and DART–HRMS (*m/z* 189.016).

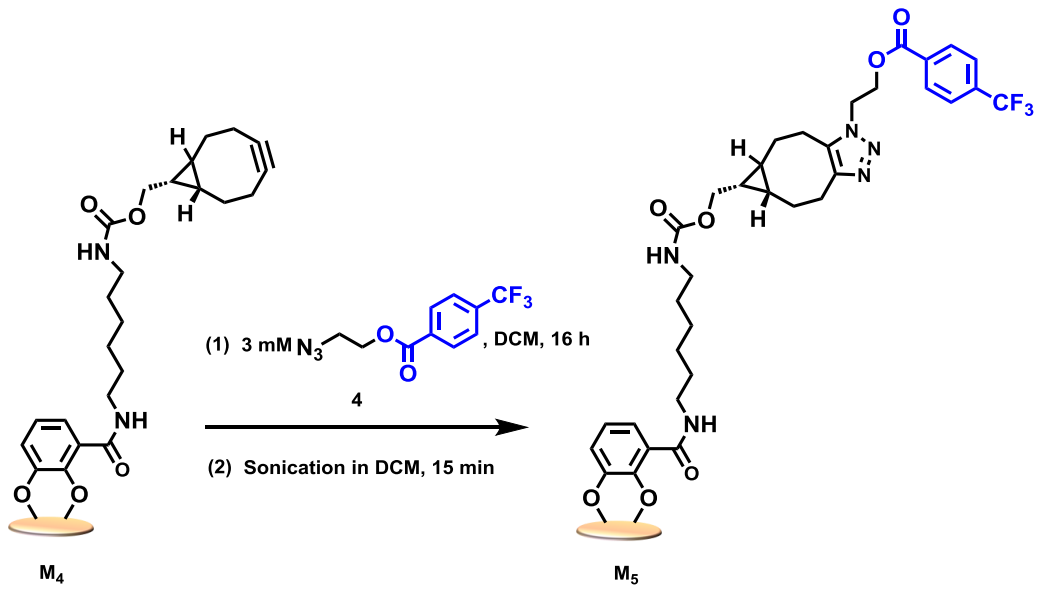

Scheme 5. Interfacial SPAAC reaction between endo–BCN-terminated surfaces and azide counterpart 4 in solution.

Interfacial SPOCQ reaction on mica. Amine terminated mica surfaces M_1 were activated by CDI coupling as described earlier and stirred with 2,3–dihydroxybenzylamine hydrobromide, to afford catechol terminated layers. These were oxidized to 1,2–dihydroxy quinones by oxidation with aqueous 50 mM $NaIO_4$ solution in 30 min. The samples were washed with copious amounts of water followed by sonication for 15 min in methanol. The resulting surfaces were then stirred with 2 to get the SPOCQ cycloaddition product in 4 h with excellent surface yields. Blank measurements were carried out rigorously to ensure no false positives resulting from physisorption and to prove the orthogonality of the reaction.

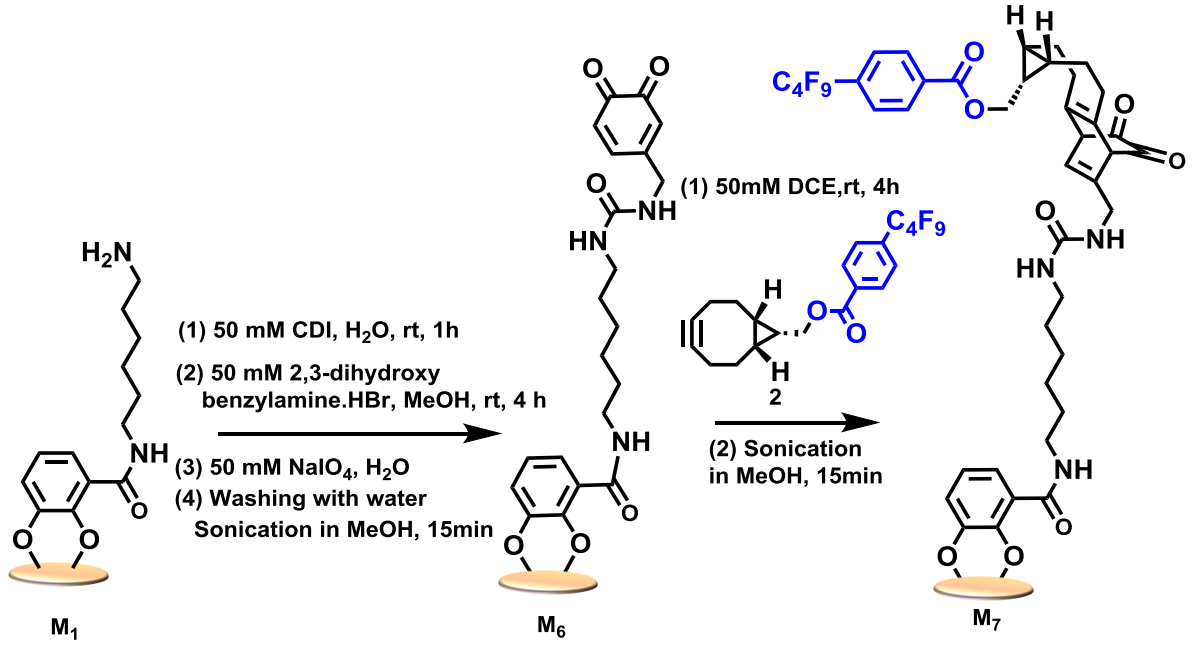

Scheme 6. Interfacial SPOCQ reaction between surfacial 1,2–quinones [M_6] and *endo*–BCN counterpart, 2, in solution.

Proof that sonication techniques are adequate to remove physisorbed moieties. To ensure that all signals are entirely due to covalently bound moieties alone, all surfaces were sonicated in corresponding solvents for 15 min. A stepwise control experiment was carried out in which *endo*–BCN-terminated surfaces M_4 was reacted with azide terminated counterpart with MS tag 4 (*m/z* 189.016) followed by sonication in dichloromethane for 15 min. These surfaces were subsequently stirred in *endo*–BCN with MS tag 2 (*m/z* 339.0062) and sonicated again. The surfaces were subject to

DART–HRMS to see if any MS–tag 2 could be detected, which would only be possible if any residual azide remained physisorbed on the surface after the sonication process. Since no trace of MS tag 2 could be detected, (Figure S6) we concluded that the sonication time and solvent chosen is adequate to remove physisorbed moieties.

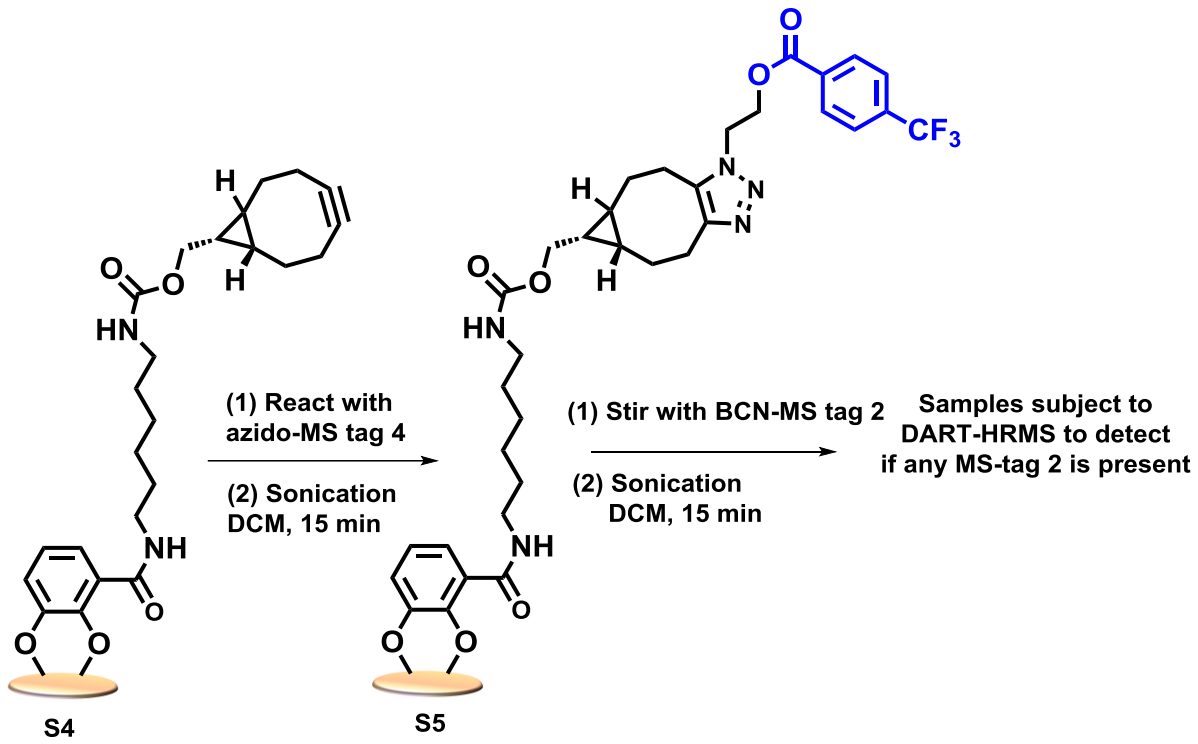

Scheme 7. Control experiment designed to detect if sonication time and solvent is adequate enough to remove all traces of physisorbed moieties after the modification.

Formation of DNA minicircles. M_1 surfaces were activated through CDI coupling as described earlier. Activated samples were stirred overnight in 100 µM aqueous solution of D1. The samples were sonicated for 10 min in water to remove physisorbed DNA molecules. Subsequent hybridization was performed with 10 µM aqueous solution of D2–D9 overnight (16 h). The samples were carefully sonicated in water and immediately used for AFM analysis.

Formation of EAD2 DNAzyme and oxidative activity on mica. M_1 surfaces were activated through CDI coupling as described earlier. Activated samples were stirred overnight in 100 µM aqueous solution of EAD2. This was followed by formation of Heme–G quadruplex by stirring the samples in a 10 mM solution of Fe(III)–protoporphyrin IX chloride (Tris–HCl, pH 8) containing 10 mM KCl for 1 h. Samples were washed with water and sonicated before use. Peroxidation reaction was carried out at 25 °C in 100 µM PBS (pH 6.0) with 5 µM ABTS diammonium salt and 5 µM H_2O_2. The modified mica samples were placed in a sealed vial and solutions of $ABTS^{2-}$ and the H_2O_2 were mixed on a mechanical stirred. Formation of the oxidized product ($ABTS^{-\bullet}$) was monitored by UV–Vis analysis (200–500 nm).of the solution at different time points (5, 15, 30 and 60 min). Blank experiments were carried out to ensure the catalytic activity was due to the DNAzymes.

2. CHEMICAL SYNTHESIS

2.1 General Remarks. Unless stated otherwise, solvents and dry solvents like dichloromethane, methanol and isopropanol were purchased from Sigma–Aldrich. Unless stated otherwise all of these chemicals were used without further purification.

2.2. Reaction Handling. Unless stated otherwise all non–aqueous reactions were performed in dried glassware under an atmosphere of argon. All flasks were equipped with rubber septa and reactants were handled using standard Schlenk techniques. Temperatures above the room temperature refer to oil bath temperatures which were controlled by a thermostat. Reactions were magnetically stirred.

2.3. ^{1}H–NMR spectra were recorded at room temperature on a Bruker AVB–400 spectrometer with ^{1}H operating frequency of 400 MHz. Unless stated otherwise all spectra were recorded at room temperature in $CDCl_3$ and all chemical shifts are given in δ units relative to the residual $CHCl_3$ (central line of singlet: δ_H = 7.27 ppm). Analyses followed first order and the following abbreviations were used throughout: s = singlet, br. s. = broad singlet, d = doublet, t = triplet, q = quartet, quin = quintet, sxt = sextet, sept = spt, dd = doublet of doublet, dt = doublet of triplet, m = multiplet, mc = centered multiplet. Coupling constants (*J*) are given in Hertz (Hz).

2.4. ^{13}C–NMR spectra were recorded at room temperature on a Bruker AVB–400 spectrometer with ^{13}C operating frequency of 101 MHz. Unless stated otherwise all spectra were recorded at room temperature in $CDCl_3$ and all chemical shifts are given in δ units relative to the $CDCl_3$ (central line of triplet: δ_C = 77.0 ppm). The following abbreviation was used throughout: s = singlet, d = doublet, dd = doublet of doublet. If no coupling constants are given, the multiplicity refers to the ^{1}H–decoupled spectra.

2.5. Synthesis of Surface Anchor 1.

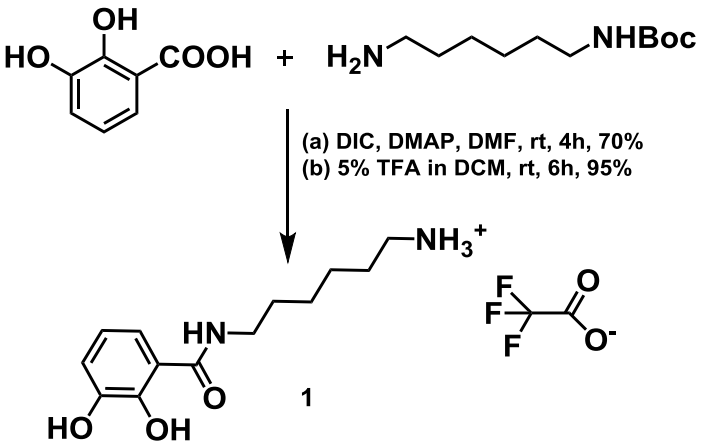

2,3–Dihydroxybenzoic acid (500 mg, 3.24 mmol) was weighed and suspended in 3 mL anhydrous DMF followed by addition of DIC (0.5 mL, 3.50 mmol), triethylamine (1 mL, 7.13 mmol) and DMAP (39 mg, 0.32 mmol). This was followed by addition of N–Boc 1,6–diaminohexane (902 mg, 3.5 mmol) and allowed to react for 3 h at room temperature, under Ar atmosphere. The reaction was monitored by TLC until completion. The solvent was removed under reduced pressure and the resultant residue was purified by column chromatography (EtOAc: Heptane 50:50 v/v) as a colorless oil, (yield: 0.798 g, 70%) and immediately used. ^{1}H NMR (400 MHz, $CDCl_3$) δ 7.03 (dd, J = 7.9, 1.3 Hz, 1H), 7.01(dd, J = 7.8, 1.3 Hz, 1H), 6.73 (t, J = 8.0 Hz, 1H), 4.62 (t, J = 6.2 Hz, 1H), 3.42 (q, J = 6.6 Hz, 1H), 3.13 (q, J = 6.6 Hz, 1H), 1.60 (d, J = 6.9 Hz, 1H), 1.46 (d, J = 6.8 Hz, 1H), 1.44 (s, 6H), 1.36 (dd, J = 5.3, 3.2 Hz, 1H).

Boc–deprotection was performed immediately using 5% TFA in DCM (3mL) for 4h. The solvent was removed under vacuum and the residue was washed with HPLC grade hexane to yield a brown solid (yield: 0.788 g, 95%). ^{1}H NMR (400 MHz, D_2O) δ 7.12 (d, J = 8.0 Hz, 1H), 6.98 (d, J = 7.9 Hz, 1H), 6.78 (d, J = 8.0 Hz, 1H), 3.29 (t, J = 7.0 Hz, 2H), 2.89 (t, J = 7.6 Hz, 2H), 1.65 – 1.41 (m, 3H), 1.32 (p, J = 3.5 Hz, 4H); ^{13}C NMR (101 MHz, D_2O) δ 170.15, 147.50, 144.85, 119.69, 119.55, 118.82, 116.73, 39.76, 39.59, 28.38, 26.85, 25.84, 25.47.

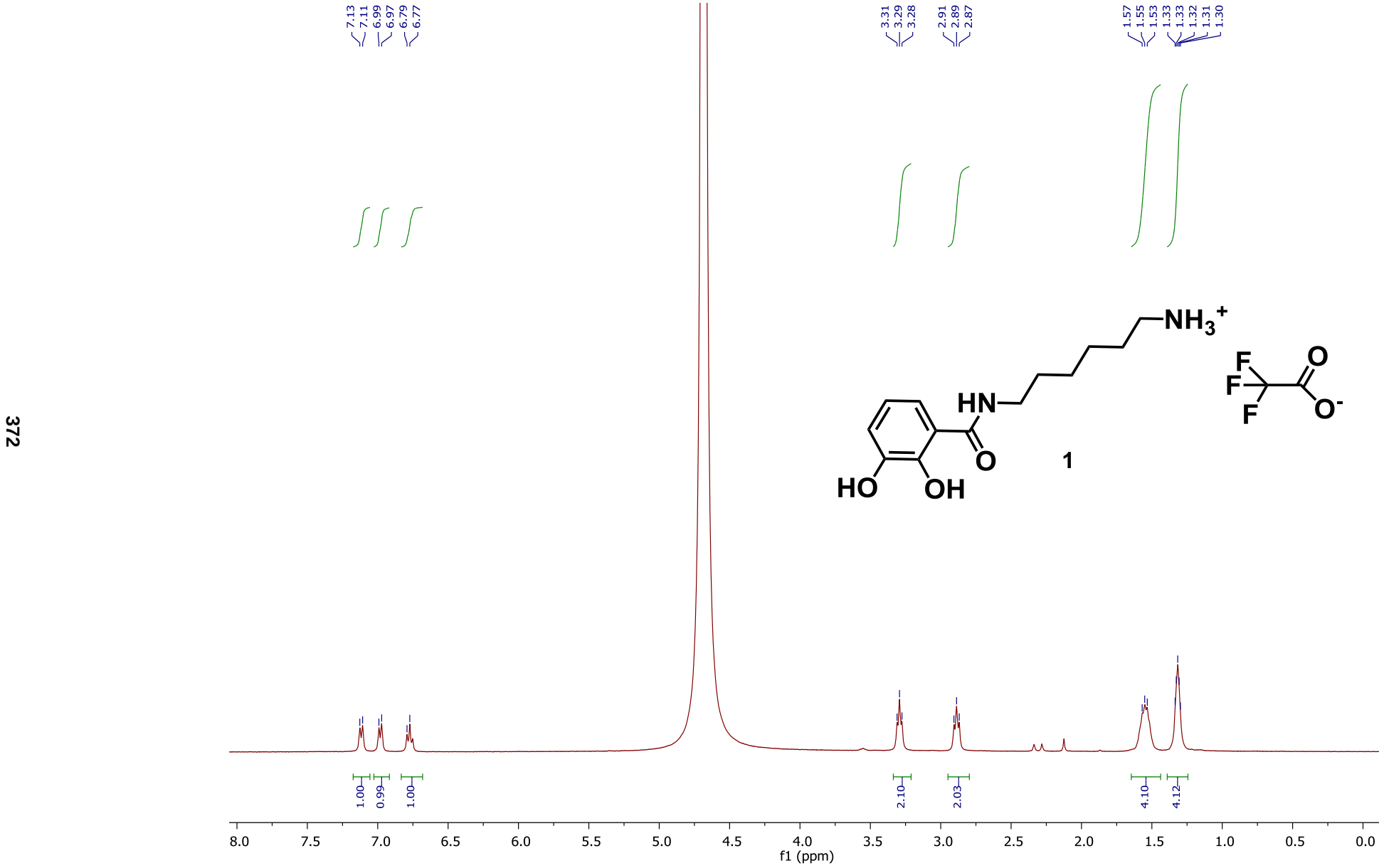
7.13
7.11
6.99
6.97
6.79
6.77
3.31
3.29
3.28
2.91
2.89
2.87
1.57
1.55
1.53
1.33
1.33
1.32
1.31
1.30
NH3+
HN
O
HO
OH
1
F
F
F
O
O-
1.00
0.99
1.00
2.10
2.03
4.10
4.12
8.0
7.5
7.0
6.5
6.0
5.5
5.0
4.5
4.0
3.5
3.0
2.5
2.0
1.5
1.0
0.5
0.0
f1 (ppm)

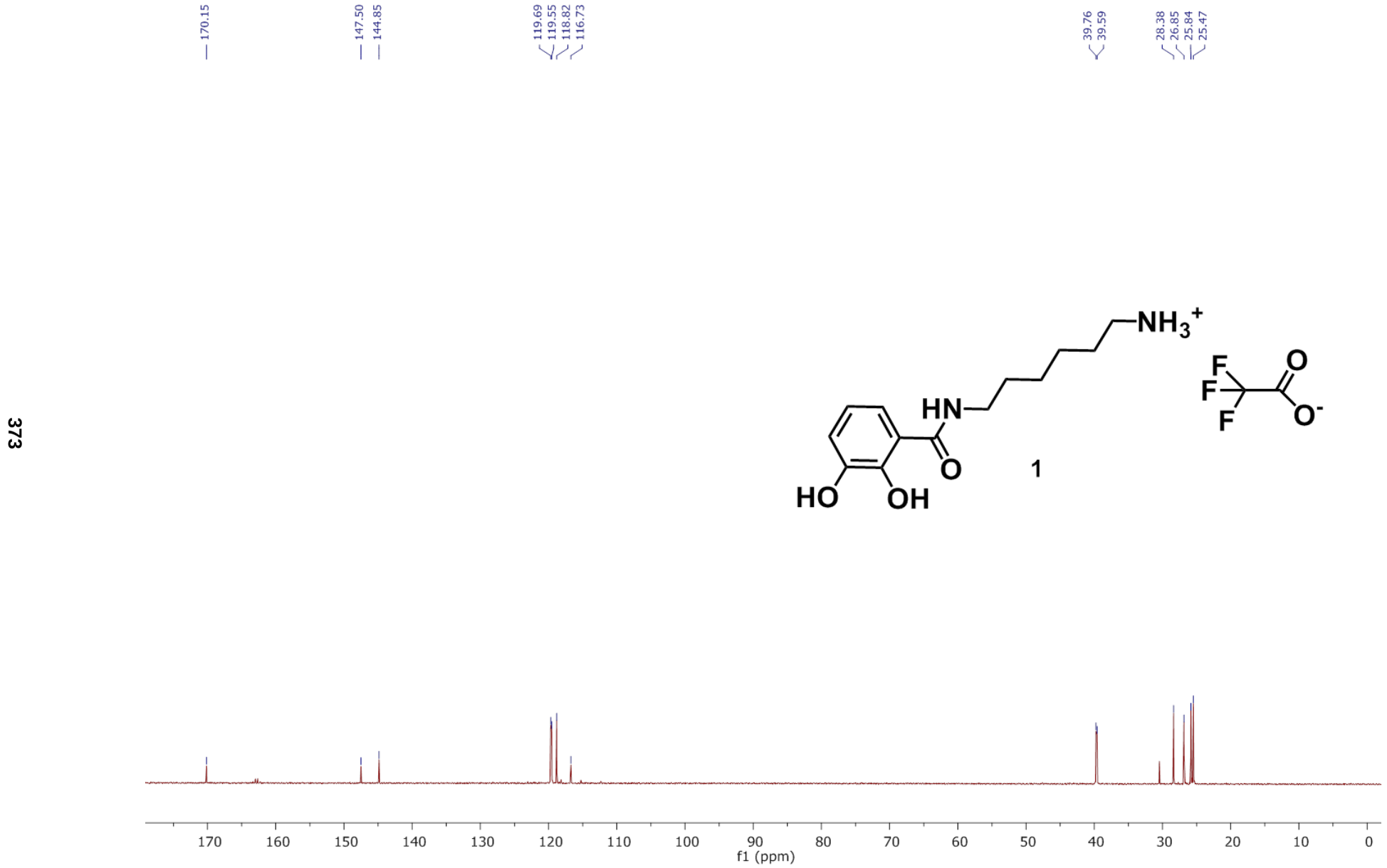
170.15
147.50
144.85
119.69
119.55
118.82
116.73
39.76
39.59
28.38
26.85
25.84
25.47
NH3+
HN
O
HO
OH
F
F
F
O
O-
1
170
160
150
140
130
120
110
100
90
80
70
60
50
40
30
20
10
0
f1 (ppm)

2.6 Synthesis of 2–azidoethanol from 2–bromoethanol.

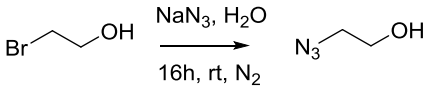

Sodium azide (15.6 g, 0.24 mol) was dissolved in 100mL milliQ water, followed by the addition of 5.67 mL of 2–bromoethanol (10 g, 0.08 mol). The mixture was heated at 80 °C overnight under N_2 flow, during which the color changed from yellow to orange. The product was extracted four times with 75 mL diethyl ether. The combined organic fractions were dried and evaporated under reduced pressure. The product was obtained as a clear oil. Yield: 54 %. The ^{1}H–NMR spectrum was in accordance with literature values (Giorgio *et al*. Molecular Pharmaceutics 2013, *10* (3), 975–978). ^{1}H–NMR (400 MHz, $CDCl_3$) δ 3.75 (m, 2H), 3.42 (t, J = 5.0 Hz, 2H), 2.66 (s, 1H).

2.7. Synthesis of 2–azidoethyl 4–(trifluoromethyl)benzoate (4).

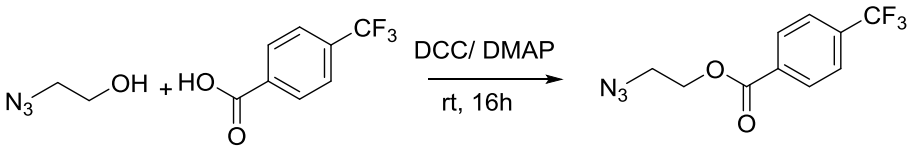

4–(Trifluoromethyl)benzoic acid (13.0 g, 68.8 mmol) was transferred to a three-necked round bottom flask (100 mL) dicyclohexylcarbodiimide (DCC) (13.60 g, 66.02 mmol) and 4–dimethylaminopyridine (DMAP) (4.00 g, 33.33 mmol) dissolved in 100 mL DCM were added to the flask. The reaction mixture was stirred for 30 min before adding 2–azidoethanol (6.66 g, 65.55 mmol). The final reaction mixture was left stirring overnight at room temperature. The reaction mixture was then filtered and evaporated under reduced pressure, forming a yellow oil. The crude product was purified by column chromatography 10:90 ethyl acetate : hexane as solvent. Yield: 35%. ^{1}H–NMR (400 Hz, $CDCl_3$) δ 8.19 (d, J = 8.4 Hz, 2H), 7.74 (d, J = 8.0 Hz, 2H), 4.54 (t, J = 5.2 Hz, 2H), 3.63 (t, J = 5.2 Hz, 2H). ^{13}C–NMR (101 Hz, $CDCl_3$) δ 165.02, 135.27, 132.74, 130.15, 127.64, 125.47, 64.09, 49.85.

3. SUPPLEMENTARY FIGURES

Supplementary Figure S1. Height profile of bare mica (M_0) showing roughness of 0.1 ± 0.01 nm across six random profiles drawn across the surface.

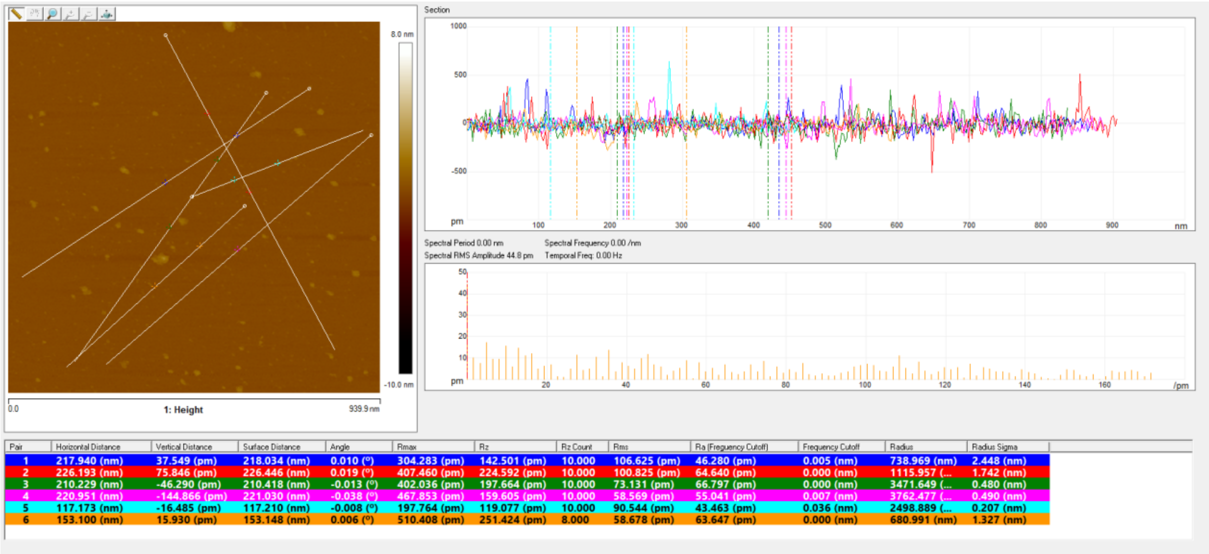

Supplementary Figure S2. Thickness of covalently bound layers of 1 as estimated across a hole on the surface of modified mica M_1.

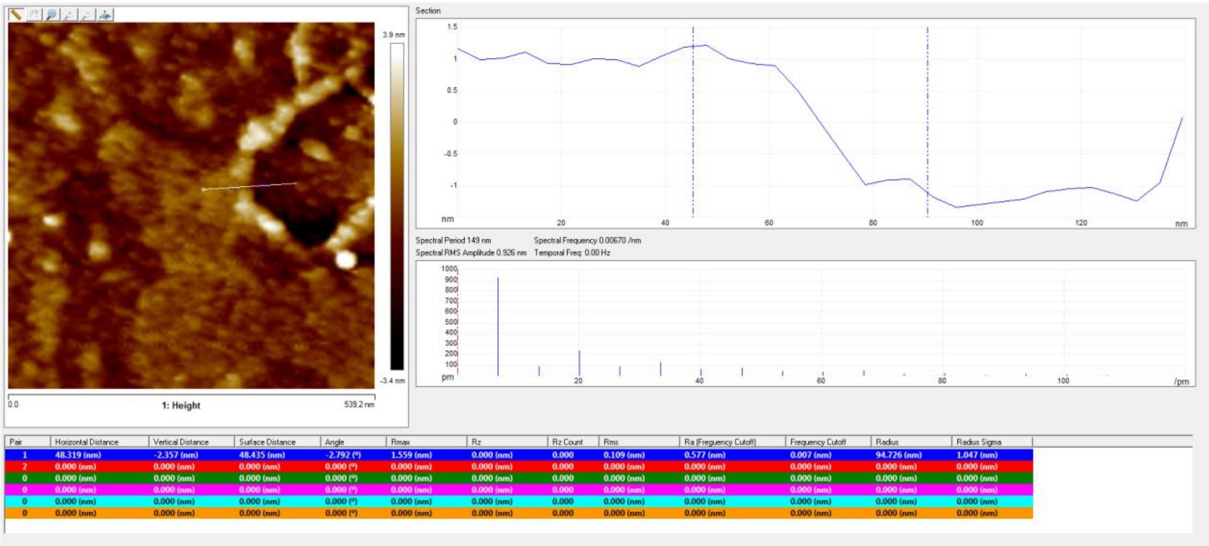

Supplementary Figure S3. Height profile of M_1 mica surface showing a roughness of 0.45 ± 0.1 nm across six random profiles drawn across the surface.

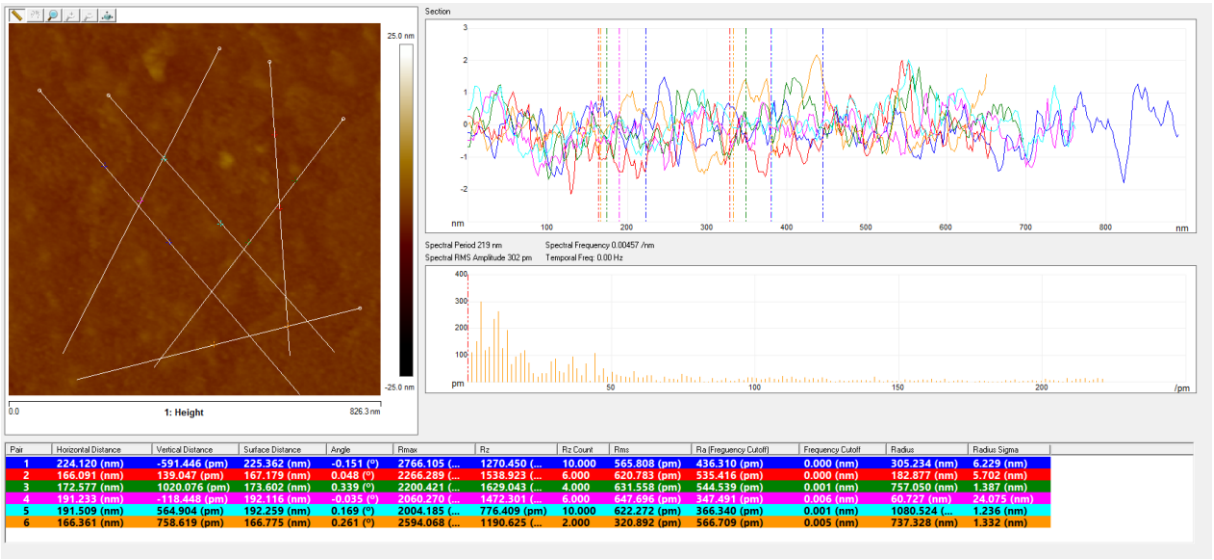

Pair	Horizontal Distance	Vertical Distance	Surface Distance	Angle	Rmax	Rz	Rz Count	Rms	Ra (Frequency Cutoff)	Frequency Cutoff	Radius	Radius Sigma
1	224.120 (nm)	-591.446 (pm)	225.362 (nm)	-0.151 (°)	2766.105 (...	1270.450 (...	10.000	565.808 (pm)	436.310 (pm)	0.000 (nm)	305.234 (nm)	6.229 (nm)
2	166.091 (nm)	139.047 (pm)	167.179 (nm)	0.048 (°)	2266.289 (...	1538.923 (...	6.000	620.783 (pm)	535.416 (pm)	0.000 (nm)	182.877 (nm)	5.702 (nm)
3	172.577 (nm)	1020.076 (pm)	173.602 (nm)	0.339 (°)	2200.421 (...	1629.043 (...	4.000	631.558 (pm)	544.539 (pm)	0.001 (nm)	757.050 (nm)	1.387 (nm)
4	191.233 (nm)	-118.448 (pm)	192.116 (nm)	-0.035 (°)	2060.270 (...	1472.301 (...	6.000	647.696 (pm)	347.491 (pm)	0.006 (nm)	60.727 (nm)	24.075 (nm)
5	191.509 (nm)	564.904 (pm)	192.259 (nm)	0.169 (°)	2004.185 (...	776.409 (pm)	10.000	622.272 (pm)	366.340 (pm)	0.001 (nm)	1080.524 (...	1.236 (nm)
6	166.361 (nm)	758.619 (pm)	166.775 (nm)	0.261 (°)	2594.068 (...	1190.625 (...	2.000	320.892 (pm)	566.709 (pm)	0.005 (nm)	737.328 (nm)	1.332 (nm)

Supplementary Figure S4. DART–HRMS extracted ion chronogram (EIC) (mass window *m/z* 339.0052–339.0072) of MS tag 4 (th. mass 339.0062) of two MS scans of SPAAC-modified mica.

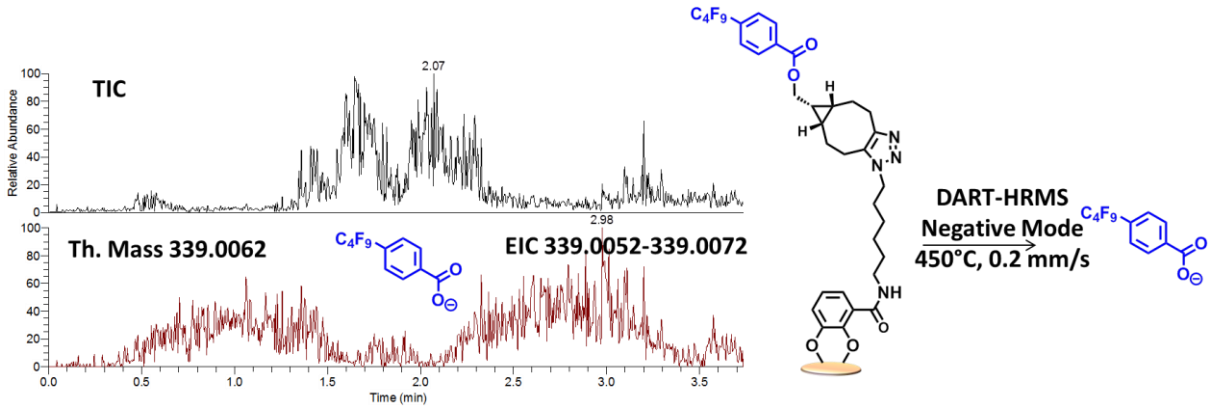

Supplementary Figure S5. DART–HRMS extracted ion chronogram (EIC) (mass window *m/z* 189.0150–189.0170) of MS tag 2 (th. mass 189.0160) of SPAAC-modified mica M_5.

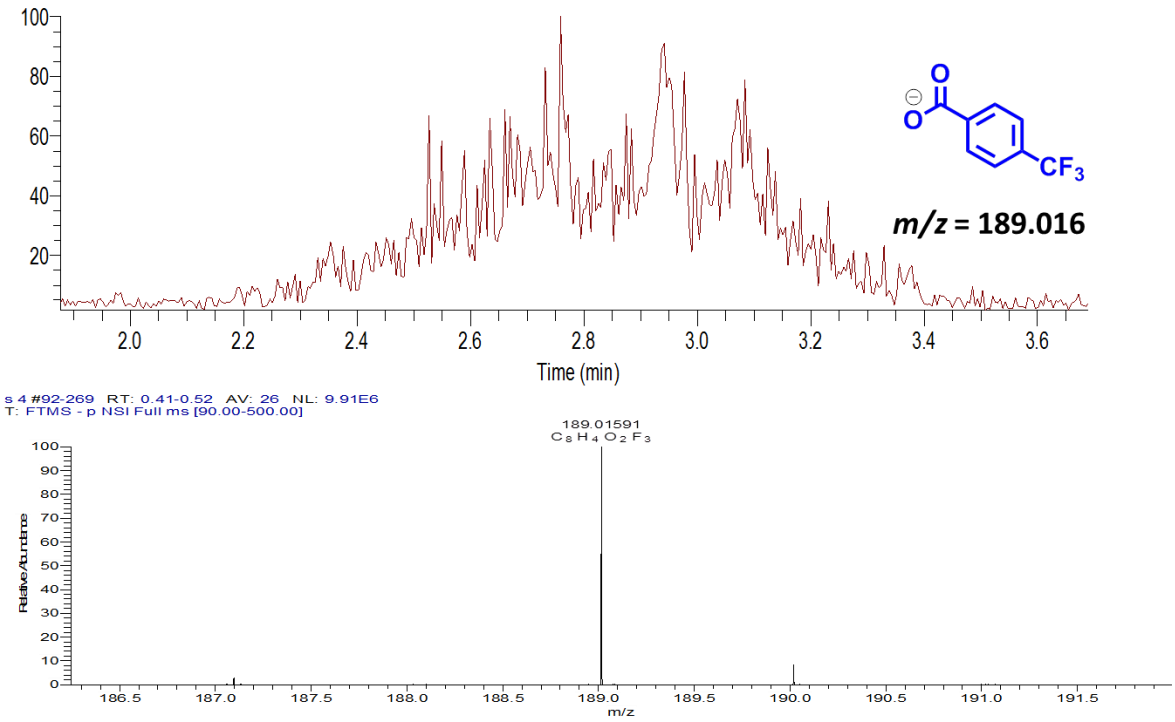

Supplementary Figure S6. Cross-over control experiment: DART–HRMS showing no trace of MS tag 2 (*m/z* 339.0062), which would have resulted if any physisorbed azide remained on the surface after sonication.

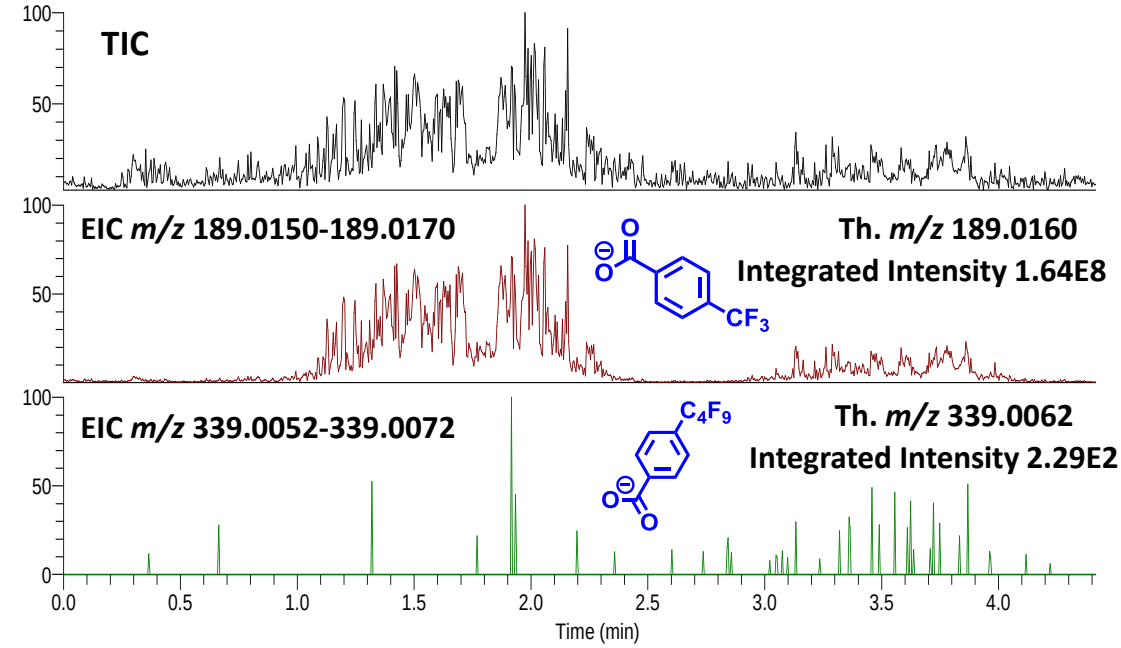

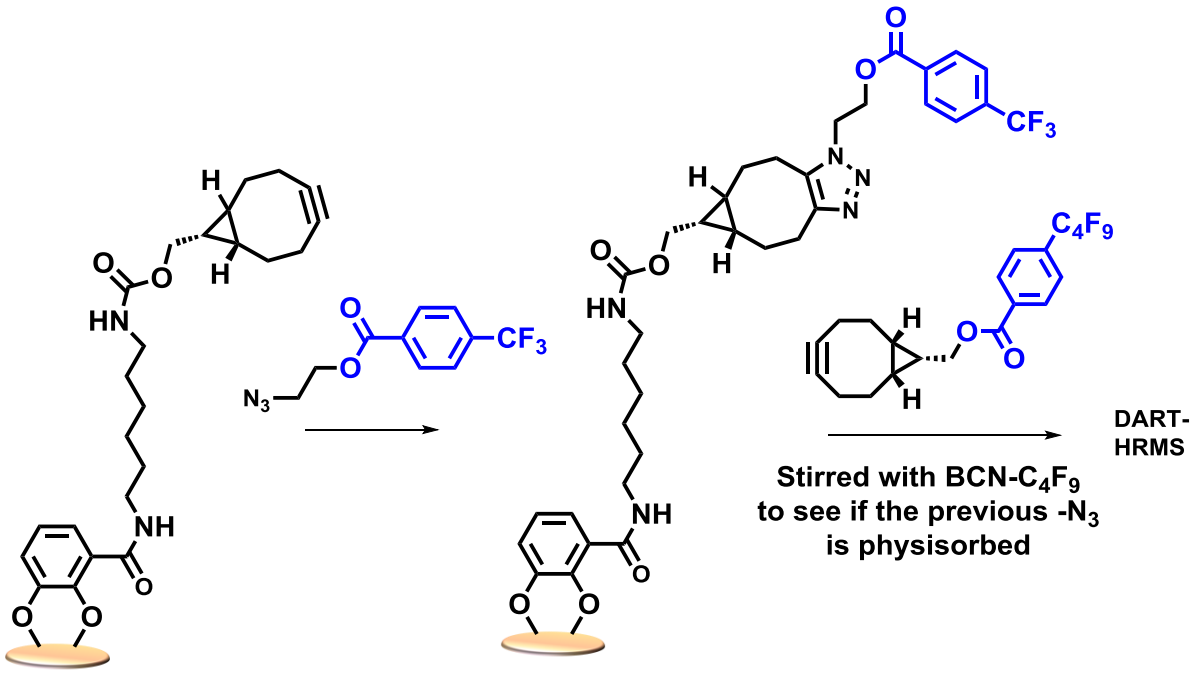

Supplementary Figure S7. 2D–height AFM image of DNA anchor D1 on mica.

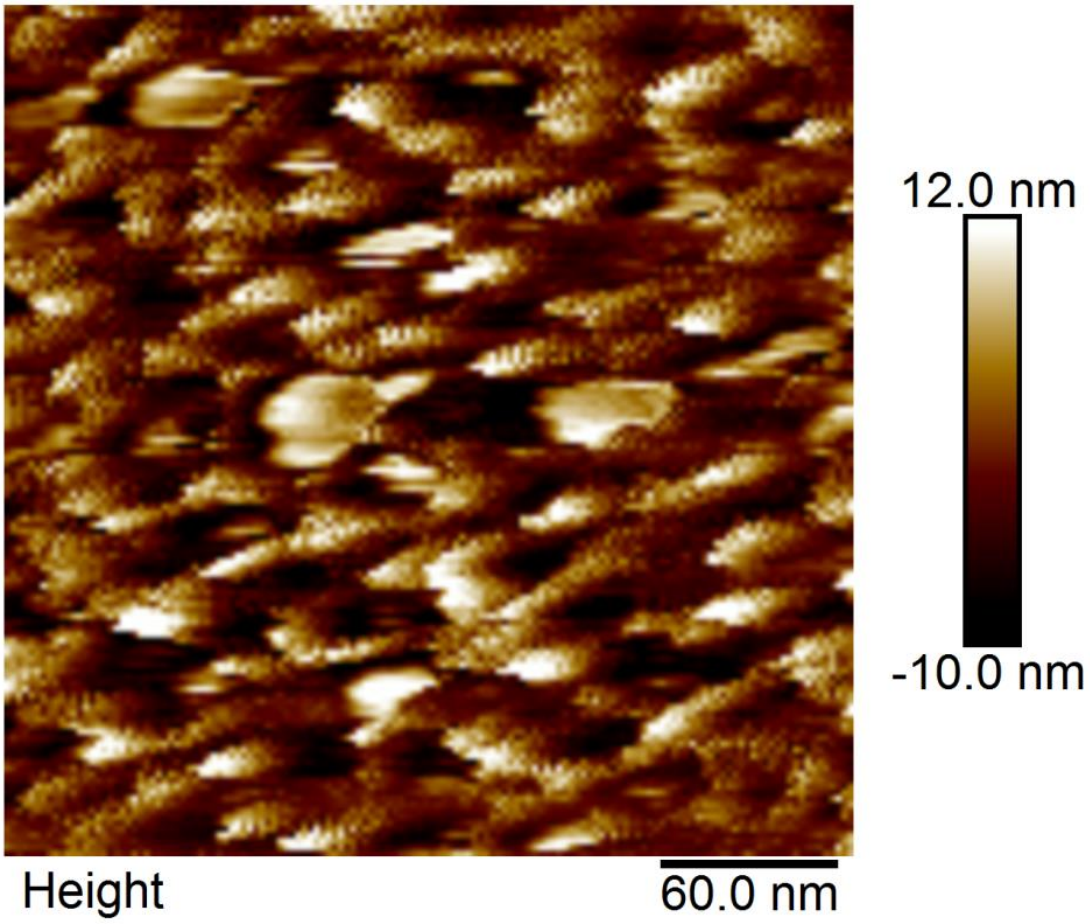

Supplementary Figure S8. Height profile of mica modified with DNA mini–circles showing roughness of 0.9 ± 0.2 nm across six random profiles drawn across the surface.

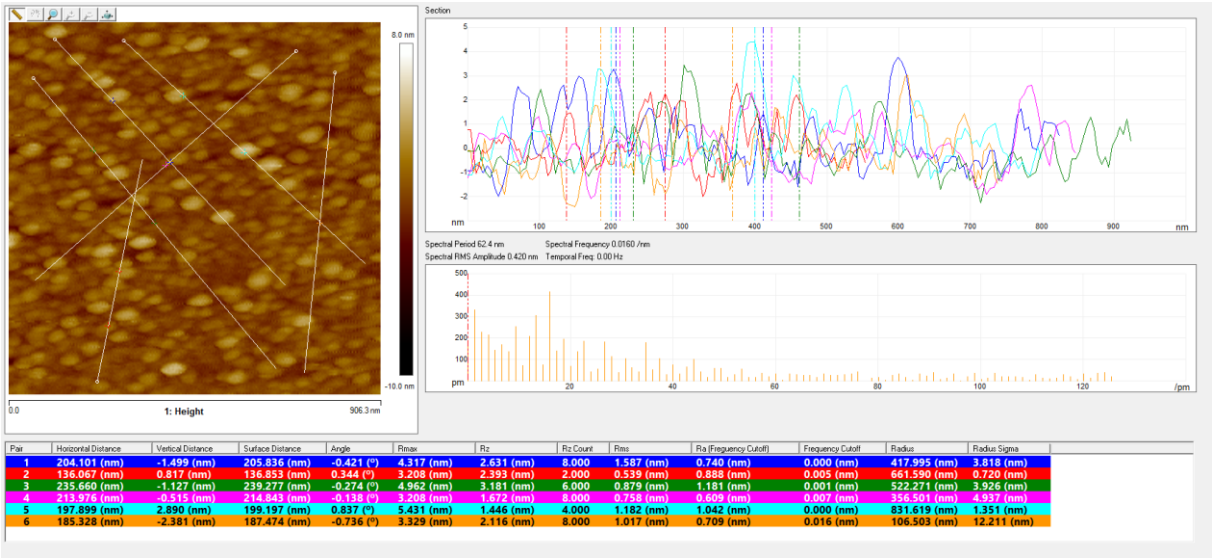

Pair	Horizontal Distance	Vertical Distance	Surface Distance	Angle	Rmax	Rz	Rz Count	Rms	Ra (Frequency Cutoff)	Frequency Cutoff	Radius	Radius Sigma
1	204.101 (nm)	-1.499 (nm)	205.836 (nm)	-0.421 (°)	4.317 (nm)	2.631 (nm)	8.000	1.587 (nm)	0.740 (nm)	0.000 (nm)	417.995 (nm)	3.818 (nm)
2	136.067 (nm)	0.817 (nm)	136.853 (nm)	0.344 (°)	3.208 (nm)	2.393 (nm)	2.000	0.539 (nm)	0.888 (nm)	0.005 (nm)	661.590 (nm)	0.720 (nm)
3	235.660 (nm)	-1.127 (nm)	239.277 (nm)	-0.274 (°)	4.962 (nm)	3.181 (nm)	6.000	0.879 (nm)	1.181 (nm)	0.001 (nm)	522.271 (nm)	3.926 (nm)
4	213.976 (nm)	-0.515 (nm)	214.843 (nm)	-0.138 (°)	3.298 (nm)	1.672 (nm)	8.000	0.758 (nm)	0.605 (nm)	0.007 (nm)	356.501 (nm)	4.937 (nm)
5	197.899 (nm)	2.890 (nm)	199.197 (nm)	0.837 (°)	5.431 (nm)	1.446 (nm)	4.000	1.182 (nm)	1.042 (nm)	0.000 (nm)	831.619 (nm)	1.351 (nm)
6	185.328 (nm)	-2.381 (nm)	187.474 (nm)	-0.736 (°)	3.329 (nm)	2.116 (nm)	8.000	1.017 (nm)	0.709 (nm)	0.016 (nm)	106.503 (nm)	12.211 (nm)

Supplementary Figure S9. Height image of bare mica, surface anchor-modified mica and mica with DNA minicircles (2D and 3D models).

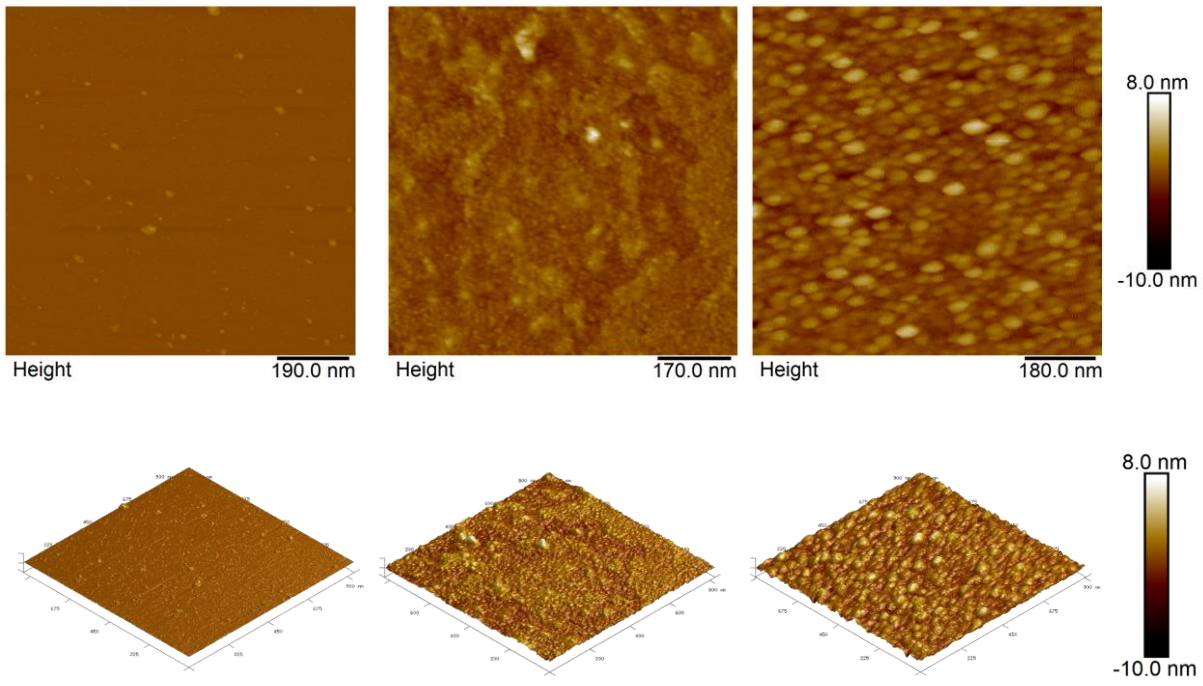

Bare mica | **Catechol modified mica** | **Mica with DNA minicircles**

Supplementary Figure S10. 3D in–phase image of different minicircles which show consistent internal diameter in agreement with theoretical value.

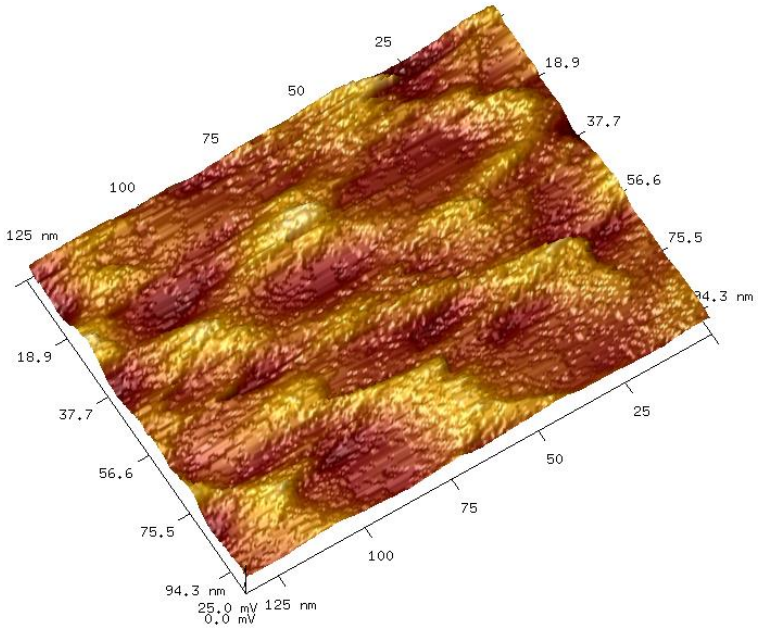

Supplementary Figure S11. In–phase images of bare mica, surface anchor modified mica and mica with immobilized DNA mini–circles (2D and 3D image).

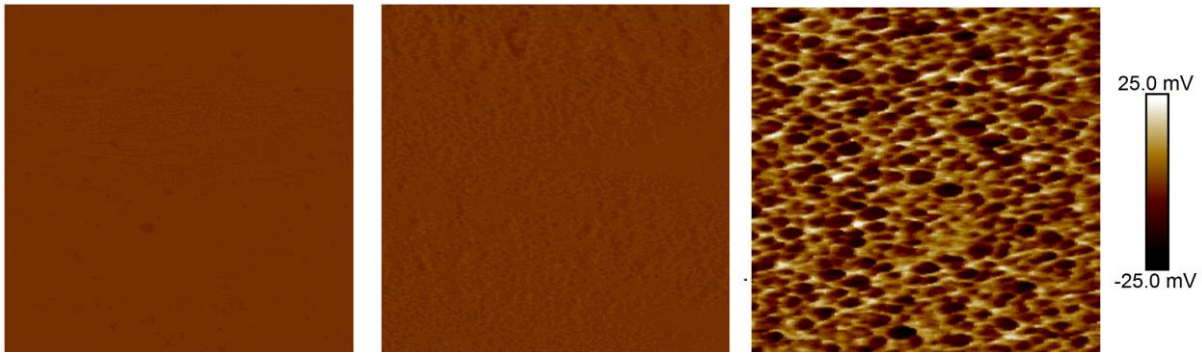

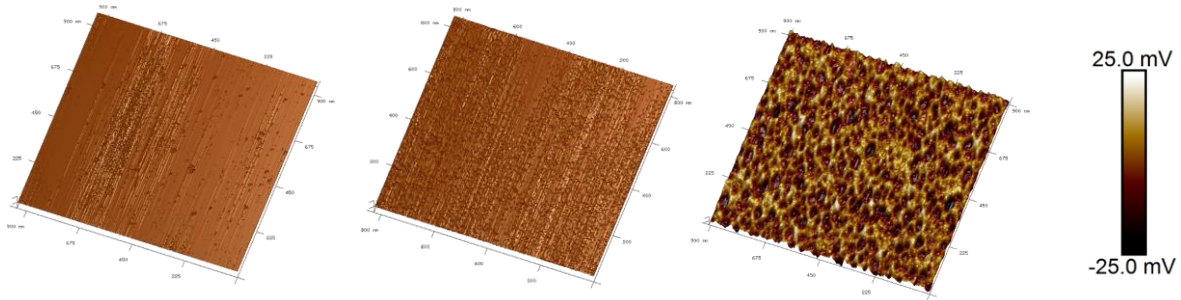

Bare mica | **Catechol modified mica** | **Mica with DNA minicircles**

Supplementary Figure S12. Profile across 2D AFM image of different mini–circles which show consistent internal diameter in agreement with theoretical value of 18 nm.

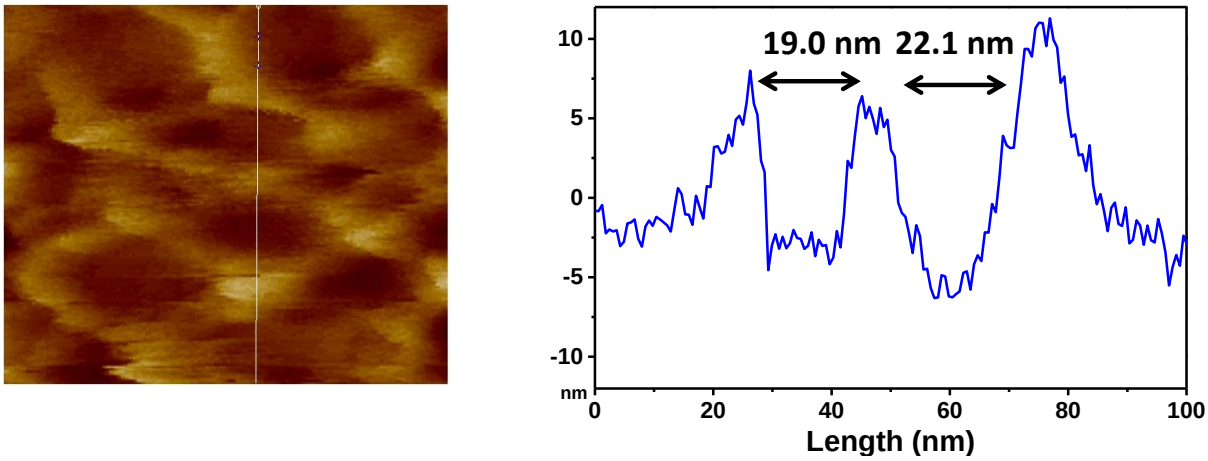

Supplementary Figure S13. 2D–height AFM profile image of single DNA mini–circle with six random lines drawn across it showing a consistent height of 4 nm.

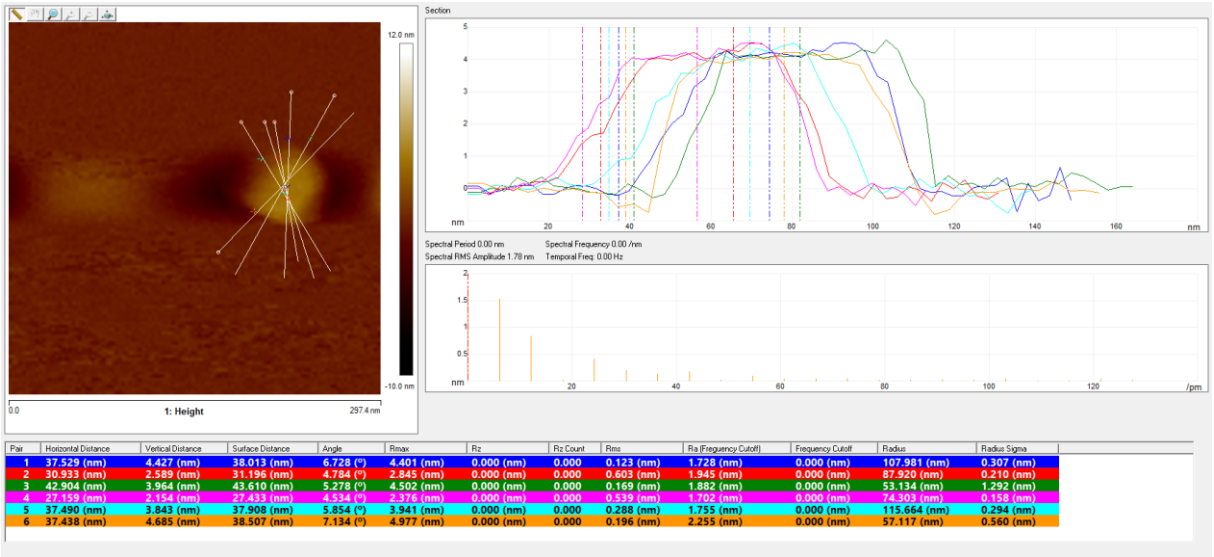

Supplementary Figure S14. 3D–height AFM image of incomplete DNA minicircles on mica obtained at lower concentration (100-fold dilution).

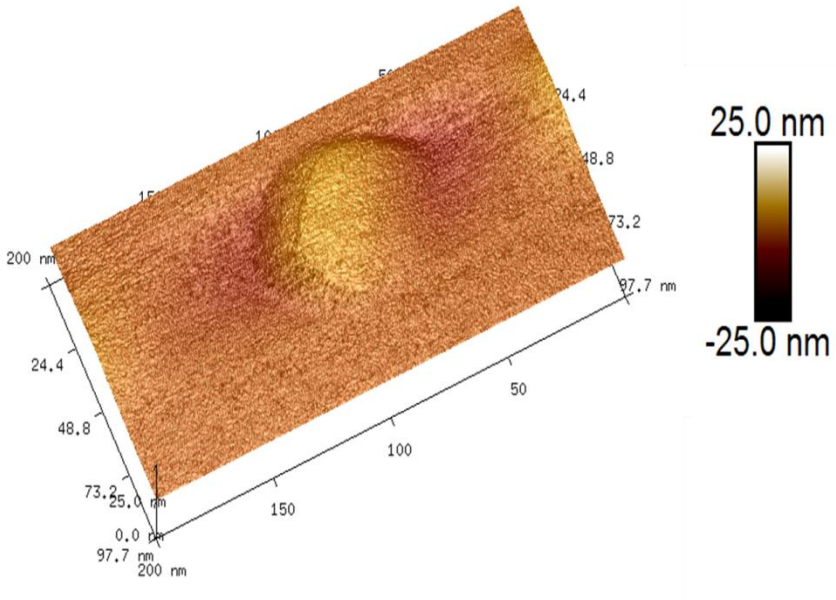

Supplementary Figure S15. 3D–height AFM image other DNA minicircles obtained at lower concentration (100-fold dilution).

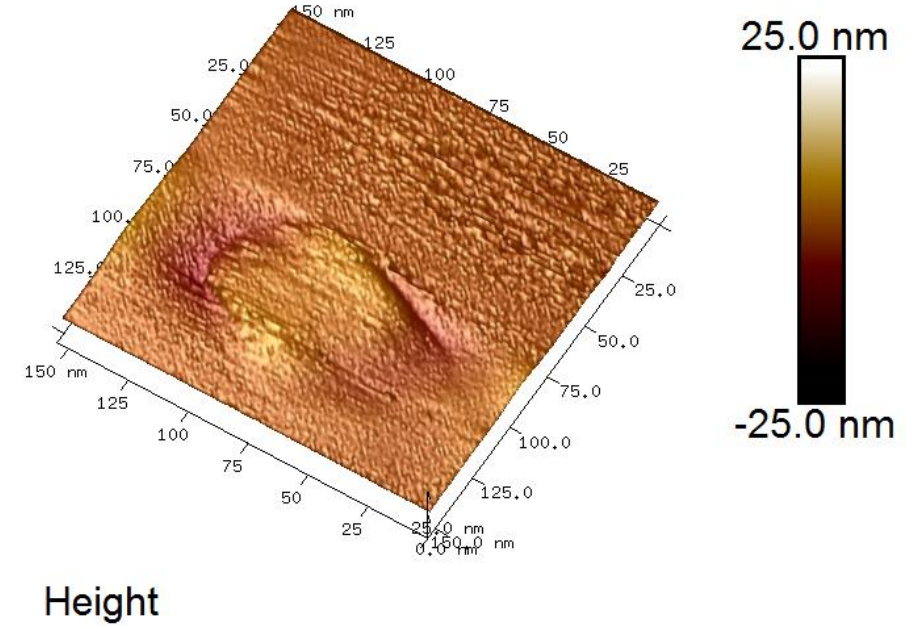

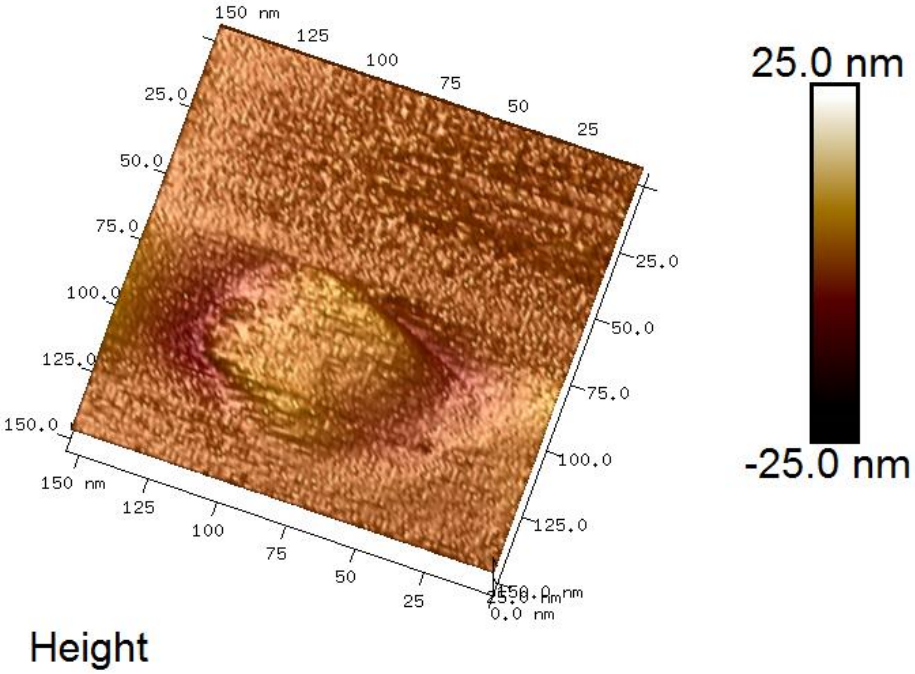

Supplementary Figure S16. 2D–height AFM image and profile of control experiment for DNA minicircles.

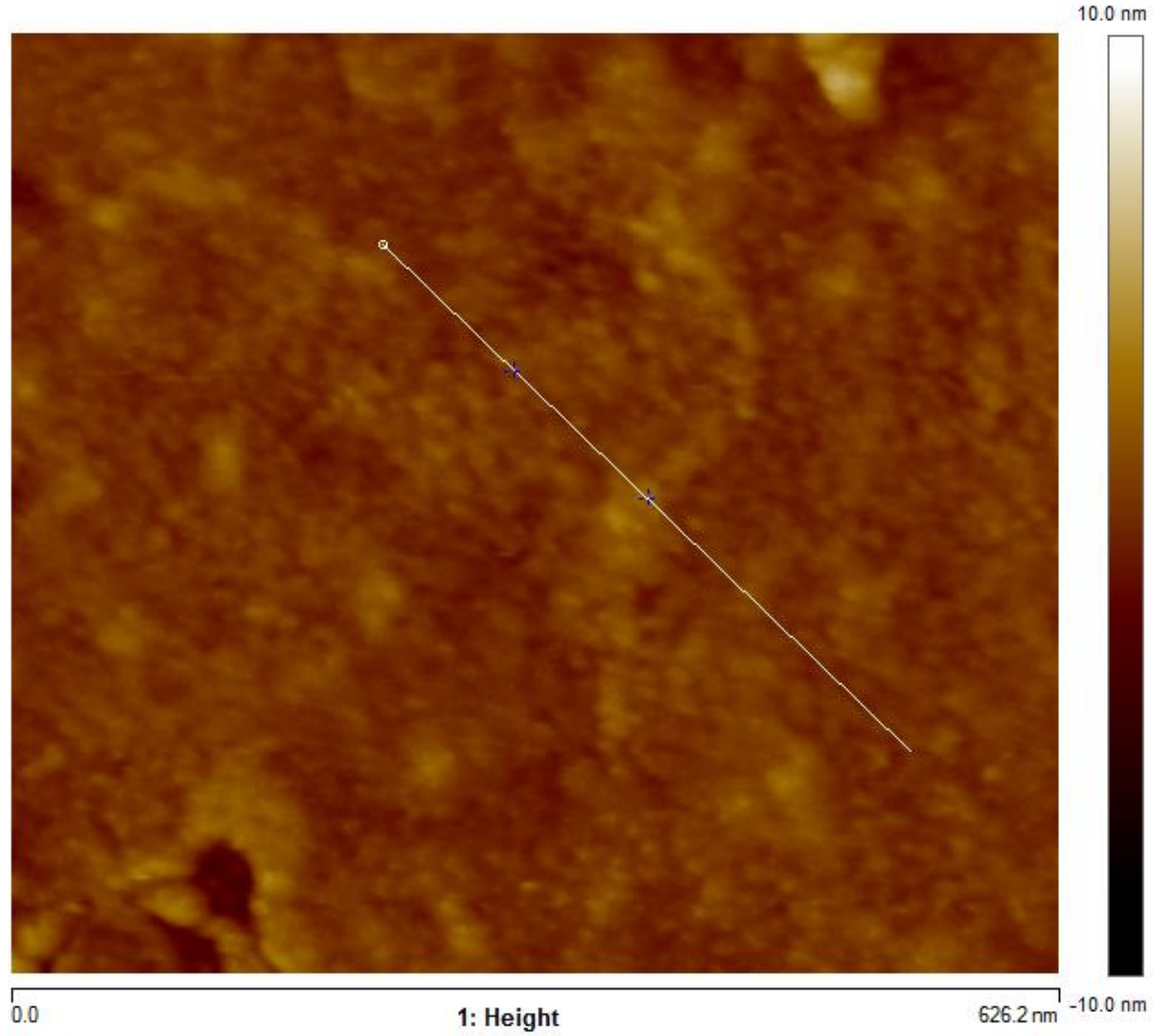

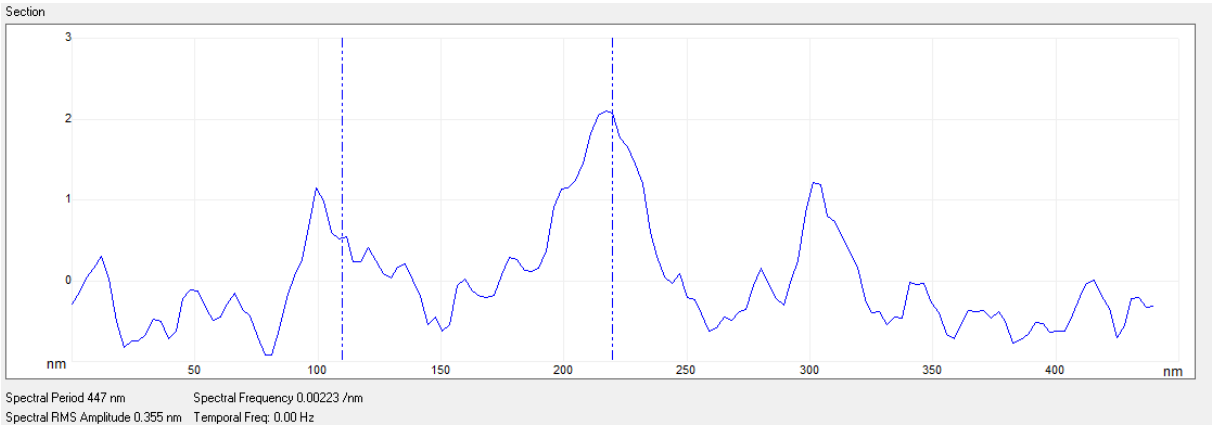

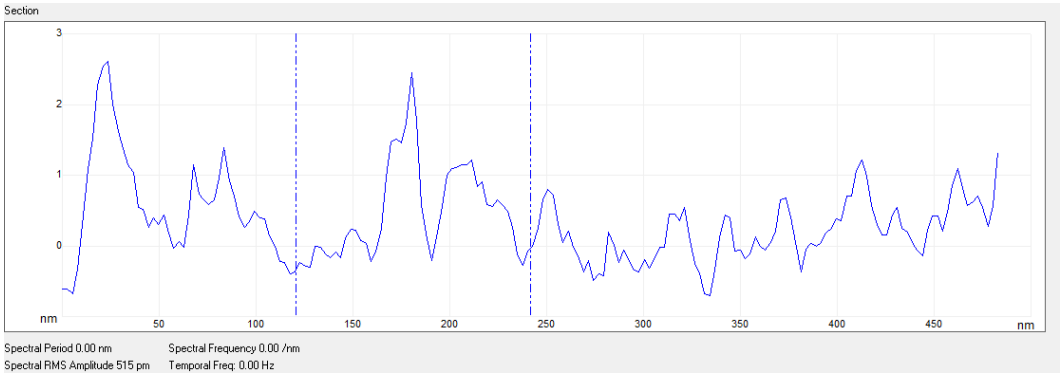

Supplementary Figure S17. DART–HRMS extracted ion chronogram (EIC) (mass window *m/z* 339.0052–339.0072) of MS tag 2 (th. mass 339.0062) of nine scans of SPAAC-modified mica.

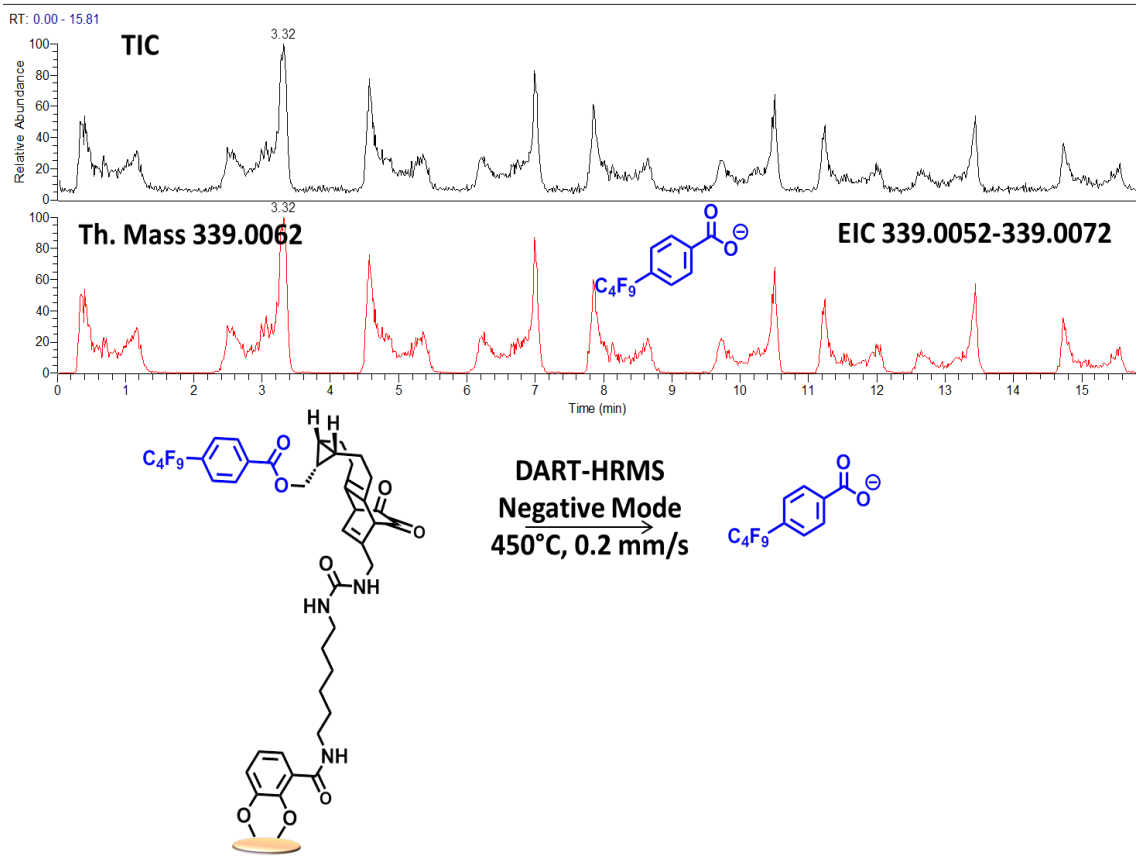

4. SUPPLEMENTARY XPS SPECTRA

S4.1 XPS Wide scan of bare mica (M_0).

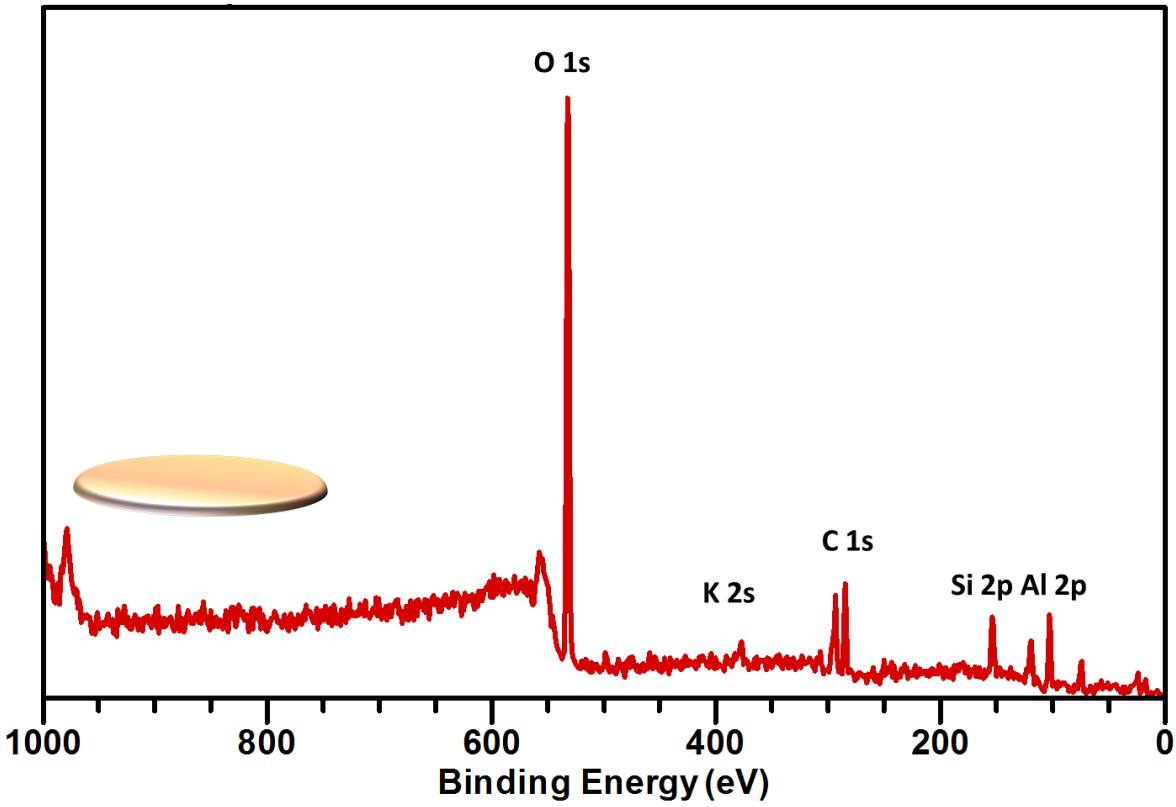

S4.2 XPS Wide scan of modified mica by 1 (M_1).

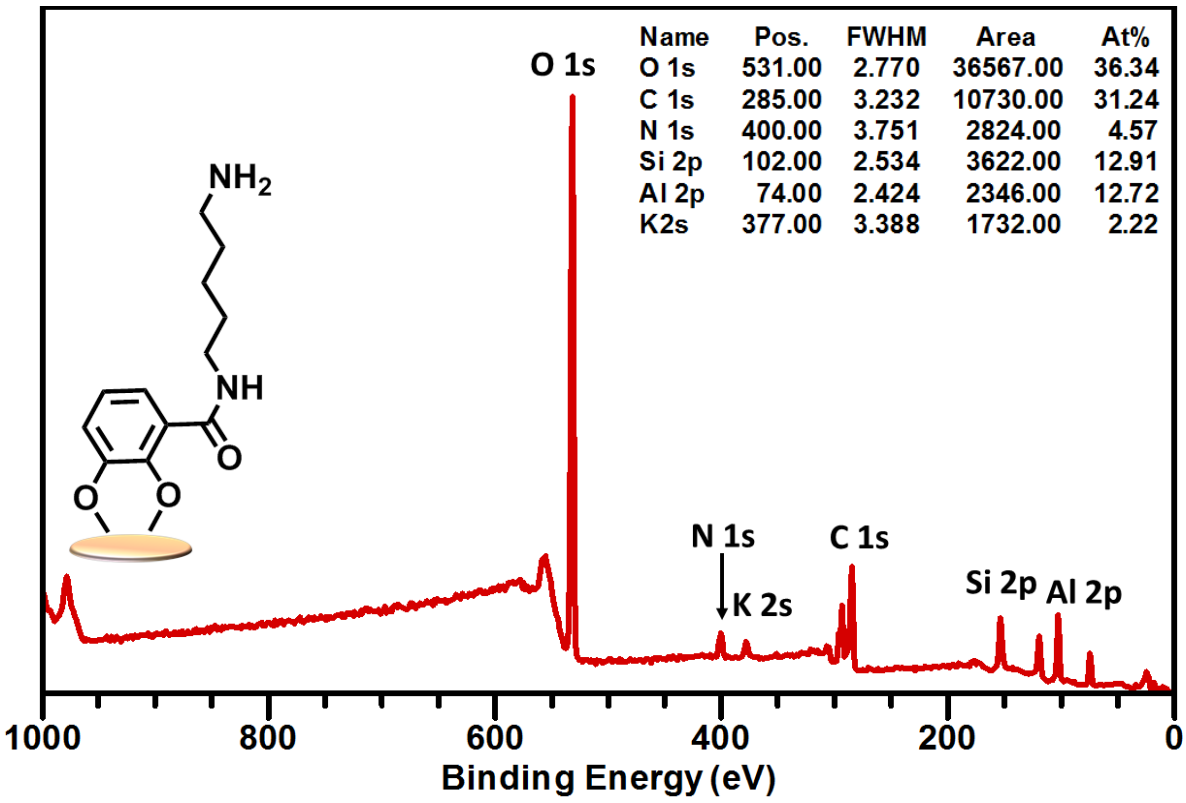

Experimental ratio (C/N) = 31.24/4.57 = 6.8

Theoretical ratio (C/N) = 13/2 = 6.5

S4.3 C 1s XPS narrow scan of M_1-modified mica.

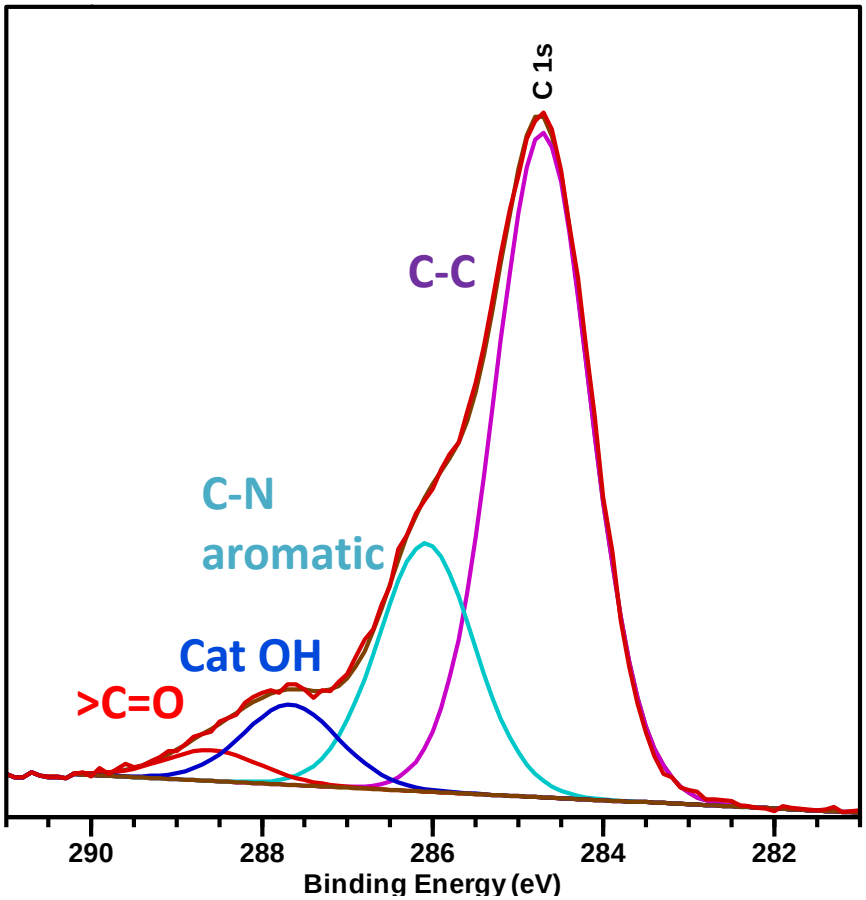

S4.4 XPS wide scan of azide-terminated surface.

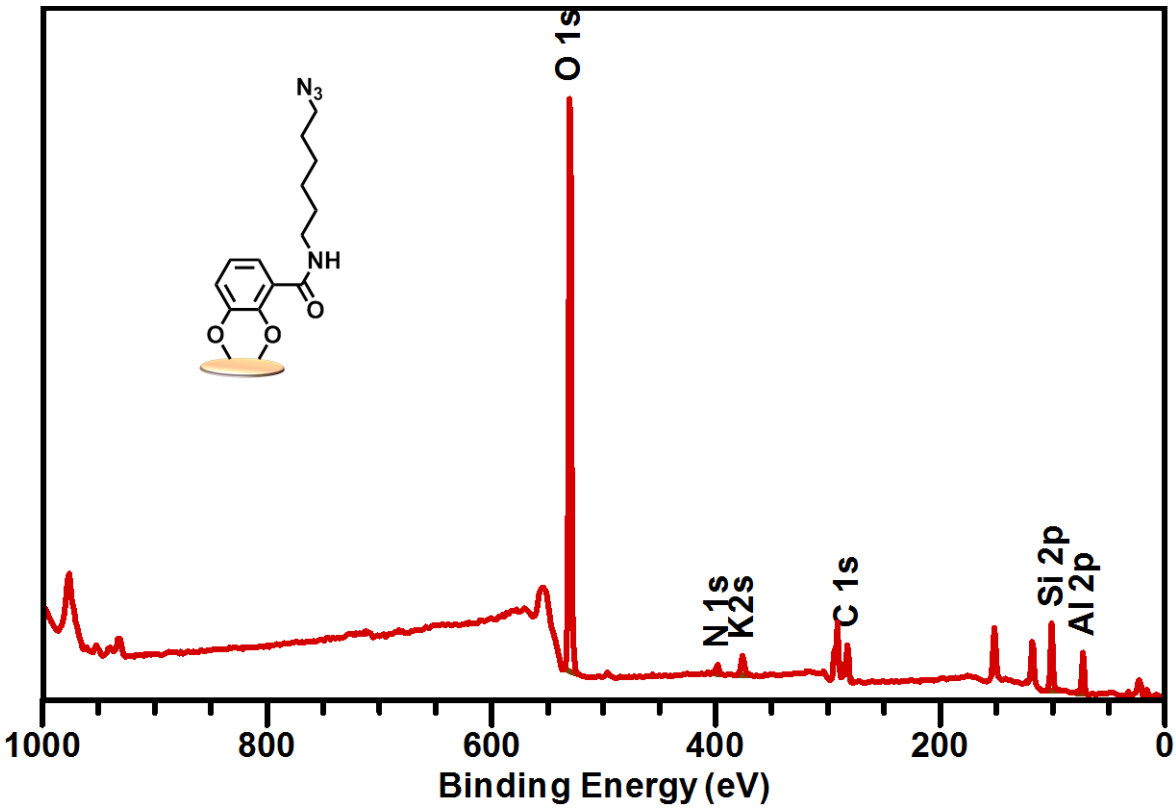

S4.5 XPS N1s narrow scan of azide-terminated surface.

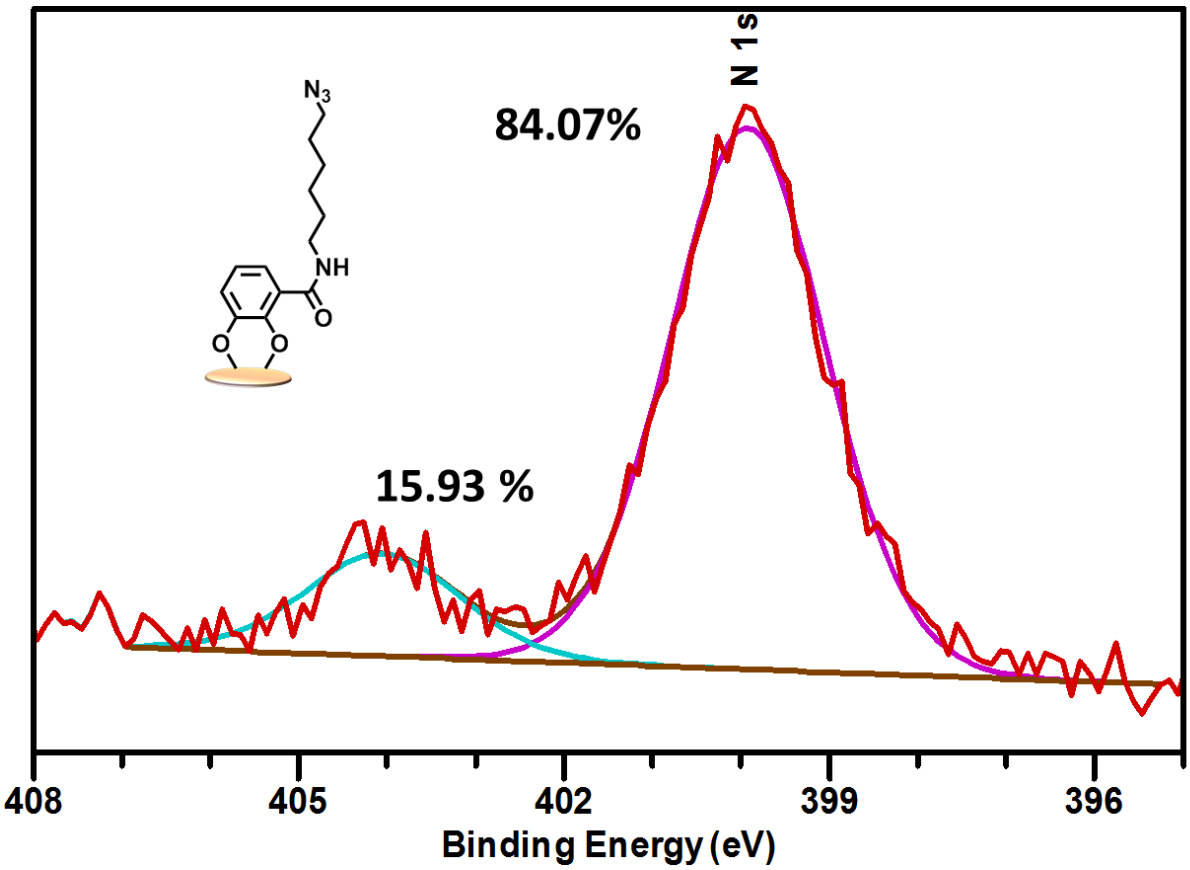

Th. ratio between middle azide N and other kinds of N = 1/3 (assuming 100% conversion of every amine termination with bottom α–amide linker N atom intact).

Obtained ratio = 15.93/84.07 = 0.19

% yield= 0.19/ 0.33 = 57.5 = ~60

S4.6 XPS Wide Scan of SPAAC on azide-terminated surface and calculation of surface yield.

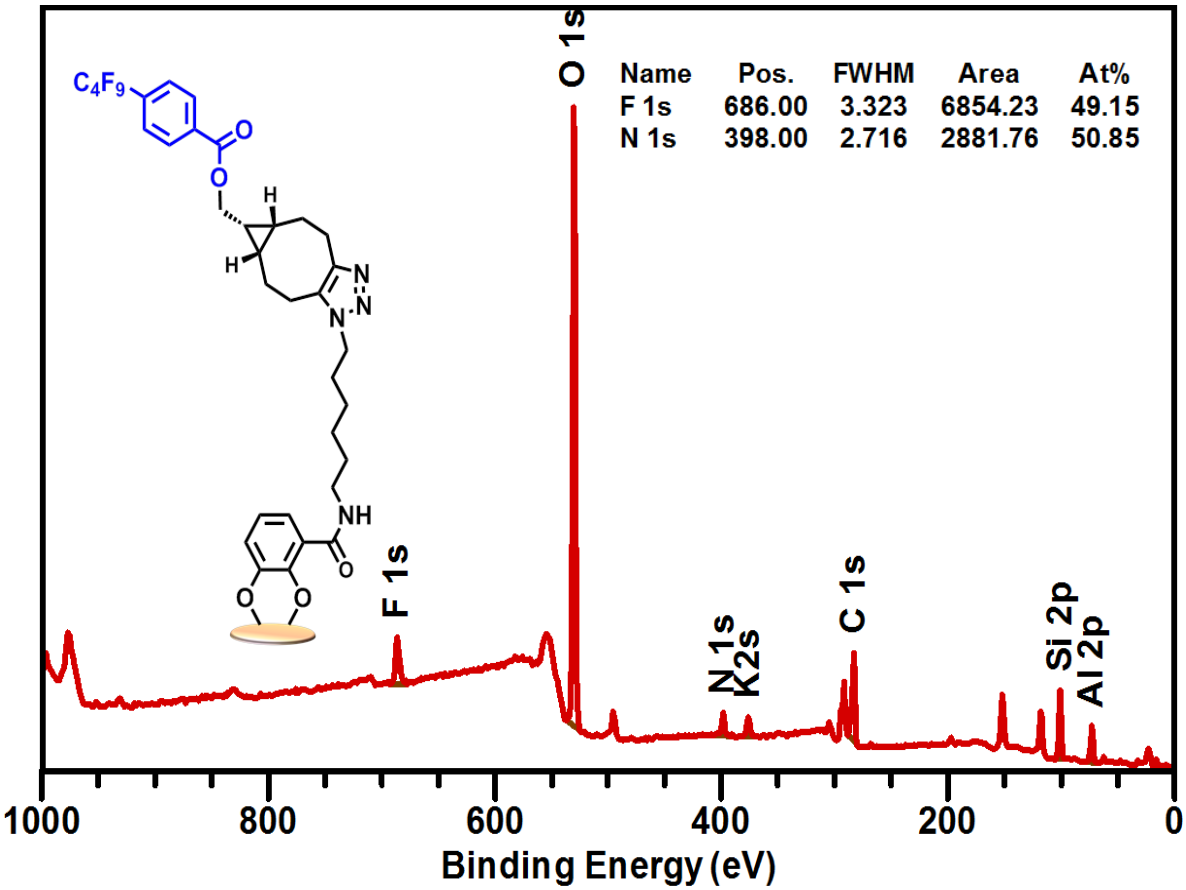

As inferred from the N1s narrow scan of azide-terminated surface, only 60% of the surfacial amines were converted to azides which are capable of further reaction with solution BCN counterpart.

% N capable of reaction = 50.85*0.60 = 31.02

Experimental ratio (F/N) = 49.05/31.02 = 1.51

Theoretical ratio (F/N) = 9/3 = 3

% yield = (1.51/3.0) * 100 = 52

S4.7 XPS C1s narrow scans of SPAAC cycloadduct (M_3) with azide initially on the surface (M_2).

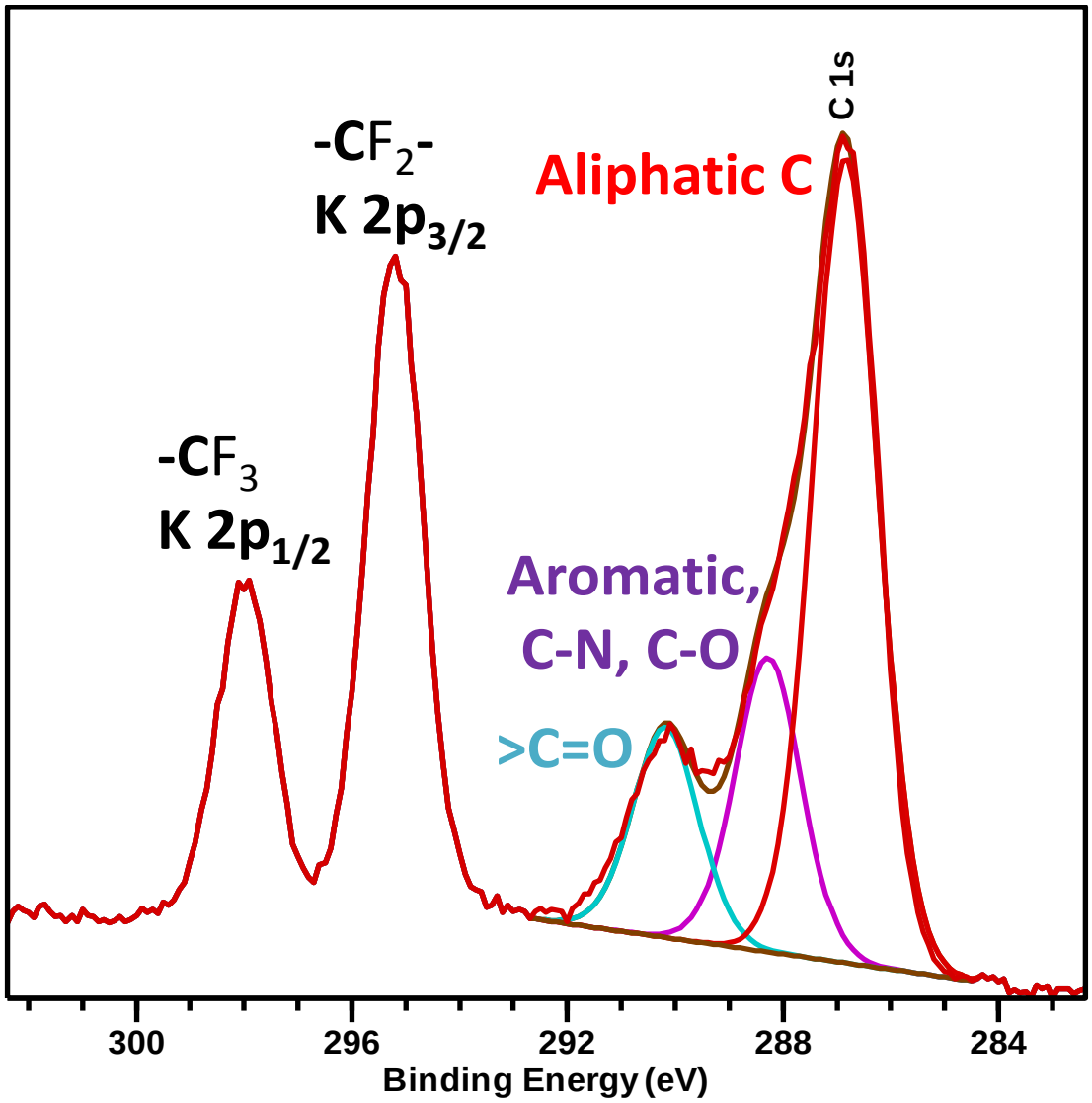

S4.8 XPS N1s narrow scans of SPAAC cycloadduct (M_3) with azide initially on the surface (M_2).

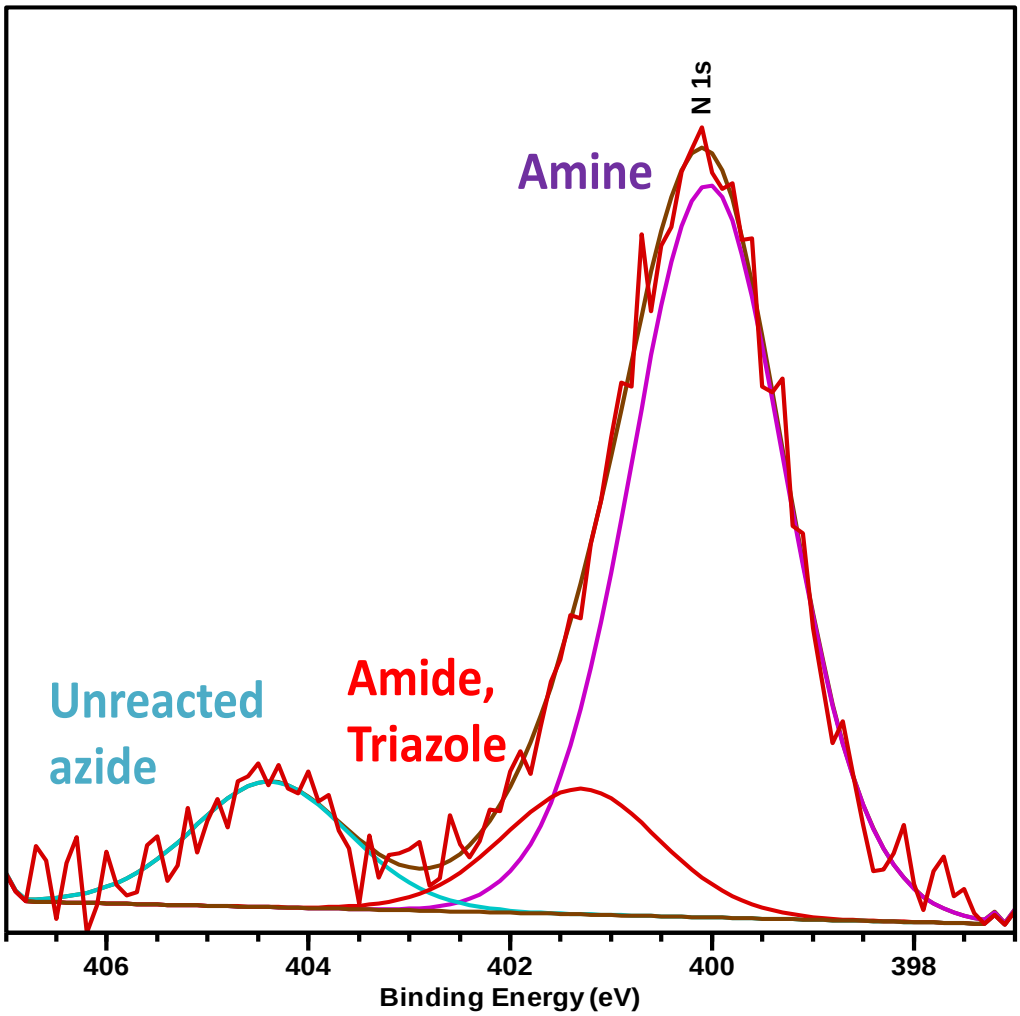

Initial number of N1s (M_1) = 2

After 60% Azide conversion (M_2)= 1 + 0.4 + (3*0.60) = 3.2

After 51% SPAAC (M_3): Total number of N1s = 1 + 0.4 + (3*0.60) = 3.2.

S4.9 XPS C1s Narrow Scan of BCN immobilized on mica surface.

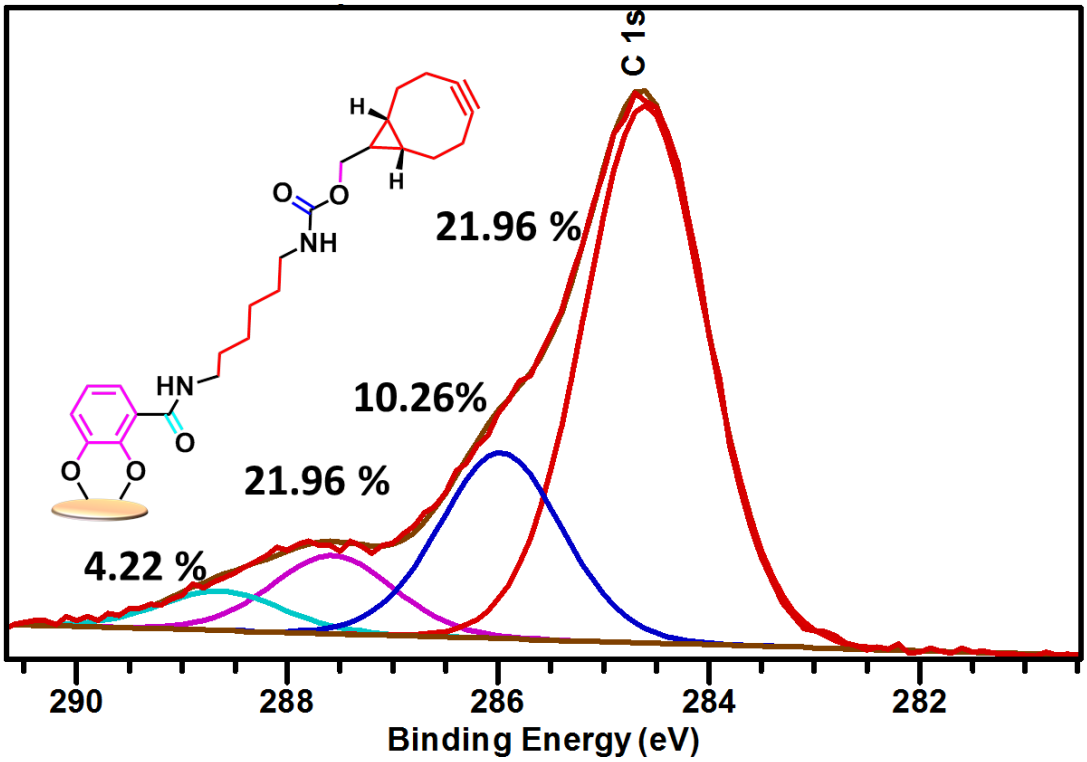

S4.10 XPS wide scan of the inverse SPAAC cycloadduct with BCN (M_5) immobilized on mica surface.

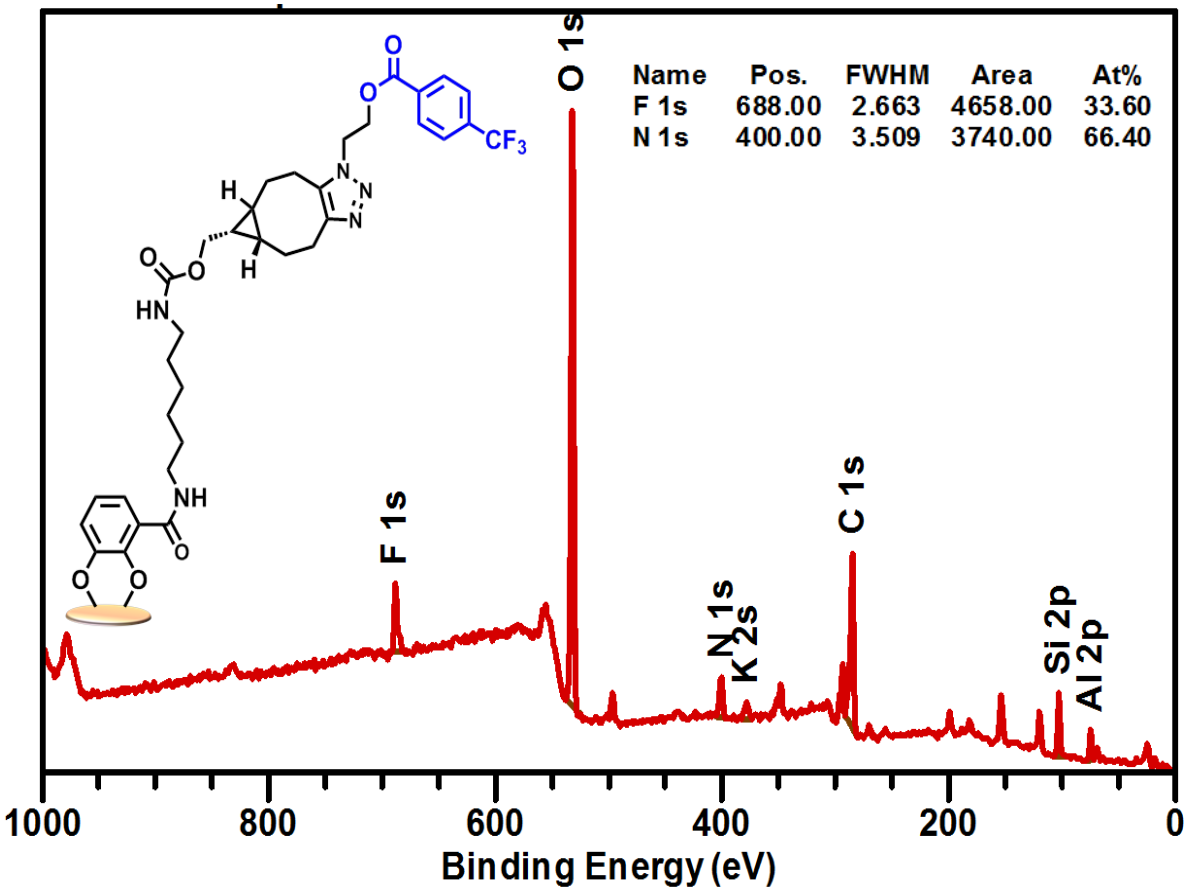

Theoretical ratio (F/N) = 3/5 = 0.6

% yield =(0.5/0.6) * 100 = 83.3

S4.11 XPS N1s narrow scans of the inverse SPAAC cycloadduct (M_5) with BCN initially on the surface (M_4).

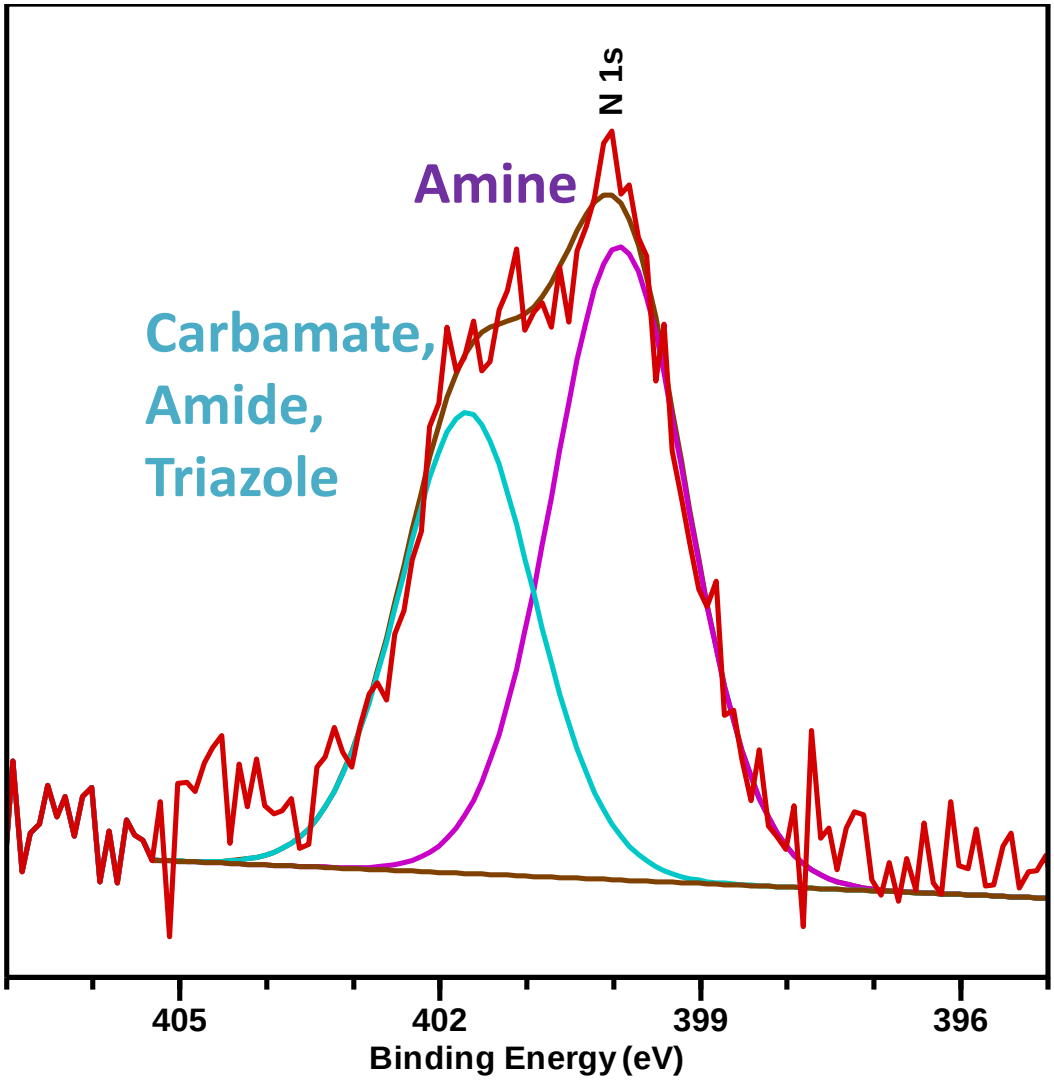

Initial number of N1s (M_4) = 2

After 83% SPAAC (M_5): Total number of N1s = 2 + (0.83*3) = 4.49

S4.12 XPS C1s narrow scans of the inverse SPAAC cycloadduct (M_5) with BCN initially on the surface (M_4).

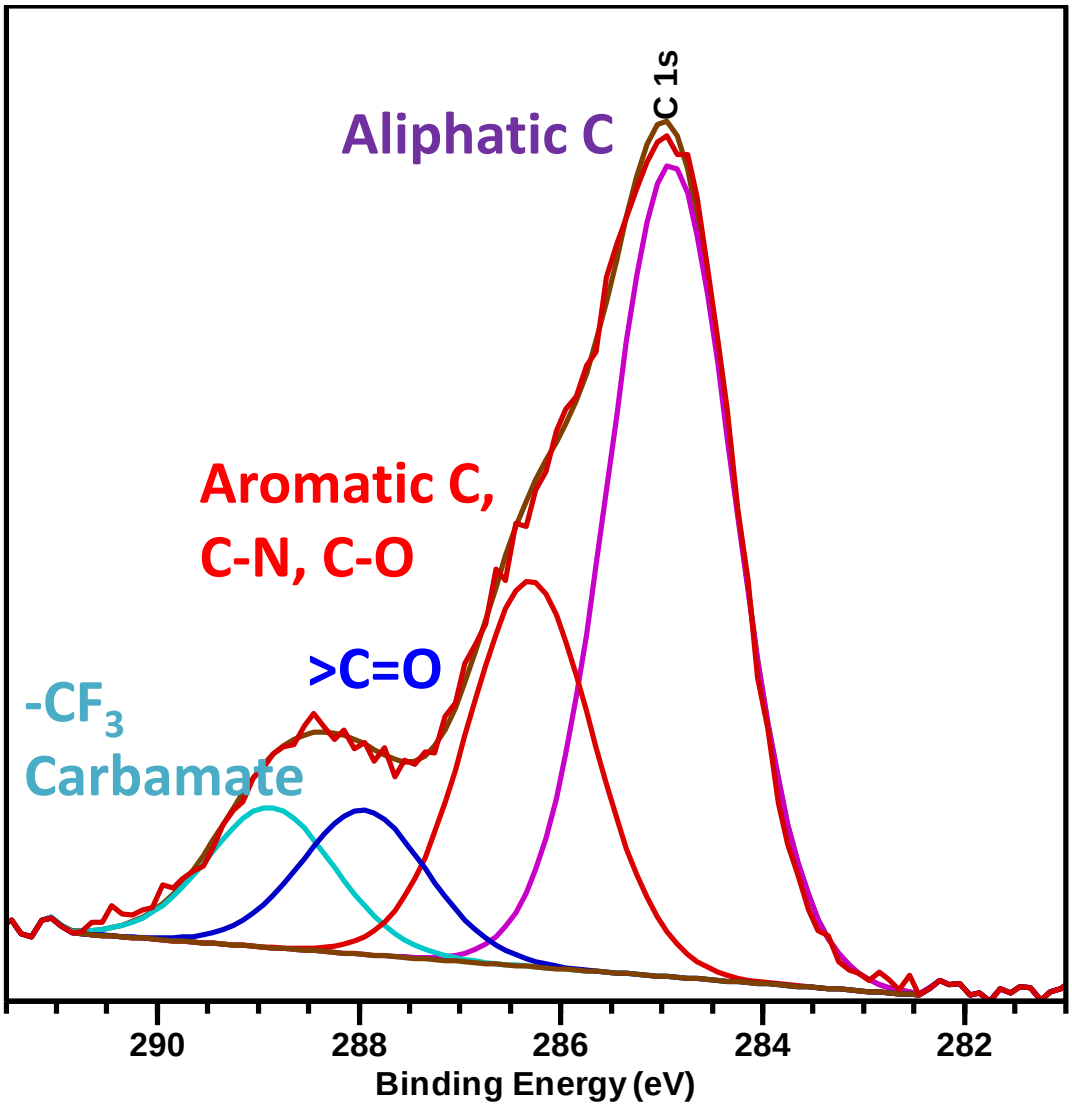

S4.13 XPS wide scan of quinone-terminated surface.

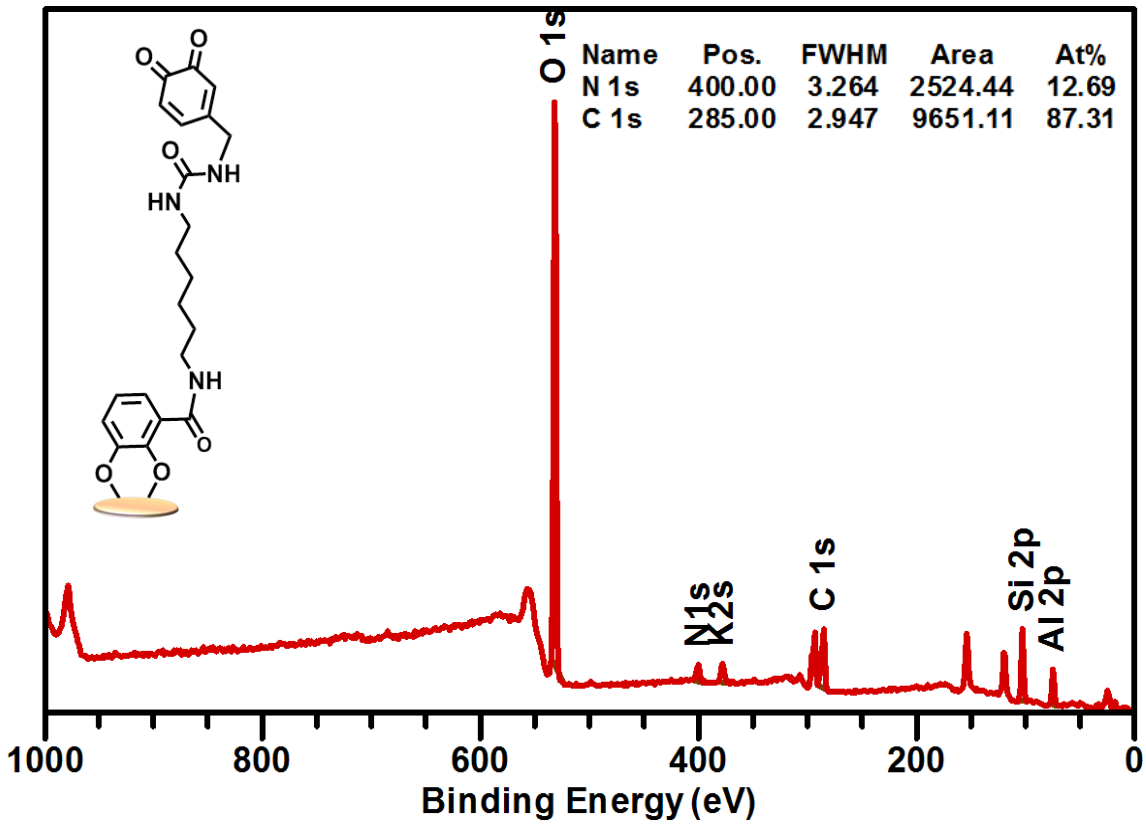

Experimental ratio (C/N) = 87.31/12.69 = 6.9

Theoretical ratio (C/N) = 21 /3 = 7

% yield quinone on surface =100

S4.14 XPS wide scan of SPOCQ cycloadduct with BCN immobilized on mica surface (M_7).

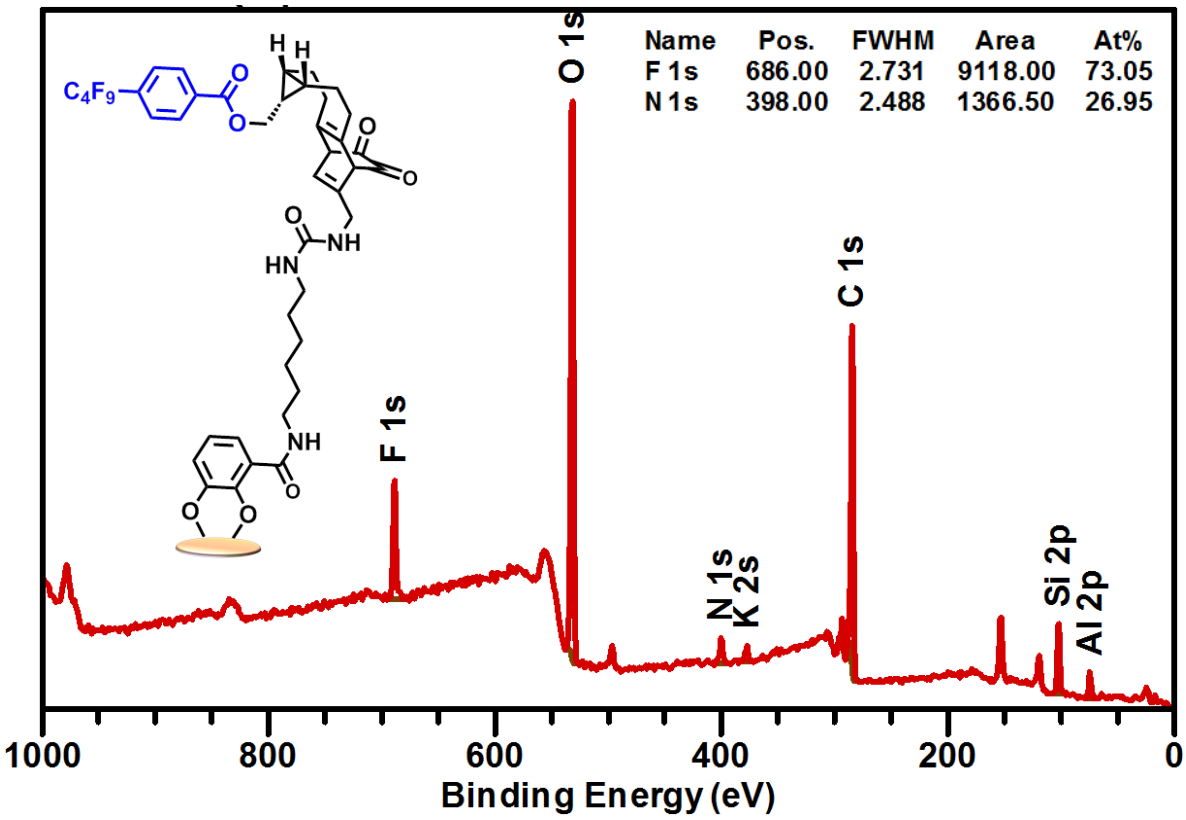

Experimental ratio (F/N) = 73.05/26.95 = 2.71

Theoretical ratio (F/N) = 9/3 = 3.0

% yield quinone on surface = 90.3

S4.15 XPS C1s narrow scan of SPOCQ cycloadduct (M_7) on surface.

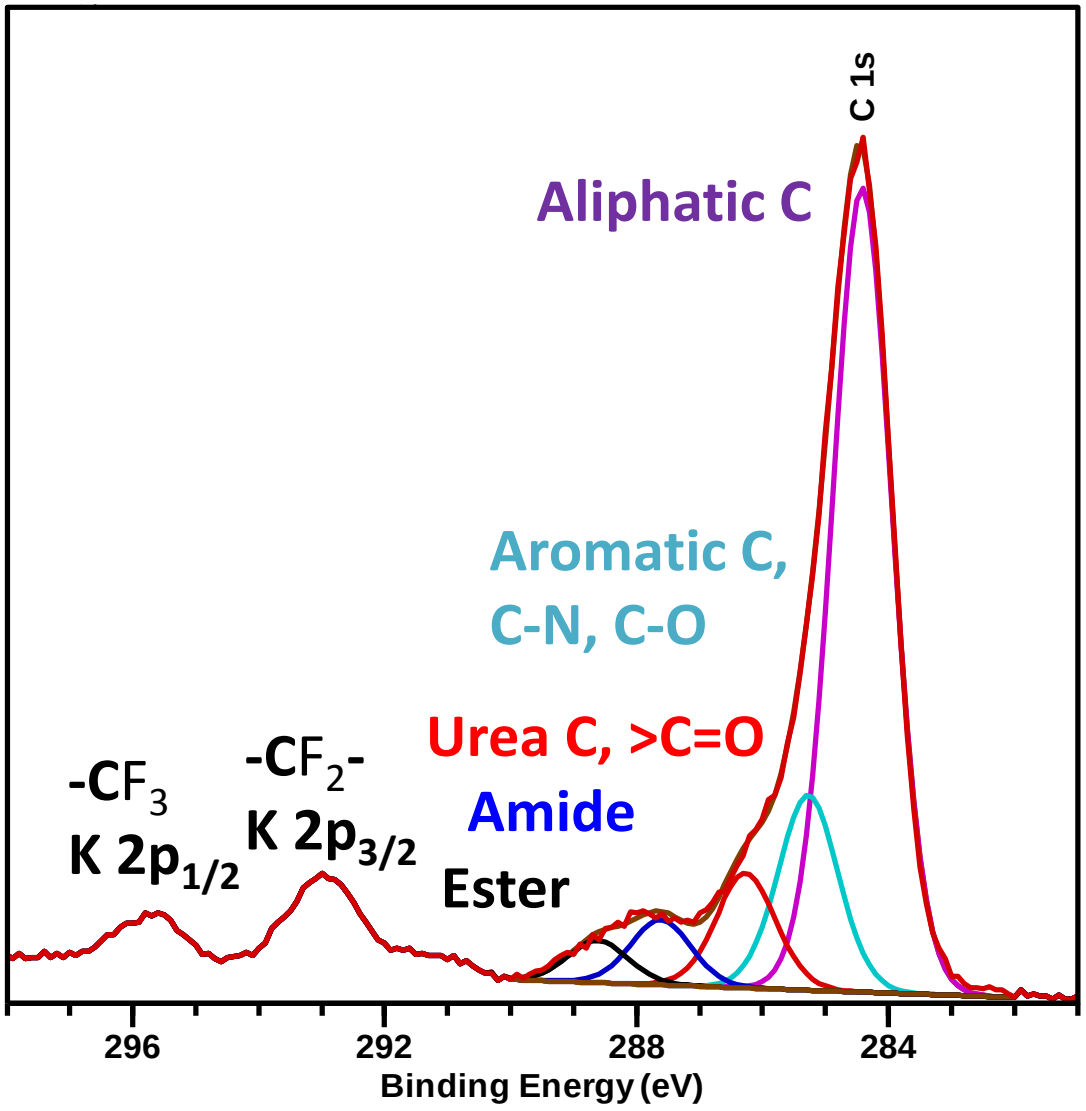

S4.16 XPS N1s narrow scan of SPOCQ cycloadduct (M_7) on surface

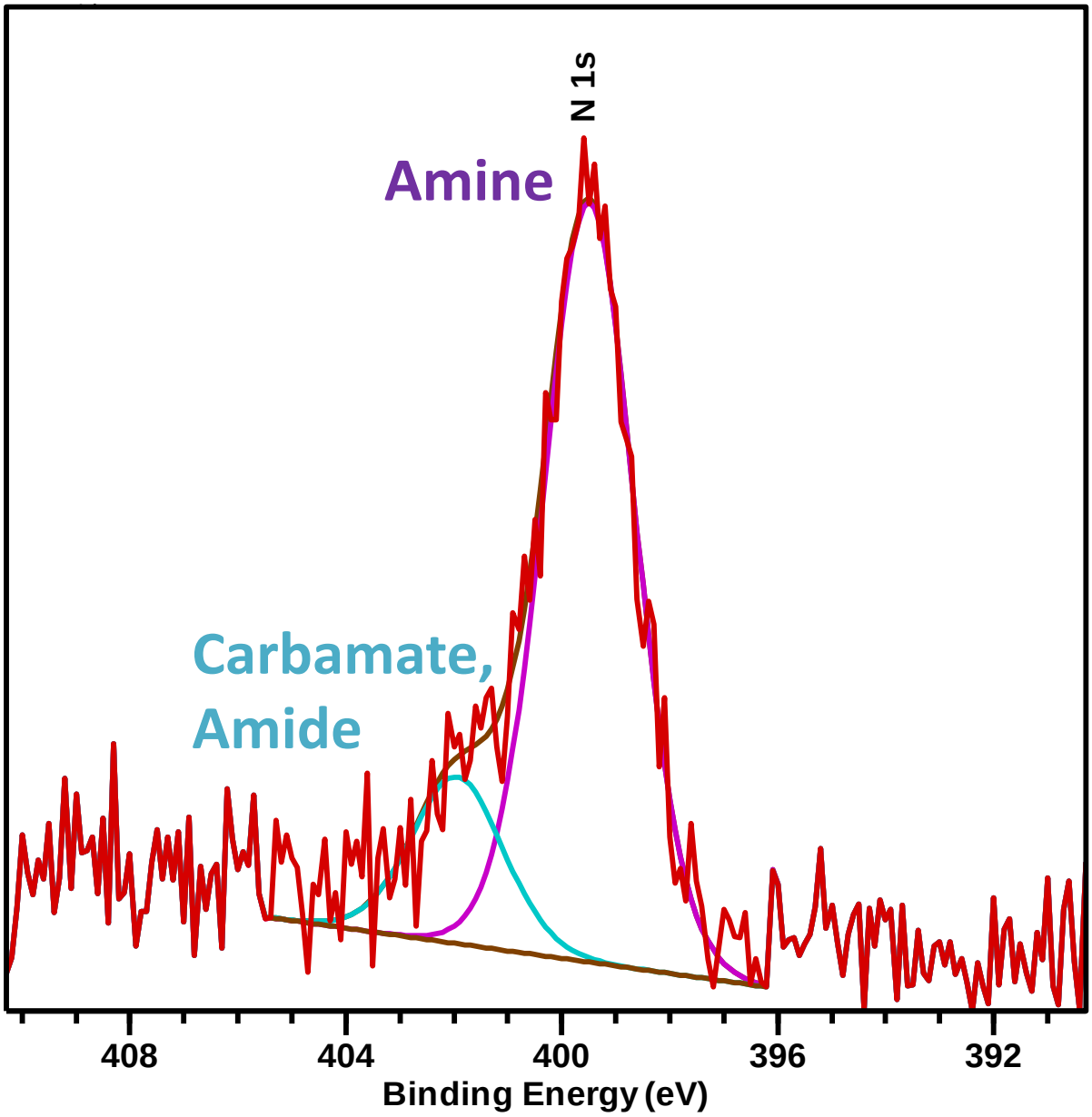

S4.17 Wide scan XPS spectra of EAD2 immobilized on mica surface (inset: Fe2p narrow spectra of the EAD2–based hGQ DNAzyme–functionalized mica).

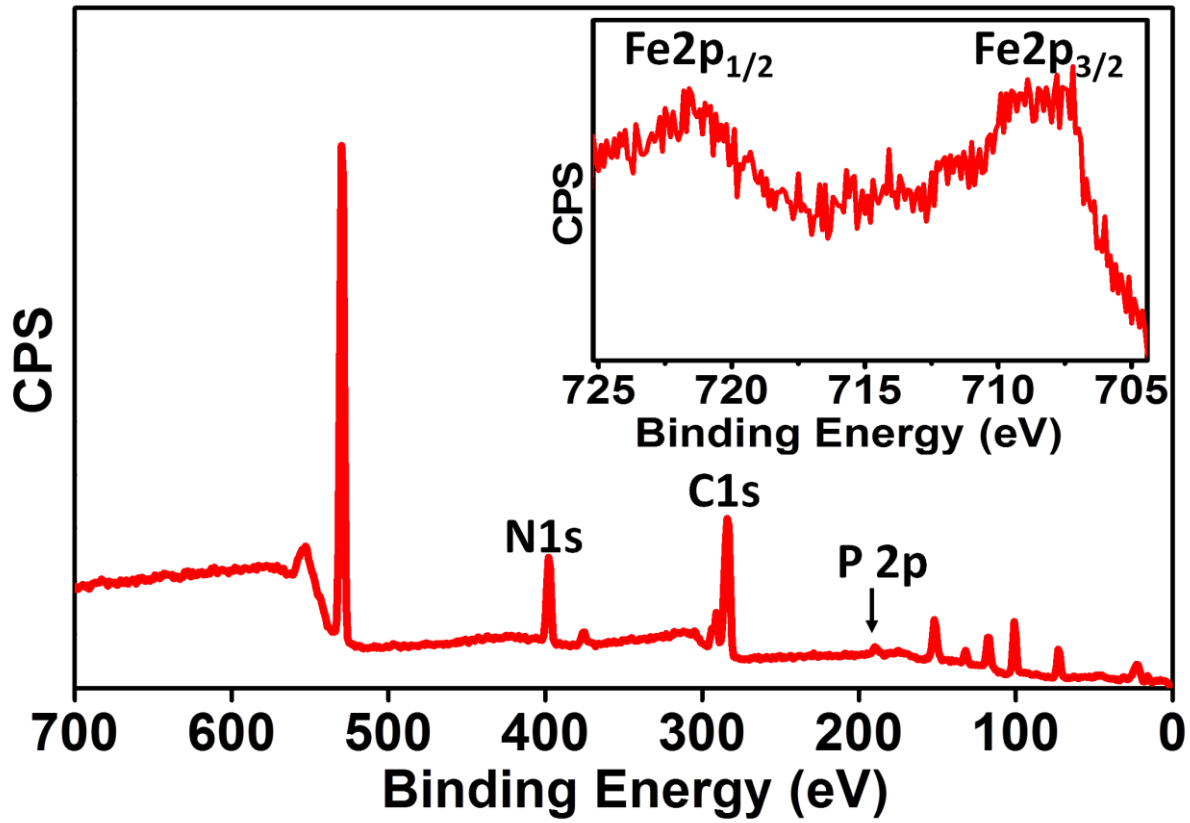

S4.18 XPS C1s narrow scan of EAD2 DNA immobilized on surface.

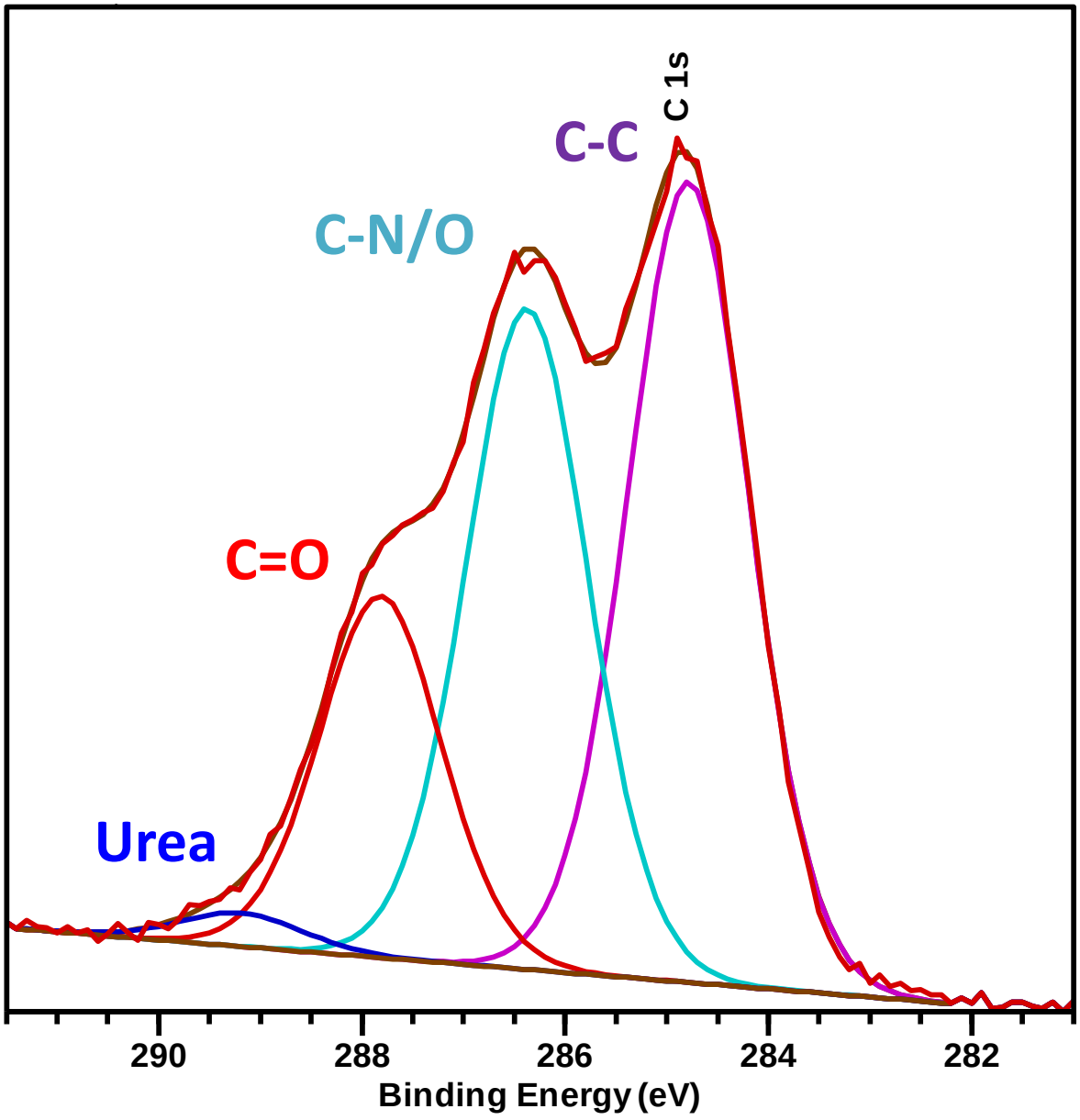

5. SUPPLEMENTARY TABLES

Supplementary Table S1. Control experiments to show importance of each modular part of surface anchor 1, thus showing the synergy between them in achieving covalent modification of mica.

SCA Data

Type of modification	SCA (°) after 1h	SCA Picture
Bare Mica (M_0)	<15	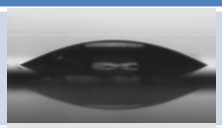
M_1	**55** (24h)	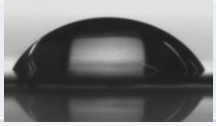
Neutralized Catechol-C_6-amine	<15 -NH_3^+ necessary condition	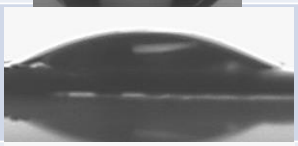
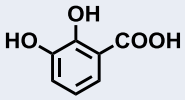	<15 -NH_3^+ necessary condition	
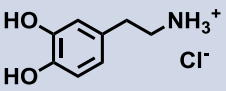	25 Amide necessary condition	
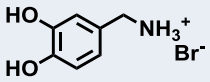	< 15 Amide necessary condition	

Supplementary Table S2. Different DNA sequences immobilized on mica surface.

DNA	Sequence
D1	5'–ATAATTACTA/5iUniAmM/CATGTCTGCG–3'
D2	5'–AGAGATTTTTATATATTTTTCGCAGACATG ATAGTAATTATTAGAGATTTTTATAT–3'
D3	5'–AAAATATATAAAAATCTCTA–3'
D4	5'–AAAAATATATAAAAA–3'
D5	5'–ATTTTTTAGAGATTTTTATATATTTTT TAGAGATTTTTATATATTTTTTAGAGATT–3'
D6	5'–ATAAAAATCTCTAAAAAATATATAAAAAT CTCTAAAAAATATATAAAAATCTCTAA–3'
D7	5'–TTTATATATTTTTTAGAGATTTTTATATA TTTTTTAGAGATTTTTATATATTTTTT–3'
D8	5'–CTCTAAAAAATATATAAAAATCTCTAAAA AATATATAAAAATCTCTAAAAAATAT–3'
GQ–anchor	5'–/5AmMC12/GCGGAGGCG–3'
GQ–Wire	5'–GCGGAGGCG–3'
EAD2	5'–/5AmMC12/CTGGGAGGGAGGGAGGGA–3'

6. DFT SIMULATIONS FOR XPS C1S NARROW SCAN ASSIGNMENTS.

6.1 DFT simulation of XPS C1s narrow scan of **M_1** surface.

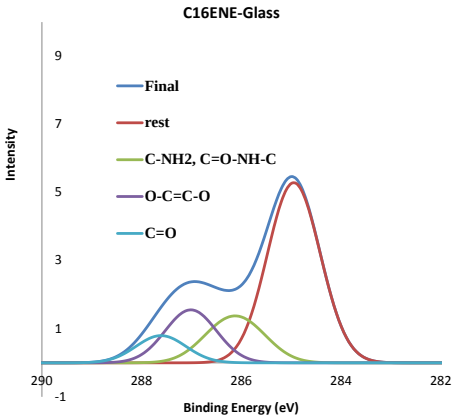

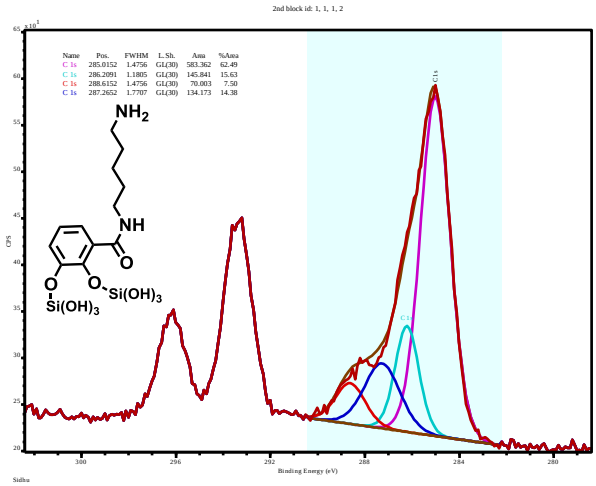

No.	1,4-6, 13-15	16,12	2,3	9
Groups	rest	C-NH2, C=O-NH-C	O-C=C-O	C=O
Theory	7 (285.0)	2 (286.1)	2 (287.0)	1 (288.6)
Expt	7.5 (285.0)	1.9 (286.2)	1.7 (287.3)	0.9 (288.6)

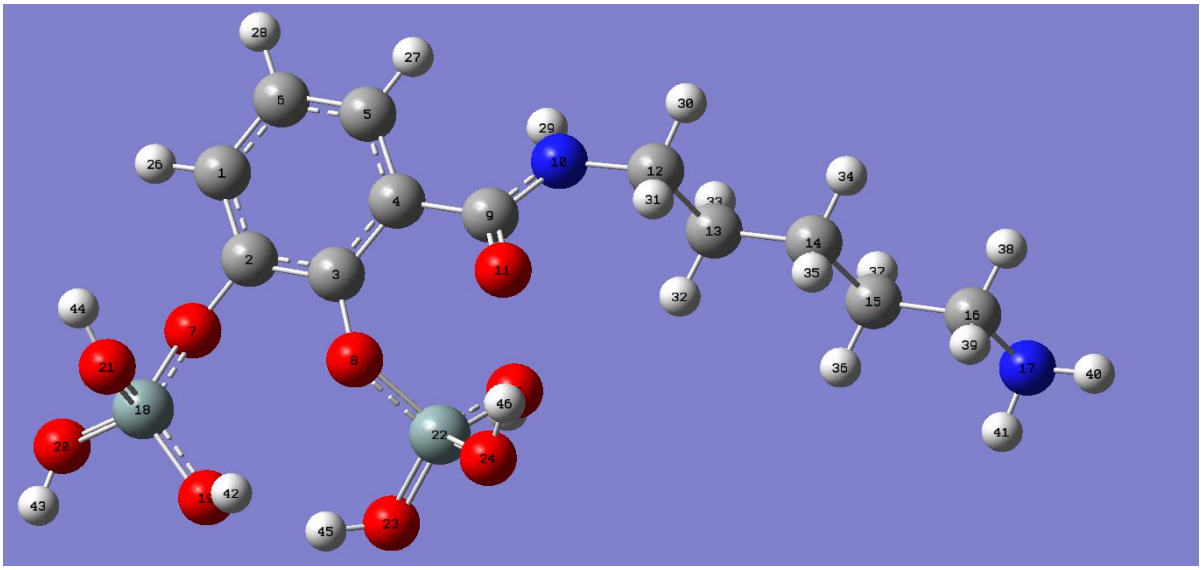

6.2 DFT simulation of XPS C1s narrow scan of **M_2**.

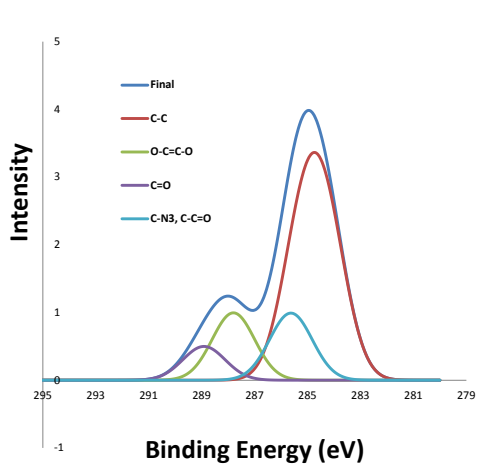

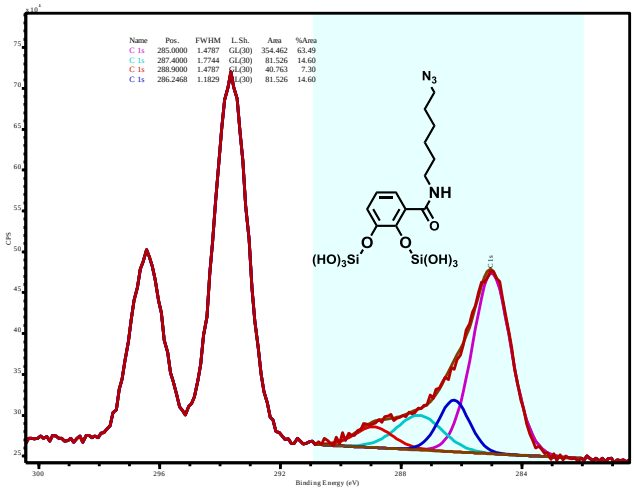

No.	1, 5-14	4, 15	2, 3	16
Groups	C-C	C-N3, C-C=O	O-C=C-O	C=O
Theory	8 (285.0)	2 (285.6)	2 (287.8)	1 (288.9)
Expt	8.2 (285.0)	1.9 (286.2)	1.9 (287.4)	0.9 (288.9)

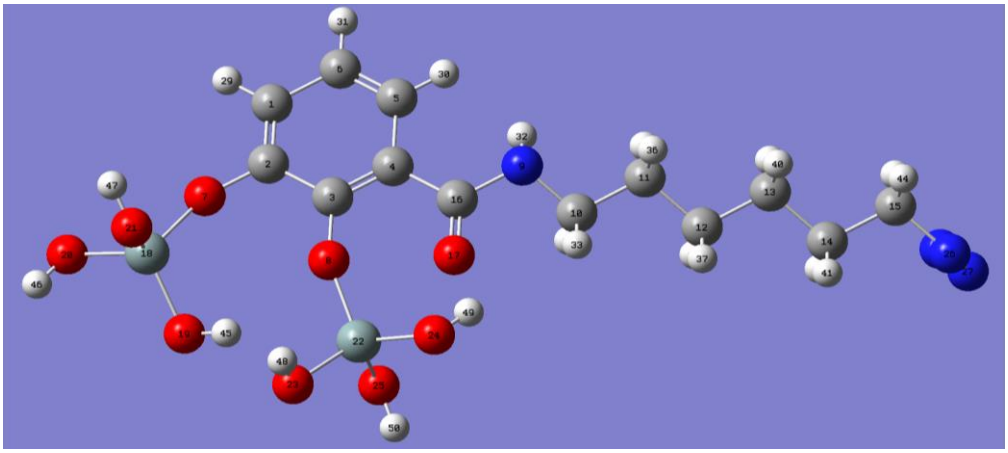

6.3 DFT simulation of XPS C1s narrow scan of **M_3**.

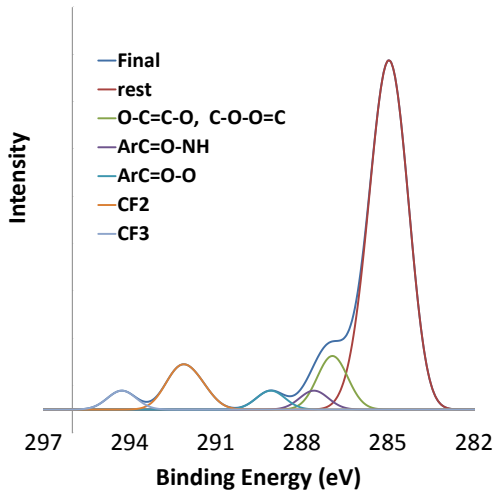

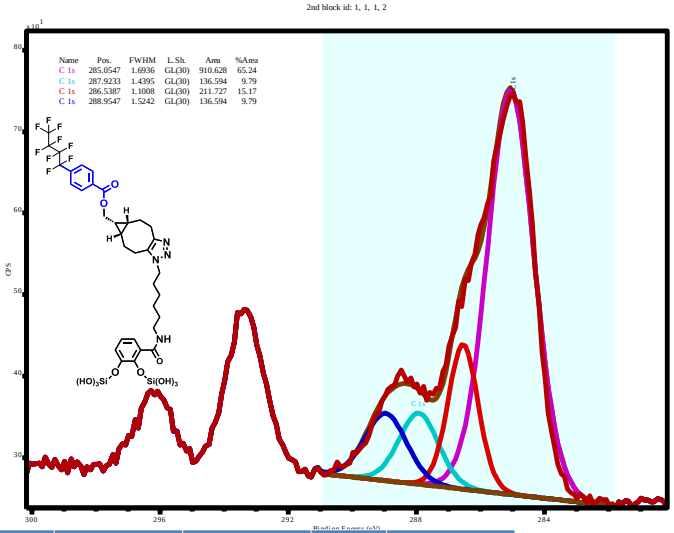

No.	5-10, 14-22, 26, 29-40,	27, 28, 23	41	3	11, 43, 44	45
Groups	C-C	O-**C**=**C**-O, C-O-O=C	ArC=O-NH	ArC=O-O	CF2	CF3
Theory	25 (285.0)	3 (287.0)	1 (287.6)	1 (289.1)	3 (292.1)	1 (294.3)
Expt	19.6 (285.0)	4.5 (286.5)	2.9 (288.0)	2.9 (288.9)	---	---

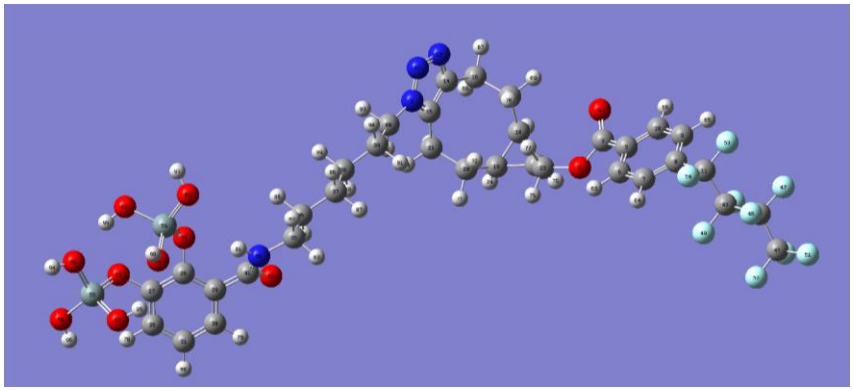

6.4 DFT simulation of XPS C1s narrow scan of **M4**.

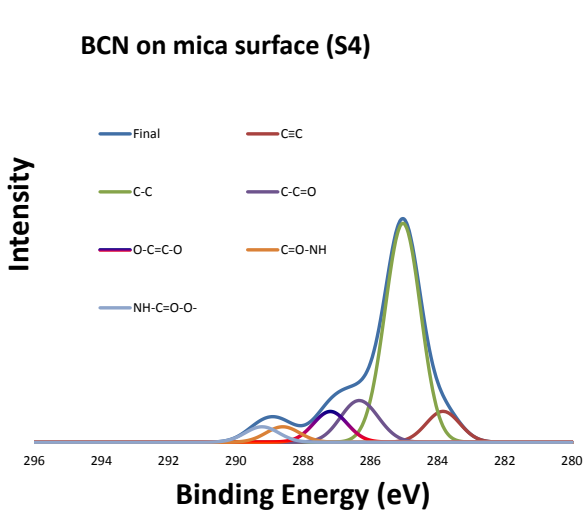

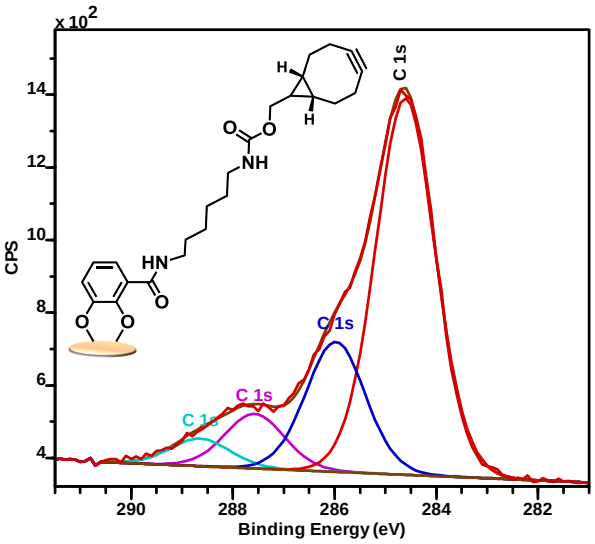

No.	30, 31	1,4-6, 13-16, 25-29, 32-33	17, 24,12,	2,3	18	21
Groups	C≡C	C-C	**C**-NH-C=O-O-**C** C=O-NH-**C**	O-C=C-O	C=O-NH	NH-C=O-O-
Theory	2 (283.8)	15 (285.0)	3 (286.3)	2 (287.2)	1 (288.8)	1 (289.2)
Expt	16.5 (285.0)		4.1 (286.4)	2.0 (287.9)	1.3 (289.0)	

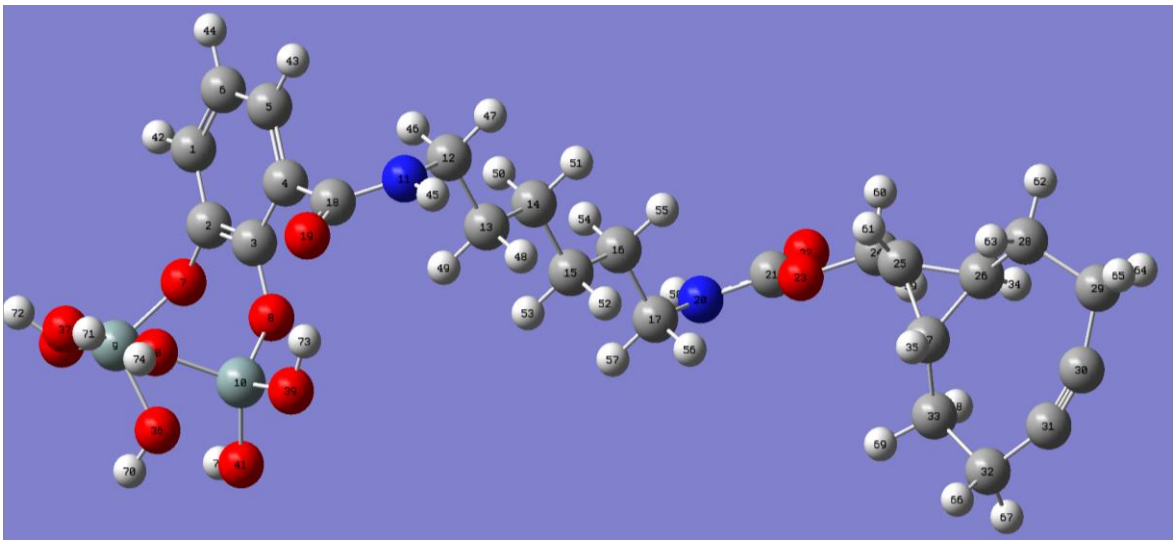

6.5 DFT simulation of XPS C1s narrow scan of **M_5**.

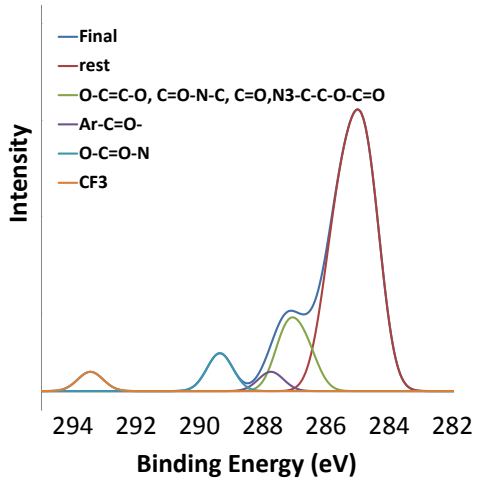

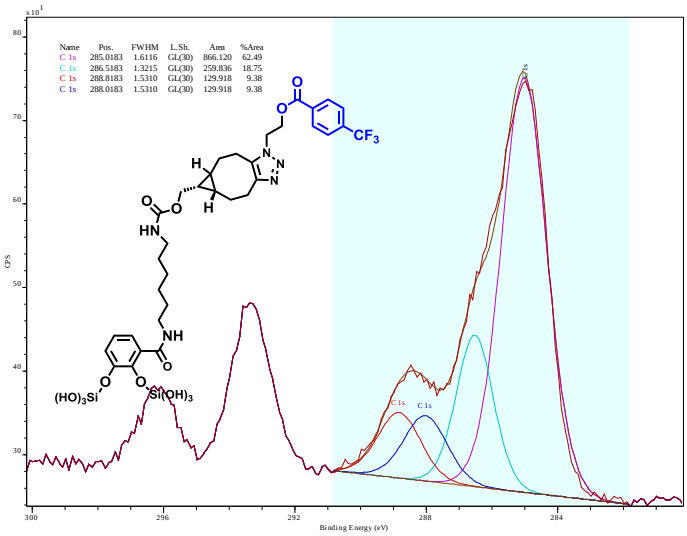

No.	1, 4-14, 22-31, 41-46	2,3,15, 16, 37,38,	16	19, 40	56
Groups	C-C	O-C=C-O, C=O-N-C, C=O,N3-C-C-O-C=O	Ar-C=O-	O-C=O-N	CF3
Theory	25 (285.0)	6 (287.0)	1 (287.7)	2 (289.9)	1 (293.4)
Expt	21.6 (285.0)	6.6 (286.5)	3.1 (288.0)	3.1 (288.8)	---

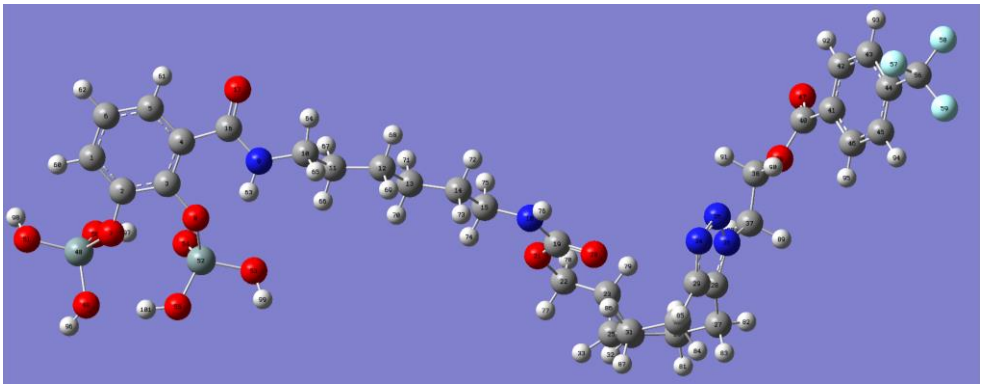

6.6 DFT simulation of XPS C1s narrow scan of **M_6**.

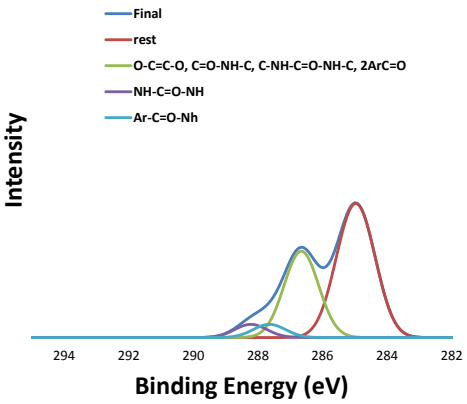

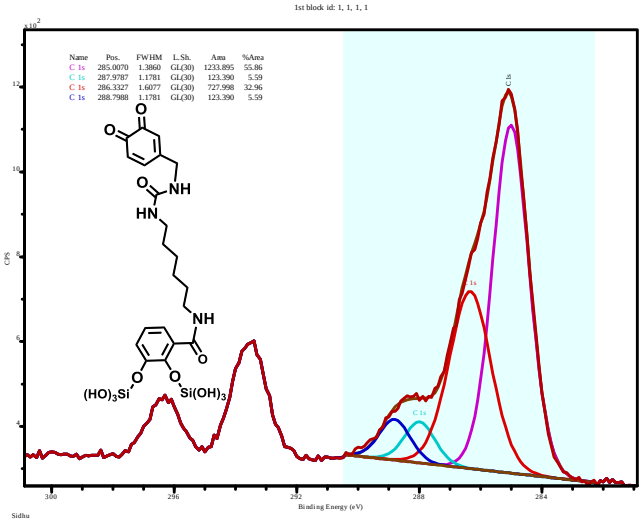

No.	1, 4,5, 6, 11-14, 21-22, 25-26	2,3,10, 15, 20, 23, 24,	17	29
Groups	rest	O-C=C-O, C=O-NH-C, C-NH-C=O-NH-C, 2ArC=O	NH-C=O-NH	Ar-C=O-Nh
Theory	12 (285.0)	7 (286.7)	1 (287.6)	1 (288.2)
Expt	11.7 (285.0)	6.9 (286.3)	1.1 (288.0)	1.1 (288.8)

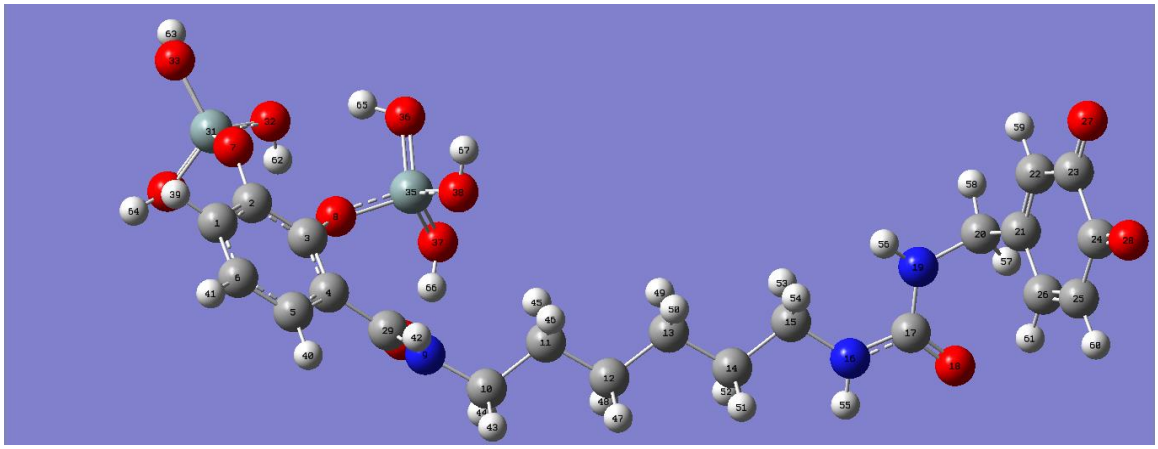

6.7 DFT simulation of XPS C1s narrow scan of **M_7**.

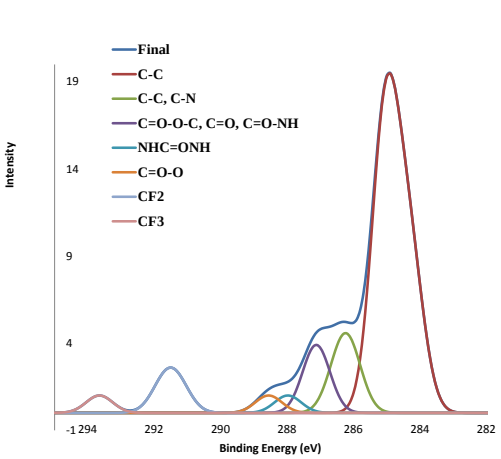

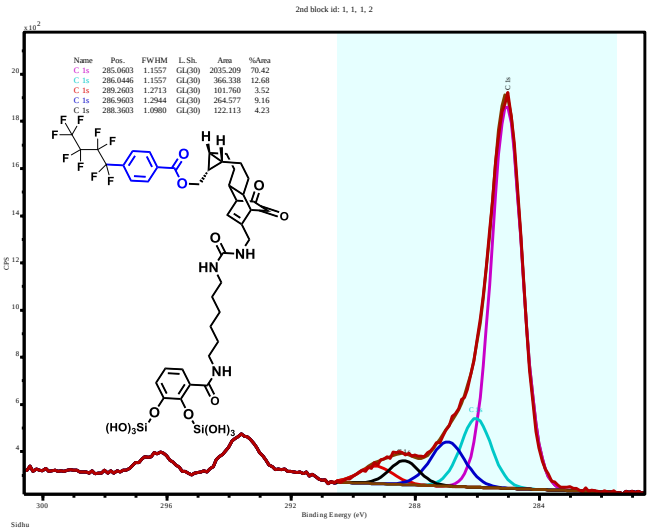

No.	1,4-6, 11-14, 20-23, 25, 28-36, 42-47,	2, 3, 10, 15, 20,	24, 26, 38, 50	17	40	53,54, 48	55
Groups	C-C	C-C, C-N	C=O-O-C, C=O, C=O-NH	NHC=ONH	C=O-O	CF2	CF3
Theory	28 (285.0)	5 (286.3)	4 (287.1)	1 (288.0)	1 (288.6)	1 (281.6)	1 (293.7)
Expt	27.4 (285.0)	4.9 (286.0)	3.6 (287.0)	1.3 (288.3)	1.6 (289.3)	--	--

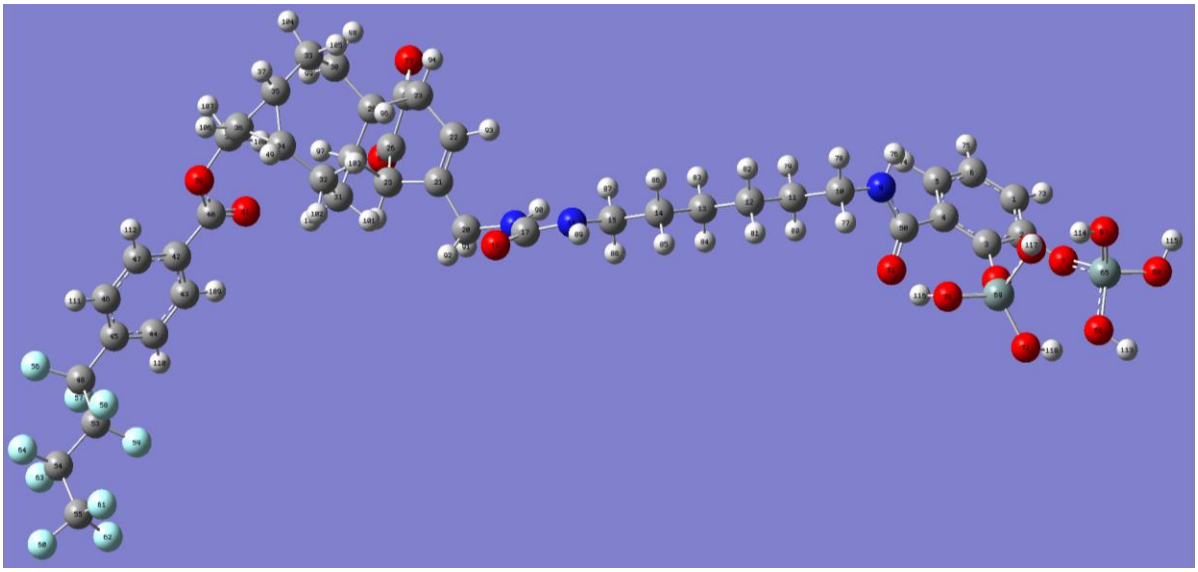

APPENDIX 6

Approach matters: The kinetics of interfacial inverse–electron demand Diels–Alder reactions

1. MATERIAL AND METHODS.

Materials. Unless otherwise specified, all chemicals were used as received without further purification. Octylphosphonic acid, hexadecylphosphonic acid, 1,1'–carbonyldiimidazole (CDI), *exo*–5–norbornene–2–methanol (racemic), hydrochloric acid, methanol, hexane, acetone, dichloromethane (CH_2Cl_2), 1,2–dichloroethane (DCE) and 2–propanol were purchased from Sigma–Aldrich. 12–Aminododecylphosphonic acid hydrochloride salt and 6–aminohexylphosphonic acid hydrochloride salt were purchased from SiKÉMIA. Aluminium pieces (99.5% purity, mirror polished, Staalmarkt Beuningen BV) were cut using mechanical cutter into exactly 2 × 1 cm dimension. For surface modification reactions, the samples were loaded onto a specially constructed PTFE wafer holder able to hold up to 16 samples at a time thus ensuring rigorous reproducibility between samples.

X–ray Photoelectron Spectroscopy (XPS) Measurements. The XPS analysis of surfaces was performed using a JPS–9200 photoelectron spectrometer (JEOL, Japan). Survey and high–resolution spectra were obtained under UHV conditions using monochromatic Al Kα X–ray radiation at 12 kV and 20 mA, and an analyzer pass energy of 50 eV for wide scans and 10 eV for narrow scans. The emitted electrons were collected at 10° from the surface normal (take–off angle relative to the surface normal 10°). All XPS spectra were evaluated by using Casa XPS software (version 2.3.15). Survey spectra were corrected with linear background before fitting, whereas high–resolution spectra were corrected with linear background. Atomic area ratios were determined after a baseline correction and normalizing the peak area ratios by the corresponding atomic sensitivity factors (1.00 for C1s, 1.80 for N1s, 2.93 for O1s, 4.43 for F1s, 1.18 for P2s and 0.75 for Al2s).

DART–HRMS Measurements. Analysis of the modified mica surfaces was performed using a DART–SVP ion source (Ion–Sense, Saugus, MA, USA) coupled to a Q–Exactive orbitrap high–resolution mass spectrometer (Thermo Fisher Scientific, San Jose, CA, USA), mounted on a motorized rail travelling at 0.2 mm/s. Thermo Scientific

Xcalibur software (V2.1.0.1139) was used for data acquisition and processing. The measurements were performed in negative mode at 450 °C using a scan range of *m/z* 188.6–189.4, a mass resolution of 70000 (FWHM) at a scan rate of 1 Hz. The ion trap was tuned with 0.1 mg/mL methanol solution of quinine (*m/z* 323.41 in negative mode) and optimized. The DART source was positioned 6.1 cm on the horizontal scale, 7 cm on the vertical scale with an angle of 45°, such that it is around 1 mm above the surface (Fig. S4.1). The distance from the surface to the ceramic tube is minimized by placing them at the edge of the moving rail so that maximum of the (4–trifluoro)methyl benzoate ion (*m/z* 189.016 respectively) would enter the MS.

Computational Procedures. All of the DFT calculations reported herein were carried out using Gaussian09. All geometries were fully optimized using the M06–2X functional[23] and the 6–311+G (d,p) basis set, which has been found to give relatively accurate energetics for cycloadditions. Analytical frequencies were calculated at this level in all cases, and the nature of the stationary points was determined in each case according to the proper number of imaginary frequencies. The intrinsic reaction coordinate (IRC) path was traced to check the energy profiles connecting each transition state to the two associated minima of the proposed mechanism. Initially, a Monte Carlo conformational search using conformer distribution option available in Spartan'14 was used (Wavefunction, Inc., Irvine, CA, USA, 2014.). With this option, a search without constraints was performed for every structure. The torsion angles were randomly varied and the obtained structures were fully optimized using the MMFF force field. Thus, different minima of energy within an energy gap of 10 kcal·mol^{-1} were generated. These structures were analyzed and ordered considering the relative energy, being the repeated geometries eliminated. In all cases, molecules with the lowest energy and an energy gap of 4.0 kcal·mol^{-1} were selected and studied quantum chemically.

Preparation of phosphonic acid monolayers. 2×1 cm Al slides were sonicated in hexane for 15 min followed by wiping with lint–free cotton swabs (Texwipe, NC, USA) to remove the polymer protection layer on top and remove any residual glue. The

surfaces were chemically activated by immersion in 1:1 (v/v) 37% HCl–MeOH mixture for 5 min, followed by washing with copious amounts of water and 2–propanol. The activated surfaces were then immersed into N_2 filled vials of 5 mM solution of 3:1 ratio of phosphonic acid derivatives (octylphosphonic acid and 12–aminododecylphosphonic acid hydrochloride salt for "free" ME (m = 7, n = 3); hexadecylphosphonic acid and 6–aminohexylphosphonic acid hydrochloride salt for "buried" ME (m = 1, n = 11) mixture in 2–propanol, heated to 50 °C for 5 min, and then left undisturbed for 5 h at room temperature to obtain self–assembled mixed monolayers.

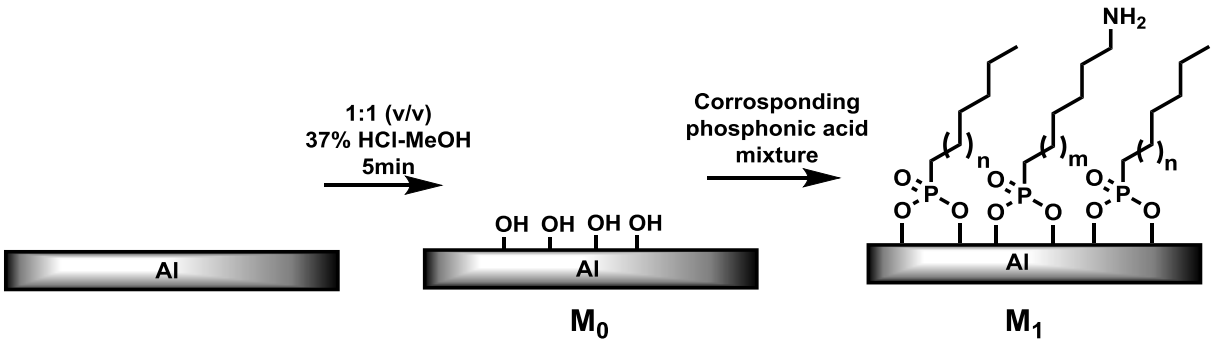

Then surfaces were taken out and sonicated successively for 5 min with 2–propanol, acetone and CH_2Cl_2. The surfaces were finally cleaned with CH_2Cl_2, air dried and stored under N_2 atmosphere. From static water contact angle (SCA) measurements, it was found that the reaction was complete after 5 h, yielding monolayers with 28–30% C as determined by XPS. Substantially longer reaction times (16 h) contributed to the formation of undesirable multilayers (42–44% C1s).

Preparation of *exo*–norbornene–terminated monolayers (M_2). Amine–terminated monolayers (M_1) were stirred with 50 mM 1,1'–carbonyldiimidazole (CDI) solution in water for 1 h to yield acyl imidazole-activated surfaces. These surfaces were immediately reacted with 50 mM *exo*–5–norbornene–2–methanol solution in DCE. This resulted in carbamate bond formation and covalent tethering of the *exo*–norbornene on the surface in 16 h. The samples were sonicated and washed with copious amounts of CH_2Cl_2, dried and stored under nitrogen atmosphere.

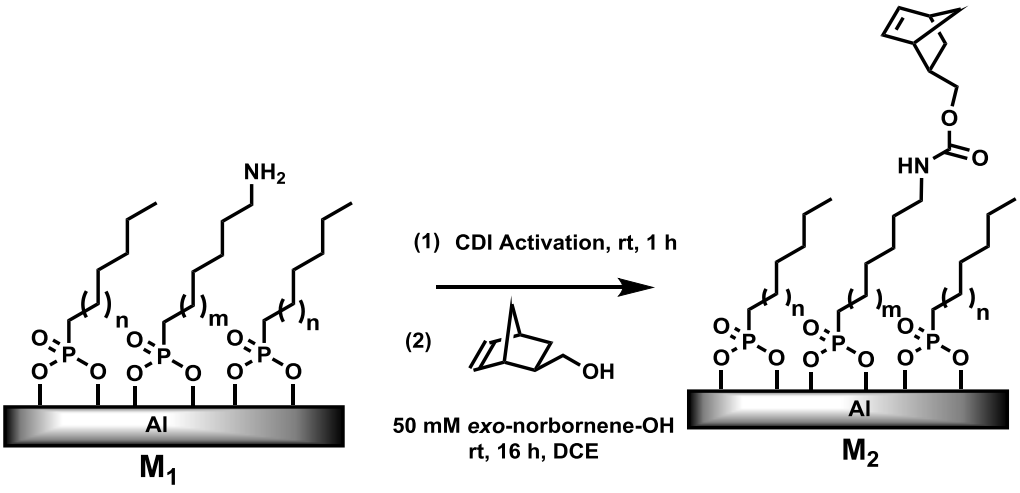

Preparation of *endo*–norbornene–terminated monolayers (M_3). Amino–terminated monolayers (M_1) were stirred with 50 mM aqueous solution of 1,1'–carbonyldiimidazole (CDI) for 1 h to yield acyl imidazole–activated surfaces. These surfaces were immediately reacted with 50 mM *endo*–5–norbornene–2–methanol solution in DCE. This resulted in covalent tethering of the *endo*–norbornene on the surface via carbamate bond in 16 h. The samples were sonicated and washed with copious amounts of CH_2Cl_2, dried and stored under nitrogen atmosphere.

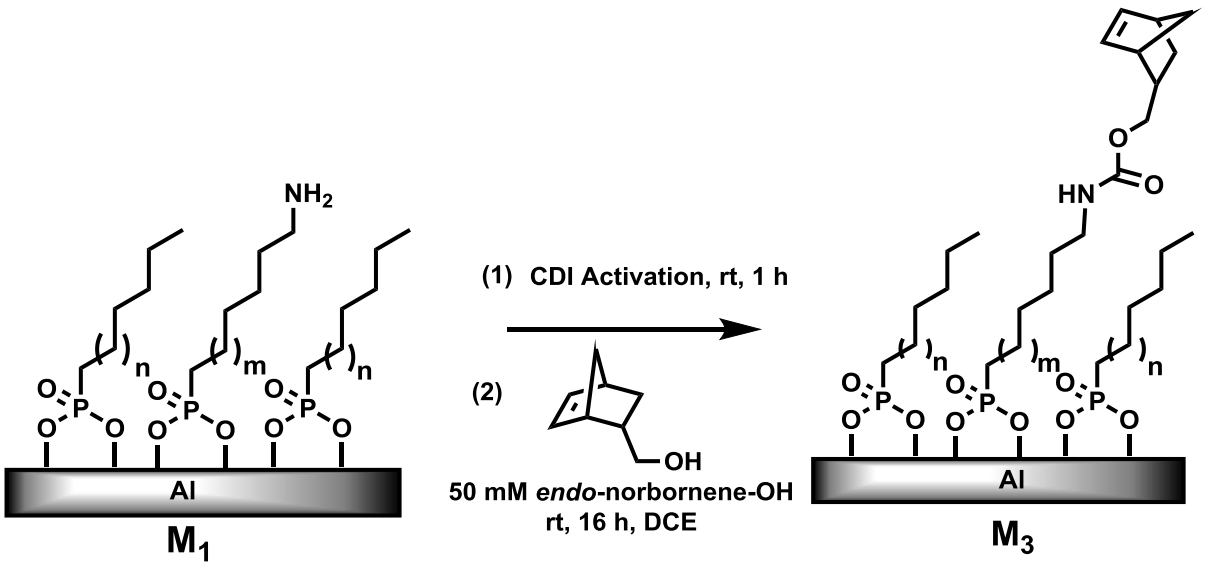

Preparation of tetrazine–terminated monolayers (M_4). Amine–terminated monolayers (M_1) were stirred with 50 mM aqueous solution of 1,1'–carbonyldiimidazole (CDI) for 1 h to yield acyl imidazole–activated surfaces. These surfaces were

immediately reacted with 50 mM (4–(6–methyl–1,2,4,5–tetrazin–3–yl)phenyl)methanamine, 1 solution in DCE. This resulted in covalent tethering of the tetrazine on the surface via urea bond in 16 h. The samples were sonicated and washed with copious amounts of CH_2Cl_2, dried and stored under nitrogen atmosphere.

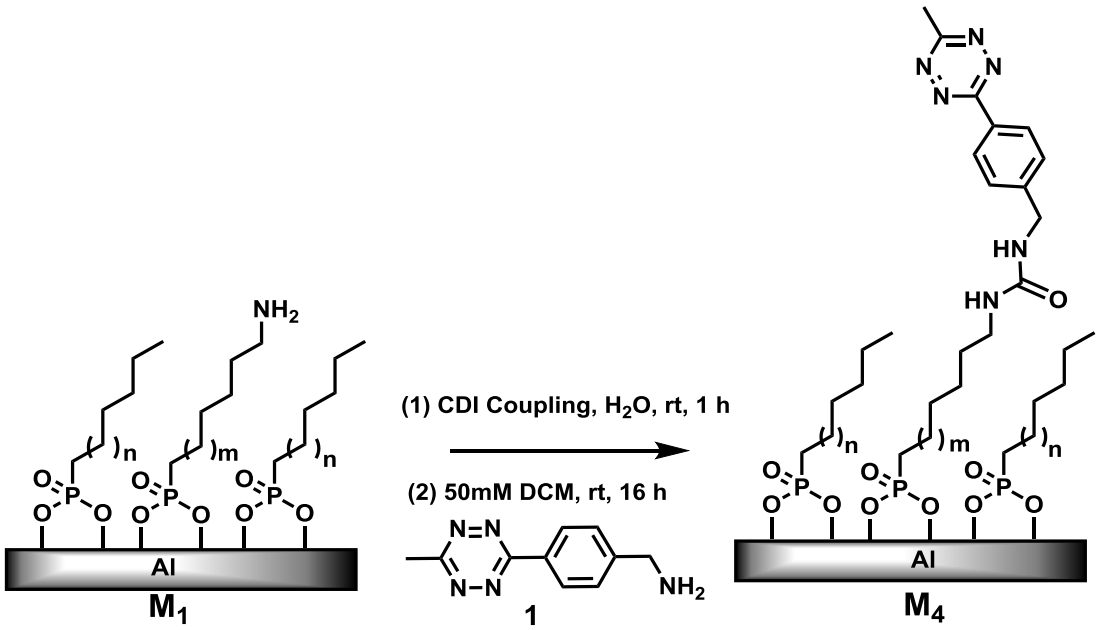

General method for IEDDA reaction on *exo–/endo–*norbornene–terminated surface: Both free and buried *exo–/endo–*norbornene–terminated surfaces were reacted with a 4–(6–methyl–1,2,4,5–tetrazin–3–yl)benzyl 4–(trifluoromethyl)benzoate solution, 3 in DCE at 30 °C. The reaction was stirred at a constant speed using a magnetic bead and stirrer and all samples were loaded in a specially constructed Teflon holder to ensure rigorous reproducibility between samples. Samples were immersed into the solution for a set period of reaction time and immediately taken out and washed with copious amounts of DCM. The samples were further sonicated in DCM to remove any physisorbed species for 15 min, dried under a dry nitrogen stream and stored for further analysis in a sealed vial.

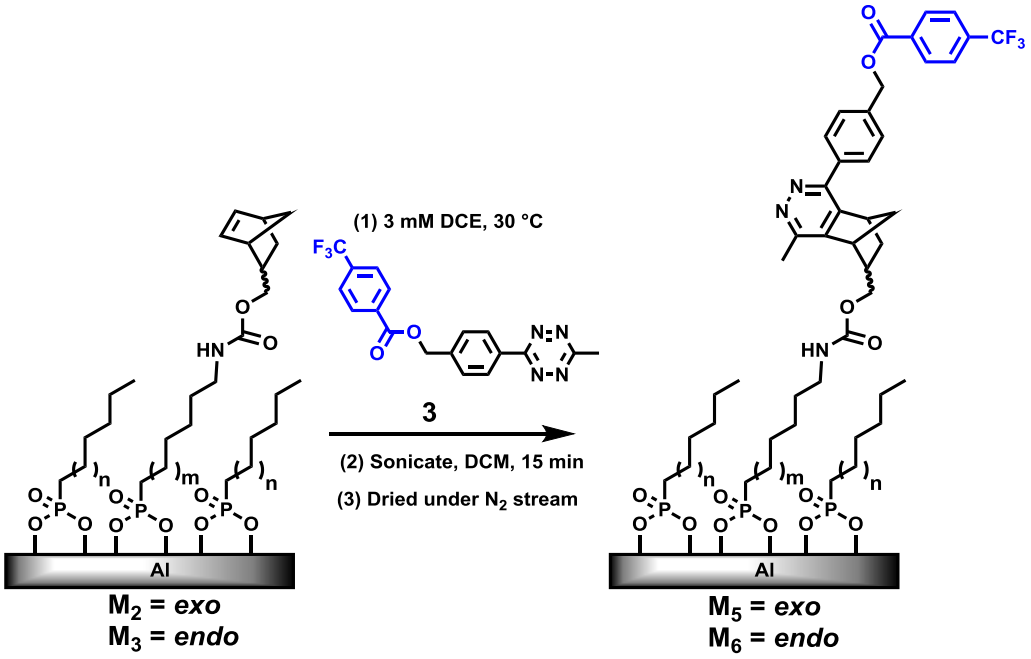

General method for IEDDA reaction on tetrazine–terminated surface: Both "free" and "buried" tetrazine–terminated surfaces were reacted with Bicyclo[2.2.1]hept–5–en–2–yl methyl 4–(trifluoromethyl)benzoate [4, *exo*–norbornene tag molecule] or Bicyclo[2.2.1]hept–5–en–2–yl methyl 4–(trifluoromethyl)benzoate [6, *endo*–norbornene tag molecule] solution in DCE at 30 °C. The reaction was stirred at a constant speed using a magnetic bead and stirrer and all samples were loaded in a specially constructed Teflon holder to ensure rigorous reproducibility between samples. Samples were immersed into above said solution for a set period of reaction time and immediately taken out and washed with copious amounts of DCM. The samples were further sonicated in DCM to remove any physisorbed species for 15 min, dried under a dry nitrogen stream and stored for further analysis in a sealed vial.

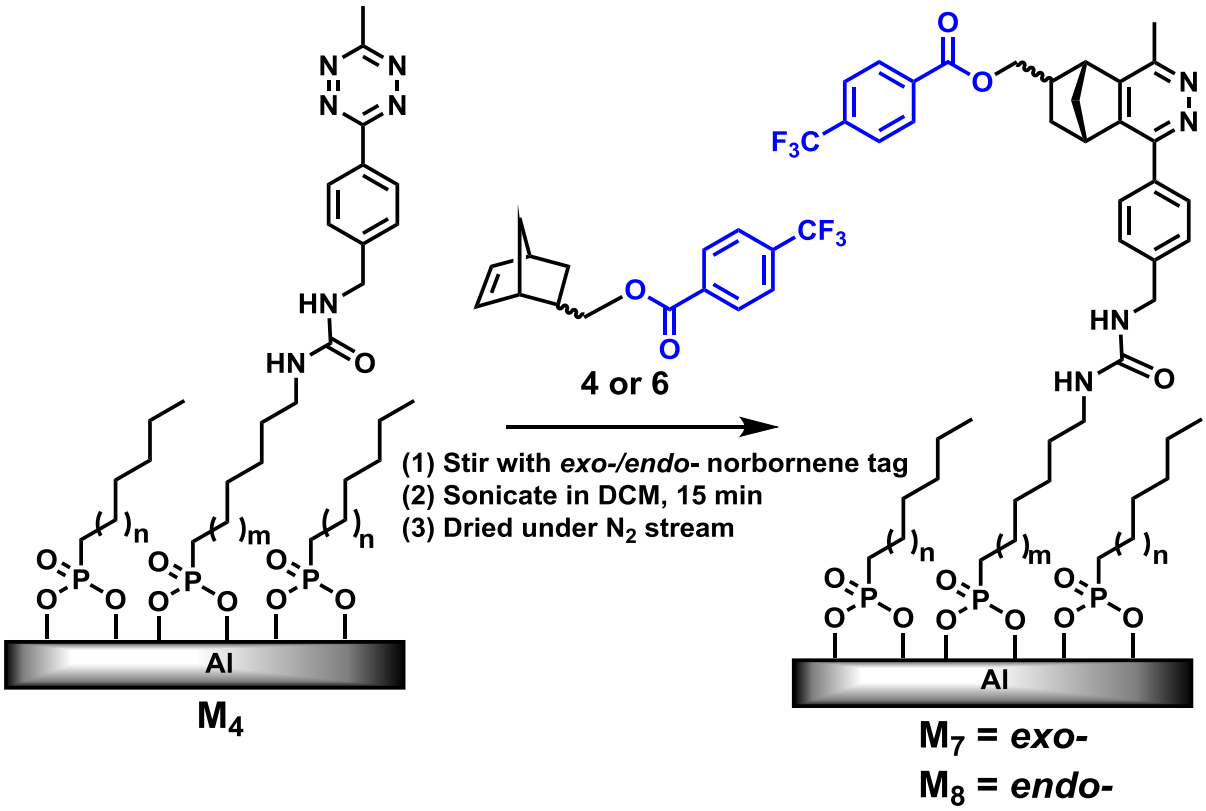

M_4

M_7 = *exo-*

M_8 = *endo-*

2. CHEMICAL SYNTHESIS

2.1 General Remarks. Unless stated otherwise, solvents and dry solvents like dichloromethane, methanol and isopropanol were purchased from Sigma–Aldrich. Unless stated otherwise all of these chemicals were used without further purification.

2.2. Reaction Handling. Unless stated otherwise all non–aqueous reactions were performed in dried glassware under an atmosphere of argon. All flasks were equipped with rubber septa and reactants were handled using standard Schlenk techniques. Temperatures above the room temperature refer to oil bath temperatures which were controlled by a thermostat. Reactions were magnetically stirred.

2.3. ^{1}H–NMR spectra were recorded at room temperature on a Bruker–400 spectrometer with ^{1}H operating frequency of 400 MHz. Unless stated otherwise all spectra were recorded at room temperature in $CDCl_3$ and DMSO–d_6 and all chemical shifts are given in δ units relative to the residual solvent [central line of singlet: δ_H = 7.27 ppm ($CDCl_3$) and 2.50 ppm (DMSO–d_6)]. Analysis followed first order and the following abbreviations were used throughout: s = singlet, br. s. = broad singlet, d = doublet, t = triplet, q = quartet, quin = quintet, sxt = sextet, sept = spt, dd = doublet of doublet, dt = doublet of triplet, ddd = doblet of doublet of doublet, ddt = doblet of doublet of triplet, m = multiplet, mc = centred multiplet. Coupling constants (*J*) are given in Hertz (Hz).

2.4. ^{13}C–NMR spectra were recorded at room temperature on a Bruker–400 spectrometer with ^{13}C operating frequency of 101 MHz. Unless stated otherwise all spectra were recorded at room temperature in $CDCl_3$ and DMSO–d_6 and all chemical shifts are given in δ units relative to the residual solvent [central line of triplet: δ_C = 77.2 ppm ($CDCl_3$) and heptet δ_C = 39.5 ppm (DMSO–d_6)]. The following abbreviation was used throughout: s = singlet, d = doublet, dd = doublet of doublet. If no coupling constants are given, the multiplicity refers to ^{1}H–decoupled spectra.

2.5. Synthesis of 3–methyl–6–phenyl methylamine–1,2,4,5–tetrazine, 1.

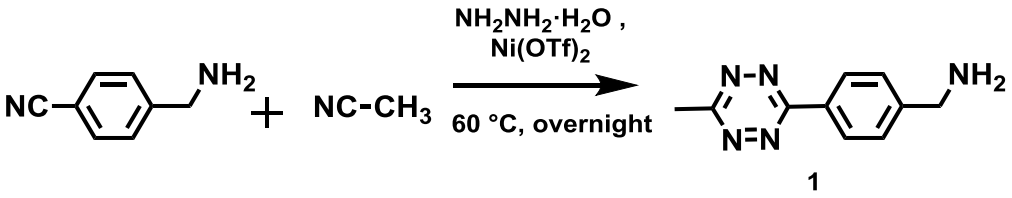

1

Metal–catalyzed tetrazine synthesis as described elsewhere[7] was applied to synthesize 3–methyl–6–phenyl methylamine–1,2,4,5–tetrazine. Briefly, 4–(aminomethyl) benzonitrile hydrochloride (1.50 g, 8.9 mmol), $Ni(OTf)_2$ (1.59 g, 4.45mmol) and acetonitrile (4.7 mL, 89 mmol) were added in a 250 mL round flask, followed adding 60% $NH_2NH_2 \cdot H_2O$ (30 mL), under N_2 flow. The mixture was stirred at 60 °C for 16 h and allowed to cool to room temperature. Sodium nitrite (14.6 g, 212 mmol) in 25 mL of water was slowly added to the reaction followed by 5 M HCl until gas evolution ceased (pH 3), in an ice bath. The product was extracted into ethyl acetate and purified by silica column chromatography (MeOH : DCM = 1:9) as a red solid. Yield: 0.56 g (27%). ^{1}H–NMR (400 MHz, DMSO–d_6), δ 2.99 (3H, s), 4.15 (2H, s), 7.71 (2H, d, J = 8Hz), 8.49 (2H, d, J = 8Hz). ^{13}C–NMR (101 MHz, DMSO–d_6), δ 20.8, 42.3, 127.6, 129.5, 131.8, 139.2, 162.3, 167.2.

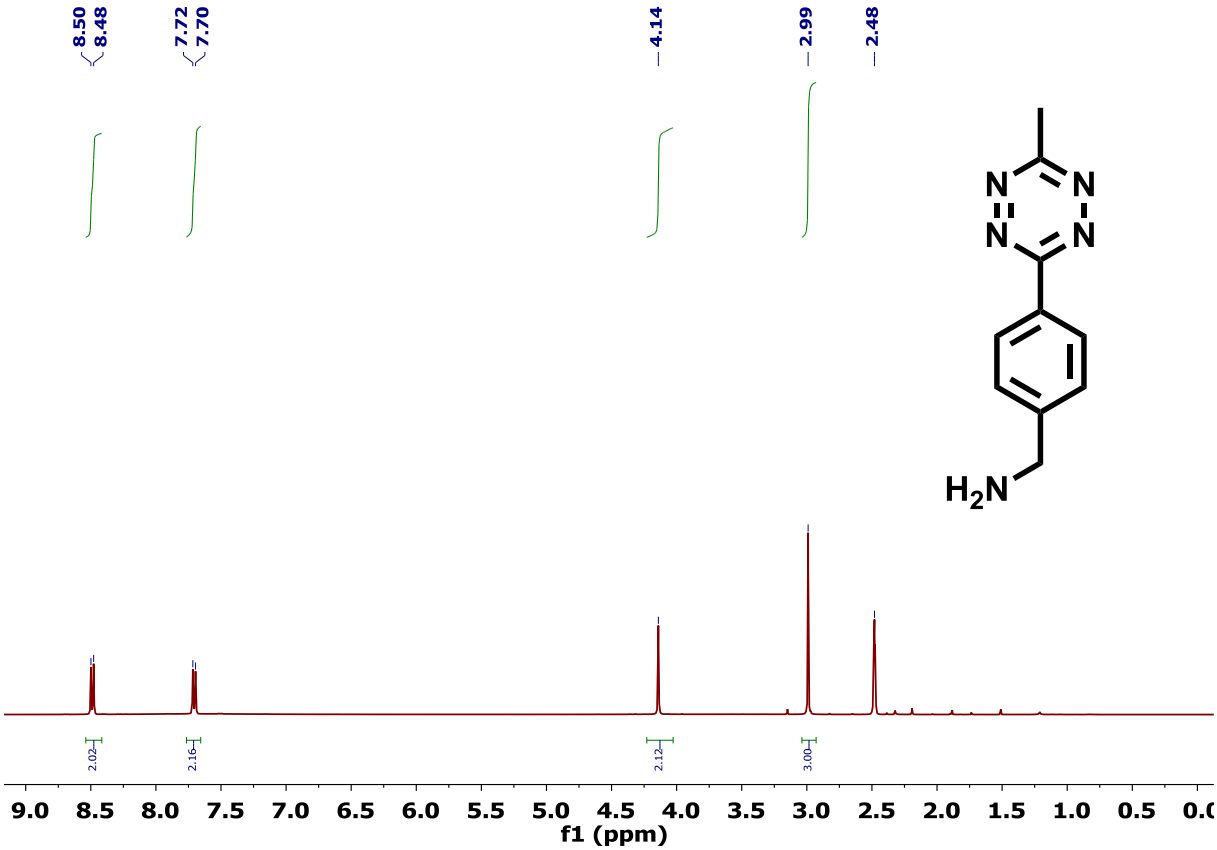
8.50
8.48
7.72
7.70
4.14
2.99
2.48
2.02
2.16
2.12
3.00
N
N
N
N
H2N
9.0 8.5 8.0 7.5 7.0 6.5 6.0 5.5 5.0 4.5 4.0 3.5 3.0 2.5 2.0 1.5 1.0 0.5 0.0
f1 (ppm)

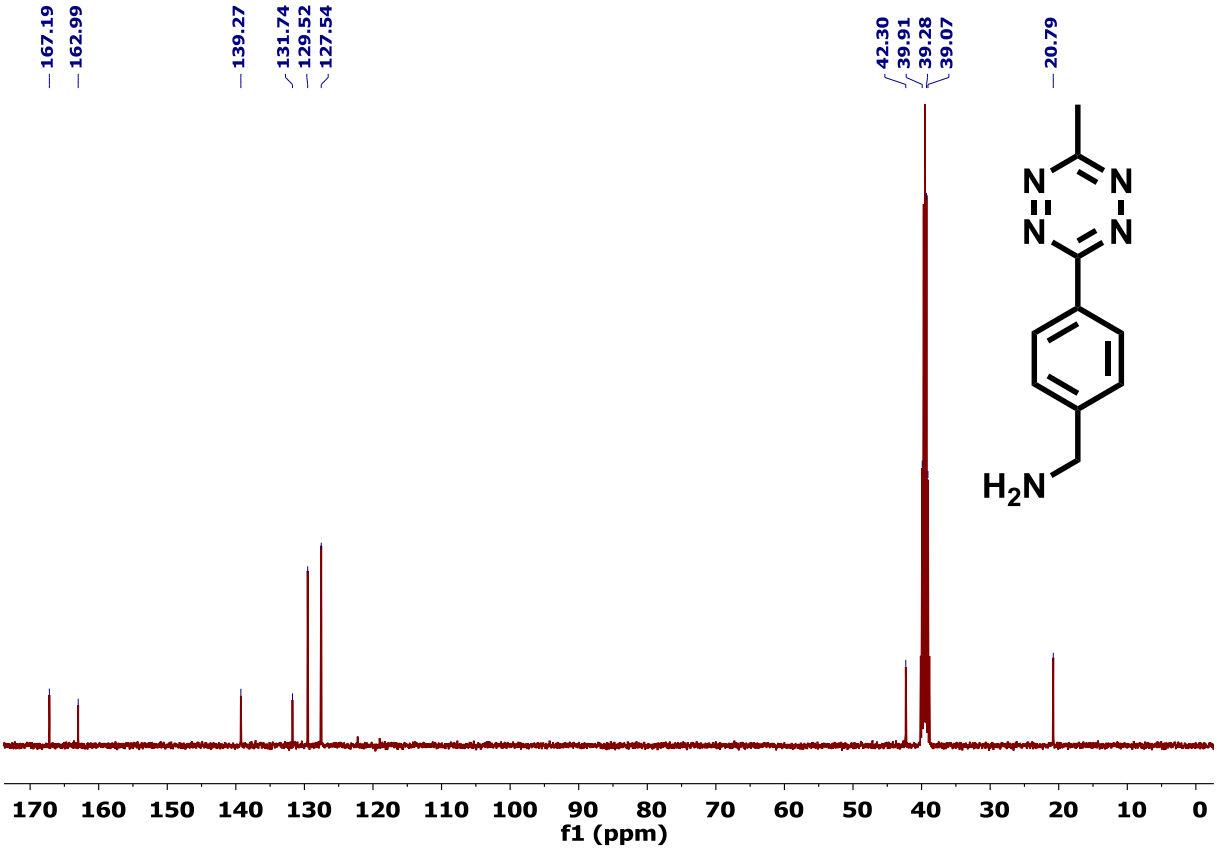
167.19
162.99
139.27
131.74
129.52
127.54
42.30
39.91
39.28
39.07
20.79
N
N
N
N
H2N
170 160 150 140 130 120 110 100 90 80 70 60 50 40 30 20 10 0
f1 (ppm)

2.6. Synthesis of 3–methyl–6–phenyl methanol–1,2,4,5–tetrazine, 2.

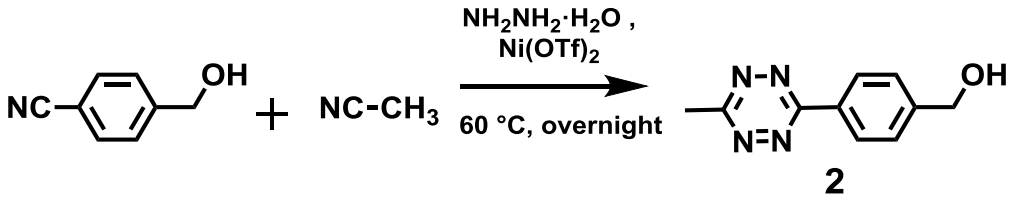

2

3–methyl–6–phenyl methanol–1,2,4,5–tetrazine was synthesized as per protocol described elsewhere.[7] Briefly, 4–cyanobenzylalcohol (0.51 g, 3.75 mmol), $Ni(OTf)_2$ (0.67 g, 1.88 mmol) and acetonitrile (1.97 mL, 37.6 mmol) were added in a 100 mL round flask, followed adding 60% $NH_2NH_2{\cdot}H_2O$ (12 mL), under N_2 flow. The mixture stirred at 60 °C for 24 h and allowed to cool to room temperature. Sodium nitrite (6.35 g, 92.0 mmol) in 14 mL water was slowly added to the reaction followed by careful addition of 5 M HCl until gas evolution ceased (pH 3), in an ice bath with stirring. The product was extracted with ethyl acetate and organic phase was dried by sodium sulfate. The product was purified using silica column chromatography (EtOAc : heptane = 1: 2.8) as a red solid. Yield = 0.33 g (41 %). ^{1}H–NMR (400 MHz, $CDCl_3$), δ 3.08 (3H, s), 4.82 (2H, d), 7.57 (2H, d, J = 8Hz), 8.55 (2H, d, J = 8Hz). ^{13}C–NMR (101 MHz, $CDCl_3$), δ 21.1, 64.7, 127.4, 128.1, 130.9, 145.6, 163.9, 167.2.

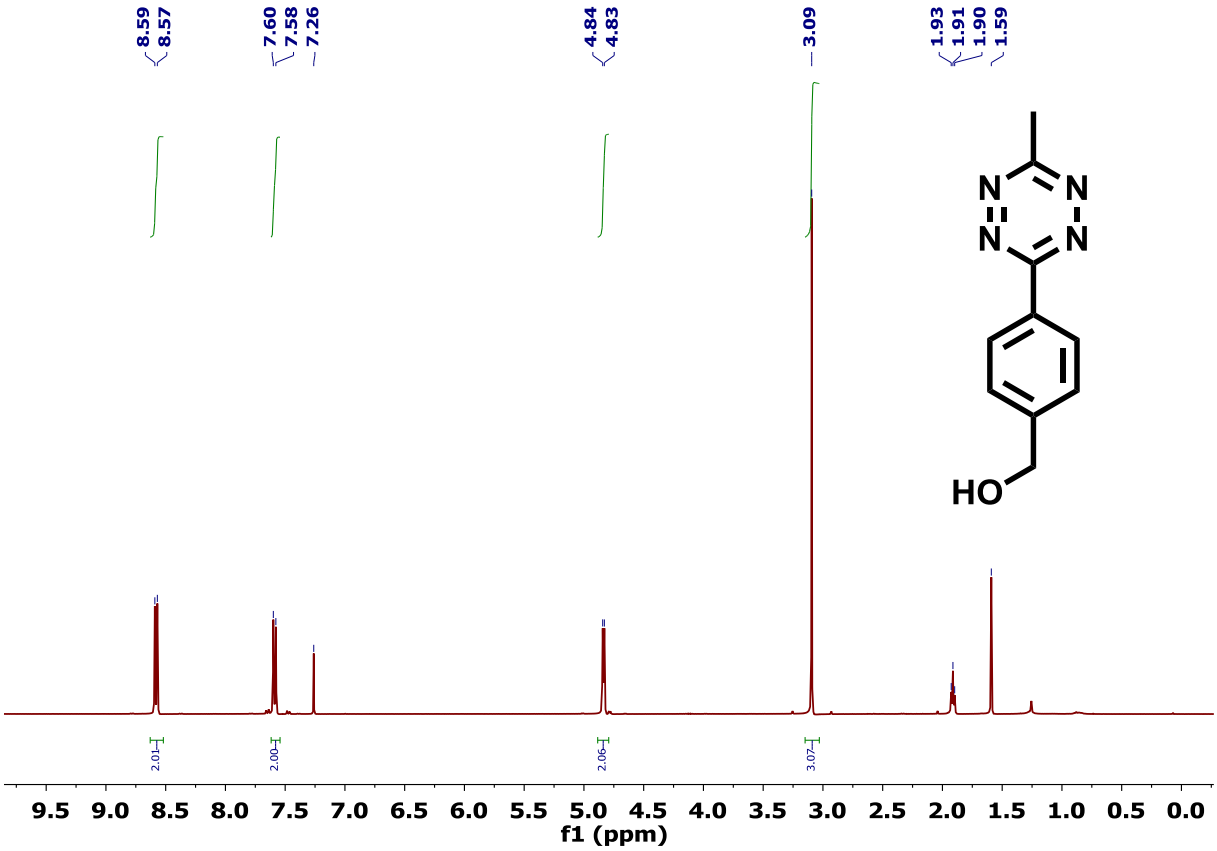
8.59
8.57
7.60
7.58
7.26
4.84
4.83
3.09
1.93
1.91
1.90
1.59
N
N
N
N
HO
2.01
2.00
2.06
3.07
9.5 9.0 8.5 8.0 7.5 7.0 6.5 6.0 5.5 5.0 4.5 4.0 3.5 3.0 2.5 2.0 1.5 1.0 0.5 0.0
f1 (ppm)

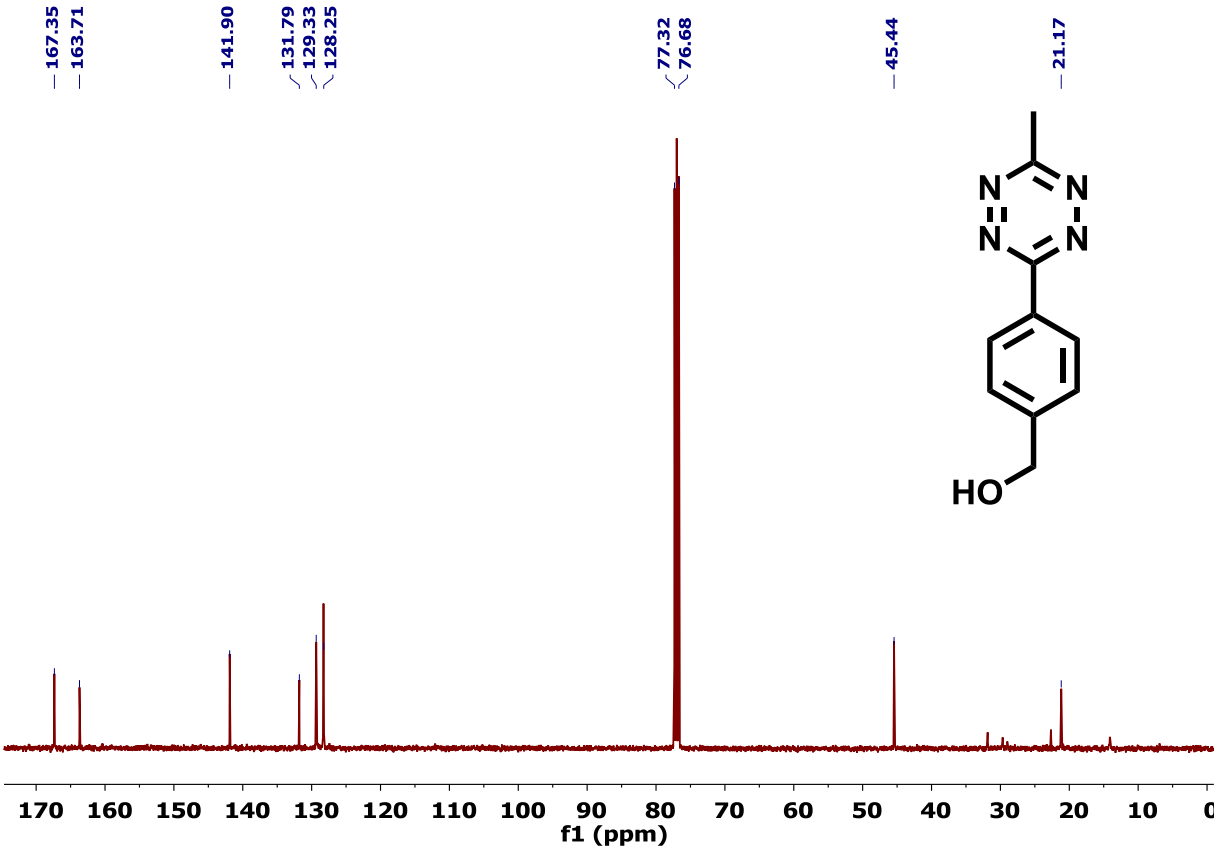
167.35
163.71
141.90
131.79
129.33
128.25
77.32
76.68
45.44
21.17
N
N
N
N
HO
170 160 150 140 130 120 110 100 90 80 70 60 50 40 30 20 10 0
f1 (ppm)

2.7. Synthesis of [3–(3–methyl–1,2,4,5–tetrazine)]benzyl(4–(trifluoromethyl)-benzoate, 3.

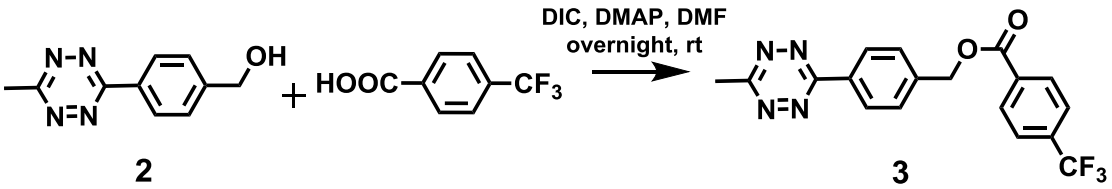

2 3

4–(Trifluoromethyl)benzoic acid (0.27 g, 1.38 mmol), DMAP (0.01 g, 0.123 mmol), 2.5 mL DMF, DIC (0.18 mL, 1.18 mmol) and compound 2 (0.21 g, 0.98 mmol) were successively added and allowed to react at room temperature for 17 h. DMF was evaporated by rotatory evaporation under reduced pressure. The mixture was extracted with EtOAc and organic phase was washed with brine, dried with sodium sulfate and concentrated by rotatory evaporation to yield an oil, which was purified using silica column chromatography (EtOAc : heptane = 1: 4) to obtain a red solid. Yield = 0.22 g (57 %). ^{1}H–NMR (400 MHz, $CDCl_3$), δ 3.11 (3H, s), 5.51 (2H, s), 7.67 (2H, d, J=8Hz), 7.73 (2H, d, J = 8Hz), 8.22 (2H, d, J = 8Hz), 8.63 (2H, d, J=8Hz).^{13}C–NMR (101 MHz, $CDCl_3$), δ 21.2, 66.5, 125.5, 128.3, 128.4, 128.7, 130.2, 131.9, 132.5, 133.1, 140.2, 163.8, 165.1, 167.4.

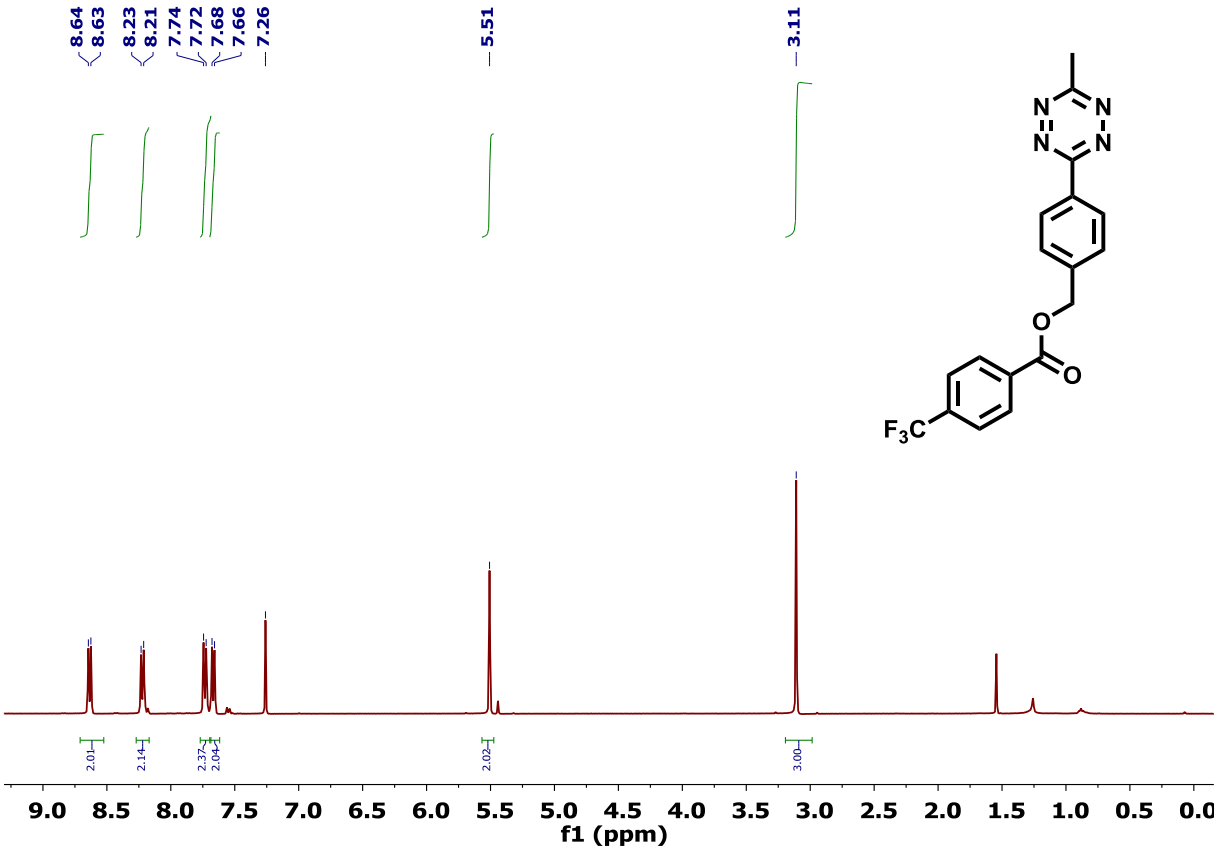
8.64
8.63
8.23
8.21
7.74
7.72
7.68
7.66
7.26
5.51
3.11
2.01
2.14
2.37
2.04
2.02
3.00
f1 (ppm)

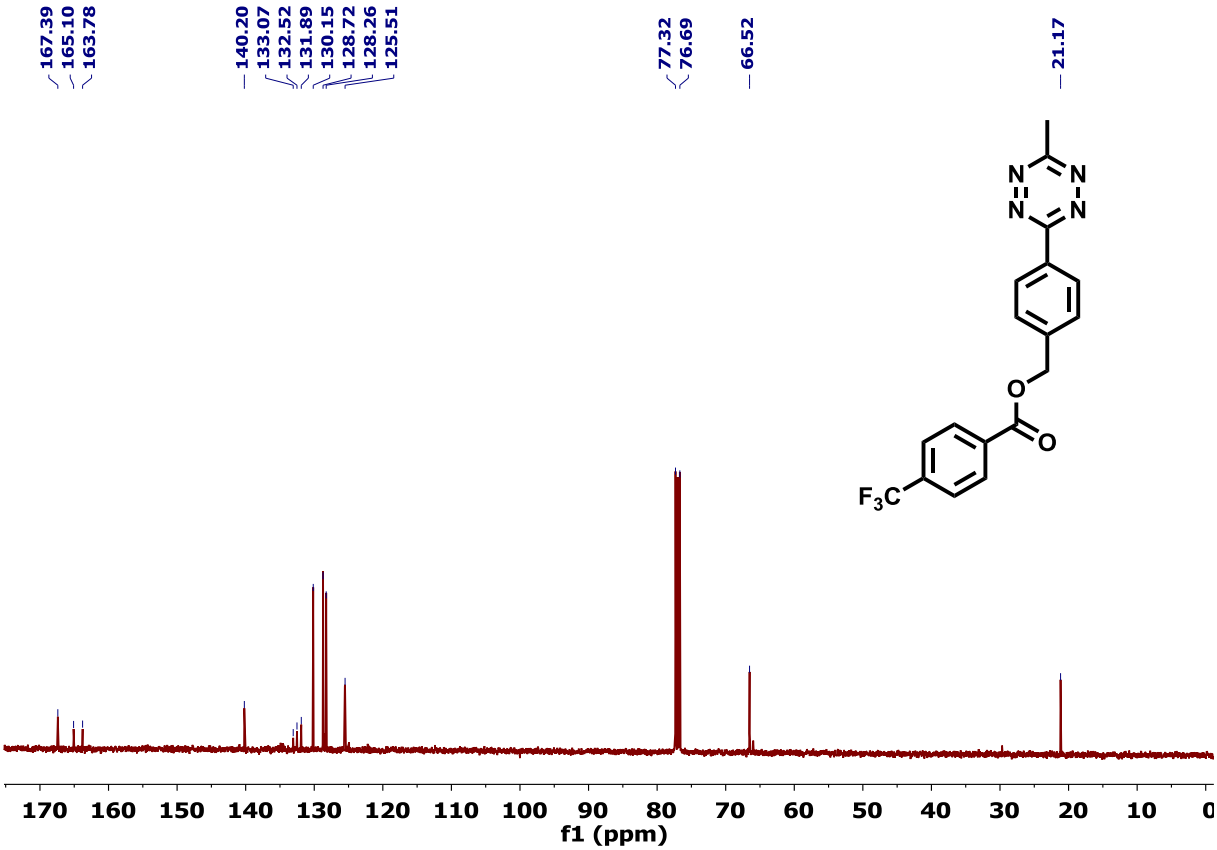
167.39
165.10
163.78
140.20
133.07
132.52
131.89
130.15
128.72
128.26
125.51
77.32
76.69
66.52
21.17
f1 (ppm)

2.8. Synthesis of (bicyclo[2.2.1]hept–5–en–2–yl)methyl4–(trifluoromethyl)-benzoate, 4.

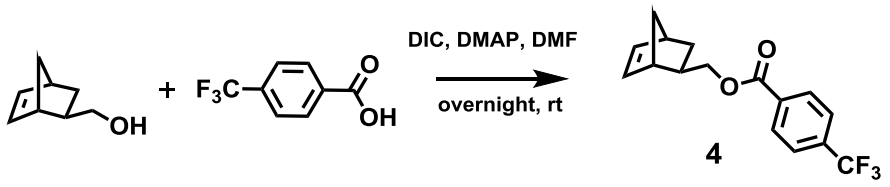

4–(Trifluoromethyl)benzoic acid (0.43 g, 2.25 mmol), DMAP (0.024 g, 0.190 mmol), 4 mL DMF, DIC (0.3 mL, 1.93 mmol) and (bicyclo[2.2.1]hept–5–en–2–yl)methanol (0.19 mL, 1.61 mmol), were successively added in a 100 mL rounded flask, and allowed to react for 16 h. DMF was removed using a rotary evaporator under reduced pressure. The mixture was extracted with EtOAc and organic phase was washed by brine, dried by sodium sulfate. The product was purified using silica column chromatography (EtOAc : heptane = 1: 4) as white solid. Yield = 0.35 g (69%). ^{1}H–NMR (400 MHz, $CDCl_3$), δ 1.23–1.40 (4H, m), 1.88 (1H, m), 2.80 (1H, s), 2.87 (1H, s), 4.25 (1H, m), 4.43 (1H, m), 6.11 (2H, m), 7.70 (2H, d, J = 8Hz), 8.16(2H, d, J = 8Hz). ^{13}C–NMR (101 MHz, $CDCl_3$), δ 29.6, 38.1, 41.6, 43.72, 45.0, 69.6, 122.3, 125.4, 130.0, 133.7, 134.52, 136.1, 137.0, 165.4.

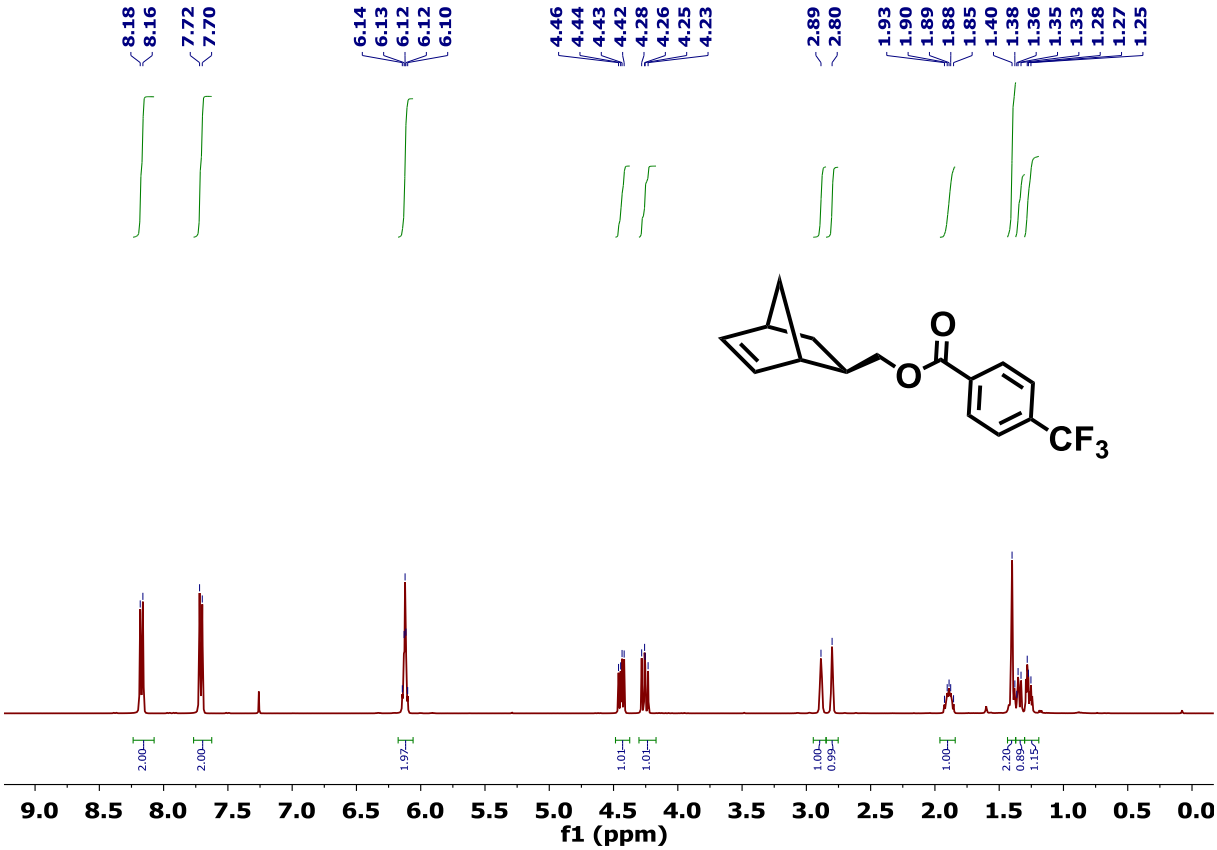
8.18
8.16
7.72
7.70
6.14
6.13
6.12
6.12
6.10
4.46
4.44
4.43
4.42
4.28
4.26
4.25
4.23
2.89
2.80
1.93
1.90
1.89
1.88
1.85
1.40
1.38
1.36
1.35
1.33
1.28
1.27
1.25
O
O
CF3
2.00
2.00
1.97
1.01
1.01
1.00
0.99
1.00
2.20
0.89
1.15
9.0 8.5 8.0 7.5 7.0 6.5 6.0 5.5 5.0 4.5 4.0 3.5 3.0 2.5 2.0 1.5 1.0 0.5 0.0
f1 (ppm)

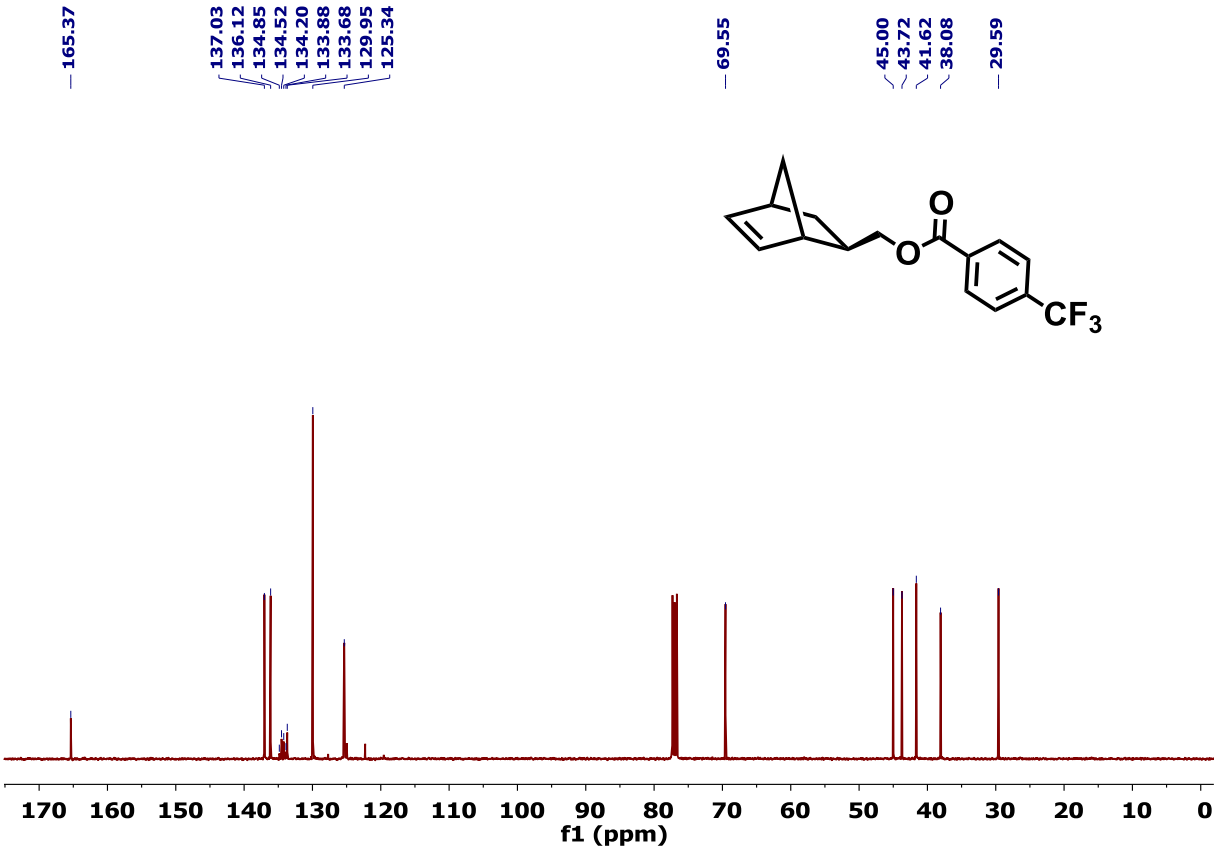
165.37
137.03
136.12
134.85
134.52
134.20
133.88
133.68
129.95
125.34
69.55
45.00
43.72
41.62
38.08
29.59
O
O
CF3
170 160 150 140 130 120 110 100 90 80 70 60 50 40 30 20 10 0
f1 (ppm)

Synthesis of (bicyclo[2.2.1]hept–5–en–2–yl)methanol, 5.

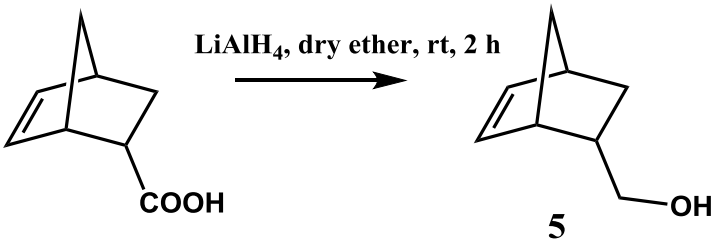

5

A commercially available mixture of *endo*– and *exo*– 5–norbornenecarboxylic acid, was subjected to column chromatography (heptane : EtOAc = 1: 4) to obtain the *endo*–norbornene carboxylic acid. Bicyclo[2.2.1]hept–5–ene–2–carboxylic acid (206.6 mg, 1.5 mmol) was mixed with $LiAlH_4$ (113.5 mg, 3.0 mmol) in 20mL dry ether for 2 h. The reaction was quenched with water and the organic product was extracted into ether followed by recovery of the product by evaporating the solvent under reduced pressure. Yield= 0.15 g (81%). ^{1}H–NMR (400 MHz, $CDCl_3$) δ 6.15 (dd, J = 5.7, 3.0 Hz, 1H), 5.97 (dd, J = 5.7, 2.9 Hz, 1H), 3.40 (dd, J = 10.4, 6.5 Hz, 1H), 3.26 (dd, J = 10.4, 8.9 Hz, 1H), 2.93 (s, 1H), 2.81 (s, 1H), 2.29 (ddt, J = 9.2, 6.6, 4.5 Hz, 1H), 1.82 (ddd, J = 11.6, 9.2, 3.8 Hz, 1H), 1.48 – 1.41 (m, 1H), 1.27 (d, J = 8.2 Hz, 1H), 0.55 – 0.49 (m, 1H).

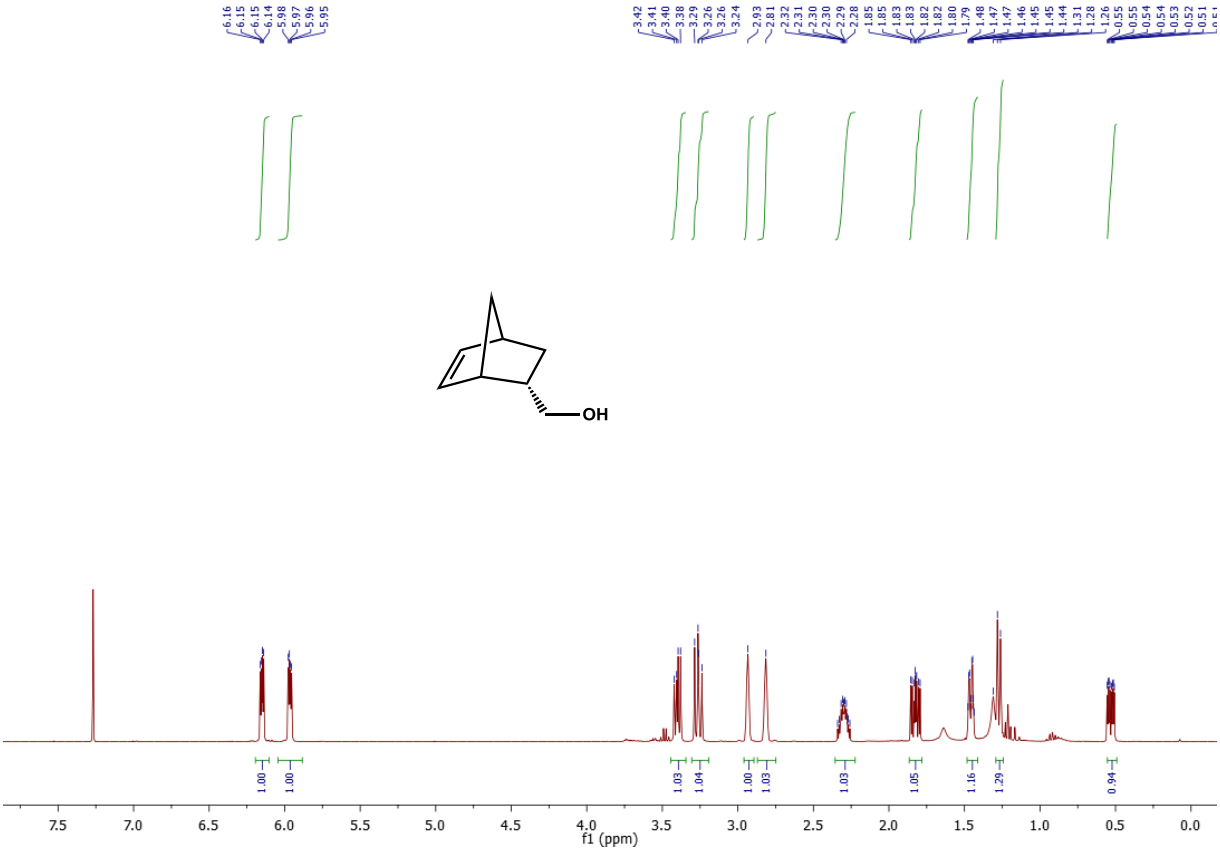

Synthesis of (bicyclo[2.2.1]hept–5–en–2–yl)methyl 4–(trifluoromethyl)benzoate, 6.

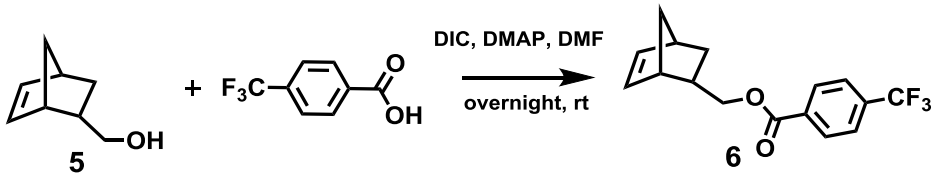

4–(Trifluoromethyl)benzoic acid (0.43 g, 2.25 mmol), DMAP (0.024 g, 0.19 mmol), 4 mL DMF, DIC (0.3 mL, 1.93 mmol) and (bicyclo[2.2.1]hept–5–en–2–yl)methanol, 5, (0.19 mL, 1.61 mmol), were successively added in a 100 mL rounded flask, and allowed to react for 24 h. DMF was removed using a rotary evaporator under reduced pressure. The mixture was extracted with EtOAc and organic phase was washed by brine, dried by sodium sulfate. The product was purified using silica column chromatography (EtOAc : heptane = 1: 4) as white solid. Yield = 0.14 g. (33%) ^{1}H–NMR (400 MHz, $CDCl_3$), δ 8.17 (d, J = 7.6 Hz, 2H), 7.72 (d, J = 7.5 Hz, 2H), 6.22 (s,

1H), 6.01 (s, 1H), 4.21 – 4.07 (m, 1H), 3.96 (t, J = 9.9 Hz, 1H), 2.98 (s, 1H), 2.87 (s, 1H), 2.57 (s, 1H), 1.93 (t, J = 10.1 Hz, 1H), 1.51 (d, J = 7.9 Hz, 1H), 1.32 (d, J = 7.8 Hz, 1H), 0.67 (d, J = 10.2 Hz, 1H). ^{13}C–NMR (101 MHz, $CDCl_3$), δ 165.30, 137.81, 134.50, 134.18, 133.78, 132.07, 129.94, 125.35, 125.01, 125.01, 122.30, 68.91, 49.44, 43.99, 42.24, 37.89, 29.69, 28.98.

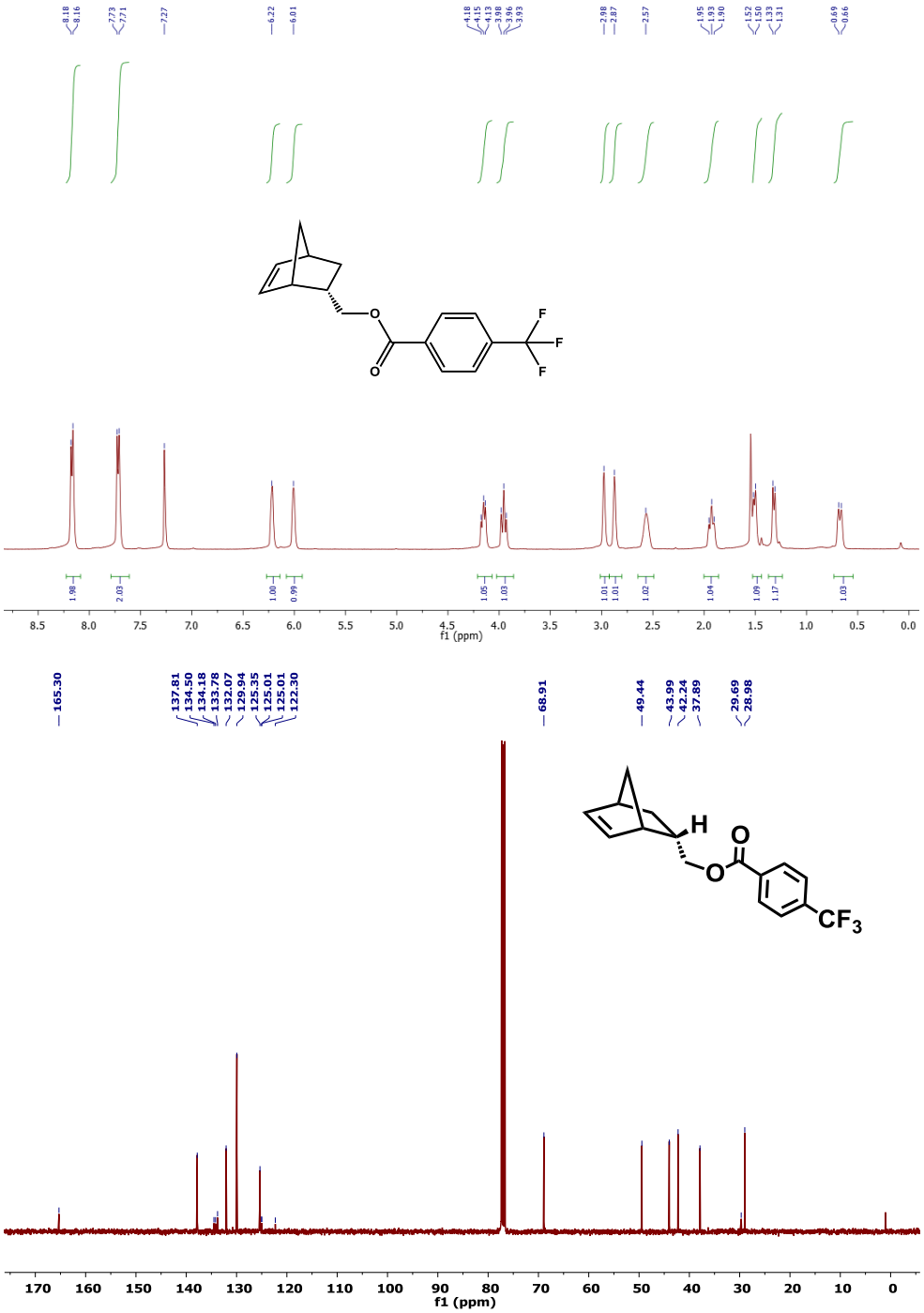

3. SUPPLEMENTARY KINETICS DATA.

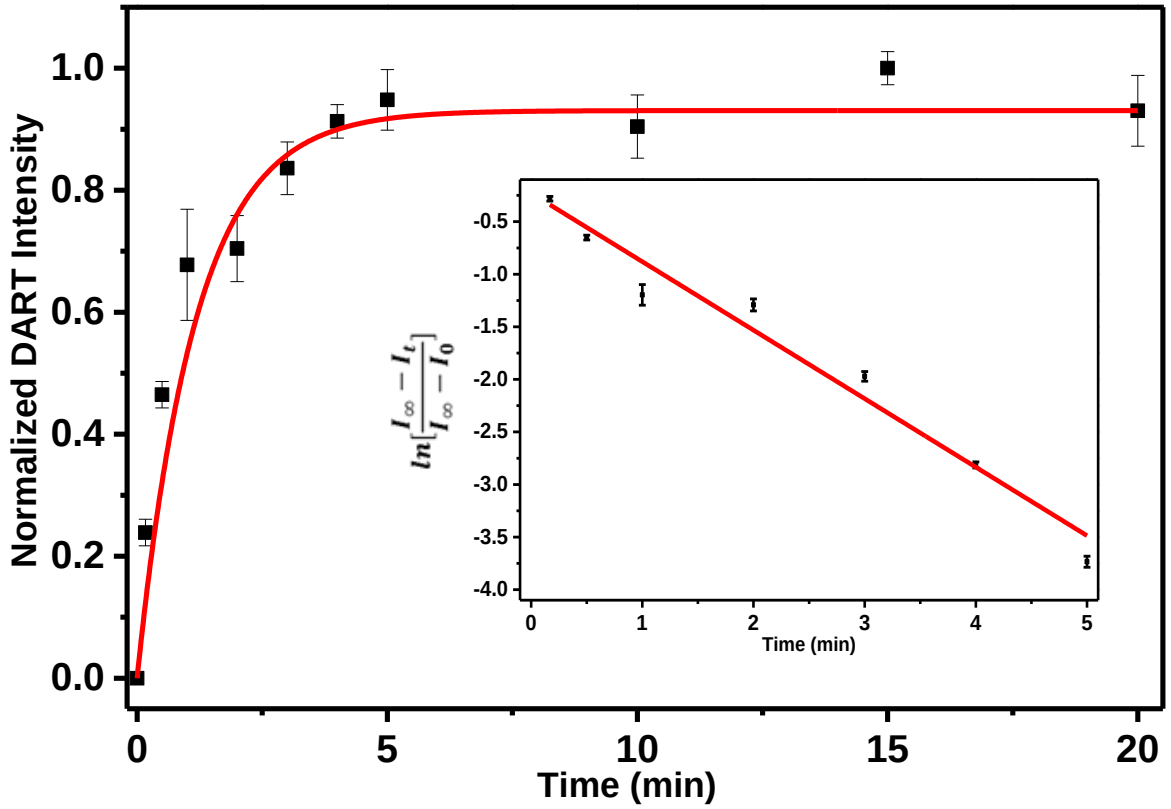

Figure S3.1. Sigmoidal plot of normalized integrated DART–HRMS intensity *vs* time (min) for "free" *exo*–norbornene-terminated surface (**M_2**) reacting with tetrazine tag, 3 in DCE solution at 30 °C. Inset: Linear plot of $ln\ |(I_\infty - I_t)\ /\ (I_\infty - I_0)|$ *vs* time (min), the slope of which is the pseudo—first order reaction rate (k′) obtained by a least–squares fit ($R^2 > 0.95$). (Each time point is an average of hexaplet samples.) The second-order rate constant is derived from here using the concentration of the other agent (typically ~3 mM, but precisely determined to 2 digits precision (e.g. 3.0 mM) in each case).

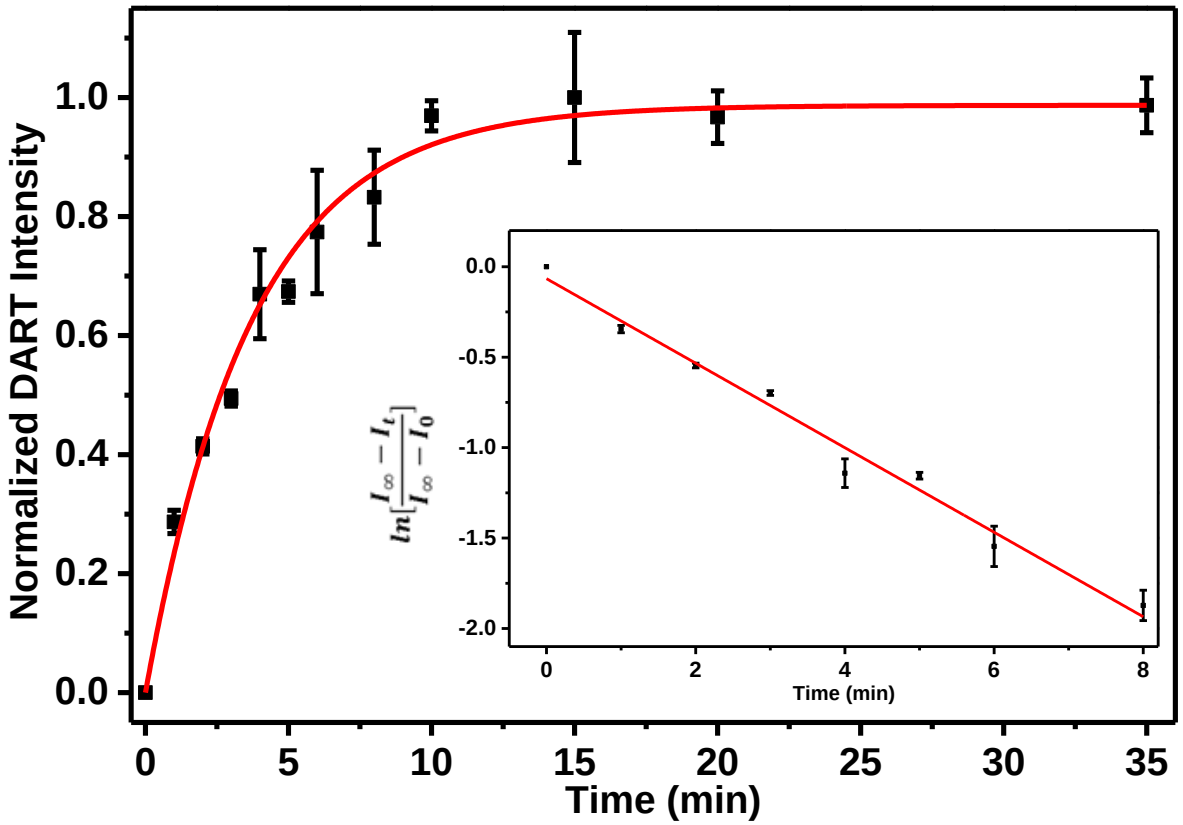

Figure S3.2. Sigmoidal plot of normalized integrated DART–HRMS intensity *vs* time (min) for "buried" *exo*–norbornene-terminated surface (**M₂**) reacting with tetrazine tag **3** in DCE solution at 30 °C. Inset: Linear plot of $ln\ |(I_\infty - I_t)\ /\ (I_\infty - I_0)|$ *vs* time (min), the slope of which is the pseudo—first order reaction rate (k′) obtained by a least–squares fit ($R^2 > 0.95$). (Each time point is an average of hexaplet samples.) The second-order rate constant is derived from here using the concentration of the other agent (typically ~3 mM, but precisely determined to 2 digits precision (e.g. 3.0 mM) in each case).

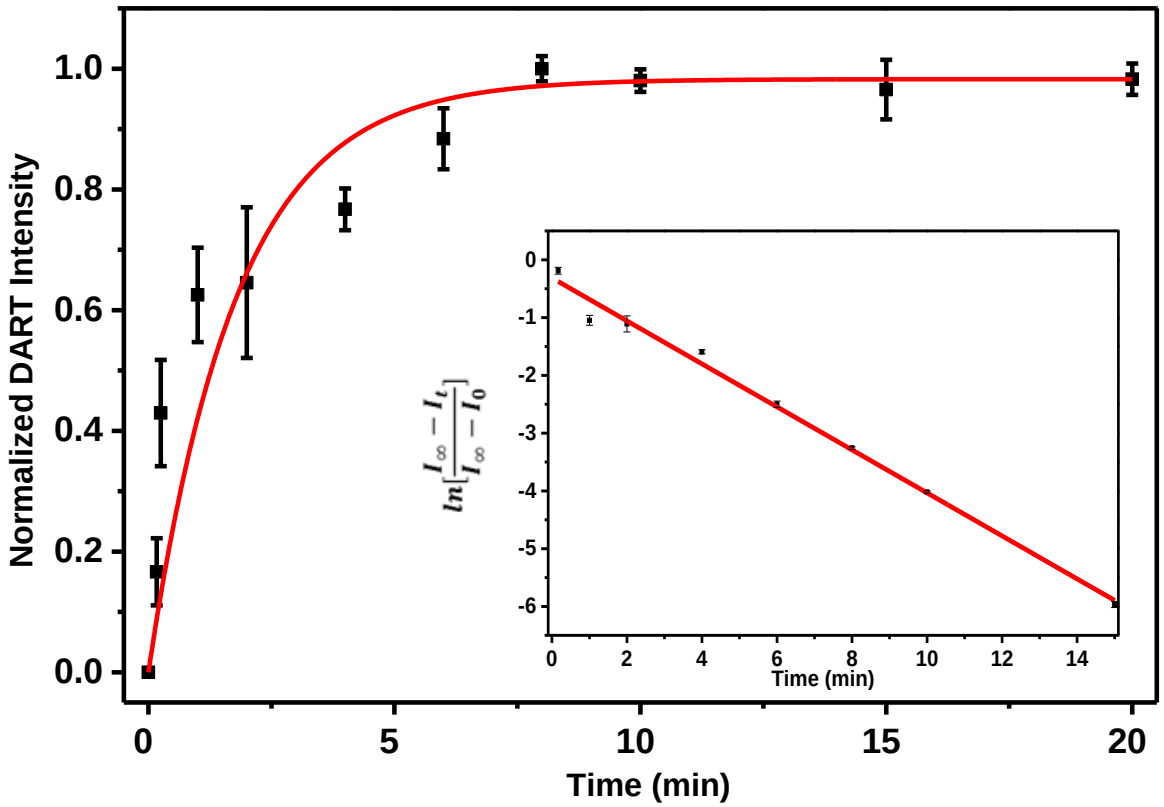

Figure S3.3. Sigmoidal plot of normalized integrated DART–HRMS intensity *vs* time (min) for "free" *endo*–norbornene-terminated surface (**M$_3$**) reacting with tetrazine tag **3** in DCE solution at 30 °C. Inset: Linear plot of *ln* $|(I_\infty - I_t) / (I_\infty - I_0)|$ *vs* time (min), the slope of which is the pseudo—first order reaction rate (k′) obtained by a least–squares fit ($R^2 > 0.95$). (Each time point is an average of hexaplet samples.) The second-order rate constant is derived from here using the concentration of the other agent (typically ~3 mM, but precisely determined to 2 digits precision (e.g. 3.0 mM) in each case).

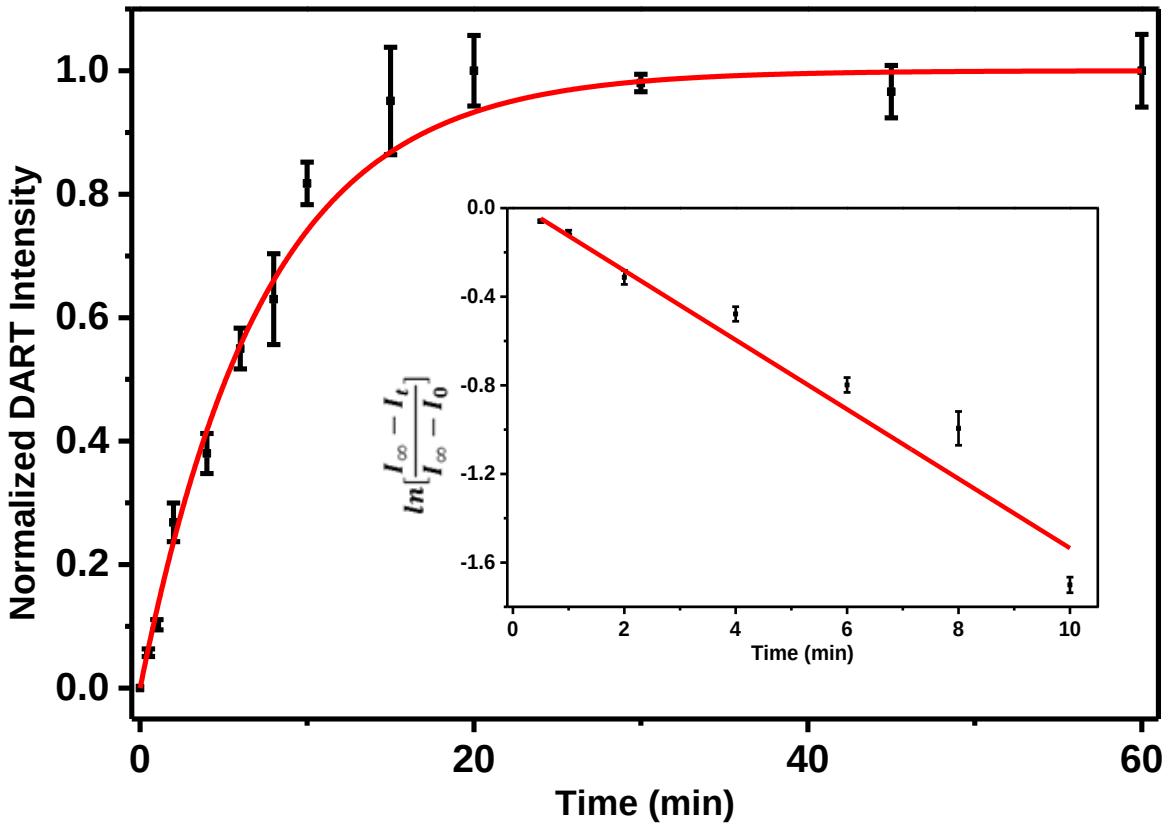

Figure S3.4. Sigmoidal plot of normalized integrated DART–HRMS intensity *vs* time (min) for "buried" *endo*–norbornene-terminated surface (**M$_3$**) reacting with tetrazine tag **3** in DCE solution at 30 °C. Inset: Linear plot of *ln* $|(I_\infty - I_t) / (I_\infty - I_0)|$ *vs* time (min), the slope of which is the pseudo—first order reaction rate (k′) obtained by a least–squares fit ($R^2 > 0.95$). (Each time point is an average of hexaplet samples.) The second-order rate constant is derived from here using the concentration of the other agent (typically ~3 mM, but precisely determined to 2 digits precision (e.g. 3.0 mM) in each case).

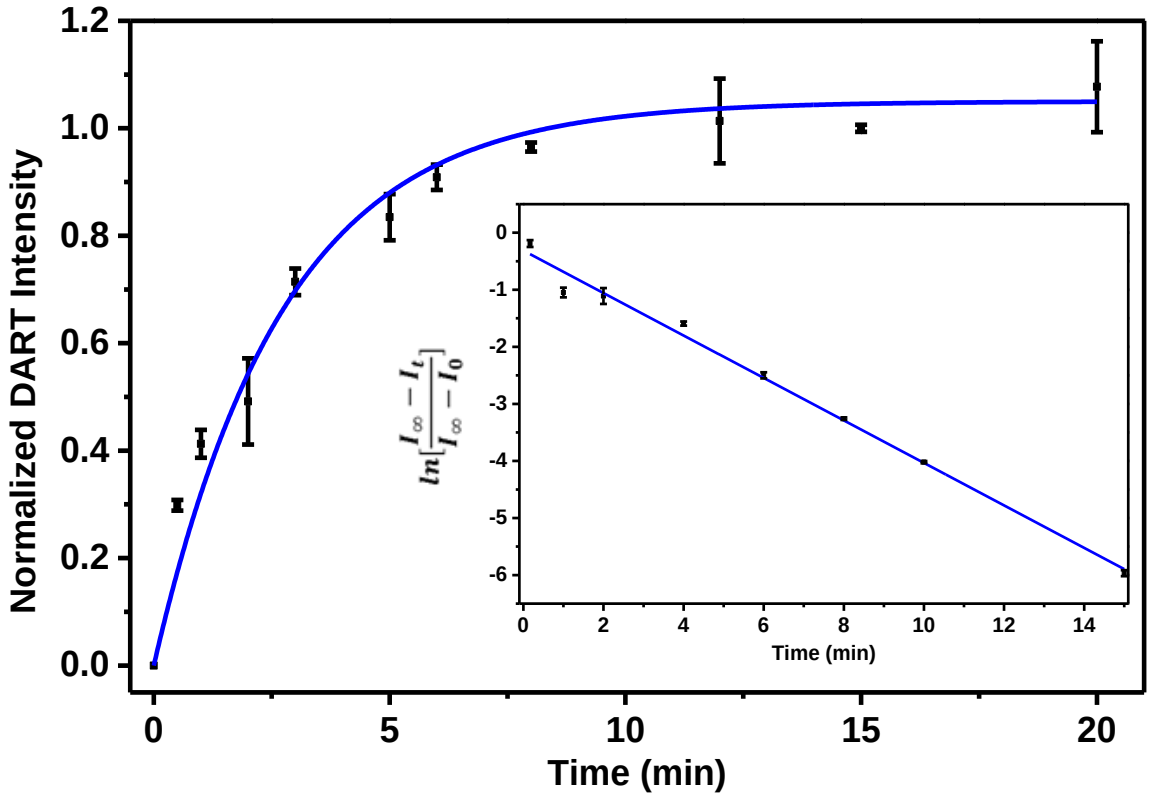

Figure S3.5. Kinetic plot of "free" tetrazine–terminated surface (**M**$_4$) reacting with *exo*–norbornene tag **4** in DCE solution at 30 °C. Inset: Linear plot of *ln* $|(I_\infty - I_t) / (I_\infty - I_0)|$ *vs* time (min), the slope of which is the pseudo—first order reaction rate (k′) obtained by a least–squares fit ($R^2 > 0.95$). (Each time point is an average of hexaplet samples.) The second-order rate constant is derived from here using the concentration of the other agent (typically ~3 mM, but precisely determined to 2 digits precision (e.g. 3.0 mM) in each case).

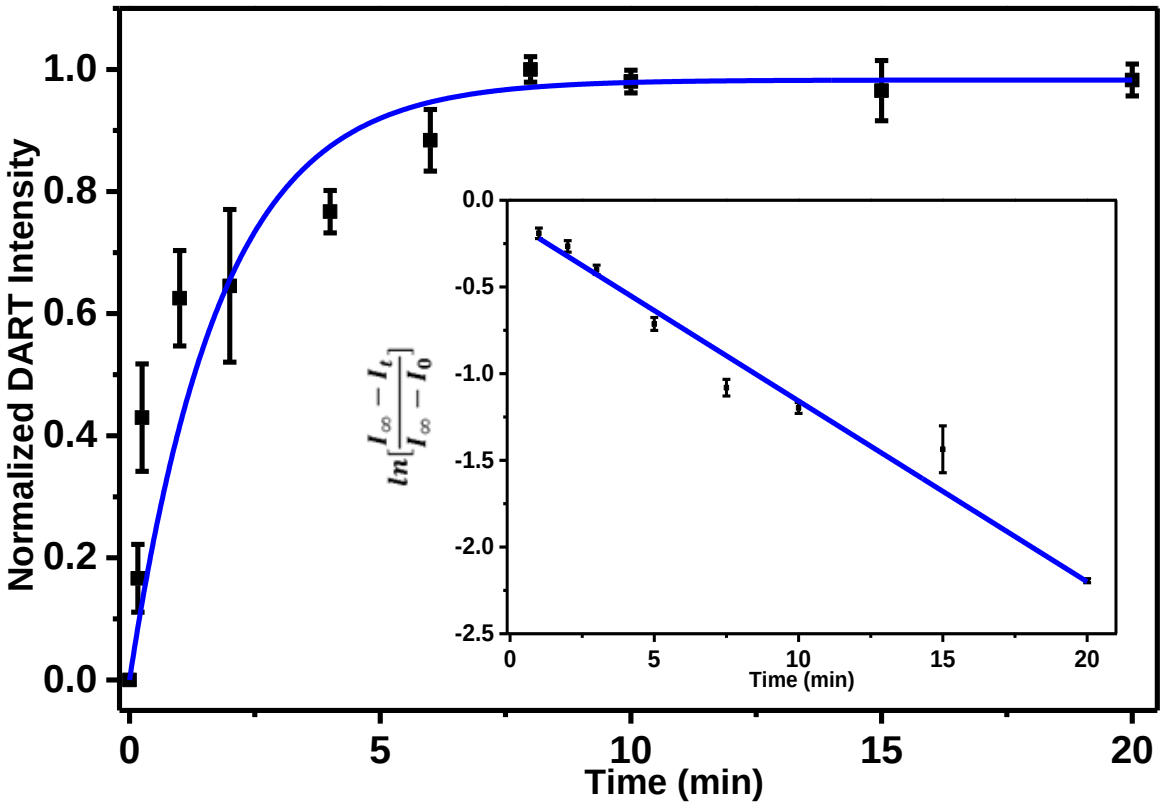

Figure S3.6. Sigmoidal plot of normalized integrated DART–HRMS intensity vs time (min) for "buried" tetrazine–terminated surface (**M$_4$**) reacting with *exo*–norbornene tag 4 in DCE solution at 30 °C. Inset: Linear plot of *ln* $|(I_\infty - I_t) / (I_\infty - I_0)|$ *vs* time (min), the slope of which is the pseudo—first order reaction rate (k′) obtained by a least–squares fit ($R^2 > 0.95$). (Each time point is an average of hexaplet samples.) The second-order rate constant is derived from here using the concentration of the other agent (typically ~3 mM, but precisely determined to 2 digits precision (e.g. 3.0 mM) in each case).

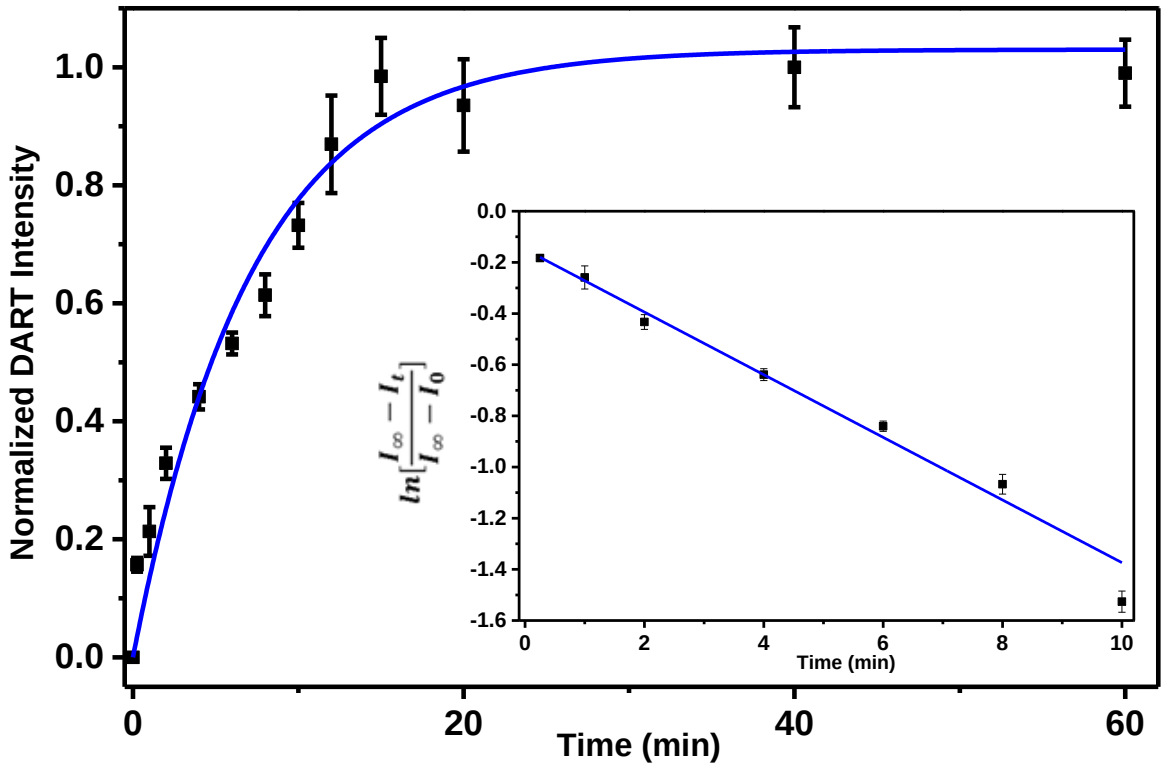

Figure S3.7. Sigmoidal plot of normalized integrated DART–HRMS intensity vs time (min) for "free" tetrazine–terminated surface (**M4**) reacting with *endo*–norbornene tag **6** in DCE solution at 30 °C. Inset: Linear plot of *ln* $|(I_\infty - I_t) / (I_\infty - I_0)|$ *vs* time (min), the slope of which is the pseudo—first order reaction rate (k′) obtained by a least–squares fit ($R^2 > 0.95$). (Each time point is an average of hexaplet samples.) The second-order rate constant is derived from here using the concentration of the other agent (typically ~3 mM, but precisely determined to 2 digits precision (e.g. 3.0 mM) in each case).

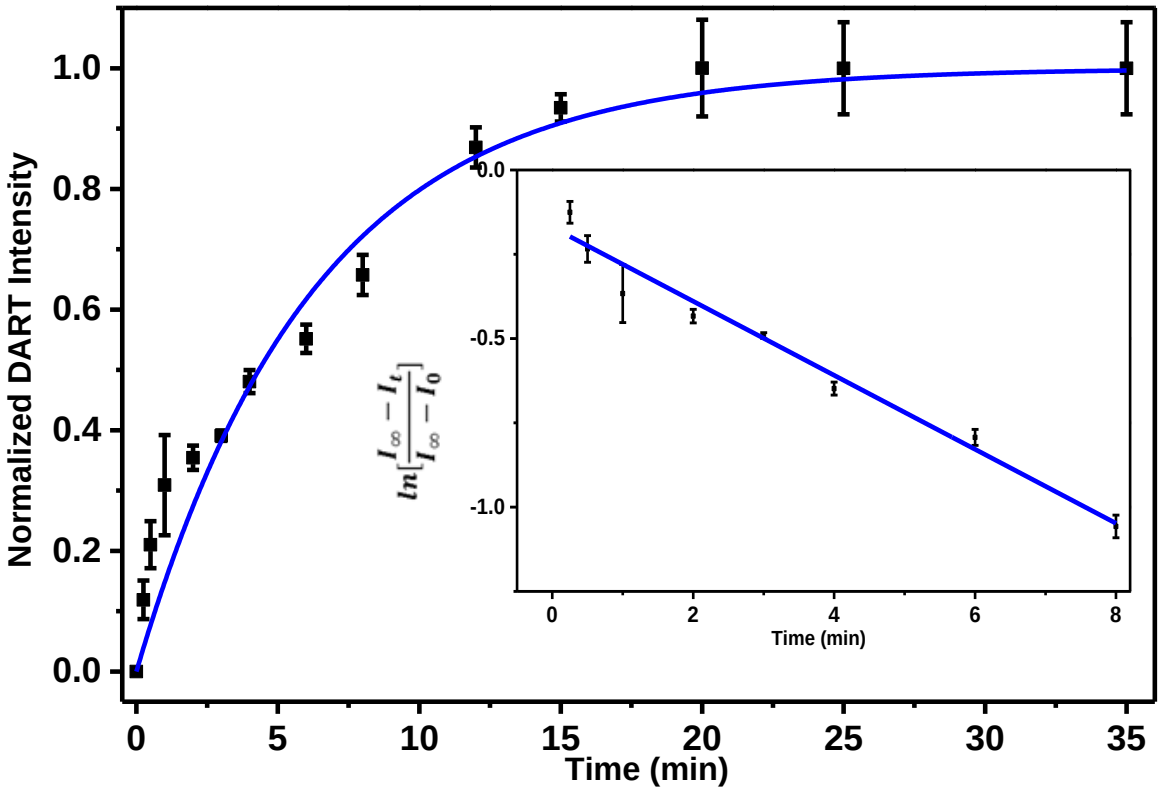

Figure S3.8. Sigmoidal plot of normalized integrated DART–HRMS intensity vs time (min) for "buried" tetrazine–terminated surface (**M**$_4$) reacting with *endo*–norbornene tag **6** in DCE solution at 30 °C. Inset: Linear plot of *ln* $|(I_\infty - I_t) / (I_\infty - I_0)|$ *vs* time (min), the slope of which is the pseudo—first order reaction rate (k′) obtained by a least–squares fit ($R^2 > 0.95$). (Each time point is an average of hexaplet samples.) The second-order rate constant is derived from here using the concentration of the other agent (typically ~3 mM, but precisely determined to 2 digits precision (e.g. 3.0 mM) in each case).

4. SUPPLEMENTARY FIGURES.

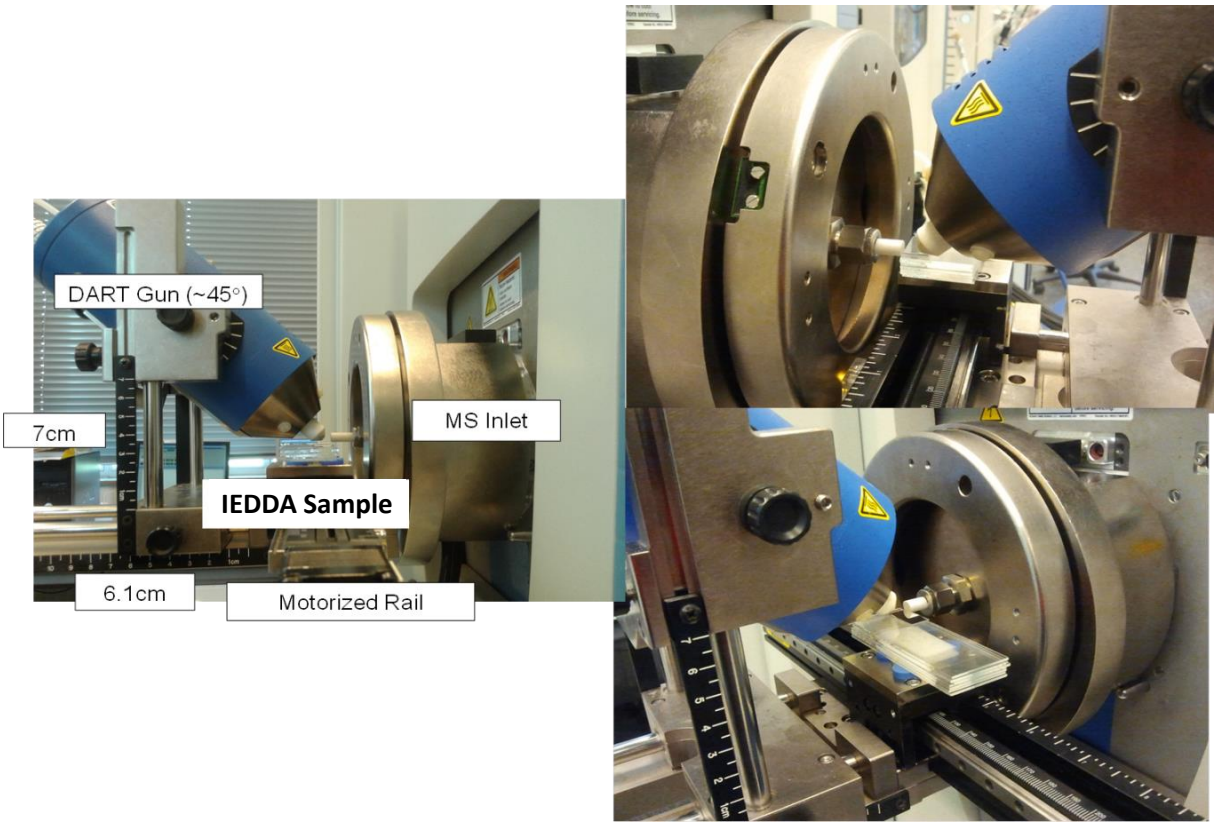

Figure S4.1. Pictures of DART setup for the kinetic analysis of organic surface reactions.

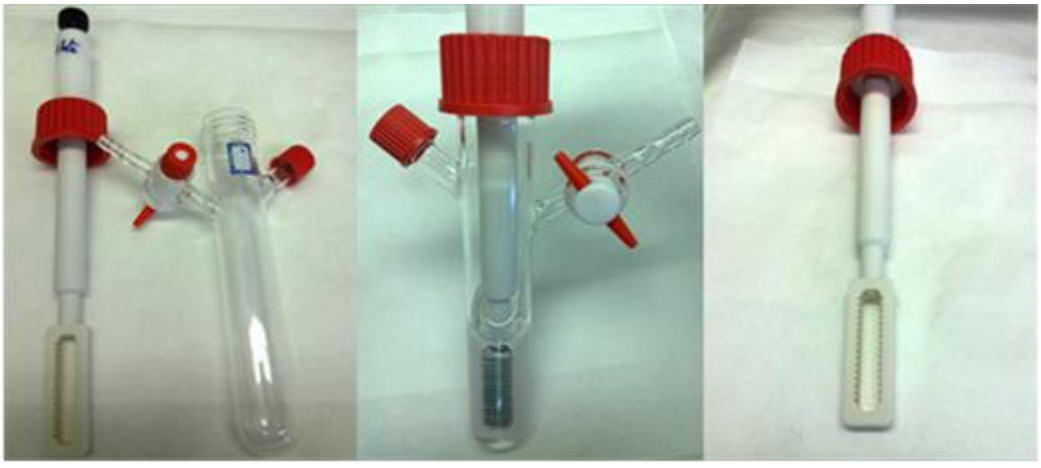

Figure S4.2. Image of the sample holder (16 slots).

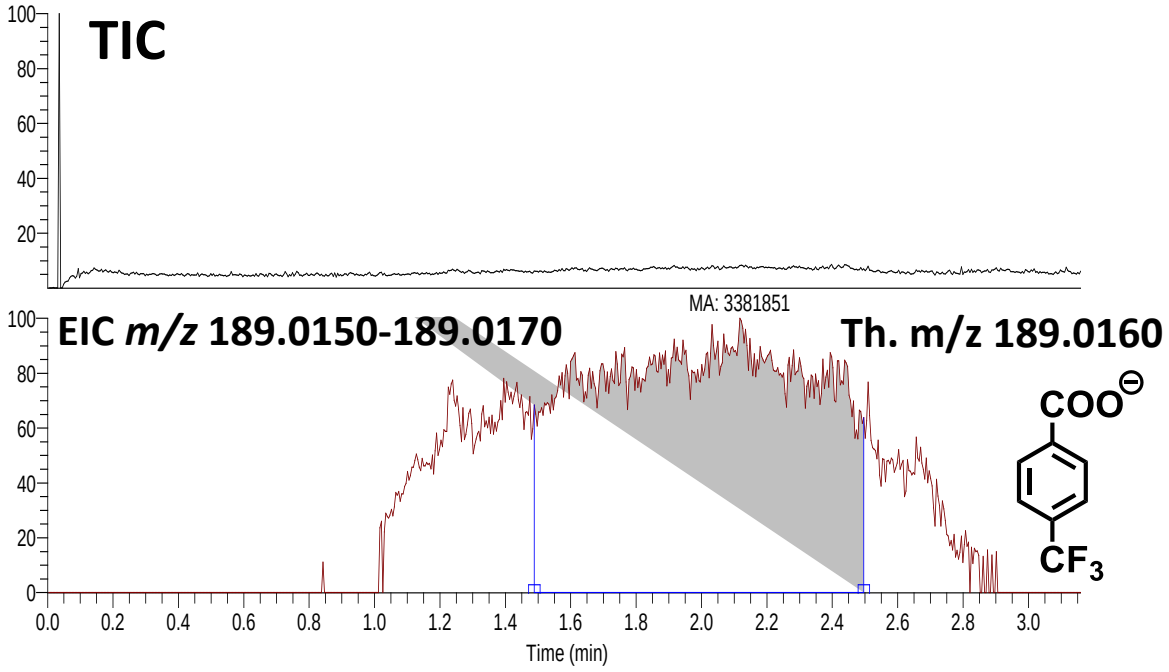

Figure S4.3. Representative spectra of a typical DART–HRMS measurement. Top: Total Ion Current (TIC); bottom: Extracted ion chromatogram (EIC) of 10 mmu window around the theoretical *m/z* of the ion of interest.

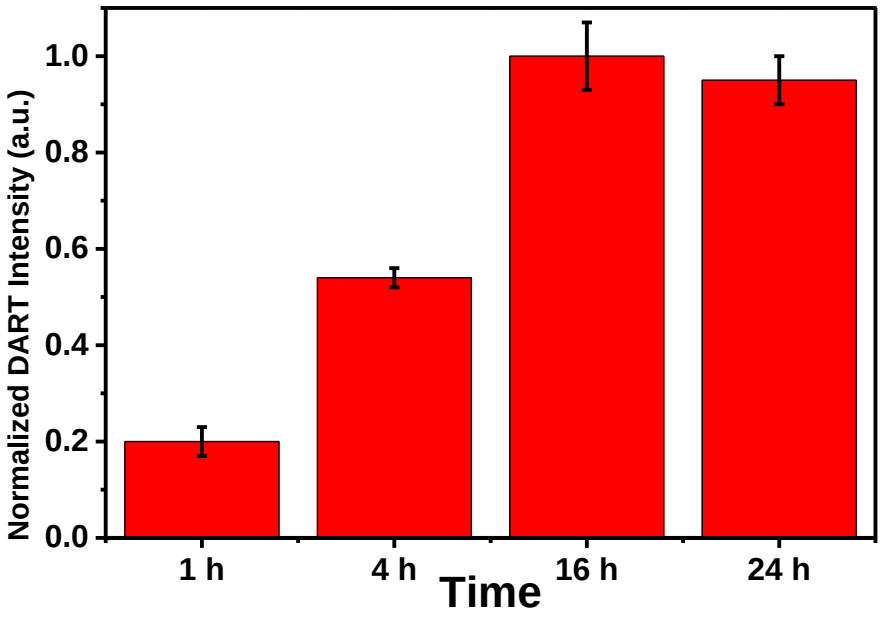

Figure S4.4. Normalized DART–HRMS intensity of MS tag with *m/z* 189.0163 after IEDDA reaction (for 20 min) on M_2 surfaces. The CDI-activated **M_1** samples were stirred in a 50 mM solution of *exo*–norbornene–OH for different times followed by stirring in a 3.0 mM DCE solution of **3** and analyzed by DART for MS tag.

5. SUPPLEMENTARY XPS SPECTRA (ALL CALCULATED ERRORS ARE AVERAGE OF 6 SAMPLES).

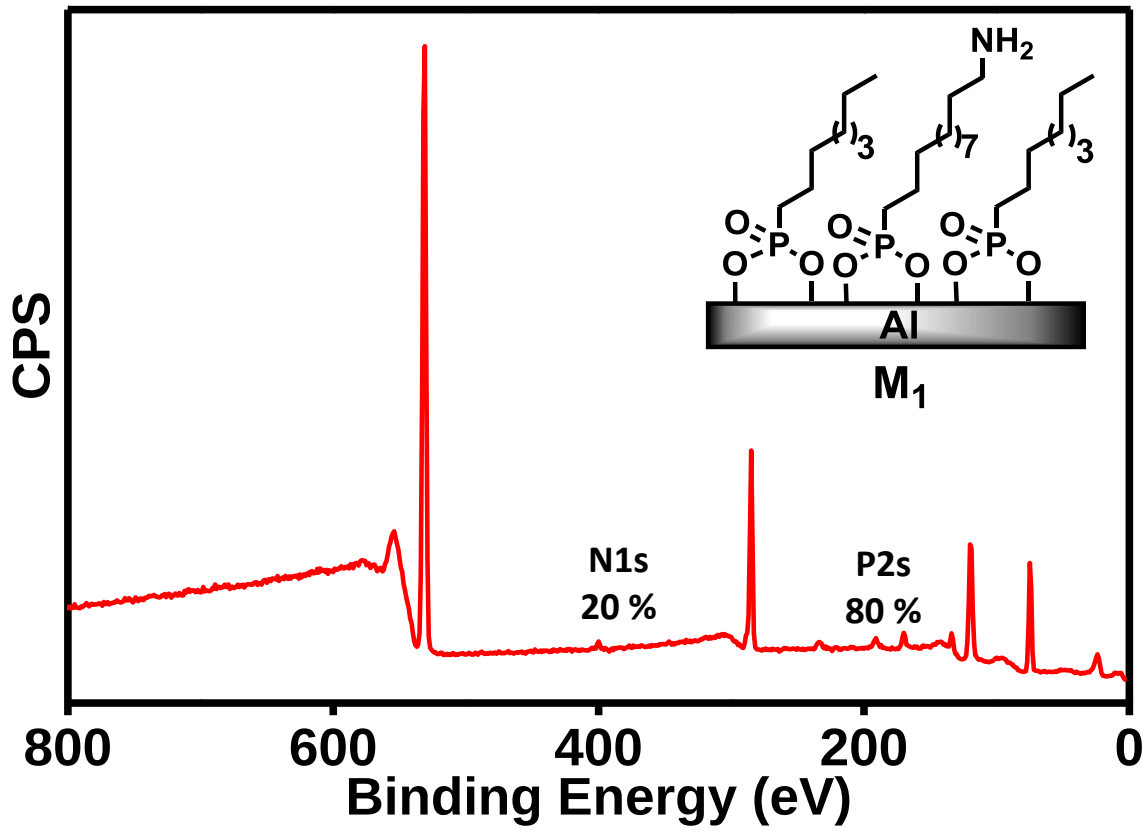

Figure S5.1. XPS wide scan of **M_1** modified Al surface for "free" microenvironment.

Theoretical N/P ratio = 1/ 4 = 0.25

Experimental N/P = 0.25 ± 0.02

⇒ 3:1 alkyl–amino terminated monolayer indeed obtained.

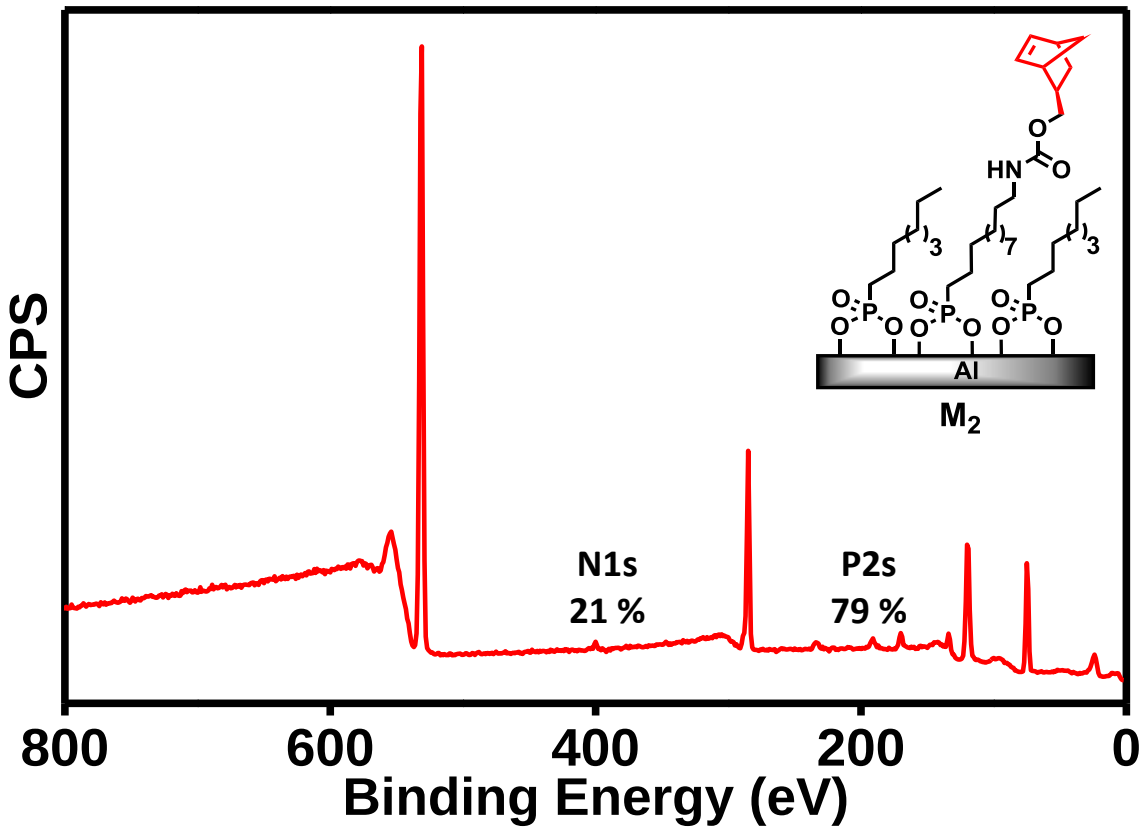

Figure S5.2. XPS wide scan of **M2** modified Al surface for "free" microenvironment.

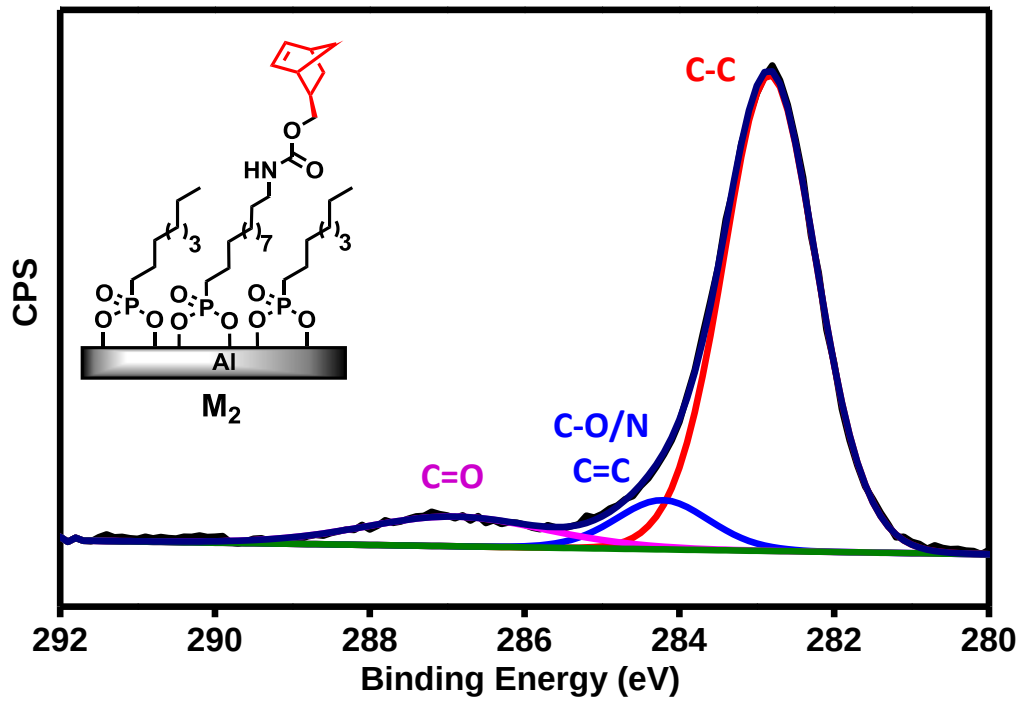

Figure S5.3. XPS C1s narrow scan of **M2** surface showing clear carbamate peak at 287.0 eV.

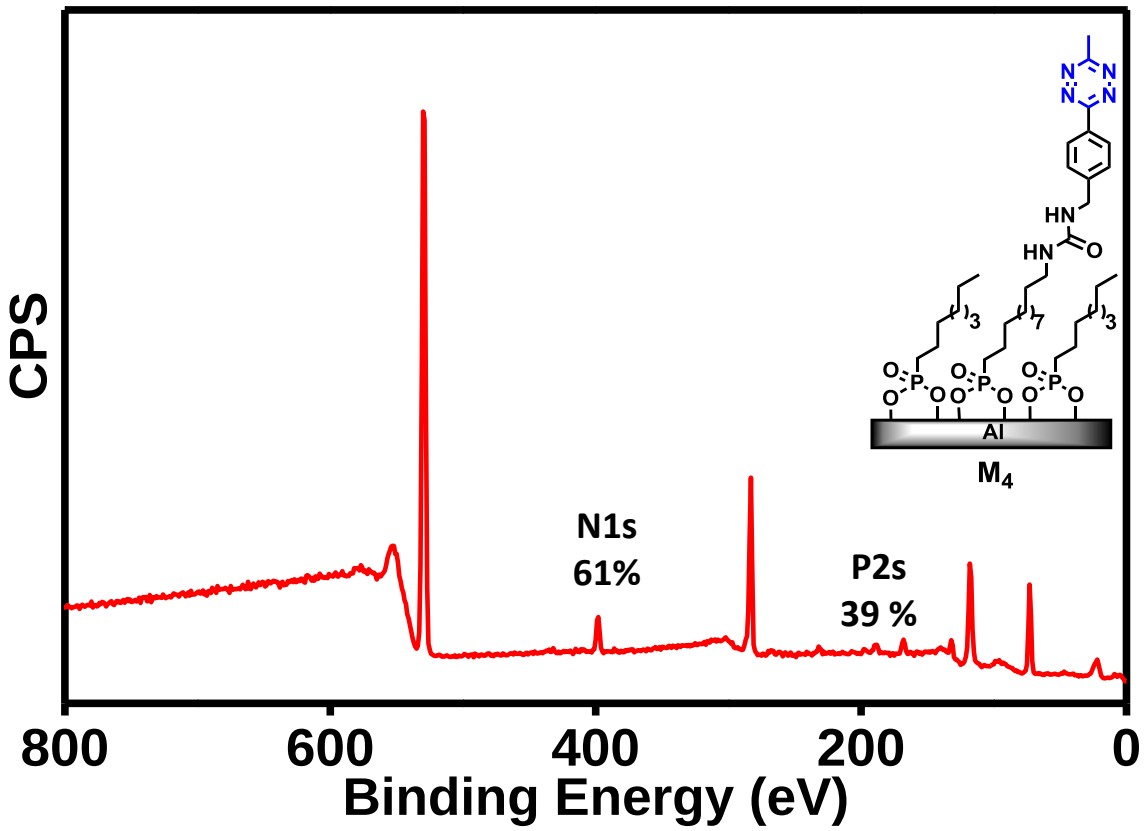

Figure S5.4. XPS wide scan of **M4** surface for “free” microenvironment.

Th. N/P = 6/4 = 1.50

Expt. N/P = 1.5 ± 0.1

Surface yield = 98 ± 2 %

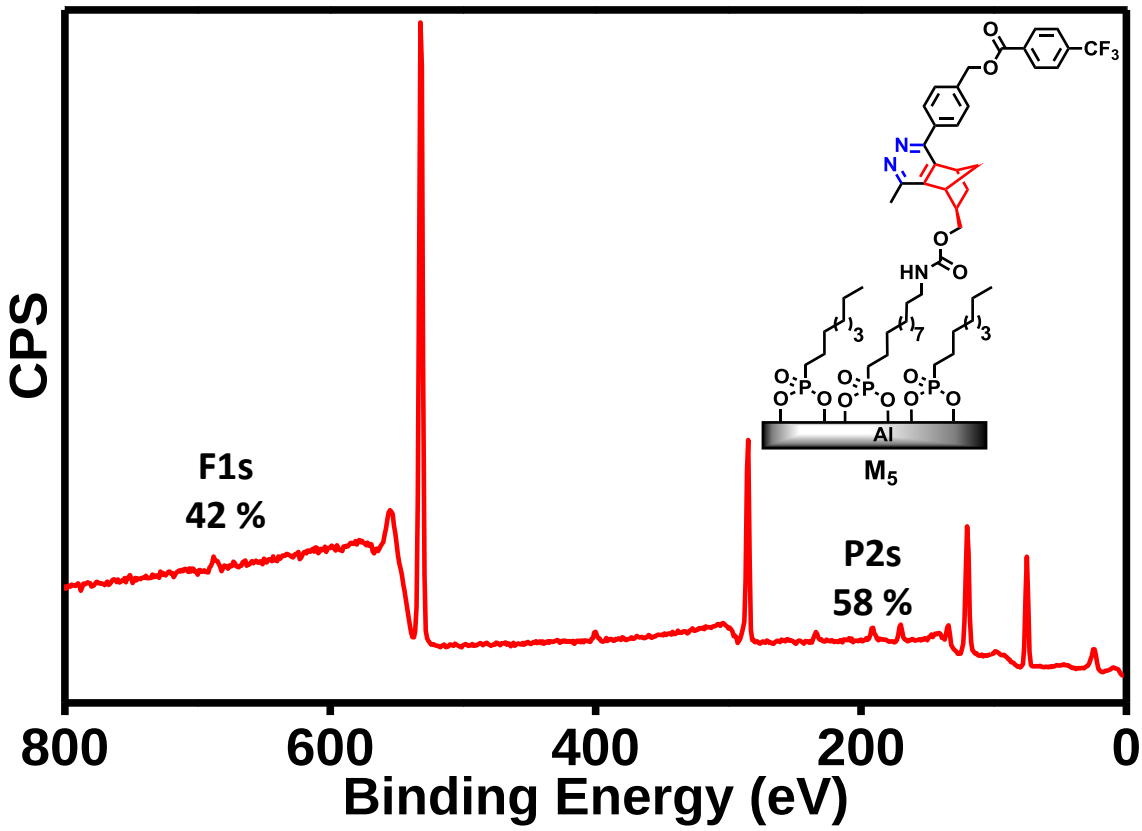

Figure S5.5. Wide scan of IEDDA cycloaddition products (**M5**) between *exo*–norbornene–terminated surface and tetrazine tag **3** for "free" microenvironment.

Th. F/P = 3/4 = 0.75

Expt. F/P = 0.76 ± 0.02

Surface yield = Quantitative

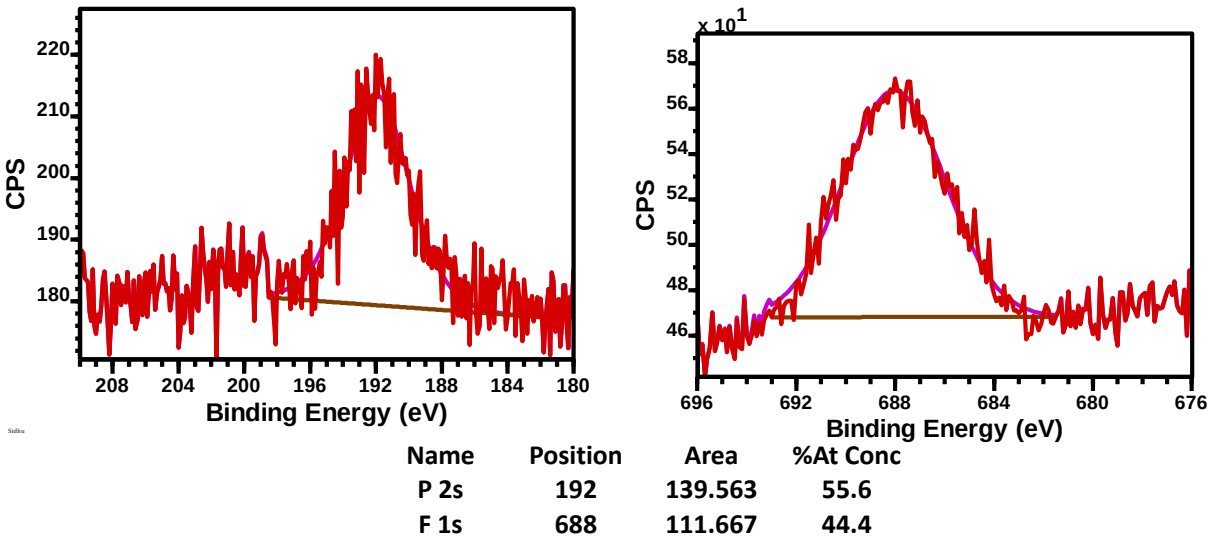

Name	Position	Area	%At Conc
P 2s	192	139.563	55.6
F 1s	688	111.667	44.4

Figure S5.6. F1s and P2s narrow scans of IEDDA cycloaddition products (**M$_5$**) between *endo*–norbornene–terminated surface and tetrazine tag **3** for "free" microenvironment.

Th. F/P = 3/4 = 0.75

Expt. F/P = 0.77 ± 0.02

Surface yield = Quantitative

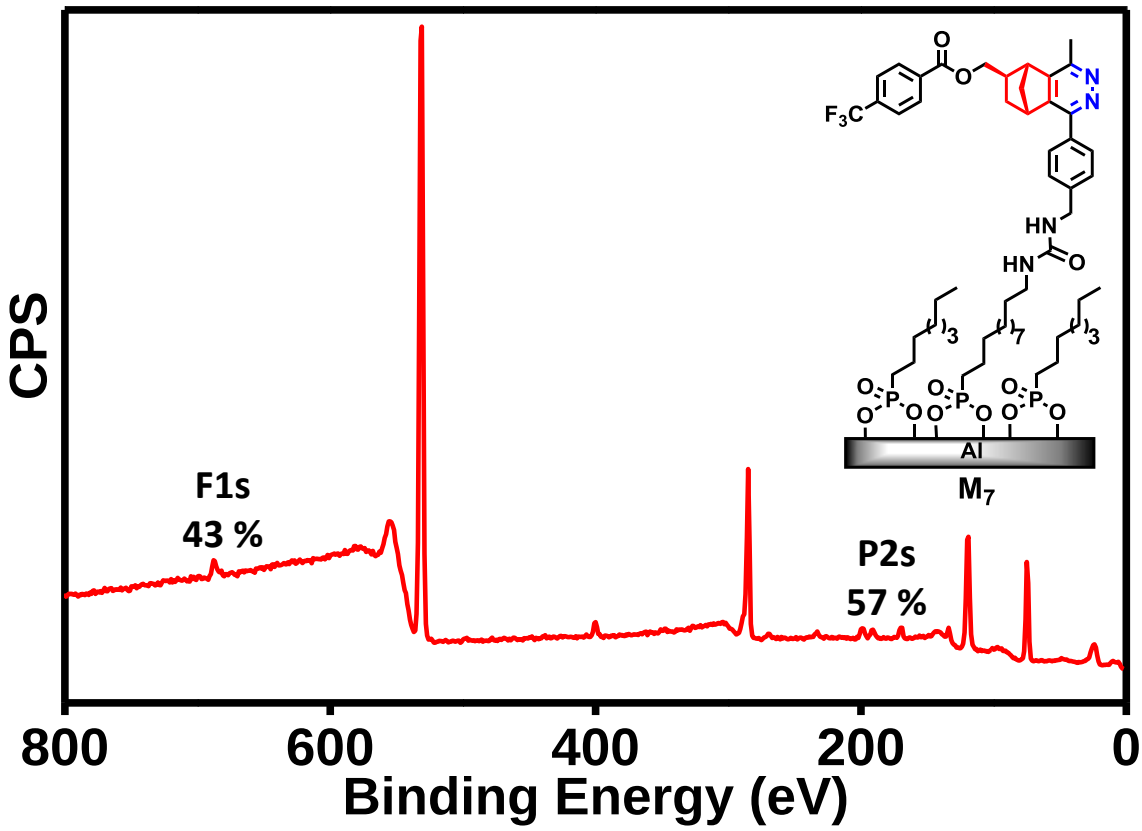

Figure S5.7. Wide scan of IEDDA cycloaddition products (**M**$_7$) between tetrazine$_{(surf.)}$ and *exo*–norbornene tag **4**.

Th. F/P = 3/4 = 0.75

Expt. F/P = 0.75 ± 0.02

Surface yield = Quantitative

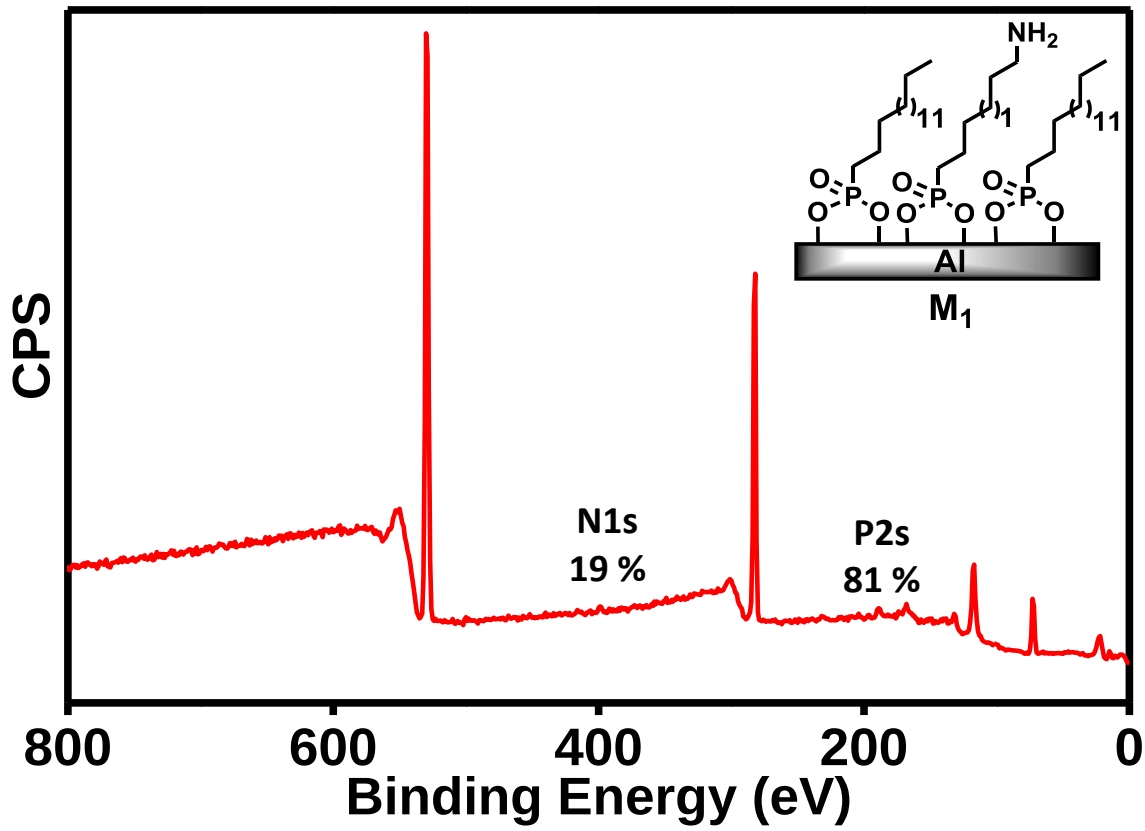

Figure S5.8. XPS wide scan of **M_1**-modified Al surface for “buried” microenvironment.

Theoretical N/P ratio = 1/ 4 = 0.25

Experimental N / P = 0.26 ± 0.02

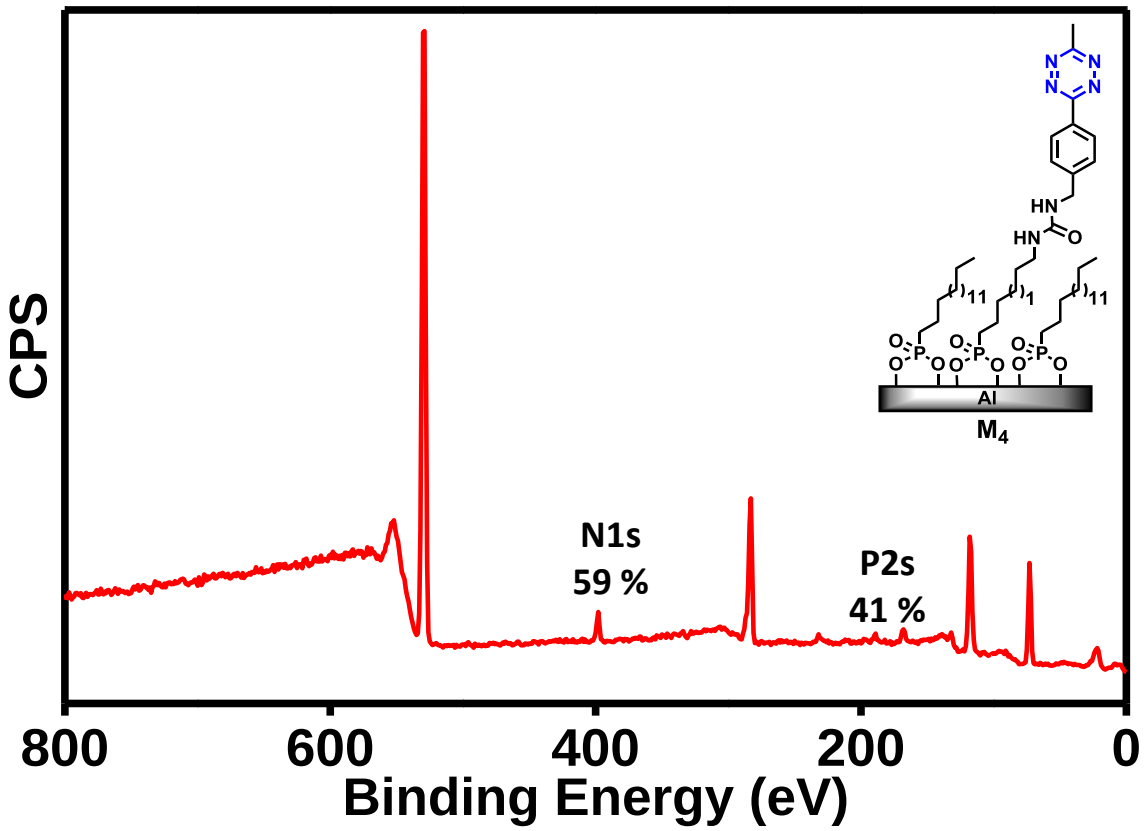

Figure S5.9. XPS wide scan of **M_4** surface for "buried" microenvironment.

Th. N/P = 6/4 = 1.50

Expt. N/P = 1.4 ± 0.1

Surface yield = 95 ± 5%

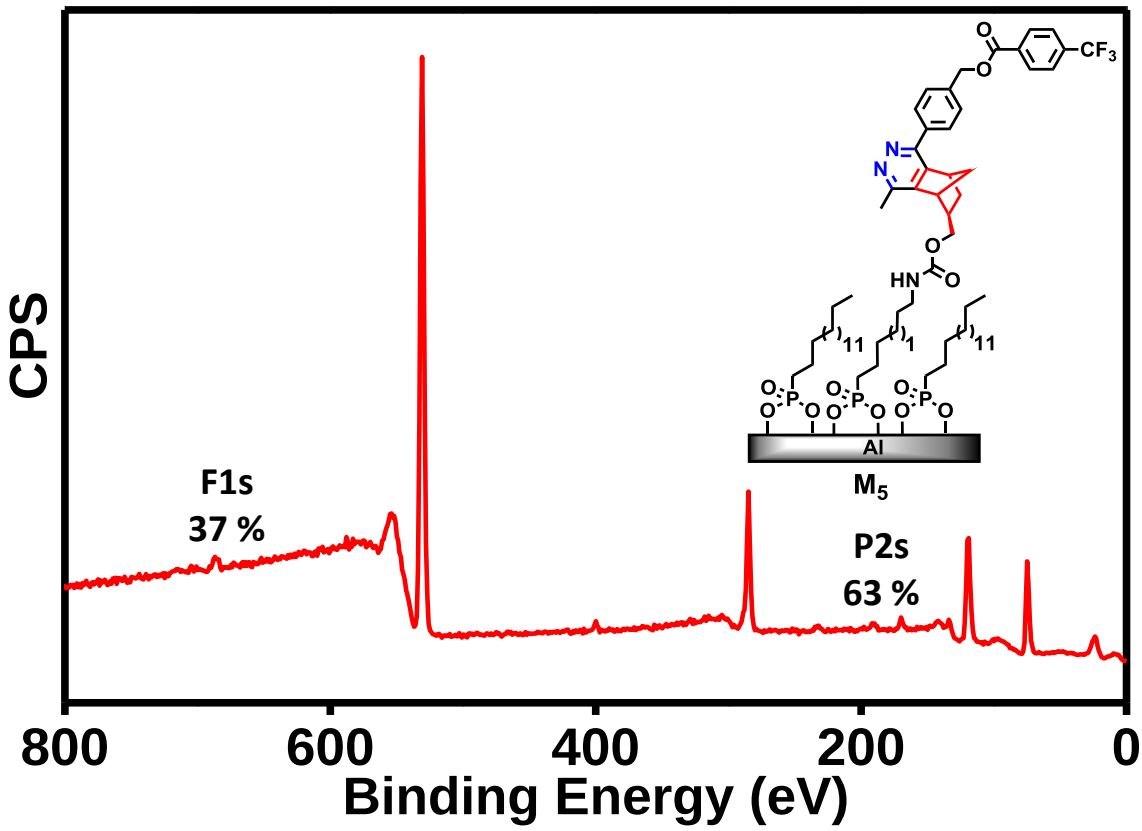

Figure S5.10. Wide scan of IEDDA cycloaddition products (**M**$_5$) between *exo*–norbornene$_{(surf.)}$ and tetrazine tag **3** for "buried" microenvironment after 15 min reaction.

Th. F/P = 3/4 = 0.75

Expt. F/P = 0.59 ± 0.02

Surface yield = 80 ± 5%

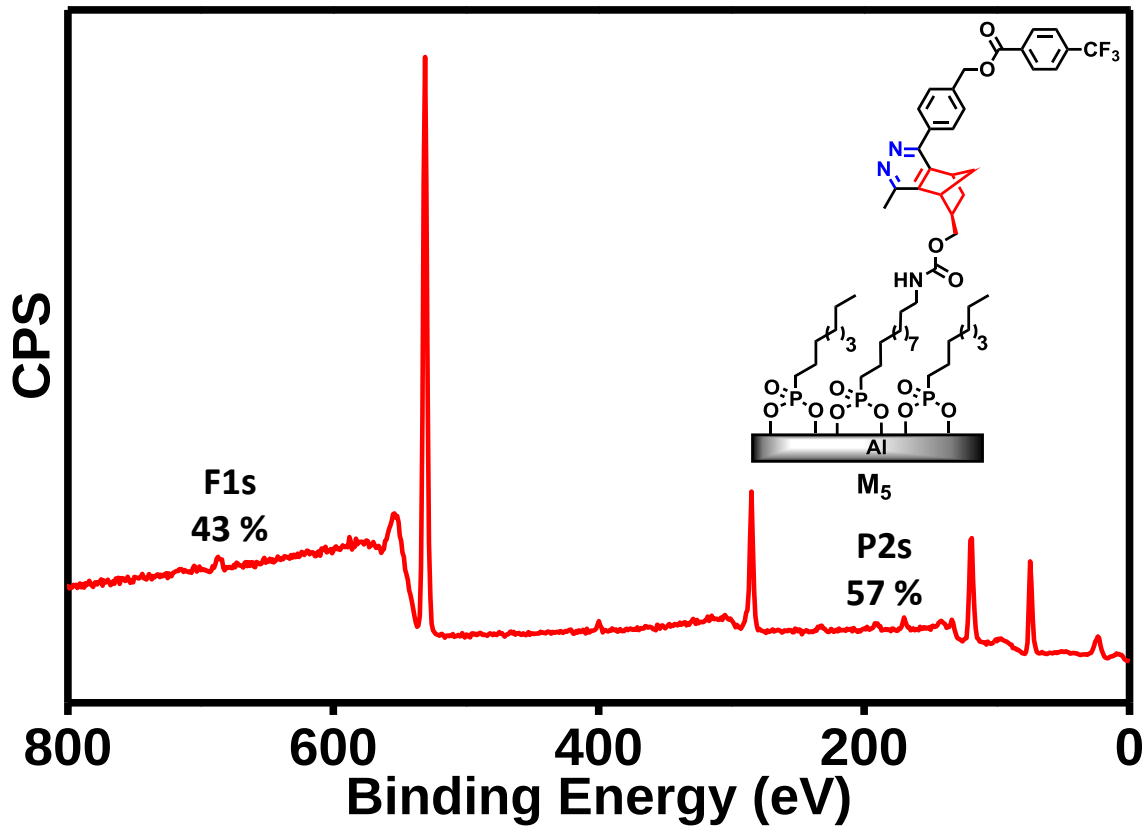

Figure S5.11. Wide scan of IEDDA cycloaddition products (**M**$_5$) between *exo*–norbornene$_{(surf.)}$ and tetrazine tag **3** for "buried" microenvironment after 1 h reaction time.

Th. F/P = 3/4 = 0.75

Expt. F/P = 0.70 ± 0.04

Surface yield = 94 ± 6 %

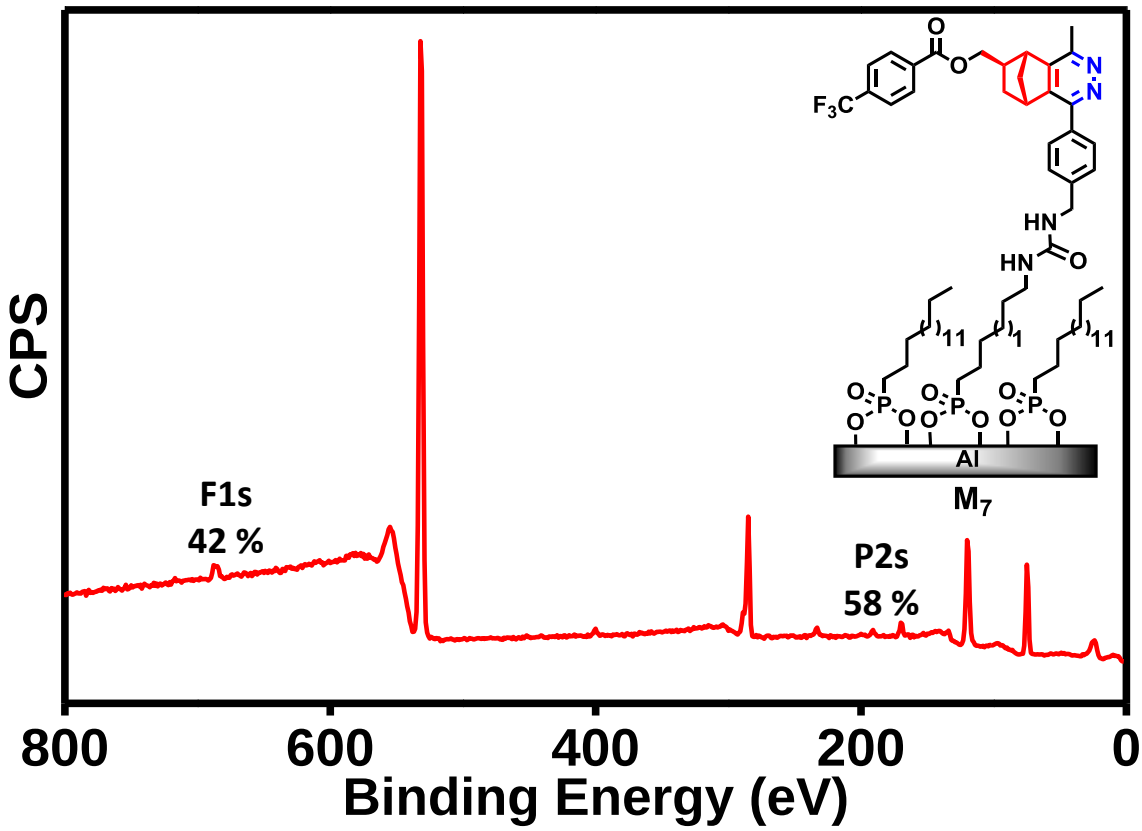

Figure S5.12. Wide scan of IEDDA cycloaddition products (**M**$_7$) between tetrazine$_{(surf.)}$ and *exo*–norbornene tag **4** "buried" microenvironment after 1 h.

Th. F/P = 3/4 = 0.75

Expt. F/P = 0.64 ± 0.07

Surface yield = 85 ± 10 %

6. SUPPLEMENTARY TABLES.

Table S6.1. Collected kinetic plots of tetrazine–norbornene IEDDA reaction for "free" or "buried" microenvironment (all $R^2 > 0.95$).

Surface group	ME	Reactant in solution	
		Exo-Norbornene	*Endo*-Norbornene
TETRAZINE	FREE	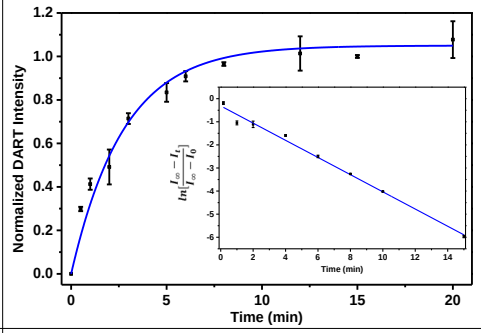	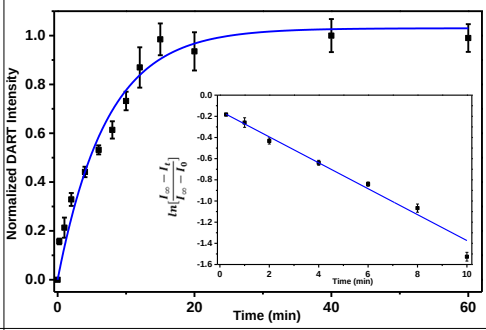
	BURIED	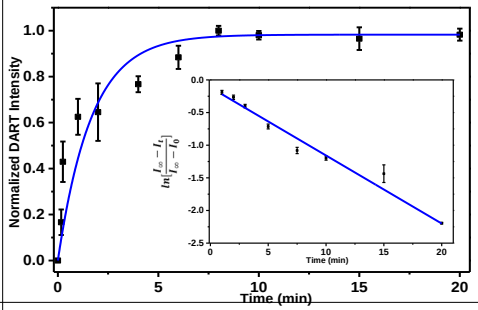	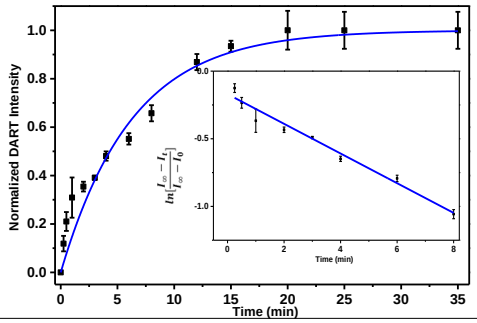
NORBORNENE		Tetrazine	
	FREE	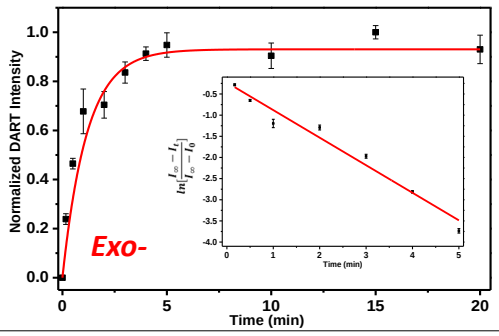	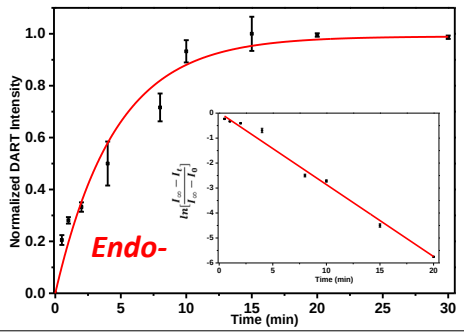
	BURIED	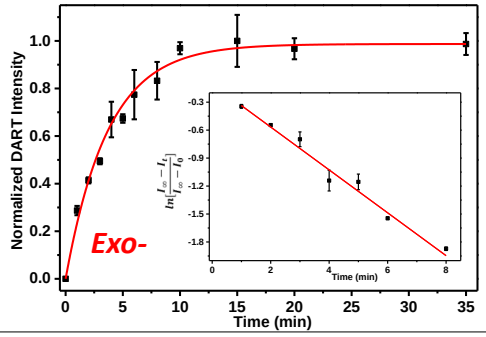	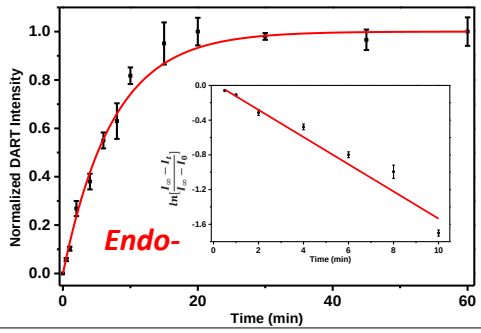

7. MATERIAL STUDIO DATA.

7.1 Al oxide (Al_2O_3) surface in bulk. All colors used are standard throughout (Grey = C, white = H, purple = P, pink = Al, red = O, fluorine = cyan).

[Any incomplete fragments and atoms are part of larger structures protruding from the adjacent box.]

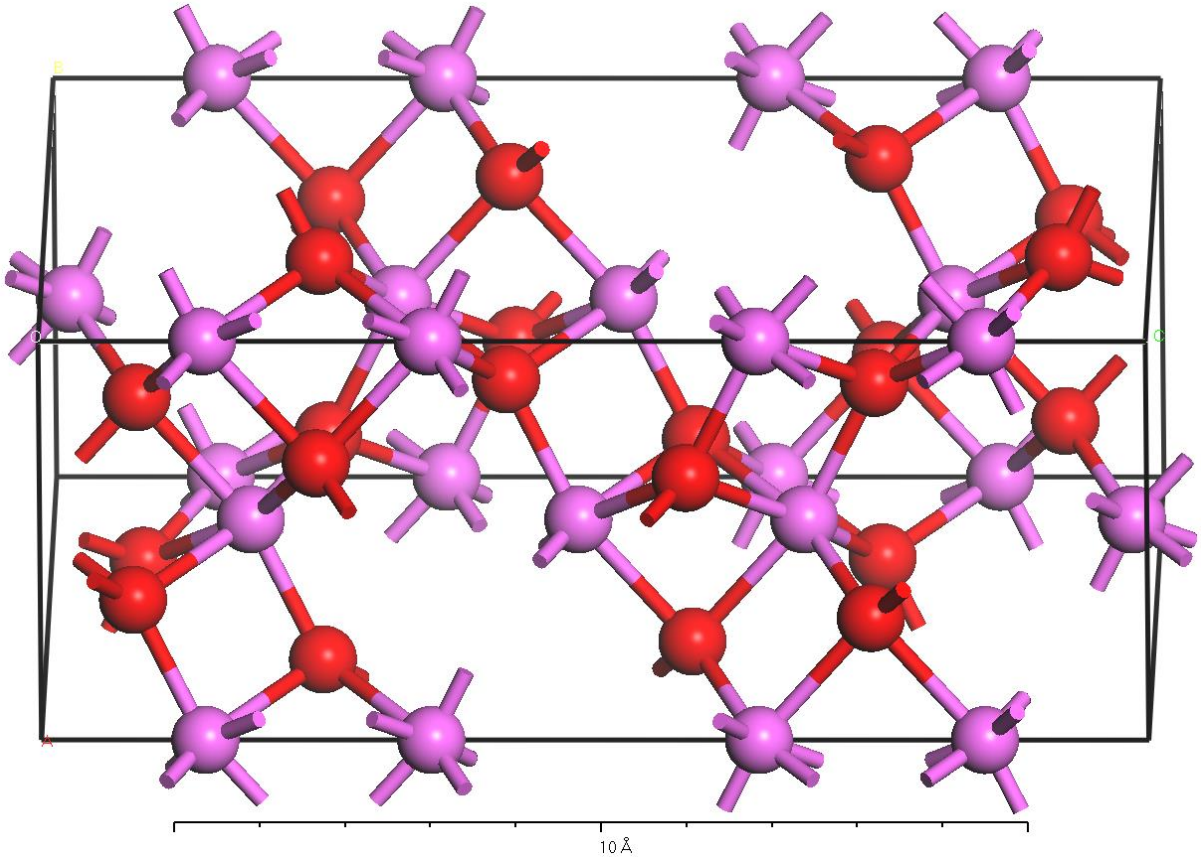

Al_2O_3 were cleaved along (h k l) = (–1 0 0) to build oxidic aluminum surfaces.

Thickness fractional = 1

Thickness (Å) = 4.121

Cap bonds on Top = O(oxygen)

7.2 Side view of cleaved Al_2O_3 surface.

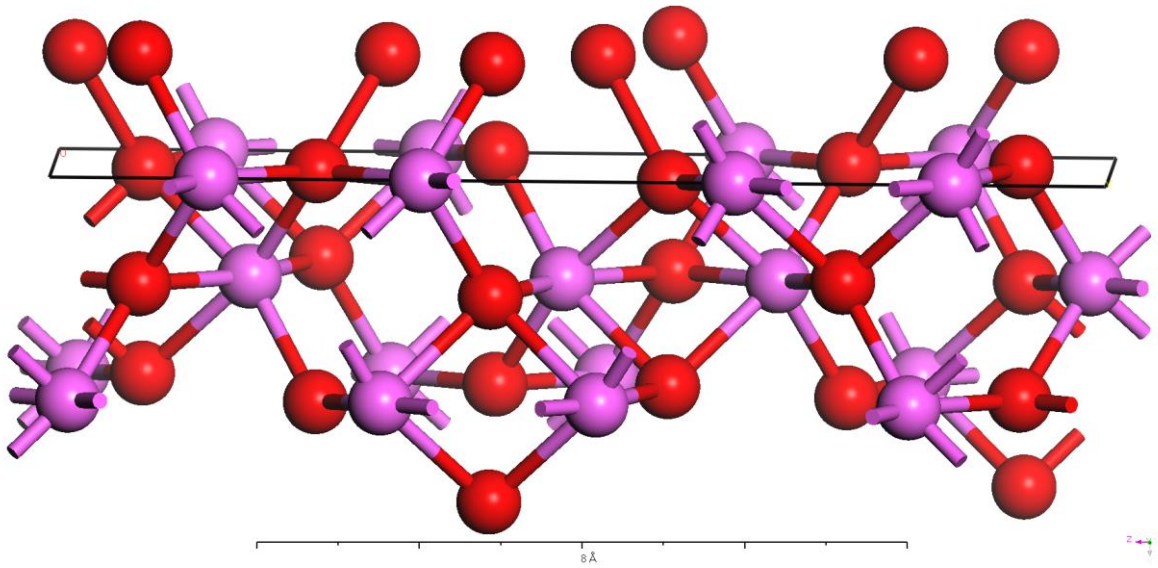

7.3 Dimensions of vacuum slab above Al_2O_3 surface for modelling alkyl groups and later IEDDA fragments.

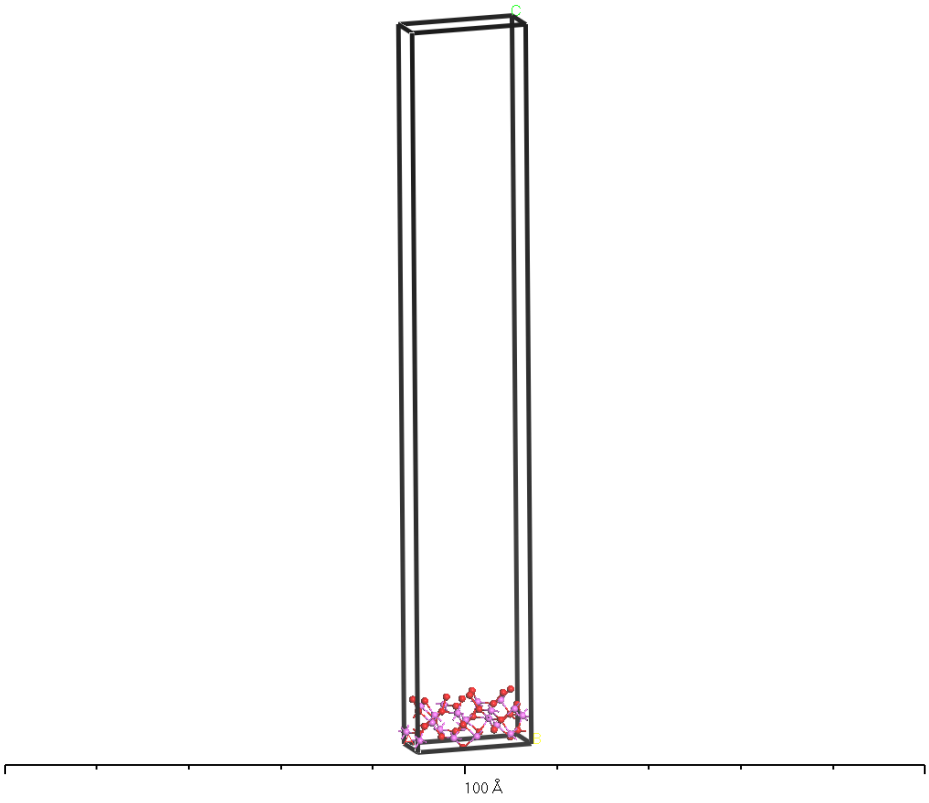

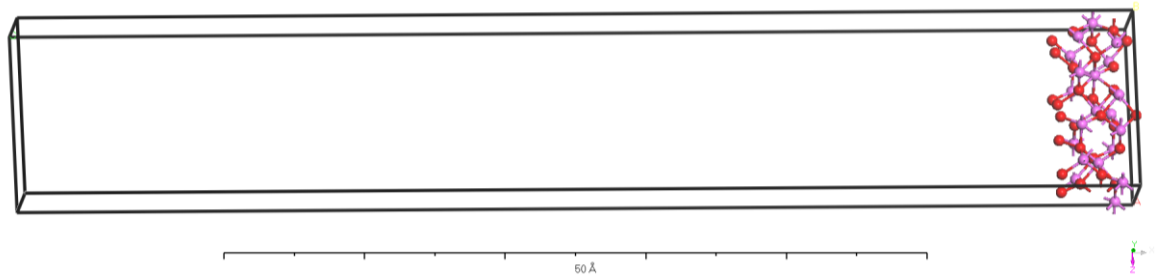

7.4 Dimensions of Al_2O_3 surface.

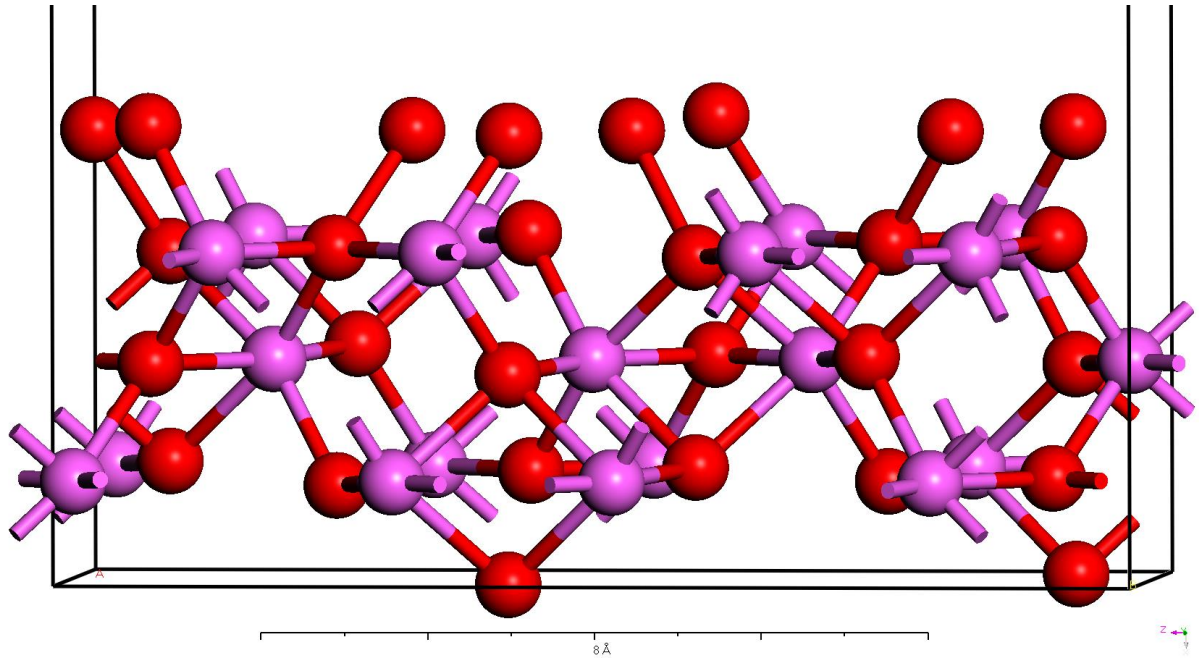

Vacuum Slab Build Dimensions

Vacuum orientation C (axis)

Vacuum thickness = 74.5048 Å

Crystal thickness = 80.00 Å

7.5 Side view of octylphosphonic acid on Al_2O_3 surface (with dimensions).

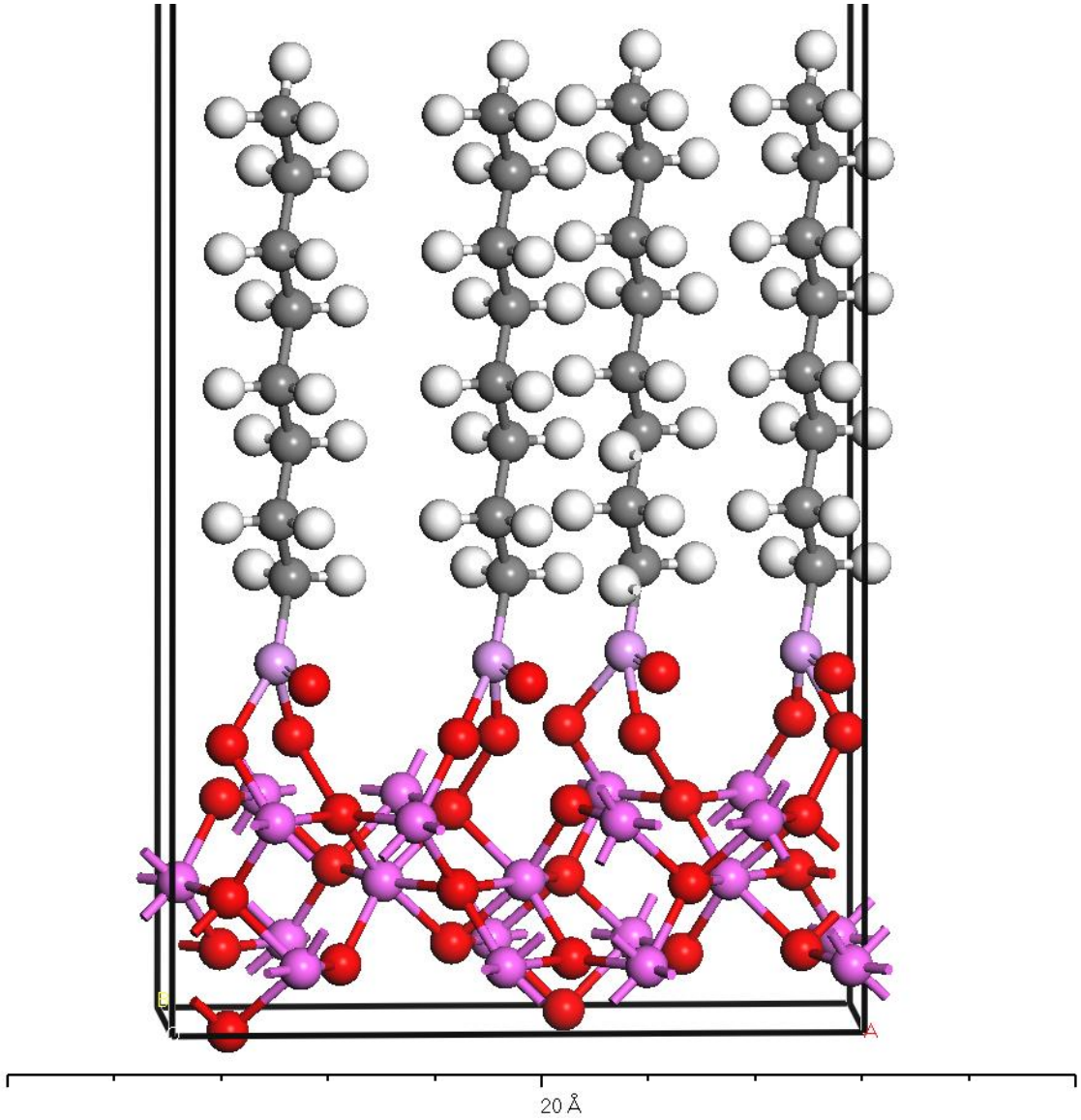

7.6 Top view of octylphosphonic acid on Al_2O_3surface (with dimensions).

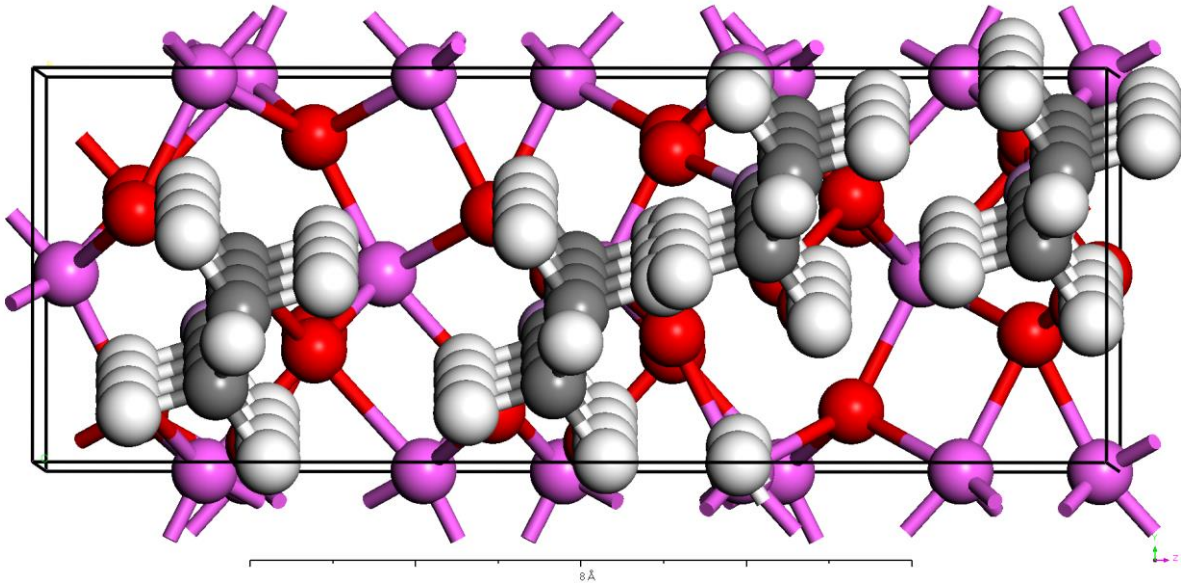

7.7 Top view of a supercell (3 x 5) of –OH terminated Al_2O_3 surface. No phosphonic acid attached (0% coverage, hydrogens of –OH highlighted with yellow, other oxygen atoms (red) are part of the Al_2O_3 surface and are unavailable to undergo reaction).

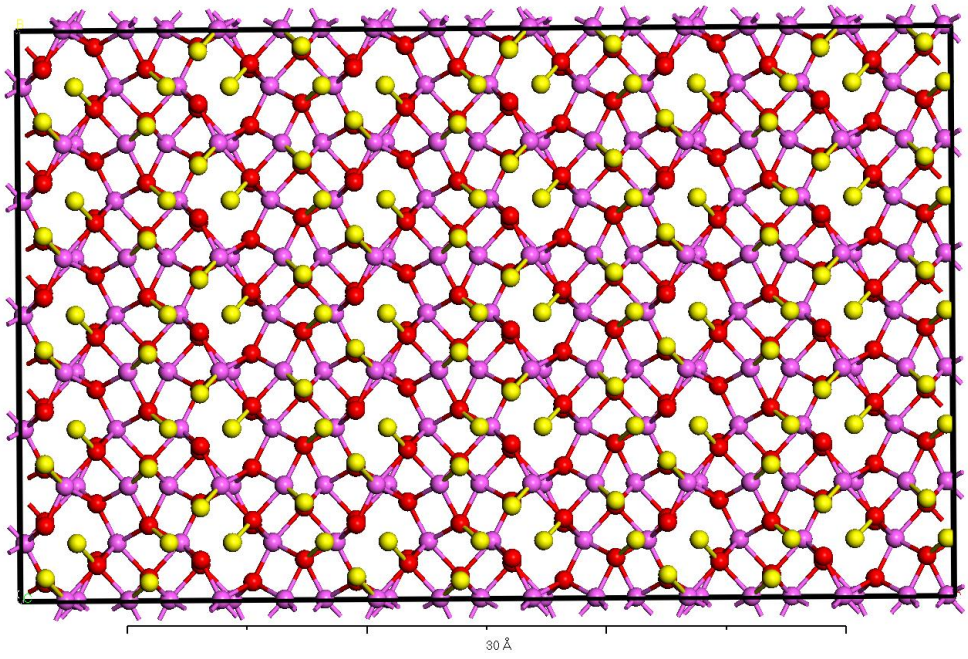

7.8 Top view of a supercell (3 x 5) of octyl phosphonic acid (100% coverage).

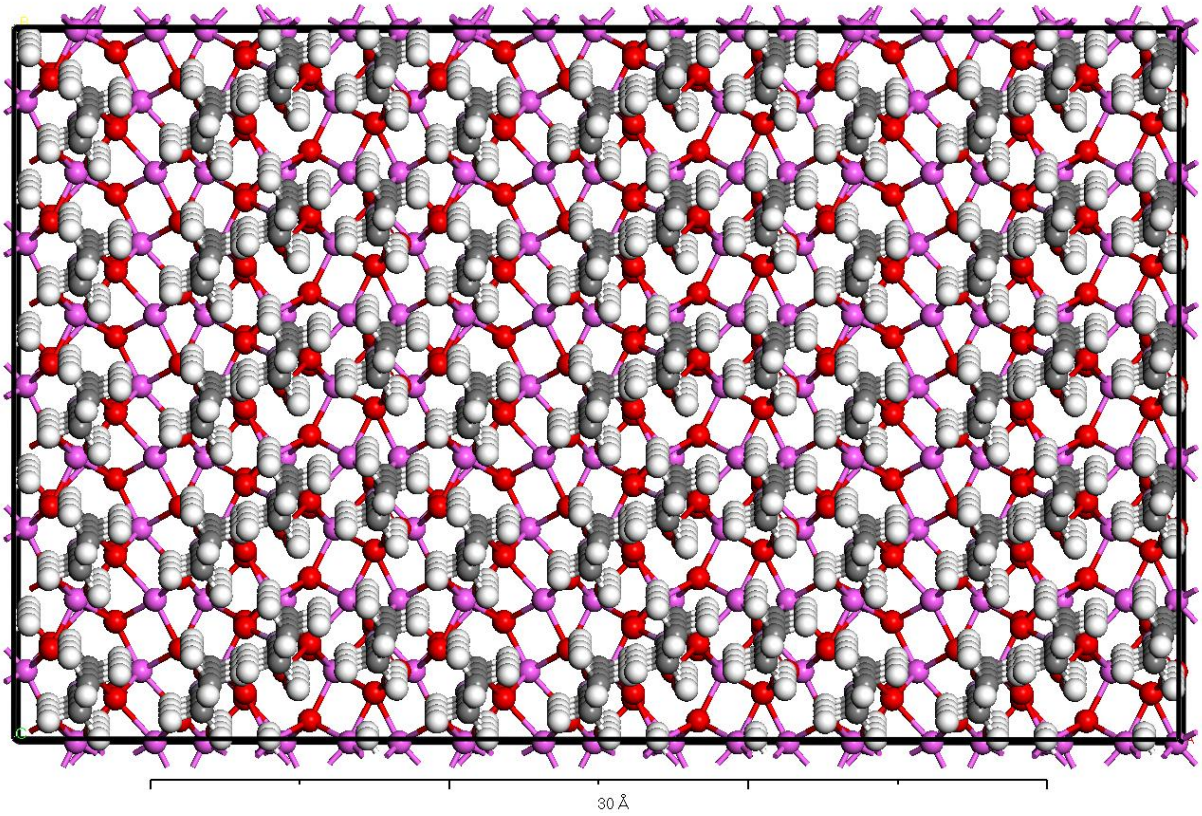

7.9 Scheme for random attachment of octyl phosphonic acid groups to obtain different % coverages. (3 different subsets of each % coverage was done to maximize randomization). (Red balls = –OH attachment, no attachment; Black balls = site of octylphosphonic acid.)

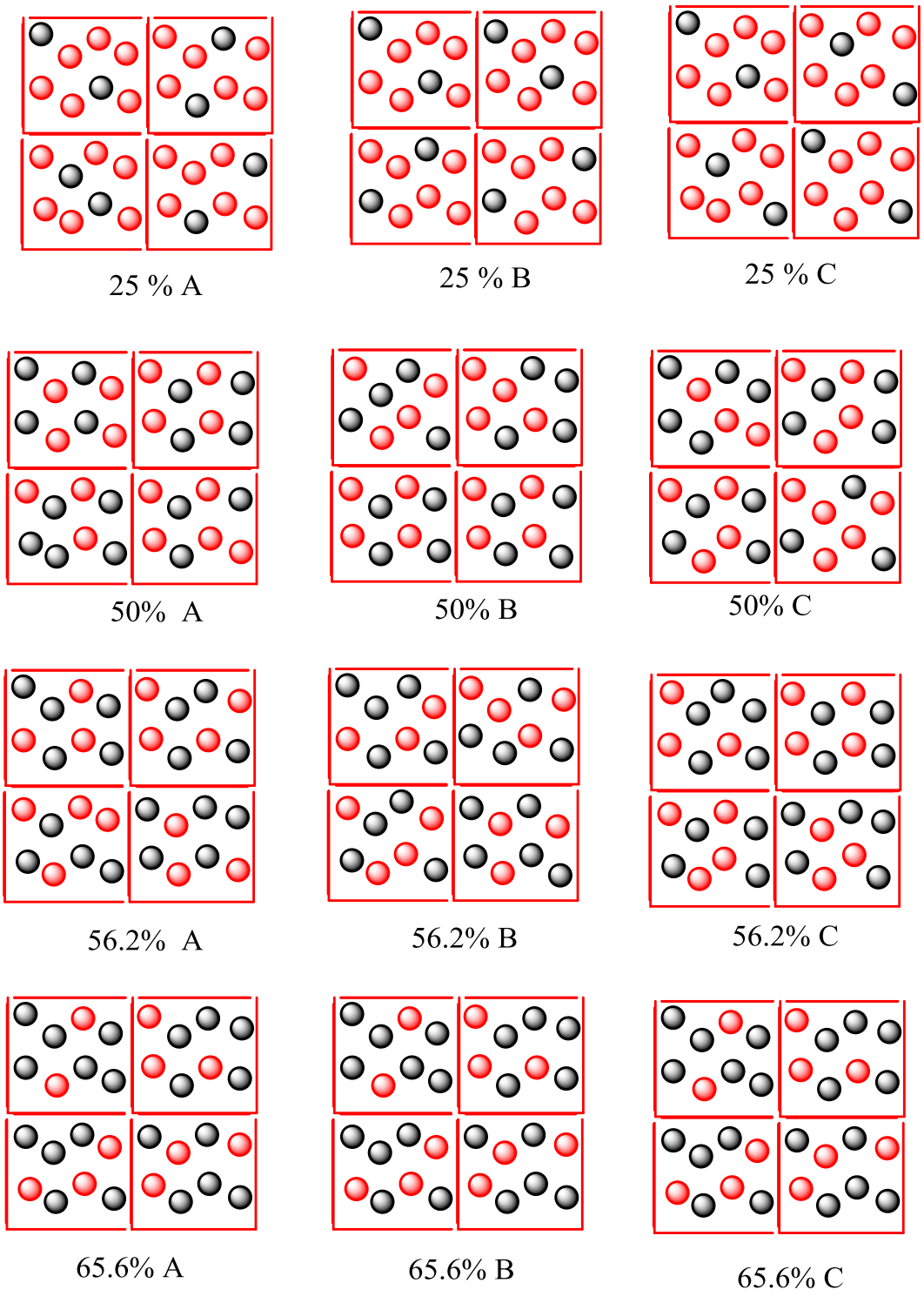

7.10 Plot of packing energy vs different surface coverages. Minimum energy denotes maximum stability. [All calculations were done on a supercell (8 x 16) with 512 chains.]

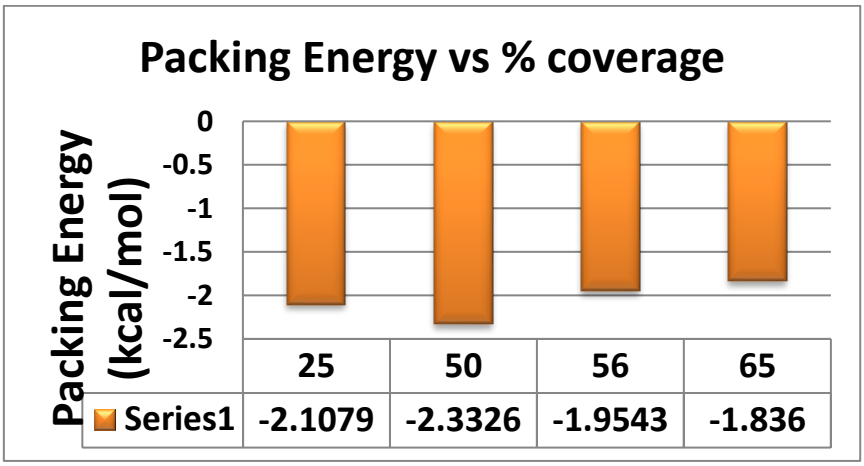

7.11 Scheme of the most stable configuration for a supercell (8 x 16) with 512 chains (50% B).

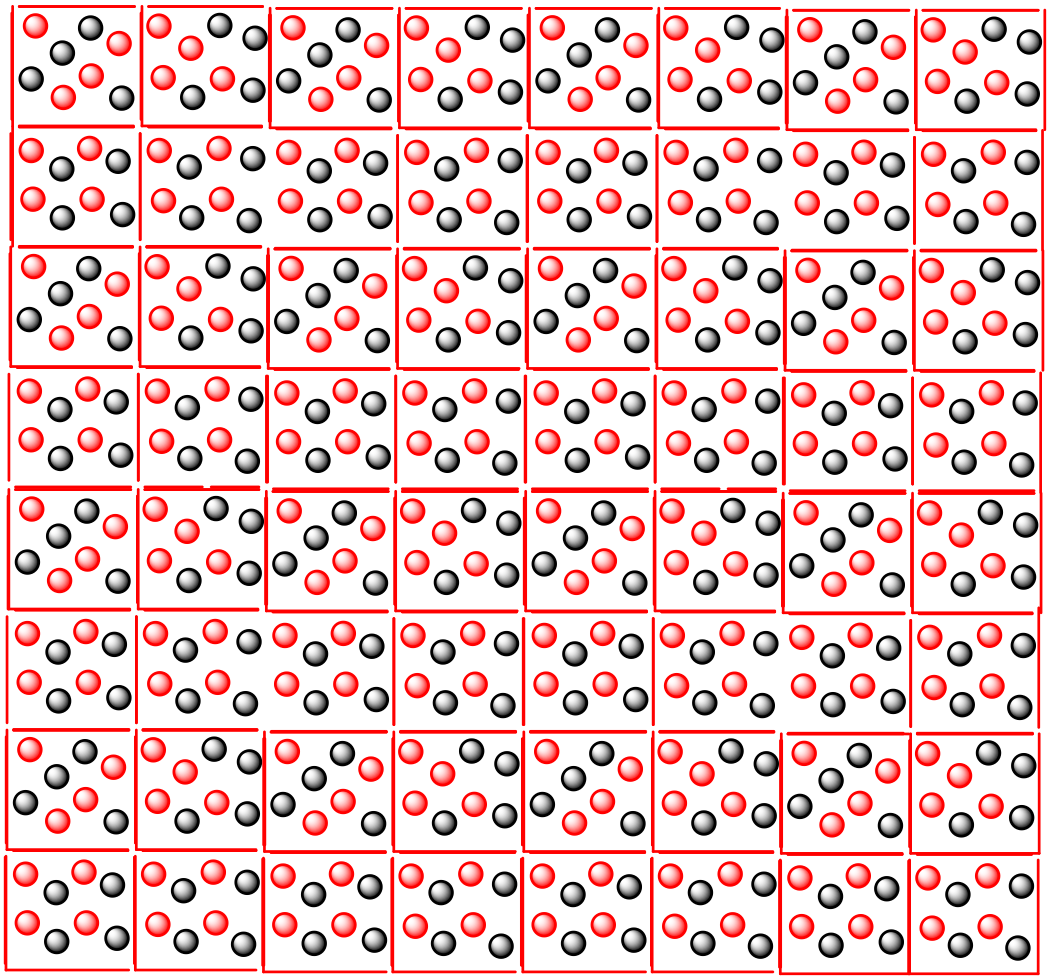

7.12 Molecular model of 50% B (1st = tilted, 2nd = across view) supercell (8 x16) after energy minimization. The picture shows the octylphosphonic acid chains attached randomly to the Al_2O_3 surface in a 50% overall coverage.

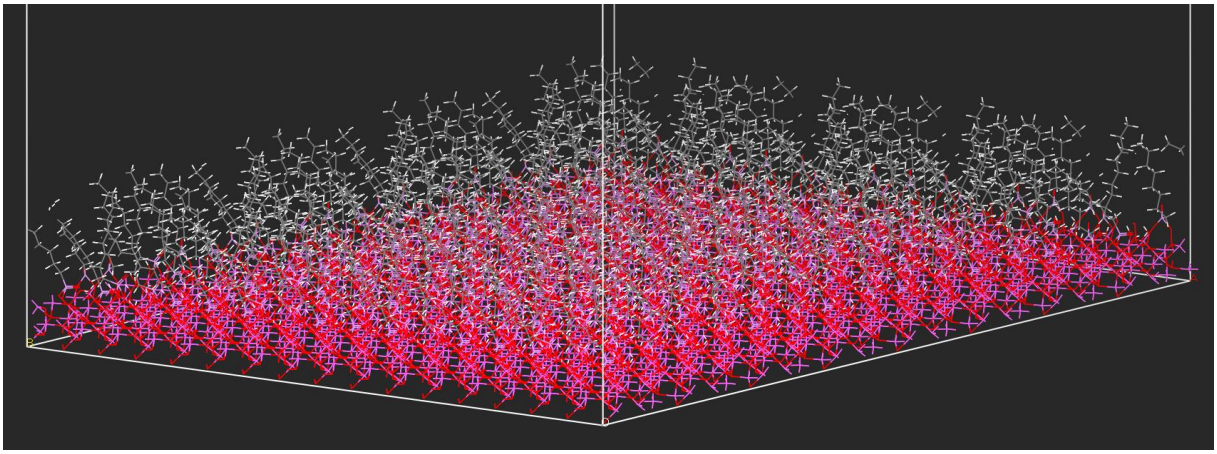

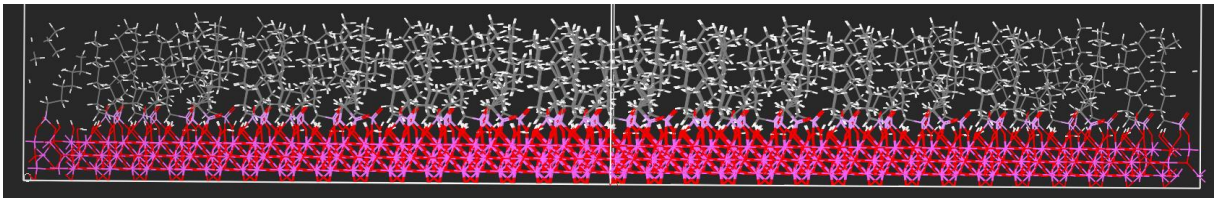

7.13 Scheme for alkyl:amine-terminated (3:1) configuration on the 50% B coverage system (blue balls shows site of *exo*–norbornene or tetrazine attachment). The reactive groups or alkyl chains are placed randomly at different positions to reduce any bias. Same configuration was kept in either case to ensure similar steric environment).

7.14 Molecular model of 50% B (1st = side, 2nd = across, 3rd = tilted view) supercell (8x16) with attached *exo*–norbornene:alkyl (1:3) after energy minimization. The picture depicts the orientation of norbornene groups with respect to the surface before performing molecular dynamics.

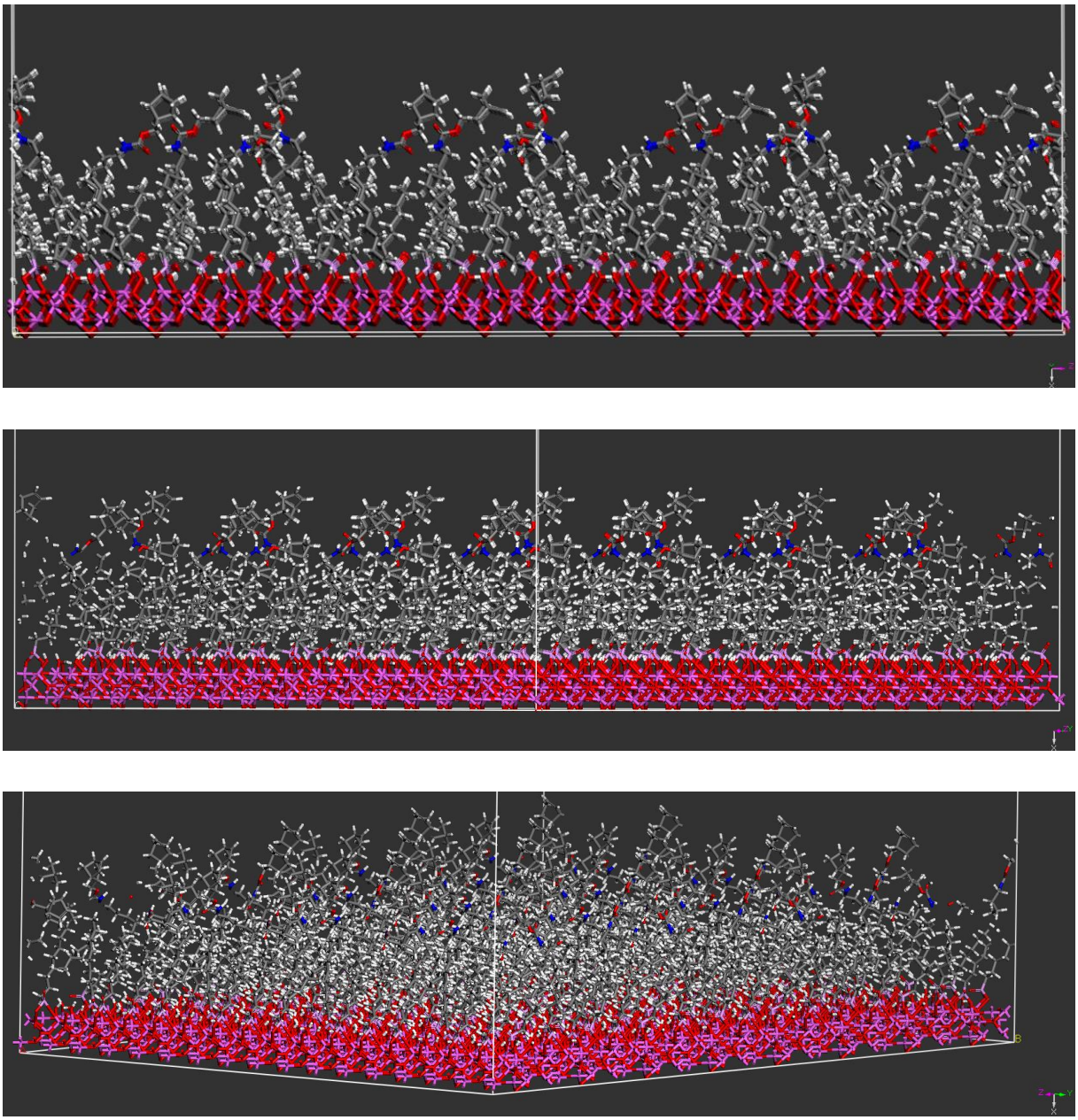

Note: For ease of model preparation, a homochiral model monolayer was used, while the experimentally prepared layers were racemic mixtures. However, given the large number of interfacial reaction sites and packing density of the attached groups, the overall effect of this chirality on the reaction rate and yield is expected to be minimal.

7.15 (a) Protocol for Molecular Dynamics on Al surface. (b) Molecular model of 50% B (1^{st} = side, 2^{nd} = across, 3^{rd} = tilted view) supercell (8x16) with attached *exo*–norbornene: alkyl (1:3) after performing molecular dynamics at 773 K. The picture depicts the orientation of norbornene groups with respect to the surface.

a)

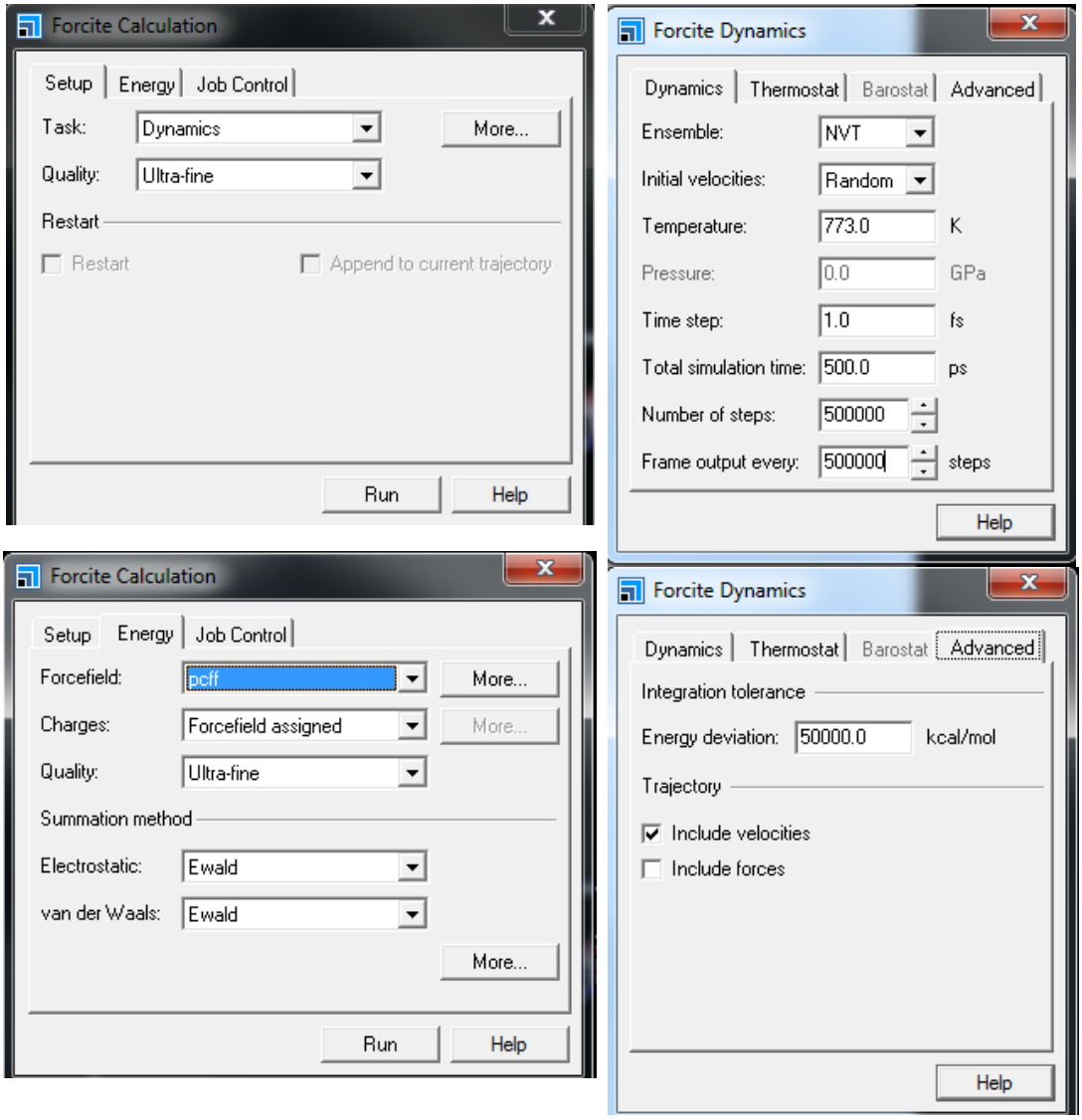

b)

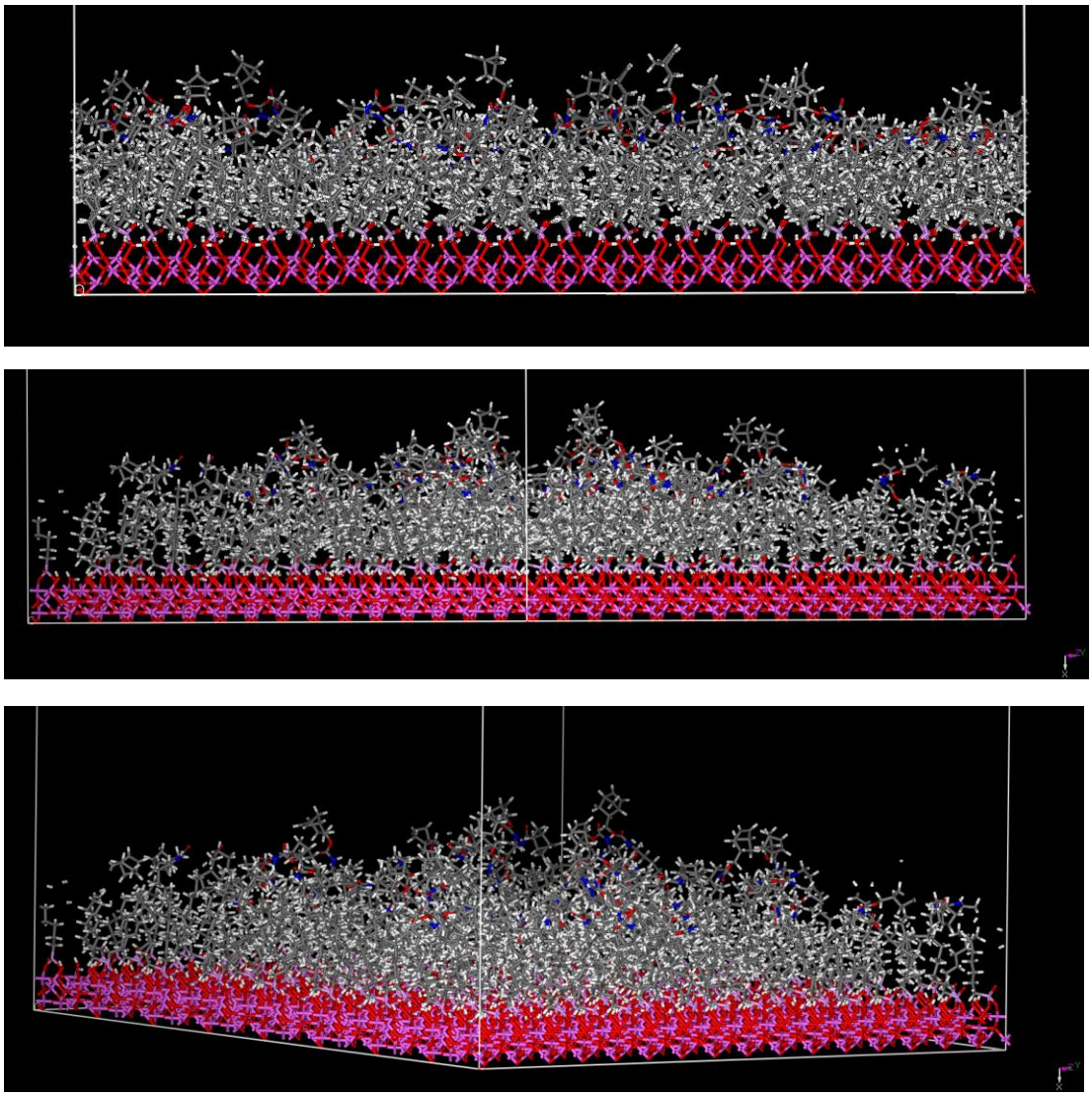

7.16 Molecular model of 50% B (1st = side, 2nd = across, 3rd = tilted view) supercell (8x16) with attached tetrazine:alkyl (1:3) after energy minimization. The picture depicts the orientation of tetrazine groups with respect to the surface before performing molecular dynamics.

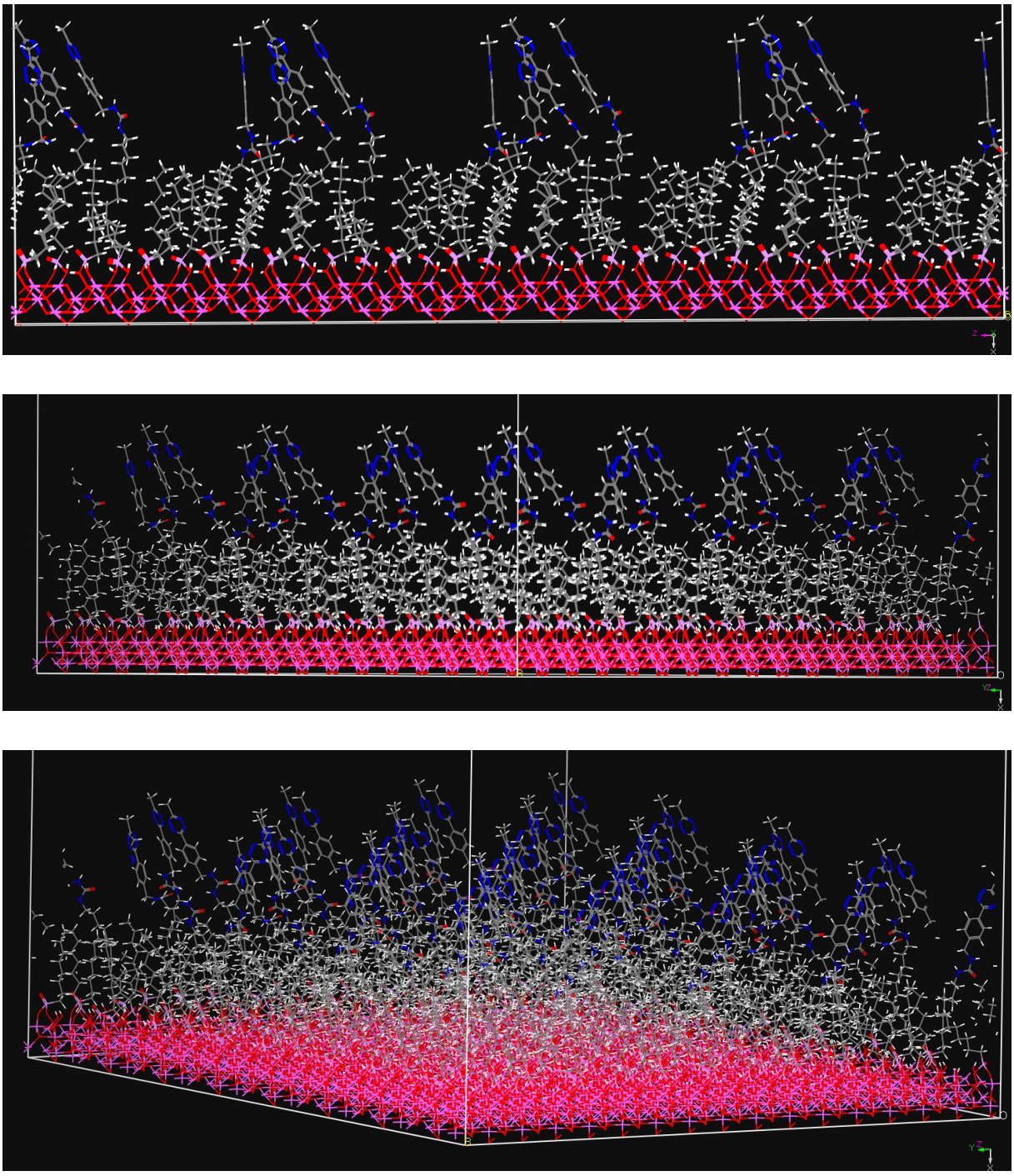

7.17 Molecular model of 50% B (1st = side, 2nd = across, 3rd = tilted view) supercell (8x16) with attached tetrazine:alkyl (1:3) after performing molecular dynamics at 773 K. The picture depicts the orientation of tetrazine groups with respect to the surface.

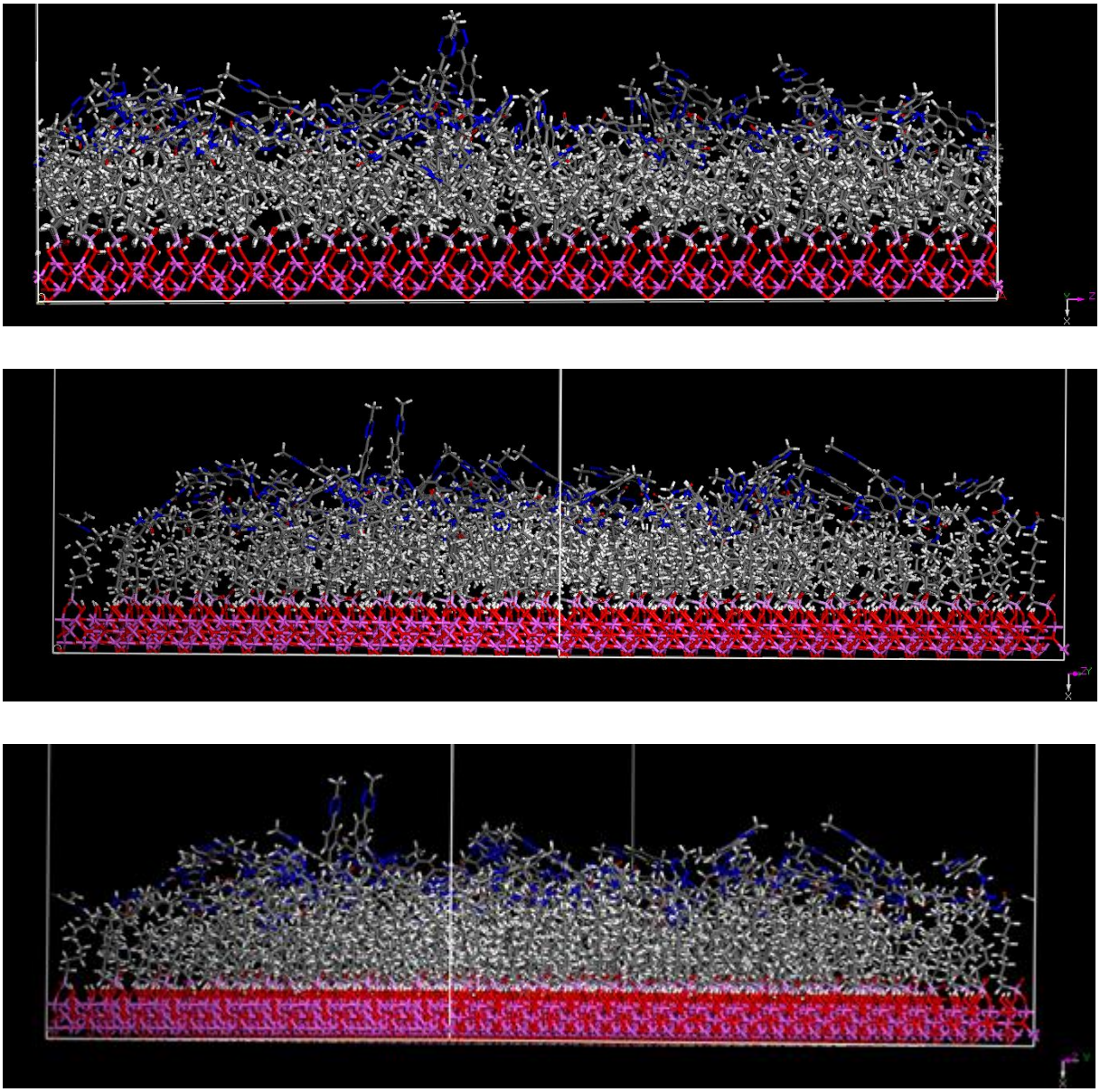

7.18 Top view of a cluster of *exo*–norbornene moieties obtained from a supercell (8x16) for *exo*–norbornene:alkyl (1:3) after performing molecular dynamics at 773 K (Figure 7.15b) displayed for understanding surface approach. [All surface atoms, alkyl linkers and microenvironment ignored for simplicity.]

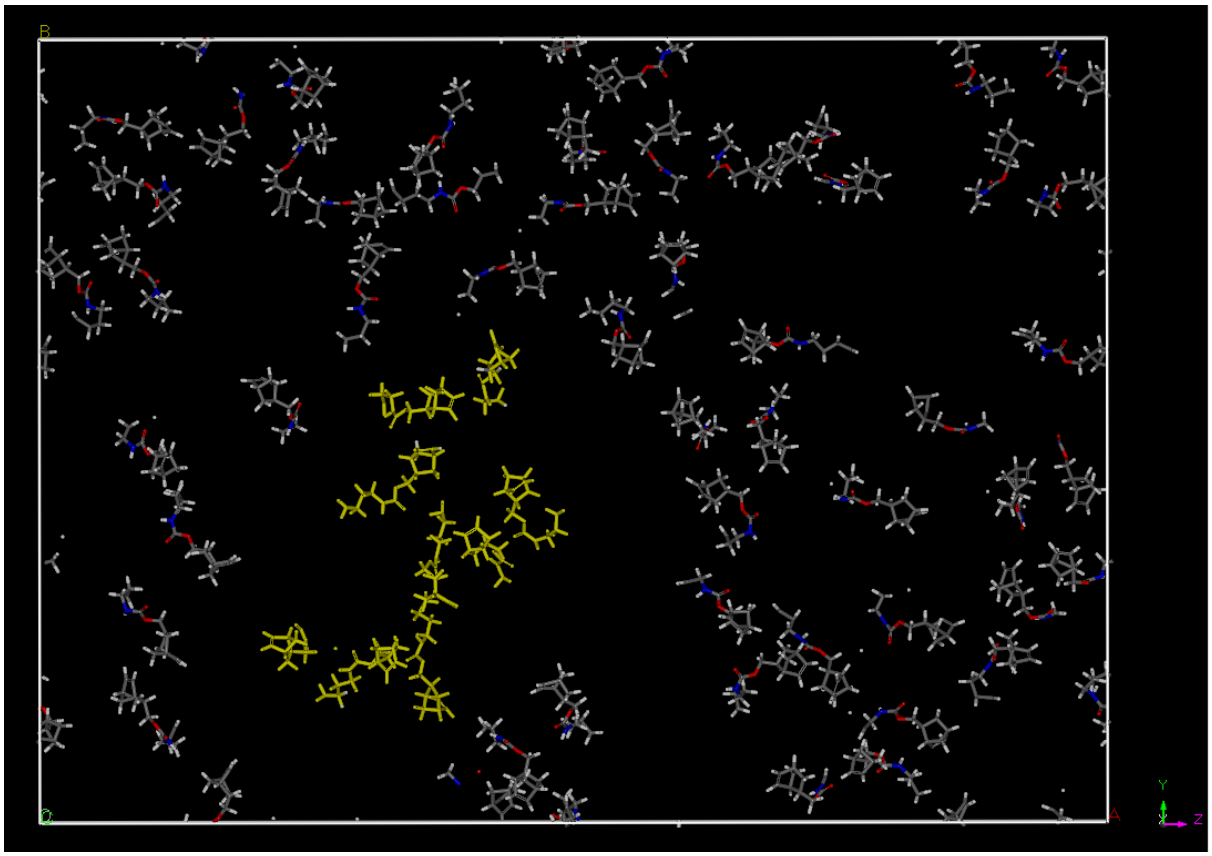

7.19 Top view of a cluster of tetrazine moieties obtained from a supercell (8x16) for tetrazine:alkyl (1:3) after performing molecular dynamics at 773 K (Figure 7.17) displayed for understanding surface approach. [All surface atoms, alkyl linkers and microenvironment ignored for simplicity.]

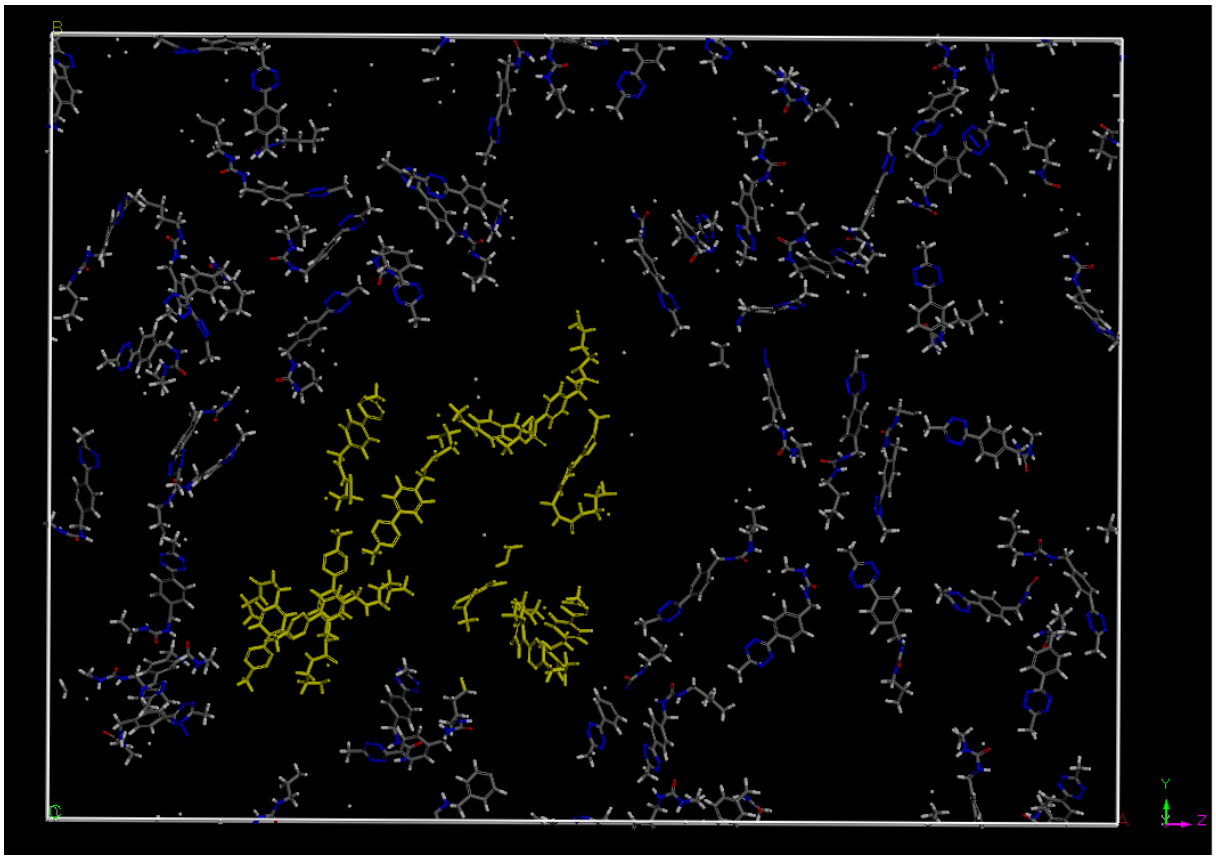

7.20 Molecular model of 50% B (1st = side, 2nd = across, 3rd = tilted view) supercell (8x16) with attached cycloadduct of *exo*–norbornene on surface with tetrazine in solution after energy minimization (1st = side, 2nd = across, 3rd = tilted view). The picture depicts the orientation of cycloadducts with respect to the surface.

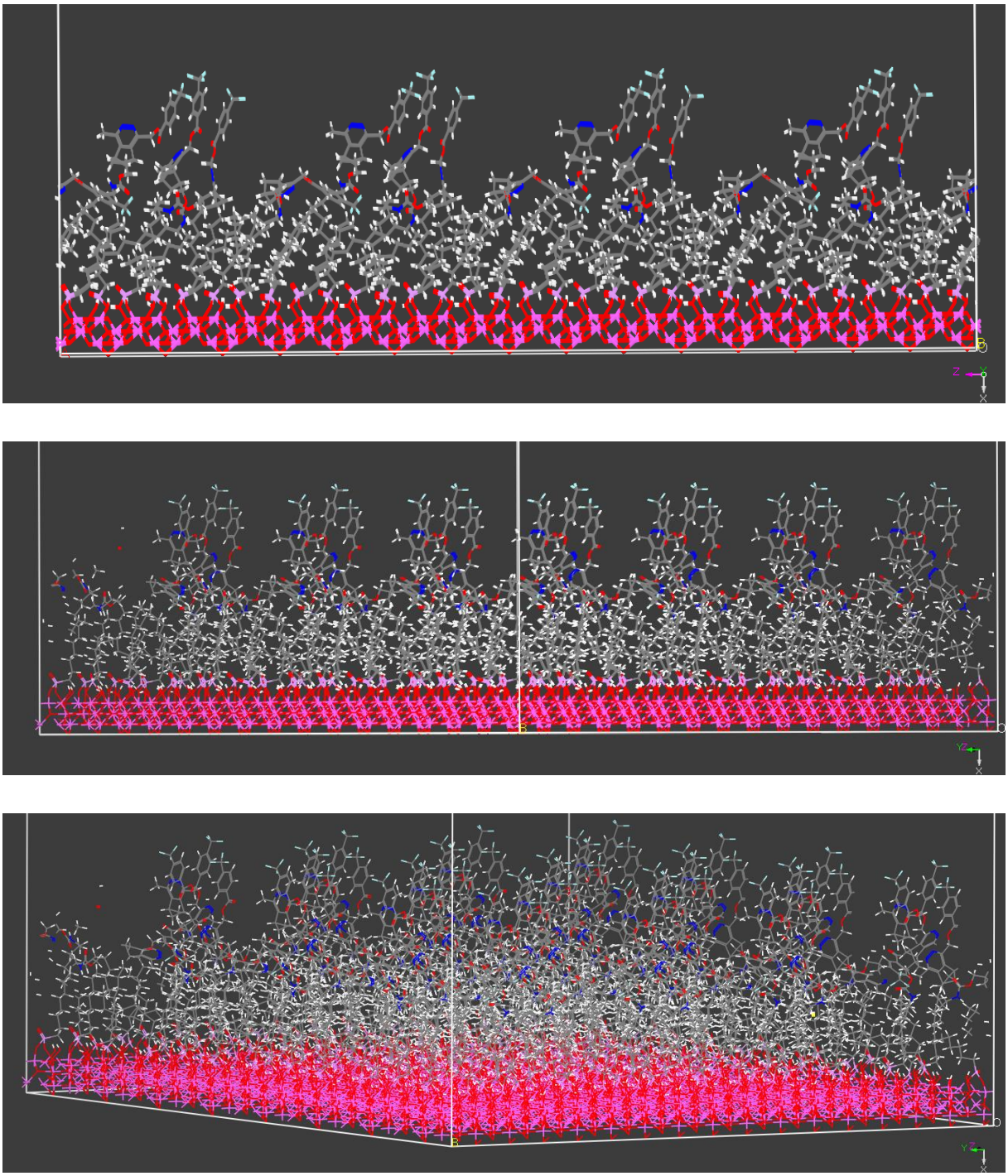

7.21 Molecular model of 50% B (1st = side, 2nd = across, 3rd = tilted view) supercell (8x16) with attached cycloadduct of tetrazine on surface with *exo*–norbornene in solution after energy minimization (1st = side, 2nd = across, 3rd = tilted view). The picture depicts the orientation of cycloadducts with respect to the surface.

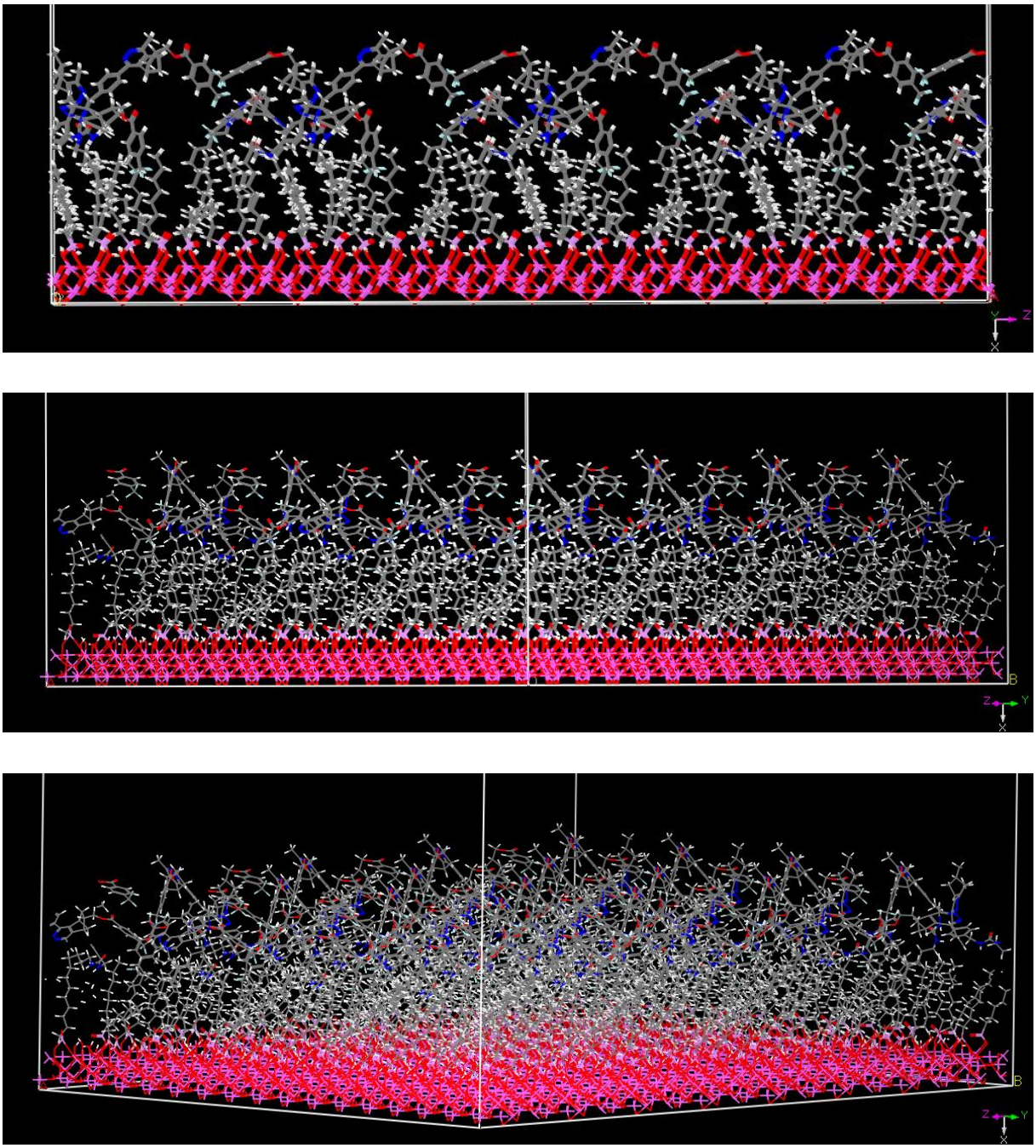

8. CARTESIAN COORDINATES OF OPTIMIZED STRUCTURES.

Reactant complex bearing tetrazine with CF_3–tag (*exo*–norbornene on surface)

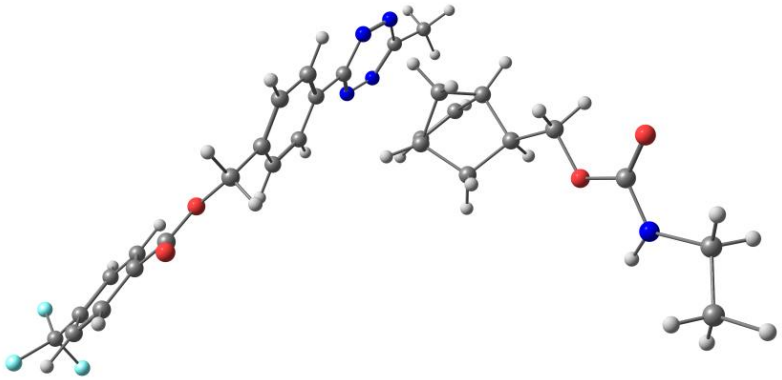

C	–4.255875000	–1.505007000	1.521287000	N	2.361110000	4.027674000	1.171977000
C	–2.141923000	–0.600621000	1.996180000	N	3.290822000	4.820735000	0.718544000
H	–2.298216000	–0.603203000	3.077186000	H	2.091169000	1.744569000	–1.979160000
H	–1.692978000	–1.560131000	1.723130000	H	4.547136000	2.707534000	–1.826684000
C	–1.271186000	0.548452000	1.570640000	C	6.024799000	–1.116590000	–0.031079000
C	–0.324048000	1.059817000	2.456260000	H	7.020232000	–0.667050000	0.017139000
C	–1.361753000	1.084762000	0.286305000	H	5.680019000	–1.285137000	0.992604000
C	0.531111000	2.080930000	2.065909000	O	6.113710000	–2.377934000	–0.705752000
H	–0.253633000	0.657736000	3.461457000	C	6.881111000	–3.307966000	–0.094255000
C	–0.516509000	2.111719000	–0.107024000	O	7.471044000	–3.121197000	0.943402000
H	–2.100006000	0.696067000	–0.404793000	O	–3.998100000	–2.466376000	2.194470000
C	0.440580000	2.612750000	0.778744000	O	–3.407247000	–0.483961000	1.336388000
H	1.269984000	2.472765000	2.753471000	C	–5.545662000	–1.308790000	0.793121000
H	–0.584391000	2.527433000	–1.104541000	C	–5.817437000	–0.145308000	0.074311000
C	1.388647000	3.653780000	0.332761000	C	–6.484513000	–2.335691000	0.857922000
C	3.208321000	5.220101000	–0.555580000	C	–7.031843000	–0.013237000	–0.584470000
C	4.315284000	6.058976000	–1.104282000	H	–5.084150000	0.649973000	0.039200000
H	4.091731000	7.117282000	–0.948636000	C	–7.697687000	–2.207248000	0.196820000
H	5.246111000	5.825999000	–0.589706000	H	–6.248062000	–3.224767000	1.429499000
H	4.416887000	5.886992000	–2.174926000	C	–7.962943000	–1.044814000	–0.519359000
N	1.231212000	4.171241000	–0.893046000	H	–7.261470000	0.887867000	–1.139840000
N	2.157144000	4.966237000	–1.345723000	H	–8.437172000	–2.996852000	0.242766000
C	4.094694000	1.966063000	–1.178535000	N	6.873282000	–4.466139000	–0.800553000
C	2.855979000	1.471266000	–1.261746000	H	6.422196000	–4.451571000	–1.702027000
C	4.843167000	1.142188000	–0.142656000	C	7.712517000	–5.593244000	–0.430222000
C	2.752296000	0.321019000	–0.273682000	H	8.714273000	–5.483285000	–0.860306000
C	3.694677000	0.824306000	0.836051000	C	7.080965000	–6.900650000	–0.883308000
C	5.061844000	–0.252778000	–0.819792000	H	6.954130000	–6.920900000	–1.969088000
H	5.745531000	1.590794000	0.271806000	H	7.715574000	–7.744220000	–0.607868000
C	3.618603000	–0.831174000	–0.866961000	H	6.101781000	–7.035791000	–0.420548000
H	1.743674000	0.031290000	0.020387000	H	7.821692000	–5.565791000	0.654203000
H	3.941800000	0.052519000	1.569050000	C	–9.249397000	–0.915471000	–1.286397000
H	3.324792000	1.713512000	1.347170000	F	–10.224947000	–1.671806000	–0.768065000
H	5.470811000	–0.123965000	–1.824537000	F	–9.096054000	–1.297390000	–2.565358000
H	3.545434000	–1.723355000	–0.238940000	F	–9.690856000	0.349465000	–1.311095000
H	3.308698000	–1.106466000	–1.875044000				

Reactant complex bearing tetrazine with CF_3–tag (*endo*–norbornene on surface)

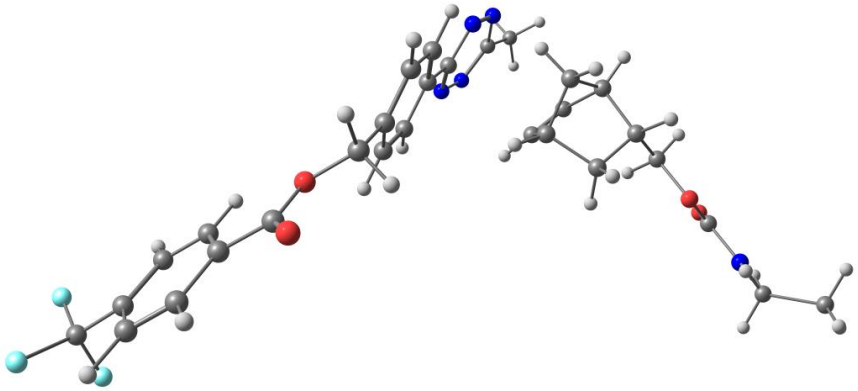

C	–4.680554000	–1.041764000	1.857276000	N	2.127157000	4.087410000	0.587023000
C	–2.596716000	–0.048058000	2.309846000	N	3.147915000	4.682267000	0.039095000
H	–2.874647000	0.307246000	3.304589000	H	2.461040000	0.822570000	–1.460429000
H	–2.177316000	–1.052148000	2.418760000	H	4.863894000	1.879183000	–1.210349000
C	–1.621333000	0.882801000	1.645140000	C	6.080044000	–0.897781000	–0.047162000
C	–0.827443000	1.728678000	2.416734000	H	5.721269000	–0.718154000	–1.063614000
C	–1.468220000	0.883287000	0.258089000	H	7.035053000	–0.379587000	0.078016000
C	0.115991000	2.553774000	1.819256000	O	6.285189000	–2.305925000	0.131684000
H	–0.947941000	1.745287000	3.494709000	C	7.156705000	–2.875122000	–0.730615000
C	–0.534592000	1.711326000	–0.346113000	O	7.743259000	–2.268293000	–1.595640000
H	–2.089005000	0.234269000	–0.348484000	O	–4.553351000	–1.761664000	2.810602000
C	0.268623000	2.549476000	0.432286000	O	–3.769587000	–0.128868000	1.491512000
H	0.735666000	3.206221000	2.421392000	C	–5.858894000	–1.057585000	0.938936000
H	–0.413205000	1.710759000	–1.422028000	C	–5.982493000	–0.148039000	–0.110038000
C	1.311855000	3.379497000	–0.204502000	C	–6.845703000	–2.015197000	1.164819000
C	3.310836000	4.558567000	–1.284008000	C	–7.096365000	–0.198484000	–0.937168000
C	4.528326000	5.162732000	–1.902563000	H	–5.213210000	0.596568000	–0.268974000
H	4.346539000	6.216625000	–2.127340000	C	–7.957317000	–2.069812000	0.337040000
H	5.365670000	5.102585000	–1.208730000	H	–6.727075000	–2.705887000	1.990564000
H	4.765342000	4.648996000	–2.832826000	C	–8.075894000	–1.158563000	–0.707873000
N	1.391636000	3.386533000	–1.540723000	H	–7.210599000	0.508534000	–1.749366000
N	2.409470000	3.985698000	–2.090666000	H	–8.733296000	–2.806699000	0.503629000
C	4.273321000	1.415870000	–0.428462000	N	7.272594000	–4.201773000	–0.472622000
C	3.057208000	0.875973000	–0.556869000	H	6.692314000	–4.578928000	0.260073000
C	4.774475000	1.077204000	0.967091000	C	8.112652000	–5.082769000	–1.263720000
C	2.722852000	0.175391000	0.748017000	H	7.491284000	–5.717692000	–1.903761000
C	3.447769000	1.095435000	1.749944000	C	9.012190000	–5.938927000	–0.381638000
C	5.066023000	–0.460855000	0.985509000	H	8.421367000	–6.571103000	0.286498000
H	5.589569000	1.689749000	1.349865000	H	9.635002000	–6.592627000	–0.995203000
C	3.651780000	–1.079225000	0.796674000	H	9.661803000	–5.308676000	0.227998000
H	1.667107000	–0.026515000	0.926727000	H	8.704064000	–4.439927000	–1.915564000
H	3.536276000	0.655344000	2.747101000	C	–9.256270000	–1.248041000	–1.634446000
H	3.011743000	2.092233000	1.818237000	F	–10.346128000	–1.716387000	–1.012310000
H	5.457607000	–0.719518000	1.973660000	F	–9.010613000	–2.075289000	–2.664129000
H	3.387035000	–1.723250000	1.637212000	F	–9.572920000	–0.057443000	–2.159702000
H	3.584982000	–1.675063000	–0.115979000				

TS with tetrazine bearing CF_3–tag (*exo*–norbornene on surface)

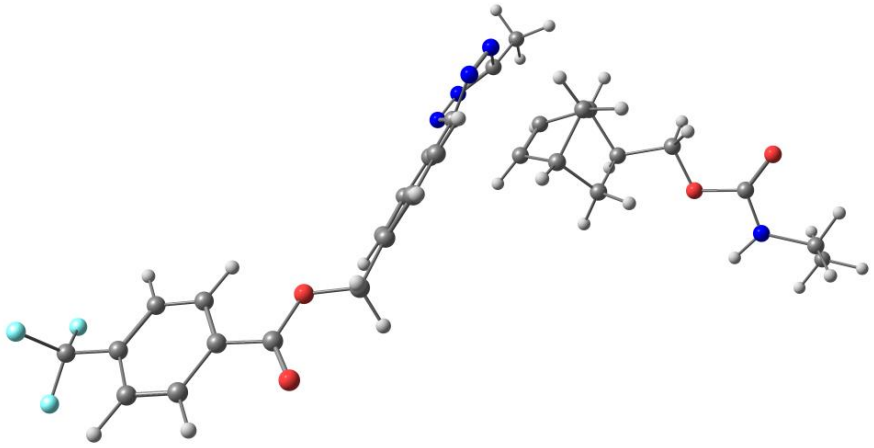

Frequency –366.6180

C	–5.090860000	–2.099630000	0.841323000	N	1.790189000	2.936210000	1.377291000
C	–2.800992000	–1.710581000	1.189831000	N	2.764449000	3.731011000	1.145660000
H	–2.864781000	–1.990657000	2.243059000	H	2.115987000	0.803547000	–1.264692000
H	–2.561417000	–2.610074000	0.616369000	H	4.067003000	2.400031000	–1.694459000
C	–1.788309000	–0.624503000	0.966759000	C	6.821994000	–0.259288000	0.058564000
C	–0.948625000	–0.217244000	1.998892000	H	7.612436000	0.465678000	–0.151573000
C	–1.659891000	–0.028026000	–0.288770000	H	6.785950000	–0.415429000	1.140108000
C	0.013757000	0.763486000	1.785307000	O	7.139102000	–1.500232000	–0.580700000
H	–1.049126000	–0.665570000	2.981682000	C	8.307703000	–2.062207000	–0.191771000
C	–0.707875000	0.955953000	–0.507761000	O	9.055916000	–1.567637000	0.618026000
H	–2.318040000	–0.334251000	–1.094660000	O	–4.964227000	–3.219322000	1.260381000
C	0.137168000	1.357295000	0.530342000	O	–4.080635000	–1.224894000	0.752465000
H	0.663524000	1.084856000	2.590329000	C	–6.384037000	–1.524596000	0.361176000
H	–0.615271000	1.426989000	–1.479021000	C	–6.476846000	–0.217153000	–0.111321000
C	1.186455000	2.374587000	0.289162000	C	–7.509409000	–2.346535000	0.396209000
C	3.099555000	3.918930000	–0.166907000	C	–7.701138000	0.270364000	–0.550542000
C	4.262373000	4.820251000	–0.446945000	H	–5.595137000	0.410182000	–0.131288000
H	3.974579000	5.854593000	–0.247266000	C	–8.732192000	–1.861953000	–0.042060000
H	5.099861000	4.566558000	0.201922000	H	–7.406705000	–3.358820000	0.767134000
H	4.560939000	4.741983000	–1.491922000	C	–8.818728000	–0.555716000	–0.515229000
N	1.103704000	3.130171000	–0.860125000	H	–7.787678000	1.282436000	–0.925442000
N	2.072601000	3.920715000	–1.090098000	H	–9.613495000	–2.491577000	–0.027253000
C	3.865200000	1.978862000	–0.716020000	N	8.503169000	–3.247233000	–0.819373000
C	2.819190000	1.095574000	–0.493708000	H	7.860059000	–3.491672000	–1.555105000
C	5.004232000	1.521719000	0.187455000	C	9.761428000	–3.962956000	–0.671607000
C	3.286672000	0.109143000	0.559572000	H	10.036578000	–3.920186000	0.383178000
C	4.244610000	0.965672000	1.404281000	C	10.879726000	–3.382488000	–1.530368000
C	5.488560000	0.200481000	–0.496092000	H	11.056480000	–2.341212000	–1.255765000
H	5.794268000	2.249084000	0.373303000	H	11.806524000	–3.939920000	–1.379722000
C	4.319144000	–0.782306000	–0.196038000	H	10.620017000	–3.426558000	–2.590406000
H	2.501663000	–0.439760000	1.077106000	H	9.575091000	–5.008412000	–0.923257000
H	4.877154000	0.350356000	2.046078000	C	–10.157540000	–0.019102000	–0.938310000
H	3.762140000	1.725031000	2.011007000	F	–10.853636000	0.446126000	0.112002000
H	5.611220000	0.352065000	–1.571883000	F	–10.913680000	–0.963172000	–1.515479000
H	4.657029000	–1.592996000	0.454371000	F	–10.043750000	0.992323000	–1.808751000
H	3.904756000	–1.231420000	–1.099306000				

TS with tetrazine bearing CF_3–tag (*endo*–norbornene on surface)

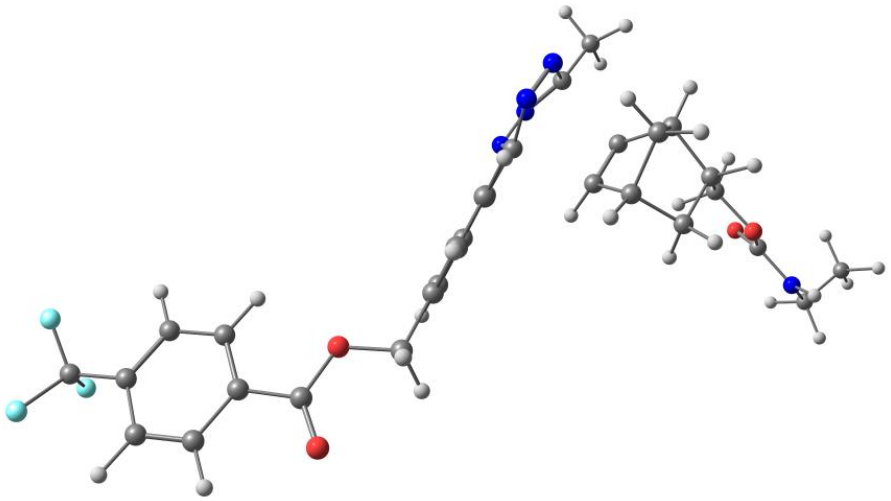

Frequency –372.4077

C	–5.114695000	–1.774703000	1.337674000
C	–2.826347000	–1.401513000	1.734440000
H	–2.966916000	–1.369211000	2.816487000
H	–2.610305000	–2.434252000	1.450174000
C	–1.747380000	–0.460554000	1.283912000
C	–1.143364000	0.416467000	2.179461000
C	–1.340567000	–0.453841000	–0.051432000
C	–0.144374000	1.286284000	1.756132000
H	–1.458021000	0.424291000	3.217684000
C	–0.351039000	0.415232000	–0.483927000
H	–1.810489000	–1.132208000	–0.755932000
C	0.253676000	1.292648000	0.420325000
H	0.321244000	1.973382000	2.452159000
H	–0.044227000	0.429380000	–1.523039000
C	1.341254000	2.192536000	–0.030175000
C	3.315256000	3.551993000	–0.740688000
C	4.517594000	4.339986000	–1.160636000
H	4.202909000	5.333748000	–1.485836000
H	5.204243000	4.454270000	–0.322799000
H	5.021321000	3.849490000	–1.993261000
N	1.488430000	2.396623000	–1.386034000
N	2.488157000	3.093195000	–1.747641000
C	4.153709000	1.622088000	–0.279270000
C	3.077369000	0.836884000	0.110851000
C	5.094385000	1.674036000	0.918657000
C	3.327585000	0.418658000	1.547290000
C	4.113092000	1.620313000	2.101975000
C	5.706075000	0.238480000	1.031955000
H	5.836027000	2.471779000	0.915592000
C	4.476397000	–0.629697000	1.428608000
H	2.452159000	0.082110000	2.100443000
H	4.622508000	1.374984000	3.036258000
H	3.527091000	2.522515000	2.241137000
H	6.430335000	0.254407000	1.851275000
H	4.634104000	–1.127917000	2.386545000
H	4.264074000	–1.400364000	0.683635000
N	1.720589000	3.200766000	0.807996000
N	2.726609000	3.901122000	0.443788000
H	2.536463000	0.192835000	–0.572838000
H	4.528323000	1.619506000	–1.295802000
C	6.425047000	–0.240351000	–0.210425000
H	5.741406000	–0.374955000	–1.052479000
H	7.213052000	0.453788000	–0.517680000
O	7.010203000	–1.506524000	0.112266000
C	7.646808000	–2.120335000	–0.912646000
O	7.749431000	–1.648905000	–2.020682000
O	–5.082291000	–2.743984000	2.048572000
O	–4.049887000	–1.001454000	1.091219000
C	–6.338761000	–1.295071000	0.626325000
C	–6.326103000	–0.144704000	–0.161215000
C	–7.508409000	–2.036627000	0.776592000
C	–7.487843000	0.261487000	–0.803325000
H	–5.411509000	0.424544000	–0.264217000
C	–8.669716000	–1.633726000	0.133811000
H	–7.490695000	–2.923017000	1.398802000
C	–8.651196000	–0.485233000	–0.651522000
H	–7.494211000	1.156382000	–1.413438000
H	–9.586603000	–2.199034000	0.244452000
N	8.128109000	–3.326308000	–0.525822000
H	8.073426000	–3.553635000	0.453902000
C	8.966099000	–4.109628000	–1.421206000
H	8.923386000	–5.147161000	–1.085667000
C	10.405726000	–3.609920000	–1.477301000
H	10.872666000	–3.656366000	–0.490975000
H	10.995425000	–4.219441000	–2.165230000
H	10.426847000	–2.576747000	–1.827798000
H	8.513275000	–4.062172000	–2.412649000
C	–9.889953000	–0.079523000	–1.400029000
F	–11.007390000	–0.479892000	–0.779116000
F	–9.914342000	–0.617589000	–2.631025000
F	–9.970731000	1.248395000	–1.555545000

Product with tetrazine bearing CF_3–tag (*exo*–norbornene on surface)

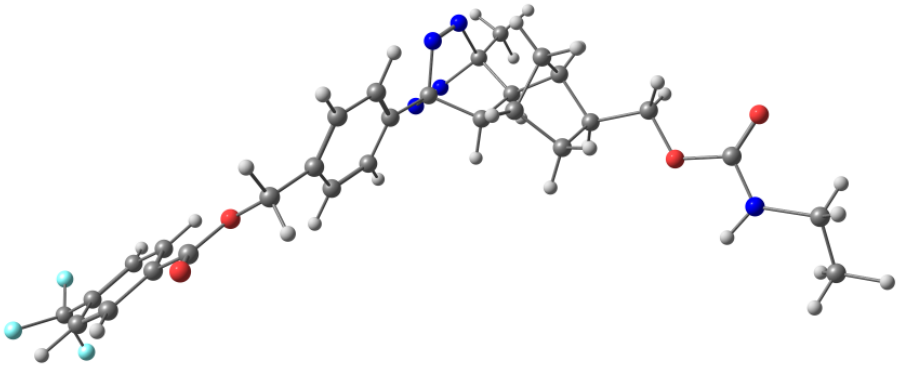

C	–5.176847000	–2.023307000	1.140721000
C	–2.882419000	–1.727946000	1.547889000
H	–3.014079000	–1.843213000	2.625448000
H	–2.679279000	–2.715636000	1.125505000
C	–1.790393000	–0.749966000	1.223783000
C	–1.000164000	–0.208486000	2.231213000
C	–1.541518000	–0.388791000	–0.101039000
C	0.031620000	0.675439000	1.927442000
H	–1.192821000	–0.471722000	3.265891000
C	–0.520078000	0.497158000	–0.408835000
H	–2.161053000	–0.798602000	–0.891447000
C	0.275691000	1.033645000	0.605332000
H	0.635293000	1.104561000	2.717345000
H	–0.343520000	0.788503000	–1.437703000
C	1.424077000	1.936925000	0.251335000
C	3.144548000	3.613898000	–0.285420000
C	4.043941000	4.790724000	–0.564764000
H	3.496695000	5.720038000	–0.402831000
H	4.904261000	4.773746000	0.105271000
H	4.388477000	4.761577000	–1.599563000
N	1.081813000	2.824510000	–0.902391000
N	1.939255000	3.661072000	–1.165083000
C	3.755917000	2.216238000	–0.600166000
C	2.687432000	1.161706000	–0.251414000
C	4.987166000	1.754038000	0.210210000
C	3.403124000	0.233562000	0.752835000
C	4.377057000	1.165583000	1.498619000
C	5.475793000	0.467505000	–0.505470000
H	5.759487000	2.514694000	0.332588000
C	4.407865000	–0.588344000	–0.081109000
H	2.727400000	–0.367317000	1.360960000
H	5.108276000	0.594421000	2.073837000
H	3.920936000	1.892848000	2.161944000
H	5.479747000	0.607546000	–1.590073000
H	4.868641000	–1.363080000	0.536972000
H	3.944248000	–1.083420000	–0.935884000
N	1.811960000	2.795131000	1.372708000
N	2.673825000	3.636655000	1.103049000
H	2.351637000	0.596164000	–1.123515000
H	3.986194000	2.237970000	–1.667807000
C	6.882634000	0.089691000	–0.086572000
H	7.610520000	0.837482000	–0.412573000
H	6.972397000	–0.018528000	0.997559000
O	7.185448000	–1.163201000	–0.707799000
C	8.378180000	–1.702601000	–0.359761000
O	9.149026000	–1.189977000	0.416160000
O	–5.146064000	–3.071536000	1.728805000
O	–4.105993000	–1.237345000	0.973786000
C	–6.407238000	–1.448468000	0.516168000
C	–6.393312000	–0.221598000	–0.145232000
C	–7.587637000	–2.180722000	0.623805000
C	–7.565377000	0.272340000	–0.701746000
H	–5.470858000	0.340235000	–0.214538000
C	–8.759628000	–1.689244000	0.067989000
H	–7.569752000	–3.128044000	1.148397000
C	–8.740601000	–0.463262000	–0.589269000
H	–7.571448000	1.227881000	–1.211466000
H	–9.685121000	–2.245241000	0.150815000
N	8.580942000	–2.874811000	–1.006556000
H	7.815861000	–3.250974000	–1.544206000
C	9.738369000	–3.704164000	–0.708328000
H	10.609984000	–3.050010000	–0.657206000
C	9.915236000	–4.762726000	–1.784884000
H	10.061467000	–4.300193000	–2.762845000
H	10.783875000	–5.383651000	–1.563002000
H	9.042234000	–5.418706000	–1.837957000
H	9.627029000	–4.171098000	0.275998000
C	–9.996386000	0.053488000	–1.233806000
F	–11.098042000	–0.391236000	–0.615152000
F	–10.087213000	–0.334950000	–2.516789000
F	–10.046183000	1.392459000	–1.230589000

Product with tetrazine bearing CF_3–tag (*endo*–norbornene on surface)

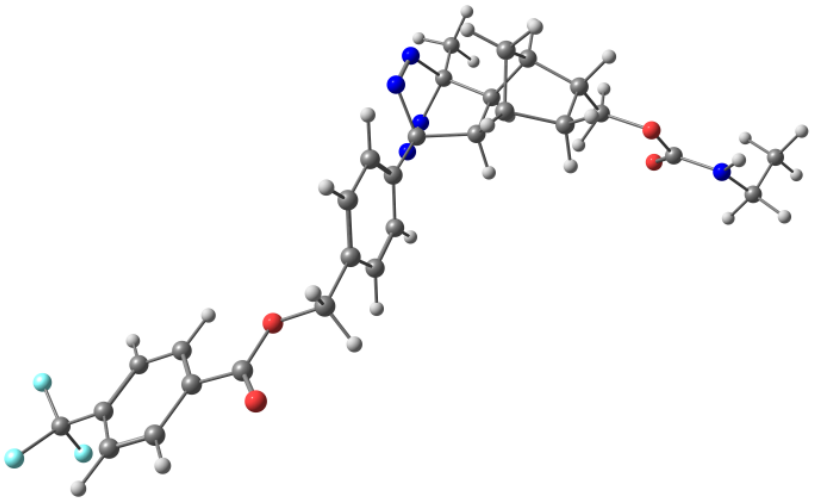

C	5.205883000	1.765797000	1.401468000
C	2.909460000	1.534816000	1.844247000
H	3.083000000	1.456609000	2.919155000
H	2.754048000	2.588032000	1.599739000
C	1.757027000	0.681835000	1.402084000
C	1.233037000	–0.297456000	2.239206000
C	1.204935000	0.854141000	0.132319000
C	0.167988000	–1.091922000	1.824611000
H	1.660629000	–0.443639000	3.225581000
C	0.147051000	0.062536000	–0.289271000
H	1.611959000	1.611011000	–0.530126000
C	–0.379846000	–0.914460000	0.557262000
H	–0.232365000	–1.857547000	2.477501000
H	–0.269080000	0.190933000	–1.281786000
C	–1.580594000	–1.703646000	0.115696000
C	–3.388678000	–3.166851000	–0.688428000
C	–4.336197000	–4.205538000	–1.232169000
H	–3.771622000	–5.067069000	–1.590557000
H	–5.017845000	–4.538990000	–0.449019000
H	–4.909863000	–3.790927000	–2.062466000
N	–1.516306000	–2.016740000	–1.344880000
N	–2.414665000	–2.750668000	–1.741674000
C	–4.046717000	–1.814428000	–0.274919000
C	–2.922093000	–0.908364000	0.259193000
C	–5.067370000	–1.831223000	0.883310000
C	–3.385064000	–0.549870000	1.688728000
C	–4.185417000	–1.787864000	2.145914000
C	–5.705312000	–0.419255000	0.970500000
H	–5.802432000	–2.634304000	0.823440000
C	–4.535695000	0.463096000	1.509318000
H	–2.581425000	–0.209829000	2.341312000
H	–4.779414000	–1.565983000	3.035874000
H	–3.603720000	–2.683479000	2.336902000
H	–6.502322000	–0.468187000	1.717791000
H	–4.798074000	0.921710000	2.463697000
H	–4.282571000	1.269948000	0.816568000
N	–1.705758000	–2.969797000	0.836868000
N	–2.614068000	–3.703598000	0.434006000
H	–2.787018000	–0.003571000	–0.338023000
H	–4.488918000	–1.435275000	–1.197240000
C	–6.331222000	0.106274000	–0.304472000
H	–5.588235000	0.347374000	–1.069292000
H	–7.043465000	–0.604788000	–0.734061000
O	–7.019078000	1.310361000	0.051029000
C	–7.598506000	1.967133000	–0.981601000
O	–7.568578000	1.581388000	–2.126407000
O	5.256200000	2.701162000	2.155689000
O	4.085794000	1.077959000	1.149677000
C	6.379121000	1.241112000	0.638060000
C	6.271110000	0.142959000	–0.213800000
C	7.600764000	1.889516000	0.805528000
C	7.390238000	–0.304400000	–0.902330000
H	5.316582000	–0.353479000	–0.330932000
C	8.720022000	1.445089000	0.116929000
H	7.655010000	2.737093000	1.477558000
C	8.606384000	0.349503000	–0.732640000
H	7.323921000	–1.159899000	–1.563241000
H	9.676285000	1.937551000	0.241595000
N	–8.190520000	3.107428000	–0.552429000
H	–8.240591000	3.255553000	0.442610000
C	–8.999750000	3.907376000	–1.459801000
H	–9.071390000	4.910248000	–1.035513000
C	–10.383671000	3.314087000	–1.701251000
H	–10.940694000	3.233219000	–0.765232000
H	–10.954810000	3.942406000	–2.387855000
H	–10.289607000	2.319901000	–2.141245000
H	–8.454023000	3.983403000	–2.401382000
C	9.797878000	–0.101797000	–1.530126000
F	10.954554000	0.209151000	–0.930449000
F	9.820383000	0.474237000	–2.743698000
F	9.793283000	–1.426781000	–1.730953000

Reactant complex with *exo*–NBN with CF_3–tag (tetrazine on surface)

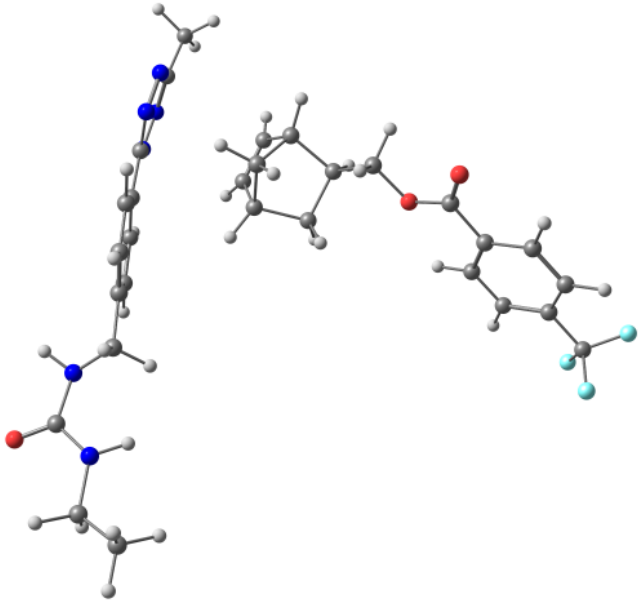

C	–3.563338000	7.893078000	–0.749028000	C	1.217437000	–2.460714000	–0.013926000
H	–2.612006000	7.618511000	–0.284384000	H	0.198262000	–4.112726000	–1.149188000
H	–3.665506000	8.976587000	–0.676215000	C	0.598449000	–1.100750000	0.418791000
H	–3.522813000	7.620754000	–1.805559000	H	–1.519794000	–0.393997000	0.167396000
C	–4.730683000	7.205522000	–0.059798000	H	–0.380011000	–1.596341000	–1.951055000
H	–5.677272000	7.481577000	–0.524898000	H	–1.858918000	–2.469030000	–1.466930000
H	–4.792535000	7.504919000	0.992078000	H	1.676451000	–2.975541000	0.833132000
C	–5.636359000	4.957747000	0.224660000	H	0.977625000	–0.289631000	–0.209166000
N	–5.365406000	3.599653000	0.264260000	H	0.818857000	–0.851126000	1.456922000
H	–6.215826000	3.057854000	0.339022000	N	–4.038580000	–3.526196000	–0.888009000
C	–4.271208000	2.975706000	–0.464146000	N	–3.799386000	–4.793291000	–0.711979000
H	–4.290833000	3.232680000	–1.530019000	H	–1.898188000	–2.201339000	2.074936000
H	–3.317662000	3.335413000	–0.058102000	H	–0.848980000	–4.489186000	1.268523000
C	–4.312356000	1.475749000	–0.299237000	C	2.265511000	–2.325498000	–1.098442000
C	–4.226838000	0.636702000	–1.407831000	H	2.666670000	–3.296825000	–1.398577000
C	–4.422341000	0.908636000	0.973236000	H	1.878223000	–1.827580000	–1.991615000
C	–4.233201000	–0.744208000	–1.255497000	O	3.337345000	–1.530879000	–0.561234000
H	–4.154206000	1.065359000	–2.401482000	C	4.364984000	–1.297282000	–1.383660000
C	–4.435601000	–0.468344000	1.133175000	O	4.429937000	–1.719226000	–2.507778000
H	–4.496624000	1.557230000	1.839431000	C	5.420430000	–0.449183000	–0.747848000
C	–4.333500000	–1.305019000	0.017786000	C	5.283623000	0.043718000	0.547382000
H	–4.160226000	–1.393423000	–2.118914000	C	6.559719000	–0.158818000	–1.497685000
H	–4.514865000	–0.907057000	2.120010000	C	6.287538000	0.832876000	1.095957000
C	–4.258935000	–2.769718000	0.195292000	H	4.395701000	–0.193327000	1.118862000
C	–3.797872000	–5.264048000	0.542026000	C	7.563700000	0.624856000	–0.951855000
C	–3.430921000	–6.696416000	0.749940000	H	6.640913000	–0.556792000	–2.501706000
H	–4.248682000	–7.341807000	0.421223000	C	7.420655000	1.115993000	0.343852000
H	–2.550969000	–6.944743000	0.156167000	H	6.194051000	1.219411000	2.102781000
H	–3.239461000	–6.879583000	1.805500000	H	8.456721000	0.853142000	–1.521500000
N	–4.404595000	–3.270984000	1.427420000	C	8.502826000	1.998295000	0.900265000
N	–4.167463000	–4.540622000	1.604940000	F	9.723526000	1.513211000	0.630659000
C	–0.842416000	–3.544218000	0.738322000	F	8.453565000	3.231219000	0.368537000
C	–1.364303000	–2.384899000	1.150110000	F	8.412062000	2.139901000	2.227910000
C	–0.033943000	–3.256037000	–0.517034000	N	–4.594470000	5.758460000	–0.171972000
C	–0.927476000	–1.308552000	0.170361000	H	–3.658353000	5.385760000	–0.137811000
C	–0.879382000	–2.124888000	–1.135136000	O	–6.729534000	5.400235000	0.518307000

Reactant complex with *endo*–NBN with CF_3–tag (tetrazine on surface)

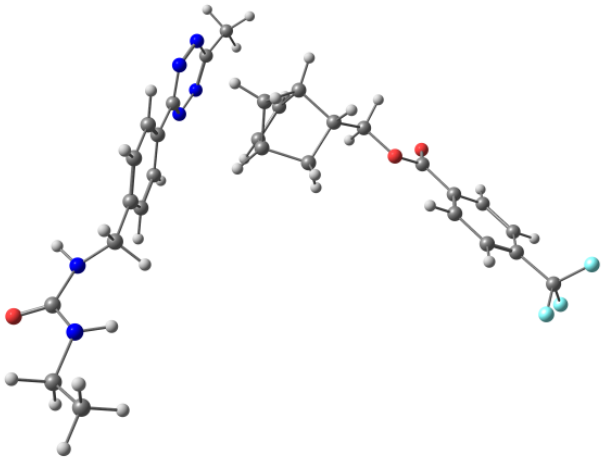

C	5.379633000	7.489755000	0.549355000	C	–1.402995000	–1.787741000	1.210413000
H	4.343666000	7.415303000	0.206483000	H	–0.513952000	–3.692356000	1.992937000
H	5.695216000	8.526050000	0.423087000	C	–0.656332000	–0.555071000	0.625701000
H	5.409506000	7.247607000	1.613562000	H	1.567132000	–0.252671000	0.458607000
C	6.287909000	6.562107000	–0.240703000	H	0.646970000	–1.380287000	2.731637000
H	7.320965000	6.643860000	0.098166000	H	1.832792000	–2.453998000	1.929514000
H	6.280228000	6.822760000	–1.304494000	H	–1.778248000	–1.558340000	2.212042000
C	6.657585000	4.174746000	–0.566654000	H	–0.744752000	0.309163000	1.286814000
N	6.110996000	2.902871000	–0.520425000	H	–1.041924000	–0.267197000	–0.354609000
H	6.808775000	2.196243000	–0.710685000	N	3.607337000	–3.827825000	0.905785000
C	5.039082000	2.514764000	0.383908000	N	3.099405000	–5.020826000	0.791397000
H	5.282450000	2.741019000	1.428824000	H	1.219750000	–1.964253000	–1.534917000
H	4.132031000	3.076153000	0.129141000	H	–0.052265000	–4.080397000	–0.606444000
C	4.735001000	1.043619000	0.234261000	C	–2.569425000	–2.261363000	0.374423000
C	4.695985000	0.205325000	1.345926000	H	–2.277744000	–2.451765000	–0.661391000
C	4.480396000	0.505929000	–1.029960000	H	–3.022560000	–3.170863000	0.778790000
C	4.394618000	–1.144250000	1.207056000	O	–3.553344000	–1.211285000	0.388293000
H	4.904068000	0.609646000	2.330661000	C	–4.671616000	–1.444398000	–0.305165000
C	4.183534000	–0.839895000	–1.177640000	O	–4.882668000	–2.461188000	–0.911296000
H	4.518527000	1.152611000	–1.899954000	C	–5.630373000	–0.297715000	–0.238329000
C	4.133509000	–1.673996000	–0.056351000	C	–5.333338000	0.866066000	0.467357000
H	4.360735000	–1.792160000	2.073893000	C	–6.844353000	–0.424532000	–0.911815000
H	3.980955000	–1.255272000	–2.156979000	C	–6.254012000	1.905405000	0.504099000
C	3.740169000	–3.090495000	–0.204284000	H	–4.385284000	0.952547000	0.981720000
C	2.750632000	–5.440695000	–0.431741000	C	–7.764700000	0.611690000	–0.877782000
C	2.084681000	–6.771943000	–0.549239000	H	–7.047912000	–1.338762000	–1.455720000
H	2.816572000	–7.568349000	–0.396161000	C	–7.462442000	1.771614000	–0.169369000
H	1.316976000	–6.872805000	0.218182000	H	–6.033399000	2.816496000	1.045749000
H	1.646742000	–6.880787000	–1.539603000	H	–8.709718000	0.528364000	–1.400837000
N	3.528794000	–3.567327000	–1.436336000	C	–8.490863000	2.864574000	–0.090863000
N	3.023243000	–4.763473000	–1.552820000	F	–9.157364000	3.006249000	–1.245151000
C	0.210225000	–3.185607000	–0.053946000	F	–9.408426000	2.606800000	0.856010000
C	0.848967000	–2.111011000	–0.527132000	F	–7.946768000	4.051530000	0.206591000
C	–0.260391000	–2.848907000	1.352281000	N	5.873425000	5.177091000	–0.051653000
C	0.824353000	–1.044292000	0.553197000	H	4.884657000	5.009199000	0.052490000
C	0.884925000	–1.927879000	1.815540000	O	7.761950000	4.379176000	–1.031303000

TS with *exo*–NBN with CF_3–tag (tetrazine on surface)

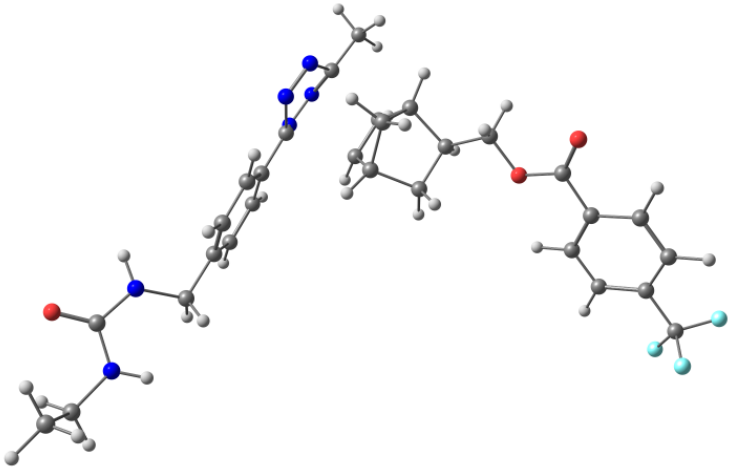

Frequency –378.5741

C	–8.661164000	5.819266000	–1.501396000	C	1.886742000	–2.128580000	–0.063670000
H	–7.705393000	6.160608000	–1.907038000	H	1.261645000	–4.096221000	–0.954610000
H	–9.382807000	6.633202000	–1.599148000	C	1.053314000	–0.814057000	–0.014412000
H	–9.013207000	4.972550000	–2.092528000	H	–1.058232000	–0.475082000	–0.693647000
C	–8.516785000	5.403765000	–0.041158000	H	0.564586000	–1.874173000	–2.307791000
H	–9.479522000	5.077334000	0.352071000	H	–0.871672000	–2.836527000	–1.929631000
H	–8.170235000	6.237592000	0.572655000	H	2.259275000	–2.398779000	0.927964000
C	–7.981927000	3.029531000	–0.190157000	H	1.429754000	–0.091612000	–0.743528000
N	–6.987481000	2.070237000	–0.170891000	H	1.075891000	–0.338557000	0.966935000
H	–7.365668000	1.134430000	–0.220050000	N	–2.825539000	–3.489032000	–0.747556000
C	–5.722230000	2.223156000	0.535535000	N	–2.117747000	–4.553622000	–0.771093000
H	–5.113139000	2.982093000	0.028965000	H	–1.159547000	–1.734140000	1.668362000
H	–5.877467000	2.556359000	1.568432000	H	0.254150000	–3.863051000	1.537954000
C	–4.971582000	0.914801000	0.525662000	C	3.076114000	–2.055892000	–0.998358000
C	–4.558492000	0.356288000	–0.685867000	H	3.631073000	–2.997026000	–1.018778000
C	–4.707481000	0.230536000	1.708846000	H	2.786151000	–1.811712000	–2.023558000
C	–3.897267000	–0.862332000	–0.713649000	O	3.943141000	–1.019749000	–0.508745000
H	–4.771188000	0.879927000	–1.612180000	C	5.049053000	–0.803340000	–1.232794000
C	–4.041120000	–0.989855000	1.690262000	O	5.320898000	–1.422115000	–2.226965000
H	–5.034816000	0.648903000	2.654635000	C	5.901376000	0.288346000	–0.670914000
C	–3.637429000	–1.545421000	0.477766000	C	5.545737000	0.989443000	0.478875000
H	–3.587090000	–1.301788000	–1.654207000	C	7.085137000	0.588453000	–1.343937000
H	–3.850806000	–1.526240000	2.611868000	C	6.375303000	1.997098000	0.956318000
C	–2.912930000	–2.837223000	0.449357000	H	4.626270000	0.744622000	0.994354000
C	–1.516949000	–4.911781000	0.404347000	C	7.914845000	1.591239000	–0.868740000
C	–0.657978000	–6.138794000	0.380341000	H	7.338287000	0.024839000	–2.233401000
H	–1.294476000	–7.024287000	0.323646000	C	7.553786000	2.289553000	0.280680000
H	–0.008488000	–6.126454000	–0.494260000	H	6.113137000	2.547829000	1.850847000
H	–0.061587000	–6.203314000	1.290062000	H	8.840318000	1.829583000	–1.378894000
N	–2.911430000	–3.600258000	1.597042000	C	8.439792000	3.407922000	0.753986000
N	–2.206315000	–4.657587000	1.574020000	F	8.252528000	4.521246000	0.026445000
C	–0.081775000	–3.332842000	0.654151000	F	8.210540000	3.732437000	2.032286000
C	–0.820166000	–2.160891000	0.731921000	F	9.737688000	3.090740000	0.646218000
C	0.833442000	–3.177715000	–0.553547000	N	–7.583546000	4.300252000	0.151357000
C	–0.377512000	–1.280134000	–0.422400000	H	–6.599874000	4.516728000	0.113963000
C	–0.021840000	–2.315904000	–1.500333000	O	–9.131265000	2.756217000	–0.481095000

TS with *endo*–NBN with CF_3–tag (tetrazine on surface)

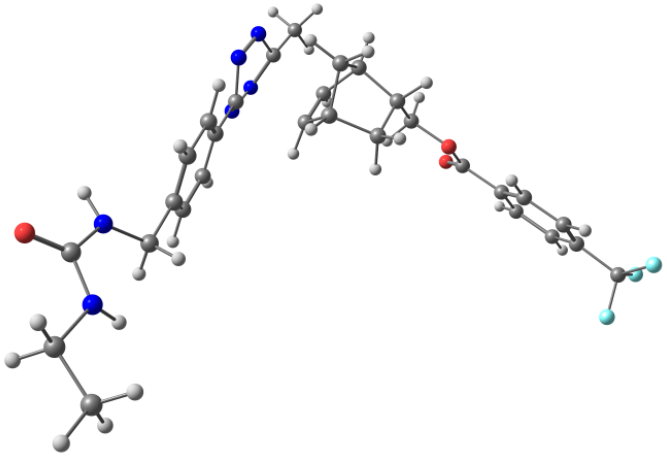

Frequency –386.0248

C	7.674873000	6.608268000	0.012944000	C	–1.737268000	–1.858180000	1.298371000
H	7.223735000	6.706301000	–0.978750000	H	–1.120508000	–3.951223000	1.810517000
H	8.356980000	7.448483000	0.148897000	C	–0.822131000	–0.617894000	1.079448000
H	6.882791000	6.682383000	0.760628000	H	1.409710000	–0.500899000	1.302998000
C	8.425425000	5.293887000	0.149248000	H	0.033709000	–1.923363000	3.128551000
H	8.874110000	5.200661000	1.138400000	H	1.278992000	–2.941276000	2.378875000
H	9.243738000	5.235626000	–0.576709000	H	–2.243083000	–1.784598000	2.265249000
C	7.977846000	2.900264000	0.213407000	H	–0.951805000	0.117583000	1.875152000
N	7.101108000	1.880164000	–0.080708000	H	–1.025872000	–0.118292000	0.129042000
H	7.523713000	0.963939000	–0.060461000	N	2.860453000	–3.626860000	0.737655000
C	5.810099000	2.028490000	–0.723375000	N	2.080926000	–4.634869000	0.840678000
H	5.252704000	2.815196000	–0.201723000	H	0.877609000	–1.536636000	–1.105564000
H	5.903826000	2.327696000	–1.776263000	H	–0.644107000	–3.570534000	–0.828745000
C	5.024174000	0.740908000	–0.646419000	C	–2.796071000	–2.047372000	0.235638000
C	4.864584000	0.085871000	0.576575000	H	–2.379425000	–2.013696000	–0.773956000
C	4.439952000	0.192908000	–1.785288000	H	–3.329774000	–2.994947000	0.353991000
C	4.134970000	–1.091045000	0.657777000	O	–3.734936000	–0.967681000	0.371003000
H	5.323524000	0.502743000	1.466751000	C	–4.729479000	–0.957375000	–0.526373000
C	3.703283000	–0.983570000	–1.711239000	O	–4.848926000	–1.783647000	–1.391564000
H	4.567991000	0.684176000	–2.744057000	C	–5.668165000	0.189487000	–0.334370000
C	3.549977000	–1.635073000	–0.488667000	C	–5.499330000	1.122787000	0.687085000
H	4.018976000	–1.603082000	1.605506000	C	–6.737536000	0.298362000	–1.220769000
H	3.262977000	–1.413206000	–2.602949000	C	–6.402760000	2.168729000	0.819086000
C	2.741829000	–2.872836000	–0.395403000	H	–4.667226000	1.025115000	1.371909000
C	1.205631000	–4.835446000	–0.191069000	C	–7.640645000	1.343151000	–1.091782000
C	0.261979000	–5.992050000	–0.066539000	H	–6.847173000	–0.443880000	–2.001801000
H	0.810281000	–6.924365000	–0.216157000	C	–7.467190000	2.271548000	–0.070226000
H	–0.180943000	–6.010694000	0.928611000	H	–6.287286000	2.898405000	1.611019000
H	–0.518946000	–5.928341000	–0.823968000	H	–8.478272000	1.435108000	–1.771817000
N	2.420974000	–3.525450000	–1.567434000	C	–8.407384000	3.439255000	0.040200000
N	1.644953000	–4.526137000	–1.464413000	F	–8.553719000	3.845451000	1.308732000
C	–0.093658000	–3.142811000	0.000563000	F	–7.958290000	4.495823000	–0.657232000
C	0.714998000	–2.024537000	–0.151407000	F	–9.626072000	3.149931000	–0.432964000
C	–0.708268000	–3.033994000	1.391781000	N	7.508648000	4.173189000	–0.022483000
C	0.614140000	–1.224334000	1.133111000	H	6.777346000	4.293564000	–0.706731000
C	0.405621000	–2.327526000	2.184573000	O	9.076116000	2.686542000	0.690857000

Product with *exo*–NBN with CF_3–tag (tetrazine on surface)

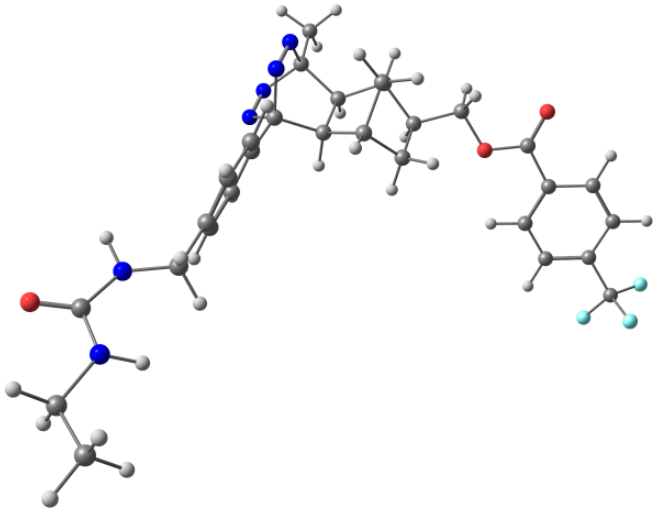

C	–8.699508000	6.147258000	–0.845695000
H	–7.771675000	6.565873000	–0.445087000
H	–9.473334000	6.910163000	–0.751034000
H	–8.551641000	5.934534000	–1.906200000
C	–9.104218000	4.889831000	–0.094278000
H	–10.028031000	4.473694000	–0.496773000
H	–9.289756000	5.110974000	0.962484000
C	–8.317374000	2.609856000	0.257228000
N	–7.228012000	1.759693000	0.290162000
H	–7.503468000	0.802193000	0.459812000
C	–6.013402000	1.953979000	–0.489564000
H	–6.231235000	2.074319000	–1.557426000
H	–5.508921000	2.866661000	–0.150223000
C	–5.079188000	0.787319000	–0.281259000
C	–4.692556000	–0.025191000	–1.341976000
C	–4.606321000	0.496106000	0.999597000
C	–3.844060000	–1.109769000	–1.134796000
H	–5.063112000	0.182396000	–2.340176000
C	–3.762322000	–0.583480000	1.212373000
H	–4.916537000	1.116024000	1.834386000
C	–3.376543000	–1.395721000	0.144123000
H	–3.561834000	–1.748109000	–1.962977000
H	–3.415129000	–0.813595000	2.212745000
C	–2.417062000	–2.529261000	0.378105000
C	–1.060130000	–4.541888000	0.793176000
C	–0.421902000	–5.881661000	1.056921000
H	–1.195837000	–6.638909000	1.187029000
H	0.206376000	–6.169849000	0.213331000
H	0.182912000	–5.838508000	1.963936000
N	–2.649192000	–3.166929000	1.710044000
N	–1.975154000	–4.170803000	1.913262000
C	–0.078287000	–3.334708000	0.729036000
C	–0.921124000	–2.073420000	0.455003000
C	0.974761000	–3.306354000	–0.399015000
C	–0.287392000	–1.477947000	–0.821076000
C	0.213366000	–2.708868000	–1.598975000
C	1.920506000	–2.133571000	–0.027933000
H	1.486930000	–4.255675000	–0.561973000
C	1.062602000	–0.875773000	–0.375999000
H	–0.934387000	–0.782625000	–1.355219000
H	0.885524000	–2.419312000	–2.409219000
H	–0.557859000	–3.348975000	–2.013900000
H	2.165958000	–2.160522000	1.037593000
H	1.520482000	–0.322803000	–1.200310000
H	0.962762000	–0.189072000	0.466196000
N	–2.542325000	–3.572319000	–0.642290000
N	–1.861952000	–4.581069000	–0.433758000
H	–0.881928000	–1.352391000	1.274584000
H	0.407194000	–3.307243000	1.707148000
C	3.224945000	–2.195873000	–0.794187000
H	3.793103000	–3.098056000	–0.553709000
H	3.074404000	–2.168404000	–1.876644000
O	3.998206000	–1.048672000	–0.407121000
C	5.183640000	–0.917099000	–1.016592000
O	5.588632000	–1.683447000	–1.849493000
C	5.943417000	0.280096000	–0.544041000
C	5.446509000	1.131251000	0.440992000
C	7.190262000	0.517877000	–1.119788000
C	6.200067000	2.223496000	0.851516000
H	4.478544000	0.934315000	0.883148000
C	7.944109000	1.607613000	–0.711974000
H	7.553715000	–0.162855000	–1.879630000
C	7.443841000	2.452842000	0.274206000
H	5.829641000	2.889243000	1.620932000
H	8.917889000	1.798239000	–1.146294000
C	8.242169000	3.660916000	0.678325000
F	9.560431000	3.426927000	0.627197000
F	8.000981000	4.702669000	–0.134670000
F	7.952588000	4.062932000	1.922566000
N	–8.069885000	3.871369000	–0.229384000
H	–7.115441000	4.196554000	–0.248618000
O	–9.419152000	2.257398000	0.631523000

Product with *endo*–NBN with CF_3–tag (tetrazine on surface)

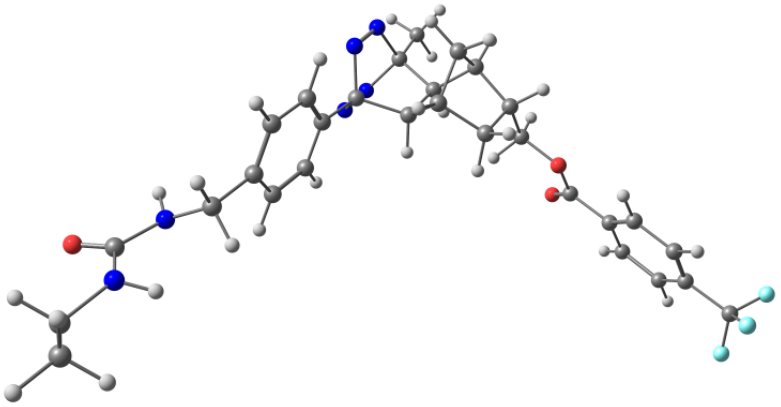

C	8.875699000	5.972721000	0.749074000	C	–1.939803000	–2.067401000	1.090071000
H	7.896680000	6.445953000	0.630002000	H	–1.469676000	–4.224267000	1.341875000
H	9.634452000	6.742381000	0.601493000	C	–0.990843000	–0.841923000	1.277640000
H	8.956346000	5.599897000	1.771955000	H	1.142298000	–0.847100000	1.919420000
C	9.066425000	4.844279000	–0.251347000	H	–0.539847000	–2.515308000	3.159412000
H	10.042834000	4.375013000	–0.130161000	H	0.808734000	–3.439244000	2.490270000
H	9.020563000	5.223459000	–1.278204000	H	–2.613418000	–2.145754000	1.948037000
C	8.174349000	2.623359000	–0.719255000	H	–1.264901000	–0.263995000	2.161512000
N	7.084969000	1.776920000	–0.628468000	H	–1.023935000	–0.164863000	0.419754000
H	7.303420000	0.847640000	–0.960575000	N	2.538908000	–3.603957000	0.803175000
C	6.065553000	1.868274000	0.407157000	N	1.809706000	–4.589837000	0.659084000
H	6.506125000	1.869343000	1.411315000	H	0.641765000	–1.253155000	–0.692968000
H	5.514534000	2.809222000	0.287953000	H	–0.730547000	–3.176043000	–1.029573000
C	5.089252000	0.724541000	0.276751000	C	–2.810375000	–1.986349000	–0.145820000
C	4.848201000	–0.138074000	1.341153000	H	–2.248554000	–1.718611000	–1.044279000
C	4.416959000	0.513303000	–0.928560000	H	–3.339349000	–2.924064000	–0.341127000
C	3.949356000	–1.193038000	1.212048000	O	–3.776002000	–0.950977000	0.098912000
H	5.372910000	0.006425000	2.279505000	C	–4.613602000	–0.689928000	–0.913925000
C	3.522254000	–0.538379000	–1.063930000	O	–4.578724000	–1.268421000	–1.966899000
H	4.610615000	1.173870000	–1.767214000	C	–5.588430000	0.394818000	–0.587032000
C	3.283449000	–1.400592000	0.007751000	C	–5.602953000	1.023718000	0.655722000
H	3.781526000	–1.871807000	2.039010000	C	–6.495169000	0.766835000	–1.578357000
H	3.020283000	–0.706296000	–2.009569000	C	–6.529051000	2.027815000	0.909382000
C	2.272537000	–2.505347000	–0.127453000	H	–4.891984000	0.727329000	1.415681000
C	0.818783000	–4.471994000	–0.413461000	C	–7.418025000	1.770511000	–1.328734000
C	0.113120000	–5.784896000	–0.637854000	H	–6.459181000	0.262134000	–2.535884000
H	0.835438000	–6.543188000	–0.942263000	C	–7.427613000	2.395590000	–0.084766000
H	–0.367882000	–6.114473000	0.283737000	H	–6.549058000	2.528554000	1.868995000
H	–0.636822000	–5.679437000	–1.423389000	H	–8.122315000	2.075506000	–2.093262000
N	2.268267000	–3.073620000	–1.510616000	C	–8.464484000	3.448720000	0.191767000
N	1.546938000	–4.055143000	–1.649419000	F	–8.687917000	4.219070000	–0.881631000
C	–0.112040000	–3.252129000	–0.134140000	F	–9.643193000	2.899951000	0.527455000
C	0.795268000	–2.023238000	0.066618000	F	–8.108308000	4.256586000	1.198713000
C	–0.968581000	–3.274886000	1.151475000	N	8.058439000	3.812893000	–0.040522000
C	0.395994000	–1.495688000	1.461586000	H	7.136737000	4.127441000	0.221077000
C	–0.003848000	–2.765762000	2.240763000	O	9.167486000	2.326026000	–1.354759000

TS *exo*–NBN with *anti* N_2 elimination (tetrazine on surface)

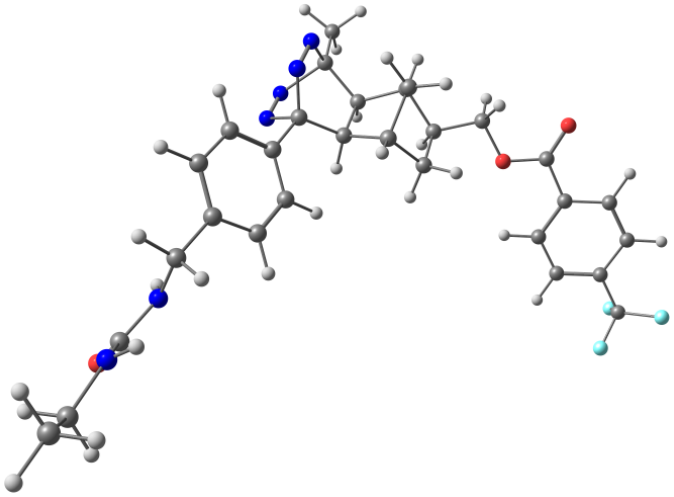

Frequency –554.5337

C	–9.796745000	5.091317000	–1.599440000	C	1.922637000	–2.158844000	0.017431000
H	–9.193838000	5.116376000	–2.511764000	H	1.519709000	–4.297726000	–0.457056000
H	–10.415996000	5.989345000	–1.588212000	C	1.066187000	–0.919666000	–0.392674000
H	–10.451831000	4.219256000	–1.643713000	H	–0.896751000	–0.881614000	–1.441823000
C	–8.918041000	5.039308000	–0.359674000	H	0.917467000	–2.564042000	–2.397906000
H	–9.521612000	5.004178000	0.547014000	H	–0.532365000	–3.467482000	–1.943088000
H	–8.290890000	5.935365000	–0.291951000	H	2.144578000	–2.150610000	1.088422000
C	–7.447068000	3.446843000	0.767993000	H	1.544381000	–0.385851000	–1.218295000
N	–6.532037000	2.420501000	0.616553000	H	0.937019000	–0.209237000	0.426317000
H	–6.265521000	2.025950000	1.508238000	N	–2.617004000	–3.674224000	–0.575415000
C	–6.502843000	1.513738000	–0.521134000	N	–1.909379000	–4.707750000	–0.308794000
H	–7.473478000	1.029736000	–0.682508000	H	–0.931056000	–1.387521000	1.224753000
H	–6.264322000	2.083319000	–1.427892000	H	0.347473000	–3.305162000	1.743772000
C	–5.434297000	0.463919000	–0.331812000	C	3.240818000	–2.237663000	–0.723524000
C	–5.715908000	–0.885853000	–0.531671000	H	3.813016000	–3.125190000	–0.441469000
C	–4.140899000	0.832857000	0.034716000	H	3.104597000	–2.252717000	–1.808094000
C	–4.727755000	–1.848359000	–0.375072000	O	3.999160000	–1.069728000	–0.371296000
H	–6.720657000	–1.189237000	–0.805921000	C	5.179345000	–0.937436000	–0.990965000
C	–3.150863000	–0.128467000	0.195296000	O	5.593805000	–1.723000000	–1.801090000
H	–3.911657000	1.880496000	0.197373000	C	5.918899000	0.288760000	–0.563229000
C	–3.431402000	–1.480567000	–0.011841000	C	5.417731000	1.154839000	0.406835000
H	–4.951722000	–2.896117000	–0.532660000	C	7.146455000	0.543727000	–1.171484000
H	–2.154511000	0.192568000	0.474712000	C	6.149593000	2.277372000	0.771581000
C	–2.405860000	–2.544782000	0.191311000	H	4.461521000	0.948057000	0.869457000
C	–1.010000000	–4.599092000	0.737061000	C	7.878069000	1.665268000	–0.810658000
C	–0.375555000	–5.905078000	1.126126000	H	7.511007000	–0.145652000	–1.923022000
H	–1.143919000	–6.669163000	1.241223000	C	7.373346000	2.525568000	0.159691000
H	0.317445000	–6.228905000	0.347378000	H	5.770770000	2.961674000	1.520586000
H	0.168892000	–5.798177000	2.065682000	H	8.830456000	1.876800000	–1.280822000
N	–2.664734000	–3.191420000	1.847585000	C	8.192567000	3.708418000	0.595381000
N	–2.009603000	–4.129279000	2.054023000	F	8.944251000	4.191622000	–0.402260000
C	–0.101138000	–3.364792000	0.748425000	F	7.426703000	4.711408000	1.044850000
C	–0.951693000	–2.114689000	0.410198000	F	9.031763000	3.381881000	1.592251000
C	0.995720000	–3.348037000	–0.338828000	N	–8.095378000	3.837005000	–0.378045000
C	–0.262729000	–1.546185000	–0.855826000	H	–7.706346000	3.566446000	–1.267846000
C	0.247872000	–2.808415000	–1.570876000	O	–7.658969000	3.959323000	1.850410000

TS *exo*–NBN with *syn* N2 elimination (tetrazine on surface)

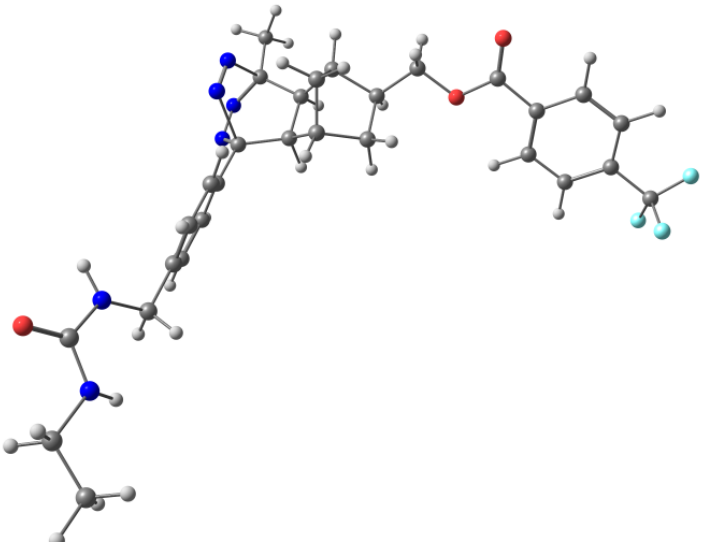

Frequency –591.7762

C	–8.719815000	6.185642000	0.042736000	C	1.907395000	–2.124733000	–0.134025000
H	–8.650789000	6.111863000	1.132058000	H	1.283889000	–4.061271000	–1.051829000
H	–9.486152000	6.926357000	–0.189196000	C	1.080858000	–0.800698000	–0.065157000
H	–7.763151000	6.547588000	–0.339176000	H	–0.969489000	–0.396044000	–0.802086000
C	–9.076945000	4.844585000	–0.576431000	H	0.649552000	–1.813170000	–2.358664000
H	–9.142237000	4.920194000	–1.662164000	H	–0.804341000	–2.751060000	–2.076818000
H	–10.055126000	4.500693000	–0.223297000	H	2.284438000	–2.405931000	0.852958000
C	–8.142717000	2.610203000	–0.832876000	H	1.483884000	–0.065536000	–0.766333000
N	–7.217331000	1.689694000	–0.397349000	H	1.097308000	–0.349201000	0.928277000
H	–7.403895000	0.746481000	–0.703485000	N	–2.626376000	–3.400478000	–0.784344000
C	–6.248401000	1.894109000	0.662342000	N	–2.001194000	–4.365449000	–0.803502000
H	–5.718388000	2.834564000	0.471233000	H	–0.720622000	–1.544507000	1.602543000
H	–6.726683000	1.974612000	1.647951000	H	0.552834000	–3.483440000	1.487984000
C	–5.248303000	0.762826000	0.692534000	C	3.099968000	–2.039162000	–1.064132000
C	–4.565508000	0.398838000	–0.469166000	H	3.658938000	–2.977969000	–1.089668000
C	–4.994331000	0.064532000	1.869215000	H	2.816004000	–1.787570000	–2.088983000
C	–3.644307000	–0.638732000	–0.449325000	O	3.960635000	–1.003723000	–0.562509000
H	–4.771876000	0.925104000	–1.395145000	C	5.058093000	–0.765212000	–1.292759000
C	–4.072591000	–0.976505000	1.894184000	O	5.325492000	–1.365026000	–2.299655000
H	–5.530242000	0.326818000	2.775277000	C	5.907534000	0.323254000	–0.720704000
C	–3.386907000	–1.333687000	0.735168000	C	5.559070000	1.001676000	0.445991000
H	–3.146907000	–0.933098000	–1.366033000	C	7.081468000	0.642860000	–1.399691000
H	–3.894960000	–1.534631000	2.805038000	C	6.388306000	2.003232000	0.932732000
C	–2.392063000	–2.445466000	0.773518000	H	4.646558000	0.741757000	0.966396000
C	–0.992545000	–4.592496000	0.683652000	C	7.911119000	1.643445000	–0.915818000
C	–0.365852000	–5.947654000	0.537552000	H	7.329085000	0.096503000	–2.301355000
H	–1.117941000	–6.718814000	0.700200000	C	7.559107000	2.316117000	0.249778000
H	0.061363000	–6.067109000	–0.459115000	H	6.134031000	2.534445000	1.841673000
H	0.430057000	–6.070723000	1.276658000	H	8.829191000	1.896062000	–1.431321000
N	–2.668448000	–3.422386000	1.686402000	C	8.426367000	3.436836000	0.751552000
N	–1.962837000	–4.506432000	1.644305000	F	9.707402000	3.278378000	0.395096000
C	–0.068406000	–3.377870000	0.593755000	F	8.028794000	4.622447000	0.260771000
C	–0.902431000	–2.075992000	0.663693000	F	8.389662000	3.538255000	2.087017000
C	0.854257000	–3.151442000	–0.630291000	N	–8.046795000	3.861017000	–0.264440000
C	–0.339471000	–1.231080000	–0.502446000	H	–7.614656000	3.939542000	0.643638000
C	0.026387000	–2.262624000	–1.583382000	O	–8.962070000	2.344399000	–1.692070000

TS *endo*–NBN with *anti* N_2 elimination (tetrazine on surface)

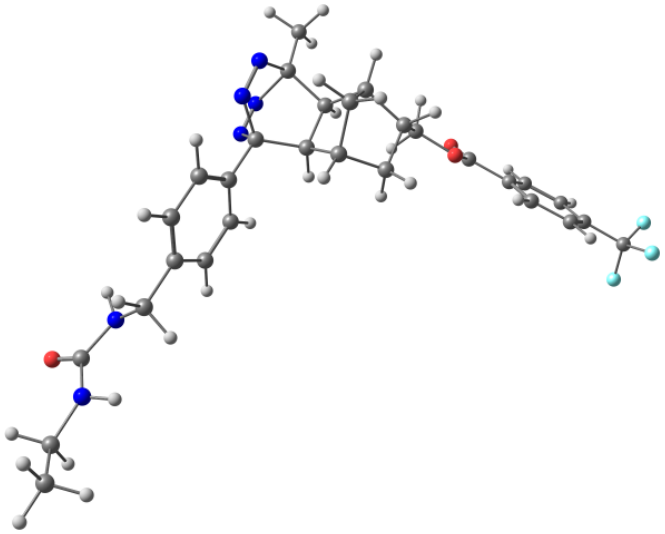

Frequency –573.4104

C	9.474340000	5.593268000	0.898949000
H	8.523668000	6.101836000	1.083161000
H	10.229650000	6.359878000	0.721058000
H	9.749588000	5.040039000	1.799002000
C	9.375886000	4.660222000	–0.296867000
H	10.325827000	4.157610000	–0.479742000
H	9.130808000	5.219049000	–1.206711000
C	8.262147000	2.586159000	–0.932311000
N	7.171371000	1.757136000	–0.741033000
H	7.255672000	0.902189000	–1.273753000
C	6.430905000	1.662623000	0.509359000
H	7.089995000	1.443516000	1.357676000
H	5.941951000	2.623414000	0.710621000
C	5.362990000	0.601204000	0.402153000
C	5.302328000	–0.452405000	1.308749000
C	4.418285000	0.663470000	–0.623966000
C	4.316682000	–1.428347000	1.200919000
H	6.037243000	–0.520055000	2.103922000
C	3.430272000	–0.304116000	–0.732368000
H	4.470434000	1.471673000	–1.345854000
C	3.371345000	–1.360278000	0.180450000
H	4.283171000	–2.258448000	1.894675000
H	2.716991000	–0.250558000	–1.547306000
C	2.303327000	–2.399351000	0.069367000
C	0.733400000	–4.359918000	–0.313303000
C	–0.018564000	–5.612923000	–0.662321000
H	0.684164000	–6.412192000	–0.895587000
H	–0.631017000	–5.929189000	0.184538000
H	–0.666806000	–5.439418000	–1.522897000
N	2.272924000	–2.960576000	–1.628161000
N	1.554020000	–3.857638000	–1.780584000
C	–0.099565000	–3.083897000	–0.136991000
C	0.854623000	–1.886179000	0.087086000
C	–0.981769000	–3.070898000	1.136776000
C	0.415122000	–1.324700000	1.459008000
C	–0.006600000	–2.590732000	2.227338000
C	–1.925778000	–1.847822000	1.061896000
H	–1.503830000	–4.009587000	1.324347000
C	–0.951455000	–0.642577000	1.241906000
H	1.168330000	–0.691735000	1.928094000
H	–0.526389000	–2.349544000	3.157575000
H	0.803542000	–3.281299000	2.445931000
H	–2.603914000	–1.904583000	1.918250000
H	–1.225840000	–0.040647000	2.109637000
H	–0.953658000	0.018384000	0.370578000
N	2.573895000	–3.562992000	0.747049000
N	1.783636000	–4.556840000	0.554609000
H	0.756154000	–1.121405000	–0.686886000
H	–0.700113000	–2.981441000	–1.043336000
C	–2.790535000	–1.778043000	–0.178228000
H	–2.227547000	–1.501150000	–1.073435000
H	–3.298276000	–2.726845000	–0.376120000
O	–3.782644000	–0.765390000	0.056704000
C	–4.673237000	–0.595328000	–0.929660000
O	–4.643598000	–1.212683000	–1.960822000
C	–5.709656000	0.429730000	–0.600967000
C	–5.696768000	1.139689000	0.597502000
C	–6.715035000	0.648814000	–1.541622000
C	–6.695546000	2.069826000	0.857739000
H	–4.909919000	0.962596000	1.319012000
C	–7.713407000	1.575130000	–1.283649000
H	–6.698260000	0.083769000	–2.465309000
C	–7.696708000	2.280011000	–0.083339000
H	–6.695693000	2.632374000	1.782780000
H	–8.498633000	1.756074000	–2.007609000
C	–8.816075000	3.237974000	0.215373000
F	–8.465203000	4.159328000	1.121262000
F	–9.222182000	3.888324000	–0.883369000
F	–9.889898000	2.596755000	0.705425000
N	8.377346000	3.628735000	–0.045109000
H	7.562590000	3.904143000	0.481330000
O	9.064691000	2.396008000	–1.825726000

TS *endo*–NBN with *syn* N_2 elimination (tetrazine on surface)

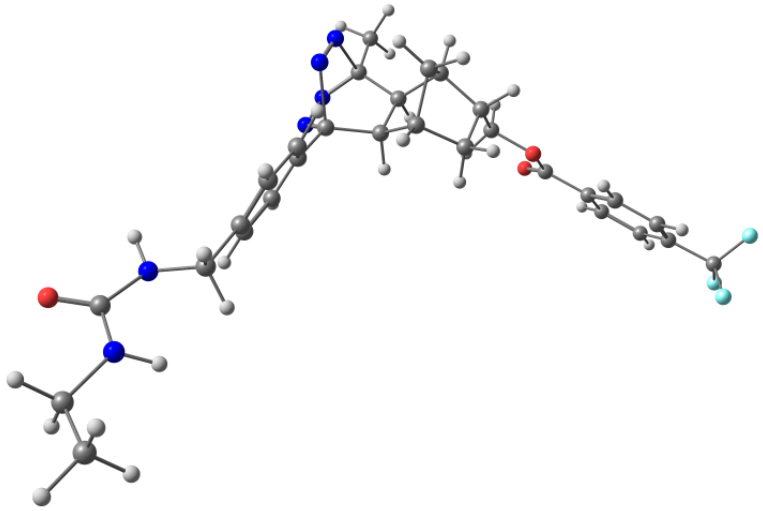

Frequency –588.4334

C	9.388627000	5.744446000	0.470775000
H	8.509392000	6.244031000	0.053981000
H	10.234976000	6.424507000	0.366615000
H	9.214311000	5.570517000	1.534412000
C	9.669000000	4.435616000	–0.249800000
H	10.545583000	3.939692000	0.167490000
H	9.877931000	4.613080000	–1.310412000
C	8.664337000	2.229413000	–0.522679000
N	7.497161000	1.488427000	–0.524746000
H	7.678942000	0.500522000	–0.636942000
C	6.308281000	1.845057000	0.235692000
H	6.540932000	2.018250000	1.293187000
H	5.890367000	2.776677000	–0.165610000
C	5.260784000	0.765473000	0.111473000
C	4.699607000	0.181988000	1.243319000
C	4.839388000	0.336353000	–1.148552000
C	3.721235000	–0.800033000	1.124696000
H	5.034952000	0.489455000	2.227978000
C	3.873208000	–0.651674000	–1.272334000
H	5.281609000	0.776401000	–2.036168000
C	3.298130000	–1.221920000	–0.134361000
H	3.312934000	–1.262769000	2.015396000
H	3.560654000	–0.998932000	–2.249510000
C	2.227290000	–2.249658000	–0.285912000
C	0.668248000	–4.277327000	–0.471926000
C	–0.057736000	–5.589295000	–0.523662000
H	0.605511000	–6.358969000	–0.916549000
H	–0.396352000	–5.879849000	0.471968000
H	–0.929002000	–5.507235000	–1.179036000
N	2.358175000	–3.052755000	–1.382126000
N	1.573509000	–4.078018000	–1.477176000
C	–0.146283000	–3.041235000	–0.088368000
C	0.784674000	–1.811933000	0.023579000
C	–0.965952000	–2.997125000	1.225841000
C	0.382308000	–1.182723000	1.378656000
C	–0.002564000	–2.385052000	2.263580000
C	–1.959877000	–1.812570000	1.103056000
H	–1.444790000	–3.939165000	1.494026000
C	–1.019358000	–0.566235000	1.151440000
H	1.108649000	–0.479312000	1.780927000
H	–0.547789000	–2.058998000	3.152579000
H	0.812749000	–3.019206000	2.588612000
H	–2.595570000	–1.826650000	1.992824000
H	–1.287114000	0.094440000	1.977145000
H	–1.072521000	0.021076000	0.230669000
N	2.496359000	–3.497486000	1.045381000
N	1.796029000	–4.403242000	0.940809000
H	0.580467000	–1.089046000	–0.772416000
H	–0.815145000	–2.942921000	–0.946119000
C	–2.888836000	–1.852288000	–0.091293000
H	–2.383470000	–1.633864000	–1.035416000
H	–3.388390000	–2.820749000	–0.189456000
O	–3.883561000	–0.836785000	0.120604000
C	–4.812601000	–0.736738000	–0.839984000
O	–4.828665000	–1.434768000	–1.818694000
C	–5.821906000	0.328589000	–0.558643000
C	–5.752384000	1.137624000	0.575746000
C	–6.852142000	0.492644000	–1.480433000
C	–6.717649000	2.111861000	0.783192000
H	–4.946460000	1.001164000	1.284810000
C	–7.821741000	1.464747000	–1.272942000
H	–6.878699000	–0.147202000	–2.353835000
C	–7.746060000	2.269029000	–0.142330000
H	–6.674856000	2.751661000	1.656791000
H	–8.625136000	1.602262000	–1.985110000
C	–8.798165000	3.308205000	0.128438000
F	–8.253083000	4.478113000	0.493378000
F	–9.569933000	3.540636000	–0.938983000
F	–9.610643000	2.933636000	1.130322000
N	8.538516000	3.529277000	–0.094604000
H	7.620524000	3.946370000	–0.090647000
O	9.728267000	1.755109000	–0.871284000

Product *exo anti* (tetrazine on surface)

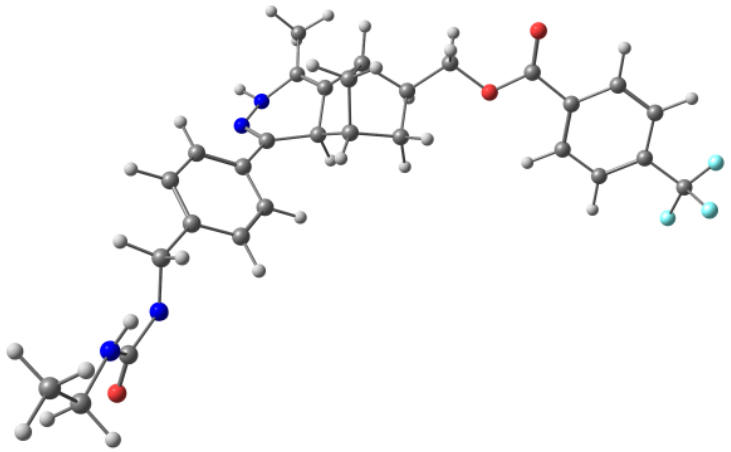

C	9.539103000	5.076685000	1.610652000
H	8.795974000	5.248509000	2.394722000
H	10.180665000	5.957696000	1.565387000
H	10.149972000	4.218501000	1.897374000
C	8.873154000	4.837219000	0.265281000
H	9.615758000	4.661406000	–0.513150000
H	8.291280000	5.713487000	–0.041160000
C	7.500201000	3.141694000	–0.829680000
N	6.553162000	2.147262000	–0.666214000
H	6.369107000	1.659491000	–1.532012000
C	6.391176000	1.372886000	0.556859000
H	7.341746000	0.941286000	0.891784000
H	6.027853000	2.031831000	1.355208000
C	5.376958000	0.276271000	0.344256000
C	5.711216000	–1.062084000	0.545052000
C	4.082643000	0.589609000	–0.066390000
C	4.776923000	–2.066644000	0.340522000
H	6.716437000	–1.321632000	0.859786000
C	3.143350000	–0.413727000	–0.268969000
H	3.813061000	1.627340000	–0.232465000
C	3.477934000	–1.757964000	–0.074269000
H	5.037029000	–3.106679000	0.488486000
H	2.144717000	–0.131742000	–0.581118000
C	2.497466000	–2.858171000	–0.311499000
C	0.915354000	–5.024161000	–0.827082000
C	0.137833000	–6.276254000	–1.117631000
H	–0.440518000	–6.165040000	–2.039294000
H	0.824130000	–7.115371000	–1.211187000
H	–0.569221000	–6.490389000	–0.311698000
C	0.174133000	–3.714315000	–0.925514000
C	1.058966000	–2.488056000	–0.572631000
C	–0.962861000	–3.627717000	0.124160000
C	0.375100000	–1.905242000	0.698027000
C	–0.174116000	–3.175450000	1.364156000
C	–1.821355000	–2.385507000	–0.208110000
H	–1.544269000	–4.545063000	0.219721000
C	–0.918896000	–1.203470000	0.257224000
H	1.035215000	–1.291274000	1.309021000
H	–0.801971000	–2.958232000	2.230414000
H	0.604846000	–3.883969000	1.657058000
H	–2.024374000	–2.335233000	–1.281860000
H	–1.380934000	–0.683729000	1.101321000
H	–0.752066000	–0.465345000	–0.529965000
N	2.961179000	–4.046873000	–0.266525000
N	2.143244000	–5.169778000	–0.515736000
H	1.039852000	–1.753262000	–1.381195000
H	–0.238712000	–3.647017000	–1.936984000
C	–3.150321000	–2.430697000	0.516157000
H	–3.759732000	–3.279984000	0.196562000
H	–3.021809000	–2.495445000	1.600176000
O	–3.854915000	–1.217342000	0.208022000
C	–5.022245000	–1.052183000	0.843697000
O	–5.464723000	–1.844759000	1.632124000
C	–5.709600000	0.220348000	0.466887000
C	–5.188742000	1.089707000	–0.490617000
C	–6.912662000	0.512064000	1.105361000
C	–5.875631000	2.253447000	–0.808661000
H	–4.255474000	0.849807000	–0.982998000
C	–7.598788000	1.676549000	0.792412000
H	–7.296749000	–0.184560000	1.840341000
C	–7.075932000	2.538617000	–0.165794000
H	–5.487541000	2.934229000	–1.556525000
H	–8.536920000	1.911465000	1.279189000
C	–7.785139000	3.827344000	–0.476353000
F	–9.095910000	3.755140000	–0.213412000
F	–7.295195000	4.844350000	0.251622000
F	–7.651135000	4.173798000	–1.763926000
N	8.023316000	3.655442000	0.331754000
H	7.522598000	3.503711000	1.193718000
O	7.844960000	3.525657000	–1.930796000

Product *exo syn* (tetrazine on surface)

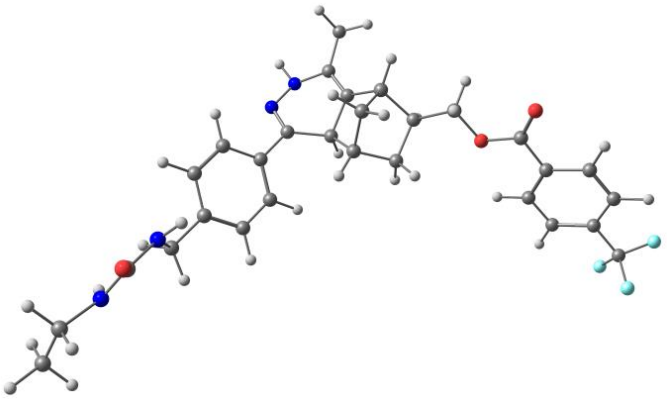

C	–9.878036000	–5.036281000	–0.964524000	C	0.086148000	2.916819000	1.372818000
H	–10.243572000	–4.318464000	–1.704465000	C	1.873707000	2.371650000	–0.150236000
H	–10.681210000	–5.748150000	–0.770504000	H	1.488812000	4.453760000	0.516051000
H	–9.034420000	–5.578101000	–1.396858000	C	0.984825000	1.117284000	0.100935000
C	–9.468441000	–4.337564000	0.321387000	H	–1.047691000	1.023020000	0.991268000
H	–9.115020000	–5.056110000	1.061591000	H	0.654209000	2.611491000	2.253671000
H	–10.319873000	–3.813221000	0.768304000	H	–0.738732000	3.561726000	1.686250000
C	–7.786416000	–2.761036000	1.114556000	H	2.150810000	2.457391000	–1.205035000
N	–6.892132000	–1.761682000	0.776896000	H	1.399572000	0.514111000	0.913383000
H	–6.346997000	–1.462795000	1.573801000	H	0.908117000	0.473719000	–0.777975000
C	–6.243317000	–1.659584000	–0.522925000	H	–0.862337000	1.812387000	–1.613952000
H	–5.750608000	–2.597731000	–0.804776000	H	0.383026000	3.796388000	–1.830364000
H	–6.998867000	–1.441610000	–1.287636000	C	3.148483000	2.366743000	0.667095000
C	–5.240008000	–0.533293000	–0.517601000	H	3.757345000	3.253376000	0.472987000
C	–3.907328000	–0.757919000	–0.839245000	H	2.945305000	2.323724000	1.740962000
C	–5.642704000	0.764494000	–0.186219000	O	3.899262000	1.200140000	0.294622000
C	–2.990810000	0.290939000	–0.839645000	C	5.042778000	1.013486000	0.966584000
H	–3.575673000	–1.759854000	–1.089584000	O	5.436766000	1.759830000	1.822584000
C	–4.735895000	1.808930000	–0.188213000	C	5.768900000	–0.220885000	0.538883000
H	–6.679520000	0.947075000	0.076704000	C	5.286124000	–1.055266000	–0.468276000
C	–3.391575000	1.588781000	–0.520594000	C	6.965425000	–0.516655000	1.187635000
H	–1.958381000	0.075101000	–1.088489000	C	6.004141000	–2.188618000	–0.825039000
H	–5.046246000	2.815471000	0.060382000	H	4.356980000	–0.812789000	–0.967241000
C	–2.437219000	2.735921000	–0.538197000	C	7.683454000	–1.650146000	0.834799000
C	–0.902713000	4.991955000	–0.658945000	H	7.318454000	0.151558000	1.963328000
C	–0.151871000	6.290850000	–0.735781000	C	7.197968000	–2.477906000	–0.171872000
H	0.475923000	6.429581000	0.148582000	H	5.645329000	–2.842376000	–1.610602000
H	0.506075000	6.303913000	–1.609414000	H	8.616870000	–1.887671000	1.329260000
H	–0.858673000	7.116091000	–0.793316000	C	7.940339000	–3.736238000	–0.526309000
N	–2.946709000	3.896541000	–0.385200000	F	9.242696000	–3.651714000	–0.228613000
N	–2.155097000	5.064319000	–0.431786000	F	7.453824000	–4.796361000	0.139564000
C	–0.107938000	3.725265000	–0.854558000	F	7.843258000	–4.022771000	–1.832171000
C	–0.969858000	2.440785000	–0.726350000	N	–8.377275000	–3.407850000	0.056522000
C	0.949605000	3.540415000	0.264057000	H	–8.375193000	–2.954572000	–0.844193000
C	–0.364179000	1.724646000	0.515501000	O	–8.025386000	–3.046662000	2.272234000

Product *endo anti* (tetrazine on surface)

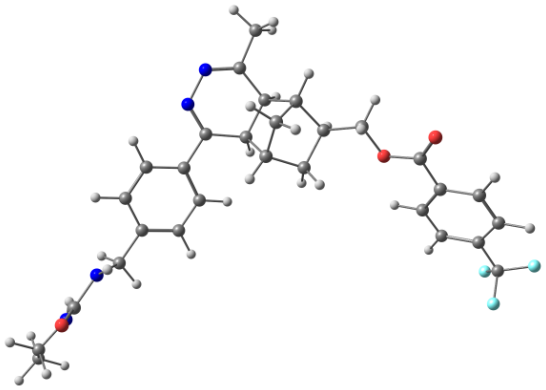

C	9.357628000	5.135499000	1.199802000	H	–1.549438000	–4.766901000	0.996423000
H	8.890113000	5.035293000	2.183585000	C	–0.842302000	–1.459812000	1.388423000
H	9.890152000	6.087255000	1.182860000	H	1.286021000	–1.698680000	1.988864000
H	10.085623000	4.330731000	1.080858000	H	–0.408890000	–3.471008000	3.014142000
C	8.320266000	5.091527000	0.090119000	H	0.854267000	–4.308708000	2.073821000
H	8.789892000	5.185967000	–0.889089000	H	–2.589222000	–2.719239000	1.773222000
H	7.613222000	5.923018000	0.185680000	H	–1.095837000	–1.038954000	2.363092000
C	6.784274000	3.494542000	–0.931532000	H	–0.828934000	–0.636389000	0.668426000
N	5.996780000	2.372167000	–0.746415000	N	2.819606000	–4.110800000	–0.331297000
H	5.582391000	2.062498000	–1.614910000	N	1.976564000	–5.234153000	–0.468306000
C	6.271530000	1.335940000	0.238037000	H	0.676051000	–1.766623000	–0.683902000
H	7.281204000	0.923233000	0.126534000	H	–0.614610000	–3.654056000	–1.253217000
H	6.201591000	1.768686000	1.243463000	C	–2.613899000	–2.271317000	–0.290443000
C	5.251342000	0.228042000	0.133545000	H	–1.956964000	–1.964245000	–1.109397000
C	5.646861000	–1.105347000	0.035382000	H	–3.208474000	–3.124015000	–0.631559000
C	3.889502000	0.523196000	0.147550000	O	–3.496253000	–1.178292000	0.008372000
C	4.707196000	–2.122070000	–0.043431000	C	–4.251175000	–0.743475000	–1.009586000
H	6.703676000	–1.350259000	0.016131000	O	–4.217608000	–1.223059000	–2.111107000
C	2.945474000	–0.493067000	0.068345000	C	–5.131175000	0.399537000	–0.618767000
H	3.568503000	1.557029000	0.217404000	C	–5.109831000	0.936854000	0.666511000
C	3.339122000	–1.831454000	–0.032159000	C	–5.979670000	0.926346000	–1.591160000
H	5.013809000	–3.156826000	–0.124860000	C	–5.940052000	2.004612000	0.981389000
H	1.895651000	–0.224528000	0.088405000	H	–4.442741000	0.521081000	1.410068000
C	2.346710000	–2.940951000	–0.137168000	C	–6.809878000	1.992115000	–1.279030000
C	0.709205000	–5.097398000	–0.488928000	H	–5.972603000	0.492523000	–2.583521000
C	–0.104502000	–6.345610000	–0.679430000	C	–6.782369000	2.526056000	0.006027000
H	0.538464000	–7.147076000	–1.037402000	H	–5.928094000	2.436838000	1.974074000
H	–0.556889000	–6.658551000	0.265812000	H	–7.469313000	2.415162000	–2.026865000
H	–0.917024000	–6.173499000	–1.391079000	C	–7.718102000	3.650971000	0.351477000
C	–0.045268000	–3.800136000	–0.330354000	F	–7.910423000	4.475000000	–0.687099000
C	0.883592000	–2.601488000	–0.009316000	F	–8.927693000	3.190560000	0.711106000
C	–0.970762000	–3.847560000	0.914044000	F	–7.262745000	4.389175000	1.371882000
C	0.493438000	–2.215057000	1.448911000	N	7.615084000	3.816210000	0.113705000
C	0.050675000	–3.569595000	2.028138000	H	7.423591000	3.419762000	1.020674000
C	–1.849911000	–2.576460000	0.979758000	O	6.739961000	4.146009000	–1.957448000

Product *endo syn* (tetrazine on surface)

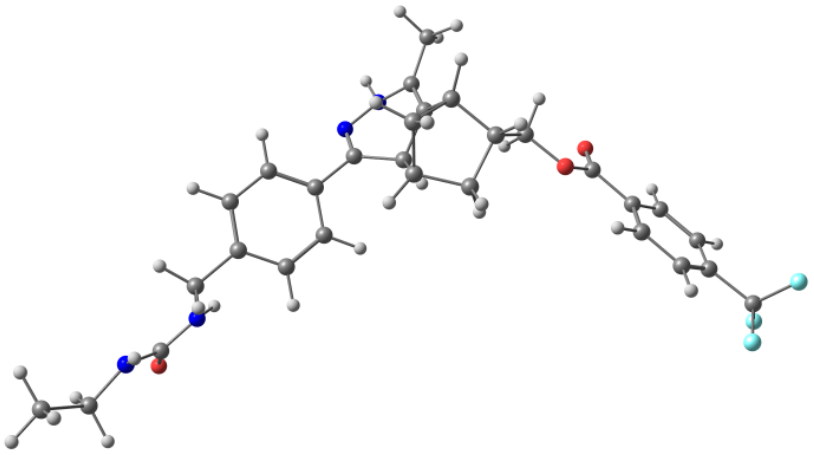

C	–9.365367000	–5.322483000	–1.261037000	C	1.898197000	2.388160000	1.060184000
H	–9.472561000	–4.808402000	–2.220510000	H	1.490226000	4.552544000	1.256364000
H	–10.206885000	–6.009006000	–1.159091000	C	0.917774000	1.196053000	1.277065000
H	–8.443778000	–5.907194000	–1.284857000	H	–1.254554000	1.287418000	1.741850000
C	–9.346086000	–4.334715000	–0.105960000	H	0.273561000	3.021842000	3.051731000
H	–9.236511000	–4.849819000	0.848364000	H	–0.959077000	3.891645000	2.099891000
H	–10.286022000	–3.773709000	–0.058933000	H	2.565896000	2.481643000	1.921613000
C	–7.895621000	–2.600563000	0.810000000	H	1.120273000	0.687186000	2.221141000
N	–6.942422000	–1.636554000	0.538638000	H	0.995630000	0.451131000	0.479718000
H	–6.601325000	–1.197578000	1.382520000	H	–0.477019000	1.641168000	–0.861606000
C	–6.006299000	–1.713226000	–0.574301000	H	0.776842000	3.615676000	–1.150992000
H	–5.476862000	–2.673214000	–0.591723000	C	2.770515000	2.238046000	–0.167325000
H	–6.558070000	–1.623643000	–1.518144000	H	2.193075000	1.987761000	–1.061682000
C	–5.013515000	–0.580142000	–0.498691000	H	3.351089000	3.141019000	–0.378795000
C	–3.647841000	–0.826938000	–0.436930000	O	3.675111000	1.154071000	0.097046000
C	–5.459266000	0.745601000	–0.488207000	C	4.483230000	0.808484000	–0.914005000
C	–2.738545000	0.226319000	–0.374113000	O	4.481629000	1.360380000	–1.981760000
H	–3.285162000	–1.849180000	–0.434852000	C	5.376230000	–0.337783000	–0.563823000
C	–4.559217000	1.794192000	–0.426814000	C	5.337957000	–0.942118000	0.690615000
H	–6.524921000	0.946425000	–0.525631000	C	6.255067000	–0.797703000	–1.543633000
C	–3.179364000	1.550228000	–0.372831000	C	6.181536000	–2.010260000	0.967748000
H	–1.681618000	–0.005959000	–0.320085000	H	4.648729000	–0.576875000	1.440522000
H	–4.900614000	2.821208000	–0.424011000	C	7.096479000	–1.864890000	–1.270124000
C	–2.227184000	2.698051000	–0.320636000	H	6.262134000	–0.310737000	–2.511013000
C	–0.659765000	4.933439000	–0.370058000	C	7.052324000	–2.465856000	–0.015145000
C	0.112414000	6.221710000	–0.399055000	H	6.157669000	–2.493579000	1.936272000
H	0.491504000	6.466159000	0.597135000	H	7.778351000	–2.237528000	–2.024854000
H	0.974358000	6.142350000	–1.067670000	C	8.000800000	–3.592775000	0.286656000
H	–0.539410000	7.028152000	–0.728679000	F	8.178415000	–4.390165000	–0.775439000
N	–2.733938000	3.863107000	–0.445392000	F	9.214247000	–3.133556000	0.633732000
N	–1.929858000	5.023255000	–0.433053000	F	7.569020000	–4.358802000	1.296546000
C	0.135033000	3.654969000	–0.265761000	N	–8.213392000	–3.427550000	–0.240847000
C	–0.762342000	2.398529000	–0.126610000	H	–7.989340000	–3.118880000	–1.174556000
C	0.964936000	3.621936000	1.044918000	O	–8.407160000	–2.708004000	1.908026000
C	–0.453374000	1.886579000	1.311466000				
C	–0.118725000	3.195040000	2.047255000				

Tautomerization *exo anti* product (tetrazine on surface)

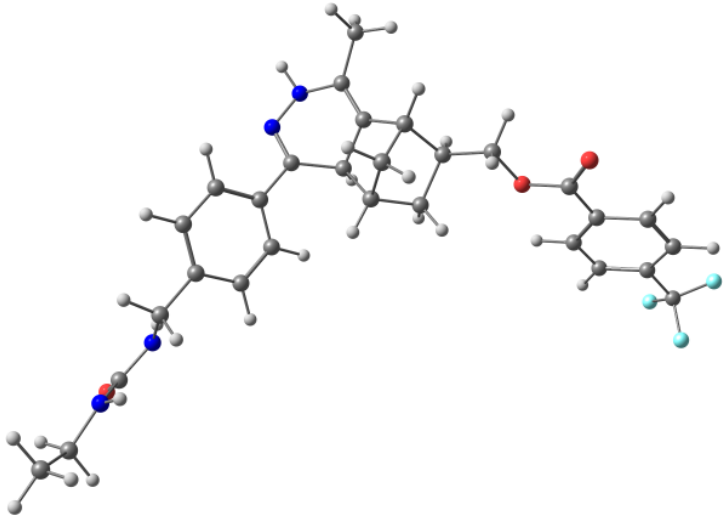

C	–9.997236000	–4.575021000	1.904652000	H	1.189078000	4.046727000	1.269324000
H	–9.183199000	–4.851981000	2.580656000	C	1.004883000	0.857829000	0.076161000
H	–10.733551000	–5.379357000	1.927924000	H	–1.089370000	0.445351000	0.687227000
H	–10.466477000	–3.665596000	2.284978000	H	0.353619000	1.780887000	2.439981000
C	–9.487563000	–4.365585000	0.488082000	H	–1.042520000	2.780203000	1.955028000
H	–10.301055000	–4.091460000	–0.183978000	H	2.193303000	2.516309000	–0.759066000
H	–9.045845000	–5.287316000	0.093829000	H	1.376982000	0.109753000	0.781986000
C	–8.069071000	–2.812588000	–0.748961000	H	1.071447000	0.427136000	–0.924655000
N	–7.013265000	–1.922264000	–0.691248000	N	–2.783847000	3.691614000	–1.270779000
H	–6.872002000	–1.450915000	–1.574042000	N	–1.811420000	4.599225000	–1.609733000
C	–6.642348000	–1.176352000	0.503667000	H	–0.621086000	1.818279000	–1.668267000
H	–7.499969000	–0.642118000	0.929721000	H	–2.232332000	5.490940000	–1.825696000
H	–6.277539000	–1.875981000	1.265845000	C	3.000222000	2.055306000	1.152657000
C	–5.537796000	–0.198758000	0.185074000	H	3.554280000	2.993896000	1.233893000
C	–5.689892000	1.162083000	0.438169000	H	2.692874000	1.755185000	2.158512000
C	–4.342389000	–0.650976000	–0.376531000	O	3.879508000	1.048202000	0.623657000
C	–4.667842000	2.056866000	0.144463000	C	4.970233000	0.793277000	1.354856000
H	–6.617836000	1.527312000	0.865647000	O	5.221134000	1.351138000	2.390264000
C	–3.319837000	0.240415000	–0.667609000	C	5.834815000	–0.266523000	0.750608000
H	–4.222990000	–1.707261000	–0.593930000	C	5.507139000	–0.895913000	–0.448535000
C	–3.470893000	1.607319000	–0.412286000	C	7.001255000	–0.608472000	1.432347000
H	–4.791026000	3.116314000	0.332967000	C	6.349554000	–1.871372000	–0.966326000
H	–2.404058000	–0.124619000	–1.120226000	H	4.600050000	–0.618803000	–0.969703000
C	–2.403507000	2.568103000	–0.782480000	C	7.843646000	–1.582356000	0.917881000
C	–0.629457000	4.654074000	–0.847138000	H	7.231985000	–0.099475000	2.359986000
C	–0.052740000	6.018774000	–0.633820000	C	7.512272000	–2.206354000	–0.280856000
H	0.106202000	6.518337000	–1.593936000	H	6.111736000	–2.364000000	–1.901021000
H	–0.724990000	6.642319000	–0.037155000	H	8.756099000	–1.852069000	1.435016000
H	0.909157000	5.956893000	–0.127033000	C	8.397124000	–3.298919000	–0.812266000
C	–0.191630000	3.498706000	–0.351911000	F	9.680982000	–3.110907000	–0.478286000
C	–0.933105000	2.212387000	–0.689302000	F	8.040807000	–4.499687000	–0.325673000
C	0.767935000	3.181107000	0.756889000	F	8.338269000	–3.388269000	–2.147382000
C	–0.432014000	1.277784000	0.447205000	N	–8.515943000	–3.279997000	0.462950000
C	–0.152054000	2.259633000	1.598174000	H	–7.914102000	–3.188094000	1.266635000
C	1.821420000	2.178566000	0.211303000	O	–8.565994000	–3.153755000	–1.805385000

Tautomerization *exo syn* product(tetrazine on surface)

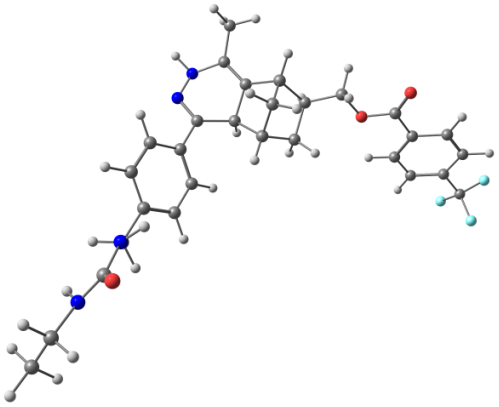

C	–10.444815000	–4.584722000	–0.676632000	C	–0.346817000	1.888179000	1.512894000
H	–10.831714000	–3.830988000	–1.368461000	C	1.753747000	2.068045000	0.341522000
H	–11.277584000	–5.228862000	–0.391356000	H	0.953522000	3.731854000	1.607216000
H	–9.705031000	–5.189140000	–1.204965000	C	1.000686000	0.772588000	–0.088248000
C	–9.831473000	–3.937718000	0.554560000	H	–1.125050000	0.224569000	0.239614000
H	–9.442969000	–4.690589000	1.240416000	H	0.094338000	1.292540000	2.315281000
H	–10.583358000	–3.362339000	1.105973000	H	–1.285844000	2.325541000	1.856795000
C	–7.902795000	–2.564850000	1.146564000	H	2.212702000	2.564226000	–0.517075000
N	–6.997021000	–1.612476000	0.721080000	H	1.329064000	–0.075122000	0.519758000
H	–6.299242000	–1.412844000	1.424001000	H	1.177936000	0.515454000	–1.134238000
C	–6.589692000	–1.434605000	–0.666266000	H	–0.487465000	1.965335000	–1.813227000
H	–6.260927000	–2.380185000	–1.113497000	H	–2.196775000	5.579077000	–1.564597000
H	–7.444396000	–1.071557000	–1.250302000	C	2.834565000	1.810470000	1.369865000
C	–5.483156000	–0.412908000	–0.752742000	H	3.345288000	2.731074000	1.663092000
C	–4.233830000	–0.749033000	–1.264674000	H	2.437685000	1.340159000	2.274241000
C	–5.701046000	0.892593000	–0.306311000	O	3.796037000	0.921883000	0.775841000
C	–3.217179000	0.198642000	–1.327724000	C	4.830124000	0.584535000	1.554349000
H	–4.052812000	–1.758001000	–1.619694000	O	4.971472000	0.981571000	2.680533000
C	–4.690598000	1.838932000	–0.370995000	C	5.788507000	–0.337114000	0.870225000
H	–6.671362000	1.159022000	0.100168000	C	5.582624000	–0.783763000	–0.433084000
C	–3.433288000	1.502705000	–0.882426000	C	6.915560000	–0.739305000	1.585228000
H	–2.255217000	–0.076677000	–1.746391000	C	6.506656000	–1.637266000	–1.023064000
H	–4.860345000	2.853438000	–0.031536000	H	4.705154000	–0.461578000	–0.978555000
C	–2.368791000	2.528804000	–0.998072000	C	7.840014000	–1.589216000	0.998268000
C	–0.666210000	4.631634000	–0.571407000	H	7.050615000	–0.373293000	2.595497000
C	–0.158544000	5.958143000	–0.099443000	C	7.629189000	–2.032181000	–0.304478000
H	–0.914123000	6.480180000	0.494903000	H	6.361923000	–1.988535000	–2.036982000
H	0.739271000	5.835571000	0.504561000	H	8.723649000	–1.902642000	1.540871000
H	0.095952000	6.593135000	–0.953118000	C	8.607988000	–2.996763000	–0.913370000
N	–2.739276000	3.707131000	–1.343294000	F	9.866264000	–2.736749000	–0.532504000
N	–1.768677000	4.672247000	–1.447546000	F	8.345451000	–4.261040000	–0.542756000
C	–0.240684000	3.421909000	–0.213939000	F	8.579750000	–2.968893000	–2.252089000
C	–0.902528000	2.191515000	–0.819251000	N	–8.715282000	–3.084622000	0.167346000
C	0.616434000	2.950832000	0.924947000	H	–8.817688000	–2.567379000	–0.692360000
C	–0.478511000	1.098042000	0.200083000	O	–7.966685000	–2.919204000	2.308466000

Tautomerization *endo anti* product (tetrazine on surface)

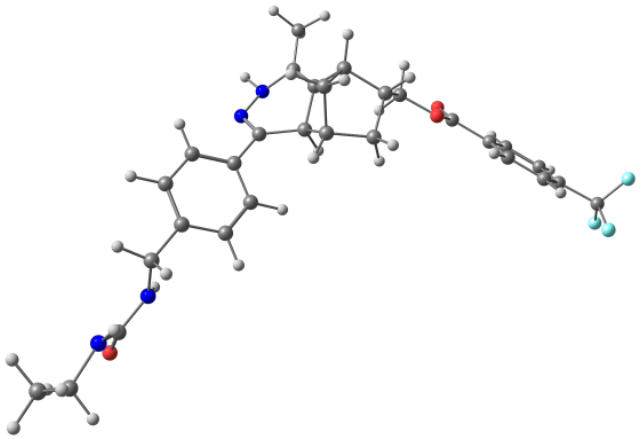

C	–10.766128000	–3.803982000	1.304083000	H	1.122088000	3.971375000	1.996837000
H	–10.162718000	–4.068474000	2.177228000	C	0.947327000	0.619693000	1.367692000
H	–11.585586000	–4.521136000	1.239656000	H	–1.257141000	0.413788000	1.564289000
H	–11.187751000	–2.809968000	1.464903000	H	–0.094944000	2.001877000	3.329193000
C	–9.936334000	–3.835556000	0.030787000	H	–1.292807000	2.939174000	2.387083000
H	–10.538546000	–3.564673000	–0.836271000	H	2.375269000	1.891815000	2.439643000
H	–9.546628000	–4.843084000	–0.153427000	H	1.093756000	–0.036411000	2.227742000
C	–8.139221000	–2.557126000	–1.018452000	H	1.200807000	0.047600000	0.470973000
N	–7.007357000	–1.792045000	–0.815969000	N	–2.239961000	3.296815000	–1.250285000
H	–6.641980000	–1.416203000	–1.679819000	N	–1.150484000	4.084126000	–1.523189000
C	–6.748420000	–1.019273000	0.392331000	H	–0.199786000	1.293260000	–0.831311000
H	–7.608702000	–0.394668000	0.659918000	H	–1.441354000	4.932610000	–1.985888000
H	–6.562855000	–1.705194000	1.228100000	C	2.798151000	2.102445000	0.368607000
C	–5.528132000	–0.154938000	0.195909000	H	2.306355000	2.061465000	–0.607319000
C	–5.626131000	1.233957000	0.183704000	H	3.324832000	3.058406000	0.441447000
C	–4.279386000	–0.745226000	–0.006076000	O	3.758766000	1.035015000	0.449758000
C	–4.500090000	2.022473000	–0.020978000	C	4.712299000	1.031721000	–0.487502000
H	–6.592696000	1.703738000	0.333166000	O	4.803306000	1.863671000	–1.350822000
C	–3.153191000	0.039834000	–0.205670000	C	5.651149000	–0.123498000	–0.340961000
H	–4.197773000	–1.827297000	–0.017127000	C	5.505657000	–1.065589000	0.674783000
C	–3.250697000	1.435096000	–0.218534000	C	6.688040000	–0.237328000	–1.265731000
H	–4.578484000	3.102617000	–0.040043000	C	6.401049000	–2.123709000	0.768411000
H	–2.193075000	–0.434885000	–0.377914000	H	4.694074000	–0.967971000	1.383791000
C	–2.058858000	2.270702000	–0.502154000	C	7.581710000	–1.293233000	–1.175902000
C	–0.145045000	4.230627000	–0.551264000	H	6.776253000	0.507395000	–2.047217000
C	0.498237000	5.579829000	–0.473111000	C	7.431406000	–2.231365000	–0.158005000
H	0.893134000	5.869002000	–1.451323000	H	6.295114000	–2.865902000	1.549589000
H	–0.220951000	6.342841000	–0.160962000	H	8.386439000	–1.396708000	–1.893618000
H	1.328319000	5.571498000	0.231903000	C	8.435508000	–3.343540000	–0.040426000
C	0.082988000	3.174938000	0.228863000	F	8.808288000	–3.805857000	–1.242170000
C	–0.673765000	1.880487000	–0.029455000	F	9.554335000	–2.932520000	0.579455000
C	0.755248000	3.040317000	1.565683000	F	7.960778000	–4.381653000	0.659544000
C	–0.497450000	1.157846000	1.335946000	N	–8.847206000	–2.871536000	0.117394000
C	–0.389242000	2.329410000	2.328840000	H	–8.380838000	–2.792621000	1.008164000
C	1.814678000	1.908893000	1.500647000	O	–8.484011000	–2.917178000	–2.127799000

Tautomerization *endo syn* product (tetrazine on surface)

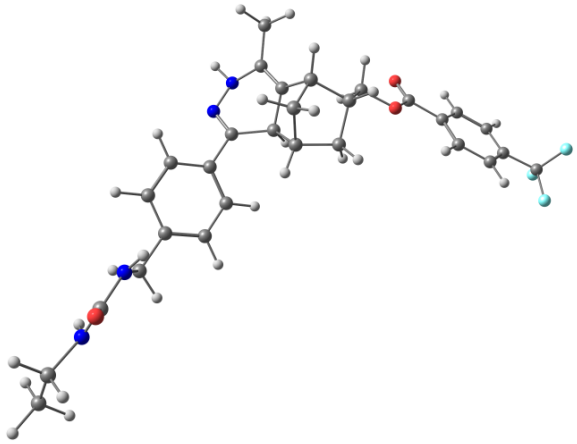

C	–10.916372000	–3.927053000	–1.105648000	O	3.728123000	0.876152000	0.550290000
H	–11.119073000	–3.185924000	–1.884176000	C	4.812962000	1.131593000	–0.188490000
H	–11.851999000	–4.444945000	–0.891016000	O	4.980286000	2.155268000	–0.796523000
H	–10.202376000	–4.653191000	–1.499333000	C	5.795084000	0.003378000	–0.169182000
C	–10.376525000	–3.267904000	0.152987000	C	5.537049000	–1.184044000	0.511674000
H	–10.174181000	–4.009177000	0.926408000	C	6.991618000	0.173419000	–0.864285000
H	–11.108129000	–2.566303000	0.568513000	C	6.479294000	–2.204890000	0.500776000
C	–8.392913000	–2.063367000	0.902733000	H	4.602133000	–1.304047000	1.043048000
N	–7.331880000	–1.258137000	0.537860000	C	7.933903000	–0.842931000	–0.875895000
H	–6.716755000	–1.063118000	1.315099000	H	7.163872000	1.105420000	–1.388363000
C	–6.727815000	–1.251557000	–0.788210000	C	7.670290000	–2.027457000	–0.193067000
H	–6.462715000	–2.264598000	–1.112842000	H	6.288604000	–3.135037000	1.020886000
H	–7.446401000	–0.848061000	–1.511757000	H	8.866221000	–0.725859000	–1.415013000
C	–5.502010000	–0.372610000	–0.788960000	C	8.723090000	–3.099760000	–0.170886000
C	–4.234254000	–0.908108000	–0.994666000	F	9.349302000	–3.205956000	–1.351460000
C	–5.626400000	0.999658000	–0.560259000	F	9.669717000	–2.838335000	0.745925000
C	–3.108590000	–0.090763000	–0.967371000	F	8.215778000	–4.303090000	0.124089000
H	–4.123699000	–1.971222000	–1.180297000	N	–9.122339000	–2.585387000	–0.138904000
C	–4.506837000	1.816605000	–0.537063000	H	–9.047117000	–2.144006000	–1.042729000
H	–6.611792000	1.422864000	–0.393066000	O	–8.655122000	–2.296400000	2.067590000
C	–3.231144000	1.279705000	–0.737453000				
H	–2.130038000	–0.522843000	–1.146785000				
H	–4.603021000	2.882071000	–0.367159000				
C	–2.037344000	2.159050000	–0.753053000				
C	–0.185948000	4.107483000	–0.225416000				
C	0.402513000	5.422323000	0.180844000				
H	–0.369816000	6.104829000	0.547449000				
H	1.148982000	5.285997000	0.962244000				
H	0.895222000	5.897670000	–0.672278000				
N	–2.172486000	3.309633000	–1.304024000				
N	–1.080563000	4.141478000	–1.310186000				
C	–0.007362000	2.922197000	0.354993000				
C	–0.690485000	1.696565000	–0.233877000				
C	0.531579000	2.532363000	1.702142000				
C	–0.613772000	0.712624000	0.966451000				
C	–0.651240000	1.656168000	2.182007000				
C	1.638396000	1.460848000	1.524585000				
H	0.814075000	3.363776000	2.347253000				
C	0.843366000	0.211749000	1.034078000				
H	–1.357801000	–0.080226000	0.963118000				
H	–0.442297000	1.135322000	3.119821000				
H	–1.581489000	2.220491000	2.269162000				
H	2.096130000	1.259317000	2.497423000				
H	0.934027000	–0.609163000	1.747745000				
H	1.206118000	–0.150175000	0.068034000				
H	–0.124217000	1.295863000	–1.089073000				
H	–1.347908000	5.061478000	–1.627871000				
C	2.728681000	1.909923000	0.577895000				
H	2.349208000	2.061600000	–0.436648000				
H	3.194740000	2.843111000	0.906841000				

9. DFT FOR XPS C1S CALCULATION

Electronic core level calculations (ECC) were used to simulate core levels of C 1s XPS spectra. All ECC were done with the GAUSSIAN09 program.[2] The effect of the bulk substrate on Al–O–P bound monolayers was mimicked by attaching the organic species to a Al $(OH_2)_2$– moiety. The geometries of the different systems were optimized at the B3LYP/6–311G(d,p) level of theory. Natural bond orbital (NBO) analysis (Glendening, E. D.; Reed, A. E.; Carpenter, J. E.; Weinhold, F. NBO, Version 3.1) was employed to obtain the core orbital energies. The simulated XPS spectra were used to facilitate the peak fitting procedure for overlapping contributions in the experimental XPS data.

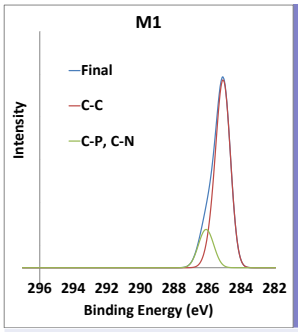

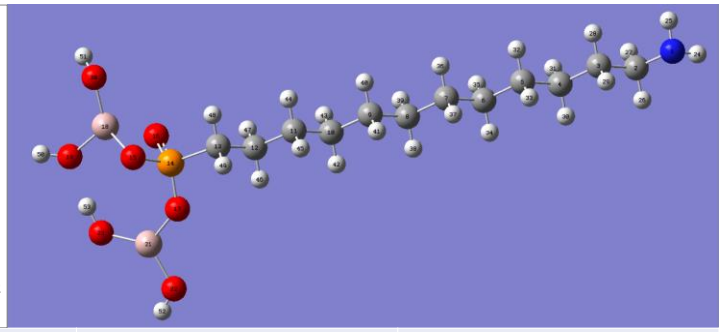

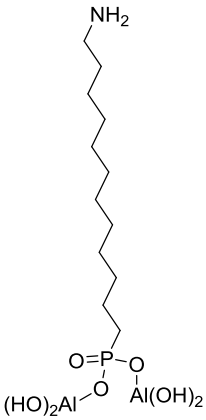

Carbon Number	3 - 12	2, 13
Functional group	**C-C**	**C-P, C-N**
Binding Energy Theory (eV)	285	286.3

Figure S9.1. Core level C1s XPS spectra (left) for the amine-terminated monolayer, simulation based on DFT calculations of the C1s core level energies for the different functional group binding energy shown in table (bottom), and [middle (Gaussview) and right(ChemDraw)) structure of model compound used for the calculation of binding energies.

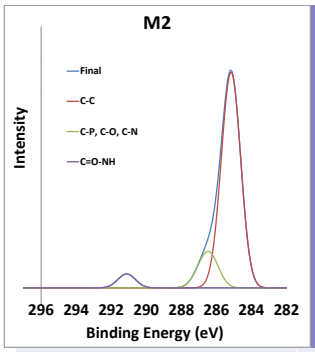

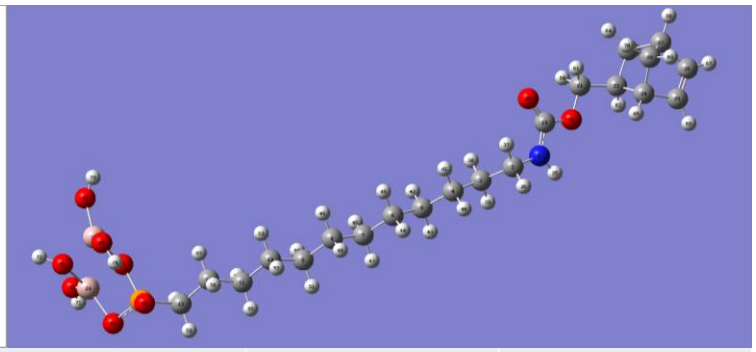

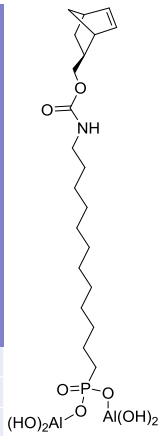

Carbon Number	3-12, 22-28	13, 21, 2	18
Functional group	**C-C**	**C-P, C-O, C-N**	**O-C=O-NH**
Binding Energy Theory (eV)	285	286.3	291.1

Figure S9.2. Core level C1s XPS spectra (left) for the *exo*–norbornene termination on an amine monolayer, simulation based on DFT calculations of the C1s core level energies for the different functional group binding energy shown in table (bottom), and [middle (Gaussview) and right(ChemDraw)) structure of model compound used for the calculation of binding energies.

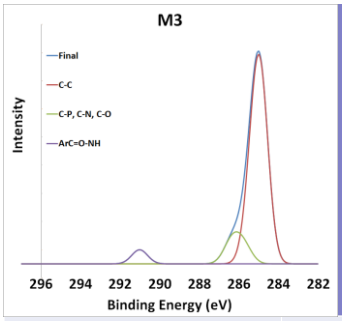

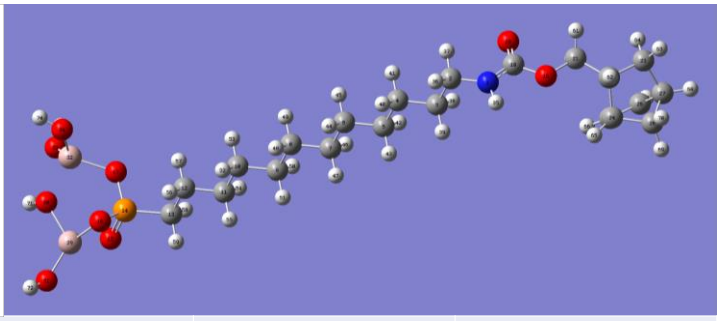

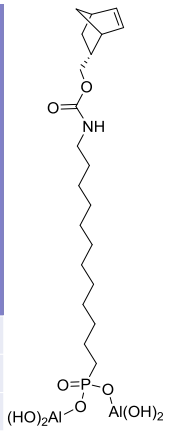

Carbon Number	3-12, 22-28	2, 13, 21	18
Functional group	**C-C**	**C-P, C-N, C-O**	**ArC=O-NH**
Binding Energy Theory (eV)	285	286.2	291.0

Figure S9.3. Core level C1s XPS spectra (left) for the *endo*–norbornene termination on an amine monolayer, simulation based on DFT calculations of the C1s core level energies for the different functional group binding energy shown in table (bottom), and [middle (Gaussview) and right(ChemDraw)) structure of model compound used for the calculation of binding energies.

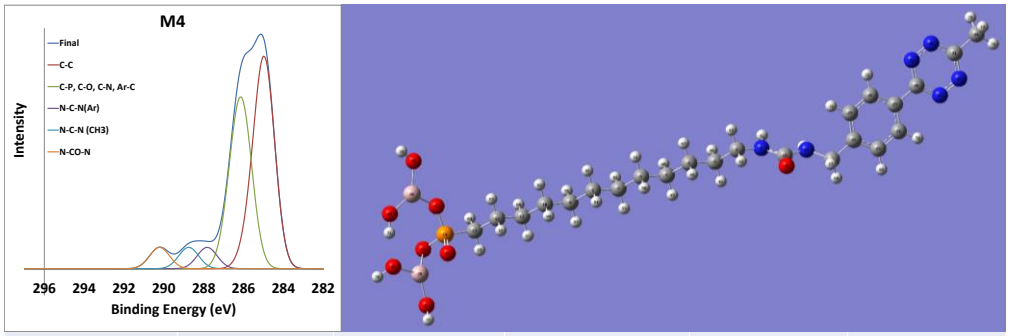

Carbon Number	3-12, 34	2,21-27	28	31	18
Functional group	**C-C**	**C-P, C-O, C-N, Ar-C**	**N-C-N(Ar)**	**N-C-N (CH3)**	**N-CO-N**
Binding Energy Theory (eV)	285.0	286.2	287.8	288.5	290.2

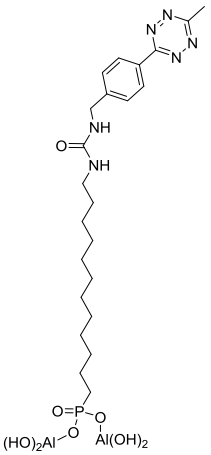

Figure S9.4. Core level C1s XPS spectra (left) for the tetrazine termination on an amine monolayer, simulation based on DFT calculations of the C1s core level energies for the different functional group binding energy shown in table (bottom), and [middle (Gaussview) and right (ChemDraw)) structure of model compound used for the calculation of binding energies.

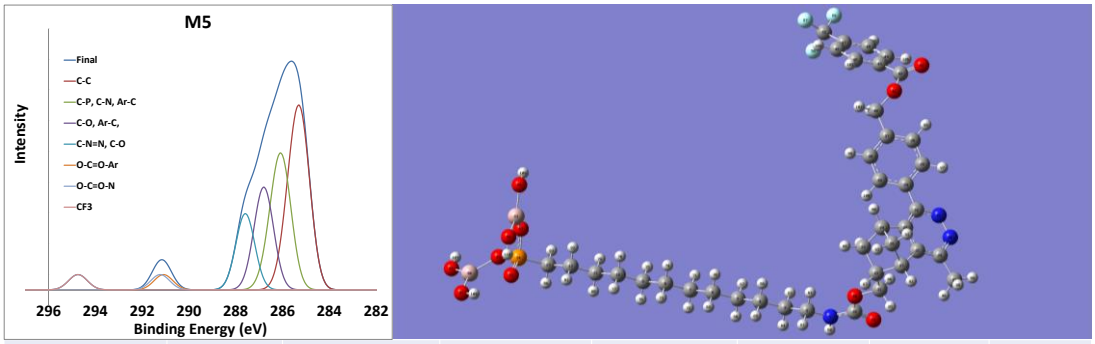

Carbon Number	3-12, 23 ,25, 28, 33	2, 13, 22, 24, 27-26, 35-36, 38-39	21, 34, 37, 45-46, 48-49	29, 32, 40, 43, 47	42	18	56
Functional group	**C-C**	**C-P, C-N, Ar-C**	**C-O, Ar-C,**	**C-N=N, C-O**	**O-C=O-Ar**	**O-C=O-N**	**CF3**
Binding Energy Theory (eV)	285.0	286.1	286.8	287.6	291.1	291.2	294.8

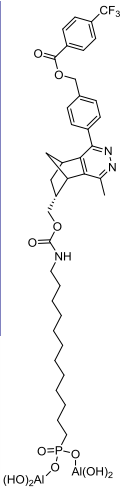

Figure S9.5. Core level C1s XPS spectra (left) for the IEDDA cycloadduct for *endo*–norbornene termination on an amine monolayer, simulation based on DFT calculations of the C1s core level energies for the different functional group binding energy shown in table (bottom), and [middle (Gaussview) and right (ChemDraw)) structure of model compound used for the calculation of binding energies.

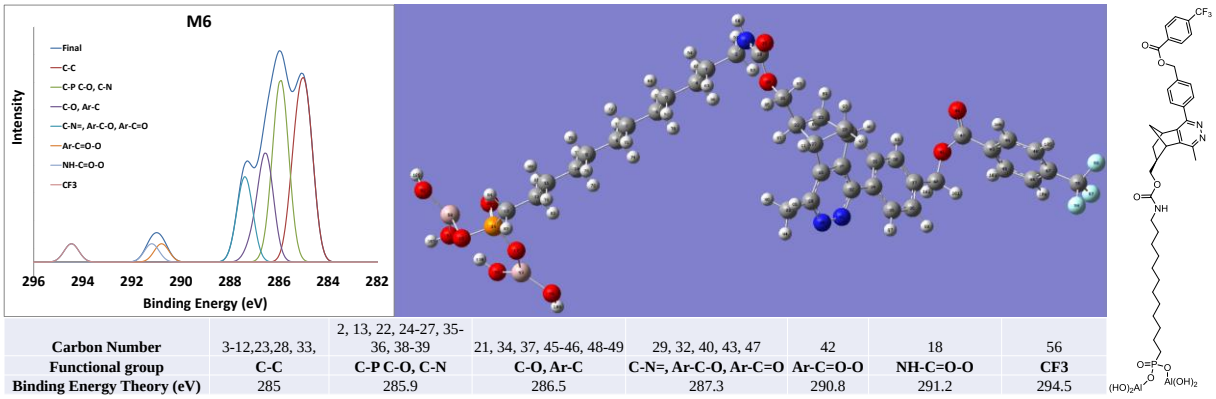

Carbon Number	3-12,23,28, 33,	2, 13, 22, 24-27, 35-36, 38-39	21, 34, 37, 45-46, 48-49	29, 32, 40, 43, 47	42	18	56
Functional group	**C-C**	**C-P C-O, C-N**	**C-O, Ar-C**	**C-N=, Ar-C-O, Ar-C=O**	**Ar-C=O-O**	**NH-C=O-O**	**CF3**
Binding Energy Theory (eV)	285	285.9	286.5	287.3	290.8	291.2	294.5

Figure S9.6. Core level C1s XPS spectra (left) for the IEDDA cycloadduct for *exo*–norbornene termination on an amine monolayer, simulation based on DFT calculations of the C1s core level energies for the different functional group binding energy shown in table (bottom), and [middle (Gaussview) and right (ChemDraw)) structure of model compound used for the calculation of binding energies.

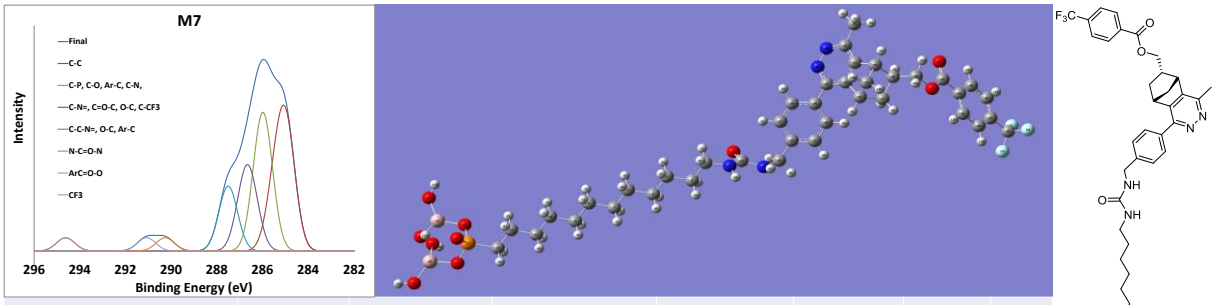

Carbon Number	3-12, 34, 37, 39	2,13,23-24,26-27, 32-33,35-36, 38,	28,31,40, 44, 47	21, 22, 25, 45,46, 48, 49	18	42	56
Functional group	**C-C**	**C-P, C-O, Ar-C, C-N,**	**C-N=, C=O-C, O-C, C-CF3**	**C-C-N=, O-C, Ar-C**	**N-C=O-N**	**ArC=O-O**	**CF3**
Binding Energy Theory (eV)	285.0	286.0	286.6	287.5	290.2	291.1	294.6

Figure S9.7. Core level C1s XPS spectra (left) for the IEDDA cycloadduct for *endo*–norbornene termination on an amine monolayer, simulation based on DFT calculations of the C1s core level energies for the different functional group binding energy shown in table (bottom), and [middle (Gaussview) and right (ChemDraw)) structure of model compound used for the calculation of binding energies.

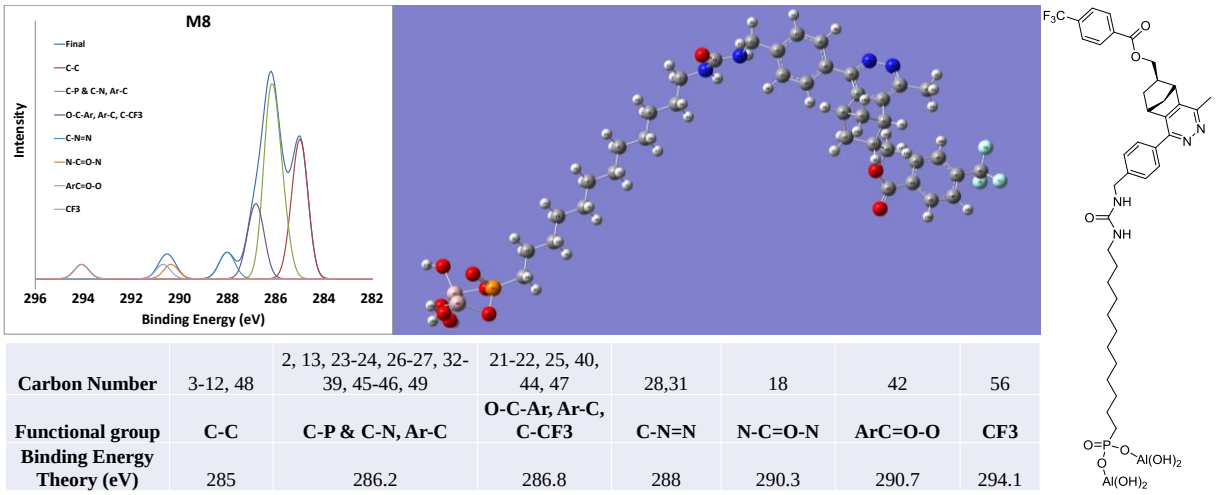

Carbon Number	3-12, 48	2, 13, 23-24, 26-27, 32-39, 45-46, 49	21-22, 25, 40, 44, 47	28,31	18	42	56
Functional group	**C-C**	**C-P & C-N, Ar-C**	**O-C-Ar, Ar-C, C-CF3**	**C-N=N**	**N-C=O-N**	**ArC=O-O**	**CF3**
Binding Energy Theory (eV)	285	286.2	286.8	288	290.3	290.7	294.1

Figure S9.8. Core level C1s XPS spectra (left) for the IEDDA cycloadduct for *exo*–norbornene termination on an amine monolayer, simulation based on DFT calculations of the C1s core level energies for the different functional group binding energy shown in table (bottom), and [middle (Gaussview) and right(ChemDraw)) structure of model compound used for the calculation of binding energies.

10. REFERENCES

(1) Sen, R.; Escorihuela, J.; Smulders, M. M. J.; Zuilhof, H. *Langmuir* **2016**, *32*, 3412.

(2) Frisch, M. J.; Trucks, G. W.; Schlegel, H. B.; Scuseria, G. E.; Robb, M. A.; Cheeseman, J. R.; Scalmani, G.; Barone, V.; Mennucci, B.; Petersson, G. A.; Nakatsuji, H.; Caricato, M.; Li, X.; Hratchian, H. P.; Izmaylov, A. F.; Bloino, J.; Zheng, G.; Sonnenberg, J. L.; Hada, M.; Ehara, M.; Toyota, K.; Fukuda, R.; Hasegawa, J.; Ishida, M.; Nakajima, T.; Honda, Y.; Kitao, O.; Nakai, H.; Vreven, T.; Montgomery Jr., J. A.; Peralta, J. E.; Ogliaro, F.; Bearpark, M. J.; Heyd, J.; Brothers, E. N.; Kudin, K. N.; Staroverov, V. N.; Kobayashi, R.; Normand, J.; Raghavachari, K.; Rendell, A. P.; Burant, J. C.; Iyengar, S. S.; Tomasi, J.; Cossi, M.; Rega, N.; Millam, N. J.; Klene, M.; Knox, J. E.; Cross, J. B.; Bakken, V.; Adamo, C.; Jaramillo, J.; Gomperts, R.; Stratmann, R. E.; Yazyev, O.; Austin, A. J.; Cammi, R.; Pomelli, C.; Ochterski, J. W.; Martin, R. L.; Morokuma, K.; Zakrzewski, V. G.; Voth, G. A.; Salvador, P.; Dannenberg, J. J.; Dapprich, S.; Daniels, A. D.; Farkas, Ö.; Foresman, J. B.; Ortiz, J. V.; Cioslowski, J.; Fox, D. J.; Gaussian, Inc.: Wallingford, CT, USA, 2009.

(3) Zhao, Y.; Truhlar, D. G. *Theor. Chem. Acc.* **2008**, *120*, 215.

(4) Liu, F.; Paton, R. S.; Kim, S.; Liang, Y.; Houk, K. N. *J. Am. Chem. Soc.* **2013**, *135*, 15642.

(5) Törk, L.; Jiménez–Osés, G.; Doubleday, C.; Liu, F.; Houk, K. N. *J. Am. Chem. Soc.* **2015**, *137*, 4749.

(6) Gonzalez, C.; Schlegel, H. B. *J. Phys. Chem.***1990**, *94*, 5523.

(7) Yang, J.; Karver, M. R.; Li, W.; Sahu, S.; Devaraj, N. K. *Angew. Chem. Int. Ed.* **2012**, *51*, 5222.

SUMMARY

Chapter 1 introduces the importance of surface functionalization and the variety of tools available to do so. The reader is then familiarized with the click concept, the development of click reactions and the reason for their prominence amongst all the other known reactions. These reactions are then reintroduced from a surface chemistry perspective along with an explanation of the tools used for analyzing them along with an introduction to direct analysis in real time–high resolution mass spectrometry (DART–HRMS). The existing challenges for efficient surface functionalization are then examined and our strategy to encounter them briefly touched upon.

In **chapter 2**, the applicability of recently introduced SuFEx reactions for quantitative surface functionalization is described. SuFExable platforms are prepared using a novel Michael addition method which allows for modularity. The quantitative nature of the reaction is illustrated using XPS and DART–HRMS is used for reaction kinetics elucidation. The interfacial SuFEx reaction is then tested for orthogonality with other click reactions *i.e.* CuAAC and SPOCQ and the applicability of such a platform shown for ferrocene immobilization.

Chapter 3 reports a novel click reaction between a strained alkene (cyclopropene) and *o*-quinones. The reaction is inspired by the SPOCQ reaction between strained alkenes and quinones, albeit free from the steric drawbacks of the latter. The kinetics of this novel reaction are elucidated in solution and on a surface and its utility demonstrated for quantitative monolayer functionalization and efficient polymer brush modification.

Taking a detour from covalent surface functionalization, **chapter 4** delves into supramolecular interactions at surfaces. A combination of XPS, DART–HRMS and GATR is used to study formation, reversible attachment and dynamicity of ureidopyrimidinone (UPy) dimers on surfaces. The yields of formed dimers is rigorously obtained using XPS wide and narrow scan spectra and the exchange rationalized using molecular dynamics. Furthermore, the kinetics of dimer formation and exchange is elucidated and used to determine the association constant (K) at surfaces.

Moving towards the application of click chemistry, in **chapter 5,** a novel strategy for on–resin peptide nucleic acid (PNA) modification is reported. The strategy makes use of an azide containing amino acid that is incorporated into the growing PNA chain during automated synthesis. This azide handle then allows for easy on–resin CuAAC

functionalization of the PNA chain with thiazole orange (TO) thus allowing facile synthesis of forced intercalation (FIT) probes that show single nucleotide polymorphism (SNP) detection ability. Furthermore, using a circular PNA–DNA hybrid design, a novel proof-of-concept PNA antisense delivery system is developed.

In **chapter 6**, the frontiers of surface functionalization are explored for a difficult to modify substrate, mica. Based on mussel adhesion, a catechol based surface anchor is designed that can be synthesized in two steps in high yields and shows facile and strong adhesion, thus forming atomically flat layers. The attachment strategy is based on a two–pronged approach, whereby after modification the surface is studded with easily modifiable amine groups. Using a combination of click tools, these amine groups are further explored and provide high yielding conjugations. Finally, to demonstrate the bio-applicability of these catechol based layers, DNA nano-constructs are self-assembled in a step-wise fashion and visualized by atomic force microscopy (AFM).

While the previous chapters have focused on the applicability and discovery of novel click reactions, **chapter 7** takes a look at the million dollar question, does the choice of surface-immobilized reactant have an influence on the yield and kinetics of an interfacial reaction? Using a combination of XPS, DART–HRMS DFT analysis and molecular dynamics, the question is answered in context of the well-known tetrazine-norbornene ligation. The reaction is further explored for various other perspectives i.e. surface orientation, reactant availability and the effect of reactant stereochemistry.

Finally, in **chapter 8** a general summary of the work is presented along with a critical discussion of the results along with novel ideas for future exploration.

LIST OF PUBLICATIONS

1) Covalently Bound Organic Layers on Mica: Formation of Atomically Flat Biofunctionalizable Surfaces.

Digvijay Gahtory, Rickdeb Sen, Rui Rijo Carvalho, Bauke Albada, Floris L. van Delft, Prof. Dr. Han Zuilhof, *Angew. Chem. Int. Ed.*, **2017**, *56*, 4130.

2) Approach Matters: The Kinetics of Interfacial Inverse-Electron Demand Diels-Alder Reactions.

Digvijay Gahtory, Rickdeb Sen, Sidharam P. Pujari, Jorge Escorihuela, Han Zuilhof, *Chem. Eur. J.* **2017**, *23*, 13015.

3) Surface-bound quadruple H-bonded dimers: formation and exchange kinetics

Digvijay Gahtory, Rickdeb Sen, Maarten M. J. Smulders and Han Zuilhof, *Faraday Discuss.*, **2017**, *204*, 383.

4) Facile functionalization of peptide nucleic acids (PNAs) for antisense and single nucleotide polymorphism detection.

Digvijay Gahtory, Merita Murtola, Maarten M. J. Smulders, Tom Wennekes, Han Zuilhof, Roger Stromberg and Bauke Albada, *Org. Biomol. Chem.* **2017**,*15*, 6710.

5) Strain-promoted cycloaddition of cyclopropenes with o–quinones: a rapid click reaction

Digvijay Gahtory, Rickdeb Sen, Andriy R. Kuzmyn, Jorge Escorihuela, and Han Zuilhof, *Angew Chem. Int. Ed.* **2018**, *accepted manuscript*.

6) SuFEx click chemistry delivers a quantitative and orthogonal platform for surface modification.

Digvijay Gahtory, Rickdeb Sen, Sidharam Pujari, Suhua Li, Qinheng Zheng, John E. Moses, K. Barry Sharpless, and Han Zuilhof, *Chem. Eur. J.* **2018**, *manuscript under review*.

7) Mild Photochemical Biofunctionalization of Glass Microchannels

Rui Rijo Carvalho, Sidharam P. Pujari, **Digvijay Gahtory**, Elwin Xander Vrouww, Bauke albada and Han Zuilhof, *Langmuir* **2016**, *32*, 2389

8) Total Synthesis of a Pyrroloindoloquinazoline Alkaloid

Digvijay Gahtory, Mangilal Chouhan, Ratnesh Sharma, and Vipin A. Nair, *Org. Lett.* **2013**, *15*, 3942

[Papers 1and 2 are shared-first author papers with Rickdeb Sen.]

OVERVIEW OF COMPLETED TRAINING ACTIVITIES

Discipline specific activities (courses, workshops, symposia, summer schools etc.)

Nanocity 2015 (**Poster**)	Amersfoort, The Netherlands	**2015**
Nanocity 2016 (**Poster**)	Amsterdam, The Netherlands	**2016**
CHAINS (**Poster and seminar**)	Veldhoven, The Netherlands	**2014–2017**
Wageningen symposium on Organic Chemistry, Royal Netherlands Society of Chemistry (KNCV) (**Seminar**)	Wageningen, The Netherlands	**2014–2017**
Advanced Chemistry	ORC	**2014–2017**

General courses (language courses, presentation courses, statistics, etc.)

VLAG PhD Week	Baarlo	**2014**
VLAG course: IP and valorization awareness	Amersfoort	**2015**
The essentials of scientific writing and presentation	Wageningen	**2018**
VLAG course: Career Perspectives	Wageningen	**2017**

Optionals (participation in discussion groups, PhD excursions, MSc courses, etc.)

PhD trip ORC Denmark and Sweden	ORC	**2017**
PhD trip ORC Canada	ORC	**2015**
Group meetings	ORC	**2014–2018**
Colloquia	ORC	**2014–2018**
Preparing PhD research proposal	VLAG/ORC	**2012–2016**

ACKNOWLEDGEMENTS

अहं ब्रह्मास्मिति (Aham Brahmāsmiti, "I am the infinite reality")

Upanishads (6th century BCE)

More than four years have passed, several papers have been published, a lot of data has been collected and conclusions have been drawn. But is that all I have done and learnt? I guess not. The more I look back at the past, more I see the modesty of my contribution to my own achievements, as those of all others who have supported me emotionally, intellectually, financially, morally or hypothetically seem more significant. And therein lies the true essence of education, as has been rightly pointed out, there lies a largely unsurmountable difference between a well–educated and a well–formed mind. And I have always strived to end up as the latter.

A house is as good as it's foundation. So the story begins all the way back home with my parents and my sweet sisters, Maneesha and Kamini, who I shall be indebted to as long as the space–time continuum exists. Words won't suffice and libraries will run out of space if I begin mentioning all those sacrifices that you have made and continue to do so. To sum it up in one sentence: all that I am and all that I ever will be is the harvest of your hard work. Not to mention your unwavering support both emotional and financial that kept me going during my highly economically mismanaged study years. Also my brother-in-law Deepak, you are one of the coolest people in the searing heat of New Delhi. Out of all my relatives, there are two individuals I cherish being family with the most after my immediate ones. That's you Guddu mama and Rekha mami from Lucknow. You have always been so kind and loving, despite my foolhardiness at times in the past, and it's a pleasure to be your nephew.

If you are one in a dataset of billion, it requires a specially trained and talented eye to spot you. Quite similar is the story of meeting my promoter Prof. Dr Han Zuilhof. After hundreds of unsuccessful PhD applications to different research groups worldwide, you gave me an opportunity to express my scientific acumen, for which I

shall forever be indebted. I will always remember your very first advice “Science is all about picking the right stones, and assembling the right team to muscle their turning”. Most importantly, I am thankful for your belief in my abilities, after the first two years were filled of nothing but failures. Your unwavering faith that unsuccessful experiments are part and parcel of research was infectious and gave me the push that I badly needed. Thereafter began the real journey of my maturity as an independent scientist, not to mention your constant reminders about my poor planning. Getting the first paper out was the highest energy barrier to cross, and once that was done, things fell in place and we produced several awesome studies. It has been a joy to work with you, discuss new ideas and learn from you at every step of the way as a student. You were always there steering the boat whenever I seemed to drift and provided the necessary impetus when morale seemed low in the team, essentially me and Rickdeb or rather Dr. Sen.

Well Dr. Sen, as they say, friends are the family you choose, and you for sure fall in that category. For the record, that eventful dinner at Florine’s defence can now officially be considered one of the defining moments of my scientific career. Another one would be the evening we scribbled on the small notebook in our office. You can be well assured that even if dementia weakens my conscious memory in old age, those two memories will always be sketched at the subconscious level. Together, we have argued philosophically without ever agreeing to the core ideology, barbecued in snow, pulled each other’s legs with the most intellectually deficient jokes ever from your side and in the meanwhile produced science that we both can be proud of. The most striking part of our collaboration was the match in our mental frequency which also was the most awesome. The most dreadful was your reluctance to work hard :). We always looked at a challenge from two different angles, but somehow always found a strategy agreeable to both. Our common passion towards problem–solving and Indian food was probably the catalyst. To summarize, peeche rahoge to peeche hi rah jaoge. Also a special thanks goes to Medea Kosian, who is the only other person (first is his mom!) able to control the mentally wild stallion that Rickdeb is.

I have always felt that the most important lessons of life are learnt from your struggles. If there is one lesson I have learnt to heart in my PhD, it's that "If we knew what it was we were doing, it would not be called research, would it?". This is because one chapter of my thesis occupies a rather large portion of neuronal space dedicated towards my scientific memory. Enter peptide nucleic acids (PNAs) based sensors. Thanks a ton Bauke for helping me completely transform the project and overcoming this challenge which at some point seemed gargantuan. Also many thanks Merita and Prof. Stromberg; it would have been impossible to make any breakthrough without your speedy synthesis of the circular PNA molecules. Especially Merita, your easy availability on the phone during the project despite your family obligations is highly appreciated.

I would also like to extend my gratitude to all the colleagues at ORC, in the past, present and future. So many thanks (as far as my memory permits) Maurice, Tom, Maarten, Floris, Cees, Louis, Teris, Michel, Esther van Andel, Esther Roeven, Bas, Tjerk, Jorin, Rui, Jorick, Ian, Jordi, Aline, Jacob, Ai, Annemieke, Pepijn and all others. A note of thanks to Andriiy and my student Reamon, whose help was very useful in my 4th paper on the novel click reaction. Also a special thanks to Sidhu for all his help in the 4 years and in my early days at ORC along with Sateesh for his awesome food and the tea/coffee–time Indian discussions that we have to this day. Thank you Sateesh for taking me to the supermarket and Kebab place in Ede on my very first evening in NL. The stomach problems I had succeeding that tasty Turkish kebab (my first ever) for several days can never be forgotten.

I have also had the pleasure to study and work with some awesome people during my study years (Bachelor's and master's). Sookhi don (Syed), you will always be one of the best friends I have ever had. Maroof, Chacha (Vikas), Shyam, Panditji (Nikhil), Pankaj, Gumphoo (Deep) and all others; it was one of the most carefree time of my life we had together those 4 years in Dehradun. I always look back at those days with nostalgia and joy. My heartfelt thanks to the old librarian lady (so sad that I don't remember your contact details anymore) who always treated me with so much

affection. Wherever you are, I wish you and your family good health and joy. Once I moved to Mohali, I was again blessed with great company. Sanjay, it's nice to see the results of my hard work on your exam sheets in your current progress. Avadesh bhai, I will always be thankful for your water cooler in the heat of Punjab. A quick note of gratitude to all others whom I befriended at NIPER. Also many thanks Prof. Chakraborti and Prof. Kartha for igniting my love towards organic chemistry through your lectures and Dr. Nair for letting me work in your laboratory. Mangilal Sir and Ratnesh Sir, your help during my master's project is one of the main reasons for the resulting publication and I am ever grateful. Sameek Singh, while we had quite some arguments during our tenure at Curadev, you greatly influenced my attitude regarding intellectual enlightenment of the human brain. I still find it surprising how you read just about anything you found on the internet till 2 PM in the night.

Finally, I come to the one person meeting whom has changed my life and perspective all together. In layman's terms, since that fateful encounter with you in the AFM room, I have found the desire and motivation to lay down my arms and surrender to mental peace. Your voice and presence is the symphony that brings me tranquility during moments of rage and arouses courage in those fearful moments of self–doubt. Being with you has put me on a trajectory of self–belief and above all the thought of finally finding my place in this chaotic and highly probabilistic universe has come home. Thank you my dearest Naoual, for being so patient with me despite my sophomoric behavior at times, your endearing belief in me and foremost, your never ending love...

Finally, to all those whom my memory may have failed, I will be forever thankful for all you have done for me. Signing off to the next step of my life with the immortal words: LIVE LONG AND PROSPER!

The only one of my kind..

Digvijay Gahtory

ABOUT THE AUTHOR

Digvijay Gahtory was born in Sitarganj, a small village in the green northern plains of India in the state of Uttarakhand (part of Uttar Pradesh back then) on 25th December 1990. After his basic school education, he did a bachelors in pharmacy (B. Pharm, 2007–2011) in the green city of Dehradun, India. Towards the end of his bachelors, he qualified the graduate pharmacy aptitude test (GPAT) with an all India rank (AIR) 91 and the national institute of pharmaceutical education and research–joint entrance examination (NIPER–JEE) with an AIR 181. Thereafter, he went on to study medicinal chemistry (M.S. 2011–2013) at NIPER, Chandigarh (the city beautiful) and developed a liking for organic chemistry.

Following a short stint (2013–2014) as a project fellow at Curadev Pharma Pvt. Ltd. in Indian Institute of technology (IIT) Kanpur, he joined the team of Prof. Han Zuilhof as a doctoral candidate (from March 2014). He has a strong interest in synthetic organic chemistry, surface modification and click chemistry. His time in Wageningen University resulted in several interesting research publications and fruitful collaborations. Other than science, he spends his time reading and thinking about history, philosophy and human nature. Personally, he is an affable individual who may seem a hard nut to crack but is much like a walnut, “hard on the outside but soft on the inside”.

The research and training presented in this thesis was financially supported by NanoNextNL (program 5A) and The Netherlands Organization for Scientific Research (NWO) via ECHO project number 712.012.006. This material reflects only the author's views and he is thus not liable for any use that may be made of the information contained therein.

Financial support from Wageningen University for printing this thesis is gratefully acknowledged.